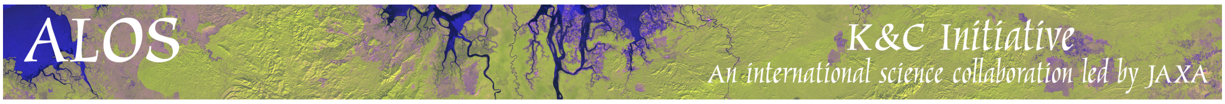

The ALOS Kyoto & Carbon Initiative

Science Team Reports
Phase 1 (2006-2008)

January, 2010

Japan Aerospace Exploration Agency
Earth Observation Research Center
2-1-1 Sengen, Tsukuba-shi
Ibaraki 305-8505, Japan

JAXA EORC, NDX-100003

The ALOS Kyoto & Carbon Initiative

Results from Phase 1 (2006-2008)

The ALOS Kyoto & Carbon (K&C) Initiative is an international collaborative project led by the Japan Aerospace Exploration Agency, JAXA. The Initiative builds on the experience gained from the JERS-1 Global Rain Forest and Boreal Forest Mapping (GRFM/GBFM) projects, in which SAR data from the JERS-1 satellite were used to generate image mosaics over the entire tropical and boreal zones of Earth. While the GRFM/GBFM projects were undertaken already in the mid 1990's, they demonstrated the utility of L-band SAR data for mapping and monitoring forest and wetland areas and the importance of providing spatially and temporally consistent satellite acquisitions for regional-scale monitoring and surveillance.

The ALOS K&C Initiative is set out to support data and information needs raised by international environmental Conventions, Carbon cycle science and Conservation of the environment. The project is led by JAXA EORC and supported by an international Science Team consisting of some 25 research groups from 14 countries.

The objective of the ALOS K&C Initiative is to develop regional-scale applications and thematic products derived primarily from ALOS PALSAR data that can be used to meet the specific information requirements relating to Conventions, Carbon and Conservation. The Initiative is undertaken within the context of three themes which relate to three specific global biomes: Forests, Wetlands and Deserts. A fourth theme deals with the generation of continental-scale ALOS PALSAR image mosaics. Each theme has identified key products that are generated from the PALSAR data including land cover (forest mapping), forest change mapping and forest biomass and structure (Forests), global wetlands inventory and change (Wetlands), freshwater resources and desertification (Deserts). Each of these products is generated using a combination of PALSAR, in situ and ancillary datasets.

This report presents results obtained by the Science Team within the first two years of ALOS PALSAR operations (Nov. 2006 - Jan. 2009).

Masanobu Shimada
Manager ALOS Science Program

Ake Rosenqvist
K&C Initiative Science Coordinator.

Table of Contents (1/2)

Forest Theme Reports

Table of Contents (2/2)

Wetlands Theme Reports

Desert Theme Report

Mosaic Theme Reports

Forest Theme Reports

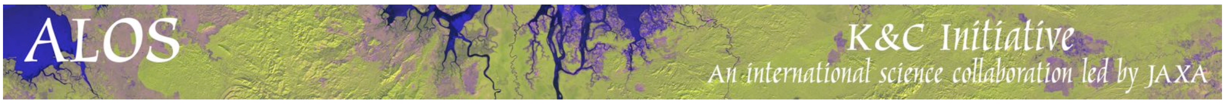

Forest Theme

Regional Mapping of Forest Growth Stage, Queensland, Australia, through Integration of ALOS PALSAR and Landsat Foliage Projected Cover

Richard Lucas *et al.*
Aberystwyth University (Wales/U.K.)

Regional Mapping of Forest Growth Stage, Queensland, Australia, through Integration of ALOS PALSAR and Landsat Foliage Projected Cover.

Richard M. Lucas, Peter Bunting and Dan Clewley,
Institute of Geography and Earth Sciences, Aberystwyth University, Aberystwyth, Ceredigion, United Kingdom, SY23 2EJ
John Armston
Queensland Department of Natural Resources and Water (QDNRW),
Climate Building, 80 Meiers Road, Indooroopilly, Queensland, 4068.
Joao Carreiras
Instituto de Investigação Científica Tropical (IICT), Departamento de Ciências Naturais,
Unidade Desenvolvimento Global, Rua João de Barros, 27, 1300-319 Lisboa, Portugal.
Arnon Accad
Queensland Herbarium, Environmental Protection Agency, Brisbane Botanic Gardens,
Mt. Coot-tha Road, Toowong, Brisbane, Queensland, 4066, Australia.

***Abstract*—Focusing on northern Australia and specifically the State of Queensland, ALOS PALSAR and Landsat-derived Foliage Projected Cover (FPC) 50 m strip mosaics were investigated for their potential for regional mapping of regrowth (non-remnant areas only) and above ground biomass (as a surrogate for growth stage) and for detecting dead standing timber, either induced naturally or through anthropogenic activities. Whilst approaches to mapping were developed and implemented at a regional level, the accuracy of the estimates was compromised by the variability in backscatter across and between strips. Current research is focusing on correction of mosaics and the collection and collation of new field and airborne datasets to support the regional mapping of growth stages, primarily between 2007 and 2011. Comparisons with historical JERS-1 SAR are also being undertaken.**

***Index Terms*—ALOS PALSAR, K&C Initiative, Forest Theme, forest growth stage, Queensland, Australia.**

I. INTRODUCTION

A. *Defining forest growth stage*

All forests can be associated with a growth stage but the spatial extent and size class distribution of trees at different stages of growth varies. Where plantations occur or forests are re-establishing on previously cleared land, relatively homogenous even-aged stands of forests occur. However, heterogeneity in the growth stage is introduced through competition and also where forests have experienced interrupted succession through processes that are natural, such as fires or drought, associated with human activities, such as grazing and selective thinning. Variability in the structure of forests at different stages of growth is also introduced at various scales through differences in physical environment and climate. Quantifying forest growth stage, particularly at regional levels, is therefore complex.

In all its forms, knowledge of the forest growth is fundamental for a number of reasons. In particular, regional estimation of growth stage can inform on the capacity of forests to recover carbon and biodiversity lost previously through deforestation and degradation activities. By understanding the impact of past land use and type as well as natural processes and events on the regrowth capacity of forests, options for greater sustainability of the land can also be developed.

B. *Remote sensing of growth stage*

Forest growth is a continuum but stages of growth are often described to more simply convey the state of the forest and methods, particularly those based on remote sensing data, vary. The scale at which forests are observed also impacts on the methods used for the description and quantification of growth stage using remote sensing data.

Detailed, albeit spatially limited, observations of individual trees and stands (e.g., in terms of height and size class distributions) can be undertaken using, for example, fine (< 1 m) spatial resolution data such as Light Detection and Ranging (LiDAR), aerial photography and/or multi/hyperspectral data (e.g., Ikonos, Quickbird, CASI [1]). More commonly, however, growth stage is defined using coarser spatial resolution optical and/or radar remote sensing data because of the requirement for characterisation and mapping across more extensive areas (e.g., for commercial forest inventory).

Many studies focusing on forest growth stage mapping have utilised optical remote sensing data, largely because of the availability of time-series, which can extend back to the early 1970s (in the case of Landsat). Using these data, the stage of growth is often defined on the basis of forest age, as estimated by comparing time-series classifications of land cover, or by establishing relationships with biophysical properties (e.g., height, density, or crown cover) that vary over the growth period. Spectral differences in reflectance may also indicate the growth stage as a function of the species composition, which may change rapidly as the forest regenerates, particularly in tropical environments [2]. Actual and relative biomass is also commonly used to indicate growth stage, although measures need ideally to be relative to the potential maximum biomass for a particular biome and environmental envelope.

With the increased availability of Synthetic Aperture Radar (SAR) data from spaceborne sensors, approaches to growth stage mapping have varied. The majority have indirectly quantified growth stage by utilising the recognised relationship between SAR backscatter and biomass or have established relationships with other structural attributes (e.g., stem number density, volume; (e.g. [3]), which vary as the forests regenerate. Time-series of SAR data have also been exploited to track the structural development of forests. Options for integrating SAR and optical data for mapping regeneration stage have also been considered. As an example, [4] combined NASA Jet Propulsion Laboratory (JPL) AIRSAR L-band HH SAR backscatter data and Landsat-derived Foliage Projected Cover (FPC) to map the extent of regrowth dominated *by Acacia harpophylla* (Brigalow) in south central Queensland, Australia. Based on the known relationship between L-band HV backscatter and biomass, several stages of regeneration were mapped.

C. Project objectives

The overall objective of the project is to investigate and demonstrate the potential of the Japanese Space Exploration Agency's (JAXA) Advanced Land Observing Satellite (ALOS) Phased Array L-band SAR (PALSAR), either singularly or in combination with optical data, for quantifying forest growth stage in northern Australia, focusing primarily on the State of Queensland and regenerating forests in particular. The study also sought to establish whether measures of growth stage might also be extracted from these data, including above ground biomass (relative to potential) or the extent of dead standing timber.

II. Background

A. Vegetation mapping in Queensland

The survey and mapping of Queensland's vegetation is a major program of the State's Environmental Protection Agency (EPA). The mapping program provides detailed information on regional ecosystems in terms of their distribution, rate of clearing and conservation status. The majority of regional ecosystem information has been produced at a scale of 1:100 000 although some coastal areas are mapped at a larger (1:50,0000) scale, including parts of Southeast Queensland and the Wet Tropics bioregions. Areas of non-remnant with vegetation (e.g., young regrowth or heavily disturbed vegetation) are not included [6]. For woody vegetation to be mapped as remnant, the dominant canopy must have > 70% of the height and > 50% of the cover relative to the undisturbed height and cover of that stratum and be dominated by species characteristic of the vegetation's undisturbed canopy. [20] provides further details on these definitions and the methodology used to survey and map vegetation in Queensland.

B. Forest growth stages in Queensland

Prior to European settlement, over 80 % of Queensland supported woody vegetation, including a diversity of forests, shrubs and heaths [5], with these ranging from tropical rainforest to low open mallee. Much of this vegetation, particularly in the northern regions, is still regarded as remnant although nevertheless suffers disturbance from natural processes (e.g., drought) or events (e.g., fire). In these areas, growth stage is more difficult to define because of the complexity of regeneration patterns associated with the differential response of species to adverse conditions and their capacity to recover, and limited knowledge of the characteristics of the mature state. A number of studies have, nevertheless, attempted to establish what is the biomass potential of these areas based on both pre-European and present-day distributions of ecosystems [6]. Differences between these two datasets may therefore provide some indication of the growth stage of forests, although factors such as fire extent, frequency and intensity are not easily accounted for.

Whilst much of Queensland is still regarded as remnant, significant clearing of vegetation has historically occurred in the south central and south-eastern regions. The Brigalow Bioregion, for example, has experienced some of the highest clearance rates with less than 15 % of forests with brigalow of gidgee (*Acacia cambagei*) as a major component occurring [7]. Other forest types that are disproportionately affected by clearing include flood and other depositional plains, which are typically dominated by *Eucalpytus* species. Within these regions, methods of clearing, and hence the subsequent regrowth of woody vegetation, vary. Where clearing occurs at the same time and over large areas, subsequent regrowth is often relatively even-aged. However, where processes such as ring-barking or stem injection occur [8], the regeneration is more piecemeal. The species composition and structure (e.g., density, canopy cover) of regenerating vegetation vary depending upon biogeographic distributions as well as the use and management of the land prior to abandonment (e.g., burning and reclearance frequency). Variations in topography, soils, geology, hydrology and climate also impact upon regrowth rates.

C. Current approaches to mapping growth stage

Within Australia, mapping of growth stage has commonly been undertaken using aerial photography, with young, early mature, mature, late mature and over-mature stages often defined. [9] suggested seven classes, with these depending largely upon the size, shape and condition of crowns. However, the mapping of equivalent classes using spaceborne sensors is more difficult and alternative approaches are needed.

For mapping the extent of early regrowth in areas where *Acacia* dominated, the method developed in [4] was based on the premise that whilst such forests typically support an FPC equivalent to forests, as defined by the Queensland Department of Natural Resources and Water (QDNRW), the size and density of stems has to be of sufficient magnitude to evoke a response at L-band and particularly at the HH polarisation where double bounce scattering between stems and the ground surface is prominent. Therefore, the extent of woody regrowth was associated with areas supporting an FPC > 12 % (approximately equivalent to 20 % canopy cover) but with an L-band HH backscatter equivalent to that of non-forest. The accuracy of classification for the Injune study area in central south east Queensland, as assessed against hyperspectral Hymap data, exceeded 80 %.

L-band SAR data also showed potential for discriminating stages of growth within the mapped area of regrowth. Modelling of L-band SAR backscatter from stands dominated by *A. harpophylla* at various stages of growth suggested that stems (which occur in clusters) individually have to be at least 2.5 m in height (which equates to about 2 - 5 cm in diameter) for the L-band backscatter to exceed that of non-forested areas. The model also indicated that volume scattering at L-band HV started to increase where trees were approaching 4 m in height, which was attributable to the increase in the size of branches within the canopy. The L-band HV backscatter was also shown by [10] to be more sensitive to increases in above ground biomass compared to L-band HH and provided an avenue for quantifying regrowth stage (i.e., by binning biomass classes). An alternative approach to tracking the development of forests is to utilise time-series of FPC on the assumption that increases and changes in spatial distribution of FPC occur as the canopy expands, particularly in open forest systems.

III. Study area

Within Queensland, the extent of vegetation has been mapped using a combination of historical aerial photography and satellite sensor data [11] by the Queensland Herbarium of the Environmental Protection Agency (EPA; Figure 1). Areas of vegetation clearance over the period 1988 to 2009 have also been mapped on an annual basis by QDNRW. By linking clearance data with the distributions of mapped ecosystems, losses of vegetation by forest type are determined and areas regarded as remnant or non-remnant defined.

Within this region, the study focused initially on the Injune Landscape Collaborative Project study area ([12,13]; Figure 2), which is located within the Southern Brigalow Belt. In the late 1990s and early 2000s, extensive clearance of forests within and below the southern section of the Injune study area occurred. However, the areas cleared were difficult to maintain as active pasture and extensive tracts of regrowth, dominated primarily by brigalow, but also other species such as Poplar Box (*E. populnea*) and Silver-leaved ironbark *(E. melanaphloia*) regenerated. Other areas of regrowth distributed throughout Queensland and for which plot-based data had been collected, were also identified, with these being associated with *Acacia*-dominated forests but also a range of other forest types.

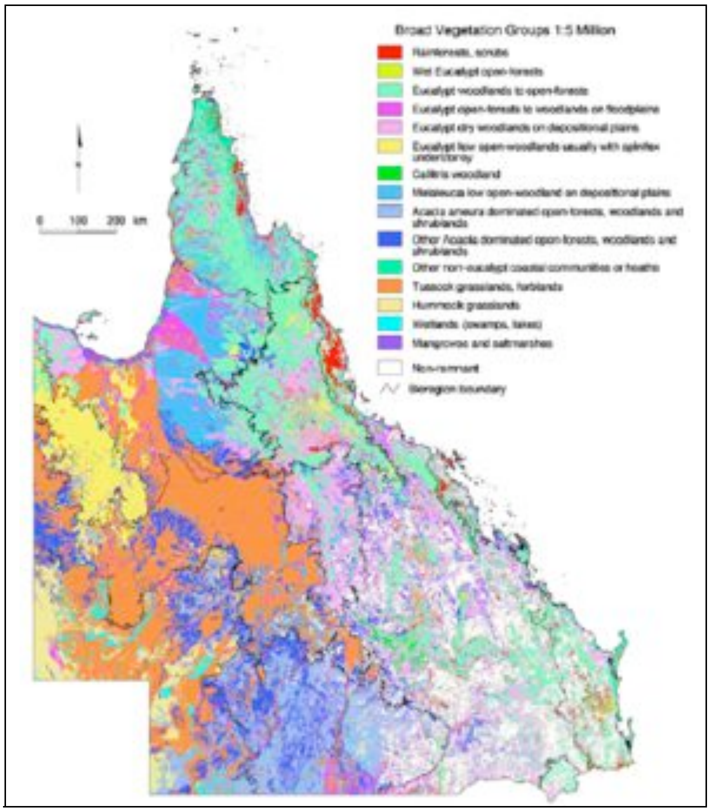

Figure 1). Mapped distribution of major forest types in Queensland, Australia [6]

IV. Available Data

A. Satellite sensor data.

For northern Australia, ALOS PALSAR fine beam dual (FBD) strip data were provided by the JAXA Kyoto and Carbon (K&C) Initiative for both 2007 and 2008. These data were provided at 50 m spatial resolution, in slant-range geometry, amplitude format, and 64 looks (4 in range and 16 in azimuth), with a swath width approximating 70 km.

Figure 2). The location of the Injune Landscape Collaborative Project and other regrowth sites in the IBRA bioregion of Brigalow Belt South, Queensland.

A regional mosaic of Landsat FPC data was also generated for 2006 by the Queensland Department of Natural Resources and Water (QDNRW) and the analysis focused on only those areas associated with non-remnant vegetation. To support the mapping of forest growth stages, a number of additional datasets were collated or collected including:

a) Compact Airborne Spectrographic Imager (CASI) and hyperspectral HyMap data, for extensive areas of regrowth within the Injune study area.
b) Plot-based measurements, including forest inventory from the Injune site [13], other regrowth sites 14], and through the TRAPS network of permanent plots [15].

These data were used to inform on the location of areas of regrowth. Additional datasets are currently in the process of being acquired.

V. METHODS

A. *Pre-processing of satellite sensor data.*

The ALOS PALSAR strip data were provided in slant range geometry, amplitude format, and were converted to intensity and calibrated (absolute calibration) using Gamma SAR processing software [16]. Geocoding of the strip data was undertaken with the Gamma Differential Interferometry and Geocoding (DIFF and GEO) suite. Initially, the geometric transformation from image to reference coordinates was undertaken by first using orbital state vectors and SRTM-derived DEM to approximate the position of each image strip and, second, establishing offsets between the ALOS PALSAR data and a SAR image simulated using the same SRTM-derived DEM to refine the registration. In this process, correlations were established between a large number of n x n windows passed over both images, with those with greatest correlation retained. However, as much of the northern Australia has very little significant relief, the refinement of the geometric transformation was undertaken (for Queensland only) by using Landsat Enhanced Thematic Mapper (ETM+) panchromatic mosaics for zones 54 to 56 and the same automated cross-correlation procedure. Each strip was then resampled using the resulting transformation. Geocoding errors were typically less than < 50 m. Across track correction and mosaicing was undertaken using Gamma and procedures developed by the European Commission's Joint Research Centre (JRC).

The Landsat FPC mosaic was generated using procedures outlined in [4,19]. As these were generated using the same Landsat sensor data associated with the panchromatic bands, the Landsat FPC and other State-wide datasets (e.g., land use change, vegetation mapping; several of which were obtained using the Landsat sensor data themselves), were also well registered and able to be integrated into subsequent analyses.

B. *Mapping regrowth and dead standing timber (non-remnant areas)*

Within the Brigalow Bioregion, and as observed using airborne SAR data, areas of regrowth dominated primarily by *A. harpophylla*, exhibited an FPC equivalent to that of forests and an ALOS PALSAR L-band HH backscatter equivalent to non-forest. To map the extent of regrowth, a rule-based classification was undertaken within Definiens Developer image segmentation and classification software, whereby areas defined as forest (FPC threshold > 12 %; equating to a canopy cover of ~ 20 %) and with a low (< ~ -14 dB) L-band HH backscatter were mapped as regrowth. Within this mapped area, relative stages of regrowth were defined by binning biomass values obtained using a relationship established with L-band HV backscatter (for low biomass forests). The same approach for mapping regrowth was applied to other sites and also to the strip mosaic of Queensland (non-remnant areas only).

Based on previous analysis of airborne data [8], areas of dead standing timber were identified as having an FPC typical of non-forest (< 12 % FPC) and an L-band HH typical of forests (e.g., > -14 dB), with this combination indicating the presence of woody material but no leaves.

C. *Biomass estimation*

For the local study areas and also for the full mosaic, above ground biomass (B) was estimated using a modification of the algorithm of [18], which included only the L-band HH and HV backscattering coefficient (σ^o) such that:

$$\mathrm{Ln}\,(B) = a_0 + a_1\sigma^o\mathrm{HH} + a_2\sigma^o(\mathrm{HV})^2 + a_3\sigma^o\mathrm{HV} + a_4\sigma^o(\mathrm{HV})^2 \quad (1)$$

where a_0 to a_4 represent equation coefficients and σ^o represents the backscatter coefficient (dB). The algorithm was re-parameterized by including measures of biomass collected for regrowth and intact forest sites (e.g., the permanent plot data acquired as part of the TRAPS network).

VI. RESULTS

A. *Regional mosaics of ALOS PALSAR and Landat FPC*

For Queensland, combined mosaics of Landsat-derived FPC and ALOS PALSAR HH and HV data were generated using both the 2007 and 2008 (Figure 3) acquisitions. Whilst at a regional level, the mosaic evidently suffers from the across track variability and the between-image differences (including, although to a far lesser degree, that associated with the Landsat FPC), unique information on vegetation and other surface structures is apparent within subsets of the mosaic (see example in Figure 4). Refinement of the strip correction and mosaicking process is ongoing with a view to generating a more seamless mosaic with standardized backscatter values.

Based on SAR simulation [13], L-band microwave interactions associated with the HH and HV data are primarily the result of double bounce scattering with the trunks and volume scattering from larger branches, respectively. By contrast, FPC is directly retrieved from Landsat sensor and ancillary (e.g., climate data; [19]) data and provides a quantitative a measure of foliage cover. The combination of these within the mosaic therefore provides a new regional data layer which can assist characterization and mapping of a range of forest structural types, including growth stage (particularly regeneration stage and standing dead or senescent timber). Unique information on the distribution and characteristics of wetlands (including mangroves) is also provided.

a)

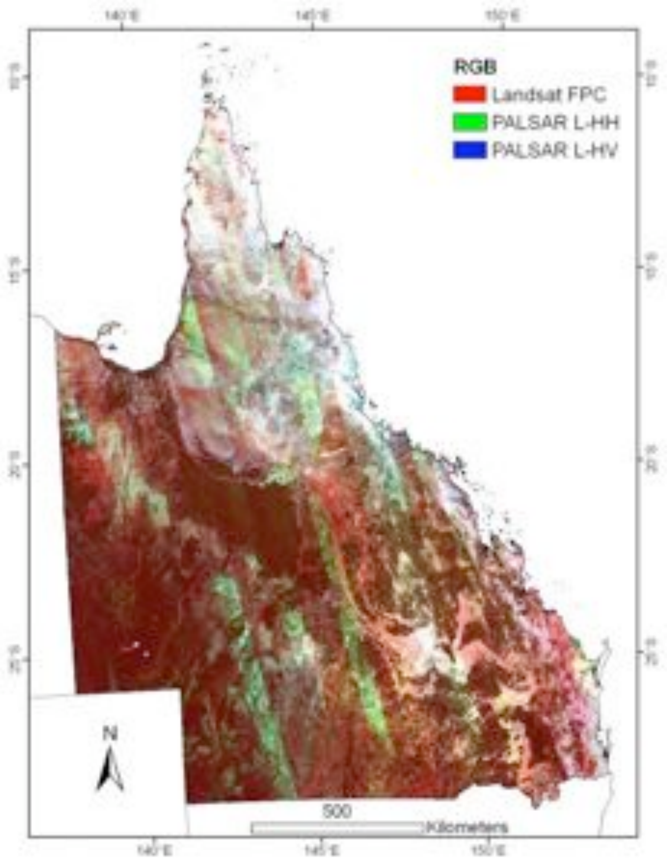

Figure 3) Landsat FPC and ALOS PALSAR L-band HH and HV mosaic of Queensland and b) a forested area in southern Queensland showing areas of closed tropical forest (pink), coastal mangrove (orange) and wooded savanna (shades of red and green)

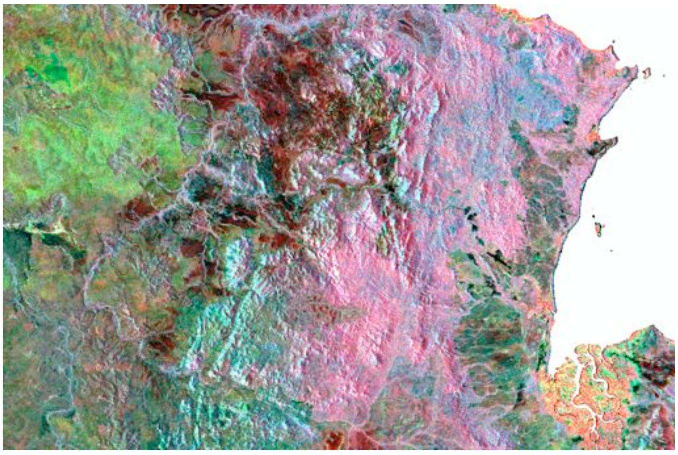

Figure 4) Landsat FPC and ALOS PALSAR L-band HH and HV mosaic of a forested area in north east Cape York Bioregion, Queensland, showing areas of closed tropical forest (pink), coastal mangrove (orange) and wooded savanna (shades of red and green)

B. Regrowth extent and growth stage, Injune

For the Injune study area, composites of Landsat FPC and L-band HH and HV data (in RGB respectively) were generated (Figure 5) which highlighted areas associated with regrowth (red).

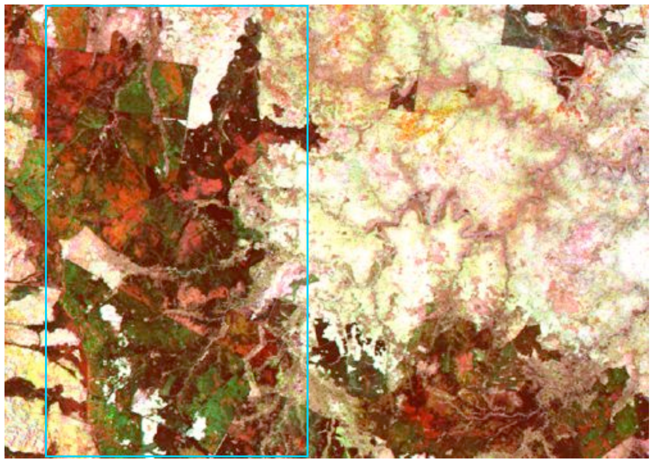

Figure 5). Subset of Landsat-derived FPC mosaic and ALOS HH and HV mosaics in RGB showing areas occupied by dead standing timber (green). Remnant vegetation supports higher FPC and HH and HV returns (shades of white).

For non-remnant forests, a diversity of information on the structure of forests within these three data layers was particularly evident. The map of regrowth extent and classification of two growth stages (Figure 6) within areas defined as non-remnant vegetation showed a close correspondence with the distribution observed within the composite image. The distribution was also similar to that mapped previously using a combination of AIRSAR L-band data and Landsat FPC over the study area.

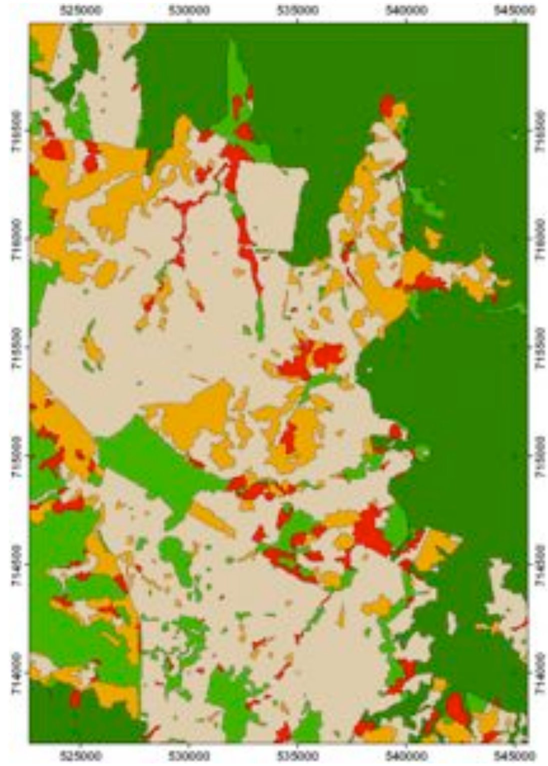

Figure 6). Classification of remnant forest (dark green), non-remnant forest (light green), early regrowth (orange) and late regrowth (red; see inset in Figure 5)

Preliminary regrowth maps have also been generated for areas regarded as non-remnant (i.e., previously cleared) in Queensland. Whilst a general correspondence between the mapped distributions of regrowth with field data and observations was noted, some discrepancies were observed. In particular, confusion between the early stages of regrowth and other vegetation types, including understorey vegetation, sand dune vegetation, heathlands and low mangroves led to the overestimation of regrowth extent. Older stages of regrowth or those occurring within areas with older remnant trees were also less well mapped. The variability in overall forest structure, which is largely associated with different species dominating regrowth and the spatial patterns of regeneration, was also considered responsible for the inconsistencies in classification, which are currently being investigated.

C. Dead standing timber

Preliminary assessments of the distribution of dead standing timber were undertaken for selected areas with ground information with a view to extrapolating to the wider area following correction of the ALOS PALSAR mosaics. Areas of of dead standing timber are noticeable in Figure 5 (dark green). Additional areas are being investigated with a view to regional mapping in Phase 2.

D. Biomass estimation

Using 10-fold cross validation, the model for retrieving biomass yielded a root mean square error of 28.5 Mg ha^{-1} and a coefficient of determination between observed and predicted of 0.48. Errors in the model were associated with discrepancies in the timing of the acquisitions of ALOS PALSAR and field data and also to within (across track) and between differences in the image data. Such issues are currently being addressed in Phase 2.

This model was nevertheless applied to the ALOS PALSAR 2007 and 2008 mosaics of Queensland to generate a preliminary map of biomass (Figure 6). The mapping largely reflected the known distribution of biomass within the region, with greater amounts associated with forests on the coastal regions towards the north and west of Australia. However, the biomass of many of the subtropical and tropical forests was under-estimated and this was attributed to the algorithm being developed primarily using data obtained for wooded savannas. The upper range of biomass (approximated here at 150 Mg $^{ha-1}$) is uncertain because of saturation of L-band SAR. Discrepancies are clearly associated with variation within and between strips.

Our studies using airborne data have suggested that different algorithms need to be developed and applied as a function of the structure of the forest (and particularly in relation to canopy closure). For this reason, revisions of the algorithm are being undertaken in Phase 2 using new collations of existing field data acquired over periods corresponding to past and future ALOS PALSAR acquisitions. New field and airborne (e.g., LiDAR) data acquisitions are also being conducted in 2009 to support this analysis.

VII. Discussion

A. Overview

Consideration of the differential interaction of microwaves with different components of the forest volume is important in understanding how and why different forest growth stages may be differentiated and mapped using SAR data. The following provides an overview of observations using airborne multi-frequency polarimetric SAR data and then discusses these in the context of mapping biomass, regrowth, dead standing timber from ALOS PALSAR data.

B. Microwave interactions

For most forests with a full canopy, a high C-band backscatter is typically observed, primarily because of volume scattering from the leaves and small branches [13]. In many ways, these data provide similar information as the Landsat FPC. However, for forests to be observed within lower frequency L- and P-band data, the size (diameter and also length) and density of stems have to be sufficient to evoke a response. This is highlighted below using two examples from woody savannas (Lucas *et al*., 2006b).

In the first example, areas of regrowth and more mature forest are not distinguishable at C-band (and also within Landsat FPC data) because the amount of foliage and small branches in the canopy is similar. However, the L- and particularly the P-band backscatter from the younger regrowth forests is lower compared to the mature forest because there is an insufficient amount of woody material for double bounce or volume scattering mechanisms to fully operate. In the second example, medium size (e.g., 5 - 10 cm diameter) trees (as delineated within hyperspectral data) are observed at L-band but not at P-band, suggesting that even less and perhaps a significant proportion of the woody material remain undetected.

This knowledge can assist with interpretation of relationship between backscatter and biomass. In closed forests, for example, saturation occurs above a certain level of biomass density as no increase in backscatter with biomass is observed. In more open forest, however, the same magnitude of backscatter may not be attained because of the lack of interaction with woody material below a certain size and density. At P-band HV, for example, 'saturation' within wooded savannas is observed at about 65 Mg ha^{-1} [10], which is lower than that typically observed for closed forests (100-150 Mg ha^{-1}) simply because the P-band is only showing sensitivity to the larger woody components and many of the smaller trees and components are simply not observed. The relatively wide spacing of trees may also reduce the overall backscatter as greater interactions with the ground surface occur.

Other factors also complicate interpretation. For example, as a greater amount of backscatter returns from ground interactions occurs in more open forests, rainfall and associated increases in soil moisture can also increase backscatter and give a false impression of increased biomass. Backscatter also increases with surface roughness and, particularly in areas of rocky terrain, can lead to inaccuracies in biomass retrieval.

C. Biomass estimation

For wooded savannas of relatively low biomass, and depending on their structure, L-band microwaves are well suited for estimating biomass because of greater interaction with a wider range of size classes (i.e., of woody branches and trunks). Differences in the biomass-backscatter relationships as a function of canopy closure are currently being evaluated but indicate that different algorithms are required for estimating the biomass of open and closed forests. This is partly evident from Figure 8 where many of the higher biomass tropical and subtropical rainforests on the east coast are (incorrectly) not associated with a high biomass value. However, wooded savannas known to support higher biomass values (e.g., the west coast of Cape York) have been identified.

Whilst the current algorithm has been developed for retrieval of biomass without consideration of forest type, the formulation of separate algorithms for open and closed forests is anticipated. However, the following needs to be undertaken:

a)

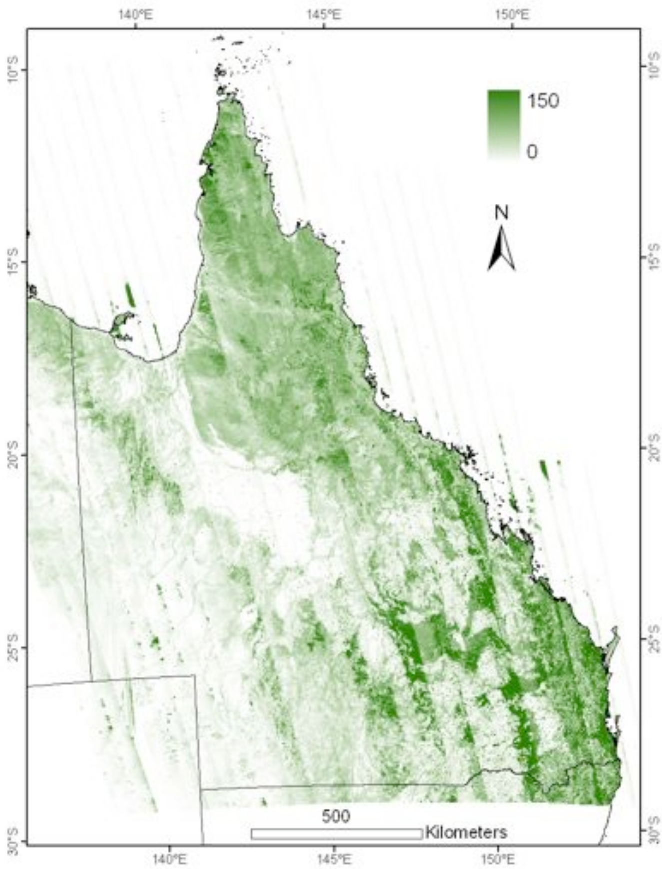

b)

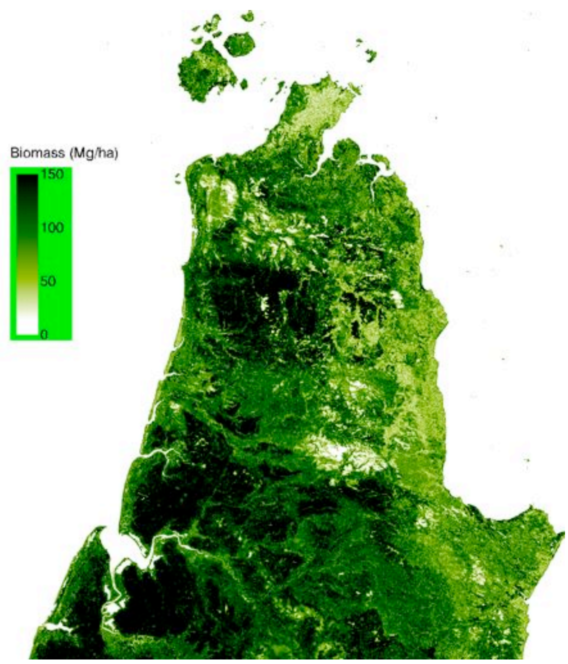

Figure 8. Preliminary estimates of biomass for top) Queensland and bottom) north Cape York based on ALOS PALSAR data acquired in 2008

a) A range of field-based biomass data needs to be collated and collected for both open and closed forests. This is currently being undertaken with focus on data acquired during the period of the ALOS operation. A proportion of the available field data was acquired prior to this period, which has led to inaccuracies in parameterization of the algorithm. This is particularly an issue in northern Australia where forests are dynamic and responding differently to processes such as drought, flooding, fires and anthropogenic disturbance.

b) Scatter in the relationships between L-band data and biomass attributed to variations within (due to cross track effects) and between the ALOS PALSAR images/strips needs to be reduced through better correction of the data.

D. Regeneration stage

The combination of L-band HH and Landsat FPC is a simple approach to the mapping of regrowth that can be applied using image pairs acquired on proximal dates. The main limitation is the inconsistency of the approach between regions. Whilst the approach provides good estimates where a relatively closed canopy, such as that typified by brigalow occurs, regrowth with sparser canopies or older regrowth is more difficult to detect. The approach to mapping is therefore being evaluated for a wider range of regrowth types and across bioregions.

E. Dead standing timber

The combination of Landsat-derived FPC and L-band HH data allowed known areas of dead standing timber to be mapped. Typically, identified areas were associated with clearance for agriculture (particularly grazing) as many trees are killed but left standing and a grass layer maintained beneath. However, where tree death occurs through natural causes such as fire, flooding or drought, regeneration often occurs either from the understorey or through epicormal growth. FPC may therefore return to levels associated with forest cover after several years of growth. Confusion with woody debris and also rocky outcrops or surfaces also occurred, although the ratio of L-band HH and HV assisted in discrimination.

Whilst in theory, the approach to classification should provide relatively consistent mapping, the high level of variability in the structure of dead standing timber (e.g., in terms of size class distributions), the causes of tree death and the nature of recovery requires adaption of algorithms which is an ongoing process. Nevertheless, the potential exists for the regional mapping of dead standing timber over time which, if combined with Landsat FPC and climate data, may provide unique insights into the longer-term response of forests to natural and human-induced (including climate) change.

VIII. CONCLUSIONS

The research has provided a first evaluation of the use of the ALOS PALSAR and Landsat-derived FPC mosaics for regional mapping of forest growth stage in Queensland, Australia. Options for quantifying the regional extent of different stages of early regrowth and standing dead or senescent timber have been presented. An algorithm for the estimation of above ground biomass has been formulated and applied regionally. Key highlights of the work are as follows:

a) The Landsat FPC and ALOS PALSAR HH and HV mosaics have provided unique regional datasets that give information on different structural attributes of woody vegetation (leaves, branches, trunks). Given the diversity of structural formations across Queensland and northern Australia in general, which are largely attributable to environmental (e.g., climate) gradients, the interpretation of these mosaics is complex. Nevertheless, our studies have shown that an enormous amount of information on vegetation and particularly growth stage and also structural type, can be extracted.

b) Options for mapping regrowth and dead standing timber in non-remnant areas have been provided. Information on the extent of regenerating forests on land cleared of vegetation since European settlement (defined as non-remnant) is required to better understand the recovery of forests following clearance and also to determine their relative biomass and contribution to regional carbon budgets. Whilst discrepancies in the extent of regrowth were observed, options exist for resolving these issues. The extent of dead standing timber, particularly over time, is important for understanding ecosystem response to climatic variation (e.g., drought cycles), particularly if integrated with time-series of JERS-1 SAR data. Detection of dead standing timber associated with human activities rather than natural events and processes appears to be more successful, although options for mapping the latter are being considered.

c) The estimation of biomass from ALOS PALSAR dual polarimetric data is feasible although better parameterisation of the model is required through use of field and airborne-derived estimates acquired over similar time-periods. Different biomass retrieval algorithms are therefore being developed, at least for closed and open forests.

Despite these advances, the provision of the regional mosaics has raised particular issues in relation to correction of the strip data and the availability of appropriate and timely ground truth data, particularly given the dynamic nature of the Australian forests. For these reasons, current research is focusing on better correction of the strip mosaic data and collection of field and airborne data in late 2008/early 2009 such that more appropriate datasets are used to support the development of mapping algorithms. Such activities include:

a) Reprocessing of the ALOS PALSAR data to reduce within (across track) and between strip variation and gaining a better understanding of the reasons for such variation through reference to meteorological and vegetation datasets.

b) Acquisition of full waveform LiDAR for 20 sites covering a range of forest structural types (from sparse open woodland to closed subtropical forests) and associated collection of ground truth (including terrestrial laser scanner data). Data have already been acquired for 19 sites and LiDAR are to be acquired for Injune (Site 20) in April, 2009 (9 years following the previous acquisition in 2000). Such data will also then be used to establish whether change can be detected (e.g., regrowth, tree mortality, woody thickening) through time-series comparison of SAR data, and in combination with the Landsat time-series.

c) Focused studies on areas in Queensland associated with change. Examples include the Bunya Mountains where woody thickening and rainforest encroachment has occurred in recent decades.

d) The advancement of algorithms for retrieving the above ground biomass of forests with modifications for closed and open forests.

These activities are being conducted currently and will also feed into the interpretation of the 2010 and 2011 ALOS PALSAR mosaics to be provided under the K&C Initiative in Phase 2.

ACKNOWLEDGEMENTS AND IMAGE COPYRIGHTS

The work has been undertaken in conjunction with the Queensland Department of Natural Resources and Water (QDNRW) and the Queensland Herbarium and has been undertaken within the framework of the JAXA Kyoto & Carbon Initiative. ALOS PALSAR data have been provided by JAXA EORC." All illustrations are copyright of the ALOS K&C © *JAXA/METI, QDNRW and Queensland Herbarium EPA*.

REFERENCES

[1] R.M. Lucas, A.C. Lee and P.J. Bunting, "Retreiving forest biomass through integration of CASI and LiDAR data". Int. J. Remote Sens., 29, 1553-1577, 2008.

[2] R.M. Lucas, M. Honzak, I. do Amaral, P.J. Curran and G.M. Foody, "Forest regeneration on abandoned clearances in central Amazonia", Int. J. Remote Sens., 23, 965-988, 2002.

[3] L.E.B. Eriksson, M. Santoro, A. Wesmann and C.C. Schmullius, "Multi-temporal JERS repeat-pass coherence for growting stock volume estimation of Siberian forest. *IEEE Trans.Geosci. Remote Sensing*, 41, 1561-1570. 2003.

[4] R.M. Lucas, N. Cronin, M. Moghaddam, A. Lee, J. Armston, P. Bunting and C. Witte, "Integration of radar and Landsat-derived Foliage Projected Cover for woody regrowth mapping, Queensland, Australia. *Remote Sens. Environ*., vol. 100, pp. 407-425, 2006.

[5] B.A. Wilson, V.J. Neldner and A. Accad, "The extent and status of remnant vegetation in Queensland and its implications for statewide vegetation management and legislation", *Rangeland J*., 24, 6-35, 2002.

[6] A. Accad, V.J. Neldner, B.A. Wilson and R.E. Niehus, "*Remnant vegetation in Queensland: Analysis of Remnant vegetation 1997-1999-2000-200-2003, including Regional Ecosystem information*. Queensland Herbarium, Queensland Environmental Protection Agency, Brisbane, 2006.

[7] R.J. Fairfax and R.J. Fensham, "Assessing woody vegetation cover change in north-west Australian savanna using aerial photography". *Int. J. Wildland Fires*, 12(4), 359-367, 2000.

[8] R.M. Lucas, A. Accad, L. Randall & P. Bunting, "*Assessing human impacts on Australian forests through integration of airborne/spaceborne remote sensing data*." In *"Patterns and Processes in Forest Landscapes: Multiple Uses and Sustainable Management*", (Eds. R. Lafortezza *et al*.), pp. 213-240, Springer, 2008.

[9] P.Gibbons and D. Lindenmayer*, Tree Hollows and Wildlife Conservation in Australia*, CSIRO Publishing, 2002.

[10] R.M. Lucas, N. Cronin, A. Lee, C. Witte and M. Moghaddam, "Empirical relationships between AIRSAR backscatter and forest biomass, Queensland, Australia". *Rem. Sens. Environ*., vol. 100, pp. 388-406, 2006.

[11] W.H. Burrows, M.B. Hoffman, J.F. Compton, P.V. Back, & L.J. Tait. Allometric relationships and community biomass estimates for some dominant eucalyptus in central Queensland woodlands. *Australian Journal of Botany*, vol 48, pp. 707-714, 2000.

[12] P.K. Tickle, A. Lee, R.M. Lucas, J. Austin and C. Witte, "Quantifying Australian forest and woodland structure and biomass using large scale photography and small footprint LiDAR". *For. Ecol. Man*., 223, 379-394, 2006.

[13] R.M. Lucas, M. Moghaddam and N. Cronin, "Microwave scattering from mixed species woodlands, central Queensland, Australia." *IEEE Trans.Geosci. Remote Sensing*, vol. 42, pp. 2142-2159, 2004

[14] J. Dwyer, Queensland University, Brisbane, Australia, personal communication, 2008.

[15] W. H. Burrows, B.K. Henry, P.V. Back, M.B. Hoffmann, L.J. Tait, E.R. Anderson, N. Menke, T. Danaher, J.O. Carter & G.M. McKeon, G.M., "Growth and carbon stock change in eucalypt woodlands in northeast Australia: ecological and greenhouse sink implications". *Global Change Biol*., 8, 769-784. 2002.

[16] Gamma Remote Sensing AG, Modular SAR Processor – MSP. Documentation User´s Guide (Version 1.1). Gümligen, Switzerland, 2007.

[17] J. Armston, R.M. Lucas, J.M.B. Carreiras & P. Bunting, "A first look at integrating ALOS PALSAR and Landsat data for assessing woody vegetation in Queensland". Proc. 14^{th} Remote Sensing and Photogrammetry Conference (CD), Darwin, Australia, 2008.

[18] S. Saatchi, Halligan, K., Despain, D. & Crabtree, R.L. (2007). Estimation of forest fuel load from radar remote sensing. *IEEE Trans. Geosci. Remote Sens*., 45(6), 1726-1740, 2007.

[19] J. Armston, R. Denham, T. Danaher, P. Scarth & T. Moffiet. (2009). Prediction and validation of foliage projective cover from Landsat-5 TM and Landsat-7 ETM+imagery. *Journal of Applied Remote Sensing,* accepted 01/2009.

[20] V.J. Neldner, B.A. Wilson, E.J. Thompson and H.A. Dillewaard, "Methodlogy for Survey and Mapping of Regional Ecosystems and Vegetation Characteristics in Queensland, Version 3.1", Queensland Herbarium, Environmental Protection Agency, Brisbane.

Richard Lucas. Received the B.Sc. degree in biology and geography (First Class) and the Ph.D. degree in the remote sensing of snow and vegetation using AVHRR and Landsat sensor data from the University of Bristol, Bristol, UK, in 1986 and 1989 respectively. He is currently Professor at Aberystwyth University in Wales, UK, where he is involved primarily in the integration of single data and time-series radar, optical (hyperspectral) and LiDAR data for retrieving the biomass, structure and speces/community composition of ecosystems ranging from subtropical woodlands to tropical forests and mangroves. His research has and continues to focus on the carbon dynamics of these systems and their response to natural and human-induced change. He has authored or co-authored over 100 journal articles, book chapters and conference papers

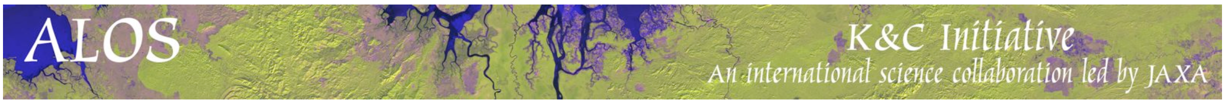

Forest Theme

Application of ALOS/PALSAR in support to Brazilian Forest Monitoring Program

Dalton Valeriano & Silvana Amaral
INPE (Brazil)

K&C Science Report – Phase 1
Application of ALOS/PALSAR in support to Brazilian Forest Monitoring Program

Dalton M. Valeriano
Instituto Nacional de Pesquisas Espaciais - INPE
Caixa Postal 515 - 12245-970 - São José dos Campos - SP, Brasil
dalton@dsr.inpe.br

Silvana Amaral[1]
Arango Sánchez Gildardo[2]
Arimatéa de Carvalho Ximenes[1]
Arley Ferreira de Souza[1,3]
[1,2]Instituto Nacional de Pesquisas Espaciais - INPE
Caixa Postal 515 - 12245-970 - São José dos Campos - SP, Brasil
[1]{Silvana, Arimatéa, Arley}@dpi.inpe.br; [2]Gildardo@dsr.inpe.br

***Abstract*— This paper presents a preliminary assessment of ALOS/PALSAR - Kyoto and Carbon Initiative radar images for the Brazilian Forest Monitoring Program. Using deforestation polygons mapped by DETER project, two ALOS/PALSAR ScanSAR images were analyzed considering the capability to detect deforestation patterns. Approximately 50% of polygons could be detected by ALOS/PALSAR images without orthoretification or radiometric calibration. Additional research efforts to develop better image products and multi-temporal approach should improve the deforestation detection capability. Considering the importance and the extension of Amazon forest and the cloud cover conditions, ALOS/PALSAR data has a strong potential to complement the Forest Monitoring Program. Having radar data operational at DETER project would also prepare the Forest Monitoring Program to integrate further radar data from planned Brazilian satellites – MAPSAR and CBERS-7.**

***Index Terms*—ALOS PALSAR, K&C Initiative, forest monitoring, DETER.**

I. INTRODUCTION

A. *Deforestation and SAR data over Brazilian Amazon*

Early deforestation stages as slash-and-burn practices were previously identified at SAR image, L band, JERS sensor as spectrally distinct from original forest cover over Brazilian Amazon [1]. L Band seemed to be very sensitive to variations between deforestation increase and primary forest [2].

Polarimetric radar data from Mapsar showed also to be very useful to detect recent deforestation over Tapajós National Forest (Pará), in the Brazilian Amazon [3]. Among polarimetric data, HH-HV showed to be the more adequate polarization to general forest mapping, it is possible to discriminate primary forest, secondary forest, bare soil, agriculture and degraded forest [4]. Preliminary investigations using ALOS PALSAR images, using only HH polarization, over Amazonia, showed distinct responses from slash-and-burn practices and also different degradation stages of the forest [5].

Comparisons between optical and radar images suggested that SAR L-band images are an important and complementary information source to land change cover mapping, specially over frequent cloud cover areas as Amazonia region [6].

This paper describes the project developed at Kyoto & Carbon (K&C) Initiative [7] where we assess the use of ALOS PALSAR K&C images for the DETER qualification procedure as initial steps to introduce ALOS PALSAR products at Brazilian Forest Monitoring Program.

B. *ALOS Imagery for forest monitoring in Brazil*

At INPE's Brazilian Amazon Deforestation Monitoring Program, the DETER System (the Real-Time Deforestation Detection System) [8] identifies and maps deforested areas in tropical Amazon forests. This system uses images from MODIS sensors on the NASA TERRA satellite and WFI on the Brazilian INPE CBERS-2B satellite. With spatial resolution limited to 250 meters, the images from these sensors allow detection of deforestation in areas greater than 0.25 km^2 (or 25 ha). In DETER, all deforestation identified in an image and not previously detected by Legal Amazon Deforestation Monitoring Project (PRODES) [9] is considered new deforestation, regardless of chronological time. The PRODES map, containing deforestation from prior years, together with non-forest areas (such as savannah, bodies of water and rocky outcrops) is used to eliminate old deforestation being identified and counted again. Identification of deforestation is performed through photo-interpretation of the MODIS image, taking into account only the portion of the image that supposedly still contains forest cover.

Every 15 days, when observation conditions are favorable, DETER produces a digital map with all deforestation occurrences observed during the preceding period. These digital maps containing Alert polygons and tables describing them are sent every 15 days to IBAMA (Instituto Brasileiro do Meio Ambiente e dos Recursos Naturais Renováveis), along with the cloud cover map for the period, thus indicating the area to be effectively monitored. The maps for the two halves of each month are integrated and, together with the cloud cover maps and images for the period, are placed on the Internet (http://www.obt.inpe.br/deter/) for consultation, where they remain available for download.

For every month, associated to DETER data, a technical report assessing DETER information and results is also published on the Internet. Based on cloud free and medium spatial resolution images (20 –30m), a sample of DETER Alert polygons is qualified. Multi-temporal and visual analysis classify DETER Alert polygons as light progressive forest degradation, moderate progressive forest degradation, high intensity forest degradation, clear cutting, or non-confirmed deforestation. Qualification results provides basic information about types of deforestation mapped by DETER and data accuracy, considering also the information about polygons area. From May to August, 2008, an average of 91% of DETER Alert polygons were confirmed as deforestation [10]. Data from field observation is also periodically obtained to improve DETER methodology and data evaluation [11]. In September 2008 INPE team went for a field expedition along the southwest of Para. With IBAMA collaboration, DETER Alert polygons were checked from a helicopter flight.

This qualification of DETER Alert polygons using optical remote sensing imagery is strongly limited by the cloud cover over the Amazon region.

A preliminary but essential application for ALOS PALSAR K&C images for deforestation monitoring could reside in qualifying DETER Alert polygons procedures. It is not expected that PALSAR imagery would provide information about different deforestation intensity, as it is usually detected by optical images and multi-temporal approach. However, radar backscatter data provides information about general forest cover condition:

- Deforested areas older than one year (PRODES mapping) presented dark patterns at L-band SAR;
- Less than one year deforestation (PRODES mapping) are detected at L-band SAR as lighter areas;
- Very recent deforestation mapped by DETER Program is discernible at L-band SAR as lighter polygons.
- Besides the clear-cut pattern, forest degradation is also detected with PALSAR Fine resolution data.

II. Description of the Project

A. *Relevance to the K&C drivers*

The use of ALOS imagery operationally at DETER system, as an improvement of the forest monitoring system, is in according to the Conservation thematic driver outlined in the K&C Science Plan [12]. To effectively monitor deforestation, specially over frequent cloud cover areas, ALOS information will be very helpful to define policy and plans of actions, either for carbon emission reduction or conservation strategies.

B. *Work approach*

This project was conducted in two parts. Initially, we had to assess ALOS PALSAR K&C imagery for deforestation detection. Secondly, some methodological development was needed to specify image processing to define the products and procedures. By the time that we finish the studies and the products and procedures tested and validated, we will be able to introduce PALSAR data operationally in the Forest Monitoring Program.

Although ALOS PALSAR Fine Mode provided an excellent spatial resolution to detailed study sites, ScanSAR data were preferred because these images cover larger extensions, essential capability when considering the Amazon forest as area of interest. Parallel to the image processing development to improve radiometric and geometric precision, we compared the ability of ScanSAR images to deforestation detection obtained from DETER system.

C. *Satellite and ground data*

For this analysis, the ALOS-PALSAR ScanSAR image of August 30, 2008 (WB1, HH polarization, slant range KC_003-21406N09S21WB1SLT1) was georeferenced (resampled to spatial resolution of 50 m) based only on the image acquisition parameters (geo_factors) with SARSCAPE software, converted to 8 bits tiff file to be integrated with deforestation data sources using geographical information systems developed by INPE (SPRING and TERRAVIEW). Every clear-cut polygon was visually interpreted over the PALSAR image, seeking to identify differences in the radar signal as lighter digital values, linear boundaries, or patterns different from the forest background and the darker pattern from older deforested areas. Comparing to radar forest backscatter, clear-cut areas present lighter patterns in PALSAR images.

DETER Alert polygons from May to August 2008 checked during the fieldwork (September, 2008) were superposed to a PALSAR K&C image from August (Figure 1). All of the analyzed DETER polygons referred to clear-cut deforestation, comprising areas that will be mostly converted to pasture, located at municipalities of Itaituba, Novo Progresso and Altamira (PA) (Figure 2).

located at municipalities of Itaituba, Novo Progresso and Altamira (PA) (Figure 2).

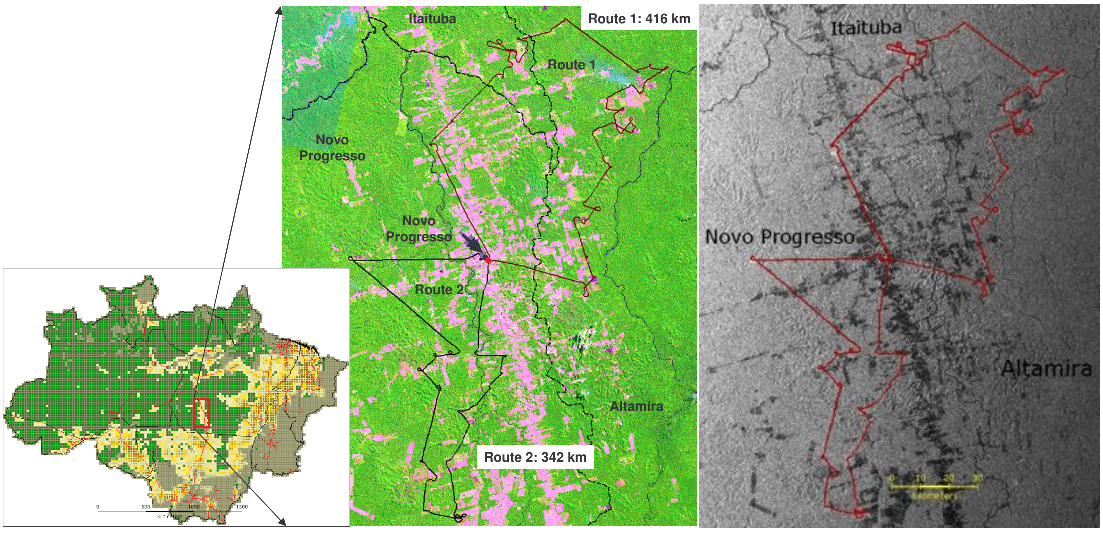

Figure 1. INPE Fieldwork location. Helicopter flight route over (a) Landsat-TM colour composition, and (b) ALOS ScanSAR image (WB1-HH–083008). Municipalities of Altamira, Novo Progresso and Itaituba – state of Pará, Brazil.

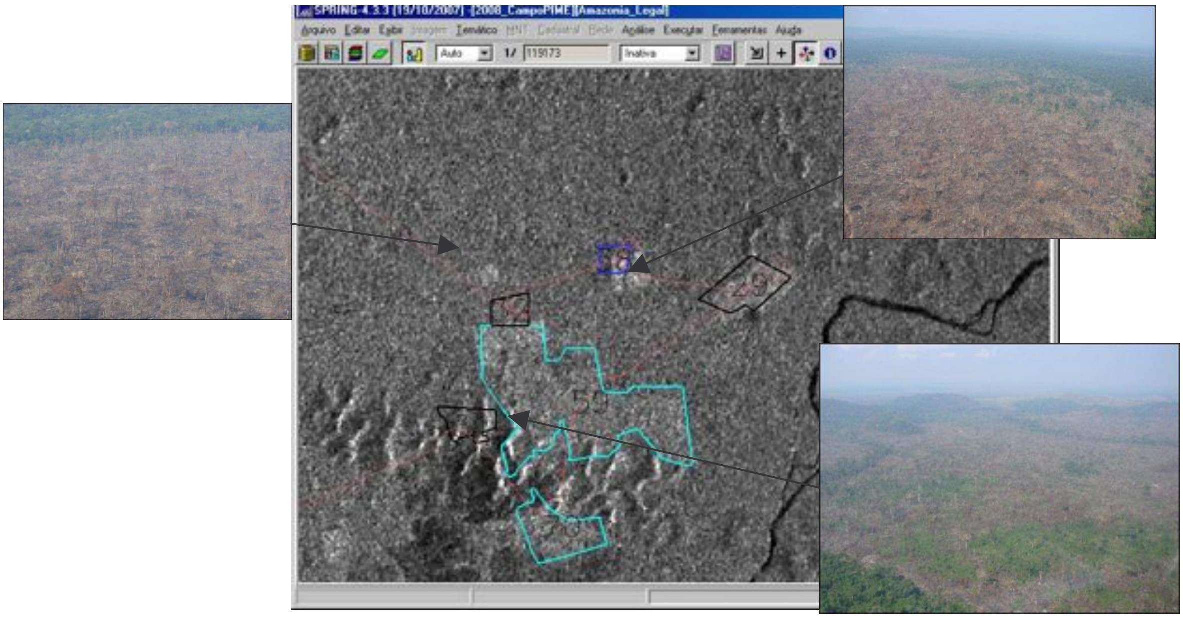

Figure 2. Example of Clear-cut Deter Alert polygons over ALOS ScanSAR image (WBS-HH–083008). Deter polygons from June (light blue), July (dark blue) and August (black) in a region close to Curuá River (Altamira-PA).

A second analysis were performed observing only DETER Alert Polygons for September 2008, over ALOS PALSAR ScanSAR image from October (10-15-2008), with the same methodological procedure. This analysis simulated the use of ALOS PALSAR at an operational approach.

III. Results and Summary

Considering the methodological part of this project, we first managed to develop a tool to store and recover every image from K&C project. An automatic procedure was implemented to regularly access JAXA ftp sites and organize the ALOS PALSAR K&C available images in a database. Using a web portal, credentialed users can consult the downloaded images by date, polarization or central geographical coordinate (Figure 3). The image swath can be visualized and the selected images can be ordered to the database manager. As soon as JAXA authorizes, this portal can be open to the Brazilian scientific community to freely access this PALSAR image database.

The analysis of ALOS ScanSAR images for deforestation detection indicated the need of additional methodology, described after the Deter comparison results.

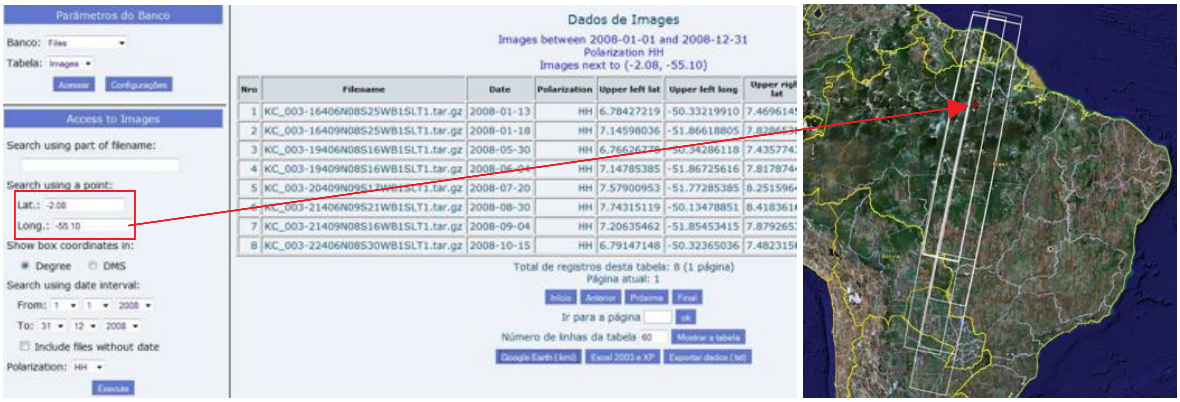

Figure 3. Web Portal to select ALOS PALSAR K&C images, verifying scenes coverage (http://www.dpi.inpe.br/sima/bancos/)

Considering only clear-cut DETER Alert polygons verified in the fieldwork (a total of 67 polygons, from May to August, 2008), ALOS-PALSAR images could register difference in image response for only 55.22% of the clear-cut polygons (Table 1).

Table 1 – ALOS-PALSAR ScanSAR image assessment for DETER clear-cut polygons verified during the fieldwork.

	Deter Clear-cut	ALOS detection	%
May	12	6	50.00
June	17	7	41.18
July	14	10	71.43
August	24	14	58.33
Total	67	37	55.22

Some factors could contribute to this result:

- The image was not properly radiometrically calibrated, there was significant difference in image illumination that difficult the interpretation.
- Clear-cut DETER polygons located in flat terrain are easier to detected than in those in hilly areas. Small hills are very frequent in the study area.
- Variation in size and shape of clear-cut polygons interferes in the radar image response.

It was observed that DETER Alert polygons detected by the ALOS (Table 2) image had an average of 4.33 km^2, in contrast to the polygons not detected in the ALOS image, that presented average areas of 2.65 km^2.

Table 2 – ALOS-PALSAR ScanSAR image assessment for DETER clear-cut polygons verified during the fieldwork.

	DETER polygons average area (km^2)	
Month	Detected	Not detected
May	7.00	3.86
June	5.51	3.21
July	2.46	1.68
August	2.35	1.83
Average	4.33	2.65

Observing DETER Alert Polygons for September 2008 over ALOS PALSAR image from October (10-15-2008), only 76 polygons from 565 where placed over the scene. Even with DETER polygons smaller than registered previously, 45% of the polygons were identified over PALSAR image (Table 2). Most of the deforestation polygons presented darker response in the PALSAR image, suggesting older clear-cut areas.

Table 3 – ALOS-PALSAR ScanSAR image (October) assessment for DETER clear-cut polygons registered for September 2008.

ALOS (10-15-2008)	DETER Polygons (Sept-2008)	%	Area (km^2)
Detected	34	44.74	0.92
Undetected	42	55.26	0.75
Total	76		

ALOS PALSAR ScanSAR images covered the north part of Amazonia, where cloud cover makes the deforestation detection difficult (Figure 3). To be used in an operational basis, ScanSAR images should be accessed and processed as soon as possible to enable DETER qualification, what is planned for the continuity of this work.

Deforestation detection by SAR L Band has also a temporal dynamic that interferes on image interpretation. Recent deforestation shows brighter pattern than the what is found on intact forest cover and it progressively becomes darker areas. This change the backscattering pattern occurs within approximately 5 months time. Such temporal variation was not enough quantified and understood, and it will be subject of further research.

Considering the results showing the potential ALOS PALSAR for deforestation detection, and the temporal variability of deforestation backscattering patterns, it is necessary to adapt the methodology for an operational forest monitoring. Change detection, multi-temporal approach should be defined, in order to compare a new radar image with previous images of the same season.

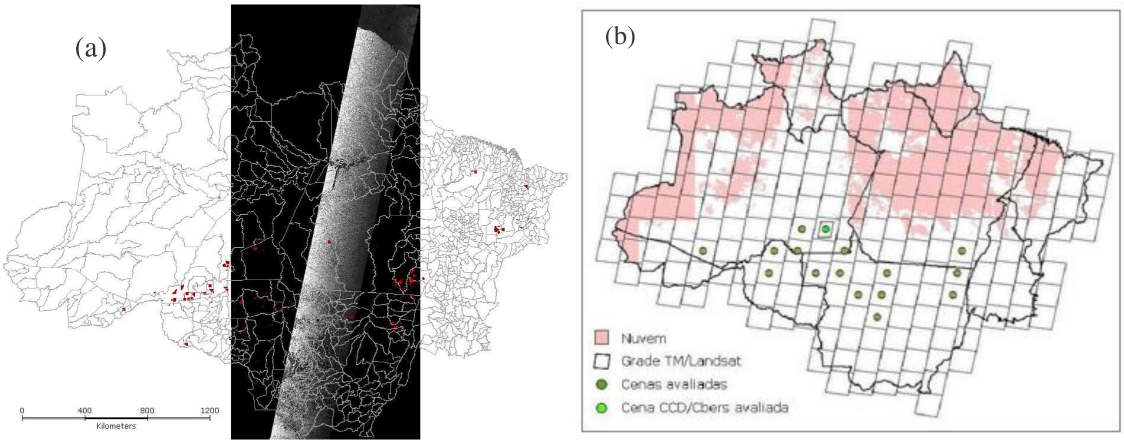

Figure 4 (a) ALOS PALSAR WB1 image (10-15-2008) coverage and DETER Alert Polygons for September 2008 (red vectors). (b) DETER Alert polygons for September qualification report: cloud cover (pink) and DETER polygons qualification sites (green dots).

IV. Final Commnents

ALOS K&C Initiative gave us the opportunity to consider the use of radar data to overcome the cloud cover problem in the Brazilian forest monitoring system. Radar data availability in a regular basis enables the development of an operational procedure to use L Band for deforestation detection.

The results obtained so far indicate that ALOS PALSAR imagery has a potential to detect only part of the deforestation polygons that are normally published as deforestation alerts. However, as the deforestation detection has to be operational and expedited, we need an uncomplicated approach, based on ScanSAR – HH polarization data, the methodology is not completely defined. We plan to build an ALOS PALSAR mosaic images for the four seasons and work with multi-temporal analysis to detect deforestation.

Another benefit from being part of ALOS K&C Initiative and conduct this project, it the construction of a radar culture, not only at the scientific level, but also in an operational basis with implications on the public awareness about the technological capability of remotely sensed monitoring of the deforestation process in Brazil. This is especially important considering that the Brazilian Spatial Program is planning to develop radar sensors onboard of Brazilian satellites in the next decade.

Acknowledgements and Image Copyrights

The authors would like to thank the INPE´s Forest Monitoring System Team that includes Maria Isabel S. Escada, Camilo D. Rennó, Taise Pinheiro, Luis E. P. Maurano, Antonio Miguel V. Monteiro, and João Vianei Soares for technical and financial support. We also thank to IBAMA and PIME Project for the fieldwork partnership. This work has been undertaken within the framework of the JAXA Kyoto & Carbon Initiative. ALOS PALSAR data have been provided by JAXA EORC.

References

[1] R. Almeida-Filho, A. Rosenqvist, Y. E. Shimabukuro, and J. R. d. Santos, "Evaluation and Perspectives of Using Multitemporal L-Band SAR Data to Monitor Deforestation in the Brazilian Amazônia," *IEEE Geoscience and Remote Sensing Letters*, vol. 2, pp. 409-412, 2005.

[2] J. B. Guerra, C. d. C. Freitas, and J. C. Mura, "Evaluating the potential of L Band POLSAR data to discriminate deforestation increment in Amazon Rain Forest," presented at 2008 IEEE International Geoscience and Remote Sensing Symposium, Boston, 2008.

[3] J. R. Santos, J. C. Mura, P. W. R., L. V. Dutra, and F. G. Gonçalves, "Mapping recent deforestation in the Brazilian Amazon using simulated L-band MAPSAR images," *International Journal of Remote Sensing*, vol. 29, pp. 4879-4884, 2008.

[4] C. C. Freitas, L. S. Soler, S. J. S. Sant'Anna, L. V. Dutra, J. R. Santos, J. C. Mura, and A. H. Correia, "Land Use and Land Cover Mapping in the Brazilian Amazon Using Polarimetric Airborne P-Band SAR Data," *IEEE Transactions on Geoscience and Remote Sensing*, vol. 46, pp. 2956-2970, 2008.

[5] D. M. Valeriano, W. R. Paradella, C. G. d. Oliveira, C. A. d. Almeida, and S. Amaral, "ALOS PALSAR data assimilation in INPE's Brazilian Amazon Deforestation Monitoring Program (PRODES and DETER)," RESTEC/Tokyo 2008.

[6] Y. E. Shimabukuro, R. Almeida-Filho, T. M. Kuplich, and R. M. Freitas, "Quantifying optical and SAR image relationships for tropical landscape features in the Amazônia," *International Journal of Remote Sensing*, vol. 28, pp. 3831-3840, 2007.

[7] M. Shimada, "PALSAR and Calibration update". *11th ALOS K&C Science Team meeting (KC#11)*, Tsukuba, Japan, Jan. 13-16, 2009. [Online] Available: http://www.eorc.jaxa.jp/ALOS/kyoto/jan2009_kc11/pdf/090113/shimada_calval_up_090113.pdf

[8] INPE, "Monitoramento da floresta amazônica por satélite, Projeto PRODES", 2008. [Online] Available: http://www.obt.inpe.br/prodes/r2007.htm

[9] INPE, "Sistema DETER - Detecção de Desmatamento em Tempo Real," 2009. [Online] Available: http://www.obt.inpe.br/deter/RelatorioMonitoramento.pdf

[10] M. I. S. Escada, T. d. F. Pinheiro, C. D. Rennó, S. Amaral, L. E. P. Maurano, and D. d. M. Valeriano, "Sistema de Avaliação dos Dados do Monitoramento da Cobertura Florestal daAmazônia por Satélite – DETER," presented at XIV Simposio Brasileiro de Sensoriamento Remoto, Natal (RN), Brasil, 2009.

[11] INPE, "FotoTeca - Banco de dados de Fotos de Campo," 2008. [Online] Available: http://www.obt.inpe.br/fototeca/fototeca.html

[12] A. Rosenqvist, M. Shimada, R. Lucas, J. Lowry, P. Paillou, B. Chapman [eds.], “The ALOS Kyoto & Carbon Initiative, Science Plan (v.3.1),” JAXA EORC, March, 2008. [Online] Available: http://www.eorc.jaxa.jp/ALOS/kyoto/KC-Science-Plan_v3.1.pdf

Dalton M. Valeriano. Biologist/Ecologist by Federal University of Rio de Janeiro (1978), Master in Remote Sensing at Brazilian Institute for Space Science (INPE) (1984), and PhD in Geography at University of California at Santa Barbara (1996). Senior Researcher at INPE, and Manager of INPE´s Forest Monitoring System

Silvana Amaral. Ecologist by University of the State of São Paulo (1988), Master in Remote Sensing at Brazilian Institute for Space Science (INPE) (1992), and PhD by Polytechnic Institute of São Paulo University (2003). Researcher at INPE since 1995, working with remote sensing and GIS for forest applications.

Forest Theme

Law Enforcement Deforestation Assessment

Humberto de Mesquita *et al.*
IBAMA (Brazil)

K&C Science Report – Phase 1
Law Enforcement Deforestation Assessment

Humberto Navarro de Mesquita Junior
Remote Sensing Center
Brazilian Institute of Environment and Natural Renewable Resources
SCEN Trecho 2 Edificio Sede Bl. "E"
Brasilia-DF, Brazil, 70818-900
humberto.mesquita-junior@ibama.gov.br

Collaborators

Marlon Crislei Silva
Remote Sensing Center
Braz. Inst. of Environ. and Nat. Renewable Resources
SCEN Trecho 2 Edificio Sede Bl. "E"
Brasilia-DF, Brazil, 70818-900
marlon.silva@ibama.gov.br

Daniel Freitas de Moraes
Remote Sensing Center
Braz. Inst. of Environ. and Nat. Renewable Resources
SCEN Trecho 2 Edificio Sede Bl. "E"
Brasilia-DF, Brazil, 70818-900
daniel.moraes@ibama.gov.br

Rodrigo Antonio de Souza
Remote Sensing Center
Braz. Inst. of Environ. and Nat. Renewable Resources
SCEN Trecho 2 Edificio Sede Bl. "E"
Brasilia-DF, Brazil, 70818-900
rodrigo.souza@ibama.gov.br

Felipe de Matos
Remote Sensing Center
Braz. Inst. of Environ. and Nat. Renewable Resources
SCEN Trecho 2 Edificio Sede Bl. "E"
Brasilia-DF, Brazil, 70818-900
rodrigo.souza@ibama.gov.br

Werner Luis Ferreira Gonçalves
Remote Sensing Center
Braz. Inst. of Environ. and Nat. Renewable Resources
SCEN Trecho 2 Edificio Sede Bl. "E"
Brasilia-DF, Brazil, 70818-900
rodrigo.souza@ibama.gov.br

Cláudio de Azevedo Dupas
Regional Laboratory of Remote Sensing and GIS
Braz. Inst. of Environ. and Nat. Renewable Resources
Alameda Tietê, 637, Cerqueira Cesar
São Paulo-SP, Brazil, 01417-020

Dalton Morrison Valeriano
National Institute for Space Research
Av. dos Astronautas, 1758 - Jardim da Granja
São José dos Campos, SP, Brazil 12227-010
dalton@dsr.inpe.br

***Abstract*— Deforestation monitoring for the Brazilian Amazon has been carried on by INPE since 1988, under the PRODES program, and recently, the DETER, both have been used by IBAMA for operational purposes and law enforcement. However, optical sensors are limited by the presence of clouds. The ALOS was launched in 2006, and its data became available to IBAMA thought the JAXA's ALOS Kyoto and Carbon Initiative project. The study site is an area of forest facing a growing pressure of deforestation. The first approach was developed with ScanSAR strip mode image was geo-rectified and DN image values were converted to the normalized radar cross section (σo), in dB, with a calibration factor of -83 dB. In the second approach we have also used five Fine Bean Single Mode Strips Slant Range data for visual interpretation and 738 were identified and it represents 15% of *posteriori* deforestation detections of DETER. The mean σ value for recent deforested area was -5.315dB and the mean so value for preserved native forest was – 7.569dB. From five fine bean strips The executed methodology, using a threshold to classify new deforested areas, has a good potential to be the base of a semiautomatic detection system for operational purposes, using ScanSAR images. The third approach was developed using a temporal RGB composition to identify possible changes in the detained areas object of a fine. This system has potential to produce data that could complement the information already available from well established optical sensor satellites monitoring systems of Brazil..**

***Index Terms*—ALOS PALSAR, K&C Initiative, Forest Theme, Law-enforcement, Monitoring, Amazon.**

I. INTRODUCTION

A. Project Purpose

The main idea of this project is to develop operational methodology to generate deforestation information for law enforcement action in the field based on SAR orbital images.

To develop this project ALOS-PALSAR images [1] provided by Kyoto and Carbon Initiative of Advanced Land Observation Satellite were proposed to be used for operational monitoring of tropical forests in Brazil. In

On the development of this project are expected to achieve some specific goals:

- Decrease de average time between the act of deforestation and the deforestation recognition by satellite images.
- Develop methodologies for detection changes applied to forest monitoring on the specialized Remote Sensing Centre on the headquarter office.
- Build-up SAR capacity to develop SAR temporal analysis by training the staff of regional offices;
- Build up a SAR image catalogue on image server data base to share satellite information to regional offices to be use on temporal series analysis;

B. The overview

Deforestation monitoring for the Brazilian Amazon has been carried on annually by INPE (National Institute for Space Research) since 1988, under the PRODES (Brazilian Amazonian Forest Monitoring by Satellite) program. More recently, the DETER (Real Time Deforestation Detection System) program was launched to give a faster response (twice a month). PRODES uses Landsat TM and Brazilian-Chinese CBERS data, while DETER is fed by the MODIS sensors on board NASA's Aqua and Terra satellites. The data from both programs have been used by IBAMA (Brazilian Institute of Environment and Renewable Natural Resources) and the Brazilian Federal Police to detect deforestation areas for operational purposes and law enforcement. However, the use of orbital optical sensors to detect deforestation in the tropical rainforest on the Amazon region is limited by the presence of clouds. Some areas remain covered for more than a year. This problem affects critically affects the time spend by the authorities mentioned above to react against the ongoing deforestation processes.

Past research has pointed out that data from SAR satellite sensors can be used to detect land cover changes in tropical forests. The Advanced Land Observing Satellite was launched in 2006, and from August 2007 its data became available to IBAMA through the JAXA's ALOS Kyoto and Carbon Initiative project (K&C). The ScanSAR-ALOS is one of the products available under the K&C. With L band and HH polarization, it is suitable for vegetation analysis.

C. The achivements

The team that proposed activity on the law enforcement deforestation assessment by PALSAR images starts became part of K&C science team on august 2007. The achievements obtained represent partially what are the expected for the the end of the project implementation.

The results presented here will show the importance of SAR images to the tropical forests monitoring (e.i. how the can contribute to anticipate the law enforcement activity and how effective ALOS-PALSAR are to identify new deforestation polygons).

Another point that should be stressed here is one of the main goals of this project, to build-up capacity to use and analyse SAR imagery. The results are scalable presented as the knowledge and the availability of SAR images were increasing along the development of the project. As mentioned before it is part result of the heuristic pyramid of knowledge that will be achieved on the end of this project. These beginning results denote that an institutional and operation use orbital SAR images for vegetation monitoring are viable.

II. PROJECT DESCRIPTION

A. Relevance to the K&C drivers

The Brazilian Institute of Environment and Natural Renewable Resources (IBAMA) is the main important institution related to environmental protection in Brazil. The institution have about 4 thousand staff people and part of that working on the law enforcement to combat the illegal deforestation. The Remote Sensing Centre of IBAMA play an important hole on training people on the use of Remote

Sensing and GIS to increase the effectiveness of the environmental protection action on the office and on the field. With the support of National Institute for Space Research (INPE), that made available optical images and promote the development of new methodologies for vegetation monitoring with satellite images, Brazilian government had improve the monitoring systems for vegetation protection.

These advances of SAR methodologies to be used to build-up operational systems to improve to monitoring of the tropical vegetation is an important approach to contribute to the reduction of the Carbon emissions as well as to the Conservation of the tropical rain forests in Brazil. These forests are playing important hole on carbon and water cycles and are considered hot spots of biodiversity conservation. The achievements already obtained confirm that we still have more to improve in the operational satellite monitoring systems using ALOS-PALSAR. The K&C science advisory panel [2] will contribute of develop SAR methodologies that can potentially be used for other countries that want establish SAR operational system to protect their tropical rainforests.

B. Study sites

The two prototypes areas on the proposed project are the Amazonian Rain Forest and the tropical rain forest, close to the Brazilian east cost hereafter called Atlantic Forest. Both areas were used to test primary methodology viability studies. On the Amazonian region four approaches were developed in scaleable increasing on area and complexity.

On the Amazonian region the study area related to the first approach is defined by a rectangle (180km by 200km) centrally located in the state of Pará, Brazil, centred coordinates of 52o 47’ 44” W and 6o 34’ 03” S (fig. 1). The second approach was conduct in some parts of Pará and Mato Grosso States (fig. 1). The third approach was conduct on the entire Amazon region. These corresponds to areas of forest that has been facing a growing pressure of deforestation, with a good amount of recent deforested areas detected by DETER. The area was selected to be used as pilot area to test new methodologies on real-time deforestation monitoring.

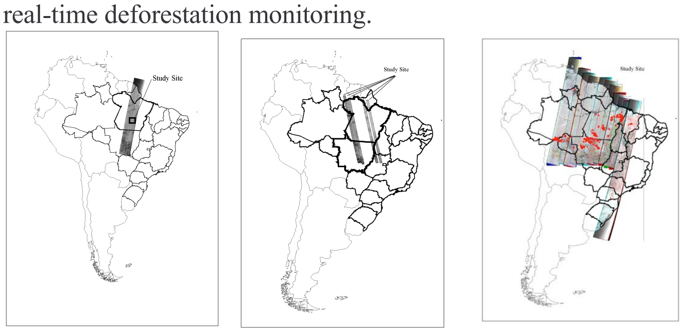

(a) (b) (c)

Figure 1. (a) Study site location in the Para State, (b) five fine bean strips in the Para and Mato Grosso States, (c) all the detained areas in the Brazilian Amazon Region ALOS K&C © *JAXA/METI.*

For the Atlantic Forest, one area on the south of Bahia and north of Minas Gerais States (fig. 2) were chosen for to test to the PALSAR ability to detect new deforestation. These areas are recognized in Brazil as an area with high pressure of deforestation and still have large size polygons of remnant natural vegetation.

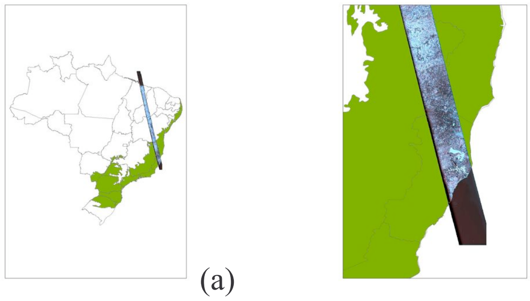

(a) (b)

Figure 2. (a) In green the old spatial distribution of Atlantic Forest biome and the position of the PALSAR strip ALOS K&C © *JAXA/METI*, (b) the zoomed area on the south of Bahia and north of Minas Gerais States.

C. The hypothesis

Seasat was launched on 1978, and was the first Earth-orbiting satellite that had the space borne synthetic aperture radar (SAR), L-band, on board. The use of L-band orbital SAR images for vegetation analysis starts with SeaSat data, developing to the SIR-A,B and C data, followed by JERS-1 and recently with ALOS PALSAR data.

The L-band SAR images have been related with the canopies and have been related with biomass estimation and structure modeling. Luckman & al. [1] developed a semi empirical model for the retrieval of above-ground biomass density on the tropical forests. Several papers were developed on this matter to understand this relationship. Neeffa & al. [4] developed a model for the tropical forest stand structure using SAR data.

Sgrenzaroli & al. [5] have shown that on the published remote sensing literature, there are several Amazon forest-mapping experiments actually deal with single SAR satellite images (i.e. JERS or European Remote Sensing – ERS), with focus on local-scale mapping. In this category, approaches based on visual inspection or automatic classification, were investigated.

Saatchi & al. [6] have studied the radar characteristics of the training sites on the State of Rondônia for land cover-type classes identification using L-band SIR-C data.

More recently, Almeida-Filho & al. [7] evaluated the potential use of orbital L-Band SAR images of JERS-1, to test a multitemporal monitoring methodology. They found that for the initial deforestation process the proposed methodology is not able to unequivocally detect areas in initial phase of deforestation, and the unambiguous detection of deforested areas is only possible if the entire clearing process has already been concluded. They also mentioned that for an operational program to monitor deforestation, based on SAR data, it is very important to have a properly geo-referenced multi-temporal database to integrate different sources of data.

The use of orbital optical sensors to detect deforestation in the tropical rainforest is usually delayed due to presence of clouds. The age of a certain deforested area is defined by the period that starts when original forest was last observed and ends when deforestation was first observed with satellite images. Recent deforested areas are considered priority for law enforcement agents because they can indicate the ongoing deforestation processes. DETER's data provides deforestation polygons with an age that can vary from 15 days up to more than a year long (fig. 3). By the beginning of the dry season most of the deforested areas detected by DETER are old (more than 90 days) due to a long period without clear images. ALOS-ScanSAR can be used to identify recent deforested areas and to reduce the interval between two observations.

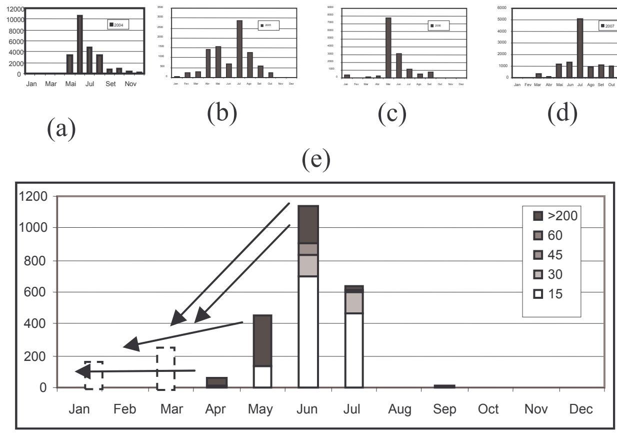

Figure 3. Monthly distribution of DETER deforestation detection in area (km2). (a) 2004, (b) 2005, (c) 2006, (d) 2007, and (e) 2007 with the proportion of the each age per month in the beginning of the dry season. Dashed columns means hypothetic scenario of PALSAR complementary data, showing some deforestation that may be able to detect during the rainy season.

D. The aproaches

On the first approach the strip of 2730km of length by 380km of swath, on wide bean mode 1 of ScanSAR images, with 100 per 100 meters resolution and HH polarization, of august 23rd, 2007. In order to validate the ALOS detection Landsat-TM images path 226 row 64 and 65 of September 2sd, 2007 and path 225 row 64 and 65 of September 27th, 2007. CBERS images path 164 row 106 and 107 of September 11th, 2006 were used to verify the forest condition one year before the ALOS image acquisition. Images were registered using orthorectified images from Geocover Landsat Facilities project (GLCF orthorectified data).

This study was conducted to test operational capability of ScanSAR images as complementary resource to the optical sensors already used in Brazil. First, an analysis was carried out in order to understand how deforested areas would show up on PALSAR sensor imagery. Than the ScanSAR strip mode image was geo-rectified and subset. DN image values were converted to the normalized radar cross section (σo), in dB, with a calibration factor of -83 dB.

The ancillary deforestation areas previously detected by PRODES were masked to eliminate old deforestation areas. An analysis was done using all DETER data sets of the year 2007. The mean sigma value was extracted for all sets of DETER deforestation detections along the year 2007 and also for the rain forest. A Lee-sigma speckle reduction filter was applied to the ScanSAR image. This image was then classified using the mean sigma value of the recent deforested areas as threshold to identify other deforested areas not detected by DETER. The CBERS 2b optical images before and after the deforestation detection by ALOS-PALSAR images were used to check the forest state (fig.4).

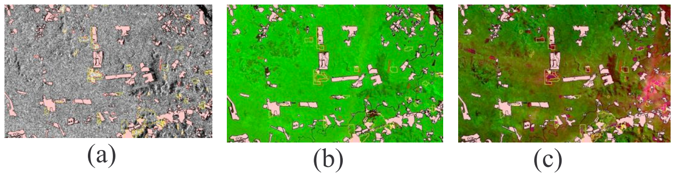

Figure 4. The yellow lines are the DETER detection polygons, the red lines are de ALOS detection polygons while the pink areas correspond the PRODES polygons. (a) ALOS ScanSAR image ALOS K&C © *JAXA/METI* used with the defined threshold value and the to identify the possible recent deforestation, (b) CBERS Image from 2006 before to characterize the situation before ALOS image acquisition, (c) Landsat image after ALOS image acquisition.

An illuminated topographic image based on the position of the PALSAR sensor was generated from the SRTM data. The simulated image was used to exclude the classified areas that could present relief related response on the ScanSAR image.

In the second approach the visual interpretation was conducted using the knowledge obtained on the first approach were some of the highlighted areas (e.i. square shape deforestation) were identified over Fine bean images overlaid by PRODES 2007 + DETER from August to December of 2007 (fig. 5).

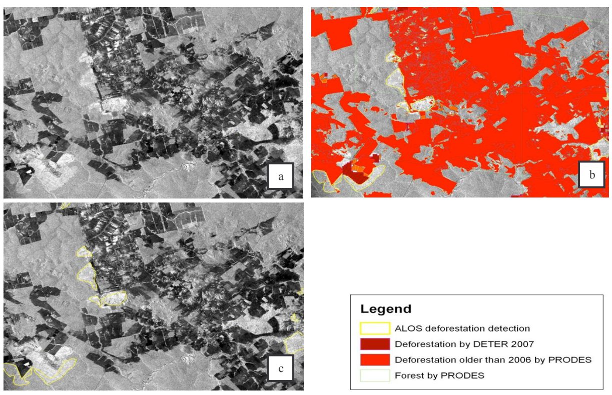

Figure 5. (a) ALOS PALSAR Fine Beam Single Mode (FBS) HH ALOS K&C © *JAXA/METI* with 50m resolution of December 2007, (b) ALOS PALSAR FBS overlaid by PRODES 2007 and accumulated DETER until December 2007, (c) ALOS PALSAR Fine overlaid by the drawn polygons detected using PALSAR image.

Field activities were developed to check the identified polygons and two data collection on helicopters were done (fig. 6). The increase in the intensity of the PALSAR images were confirmed was areas of disturbance of the forest structure and some fail trees were found.

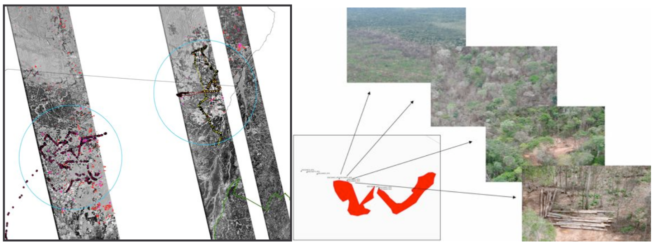

(a) (b)

Figure 6. (a) ALOS PALSAR Fine Beam Single Mode (FBS) HH strip ALOS K&C © *JAXA/METI* and the helicopter autonomy 150miles in blue and dots showing the GPS tracks, (b) ALOS PALSAR HH deforestation detection polygon and the time synchronized pictures taken by the helicopter.

On the third approach on the Amazonian region ALOS-ScanSAR images were used to build-up temporal color composites, this methodology were used together with visual interpretation inside of the detained areas were a fine were applied by the enforced law agents of IBAMA. Figure 7 are showing one example of temporal color composite applied in one of the eleven strips that cover all the detained areas.

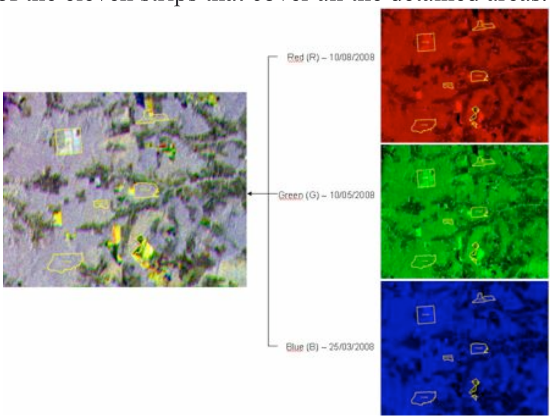

Figure 7. Temporal RGB composition using tree ScanSAR Strip images of tree different dates were DN of images show changes with different colors ALOS K&C © *JAXA/METI*.

The ALOS-ScanSAR images of December 2008 and January 2009 were used to detect new deforestations on the cloudy season on the Amazonian region.

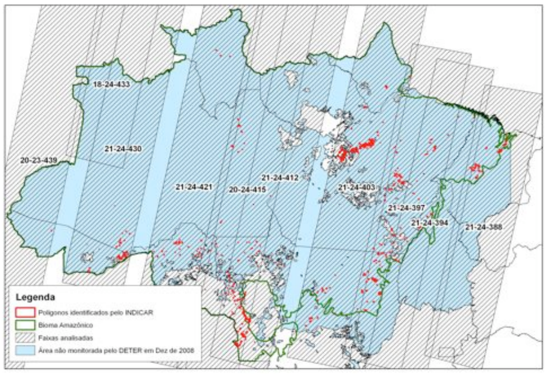

Figure 8. (a) ALOS-ScanSAR strips, in blue the cloud cover on December by DETER monitoring system, in red new deforestation detections by ALOS.

On the figure 8 the temporal composites were used to detect new deforestations where that the optical system DETER can not detect due to the presence of clouds from October to December.

III. Results

On the first approach, DETER polygons were used to extract average values inside these areas, was possible to recognize that most of older deforestations in the same year were low values compared with the very recent detections. The figure 9 shows the average sigma values obtained for old deforestations (may be crops or pasture) compared with one year old deforested areas detected by DETER system using Terra-MODIS images and the signal obtained for primary forest.

Class	Area	Min	Max	Mean	Std
DETER Recent (1)	2279	-12,330	4,204	-4,992	1,893
Forest PRODES (2)	132020769	-15,520	0,178	-7,254	1,818
Deforest PRODES (3)	162780000	-20,374	0,899	-11,020	2,505

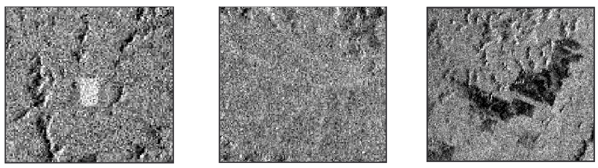

(1) **(2)** **(3)**

Figure 9. Comparison between very recent deforestation from DETER of the year 2007, Deforestation detected with PRODES system from 1997 to 2006 in average and the remnant primary forest identified by PRODES database.

The results showed that areas corresponding to old deforestation are related to low dB values, while recently deforested areas are related to high dB values. The mean σο value for recent deforested areas was -5.315dB and the mean σo value for preserved native forests was - 7.569dB.

Based on the threshold value classified ALOS image, 1476 polygons were generated. Using the arbitrary criteria that more than 10 degrees slope can be affected with an increased brightness, 1239 polygons on slope areas were eliminated. From the resultant 237 polygons, 133 were confirmed to be over the relief but were not eliminated because they were geographically displaced, one was a false detection, and 99 were confirmed deforestations. From the 99 deforested polygons, 19 were coincident with PRODES from the year 1997 to 2006 and 55 polygons with PRODES 2007 (finished on august 2007), 4 were on areas of non forest (neither considered by PRODES nor DETER) and 17 are new detections of ALOS, not detected by any other optical system.

On the second approach five strips of Fine Bean Single Mode, polarization HH with 50m resolution on the month December 2007 and January 2008 were used to detect possible recent deforestation by visual interpretation based on the knowledge acquired on the approach number one. Overlaid the PALSAR images with PRODES 2007 and year before and accumulated DETER from August to December 2007, 738 polygons were generated (Table 1). These polygons were compared with the posterior detection made by DETER from January to September of 2008, were 1346 polygons were identified on the same area monitored by ALOS. From the total DETER polygons 207 (15.38%) were intersected with ALOS PALSAR polygons, 878 (65.23%) were polygons that their areas were monitored month(s) before in the year 2008 and were not detected (possible these polygons occurred after ALOS PALSAR detection), and 261 (19.39%) had their areas covered by clouds until their detection by DETER, we are not able to define when it occurs in relation to ALOS PALSAR detections (tab.2).

Table 2 – Comparison between the ALOS-PALSAR and optical capabilities by DETER system with MODIS images.

	DETER	ALOS	Intersect	MAR	ABR	MAY	JUN	JUL	SEP
FBS60	139	215	21	1	0	0	0	9	11
FBS62	137	100	13	11	0	0	0	1	1
FBS69	409	290	111	48	14	34	4	7	4
FBS70	437	77	41	8	12	19	2	0	0
FBS71	224	56	21	3	9	6	2	1	0
Total	**1346**	**738**	**207**						

Without clouds month(s) before DETER detection in 2008

	JAN	FEB	MAR	APR	MAY	JUL	TOTAL
FBS60	2	23	3	0	44	16	**88**
FBS62	50	53	0	2	5	0	**110**
FBS69	0	113	19	15	1	54	**202**
FBS70	0	257	3	47	0	15	**322**
FBS71	0	117	0	37	0	2	**156**
							878

Covered by clouds until their detection by DETER

	JAN	FEB	MAR	APR	MAY	JUL	TOTAL
FBS60	0	0	26	0	0	4	**30**
FBS62	0	12	0	0	0	2	**14**
FBS69	0	0	54	5	1	36	**96**
FBS70	0	0	38	28	0	8	**74**
FBS71	0	0	24	23	0	0	**47**
							261

The new deforestation detections produced by ALOS-PALSAR.on December 2007 and January 2008 were compared with the posterior detections produced by DETER. As DETER is based on optical sensor MODIS several detections cannot be detected when the specific region were cover by clouds. The increase of the coincidences from March to September of 2008 is old detections that occur before ALOS detections.

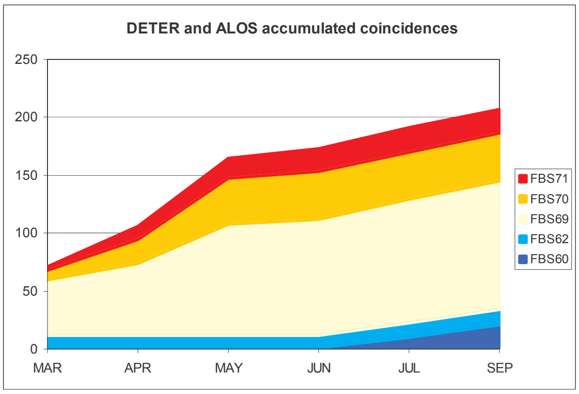

Figure 10. The accumulated coincidences between ALOS December 2007 and posterior DETER detection along 2008 year.

Seeking for changes we could find an area that were checked by optical images in other to generate an indicative of changes that may represent an break down in a detained areas after received a fine by the IBAMA´s enforced law agent. The Figure 11 is presenting an example of changing detection. This methodology still need much field activities to determine the level of changes ALOS PALSAR are identifying and how it can be used by the enforced law agents to return in the detained areas.

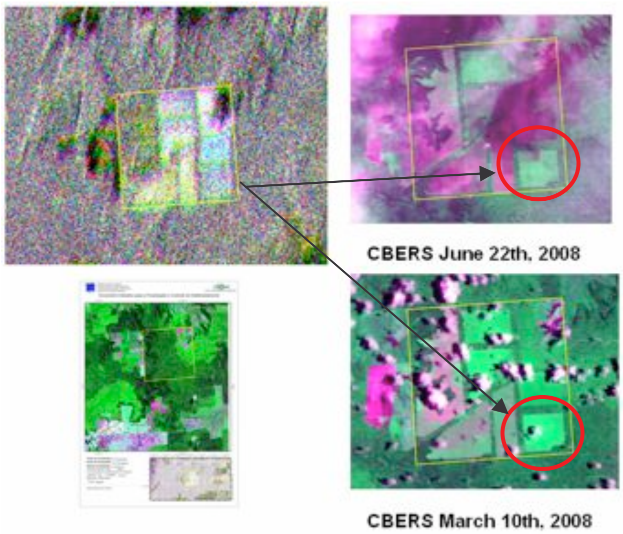

Figure 11. Up left ALOS ScanSAR temporal composites, on the right CBERS images used to confirm the changes detected by ALOS and a Indicative of temporal changes in detained areas.

An approach were also developed on the prototype area of Atlantic Forest to analyse the capability of Fine Bean Dual Mode strip mode K&C data to detect new deforestations. The area analysed on the south of Bahia shows a potential to analyse large size deforestation polygons (fig. 12).

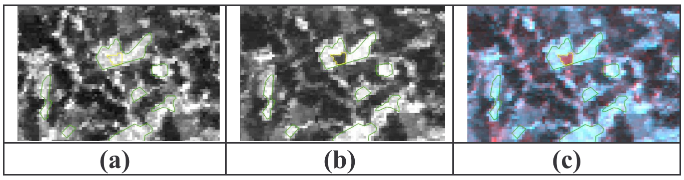

Figure 12. (a) the situation at july 2007, (b) at july 2008 and (c) the temporal change in one year time change.

IV. Discussions

The mean σ_o value for recent deforested areas, for preserved native forests and old deforested areas are similar to those found by other authors are shown on the Table 3.

Table 3 – Comparison between the sigma values obtained from different studies: (1) present study, (2) Sgrenzaroli & al. [5], (3) Saatchi & al., [6] and (4) Luckman & al. [3].

Covarage Type	1	2	3	4
Primary Forest	-7,254	-7.71dB	-9.71	-8.3 to 7.1
Recent deforestation	-4,992	----	-5.75	----
Old deforestation (may be crop or pasture)	-11,020	-1.11dB	- 14.45	-11.9 to -10.7

Almeida-Filho & al. [7] notice the importance of high quality georegistration on the several databases in order to implement an operational monitoring system. In this study the georegistration was a very limiting factor and was solved by using the recent implementation of the geocoded methodology.

V. Conclusions

The executed methodology, using a threshold to classify new deforested areas, has a good potential to be the base of a semiautomatic detection system for operational purposes, using ScanSAR images. This system has potential to produce data that could complement the information already available from optical sensor satellites (CBERS-CCD, Landsat-TM and Terra-MODIS images). The resulted monitoring system, combining optical and SAR data, would decrease the average age of the deforested areas. As a result, the response time related to law enforcement activities to combat illegal logging would decrease.

Two points need to be stressed here. One is the new detections of ALOS images which were not detected by any other optical systems. These detections are probably related to very recent deforestations that may have occurred some days before ALOS image acquisition. The second point is the number of ALOS detection coincident with PRODES 2007, these detections can be used to the enforcement law agents, because these polygons where not detected by DETER until the end of the year when the mask were changed to the PRODES 2007 database.

The DETER detections were always correct and the area not covered by clouds before DETER detections means that there was no deforestation on this areas. This presumption presumes that detection recognized after are new very recent deforestations.

In the third approach the no changes can not be necessarily defined us compliment determined in the detained areas, us well us, some cases of changes need to be studied to determine the level of change can be related to re-growth process.

The approaches reveled that there are simple methodologies that can be applied on operational systems but it still need implementation for semi-automatic processing. The improvement on software development for fast processing will be need for implementation of rapid response SAR based vegetation monitoring. Looking forward, another extension needed is to increase the number of regional offices that can use the PALSAR images as a resource for historical time series analysis.

Acknowledgements

This work has been undertaken within the framework of the JAXA Kyoto & Carbon Initiative. ALOS PALSAR data have been provided by JAXA EORC. Thanks to the Brazilian National Institute for Space Research (INPE) to be a partner and to provide CBERS-2 (Chinese Brazilian Earth Resources Satellite) and Landsat-TM images, DETER and PRODES data; and to National Aeronautics and Space Agency (NASA) for making Terra-MODIS images available through the Earth Observation Distribution System (EODIS).

References

[1] M. Shimada, "PALSAR and Calibration update". *11th ALOS K&C Science Team meeting (KC#11)*, Tsukuba, Japan, Jan. 13-16, 2009. [Online] Available: http://www.eorc.jaxa.jp/ALOS/kyoto/jan2009_kc11/pdf/090113/shimada_calval_up_090113.pdf

[2] A. Rosenqvist, M. Shimada, R. Lucas, J. Lowry, P. Paillou, B. Chapman [eds.], "The ALOS Kyoto & Carbon Initiative, Science Plan (v.3.1)," JAXA EORC, March, 2008. [Online] Available: http://www.eorc.jaxa.jp/ALOS/kyoto/KC-Science-Plan_v3.1.pdf

[3] Luckman A.; Baker, J.; Hozák, M.;Lucas, R., 1998 - Tropical Forest Biomass Density Estimation Using JERS-1 SAR: Seasonal Variation, Confidence Limits, and Application to Image Mosaics. *Remote Sensing of Environment 63:126-139*.

[4] Neeffa,T.; Dutra, L.V.; Santos J.R.; Freitas, C.C.; Araujo, L.S.; 2003. Tropical forest stand table modelling from SAR data. *Forest Ecology and Management, 186:159–170*.

[5] Sgrenzaroli, M.; Baraldi, A.; De Grandi, G.D.; Eva, H.; Achard F.; 2004. A Novel Approach to the Classification of Regional-Scale Radar Mosaics for Tropical Vegetation Mapping. *IEEE Transections on Geoscience and Remote Sensing*, 42(11):2654-2669

[6] Saatchi, S.S.; Soares, J.V.; Alves, D.S., 1997. Mapping Amazon Deforestation and Land Use in Amazon Rainforest by Using SIR-C Imagery. *Remote Sensing of Environment*. 59:191-202.

[7] Almeida-Filho, R.; Rosenqvist, A.; Shimabukuro Y.E.; Santos J. R.; 2005. Evaluation and Perspectives of Using Multitemporal L-Band SAR Data to Monitor Deforestation in the Brazilian Amazônia. *IEEE Geoscience and Remote Sensing Letters*, 2(4):409-412.

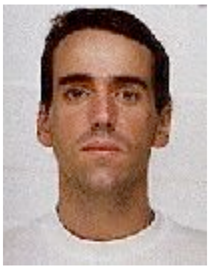

Humberto Navarro de Mesquita Junior is head of Remote Sensing Center (CSR) of Brazilian Institute of Environment and Natural Renewable Resources (IBAMA). Dr. Humberto had his Bachelor in Biology n 1994, During the Master or Ecology at University of São Paulo were trained on Image Processing at University of Indiana, USA. The doctorate was on the Landscape Ecology Lab and partially research spatial modeling at Geography department of Edinburgh University. From 2000-2002 on the second research opportunity of JERS-1 became member of Monitoring of Tropical Rain and Boreal Forest Environments initiative in 2007 became PI member of ALOS K&C initiative.

Marlon Crislei Silva is coordinator of the data management and software development in CSR-IBAMA. Agriculture-measurer Engineer finished the master on GIS on the Federal University of Viçosa.

Daniel Freitas de Moraes is environmental analyst of CSR-IBAMA and member of Amazonian Monitoring group. Bachelor on Biology specialized on Remote Sensing and GIS.

Rodrigo Antonio de Souza is environmental analyst of CSR-IBAMA and member of Amazonian Monitoring group. Bachelor on Biology and ;master on Conservation Biology with emphasis on GIS at Federal University of Minas Gerais.

Felipe de Matos is environmental analyst of CSR-IBAMA and member of Amazonian Monitoring group. Bachelor on Geography specialized on Remote Sensing and GIS.

Werner Luis Ferreira Gonçalves is environmental analyst of CSR-IBAMA and member of Amazonian Monitoring group. Bachelor on Geography specialized on Remote Sensing and GIS.

Cláudio de Azevedo Dupas is coordinator of Remote Sensing and GIS laboratory of São Paulo State office of IBAMA and member of Atlantic Forest group. Bachelor on Biology, and master on Remote Sensing at International Institute for Geo-Information Science and Earth Observation (ITC), Nerderlands.

Dalton Morrison Valeriano is the coordinator of the Amazonian Monitoring Program at National Institute for Space Research (INPE). Graduated in Ecology, master in Remote Sensing at INPE, and the Doctorate on Geography in University of California at Santa Barbara, USA.

Forest Theme

Tropical Forest and Wetlands Mapping, Case Study Borneo

Dirk Hoekman *et al.*
Wageningen University/SarVision (The Netherlands)

K&C Science Report – Phase 1
Tropical Forest and Wetlands Mapping, Case Study Borneo

Science Team member name
Dirk Hoekman Wageningen University, Dept. of Environmental Sciences,
Droevendaalsesteeg 4, 6708 PB Wageningen, The Netherlands, email: dirk.hoekman@wur.nl

Name of collaborators
Marcela Quiñones and Martin Vissers
SarVision, Agrobusiness Park 10, 6708 PW, Wageningen, The Netherlands, email: vissers@sarvision.nl

***Abstract*—The production of spatially detailed maps of (very) large areas, and time series of these maps, requires dedicated processing approaches. This paper introduces finite mixture modelling and Markov Random Field classification as a tool for production and mosaicing of detailed thematic maps. Results are shown for a multi-temporal classification of the entire island of Borneo for the year 2007 using 50 m resolution PALSAR FBS an FBD strip data. First results indicate that more than 20 classes of forest and land cover can be distinguished well, even though strips have been collected over a 46-day cycle of observation.**

Validation of the Borneo map is still ongoing using large ground data sets and other reference sets spread over Borneo. It is pursued to develop legends in compliance with LCCS and IPCC guidelines. These results may be of key interest to develop REDD projects for the humid tropics.

Maps created for the Central Kalimantan prototype area indicate good results for LULC mapping, flood frequency mapping and peat swamp hydrology may be obtained. These maps are already used by local organisations.

***Index Terms*—ALOS PALSAR, K&C Initiative, Tropical Forest**

I. INTRODUCTION

Significance of tropical rain forests

Deforestation and degradation of tropical rain forests is continuing and currently may occur faster than ever before. It threatens the livelihoods of millions of people depending on the forests, and threatens biodiversity conservation, carbon storage capacity, and other important functions these forests provide.

Environmental awareness and consumer demand for more socially responsible products from tropical forest areas increased in recent years. As a result, all biofuel for the European market for example should be produced in compliance with forthcoming EC regulations on greenhouse gas emission reduction. This will prohibit conversion of tropical forest to biomass plantations.

Moreover, agreements are negotiated under the UN Framework Convention on Climate Change (UNFCCC) to compensate tropical nations for reduced emissions from deforestation and forest degradation (REDD).

The availability of credible and regularly updated spatial information on forest and land use/cover change will be a precondition for successful implementation of initiatives such as mentioned above. In cloudy tropical forest areas new radar satellite imaging techniques will play a key role as one of the most objective methods to measure forest, land cover, biomass and hydrological changes.

Information needs

Ongoing consultation with potential user organisations indicates that satellite observations are needed, as area change is typically dynamic and covers large geographic areas. It is the only objective approach to support reduced deforestation and sustainable biomass production projects in developing countries, providing proof that deforestation rates have decreased and that plantations have been developed inside or outside forest areas.

The following satellite based information maps are required:

- Land use/cover
- Land use/cover change (including deforestation and degradation)

Emerging international guidelines require that these maps are made available at multiple time intervals using a transparent and consistent methodology. Spatial resolution in the order of 10-100 m is sufficient.

High attention and expectation for the inclusion of forest degradation in payment agreements for reducing emissions from deforestation and forest degradation requires new approaches for mapping crown canopy structure of (tropical) forests at high spatial detail. To monitor forest degradation (canopy openings) details smaller than 20m should be clearly visible requiring a spatial resolution of less than 5m; 1-2 m would be ideal. Permanent clouds are making optical satellite imagery useless; again the use of radar satellite imagery is needed (Figure 1).

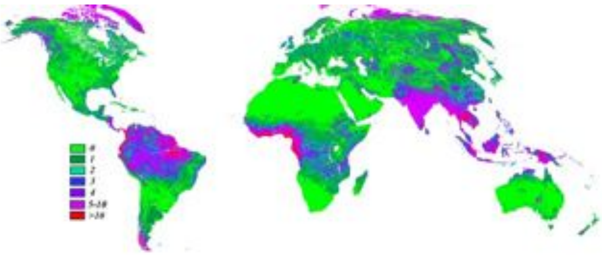

Figure 1. Persistent cloud cover prevents optical remote sensing monitoring of the world's tropical rain forest areas. The colour code shows the estimated number of months per year LANDSAT fails to deliver useful images (Source: [2]).

II. PALSAR STRIP DATA HANDLING AND MOSAICING

The production of a high resolution continental scale map requires the use of a very large number of (radar) images. Within K&C this problem is mitigated by using strip data, which have the same swath width as standard PALSAR radar images (i.e. 70 km, for Fine Beam data), but may span the entire area of interest (up to several thousands of km). For a complete coverage of the entire area of interest many strips may be needed. Borneo, for example, requires 22 of such strips (Figure 2). Often a single coverage will not suffice to meet the required information needs. For forest and land cover mapping in tropical rain forest areas it is advantageous to combine wet and dry season observations, and to combine HH and HV polarisation. For monitoring tropical forest cover change repetitive yearly observation is needed. Very dynamic areas, notably wetlands and agricultural areas, may require even more observations per year to fulfill specific information needs.

Figure 2. Three strips of radar data projected over Borneo and displayed in Google Earth.

For our work in Insular SE Asia and PNG systematic observations were used for modes summarised in Table 1. The selected cycles are shown in Table 2. To be able to produce a 2007 forest and land cover map of Borneo, for example, all the strips collected during the ascending passes of cycle 9 (FBS mode) and cycle 13 (FBD mode) should be used. For technical reasons which are not discussed here, it is not always possible to collect radar data for every pass of the satellite over the area of interest. The success rate in some areas of the world may even drop below 80%. Consequently, most mosaics cannot be created with strips collected within one cycle of systematic observation. In such a case replacement data may be available from a preceding or following cycle. For example, when strips are missing from the FBS cycle 9 these can be replaced from the FBS cycle 8 acquisitions.

Table 1. PALSAR default observation modes

Polarization	Incidence range	Swath width	Resolution (4 looks)
(FBS) HH	36.6°~40.9°	70 km	10 m
(FBD) HH+HV	36.6°~40.9°	70 km	20 m
ScanSAR (HH)	18.0°~43.0°	361 km	~100 m

Table 2. Selected cycles for this study

Default mode	Polarisation	Cycles 2007	Cycles 2008
FBS	HH	9	17
FBD	HH+HV	13	21
ScanSAR	HH	7-16	

The time structure within one cycle is such that the time elapsed between observations of adjacent strips is 17 days or 29 days. This can be explained as follows. Starting East and moving West adjacent strips make jumps of 17 days. For example when RSP412 is the first strip acquired, the adjacent strip RSP413 is collected 17 days later and strip RSP414 34 days later. The next strip RSP415 is collected 3x17 = 51 days later, but this is in the next cycle. To remain in the same cycle 46 days can be subtracted and a jump of 5 days with respect to the first strip RSP412 remains, which is -29 days with respect to the previous strip. For the Borneo mosaic of 2007 4 (out of 22) replacement strips have been collected from cycles 12 and 14 for FBD mode and 3 (out of 22) from cycles 17 and 18 (one year later!) for FBS mode.
The time laps are an inherent feature of any mosaic and these have to be dealt with carefully within classification procedures.

Backscatter of terrain is modulated by the surface geometry of hills and mountains. This modulation is a function of slope steepness, slope orientation and the scattering mechanism of the terrain. Results for an area in central Borneo which is almost completely covered by dense forest are shown in the Figures 3 and 4. In Figure 5 the entire mosaic, which is a multi-temporal aggregate of FBS and FBD data, is shown.

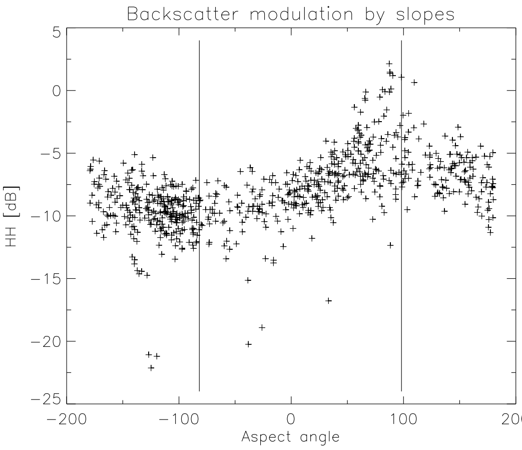

(a)

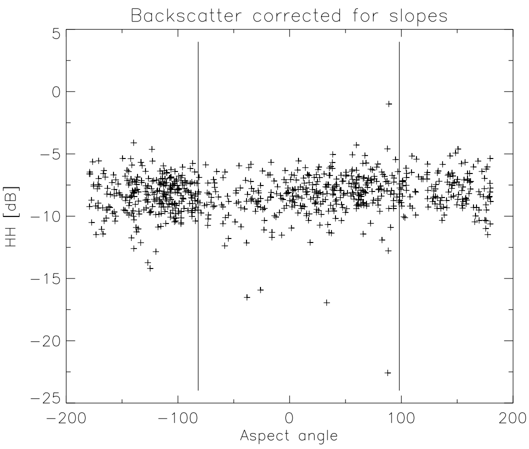

(b)

Figure 3. Slope correction for all pixels in a small test area in a mountainous section of central Borneo; (a) backscatter (gamma in dB) as function of slope aspect; (b) idem, after correction (Note: the vertical lines present the radar orientation angles).

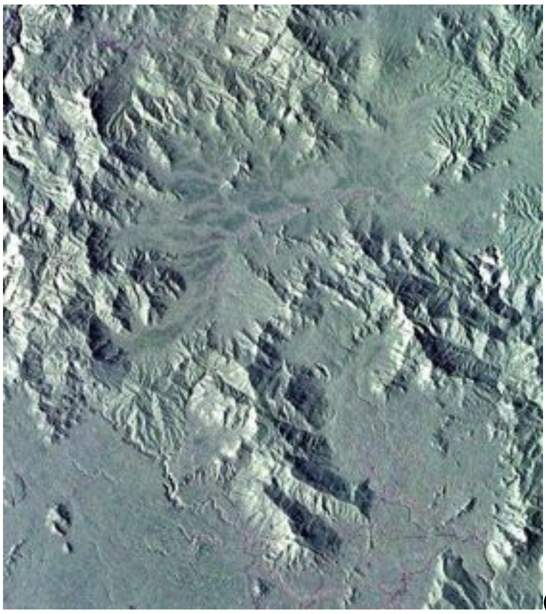

(a)

(b)

Figure 4. (a) PALSAR FBS/FBD aggregate for an area (~42x46km) typical for the mountainous forested terrain in the centre of Borneo; (b) idem, relief corrected. Some effects of overlay and shadow remain visible and are masked after classification. ALOS K&C © *JAXA/METI*

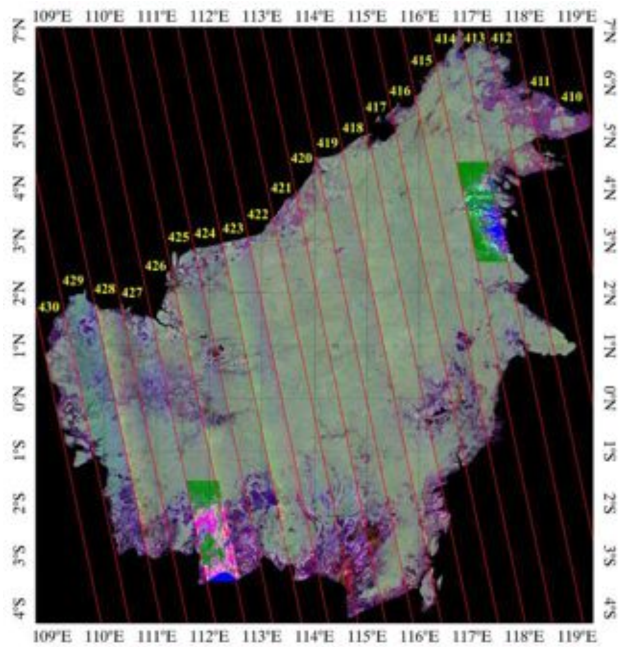

Figure 5. FBS/FDB mosaics of Borneo after radiometric balancing and slope correction. The RSP strips and two patches of classified data are superimposed. ALOS K&C © *JAXA/METI*

III. CLASSIFICATION METHODOLOGY

Several approaches for continental scale mapping (and monitoring) have been tested. The most promising and by far the most accurate approach is based on (unsupervised) mixture modelling followed by Markov Random Field (MRF) classification. The approach has been tested very successfully on agricultural areas [3, 4, 5]. The approach is ideal for the complex and heterogeneous landscapes encountered in the tropics, where ground truth is often very limited or missing.

In mixture modelling the feature space is assumed to be a superposition of a certain number of clusters, each cluster having a certain pre-defined type of distribution, and pixels belong to one or more clusters. The model can be made for any number of pre-defined clusters. In case ground truth is available the optimum number of clusters can be found by trial-and-error and clusters, or aggregates of clusters, can be labelled with a class name. An example is given in Figures 6 for a polarimetric PALSAR image.

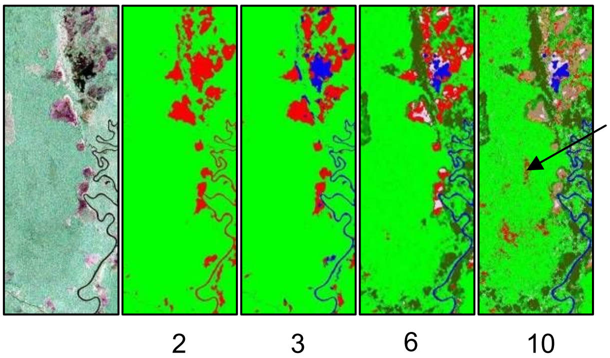

Figure 6. Mixture modelling followed by Markov Random Field classification of a small part of a polarimetric image over Central Kalimantan. Models of increasing complexity reveal a hierarchy of classes. For example, model 2 shows forest non-forest, model 3 adds the class water, while in model 10 re-generating forests can be distinguished (black arrow). Note that model 2 has 43 parameters, increasing to 219 parameters for model 10 and that the model number equals the number of clusters g. ALOS K&C © *JAXA/METI*

In case the complexity of the terrain is not well-known the optimum number of clusters can be computed from the so-called Bayesian Information Criterion (BIC). Figures 7a and 7b show the value of BIC as a function of the number of clusters g for a (complex) disturbed peat swamp forest terrain and an almost undisturbed mountain forest area, respectively. The results indicate, for the peat swamp area, that many clusters are needed to describe the information content of the image appropriately. Consequently, when ground truth is available many different classes could be distinguished. For the mountain forest area the result indicates that at least several classes (i.e. forest types) can be distinguished. *It should be noted that the latter classes may not be present in the peat swamp area, and vice versa.*

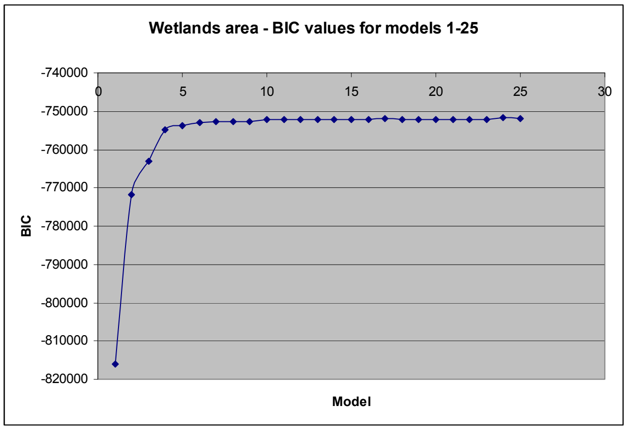

Figure 7a. BIC as a function of mixture model number g for a complex disturbed peat swamp area in Central Kalimantan (2007 FBS-FBD composite). The result indicates at least 25 clusters are needed to describe feature space.

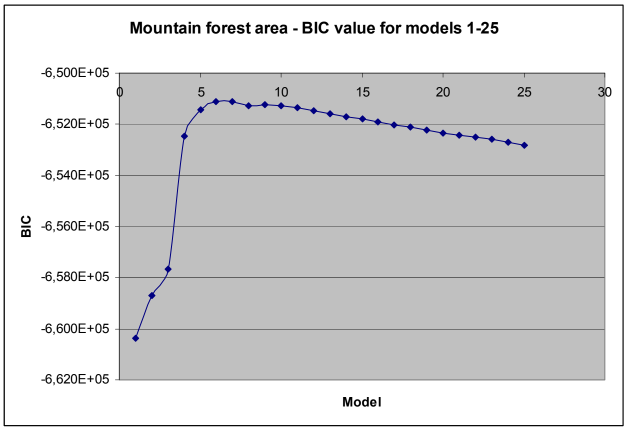

Figure7b. BIC as a function of mixture model number g for a typical undisturbed forest area in the heart of Borneo (2007 FBS-FBD composite). The result indicates that ~7 clusters are sufficient to describe feature space.

IV. MAP FRAGMENTS OF FOREST AND LAND COVER

A first series of map fragments for Borneo have been produced according the methodology introduced in Sections 2 and 3. This involves the following steps:

1. Selection of strip data and, when necessary, replacement data;
2. Radiometric balancing, orthorectification and relief correction;
3. Cluster analysis in key ecological, deforestation and agricultural regions;
4. Selection of key clusters for the description of the entire Borneo data set;
5. Aggregation of key clusters into broad classes;
6. Classification and outlier analysis;
7. Evaluation of results and legend using reference data;
8. Optionally, refinements follow by (iteratively) repeating steps 3-7.

A first iteration of cluster analysis in 14 key areas yielded the following tentative legend (Table 3). It comprises classes typical for wetland areas, namely the mangroves and the peat swamps, several typical dry land forest areas, and other more general broad classes. The latter includes the class "other land cover types or mixed".

The "class other land cover types or mixed" contains either (1) very fragmented small areas of mixed cover type which can not be classified well because of the abundance of mixed pixels, or (2) it contains an area for which an adequate representative cluster has not been selected yet. Since such an area can be detected, as a result of the outlier analysis, and the unknown area can be identified on the basis of appropriate reference data, the legend can be extended in the next iteration.

Table 3. Draft legend Borneo

	Wetland areas
	Mangrove 1 (Nipah)
	Mangrove 2
	Peat swamp less dense
	Peat swamp low pole
	Burnt (peat) forest and bare
	Burnt shrubs and bare
	Forest and forest on peat/heath
	Dry land forest areas
	Forest - Lower biomass and/or degraded
	Forest - Higher Biomass
	Deforestation types
	Global types
	Riverine-riperian and swamp forest
	Shrub land
	Shrub land – other types
	Bare
	Tree plantations and Palm oil
	Dry land agriculture
	Sawah
	Water
	Other land cover types / mixed
	No data (radar shadow and layover)

Selected results are shown in Figures 8-10.

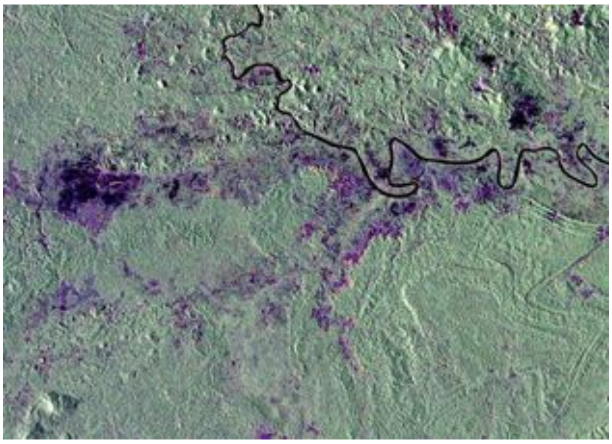

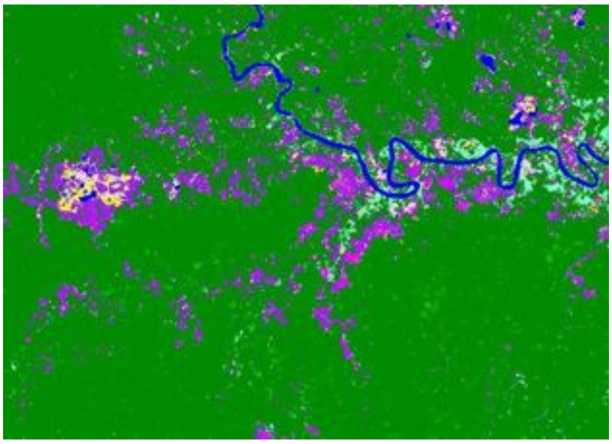

Figure 8. (a) PALSAR mosaic for an area (~43x31km) typical for deforestation in hilly/mountainous forested terrain in Borneo; (b) idem, classification. ALOS K&C © *JAXA/METI*

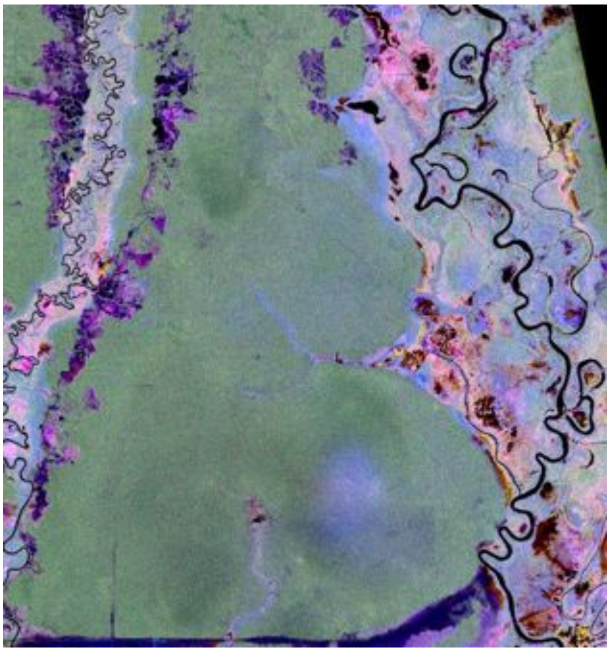

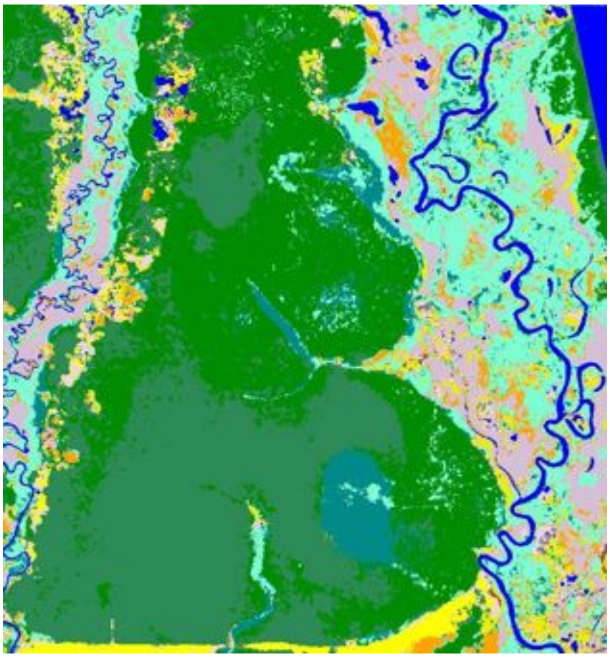

Figure 9. (a) PALSAR mosaic for the Mawas area in Central Kalimantan (~58x62km), which is typical for a (fairly) undisturbed peat swamp forest ecosystem; (b) idem, classification. ALOS K&C © *JAXA/METI*

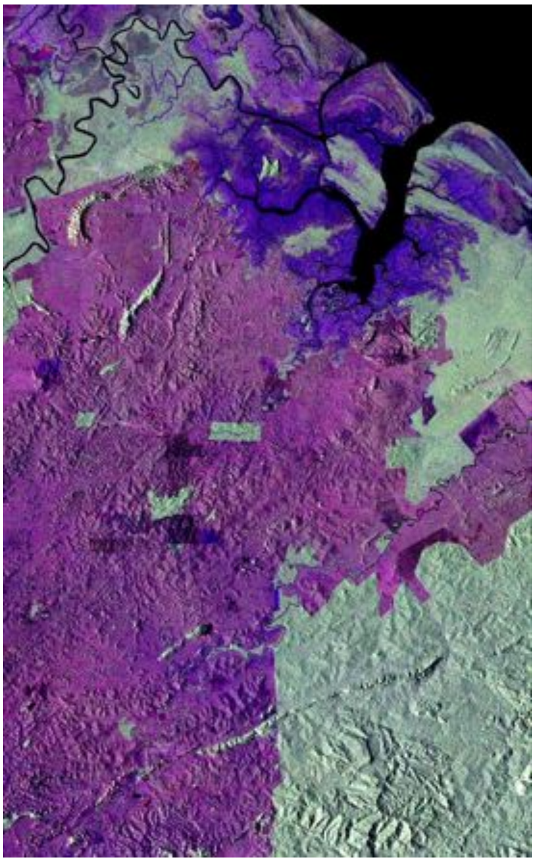

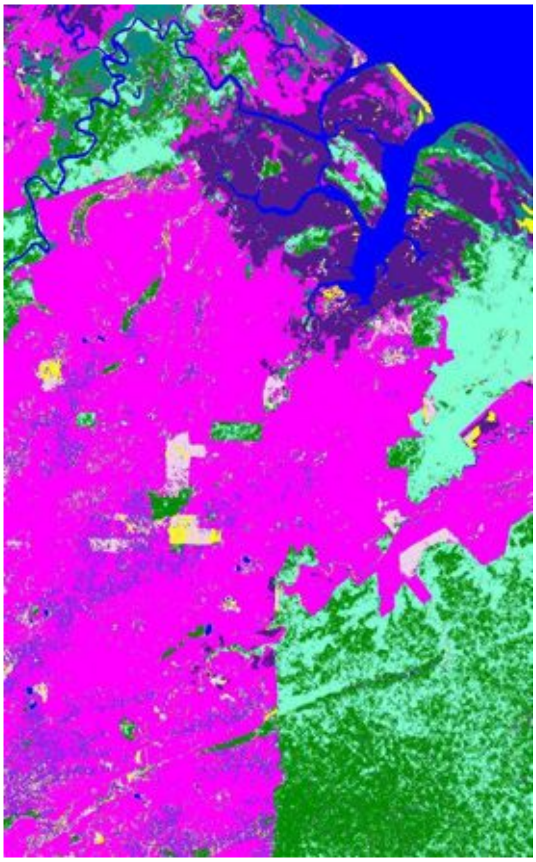

Figure 10. (a) PALSAR mosaic showing an old oil palm plantation development area and mangroves (Nipah) in Sabah (~58x32km); (b) idem, classification. ALOS K&C © *JAXA/METI*

V. FIELD DATA AND VALIDATION

For K&C dedicated data collection campaigns have been made (1) to collect extensive ground truth and reference data over Borneo in the framework of a systematic validation study funded by the Netherlands government; (2) to collect ground water level data in wetland areas to calibrate PALSAR for flooding fraction and ground water level [6, 7]. An accuracy assessment will be made for the Borneo map, as well as for each individual class of this map [8]. Guidelines provided by GOFC-GOLD [9] and GlobCover 2006 [10] for global mapping will be followed as much as possible. These state, for example, that the creation of an international expert network is the key element of the validation process [10]. This is also pursued within this project. An extensive partnership network of local end users in Insular SE Asia is already in place.

Within K&C it is pursued to produce maps to support UN conventions and development of REDD projects. Hence, two types of legend are under consideration: (1) using IPCC classes and (2) using the FAO LCCS system.
For validation the following reference data sets have been collected:

- Landsat
- MODIS 2007 (year aggregate)
- Ministry of Forestry classification, 2005

- NRM classification, 1997
- GlobCover, 2006
- Selected validation data set (samples)

Because of rapid changes in vast areas many of the reference data, even those of the Ministry of Forestry, are already outdated. This forms a major complication in the validation process. Nevertheless, the first results (presented as maps during the conference) are promising.

VI. MAPS OF PROTOTYPE AREA

It is intended to produce high resolution continental scale maps according methodologies and validation procedures introduced in Chapter 3 and Chapter 5, respectively, as the final K&C products. For development and evaluation purposes, however, several tentative products have been made at regional and local scale. These have been presented as K&C mid-term products (or posters), and will be briefly summarised in this section.

(A) LULC map Central Kalimantan

The main product development area of this project is in Central Kalimantan. In this area the intended methodology based on mixture modelling and Markov Random Field classification has been tested first. Use was made of the FBD mosaic produced by the K&C mosaicing theme, and a Scansar (WB1 HH) image of the wet season. Relief correction is not necessary since the terrain (a wetland area) is flat. An accurate forest and land use/cover map with more than 20 classes resulted (Figure 11).
This map is currently used for spatial planning in the Ex Mega Rice Project area (EMRP) by the provincial government of the Central Kalimantan, and has replaced older maps based on LANDSAT. The information is applied, among others, for ecological restoration and conservation of wild orangutan populations. Dedicated ground truth collection and evaluation based on reference data (Table 4) reveals an accuracy of at least 84%. In [11] full details on the production and accuracy assessment are reported.

Table 4. Reference data used for evaluation of the prototype area land use / land cover map of the Ex Mega Rice Project area in Central Kalimantan.

Reference data
• LANDSAT-7 ETM: Path row 118-062. 2000-07-16
• MODIS Tree cover percentage, University of Maryland / SDSU MODIS VCF 2005.
• Fire hotspot data. Database NASA/ University of Maryland MODIS, ESA/ESRIN AATSR, January 2004 – June 2007
• Other LULC maps:
• Ministry of Forestry Peta Penuputan Lahan Provinsi Kalimantan Tengah 2003
• Ministry of Forestry / BAPPEDA Peta Kawasan Vegetasi 2003
• Bakosurtanal Liputan Lahan 1:250,000 LULC map 2003EU

(B) Flood frequency map Central Kalimantan

There is a large demand for inventory and physical characterization of peat swamp forests in South-East Asia in support of hydrological modelling, management, protection and restoration. The current loss of peat swamp forest causes enormous emissions of CO_2 at the global level.
The need for such data is particularly high in the main product development area of this project, in Central Kalimantan, where the Mega-Rice Project was located. For the Central-Kalimantan prototype area a series of flood event maps have been produced for the period November 2006 until December 2007 (Figure 12). Use is made of systematic and frequent observation by PALSAR radar (Table 5) and the previously produced LULC map (see above). The approach is based on land cover dependant backscatter fluctuation caused by flooding or peat soil ground water level change. In [12] full details on the production and accuracy assessment are reported.

Table 5. Input data used for the production of the Central-Kalimantan flood frequency map.

ALOS PALSAR ScanSAR HH (WB1); EOC standard product Level 1.5;		
11-11-2006	27-12-2006	11-02-2007
29-03-2007	14-05-2007	14-08-2007
29-09-2007	14-11-2007	30-12-2007

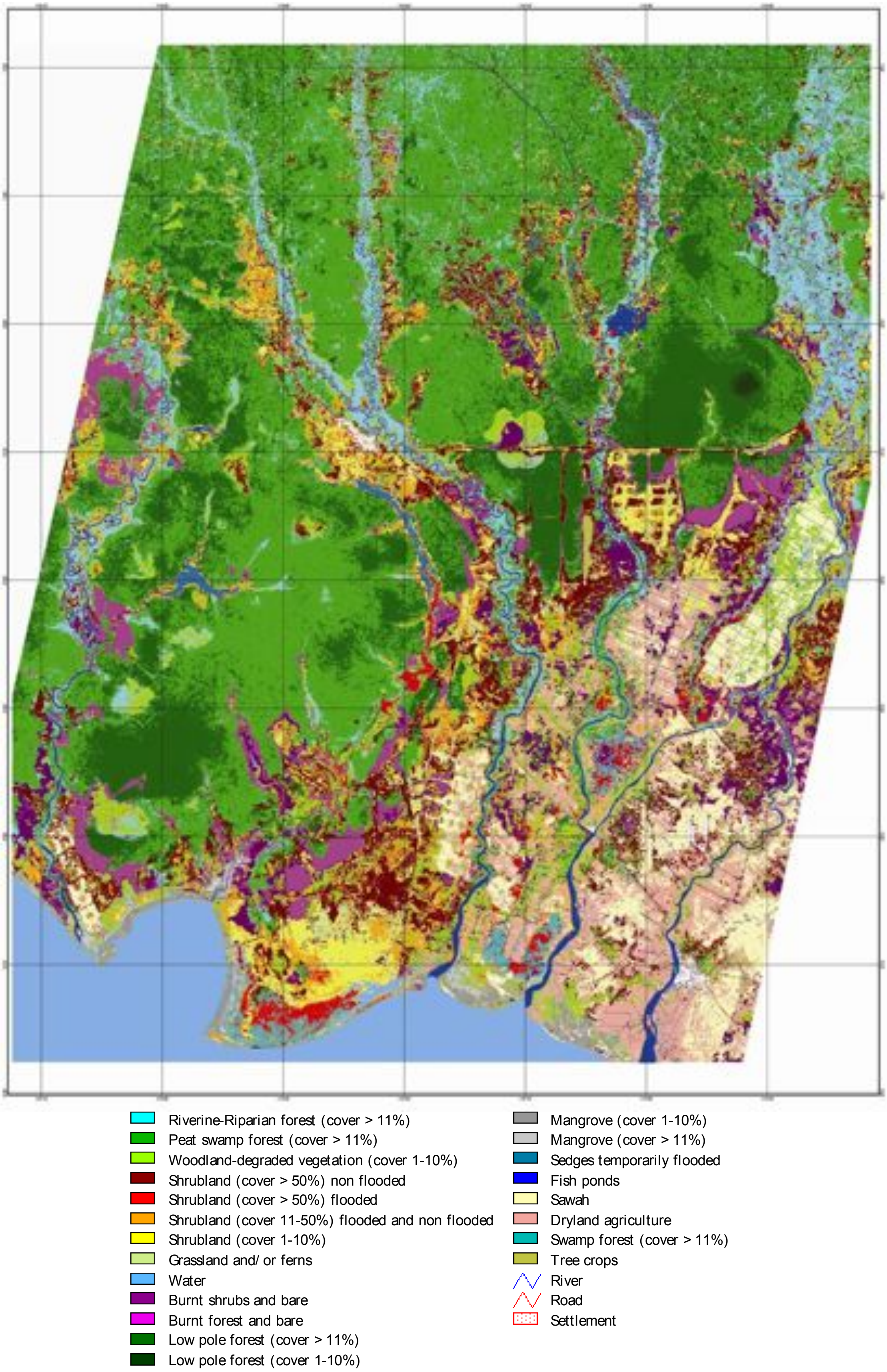

Figure 11. Map of forest and land use/cover 2007 of the main product development area (the EMRP project area and Sebangau) in Central Kalimantan based on FBD and WB1 HH data (K&C mid-term product 1).

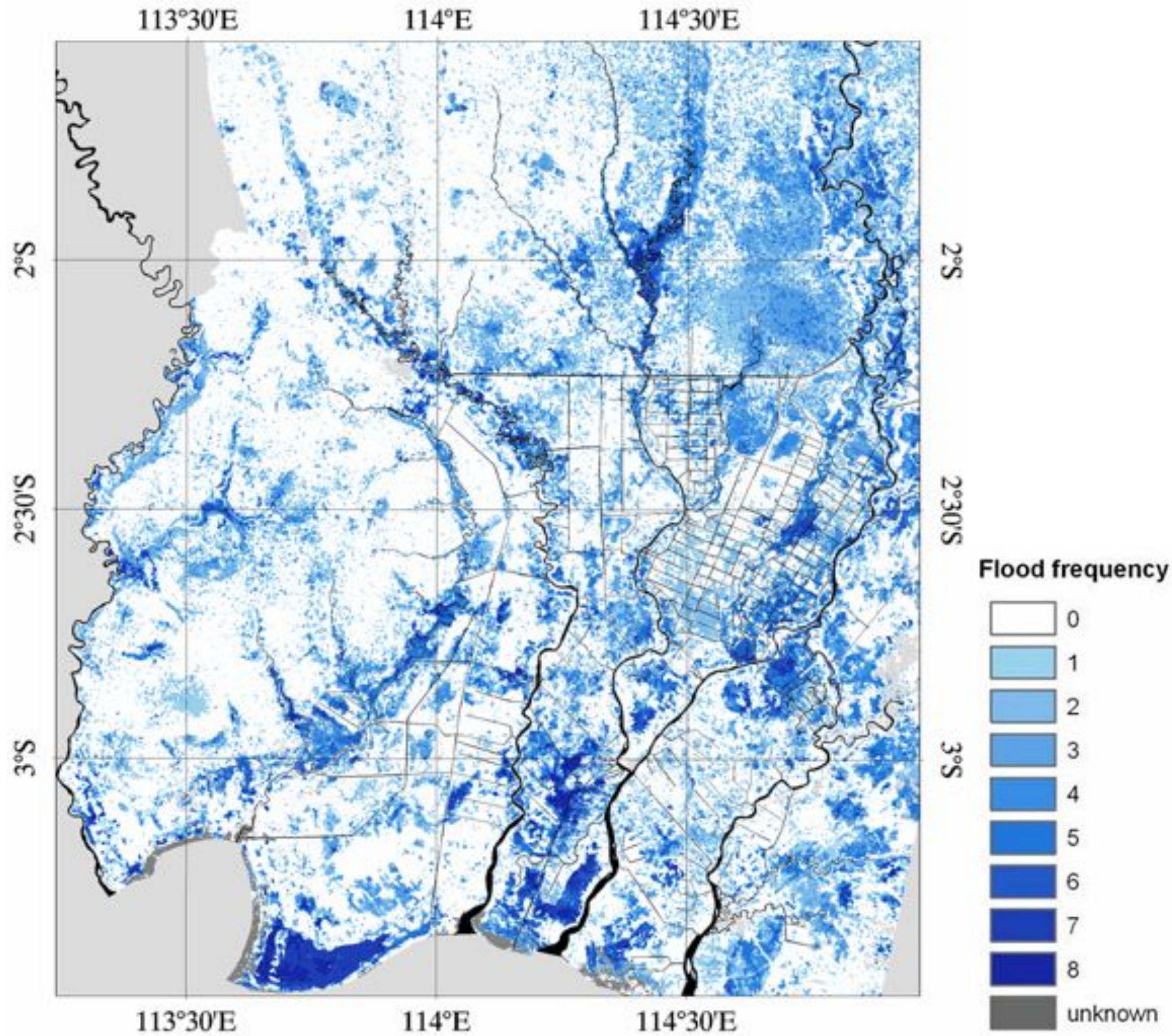

Figure 12 Map of flooding frequency in 2007 of the main product development area (the EMRP project area and Sebangau) in Central Kalimantan based on 9 PALSAR WB1 HH images (K&C mid-term product 2).

VII. FIRST RESULTS PEAT SWAMP HYDROLOGY

To study peat swamp hydrology, ecology and radar wave interaction in a systematic way a dedicated research station has been established in the Mawas peat swamp forest conservation area, which is located some 80 km east of Palangkaraya, in the province Central Kalimantan. The main feature is a research bridge, 23 km in length, crossing an entire peat dome. Instruments placed along this bridge automatically measure rainfall and water level every hour. In December 2004, an airborne radar survey (the ESA INDREX-2 campaign) was carried out along this bridge to test a variety of advanced imaging radar techniques [13], [14]. The intention is to collect field data over an extended period (i.e. 10 years) to develop hydrological modelling, examine relationships between hydrological, soil and vegetation characteristics, study carbon sequestration and to relate biomass and water (flooding) levels to L-band radar observations of the ALOS PALSAR instrument [6], [7].

(A) Hydrological characterisation

Peat domes are formed in ombrogenous peat swamp areas, which are purely rain-fed and, consequently, nutrient poor. Vegetation types are located in concentric zones, with the 'poorer' forest types located towards the centre of the dome. To characterize the hydrology of such a dome, where water is flowing from the top in the centre towards the edges, the water level variation along the flow is monitored. An example result for one of the instruments along the bridge is shown in Figure 13.

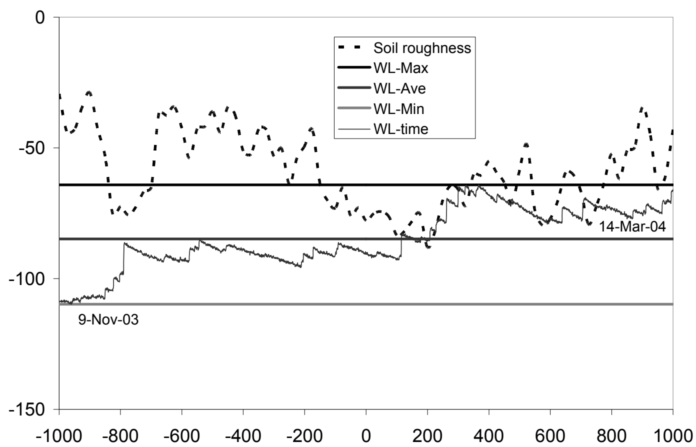

Figure 13. Water table variation WL-time (solid curve) and peat soil surface roughness (dashed curve). The vertical axis shows water level and soil surface height (both in cm). The horizontal axis shows horizontal distance (in cm) along the soil surface roughness profile (i.e. from -1000 to 1000 cm) as well as time (i.e. from 9-Nov-03 to 14 Mar-04). The position of the water table measurement is at the centre of this profile. These measurements are made every hour. The results for the period 9 Nov2003 until 14 March 2004 are shown (also along the horizontal axis). The three horizontal lines show the maximum (WL-Max), average WL-Ave) and minimum (WL-Min) water level. The percentage terrain flooding, thus, can be deduced from the combined roughness and water table measurements.

(B) Mawas ALOS PALSAR observation example

In the JERS-1 image of January 1998 (dry period) shown in Figure 14 the area demarcated by the red line is an area within the Mawas area suffering from excess drought. In the PALSAR image of 9 November 2006 (dry period) this area has decreased above the main east-west canal because of the construction of dams in the canal going North (canal Neraka). In the area south of the main east-west canal a large network of canals is still present and the continued drainage has worsened the situation. Note the very low radar backscatter (intense black) caused by very dry bare peat areas and the bright white area, which is a strongly degraded open forest with fire damage. The areas demarcated in blue are hydrologically intact, allowing forests previously damaged to regenerate.

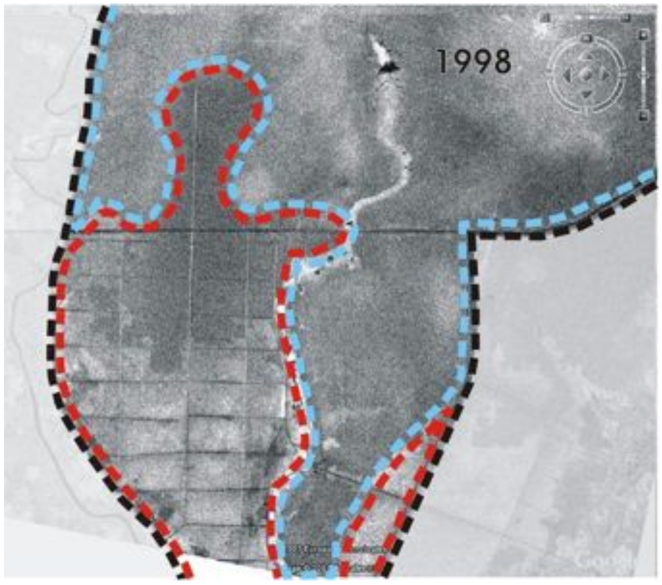

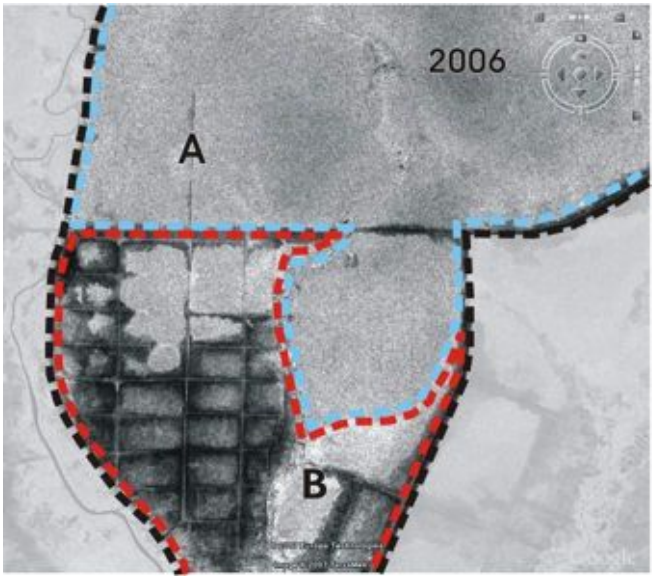

Figure 14. Peat swamp degradation (B) and restoration (A) in the Mawas area between 1998 (JERS-1) (left) and 2006 (PALSAR) (right). The red area is degraded, the blue area is intact or regenerating.

VIII. DISCUSSION AND CONCLUSIONS

The demonstrated methodology for continental wide mapping of forest and land cover at high resolution yields very promising results, and is generally applicable. These results are especially relevant for the humid tropical rain forest areas where other (optical) techniques have a poor performance because of persistent cloud cover. For monitoring, or the development of future REDD projects, radar observation seems to be irreplaceable.

The tentative legend shown already contains six forest types which have typical biomass ranges, and which can be mapped fairly accurate. Since more classes can be differentiated (on the continental scale) than initially foreseen, more validation effort is required. The (ongoing) validation study likely may reveal that more types of deforestation, tree plantations and shrubs can be differentiated.

First validation results show good agreement with the maps of the Ministry of Forestry which are based on visual interpretation of Landsat, but in general are outdated. The PALSAR maps would be perfect to improve GlobCover [10] in tropical rain forest areas with persistent cloud cover.

Maps of the Central Kalimantan prototype area indicate high accuracy for LULC mapping (over 84% for 20 classes), flood frequency mapping and peat swamp hydrology may be obtained. These maps are already used by local organisations.

It is expected that more characteristics of agricultural and peat forest areas can be obtained when the PALSAR ScanSAR cycles are included in the classification (or parameter retrieval) procedures. These features are mainly related to cropping cycles, hydrological/seasonal cycles and flooding events.

The work will be continued within the extension (phase 2) of the JAXA Kyoto & Carbon Initiative.

IX. ACKNOWLEDGEMENTS

This work has been undertaken in part within the framework of the JAXA Kyoto & Carbon Initiative. ALOS PALSAR data have been provided by JAXA EORC. The (ongoing) validation study of the Borneo map is coordinated by the Netherlands Agency for Aerospace Programmes (NIVR) and funded by the Netherlands Government, Ministry of Housing, Spatial Planning and the Environment.

REFERENCES

[1] A. Rosenqvist, M. Shimada, R. Lucas, J. Lowry, P. Paillou, B. Chapman [eds.], "The ALOS Kyoto & Carbon Initiative, Science Plan (v.3.1)," JAXA EORC, March, 2008. [Online] Available: http://www.eorc.jaxa.jp/ALOS/kyoto/KC-Science-Plan_v3.1.pdf

[2] Friedl in: M. Hansen, M. Herold, R. Ridder, and C. Schmullius, Land cover recommendations, Global Vegetation Monitoring Workshop, Missoula, August 2006.

[3] Hoekman, D.H., T. Tran, and M.A.M. Vissers, 2007a, Unsupervised full-polarimetric segmentation for evaluation of backscatter mechanisms of agricultural crops, *Proc. of POLinSAR 2007 Workshop,* ESA SP-644, 22-26 Jan 2007, Frascati , Italy (CD-ROM).

[4] Hoekman, D.H., T. Tranh, and M.A.M. Vissers, 2007b, Unsupervised full-polarimetric segmentation of agricultural crops at the DEMMIN test site, AGRISAR and EAGLE Campaigns Final Workshop, 15-16 October 2007, ESTEC, Noordwijk, The Netherlands (CD-ROM).

[5] Tran, N.T., R. Wehrens, D.H. Hoekman, and L.M.C. Buydens, 2005, Initialization of Markov Random Field Clustering of Large Remote Sensing Images, *IEEE Transactions on Geoscience and Remote Sensing*, Vol.43, No.8, August 2005, pp.1912-1919.

[6] Hoekman, D.H., 2007, Satellite radar observation of tropical peat swamp forest as a tool for hydrological modelling and environmental protection. *Aquatic Conservation: Marine and Freshwater Ecosystems*. Special edition title "Satellite-based radar – developing tools for wetlands management", Vol.17, pp.265-275.

[7] Hoekman, D.H., and M.A.M. Vissers, 2007, ALOS PALSAR radar observation of tropical peat swamp forest as a monitoring tool for environmental protection and restoration, Proceedings of the IEEE International Geoscience and Remote Sensing Symposium, 23-27 July 2007, Barcelona, Spain (CD-ROM).

[8] Foody, G.M., 2008, Harshness in image classification accuracy assessment, International Journal of Remote Sensing, Vol.29:11, pp.3137-3158.

[9] GOFC-GOLD, 2006, Report 25; Global Land Cover Validation: Recommendations for Evaluation and Accuracy Assessment of Global Land Cover Maps, A. Strahler *et al*., March 2006.

[10] GLOBCOVER, 2008, Products Description and Validation Report, P. Bicheron *et al*., December 2008;

ftp://uranus.esrin.esa.int/pub/globcover_v2/regional/

[11] SarVision, 2008a, Mid-2007 Revised Land use/cover map, Ex-Mega Rice Project area and Sebangau, Central Kalimantan, Final Version, SarVision report, 28 May 2008, Wageningen, The Netherlands, 43 pages.

[12] SarVision, 2008b, Flood analysis, Ex-Mega Rice Project area and Sebangau, Central Kalimantan, SarVision report, 23 May 2008, Wageningen, The Netherlands, 30 pages.

[13] Hajnsek, I., F.Kugler, K. Papathanassiou, R. Scheiber, R.Horn, A. Moreira, D.H. Hoekman, M. Davidson, and E.P.W. Attema, 2005, INDREX 2 – Indonesian airborne radar experiment campaign over tropical forest in L- and P-band, POLinSAR 2-nd Int. Workshop on Applications of Polarimetry and Polarimetric Interferometry, ESA-ESRIN, Frascati, Italy, 17-21 January 2005, *ESA report SP-586* on CD-ROM

[14] Hajnsek, I, and D.H. Hoekman, 2006, Final Report, INDREX II – Indonesian Radar Experiment Campaign over Tropical Forest in L- and P-band, Version 1, 14 June 2006; ESA Contract RFQ/3-11077/04/NL/CB; Report ESA, DLR and Wageningen University; 142 pages.

Dirk H. Hoekman received his M.Sc. degree E.E. from Delft University of Technology, Dept. of Electrical Engineering, The Netherlands in 1981 and his Ph.D. degree from Wageningen University, The Netherlands in 1990. He is employed at Wageningen University since 1981 where he currently holds the position of Associate Professor in remote sensing with main interests in the physical aspects of remote sensing, microwave remote sensing and applications of remote sensing in forestry, agriculture, (agro-)hydrology, climate studies and environmental change. He was scientific co-ordinator for the ESA/INPE Amazonian expedition (1986) and the ESA/JRC AGRISCATT campaign (1987-1989); co-ordinating investigator for the international test site Flevoland for the JRC/ESA MAESTRO-1 campaign (1989-1991); for tropical rain forest sites in Colombia and Guyana, including ESA's SAREX-92 campaign (1992-1993) and NASA's South-American AIRSAR Deployment (1993); scientific co-ordinator for the EC programme TREES'94 ERS-1; and co-ordinating investigator for tropical rain forest sites in Indonesia, including NASA's PACRIM-2 campaign (2000) and ESA's INDREX-1 and -2 campaigns (1996, 2004). He is currently co-ordinating research programmes to support the realisation of operational wide-area radar monitoring systems for sustainable forest management and UN REDD; and exploring the scientific use of ALOS PALSAR for tropical peat swamp forest hydrology and forest cover change monitoring in Indonesia and the Amazon in the framework of the JAXA Kyoto&Carbon Initiative.

Marcela J. Quiñones received the B.Sc. degree in biology from Los Andes University, Bogotá, Colombia in 1987, the M.Sc. degree in Remote Sensing and GIS for forestry applications in 1995 from the International Institute for Aerospace Survey (ITC), Enschede, The Netherlands and the PhD degree in Environmental Sciences at Wageningen University in 2002. Now she is a researcher at SarVision working on the application of remote sensing data for the Amazon region. She has been involved mainly in research projects for resource management, ecology and land use planning in the Colombian Amazon. Her main interest is the establishment of operational accurate remote sensing monitoring systems in the Amazon region for studies of ecosystem dynamics, deforestation and fire detection.

Martin A.M. Vissers is an agricultural engineer from Wageningen University (WU), The Netherlands, graduated in Land and Water Management, 1987. He specialized in remote sensing data handling and archiving, image processing, software development, field work and radar remote sensing techniques. He was involved in many scientific remote sensing campaigns. In 1995 he founded his company "Vissers DataManagement", a small business dedicated to digital image processing, data-handling and remote sensing field campaigns. He executed several contracts for ESA-ESTEC, Wageningen University and other institutes and companies in the field of remote sensing. Since April 2000 he is managing director of SarVision BV, a company he co-founded. Beside responsible for management he executed several major contracts for ESA-ESTEC, WWF, VROM, CKPP and he was involved in several remote sensing campaigns (fieldwork as well as data processing).

Forest Theme

Monitoring Indonesian Forests with ALOS PALSAR

Shaun Quegan *et al.*
University of Sheffield (U.K.)

K&C Science Report – Phase 1
Monitoring Indonesian Forests with ALOS-PALSAR

Shaun Quegan, Martin Whittle
CTCD-NCEO, University of Sheffield, Hicks Building, Hounsfield Rd, Sheffield S3 7RH
s.quegan@sheffield.ac.uk

Yumiko Uryu
WWF Indonesia, yumuryu@yahoo.com

Abstract— Deforestation in the Sumatran province of Riau is found to cause an initial marked increase in HH backscatter. Large areas can therefore be rapidly surveyed for evidence of deforestation by measuring temporal variability in a time-series of ScanSAR data. Regions of anomalous change can then be subjected to temporal analysis to find the timing of deforestation events to within 46 days. Algorithms to perform these operations automatically have been implemented and are currently being assessed and refined using field data. Comparable results for annual change are also achievable using Fine Beam Dual (FBD) data, but this involves more substantial data handling and cannot localise the time of deforestation. Though the analysis has been developed only over Riau, it is expected to be generic and transferable, and will be tested in other regions once suitable data are acquired, with the intention of extending it to the whole of Indonesia.

Index Terms— **ALOS PALSAR, K&C Initiative, change detection, ScanSAR, tropical deforestation**

I. INTRODUCTION

A. *Project objectives*

The objectives of this project are:

1. To demonstrate that ALOS ScanSAR and FBD data can successfully detect natural forest cover change in Indonesia, where cloud and haze hamper natural forest monitoring based on optical remote sensing data.
2. To assess the ability of ALOS data to detect key natural forest and land cover types in Indonesia.
3. To develop software that permits ALOS-based forest monitoring to be carried out in a scientifically robust manner at technician level.
4. To provide the Indonesian and global community with tools for using ALOS-PALSAR data that allow transparent, accurate and frequent tracking of natural forest cover change independently of cloud and haze and that can be used as a basis for action on biodiversity conservation, forest carbon management, etc.

Up to now, work has been directed primarily toward the first and third objectives, with particular emphasis on the analysis of ScanSAR time series. The analysis this involves also contributes to meeting the second objective. Our immediate aim is to be able to detect all new deforestation occurring from the start of the ALOS time-series so that it can be reported on at 46 day intervals, and the current drive is focussed on developing the machinery needed to achieve this goal.

Up to now, we have carried out a case study applied to a single time-series of ScanSAR data for the year 2007, in order to develop methods that highlight regions showing evidence of deforestation and track the progress of these events. These methods should be able to analyse a year's ScanSAR images for a single scene within 12 hours. A more rapid but approximate analysis should be achievable within an hour.

B. *Scientific findings*

Analysis of PALSAR data seems to indicate that multi-temporal ScanSAR data is as capable of measuring deforestation as Fine Beam Dual (FBD) data. This provides major advantages, particularly coverage of wider areas and the ability to locate the timing of deforestation events to within 46 days. Deforestation in Riau (the test area) typically leads to an *increase* in HH backscatter, but at the moment we have no datasets long enough to know how the signal subsequently develops over longer periods. Evidence from Brazil (backed up by physical argument) suggests that the signal will decline with time to values well below that of mature forest. The characteristic signal of a deforestation event indicates that large areas can be rapidly surveyed for evidence of deforestation by measuring temporal variability in a time-series of ScanSAR data. Detected regions of change can then be subjected to temporal analysis to find the actual timing of the event. These operations can be realised by automatic algorithms which have been implemented and are currently being tested. Up to now, the analysis has been developed only over Riau, but we expect it to be generic and transferable, and it will be tested elsewhere once suitable data are acquired, with the intention of extending it to the whole of Indonesia.

II. DESCRIPTION OF THE PROJECT

A. *Relevance to the K&C drivers*

The project was designed to gain better understanding of the land carbon cycle, and in doing so derive information relevant to UNFCCC reporting under Land Use, Land Use Change and Forestry. Its original focus was meant to be temperate forest, but this was modified for three reasons: (1) the greater importance of tropical land use change for the global carbon budget; (2) the proposal for the post-2012 Reduction of Emissions from Deforestation and Degradation mechanism at the Bali COP-12; (3) development of good working links between the University of Sheffield and WWF Indonesia, which gives a means to link technical developments to ground data, provides access to important institutional links in Indonesia, and supports applications on the ground.

The key initial aim of the project was to develop methodology to map changes in forest cover using ALOS PALSAR data. The expectation was that multi-temporal (annual) FBD data would be crucial for this, but investigations at the Riau test site in Sumatra suggest that equivalent, and in fact more powerful, results may be obtained using 46-day repeat ScanSAR data. We also aimed to develop methods to estimate product accuracy, and thence to generate maps of forest cover and maps of forest changes, together with corresponding accuracy assessments. Substantial progress has been made in developing methods to detect deforestation and locating the times of these changes. We are currently planning work in Sumatra to test the performance of the algorithms and optimize the parameters used in them. We then intend, with the help of JAXA, to extend the methods to the whole of Indonesia.

B. *Work approach*

The work has benefited greatly from access to the WWF 2007 land-cover database for Riau & Jambi [1]. This provides detailed information about vegetation types covering the region and is based on remote sensing data nominally for 2007. We also have ALOS ScanSAR and Fine Beam Dual images for much of the same region spanning the same year. With the help of the WWF database we can identify primary forest regions and assess their normal characteristics. It also allows us to reduce the processing task, since for deforestation studies we can ignore areas already known to have other types of land cover. This is very helpful, since a single ScanSAR image typically contains $\sim 19\times10^6$ pixels, and a long time-series of images represents a significant amount of data processing. The approach we have developed is to detect anomalous changes in regions labelled as forest; these are likely to indicate deforestation events. Subsequent operations aim test this hypothesis and determine when the changes occurred. The wider challenge is to extend the methods to regions outside the database where there may be less prior knowledge about forest cover.

Temporal variability within a time-series of images can be charted by recording the temporal standard deviation at each pixel. Seasonal fluctuations together with slow changes over the period of the time-series may contribute to this, hence to detect deforestation we need a more specific temporal signature. Initial searches used colour-coded combinations of images in conjunction with the WWF land-cover database to survey the type of changes that occur and to identify suspect regions within designated primary forest areas for more detailed study.

Each pixel of a ScanSAR image covers a region of size 100m × 100m and we have made the assumption that under deforestation enough of each pixel is cleared within the 46-day cycle to change significantly the scattering coefficient between successive images in the time-series, thus generating a step in the intensity (more subtle effects due to partial clearance or forest degradation will be studied later). In practice the algorithms use a window to average over squares of 5×5 pixels and we are thus currently working at a spatial resolution of 500m × 500m per cycle.

A preliminary routine (*changemap*) distinguishes positive from negative changes that exceed a threshold value. Areas of positive change are picked out as regions of suspected deforestation. This increase is thought to be due to the practice of leaving tree stumps and other detritus behind after felling. The stumps in particular would lead to high backscatter due to the double bounce mechanism. In other areas of the world, alternative management practices may instead lead to a negative change, and partly for this reason it is worth retaining the possibility of studying both types of change.

A more specific routine (*stepmap*) fits a step function to window-averaged data and filters out regions of positive or negative step-size that exceed a given threshold value. This routine picks out many areas in common with *changemap* and some that are different. It also produces extra valuable data on the time of step. However it is relatively slow, taking about 16 × the CPU time of *changemap*. A third routine (*noisemap*) has also been developed to look more generally at regions of anomalous behaviour, particularly with a view to isolating regions that might lead to false detections. This routine is relatively fast and may be used to initially screen large areas for possible regions of interest. Inside the WWF database region it is possible to focus only on known forest areas, but in regions without prior knowledge of land cover a means of locating regions of interest will be needed. Using *noisemap*, pixels that do not include any period of scattering that exceeds the normal standard deviation can be identified and ignored, allowing use of the relatively slow *stepmap* to focus only on the remaining areas.

C. *Satellite and ground data*

In the initial phase of program development we have concentrated on a set of eight ScanSAR images centred on Lat. 1.728 S, Long. 102.332 E that partially overlap the WWF land-cover database for Riau [1]. This is the complete set of 46-day ScanSAR images for 2007, and they are all acquired with the same geometry. Using such a limited dataset was necessary because data quota limitations prevented more extensive coverage. However, it has been sufficient for developing methods that should have much wider applicability.

In addition, we have nearly full coverage of Riau by FBD data from June to August 2007; a missing strip had to be filled with November data.

Before analysis the eight ScanSAR images were accurately co-referenced using Gamma software. A multi-channel filter [2] was then applied to remove speckle. The IDL code for this procedure has been structured to work automatically with a large number of images and delivers de-speckled files of the same name with modified extensions. The routine also finds the combined intersection areas of all input files and applies to all results. In other words, any regions that are not covered by all input files are removed. Processing takes less than 1 hour for 8 images and intermediate processing files are not currently saved. However, if a significantly longer time base is available it may be worthwhile to implement an iterative procedure to speed the processing of new images [3], which would require the archiving of some intermediate files. The resulting average image is shown in context with the database in Figure 1.

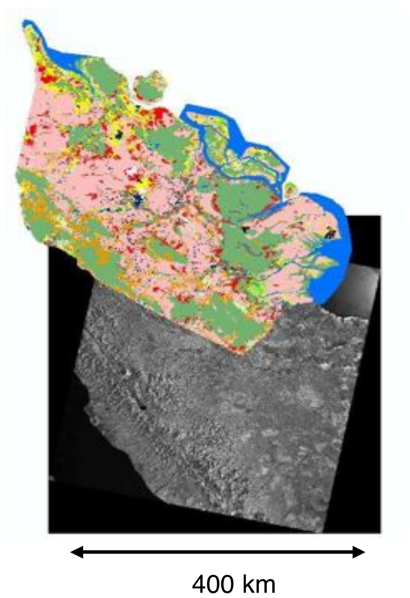

Figure 1. A de-speckled and averaged PALSAR ScanSAR image of the Riau and Jambi regions of Sumatra overlaid by the WWF 2007 land-cover database. Images obtained Jan – Dec 2007, ALOS K&C © *JAXA/METI*

1) Regions

From the preliminary analysis using colour-coded combinations of images in conjunction with the WWF land-cover database, ten regions are discussed here, as detailed in Table 1. For each of these regions, the intensities of a 5×5 window of pixels are plotted for comparison as a time-series in the Appendix. Two of these (Regions 1 and 3) have all the hallmarks of deforestation events: 1) the intensity changes abruptly over a 46-day period in a region designated as forest; 2) the regions have an angular appearance; 3) they are close to known cleared areas and plantations. In addition, for region 1 the progressive nature of the event is consistent with sequential forest clearance. For comparison, apparently undisturbed regions immediately adjacent to regions 1 and 3 have also been investigated – these have a slow, probably seasonal intensity variation indistinguishable from other regions of primary forest. Regions 5 – 10 have all been chosen because they belong to regions of relatively high temporal standard deviation. These types of region could potentially be wrongly identified as deforestation; it is therefore important to know their characteristics.

Table 1 Regions investigated in detail.

	Latitude South	Longitude East	
Region 1	0˚ 34’ 36.13”	102˚ 20’ 39.63”	Suspected deforestation
Region 2	0˚ 33’ 10.18”	102˚ 39’ 31.80”	Adjacent forest to region 1
Region 3	0˚ 13’ 28.30”	102˚ 54’ 25.47”	Suspected deforestation
Region 4	0˚ 12’ 31.12”	102˚ 55’ 10.97”	Adjacent forest to region 3
Region 5	0˚ 15’ 28.30”	102˚ 49’ 47.49”	A forest region with unusually high s.d.
Region 6	0˚ 11’ 44.51”	102˚ 40’ 48.73”	River and associated forest
Region 7	0˚ 25’ 29.81”	102˚ 49’ 57.83”	An anomalously bright region
Region 8	0˚ 18’ 30.91”	102˚ 35’ 13.05”	Probable flood plain
Region 9	0˚ 18’ 30.94”	102˚ 33’ 39.42”	As above
Region 10	0˚ 42’ 36.26”	102˚ 58’ 44.65”	Paddy fields

The WWF database is very detailed and for the purposes of the current study the regions have been amalgamated into just nine groups as shown in Table 2.

Table 2 WWF database amalgamated regions

Landcover	**Fill**
Primary Forest (all types)	
Shrub,Grass& Fern	
Regrowth (All types including Forest, Shrubs, Semak, Belukar Muda)	
Plantation (Rubber, Oil Palm, Acacia, Coconut)	
Paddy fields	
Water	
Agricultural (mixed agriculture, mixed garden)	
Cleared, cleared post acacia harvested, etc.	
Burnt	
Built	

All the regions given in Table 1 lie within the database. Here, in Figure 2 we show the context of the two regions of main interest. The land-cover maps are superimposed on composite ScanSAR images colour-coded to reference the beginning, middle and end of the cycle. In these images the regions of interest lie at the image centres. Region 1 changed relatively late in the year (see Appendix) and appears as a bluish patch in Figure 2(a), region 3 changed closer to mid-cycle and appears as a greenish patch in Figure 2(b).

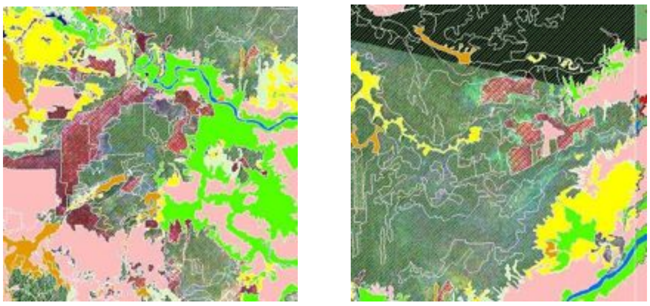

(a) (b)

Figure 2 (a) A small section of a time-averaged de-speckled PALSAR ScanSAR image surrounding region 3 showing texture probably associated with plantation drainage. (b) A high resolution FBD image of the same area where the colour derives from polarisation channels shown as: HH-red, HV-green, HH/HV-blue. Images obtained Jan – Dec 2007, ALOS K&C © *JAXA/METI*

2)Normalisation

An initial view of the areas that are subject to change can easily be obtained from the temporal standard deviation for each pixel. However, over a whole year, it is evident that the average backscatter of the forest regions changes significantly. Most of our work has therefore been carried out with images corrected for this (probably) seasonal variation by normalising intensities relative to the forest background. Deviations relative to this background that lie within areas designated as primary forest then highlight regions of interest. By masking out non-forest regions these can easily be isolated and identified, as shown in figure 3.

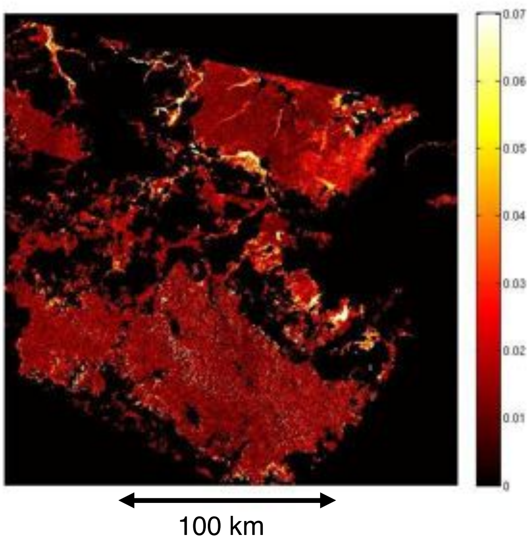

Figure 3. Temporal standard deviation map of areas labelled as forest in the WWF database that overlap with the image region. Areas outside the forest or image are shown in black and the standard deviation of other regions is indicated by the colour-bar, with regions of highest standard deviation shown in white. Images obtained Jan – Dec 2007, ALOS K&C © *JAXA/METI*

3)Tools

Three MATLAB routines have been developed and are described briefly below. The routine *noisemap* was originally designed to seek anomalous areas that might confuse the step fitting routine. In particular, if steps are found in data with overall high or low average values compared to forest they are unlikely to be part of the forest. Strongly fluctuating data might also lead to an erroneous fit. All of these routines incorporate user-defined window-averaging and a detection threshold value, T_d, expressed in units of the forest temporal standard deviation SD_F:

$$T_d = T_h / SD_F \qquad (1)$$

where T_h is the threshold expressed as an intensity and the standard deviation is obtained from the fluctuations over the full extent of forest available in the image according to the WWF database.

Table 3a noisemap

Inputs	Meaning
a	The set of N images, i.e. time-series data
Tnorm	Forest intensity normalization data
mask_stat	Forest intensity statistics
T_d	A detection threshold; see Eq. (1)
nwin	A window size for spatial averaging

Outputs	Output pixels are set = 0 unless the following criteria are met:
hav	Pixels with average intensity > mean + T_h
lav	Pixels with average intensity < mean - T_h
nz	Pixels with a noise metric nz > mean + T_h
sdev	Pixels with temporal standard deviation > mean + T_h
nzmin	Pixels with a temporal minimum value < mean - T_h
nzmax	Pixels with a temporal maximum value > mean + T_h

The noise metric was designed to discriminate between a step function response and strong temporal fluctuations. It can be represented as

$$nz_{ij} = \frac{1}{N}\sum_{k=1}^{N-1}\left|\Delta\sigma_{ijk}\right|, \qquad (2)$$

where σ_{ijk} is the (i, j)'th pixel of the k'th image and $\Delta\sigma_{ijk} = \sigma_{ijk} - \sigma_{ijk-1}$ is the change in intensity between images. It is strongly correlated with other noise measures such as the standard deviation, but it may have a specific use in avoiding false positives, as we show later.

The routine *changemap* fits a straight line to the window-averaged intensity time-series. The input arguments are similar to those for *noisemap*, but include an additional mask, represented here as M, that limits the area over which the calculations are performed. This may be a mask obtained from regions of the WWF database (particularly forest) or it may be obtained from regions identified by *noisemap* as having, e.g., a significantly high standard or other deviation from the norm. Note that the criterion for detecting positive change ("*cpos*") in Table 3b could equally be expressed as "pixels with a fitted final image intensity > Tsd," and similarly for cneg.

Table 3b changemap

Inputs	Meaning
a	The set of *N* images, i.e. time-series data
Tnorm	Forest intensity normalization data
mask_stat	Forest intensity statistics
Tsd	A threshold relative to forest standard deviation
nwin	A window size for spatial averaging
M	A mask determining a region to be analysed

Outputs	Output pixels are set = 0 unless the following criteria are met:
cpos	Pixels with positive change gradient > T_h / N
cneg	Pixels with negative change gradient < - T_h / N
C1pos	Pixels with fitted 1^{st} image intensity > mean + T_h
C1neg	Pixels with fitted 1^{st} image intensity < mean – T_h

The routine *stepmap* fits a step function to the window-averaged intensity time-series using the matlab routine *fminsearch*; this in turn uses a Nelder-Mead simplex algorithm to optimise the fit. The routine is initialised by finding the time of maximum change, the initial value and the final value. The fit is relatively slow compared to *changemap* and overall timings for this routine are roughly 16 × those for *changemap*. Like *changemap*, the input arguments include a mask, M, that limits the area over which the calculations are performed. In the absence of any prior knowledge of forest cover, it currently seems as though this mask can best be chosen using values of *nzmax* from *noisemap* with a suitable threshold. This quantity simply identifies the maximum value for a window-averaged pixel in the time series; clearly, unless some values in the time-series are above a given threshold, there is no point in applying a step fit.

For a set of 8 images of size 400x400 pixels in the absence of any masks, timings obtained for Region 1 on our high-performance computing system (http://www.shef.ac.uk/wrgrid/iceberg) were: *noisemap* ~ 19.3 s, *changemap* 85.3 s and *stepmap* 1375.6 s. These would scale to roughly 39 min, 2.85 hr & 45.85 hrs respectively for the full image size. With masking provided by *noisemap* the values recorded for Region 1 were *changemap* 18.3 s and *stepmap* 302 s, which scale to a more manageable 37 min and 10.1 hrs respectively for full images.

Example fits using a line and a step function are shown in figure 4 for the data of Region 1.

Table 3c stepmap

Inputs	Meaning
a	The set of *N* images, i.e. time series data
Tnorm	Forest intensity normalization data
mask_stat	Forest intensity statistics
Tsd	A threshold relative to forest standard deviation
nwin	A window size for spatial averaging
M	A mask determining a region to be analysed

Outputs	Output pixels are set = 0 unless the following criteria are met:
spos	Pixels with positive step change > mean + T_h
sneg	Pixels with negative step change < mean + T_h
bpos	Pixels with baseline > mean + T_h
bneg	Pixels with baseline < mean – T_h
tpos	Returns the image number for the time of greatest change if spos>0
tneg	Returns the image number for the time of greatest change if spos<0

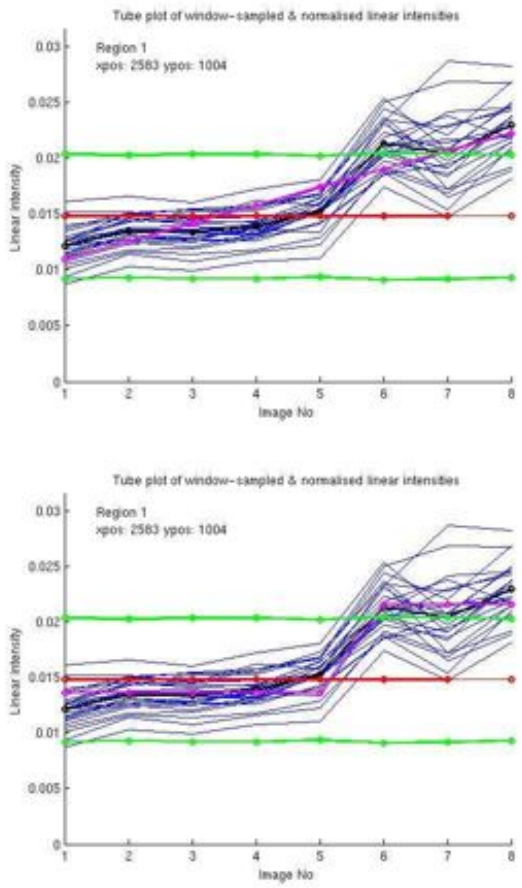

Figure 4. Fitting of normalized intensity time series for a region suspected of being subject to deforestation: (a) by a simple line (b) by a step function. Each fit is shown as a magenta line. Blue lines represent the normalized intensity over the whole series for 25 individual pixels centred at 0.576703 S, 102.677675 E; the average of these is shown as a black line. The red line shows the forest mean intensity and the green lines represent 1 standard deviation either side.

III. RESULTS AND SUMMARY

1) Results

The results of the stepfitting exercise are illustrated in Figure 5 for two different threshold levels. In Table 4 the numbers of pixels for each category are recorded. It can be seen that, of the 4481 pixels assigned, 2491 lie within the known forest, leaving 1990 outside. This means that, in the absence of any prior land-cover knowledge, the false-positive ratio is at least 44.4%. For a higher threshold level the total number of hits decreases to 1353 of which 641 lie outside the known forest so that the false-positive ratio has increased to 47.3%. An associated map of the step timings is shown for Figure 6 for the higher threshold. A comparison with figure 5 shows that the areas chosen outside the forest return an early step time & this may be a way of distinguishing some false from true positives.

Table 4 Pixel counts for detections with *changemap* and *stepmap* and the number of overlaps with each other and the forest class.

(a) with thresholds set low at 0.5, 0.35, 0.65

Count	Forest	*cpos*	*spos*
Forest	57009	5552	2491
cpos	5552	9279	3529
spos	2491	3529	4481

(b) with thresholds set high at 1.0, 0.75, 0.75

Count	Forest	*cpos*	*spos*
Forest	57009	1353	712
cpos	1353	1917	960
spos	712	960	1353

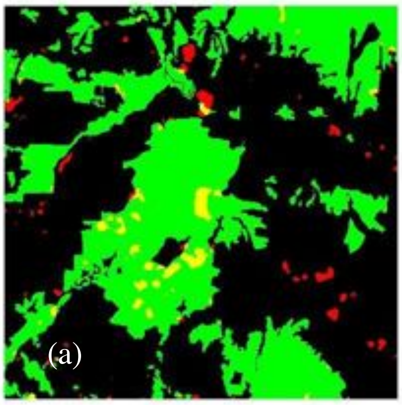

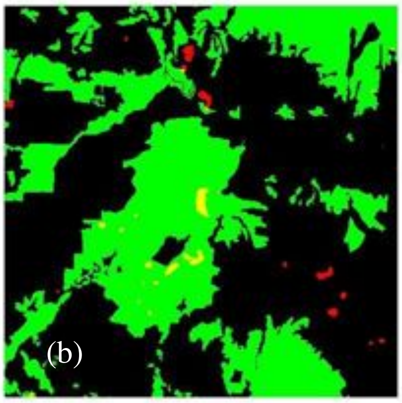

Figure 5. An image centred on region 1 using the routine *stepmap* overlaid on the primary forest regions (shown green). Non-zero values of *spos* are shown red or yellow where they overlay forest regions: (a) with threshold set at 0.65 standard deviations (b) with threshold set at 1.0 standard deviations.

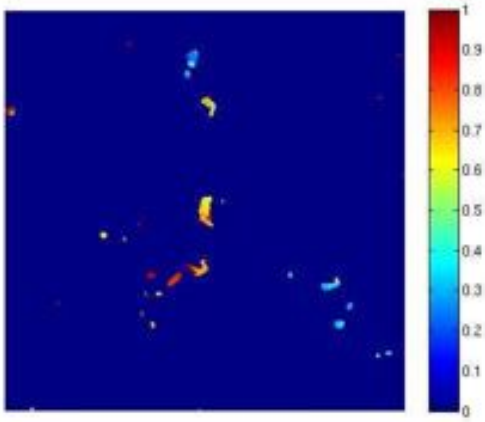

Figure 6. An image associated with 4(b) showing the time of step for the regions highlighted. The colour-bar represents a continuous advancing time scale with 0 meaning no image and images 8 mapped on to 1. It thus represents advancing time with are mapped on to the scale 0-1.

In figure 7 the low threshold map of Figure 5(a) is overlaid by the primary forest regions and the noise metric, *nz* (Eq. (1)), which takes the blue channel. Where the noise metric overlays the high-step regions outside the forest the colour becomes pink, and it can be seen that many of these likely false-positive areas have been picked out in this colour. These areas appear to be associated with paddy fields (compare with Figure 2(a)). The intensity plot shown as region 10 in the Appendix demonstrates that paddy fields can show very strong fluctuations, which suggests that *nz* may indeed be a useful tool for reducing this particular source of false positives.

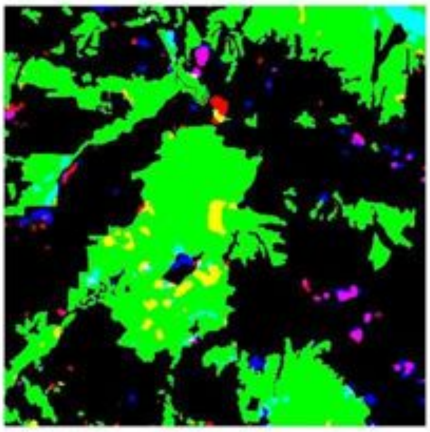

Figure 7 An image centred on region 1 using the routine *stepmap* overlaid on the primary forest regions (shown green). Non-zero values of *spos* are shown red or yellow where they overlay forest regions. Overlaid in blue are pixels with high values of *nz*; where coincident with the step-fitted regions these show as pink. Virtually none of the regions identified as suspect in the forest are overlaid by this metric (where they would appear white in this image). The *stepmap* and *noisemap* thresholds were set at 0.65 and 1.0 standard deviations respectively.

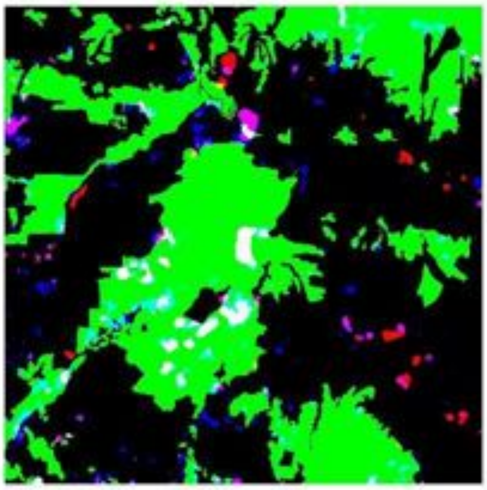

Figure 8 An image centred on region 1 using the routine *stepmap* overlaid on the primary forest regions (shown green). Non zero values of *spos* are shown red or yellow where they overlay forest regions. Overlaid in blue are pixels with high values of cpos; where coincident with the stepfitted regions these show as pink. Most of the regions identified as suspect in the forest are overlaid by this metric (where they appear white in this image). The *stepmap* and *noisemap* thresholds were set at 0.65 and 1.0 standard deviations respectively.

In figure 8 the low threshold map of Figure 5(a) is overlaid by the primary forest regions and high values of *cpos*, which indicates a high level of change over the time-series (see Table 3b). Where this overlays *spos* (the high-change step-fit metric Table 3c) within the primary forest region the result is white, and where it overlays *spos* outside the forest region the result is pink. The white areas suggest that *changemap* matches the results of *stepmap* within the forest regions and supports its use as a quick but possibly rough tool for locating suspect areas. Note that the pink areas in figure 8 tend to complement those in figure 7. A number of red areas remain and thus *changemap* may also be useful in combination with *stepmap* to cut down the false positive ratio.

In figure 9, the results of step fitting are again combined with the noise function *nz* and the primary forest mask for Region 3 and its surroundings. In this figure the angular areas shown black are designated “cleared post acacia harvested” in the WWF database (see figure 2b) and are picked out well by plotting the *hav* metric of *noisemap*. Red areas identified by *stepmap* overlap some of these regions and also extend into the forest, where they show as yellow. Region 3 itself shows yellow in the centre of figure 9(a). The noise metric *nz* has again been successful in picking out some erroneously identified regions outside the forest area (where blue and red combine to give pink) but has not picked out the mottled region inside the forest boundary in the lower-right quadrant (a typical locality has the position: 0° 16’ 59.61’’ S, 102° 57’ 26.41 E”). This is labelled in the WWF database as “swamp forest very open canopy”. This region is also picked out by *changemap* and so it is a probable false positive area that we cannot currently reject by using alternative metrics. An associated map of the step timings is shown in Figure 9(b), where it is clear that this mottled region stands out in red (meaning the step was fitted at the end of the sequence) while the more likely suspects for deforestation changed around mid-sequence and are coloured blue or yellow. Time-series plots for this region show a steady increase in intensity over the year, suggesting that *stepmap* has erroneously fitted a region of change with a step at the sequence end. This is a problem that may be remedied by using a longer time-sequence but alternative means of identifying these difficult areas are also being sought.

We have already made some comparisons with Fine Beam Dual (FBD) images, and expect to extend this, particularly with a view to developing the second objective of the project. A large region to the north-west of region 3 has clearly been affected by plantation work, as evidenced by linear features that are probably due to drainage channels. These have not been picked out by our analysis so far because the forest region was probably cleared after the images used to compile the WWF database, but before 2007. These are shown more clearly in figure 10(a) and compared with a higher resolution FBD image in Figure 10(b). These features could probably be picked out on a ScanSAR images by using a texture filter, and this will be investigated during the next phase of the work.

Although the exact location of Region 3 is seen to be within the WWF-designated primary forest area in Figure 9(a) in the FBD image (acquired 27/07/2007), in Figure 10(b) it is clearly seen to be part of the plantation, but also coloured blue. The intensity plot for this region (shown in the Appendix) shows that the event occurred between images 3 and 4, which were acquired in May (03/05/2007) and June (18/06/2007) respectively – i.e. before the FBD image. The evidence could suggest that primary deforestation occurred in June and the ground was quickly turned to plantation by July, or more likely (since much of the plantation seems established) that Region 3 is actually a plantation management event in a pre-existing plantation rather than deforestation. If this is true the WWF database is in error; currently planned fieldwork will establish this. This clearly highlights the importance of FBD images to support or refute the results of temporal ScanSAR analysis.

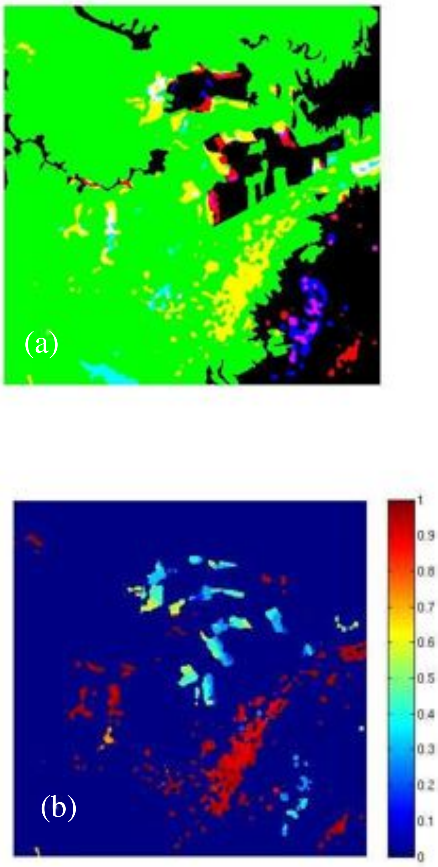

Figure 9(a) An image centred on region 3 using the routine *stepmap* overlaid on the primary forest regions (shown green). Non-zero values of *spos* are shown red or yellow where they overlay forest regions. Overlaid in blue are pixels with high values of *nz*; where coincident with the stepfitted regions these show as pink. Here, some regions show white where forest regions are overlaid by both metrics. A mottled region (lower centre right) shows yellow, but seems unlikely to be due to deforestation. The *stepmap* and *noisemap* thresholds were set at 0.65 and 0.5 standard deviations respectively. (b) The same image showing the time of step for the regions highlighted. The colour bar represents a continuous advancing time scale with 0 meaning no image and image 8 mapped on to 1. It thus represents advancing time mapped onto the scale 0 -1. The mottled region shown as red in this figure indicates that a step has been fitted right at the end of the time-series.

2) Potential difficulties

We have seen that the high level of false positives recovered in Region 1 can be significantly reduced by using other metrics. The mottled (assumed) false-positive area in Region 3 currently can only be recognised from its very late time-of-step. This is quite possibly the result of the step fitting routine attempting to fit something which is not a step, and investigating this will be a priority. We are surer of the results that give a clear step signal in mid time-series, when there are data either side of the step to inform the routine. However, the hope would be to identify regions that are being deforested during the most recent cycle, rather than those that have already been deforested, say 6 months ago. A single step at the end of a sequence may therefore be insufficient for an unambiguous identification of deforestation. Regions that fluctuate wildly in scattering intensity or have an annual spiky variation (like paddy fields) can be discounted, but regions that have shown low variation in the past and suddenly change are clearly of interest. An ability to recognise and map primary forest regions without prior knowledge forms part of the second objective of this project and clearly is important to the wider application of the approach described above.

Further investigation is needed into how the analysis is affected by use of the known forest variation to normalise data and detect changes relative this background. It is well known that rainfall varies markedly over Sumatra and so it may be expected that the annual variation of backscatter from forest may vary from place to place. In the absence of this knowledge we may be forced to normalise with respect to some local average or even with respect to the whole temporal image variation. To this end it may be worth studying the annual variation of other land-cover categories for comparison.

3) Summary

The characteristic sharp increase in backscatter caused by tropical deforestation allows large areas to be surveyed rapidly for evidence of deforestation by first measuring temporal variability in a time-series of ScanSAR data to detect regions of interest, then temporal analysis in these regions to locate the time of the event to within 46 days. This process has been implemented as an automatic algorithm, which is currently being assessed in a case study using ground data from Riau.

Data have already been obtained to extend the time-series for the current ScanSAR scene. These will be processed with an updated algorithm, together with the images used here, to assess the findings in this report; this is expected to show that an extended series gives better confidence in the results. We then aim to analyse the whole scene and, depending on data availability, extend the analysis to the whole of the area covered by the WWF database.

Up to this point, our analysis has been developed only over Riau, but we expect it to be generic and transferable, and we will test it in other regions once suitable data are acquired, with the intention of extending it to the whole of Indonesia. This will require methods to define a prior approximate map of primary forest, which can be based on optical or radar data. This will be investigated in the next phase of the work.

The work described in this report has its most important application in understanding the tropical carbon balance and in its contribution to the proposed UNFCCC Reduced Emissions from Deforestation and Degradation mechanism. The PALSAR sensor appears to be an extremely powerful tool for tracking tropical deforestation, but it is critical for its general acceptance that well-founded methods to use the data are developed, tested, demonstrated and made available in a form that can readily be applied by the tropical forest nations themselves. This work aims to make progress towards supplying both the necessary tools and confidence in their ability to deliver the required information.

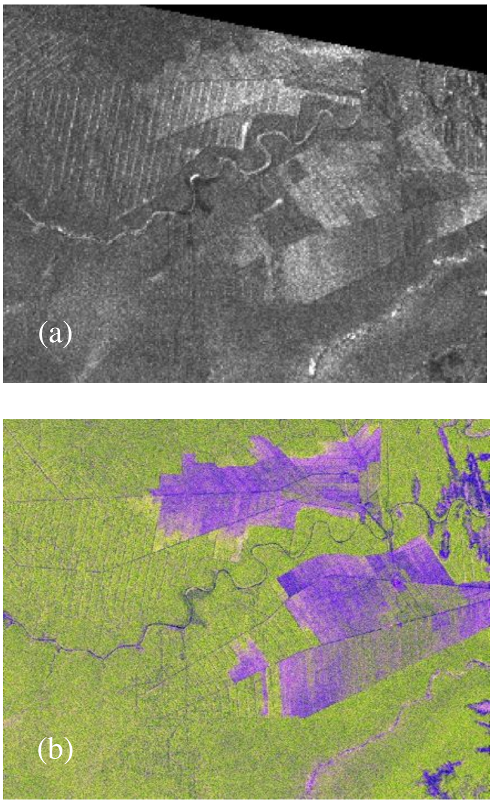

Figure 10 (a) A small region of a time-averaged de-speckled ScanSAR image surrounding region 3 showing texture probably associated with plantation drainage. PALSAR in ScanSAR mode acquired Jan-Dec 2007 © *JAXA/METI* (b) A high resolution FBD image of the same area where the colour derives from polarisation channels shown as: HH-red, HV-green, HH/HV-blue. PALSAR in FBD mode acquired July 2007 © *JAXA/MET*

IV. MISCELLANEOUS

1) Appendix

This Appendix displays time-series plots for the ten regions detailed in Table 1. The 25 lines shown in each plot correspond to the individual pixels in a 5×5 window centred on the central pixel of each region. The red and green lines show the mean and one standard deviation values for the whole image (excluding pixels with value zero).

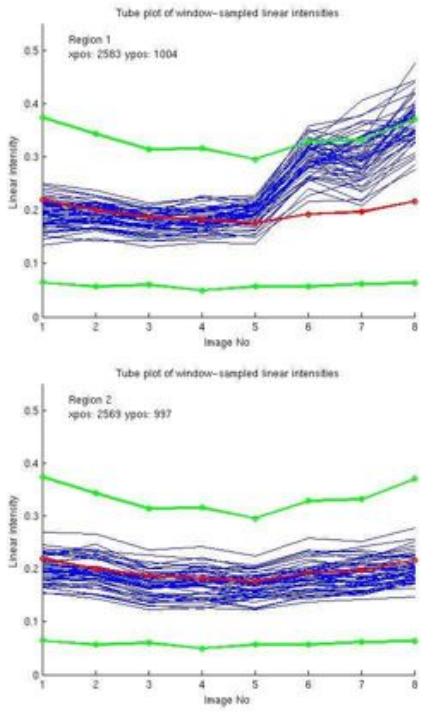

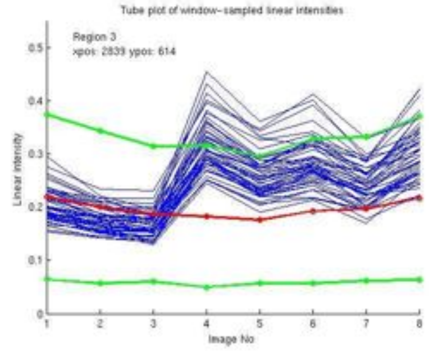
Tube plot of window–sampled linear intensities
Region 3
xpos: 2839 ypos: 614
Linear intensity
Image No

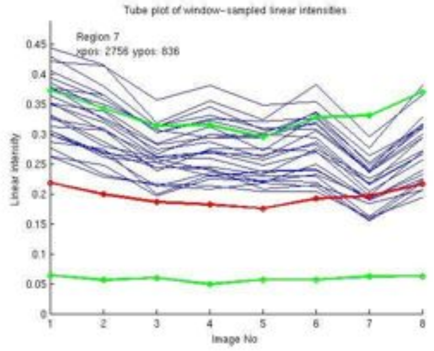
Tube plot of window–sampled linear intensities
Region 7
xpos: 2756 ypos: 836
Linear intensity
Image No

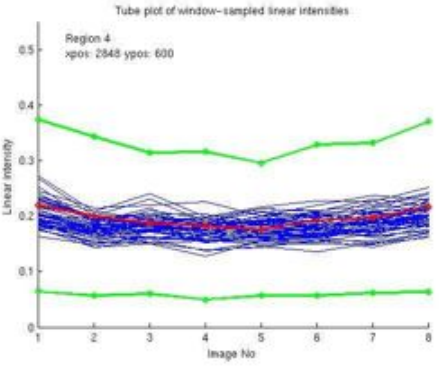
Tube plot of window–sampled linear intensities
Region 4
xpos: 2848 ypos: 600
Linear intensity
Image No

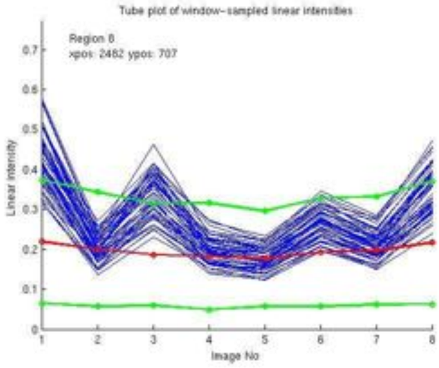
Tube plot of window–sampled linear intensities
Region 8
xpos: 2482 ypos: 707
Linear intensity
Image No

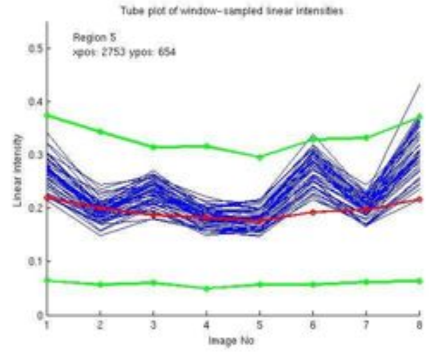
Tube plot of window–sampled linear intensities
Region 5
xpos: 2753 ypos: 654
Linear intensity
Image No

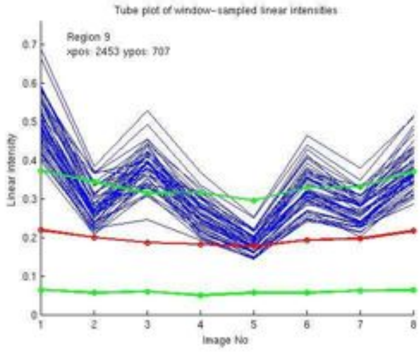
Tube plot of window–sampled linear intensities
Region 9
xpos: 2453 ypos: 707
Linear intensity
Image No

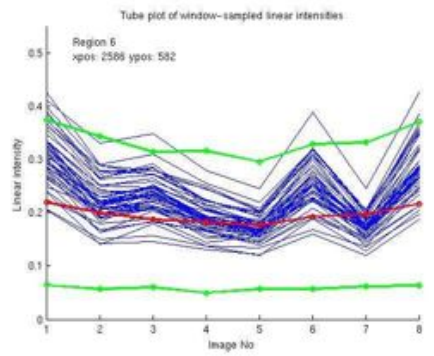
Tube plot of window–sampled linear intensities
Region 6
xpos: 2586 ypos: 582
Linear intensity
Image No

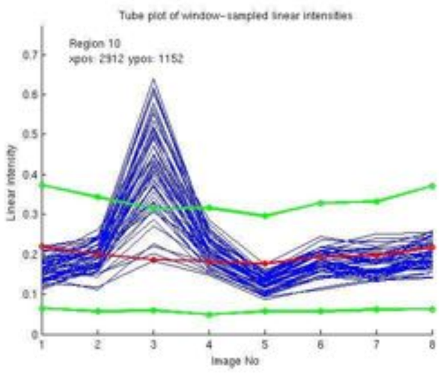
Tube plot of window–sampled linear intensities
Region 10
xpos: 2912 ypos: 1152
Linear intensity
Image No

References

[1] Y. Uryu, C. Mott, N. Foead, K. Yulianto, A. Budiman, Setiabudi, F. Takakai, Nursamsu, Sunarto, E. Purastuti, N. Fadhli, C. M. B. Hutajulu, J. Jaenicke, R. Hatano, F. Siegert, and M. Stüwe, "Deforestation, Forest Degradation, Biodiversity Loss and CO2 Emissions in Riau, Sumatra, Indonesia. WWF Indonesia Technical Report," Jakarta, Indonesia 2007.

[2] S. Quegan and J. J. Yu, "Filtering of Multichannel SAR images," *IEEE Transactions on Geoscience and Remote Sensing*, vol. 39, pp. 2373-2379, 2001.

[3] S. Quegan, J. J. Yu, and T. LeToan, "Iterated multi-channel filtering of SAR images," Proc. IGARSS 2000., Honolulu, HI, USA, IEEE 2000.

Biographies

Shaun Quegan received the B.A. (1970) and M.Sc. (1972) degrees in mathematics from the University of Warwick. His Ph.D., awarded by the University of Sheffield in 1982, was concerned with atmospheric modelling. Between 1982 and 1986 he was a Research Scientist at Marconi Research Centre, and led the Remote Sensing Applications Group from 1984-86. He established the SAR Research Group at the University of Sheffield in 1986, whose success led to his Professorship awarded in 1993. In the same year he helped to inaugurate the Sheffield Centre for Earth Observation Science, of which he remains the Director. In 2001 he became the Director of the UK National Environmental Research Council Centre for Terrestrial Carbon Dynamics, which is concerned with assimilating Earth Observation and other data into process models of the land component of the carbon cycle. In addition, since 2008 he has led the Carbon Cycle Theme of the UK National Centre for Earth Observation. He has served on many national and international committees, including the JAXA Kyoto and Carbon Initiative, the ESA Earth Science Advisory Committee (2003-2007) and as Chairman of the Terrestrial Carbon Observations Panel (2002-2007). He was also a co-proposer and member of the Mission Assessment Group for the BIOMASS mission, currently under Phase-A study with ESA. His earlier interests in the physics, systems and data analysis aspects of radar remote sensing are now subsumed in the more general aim of exploiting general EO technology to study the Earth's carbon cycle.

Martin Whittle received a B.Sc. in Chemistry in 1974 and a Ph.D. in 1979 awarded by University of Manchester. He is a researcher with a background in laser light scattering, infra-red photo-ionisation, computer simulation of liquids, gels, emulsions and slurries including electrorheological systems. He has also worked in data mining of web-search databases and virtual screening with a variety of techniques including data fusion in a drug-discover context.

Forest Theme

Detection of Deforestation in Swedish Forests

Johan Fransson *et al.*,
SLU/CTH/Gamma RS (Sweden/Switzerland)

K&C Science Report – Phase 1
Detection of deforestation in Swedish forest

Johan E.S. Fransson

Swedish University of Agricultural Sciences, Department of Forest Resource Management, SE-901 83 Umeå, Sweden,
Email: Johan.Fransson@srh.slu.se

Håkan Olsson[1], Leif E.B. Eriksson[2], Lars M.H. Ulander[2], Maurizio Santoro[3]

[1] Swedish University of Agricultural Sciences, Department of Forest Resource Management, SE-901 83 Umeå, Sweden,
Email: Hakan.Olsson@srh.slu.se

[2] Chalmers University of Technology, Department of Radio and Space Science, SE-412 96 Göteborg, Sweden,
Email: leif.eriksson@chalmers.se , lars.ulander@foi.se

[3] GAMMA Remote Sensing, Worbstrasse 225, CH-3073 Gümligen, Switzerland, Email: santoro@gamma-rs.ch

***Abstract*—An extensive dataset of ALOS PALSAR L-band Synthetic Aperture Radar (SAR) backscatter images is investigated for clear-cut detection in Swedish forest. SAR data were available for the counties of Västerbotten and Västra Götaland as well as for two local test sites (Remningstorp and Krycklan). A strong forest/non-forest contrast and temporal consistency were found for the Fine Beam Dual HV-polarized backscatter in summer/fall. Thus, a simple thresholding algorithm could be used for clear-cut detection. Using the ALOS PALSAR data and methods applied so far, most pixels in the clear-felled areas could be correctly classified as changed. For the county of Västerbotten in northern Sweden, up to about 50% of the pixels were correctly classified as changed for about 90% of the clear-felled areas using a 2 dB threshold. The results were less good for the county of Västra Götaland in southern Sweden, where only up to about 40% of the pixels could be correctly identified as changed for about 65% of the clear-felled areas. For the south county, also much over classification of non changed areas occurred. It would still be possible to use the ALOS PALSAR data in a sampling routine, where changed areas are checked against cutting permits and samples of the remaining detected changes should be checked *in situ* for determining type of change. In the extension phase of the project, an up scaling of the mapping of clear-cuts, and possibly also biomass, to all of Sweden is planned. There is also a need for further algorithm development.**

***Index Terms*—ALOS PALSAR, K&C Initiative, boreal forest, forest theme, deforestation, clear-cuts, Sweden.**

I. INTRODUCTION

In Sweden, a nationwide coverage of satellite data is acquired annually by the government. The images are used by the Swedish Forest Agency for change detection in order to find clear-felled areas and subsequent verification of the cutting permits of about 70,000 clear-felled areas yearly. In combination with about 50,000 National Forest Inventory (NFI) field plots, the images are also used for producing nationwide forest maps, and for post stratification of forest variable estimates from the NFI plots. At present, optical satellite imagery are used. Sweden is, however, characterized by frequent cloud-cover and long periods of reduced solar illumination. In order to obtain the about 200 cloud-free SPOT scenes that are needed for a nation-wide coverage, about 6,000 programming attempts of the SPOT satellite are needed. In this respect it is of interest to investigate space borne Synthetic Aperture Radar (SAR) as a future complement for forest monitoring due to its independence of cloud cover and thus the possibility to obtain the needed imagery in a foreseeable way.

It is of particular interest to investigate the usefulness of L-band SAR sensors, for which the backscattered signal has shown a high sensitivity to forest structural properties, in particular for the cross-polarized return (see e.g. [1-8]). This has motivated further investigation of the usefulness of the Advanced Land Observing Satellite (ALOS) Phased Array L-band type Synthetic Aperture Radar (PALSAR) images for forest change detection and mapping. Logging activities and fire scars are characterized by noticeable decrease of the backscatter. The backscatter difference before and after the forest cover change has been devised to be a tool for mapping clear-cuts and deforestation in boreal [9-13] and tropical forest [14-17]. Several studies, however, highlighted the importance of the environmental conditions at the time of image acquisition, concluding that data acquired under dry conditions perform better than in case of wet conditions [14, 15, 18, 19]. The importance of a multi-polarization and multi-sensor approach for mapping of reforestation and disturbance has been reported by [11, 14, 20].

Although a few algorithms have been presented to detect deforestation, no large area applications of deforestation mapping using change detection with SAR data has been reported in literature yet. To fulfill the goals of the K&C Initiative project (see Section II), efforts had to be paid to the development of an algorithm for mapping deforestation at regional level. A further challenge was represented by the availability of temporally dense time series of data, which required a thorough investigation of ALOS PALSAR backscatter signatures in order to be able to develop a robust deforestation change detection algorithm [23].

II. DESCRIPTION OF THE PROJECT

A. *Relevance to the K&C drivers*

The prime scope of this K&C Initiative project was to develop, verify and demonstrate a methodology for detection and delineation of deforestation (primarily clear-cuts) in managed forest regions in Sweden using multi-temporal ALOS PALSAR data. Methods for detecting land use change are of prime interest for green house gas reporting. In the case of Sweden most changes in mature forest will be clear-cuts, which are re-planted after a few years. It is of interest to develop a system that can detect all clear-felled areas and sort out the large majority of legal fellings by comparisons with granted cutting permits. The remaining detected forest changes are likely to be illegal fellings, large damages or permanent land cover changes and should, thus, be visited in field.

B. *Work approach*

To demonstrate the potential of ALOS PALSAR imagery to map deforestation, the counties of Västerbotten and Västra Götaland, in the north and in the south of Sweden, respectively, were selected (Fig. 1). These counties will be referred to as prototype areas, in agreement with the nomenclature adopted in the K&C Initiative (see also [21]). The two counties are covered predominantly by forests as shown in Table 1 and in Section II.C, Figs. 6 and 7). The county of Västerbotten consists of boreal forest, whereas the county of Västra Götaland is located within the hemi-boreal forest zone. The average annual timber production is substantially higher and the clear-felled areas are generally smaller but more frequent in Västra Götaland than in Västerbotten.

Detection of deforestation was based on multi-temporal datasets of ALOS PALSAR images acquired in different seasons and with different polarizations (as further described in Section II. C). The deforestation part of the work approach was arranged in four parts:

- Analysis of ALOS PALSAR backscatter signatures to understand which type of backscatter could be more suitable for detecting deforestation;
- Development of an algorithm for the detection of deforestation using time series of ALOS PALSAR data;
- Generation of deforestation maps using the developed algorithm;
- Accuracy assessment of the produced deforestation maps.

A detailed analysis of the temporal signatures at the two test sites of Remningstorp (Lat. 58°30’ N, Long. 13°40’ E) and Krycklan (Lat. 64°14’ N, Long. 19°50’ E) in the prototype areas (Fig. 1) has been recently reported in [23].

Table 1. Statistics on forest status and clear-cut activities for the prototype areas [22].

	Västerbotten	Västra Götaland
Area of forest land	3.2 10^6 ha	1.3 10^6 ha
Proportion of forest land	57.7%	54.3%
Notified clear-cuts in 2007	5,033	6,025
Area of notified clear-cuts in 2007	27,289 ha	15,805 ha

Figure 1. The K&C Initiative prototype areas in Sweden and local test sites.

In this K&C science report, we summarize the main findings, highlighting those that were relevant for the development of the change detection methodology.

- The HV-backscatter is more sensitive than the HH- and VV-backscatter to forest growth stage, i.e. stem volume or biomass (see e.g. Fig. 2).
- The HV-backscatter has a very high temporal consistency under unfrozen conditions (Fig. 3). No HV-backscatter data were acquired under frozen conditions.
- The HH-backscatter presents clear seasonal dependencies. The sensitivity to different growth stages is higher for unfrozen conditions. For unfrozen conditions the backscatter of dense mature forest is consistent, whereas it is affected by the wet or dry weather conditions in regrowing young forest (Fig. 4).
- The sensitivity of the backscatter to forest growth stage increases slightly between 21.5 and 41.5 degrees look angle, both at HH- and HV-polarization.
- The backscatter signatures do not change significantly between 20 m pixel size (ALOS PALSAR path data) and 50 m pixel size (K&C ALOS PALSAR strip data).

The strong sensitivity of the ALOS PALSAR HV-backscatter data acquired under unfrozen conditions to forest growth stage and the strong temporal consistency suggested that a simple change detection algorithm based only on HV-backscatter would be sufficient to detect deforestation. It is, however, foreseen in the extension phase to look at possible improvements, e.g. by also including HH-backscatter in the detection algorithm.

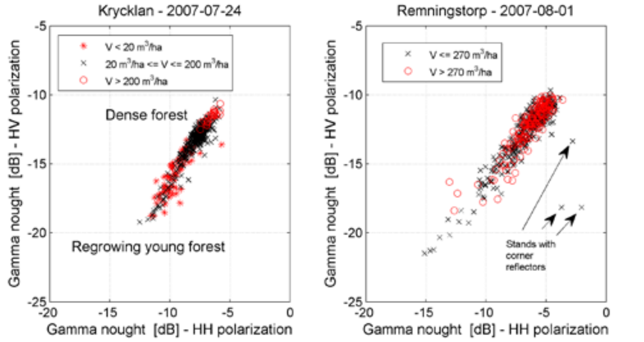

Figure 2. Scatterplot of HH- and HV-backscatter for the test sites of Krycklan and Remningstorp. The SAR images were acquired under unfrozen conditions. Acquisition mode: Fine Beam Dual at 34.3 degrees look angle [23].

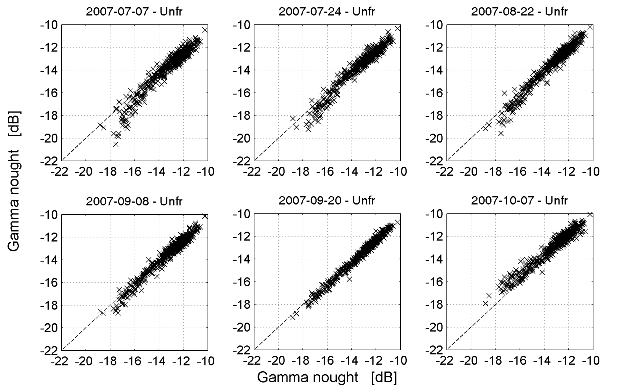

Figure 3. Scatterplot of HV-backscatter for the test site of Krycklan for six different dates with reference to a common date (2007-08-05). The SAR images were acquired under unfrozen conditions (Unfr). Acquisition mode: Fine Beam Dual at 34.3 degrees look angle [23].

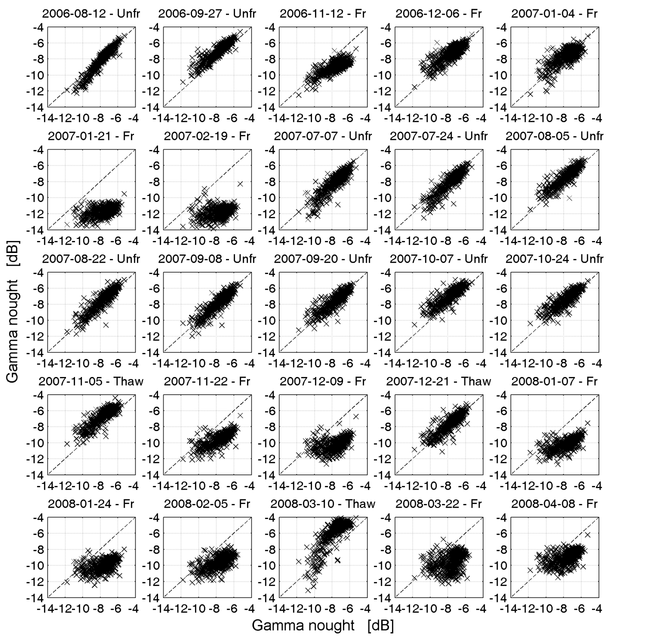

Figure 4. Scatterplot of HH-backscatter for the test site of Krycklan for 25 different images plotted along the y-axis with respect to a common date (2006-06-07) plotted along the x-axis. Acquisition mode: Fine Beam with 34.3 degrees look angle [23].

The change detection algorithm was developed based on the multi-temporal dataset of ALOS PALSAR HV-backscatter images available over the two prototype areas (see Section II. C). For each summer/fall during 2007 and 2008 several backscatter measurements were available for all points on the ground within the prototype areas. As a time series of backscatter measurements was available it was suggested to develop a slightly more complex algorithm than just adopting a simple two-date change detection algorithm.

The multi-temporal approach was based on the temporal consistency of the backscatter difference for each combination of backscatter measurements for a given point. If the backscatter difference for all image pairs covering the felling date of a forest was consistently above a certain level (e.g. 2 or 3 dB), while the difference for image pairs acquired before and after the felling date was small, the pixel was classified as "change". Support to this approach is illustrated in Fig. 5 that shows the temporal signatures of the HV-backscatter for a set of polygons clear-felled between 2006 and 2008 within a 50×50 km^2 large area in Västerbotten. Red crosses refer to polygons clear-felled between the two image acquisition dates reported on the plot axes. Black crosses refer to polygons clear-felled before both image acquisition dates (lower backscatter) and green crosses refer to polygons reported as clear-felled in the reference dataset but not yet clear-felled at the time of both acquisitions (higher backscatter). Unchanged polygons between image acquisitions were mostly along the 1:1 line, confirming the temporal consistency of the HV-backscatter. A few of the unchanged polygons were off the 1:1 line probably because of errors in the reference dataset or because felling had started at the time of the second image date, but had not yet been completed or registered. Polygons clear-felled between image acquisitions present a clear drop in most cases larger than 2 dB. Very few of these cases show a small variation of the backscatter, which could be related to the small size of the polygon, thus altering the temporal signatures of the backscatter in case of change.

An issue that had to be taken into account when developing the change detection algorithm concerned intercepts and slopes in the trend of co-plotted backscatter measurements. These can be due to the effect of large area variations of the environmental conditions or non-perfect data calibration. Such deviations can disturb the analysis if not accounted for. For example, if the second image of a pair has a consistently higher backscatter compared to the first image (e.g. top-left scatterplot in Fig. 5), clear-cuts occurred between the two acquisitions might not be detected because the backscatter difference might be too small. This suggested that it makes more sense to use the variation of the backscatter with respect to a reference level rather than the simple backscatter difference between the image acquisitions. The reference level can be obtained by fitting a linear or non-linear regression model to the pairs of backscatter values as shown by the solid red line in the top-left scatterplot of Fig. 5 and measure the difference between the backscatter on the first date and the model-based value for the second date, i.e. the model residual.

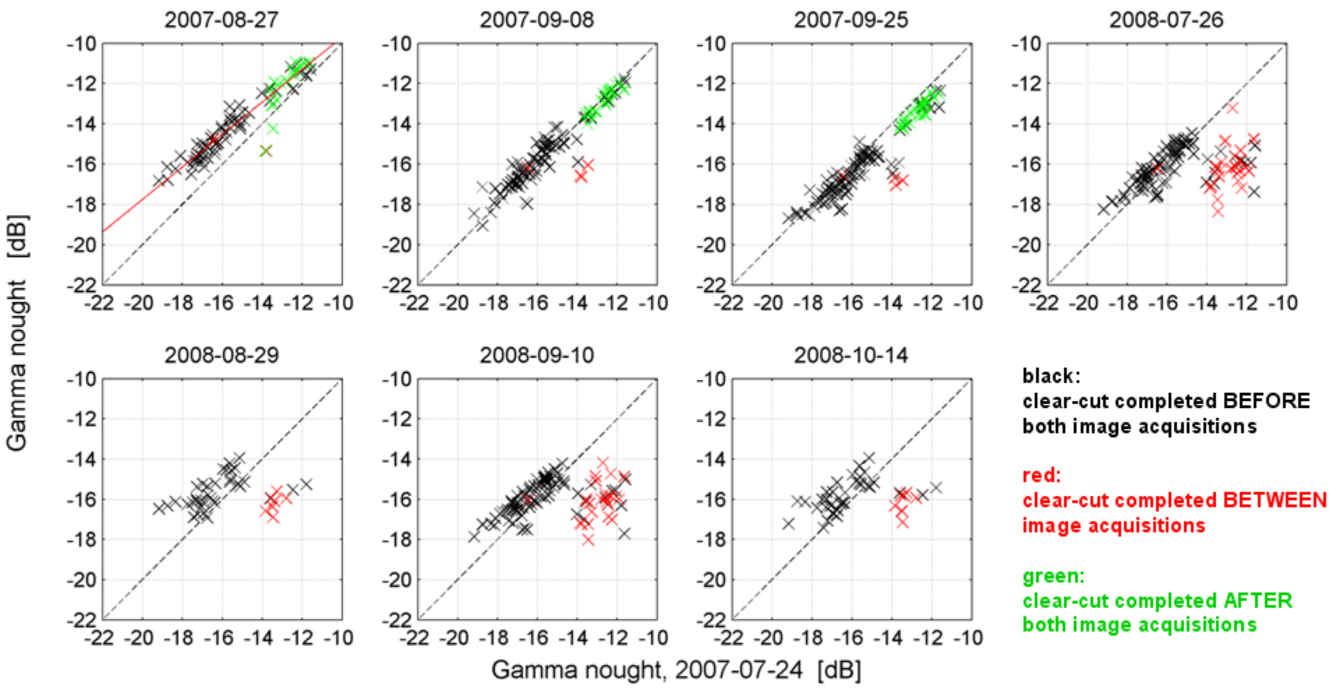

Figure 5. Scatterplots of HV-backscatter for clear-cuts in Västerbotten occurred between image acquisitions (red crosses) and outside the interval between the two image acquisitions (black and green crosses).

An issue that had to be taken into account when developing the change detection algorithm concerned intercepts and slopes in the trend of co-plotted backscatter measurements. These can be due to the effect of large area variations of the environmental conditions or non-perfect data calibration. Such deviations can disturb the analysis if not accounted for. For example, if the second image of a pair has a consistently higher backscatter compared to the first image (e.g. top-left scatterplot in Fig. 5), clear-cuts occurred between the two acquisitions might not be detected because the backscatter difference might be too small. This suggested that it makes more sense to use the variation of the backscatter with respect to a reference level rather than the simple backscatter difference between the image acquisitions. The reference level can be obtained by fitting a linear or non-linear regression model to the pairs of backscatter values as shown by the solid red line in the top-left scatterplot of Fig. 5 and measure the difference between the backscatter on the first date and the model-based value for the second date, i.e. the model residual.

Based on this rationale the multi-temporal clear-cut detection method was setup as follows:

- The prototype area was first divided into areas of smaller size. The size was a trade-off between having on one hand a large number of measurements for accurate estimation of the regression model coefficients that describe the backscatter trend of two acquisitions and avoiding on the other hand that large-scale spatial variations of the environmental conditions (e.g. thaw in one area and dry conditions in another) might distort this trend. Dividing the prototype areas into 50×50 km^2 large tiles seemed to be reasonable.
- Given a tile, for each combination of images the coefficients of the regression model relating the backscatter at the two dates were estimated. For each pair of images the regression coefficients were estimated using the measurements of all pixels labeled as forest in a forest/non-forest map available from the Swedish National Land Survey. A linear regression model seemed to be sufficient. The residuals were then computed. It was assumed that within the tile the number of pixels subject to change was negligible with respect to the total number of pixels labeled as forest so that no a priori information on the actual forest cover at the time of image acquisitions was required to determine the estimates of the regression coefficients.
- For each pixel the temporal evolution of the residuals was analyzed with respect to a threshold value according to the basic idea presented at the beginning of this Section.

To test the sensitivity of the classification to the threshold, three threshold values were used: 2 dB, 2.5 dB and 3 dB. The maps of detected deforestation were finally mosaiced together and majority filtering was applied. The filter was designed to remove isolated pixels up to groups of three neighboring pixels. This implies that detected deforestation smaller than 1 ha has been neglected.

C. Satellite and ground data

For this K&C project, image strips have been provided by JAXA in form of multi-look amplitude images in slant range geometry with approximately 50 m pixel size [24]. Absolute calibration of the data was performed by using the updated calibration coefficients published in [25]. For each of the years 2007 and 2008, one cycle of images acquired in FBS34 mode during winter and two cycles of images acquired in FBD34 mode during summer/fall have been delivered. In total, data from six ALOS repeat-pass cycles have been obtained. For each season a complete coverage of the prototype areas was obtained. Because of the strong multi-looking applied, no action was taken to further reduce speckle effects. All image strips have been geocoded to 50 m pixel size in order to adhere to the original size of the data. To increase the geolocation accuracy co-registration of neighboring strips was applied after geocoding. Final co-registration errors were less than the pixel size. Topographic normalization of the backscatter for local incidence angle and pixel area was applied. For details on the processing it is referred to [23]. Figs. 6 and 7 show two mosaics in form of RGB color composites obtained from K&C ALOS PALSAR strip data. The red areas, overlaid on the mosaic, correspond to detected changes between summer 2007 and fall 2008. Red corresponds to the HH-backscatter, green to the HV-backscatter and blue to their ratio. Forests appear in green. Bare surfaces, agricultural fields and marshes appear in purple. Rivers, lakes and the sea appear in blue. Urban settlements appear in yellow/pink.

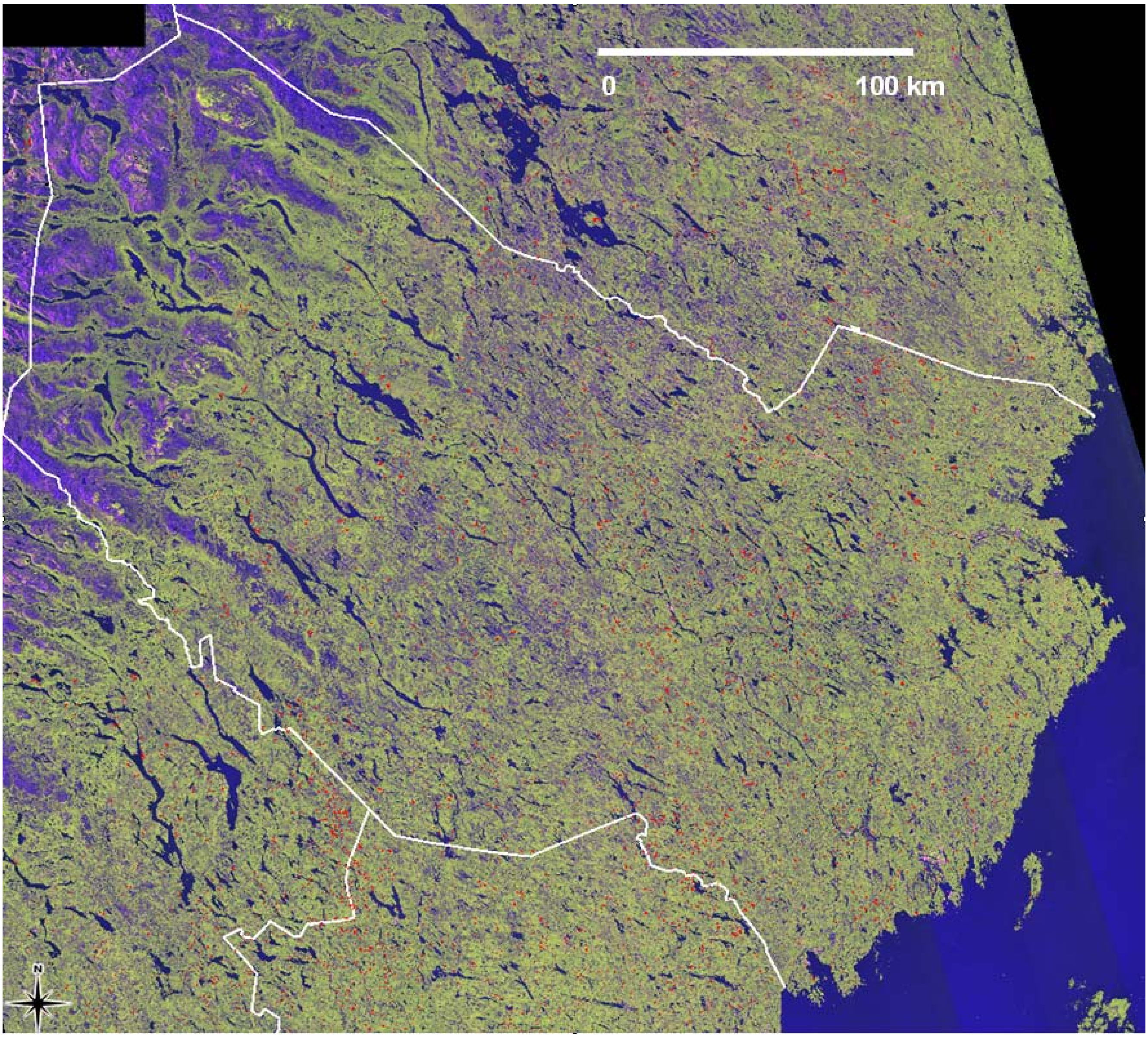

Figure 6. False color composite of ALOS PALSAR HH-backscatter (red), HV-backscatter (green) and backscatter ratio HH/HV (blue) for the county of Västerbotten. Time frame of ALOS PALSAR dataset: July 2007 - October 2008. The areas detected as deforestation during the time frame of the ALOS PALSAR dataset are overlaid in red. ALOS PALSAR images © JAXA/METI.

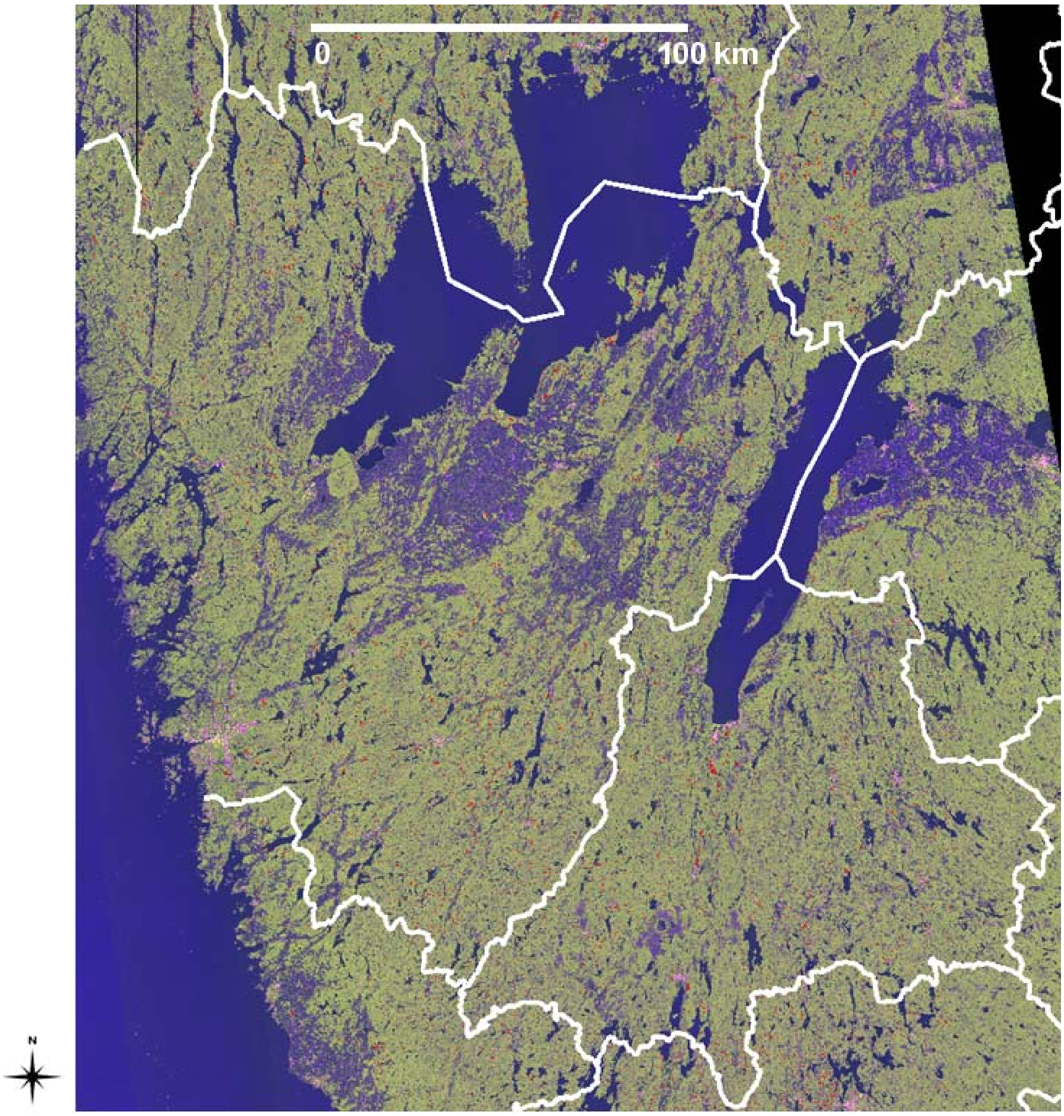

Figure 7. False color composite of ALOS PALSAR HH-backscatter (red), HV-backscatter (green) and backscatter ratio HH/HV (blue) for the county of Västra Götaland. The false color composite includes the entire county of Västra Götaland (west) as well as the county of Jönköping (south-east). Time frame of ALOS PALSAR dataset: July 2007 - October 2008. The areas detected as deforestation during the time frame of the ALOS PALSAR dataset are overlaid in red. ALOS PALSAR images © JAXA/METI.

To avoid that changes occurring in other land covers such as cropland would be confused with the detection of deforestation, a forest/non-forest map provided by the Swedish National Land Survey was used to mask out non-forested areas. Temporal signatures of the backscatter for agricultural fields and clear-cut areas are in fact similar, i.e. sudden decrease of backscatter at harvest.

For the establishment of the algorithm and the validation of the detected changes a GIS layer of forest polygons subject to felling between 2006 and 2008 was available from the Swedish forest company Sveaskog. All polygons were larger than 2 ha. For each polygon the date of completion of the clear-felling was reported. The dataset included 1068 polygons for the county of Västerbotten, but only 65 polygons for the county of Västra Götaland. Of these 341 (Västerbotten) and 29 (Västra Götaland) polygons were clear-felled during the period of the HV-backscatter data acquisition, i.e. July 2007 to October 2008. These sets were considered for the accuracy assessment. The remaining clear-fellings took place before July 2007.

Fig. 8 shows the size distribution of the clear-cuts for the validation data available from the two counties. Clear-cuts in the Västerbotten county are on average larger, several exceeding 20 ha. In the Västra Götaland county the clear-cuts are smaller, none of them available in the reference dataset being larger than 20 ha. This aspect might be of importance considering that the pixel size of the ALOS PALSAR K&C strip data is 50 m, i.e. 1 ha corresponds to 4 pixels. In the following, it is primarily referred to the results obtained in the county of Västerbotten because of the larger number of reference polygons as well as the larger distribution of polygon sizes.

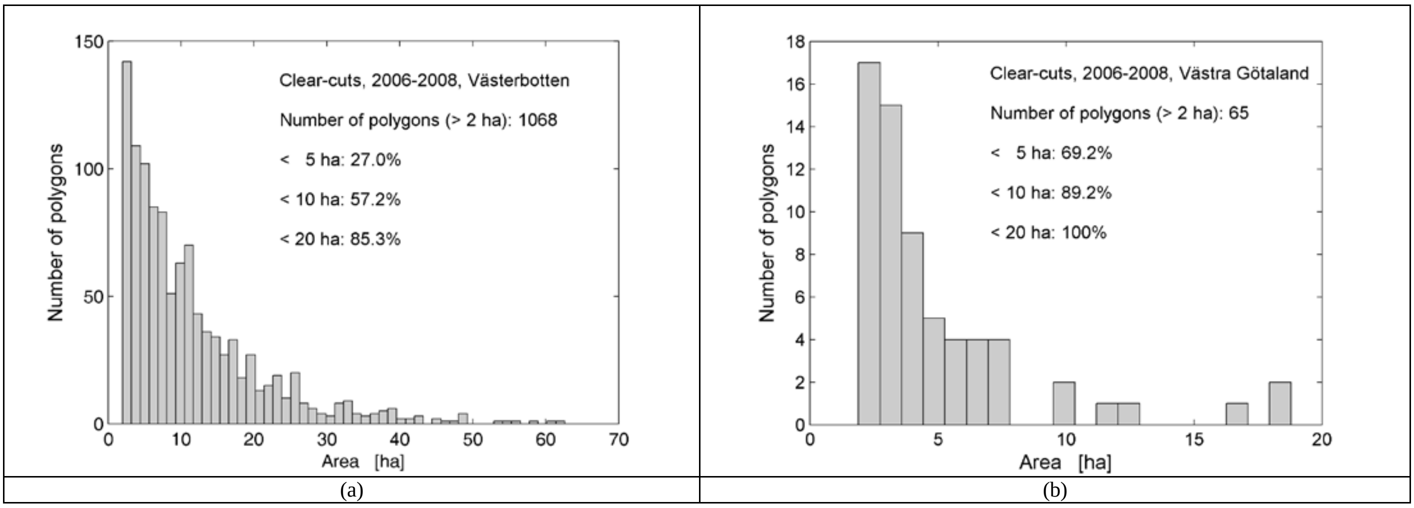

Figure 8. Distribution of the size of the clear-cuts in the GIS database used for validating the developed methodology for detection of deforestation in the two prototype areas, (a) Västerbotten, (b) Västra Götaland.

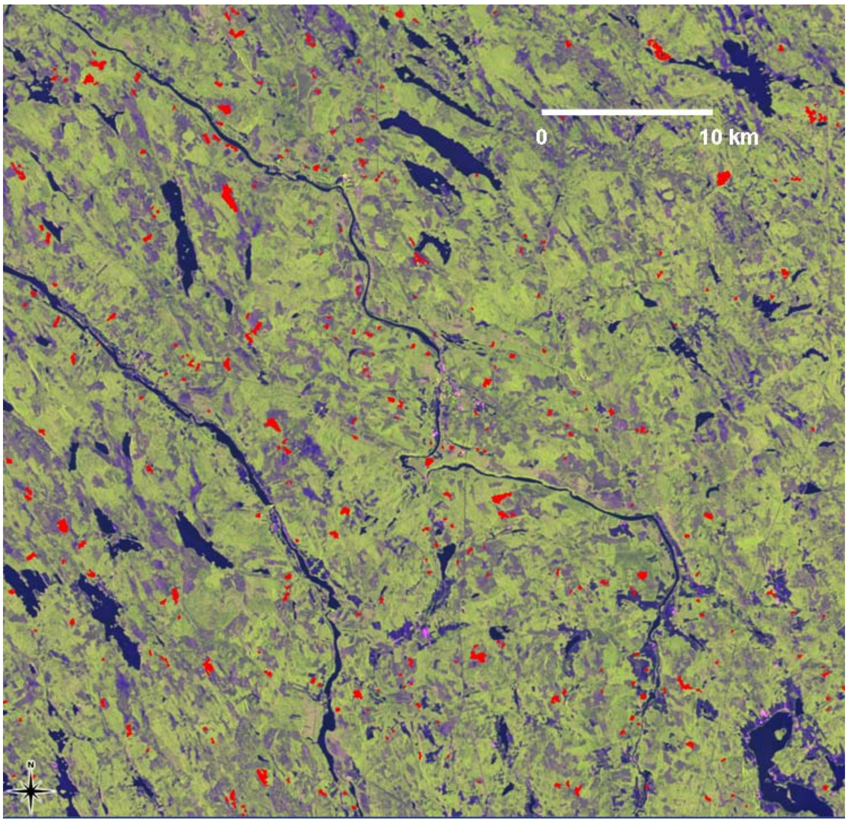

Figure 9. Subset of the image shown in Fig. 6 centered at the test site of Krycklan (Lat. 64°14' N, Long. 19°50' E), Västerbotten. ALOS PALSAR images © JAXA/METI.

III. Results and Summary

The output of the change detection algorithm applied in this study consisted of maps of detected changes, i.e. detected deforestation, in the forested areas of the prototype areas, i.e. the Västerbotten county and the Västra Götaland county. The extent of the ALOS PALSAR strips also allowed mapping the Jönköping county, located south-east of the Västra Götaland county. The accuracy assessment, however, has been carried out for the prototype areas. The maps overlaid on the false color composite of ALOS PALSAR HH- and HV-backscatter imagery are illustrated in Figs. 6 and 7. For each pixel detected as change, the dates of the two images comprising the detected change were also reported. Fig. 9 shows a zoom of the image shown in Fig. 6 around the test site of Krycklan.

The scope of the accuracy assessment of the deforestation maps was twofold

1) For a given detection threshold verify whether a clear-cut had been detected and determine a measure of the agreement in terms of correctly detected pixels. In this way, information was obtained on the capability of the 50 m resolution ALOS PALSAR K&C strip data to detect as well as to delineate clear-cuts.

2) Verify the sensitivity to the different detection thresholds. In this way, information was obtained on the robustness of the change detection algorithm and whether improvements to the simple approach are required.

Fig. 10 gives an example of the performance of the change detection algorithm based on a time series of ALOS PALSAR HV-backscatter data for the county of Västerbotten. On the x-axis the percentage of pixels detected as deforestation (i.e. correctly classified) is reported for each of the reference polygons. On the y-axis the size of the polygons is reported. For Fig. 10 the detection result was based on the 2.5 dB threshold. The scatterplot shows that a large number of polygons were not only detected but also rather well delineated. Polygons showing less than 50% of correctly classified pixels are less compared to those including more than 50% of correctly classified pixels. When relating the percentage of correctly classified pixels to the size of the polygons no significant trend was seen, i.e. the classification accuracy did not improve when considering only larger polygons.

Fig. 10 also shows a certain number of polygons with zero percentage of pixels classified as deforestation. These 25 polygons were reported as clear-felled during the acquisition period of the HV-backscatter data, but were not detected by the change detection algorithm. A closer look at these polygons revealed that most of them were between 2 and 3 ha large, so that edge effects might have distorted the backscatter difference. Part of the largest polygons were actually detected with the 2.0 dB threshold, thus confirming the indication reported in Fig. 5 that not all clear-cuts present a strong variation of the HV-backscatter. This issue needs to be looked at in more detail in future work dealing with the improvement of the detection algorithm. Finally, for two polygons the felling date was reported to be two days after the date of the first ALOS PALSAR backscatter dataset. It is likely that the forest in the polygon had already been clear-felled at the time of the first image acquisition.

As outcome of these observations it might be stated that:

- The GIS database of clear-cut polygons (in Västerbotten) is reliable as validation dataset;
- The impact of the spatial resolution of the ALOS PALSAR backscatter dataset on the detection accuracy is not marginal for clear-cuts smaller than 5 ha;
- The detection accuracy seems to be reasonable even if the algorithm is simple and uses a global threshold.

Further investigation on the detection accuracy is reported in Table 2, which gives a more general overview on the classification accuracy, also in terms of detection errors.

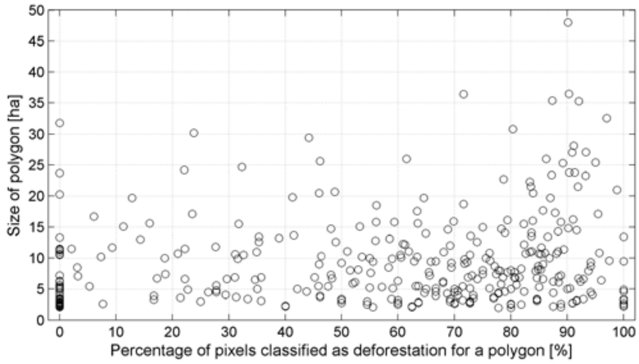

Figure 10. Polygon-wise percentage of correctly detected pixels in relation to area of the polygon. Prototype area: Västerbotten. Number of polygons: 341.

In Table 2, the total percentage of correctly detected pixels refers to the number of pixels detected as clear-cut and being actually reported as clear-felling within the temporal interval of ALOS PALSAR data for the specific pixel. The total error percentage is expressing the number of pixels classified as clear-cut for polygons that were clear-felled before the start of the time series of ALOS PALSAR data for the specific pixel. Table 2 shows that for increasing classification threshold the classification accuracy decreases from 78.2% to 57.4%, while the classification error also decreases from 9.7% to 3.0%. The detection of deforestation seems therefore to perform better when using lower threshold values, even though the detection errors increase with decreasing threshold value. Possible causes for the limited accuracy are

- Spatial resolution of the ALOS PALSAR dataset;
- Edge effects (edge erosion on the reference dataset was not performed);
- The simplicity of the change detection algorithm.

To assess the importance of each of these factors, the following studies could be considered in the K&C Initiative extension phase:

- Apply the change detection algorithm to ALOS PALSAR path data at 20 m spatial resolution (or similar);
- Apply edge erosion to the reference dataset and possibly exclude those polygons that do not cluster;
- Improve the change detection algorithm. In its current version the algorithm makes use of a global threshold for the entire prototype area. It is likely that the detection accuracy might increase if the algorithm is made adaptive to the local properties of the backscatter following spatial variations of the environmental conditions.

To provide indications on the capability of the change detection algorithm applied to ALOS PALSAR HV-backscatter data (acquired under unfrozen conditions), Fig. 11 shows the percentage of polygons for which the percentage of pixels classified as deforestation is above a certain threshold. When this requirement is satisfied, the polygon is referred to as "correctly classified". One plot is reported for each prototype area and in each plot the trend is reported for the three different thresholds applied to the detection of deforestation.

Table 2. Global figures of detection accuracy for the three different classification thresholds. Prototype area: Västerbotten.

Classification threshold	Percentage of correctly detected pixels (reference dataset: 341 polygons)	Percentage of erroneously detected pixels (reference dataset: 727 polygons)
2.0 dB	78.2%	9.7%
2.5 dB	68.4%	5.0%
3.0 dB	57.4%	3.0%

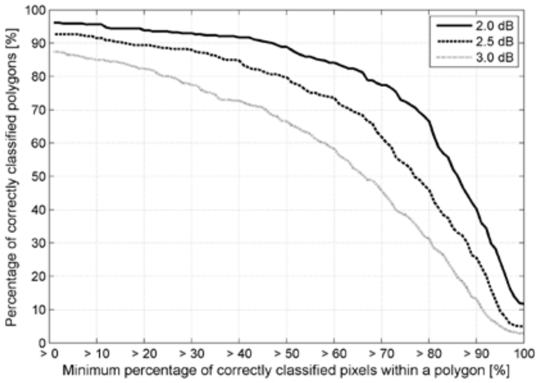

(a)

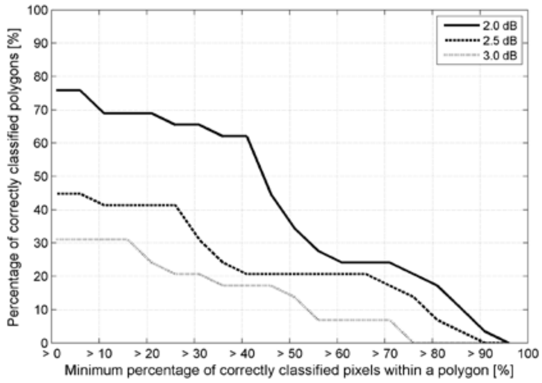

(b)

Figure 11. Percentage of correctly classified clear-cuts as a function of the minimum percentage of pixels correctly classified within the polygon for the prototype areas (a) Västerbotten, (b) Västra Götaland.

Fig. 11 a shows that in the Västerbotten county for 2.0 and 2.5 dB threshold and up to about 50% correctly classified polygons, the classification accuracy is about 90%. If a polygon is defined as correctly classified when more than half of the pixels within the polygon are correctly detected, then the classification accuracy decreases remarkably. For 3 dB threshold the decrease is steady and in general the detection accuracy is lower compared to the smaller thresholds of 2.0 and 2.5 dB. The accuracy assessment in the Västra Götaland county showed a similar trend, although the overall accuracy was lower compared to the Västerbotten county. Nevertheless, it must be reminded that the number of polygons in Västra Götaland was small (only 29), i.e. the significance of the results appears to be rather limited. Combining these observations with those reported in the two previous paragraphs, it is concluded that

- With the HV-backscatter from ALOS PALSAR K&C strip data it is possible to roughly delineate forest cover changes but not to fully match the extent of the deforestation;
- The accuracy of the detection depends on the classification threshold;
- Higher accuracy seems achievable with a threshold between 2.0 and 2.5 dB.

To gain further insight on which detection threshold is more suitable to use in order to achieve a more accurate detection of deforestation, Fig. 12 reports the total area classified as change in relation to the detection threshold used for classification. Fig. 12 shows that for both prototype areas the total area detected as change decreases significantly, in particular when going from 2.0 to 2.5 dB. Considering that the figure of notified areas of felling in each county as reported in the Statistical Yearbook of Forestry 2008, published by the Swedish Forest Agency [22], is 273 km^2 for Västerbotten and 158 km^2 for Västra Götaland, it is obvious that the estimates corresponding to the 2.0 dB level are extremely biased.

The algorithm detected far more areas of change than in reality, which could be related to speckle noise or not fully compensated effects of the environmental conditions on the backscatter. Another issue that might explain the large discrepancy is the accuracy of the forest/non-forest map used as basis for selecting the areas on which the algorithm should be applied. Several small parcels were detected as forest cover change in areas of patched land-cover, as well as along the border between forest and fields or roads or urban settlements. These results indicate that a more in depth study on the reasons of the mismatches should be considered in the extension phase.

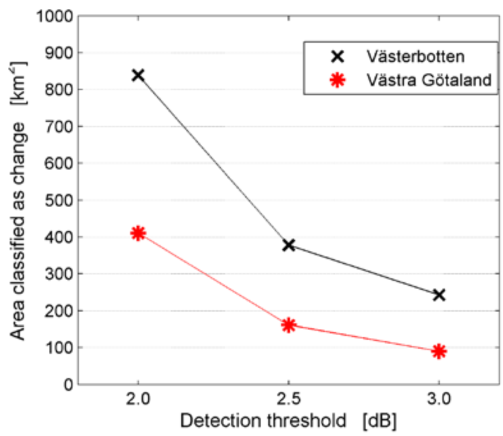

Figure 12. Total area classified as change, i.e. clear-felled areas (deforestation), for the three different detection thresholds used.

For the simple algorithm developed during the first phase of this K&C Initiative project, it seems that a classification based on a global threshold close to 2.5 dB is sufficient for obtaining a first-order, but nonetheless reasonable estimate of the total area subject to change during the acquisition period of the ALOS PALSAR data used in this study. Assuming that an extrapolation from the values reported above (which are valid for a period of 12 months) over the 15 months for which ALOS PALSAR data were available can be considered as a good approximation of clear-felled areas that deforestation occurred during this time frame, we obtain 360 km^2 and 200 km^2 in Västerbotten and Västra Götaland, respectively. Considering the result based on a threshold value of 2.5 dB, the total area of detected changes from the ALOS PALSAR HV-backscatter data is 378 km^2 and 161 km^2 respectively, which corresponds to a +5% difference for the Västerbotten county and a -20% difference in the Västra Götaland county.

Future studies should investigate whether the smaller size of the clear-cuts in the Västra Götaland county can explain the larger discrepancy and whether the method for change detection needs to be improved following the indications mentioned so far (e.g. inclusion of the HH-backscatter in the change detection algorithm, adaptation of the threshold to the local conditions).

In summary, it was found that K&C ALOS PALSAR HV-backscatter strip data acquired during unfrozen environmental conditions was a stable data source for change detection of clear-cuts. It was also shown that large area change detection of clear-cuts could be performed using these data. For the prototype area of Västerbotten in northern Sweden, up to about 50% of the pixels were correctly classified as changed for about 90% of the clear-felled areas using a simple thresholding algorithm with a threshold value of about 2 dB. The results were only partly satisfying for the prototype area of Västra Götaland in the southern Sweden. Here, up to about 40% of the pixels could be correctly identified as changed for about 65% of the clear-felled areas. This might be due to the limited reference dataset of clear-felled polygons, smaller stand size and maybe also the wetter soil conditions and the more abundant ground vegetation in these areas. In the extension phase of the K&C Initiative project, an up scaling of the mapping of clear-cuts, and possibly also biomass, to all of Sweden is planned. This phase will also involve further algorithm development. The possibility to timely find changed areas is of great interest for providing a sampling frame for *in situ* verifications of land cover changes.

Acknowledgements

This work is financially supported by the Swedish National Space Board and Hildur and Sven Wingquist's Foundation for Forest Research. The authors gratefully acknowledge the forest company Sveaskog and Anders Krantz for providing the GIS layer of clear-cut polygons. This work has been undertaken within the framework of the JAXA Kyoto & Carbon Initiative. ALOS PALSAR data have been provided by JAXA EORC within the ALOS Kyoto & Carbon Initiative and the ALOS Calibration and Validation activities. Weather data were provided by the Swedish Meteorological and Hydrological Institute (SMHI) and the Svartberget research station, SLU. The DEMs were obtained from the Swedish National Land Survey.

References

[1] M. C. Dobson, F. T. Ulaby, T. Le Toan, A. Beaudoin, E. S. Kasichke, and N. Christensen, "Dependence of radar backscatter on coniferous forest biomass," *IEEE Trans. Geosci. Remote Sensing*, vol. 30, pp. 412-416, 1992.

[2] K. J. Ranson and G. Sun, "Mapping biomass of a northern forest using multifrequency SAR data," *IEEE Trans. Geosci. Remote Sensing*, vol. 32, pp. 388-396, 1994.

[3] E. Rignot, J. Way, C. Williams, and L. Viereck, "Radar estimates of aboveground biomass in boreal forests of interior Alaska," *IEEE Trans. Geosci. Remote Sensing*, vol. 32, pp. 1117-1124, 1994.

[4] Y. Wang, F. W. Davis, J. M. Melack, E. S. Kasischke, and N. L. Christensen Jr., "The effects of changes in forest biomass on radar backscatter from tree canopies," *Int. J. Remote Sens.*, vol. 16, pp. 503-513, 1995.

[5] P. A. Harrell, E. S. Kasischke, L. L. Bourgeau-Chavez, E. M. Haney, and N. L. Christensen Jr., "Evaluation of approaches to estimating aboveground biomass in southern pine forests using SIR-C data," *Remote Sens. Environ.*, vol. 59, pp. 223-233, 1997.

[6] J. E. S. Fransson and H. Israelsson, "Estimation of stem volume in boreal forests using ERS-1 C- and JERS-1 L-band SAR data," *Int. J. Remote Sens.*, vol. 20, pp. 123-137, 1999.

[7] J. T. Pulliainen, L. Kurvonen, and M. T. Hallikainen, "Multitemporal behavior of L- and C-band SAR observations of boreal forests," *IEEE Trans. Geosci. Remote Sensing*, vol. 37, pp. 927-937, 1999.

[8] M. Santoro, L. Eriksson, J. Askne, and C. Schmullius, "Assessment of stand-wise stem volume retrieval in boreal forest from JERS-1 L-band SAR backscatter," *Int. J. Remote Sens.*, vol. 27, pp. 3425-3454, 2006.

[9] E. S. Kasischke, L. L. Bourgeau-Chavez, N. H. F. French, P. Harrell, and N. L. Christensen Jr., "Initial observations on using SAR to monitor wildlife scars in boreal forests," *Int. J. Remote Sens.*, vol. 13, pp. 3495-3501, 1992.

[10] S. M. Yatabe and D. G. Leckie, "Clearcut and forest-type discrimination in satellite SAR imagery," *Canadian Journal of Remote Sensing*, vol. 21, pp. 455-467, 1995.

[11] K. J. Ranson, G. Sun, K. Kovacs, and V. I. Kharuk, "Utility of SARs for mapping forest disturbance in Siberia," *Proc. IGARSS'02*, Toronto, 24-28 June, 2002.

[12] G. Sun, L. Rocchio, J. Masek, D. Williams, and K. J. Ranson, "Characterization of forest recovery from fire using Landsat and SAR data," *Proc. IGARSS'02*, Toronto, 24-28 June, 2002.

[13] C. Thiel, P. Drezet, C. Weise, S. Quegan, and C. Schmullius, "Radar remote sensing for the delineation of forest cover maps and the detection of deforestation," *Forestry*, vol. 79, pp. 589-597, 2006.

[14] E. Rignot, W. A. Salas, and D. A. Skole, "Mapping deforestation and secondary growth in Rondonia, Brazil, using Imaging Radar and Thematic Mapper data," *Remote Sens. Environ.*, vol. 59, pp. 167-179, 1997.

[15] F. Ribbes, T. Le Toan, J. Bruniquel, N. Floury, N. Stussi, S. C. Liew, and U. R. Wasrin, "Deforestation monitoring in tropical regions using multitemporal ERS/JERS SAR and INSAR data," *Proc. IGARSS'97*, Singapore, 3-8 August, 1997.

[16] S. Takeuchi, Y. Suga, Y. Oguro, and T. Konishi, "Monitoring of new plantation development in tropical rain forests using JERS-1 SAR data," *Adv. Space Res.*, vol. 26, pp. 1151-1154, 2000.

[17] T. Igarashi, M. Shimada, Å. Rosenqvist, T. Hashimoto, T. Tadono, M. Matsuoka, and H. Yamamoto, "Preliminary study on data sets of ADEOS-II and ALOS dedicated to terrestrial carbon observation," *Adv. Space Res.*, vol. 32, pp. 2147-2152, 2003.

[18] T. M. Kuplich, V. Salvatori, and P. J. Curran, "JERS-1/SAR backscatter and its relationship with biomass of regenerating forests," *Int. J. Remote Sens.*, vol. 21, pp. 2513-2518, 2000.

[19] J. R. Santos, M. S. Pardi Lacruz, L. S. Araujo, and M. Keil, "Savanna and tropical rainforest biomass estimation and spatialization using JERS-1 data," *Int. J. Remote Sens.*, vol. 23, pp. 1217-1229, 2002.

[20] L. Pierce, P. Liang, and M. C. Dobson, "Regrowth biomass estimation in the Amazon using JERS-1/RADARSAT SAR composites," *Proc. IGARSS'02*, Toronto, 24-28 June, 2002.

[21] A. Rosenqvist, M. Shimada, R. Lucas, J. Lowry, P. Paillou, and B. Chapman, "The ALOS Kyoto & Carbon Initiative, Science Plan (v.3.1)," JAXA EORC, 2008 http://www.eorc.jaxa.jp/ALOS/kyoto/KC-Science-Plan_v3.1.pdf.

[22] -, "Statistical Yearbook of Forestry 2008." Jonköping: Swedish Forest Agency, 2008, pp. 334 http://www.skogsstyrelsen.se/statistics.

[23] M. Santoro, J. E. S. Fransson, L. E. B. Eriksson, M. Magnusson, L. M. H. Ulander, and H. Olsson, "Signatures of ALOS PALSAR L-band backscatter in Swedish forest," *IEEE Trans. Geosci. Remote Sensing*, in press.

[24] Å. Rosenqvist, M. Shimada, N. Ito, and M. Watanabe, "ALOS PALSAR: A Pathfinder Mission for Global-Scale Monitoring of the Environment," *IEEE Trans. Geosci. Remote Sensing*, vol. 45, pp. 3307-3316, 2007.

[25] M. Shimada, O. Isoguchi, T. Tadono, and K. Isono, "PALSAR radiometric and geometric calibration," *IEEE Trans. Geosci. Remote Sensing*, in press.

Johan E.S. Fransson was born in Karlshamn, Sweden, in 1967. He received the M.Sc. in forestry and Ph.D. in forestry remote sensing from the Swedish University of Agricultural Sciences (SLU), Umeå, Sweden, in 1992 and 1999, respectively. Since 1993, he has been with the Department of Forest Resource Management, SLU, Umeå. In 2000 and 2002 he was appointed as Assistant Professor and Associate Professor in forestry remote sensing, respectively. Dr. Fransson became the Head of the Department in 2008. His main research interest concerns analysis of SAR images for forestry applications. Dr. Fransson received the International Space University Certificate from the Royal Institute of Technology in Stockholm, Sweden, in 1995 and the award from “Kungliga Skytteanska samfundet” to a younger researcher at SLU, Umeå, in 2002.

Forest Theme

Boreal Forest Mapping in Siberia

Christian Thiel, Christiane Schmullius & Maurizio Santoro,
FSU-Jena/Gamma RS (Germany/Switzerland)

K&C Science Report – Phase 1
Forestry Theme – Boreal Forest Mapping in Siberia

Christian Thiel
Friedrich-Schiller-University Jena, Loebdergraben 32, Christian.Thiel@uni-jena.de

Christiane Schmullius
Friedrich-Schiller-University Jena, Loebdergraben 32, c.schmullius@uni-jena.de

Maurizio Santoro
Gamma Remote Sensing, santoro@gamma-rs.ch

***Abstract*—This report provides on overview on the accomplished work done by the Friedrich-Schiller-University in the framework of the K&C initiative. Major aim was the derivation of forestry related thematic information over the whole prototype area which is located in Central Siberia. First of all a sophisticated SAR data processing chain had to be developed to handle the large amount of data. Afterwards four diverse classification strategies have been developed. These strategies comprise multitemporal methodologies, change detection and the implementation of interferometric coherence. In particular the latter strategy proved being valuable and having the potential for operational implementation.**

***Index Terms*—ALOS PALSAR, K&C Initiative, Forest Theme, Forest Cover Mapping, Change Mapping, Coherence, Siberia**

1. INTRODUCTION

SAR DATA offer great potential for forest cover mapping, forest disturbance mapping (e.g. logging, forest fire, and wind damage) and forest biomass assessment. Lower radar frequencies turned out to be of particular adequacy. E.g. L-band SAR backscatter data acquired by the JERS-1 SAR was found to be suitable for mapping forest cover in the boreal zone. Radar backscatter and interferometric coherence have been successfully implemented. The launch of ALOS PALSAR offers new dimensions regarding spaceborne SAR data driven investigations. Compared to its antecessor JERS-1, PALSAR features a much increased performance in terms of image radiometry, geometry, and orbit steadiness. The controlled interferometric baseline combined with the well-defined observation strategy over the boreal zone greatly increases the potential of interferometry based SAR data examinations.

The report first investigates the use of backscattered intensity and then evaluates the additional information obtained through synergistic use of intensity and coherence for large area forest monitoring in Siberia. Regarding the intensity a multitemporal approach and a change detection method have been developed. These mapping exercises are conducted on a pixel level. The mapping by means of intensity and coherence is based on image segments.

2. SAR DATA PROCESSING

A. *SAR DATA PRE-PROCESSING*

The SAR pre-processing comprehends the processing steps summarised in Figure 1. Unfortunately, still (also at cycle 20) partially erroneous data (intensity ramps) were delivered. These intensity ramps at the edges of the data stripes could appear at far and near range as well at both azimuth sides. The magnitude and the width of the erroneous parts were varying. For sustaining as many rows and lines as possible, an interactive approach was chosen instead of a fixed cutting scheme (compare Figure 2).

The DEM based (SRTM, 90 m) orthorectification is described by Wegmüller 1999. Each strip was processed separately; one lookup table was applied to both polarisations. Regarding topographic normalisation pixel area correction and angular adjustment as proposed by Castel at al. 2001 was implemented:

$$A_{slope} = \frac{az \cdot r}{\cos(\psi)} \tag{1}$$

where az and r denote azimuth and range pixel spacing respectively, and ψ represents the projection angle, which is defined as angle between surface normal and image plane normal. The true local SAR pixel size A_{slope} is then used to correct for topography induced pixel area distortions as follows:

$$\sigma^0{}_{cor} = \sigma^0 * \frac{A_{flat}}{A_{slope}} \tag{2}$$

where A_{flat} is the SAR pixel size for flat terrain, σ^0 is the backscattering coefficient, and $\sigma^0{}_{cor}$ the corrected backscattering coefficient. The angular adjustment utilises the incidence angle θ_{ref} for flat terrain and the actual local incidence angle θ_{loc} to minimise variations in backscatter which are caused by topography driven variations of backscattering mechanisms.

$$\sigma^0{}_f = \sigma^0{}_{\theta_{cor}} \left(\frac{\cos\theta_{ref}}{\cos\theta_{loc}} \right)^n \tag{3}$$

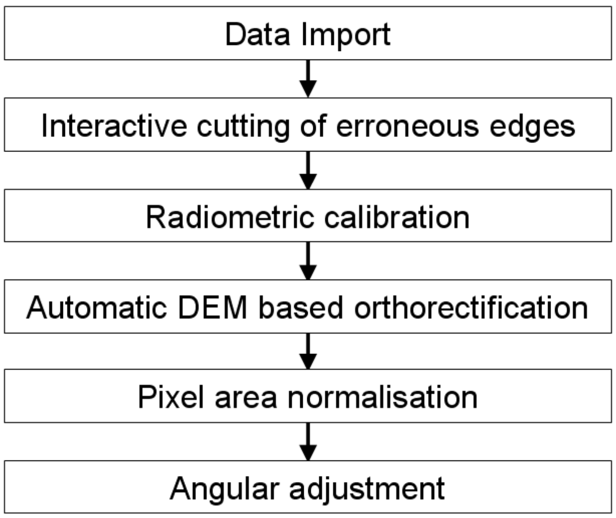

Figure 1: Scheme of K&C SAR data strip pre-processing

The geocoding accuracy was not checked in detail but can be assumed being high. The RMS errors between the automatically detected GCPs and the computed polynomials are in the order of 0.3 pixels. Geocoding details are preserved for each single strip and can be delivered if required. Figure 2 demonstrates this high geolocation precision. The black vertical fissure is due to missing data between the two strips. At the position were both data strips connect no geolocation offset is detectable. Additionally, no offsets have been detected during the multitemporal data examinations.

B. MOSAICING PROCEDURE

Mosaicing was conducted after SAR data pre-processing. Four mosaics, one for each cycle (08, 12, 13, and 20), have been processed. Areas with no data have been masked out. Histogram adaptation or similar radiometric adjustments have not been utilised. In the overlap area between two stripes feathering was applied with a maximum of 50 pixels (50 pixels when the data overlap was at least 50 pixels). Eventually, the mosaics from the cycles 12, 13, and 20 have been combined to one single multitemporal mosaic to achieve the maximised spatial coverage for prototype area-wide landcover classification. The intensities are scaled in dB.

C. FINAL DATA SETS

Figure 3 and Figure 4 provide an overview on the processed data for the K&C prototype area. Data has been processed up to ~62°N, while the prototype area extends to 65°N. However, due to geocoding problems (only minor relief north of 62°N and no adequate DEM available) it was considered to exclude the northern part of the prototype area for the time being.

None of the cycles provides a complete spatial coverage. Thus, multitemporal classification is not feasible for the whole prototype area. The lowest coverage was achieved for cycle 8. By means of combining all summer acquisitions an almost complete coverage of the prototype area can be achieved (see section 3.B).

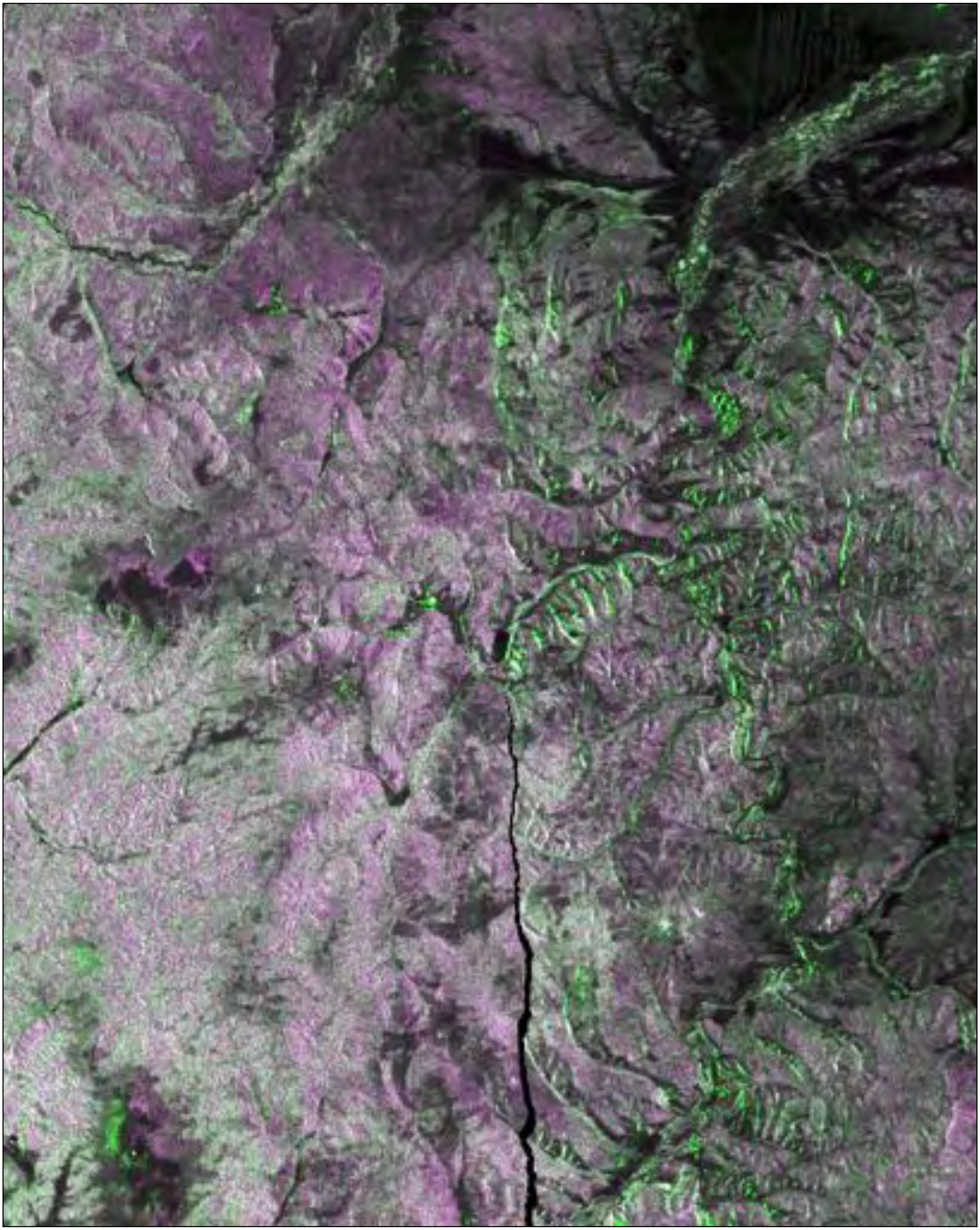

Figure 2: PALSAR HV/HH/HV composite for demonstration of high geolocation precision, ALOS K&C © JAXA/METI

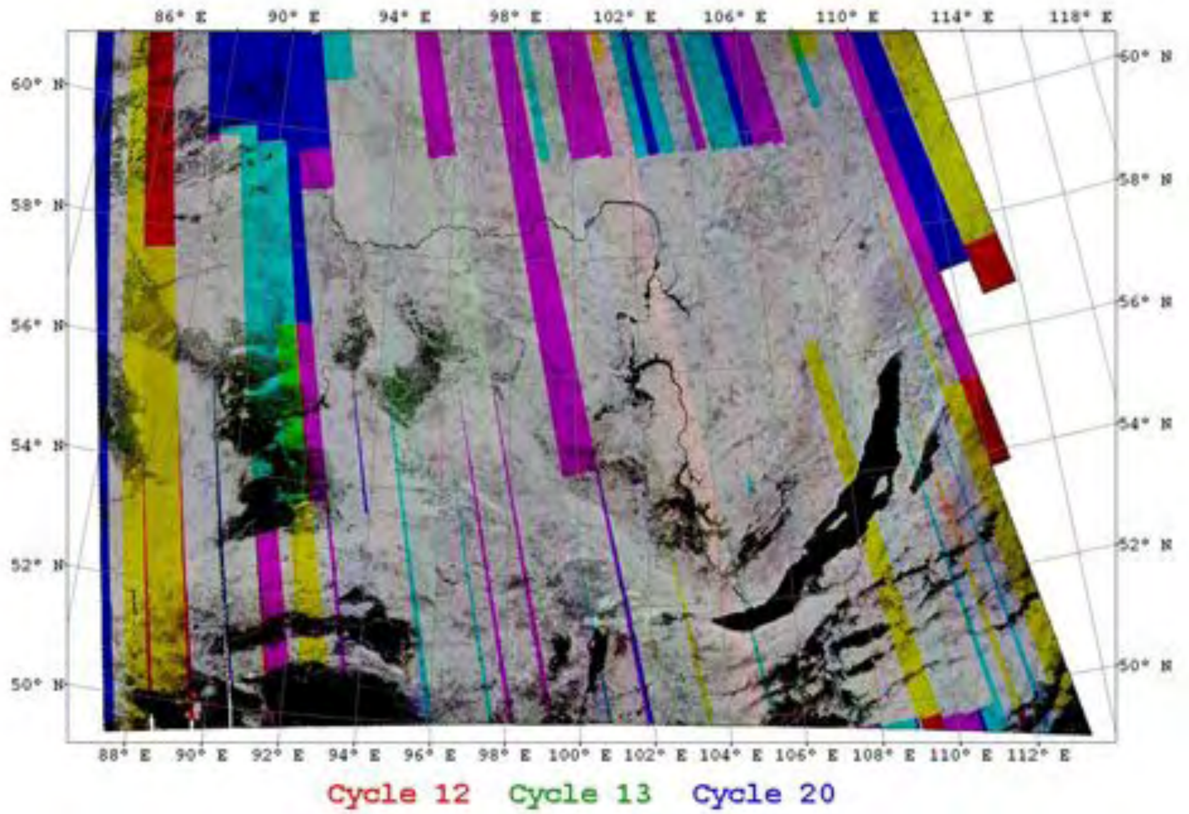

Figure 3: Processed summer FBD data in Siberia, ALOS K&C © JAXA/METI

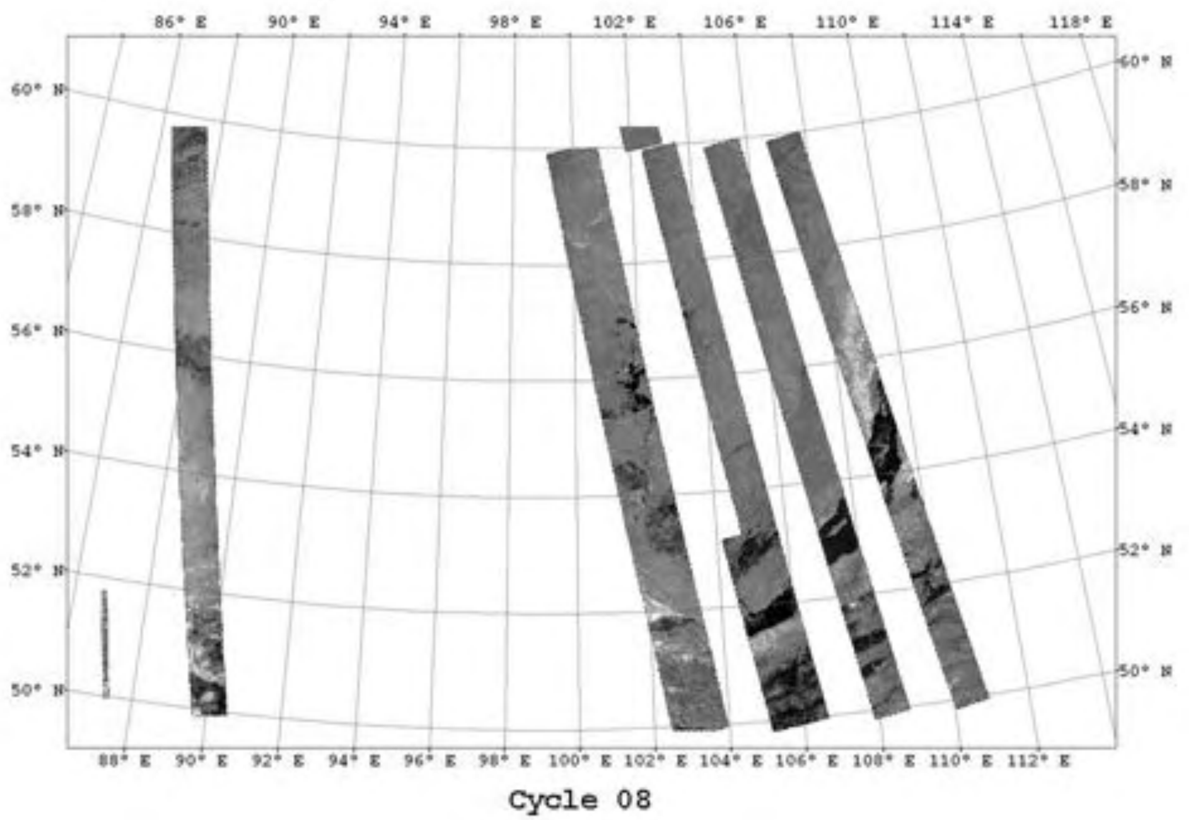

Figure 4: Processed winter FBS data in Siberia, ALOS K&C © JAXA/METI

3. CLASSIFICATION

A. MULTITEMPORAL CLASSIFICATION

CLASSIFICATION METHODOLOGY

The multitemporal classification makes use of the characteristic temporal backscattering variations of the considered classes. Thus, additionally to the multitemporal dataset, simple multitemporal metrics have been computed. The following table summarises the utilised data layers. The multitemporal metrics have been computed for both polarisations separately.

Basing on these preconditions suited and robust metrics have been selected and thresholds for the considered classes have been defined. These thresholds are summarised in the following table. All conditions per line in the table must be fulfilled. The classes water and settlement are defined manifold. In these cases at least on of the definitions must be fulfilled. However, at some positions within the test area higher backscatter values occur at water bodies. This is due to an uneven water surface caused by wind or currents (in particular at river junctions). To overcome the wind problem the minimum backscatter for HH was chosen. However, the current problem could not be completely solved in doing so.

PALSAR Data	Multitemporal Metrics
FBD HH/HV Cycle 12 (early summer 2007) FBD HH/HV Cycle 13 (late summer 2007) FBD HH/HV Cycle 20 (early summer 2008)	Minimum Mean Maximum Standard Deviation (averaged by 5x5 matrix)

Aim of the multitemporal classification was to separate as many land cover types as possible. The classification considers the land cover types water, agriculture, settlement, clear-cuts & burnt areas, three forest classes, and a class containing recent changes such as new clear-cuts (formed between cycles 12 and 20) and fire scars. The following table collects typical relative values for the available data layers from very high (++) to very low (--), 0 means medium values. These ratings are basing on fundamental knowledge and the examination of the available data.

Potential misclassifications concern agricultural fields featuring a smooth surface and low temporal variations. Forests are characterised by very stable backscatter. In comparison to other land cover types the backscattering intensity is high, in particular at cross polarisation. The amount of backscatter is a function of forest biomass, whereby saturation occurs already at rather low biomass levels. Nevertheless three forest classes have been established against different backscattering levels. Forest 1 is forest with no evidence (related to PALSAR data) for disturbances, forest 2

	HH Min	HH Mean	HH Max	HH Std.	HV Min	HV Mean	HV Max	HV Std.
Water	--	-	0	-	--	--	-	0
Agriculture	--	--	0	++	--	-	0	0
Forest 1 (dense, high biomass)	+	+	+	--	++	++	++	--
Forest 2 (low biomass)	0	0	0	--	0	0	0	--
Forest 3 (very low biomass)	-	-	-	-	-	-	-	-
Clear-cuts & burnt areas	--	-	-	-	--	--	-	-
Settlement	++	++	++	+	0	+	+	+
New clear-cuts and fire scars	--	0	+	++	--	0	++	++

	HH Min	HH Mean	HH Max	HH Std.	HV Min	HV Mean	HV Max	HV Std.
Water (Def. 1)	< -19 dB					< -26 dB		
Water (Def. 2)	< -16 dB			< 1.0		< -26 dB		
Water (Def. 3)	< -19 dB				< -30 dB			
Forest 1 (dense, high biomass)		< -2 dB					> -14 dB	< 1.2
Forest 2 (low biomass)		< -2 dB					> -17 dB	< 1.0
Forest 3 (very low biomass)		< -2 dB					> -20 dB	< 0.8
Settlement (Def. 1)		> -1 dB	> 0 dB	> 1.0				
Settlement (Def. 2)		> -3 dB	> -2 dB	> 2.0				
New clear-cuts and fire scars		< -4 dB				> -18 dB	> -14 dB	> 1.2
Clear-cuts & burnt areas		> -9 dB		< 2.0				
Agriculture		< -9 dB		> 2.0				

corresponds to former clear-cuts or fire scars with considerable regrowth and forest 3 is related to initial regrowth or other temporally stable forestry related classes with low to medium cross polarisation backscatter.

Settlements typically feature very high HH backscattering intensities. This particularly applies if geometric features of the settlements allow the generation of double bounce. Although settlements and their entities are rather stable in time, the backscattering intensity varies considerably. On the one hand, very high backscatter causes a high potential for very high variations, on the other hand, the amount of double bounce is driven by a number of variable conditions such as surface moisture or local incidence angle. In summary, only the parts of the settlements causing double bounce are detected as settlements. The other parts do not feature settlement specific backscattering signatures. Texture was not considered, as 50 m ground resolution cannot resolve relevant settlement objects.

New clear-cuts and fire scars must feature forest typical backscattering signatures at least at one (the first) acquisition date, thus maximum backscatter must be the same as for forest. The conversion from forest to non-forested areas causes high backscatter variations.

The remaining and so far not classified areas are agricultural land and clear-cuts / burnt areas with a maximum HV backscatter below -20 dB (minor volume scattering). This mixture can be segregated by the fact, that agricultural land is characterised by high temporal changes and thus high backscatter variations. Additionally, the mean HH backscatter is much lower compared to clear-cuts and burnt areas in particular. Although this multitemporal classification approach shows promising results (see below), the dataset in terms of the multitemporal dimension is not sufficient. For the derivation of multitemporal metrics with statistical significance many more acquisitions would have been required. The accuracy of all classes would benefit from such an extension of the data set. Still it could be demonstrated, that in principle an operational classification approach basing on multitemporal PALSAR data is feasible.

TEST AREA AND RESULTS

As a multitemporal dataset is required, the classification approach could not be applied to the whole prototype area. Thus, a spatial subset was created. The area covered by the tracks 467 and 468 of cycle 08 was taken as subset from 54°N to 60°N (see Figure 5). For this area data from all cycles (8, 12, 13, and 20) were available. Unfortunately, as emerged during the classification process, a single winter intensity scene (cycle 08) does not add supplementary information. Thus, data from cycle 08 was neglected.

Figure 5 provides an RGB composite of the whole subset and the final map. Figure 6 provides the same information for a part of the subset. Accuracy assessment has not been accomplished so far. However, at first view the classification results seem to be promising. The greatest potential for misclassifications lies in the fuzziness of the classes related to diverse biomasses. Thus, the classes forest 3 and clear-cuts & burnt areas contain thematically similar land cover types and could be merged later on. Also, the subdivision of the three forest classes was conducted arbitrarily. No scientific, political or economical definition of the class forest was considered. The class settlement is obviously heavily underestimated.

B. CLASSIFICATION OF BASIC LANDCOVER FOR WHOLE PROTOTYPE AREA

CLASSIFICATION METHODOLOGY

Mapping was conducted by means of thresholds using one single mosaic (FBD intensities) for the whole prototype area. This mosaic contains data from three different observation cycles; the focus was put on filling data gaps. As none of the cycles is delivered completely, the mosaic contains data from two different years. This approach can provide a map with the most complete coverage of the prototype area but with the lowest accuracy.

Figure 7 (top) shows a composite of the complete mosaic. As no histogram adaptation was conducted during the mosaicing process, some of the strips do not fit into the mosaic regarding their radiometry. This is most likely due to varying weather condition at the diverse acquisitions. Moreover, it can be observed, that the radiometric difference between two adjacent strips is varying, which complicates histogram matching efforts.

Aim of the multitemporal classification was to separate only basic land cover types. The classification considers the land cover types water, forest/settlement, and very low biomass (agriculture, clear-cuts, fire scars, steppe etc.). The following table collects typical mean relative values for the available data layers from very high (++) to very low (--), 0 means medium values. These ratings are basing on basic knowledge and examination of the available data.

	HH	HV
Water	--	--
Forest/Settlements	+	++
Very low biomass	-	-

As relatively broad classes have been considered, the signature spectrum of these classes exhibit great potential for overlaps. This is particularly true for the classes water and very low biomass. However, as no multitemporal metrics can be computed, the separation of more classes is not feasible. The table below summarised the thresholds for the classification. All conditions per line in the table must be fulfilled.

	HH	HV
Water	< -19 dB	< -26 dB
Forest/Settlements	> -8 dB	> -20 dB
Very low biomass	Remaining values	Remaining values

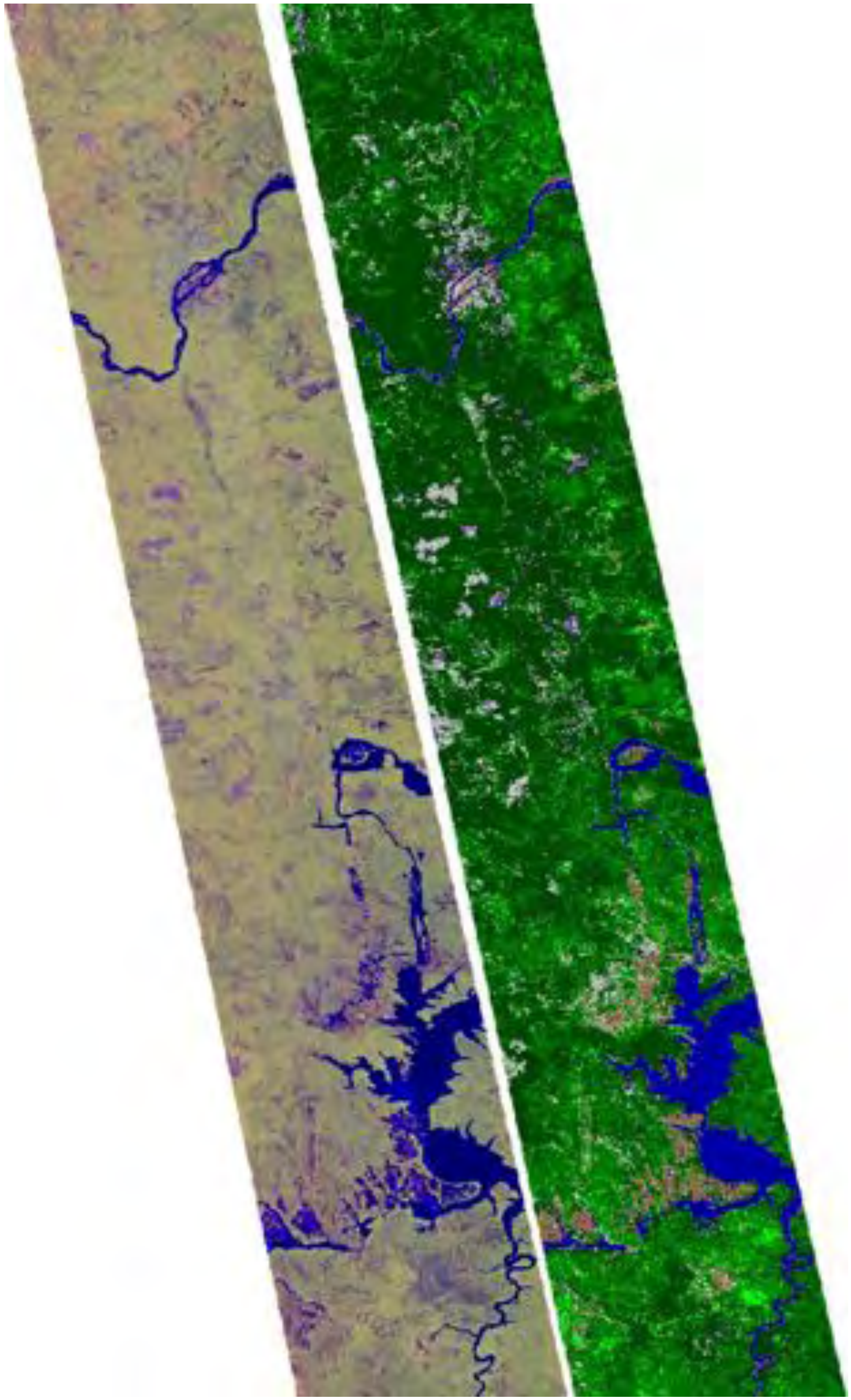

Figure 5: SAR data (left) and classification result (right) for the whole subset. SAR data composite and map colour coding as at Figure 6. (Tracks 467 and 468, 54°N-60°N), ALOS K&C © JAXA/METI

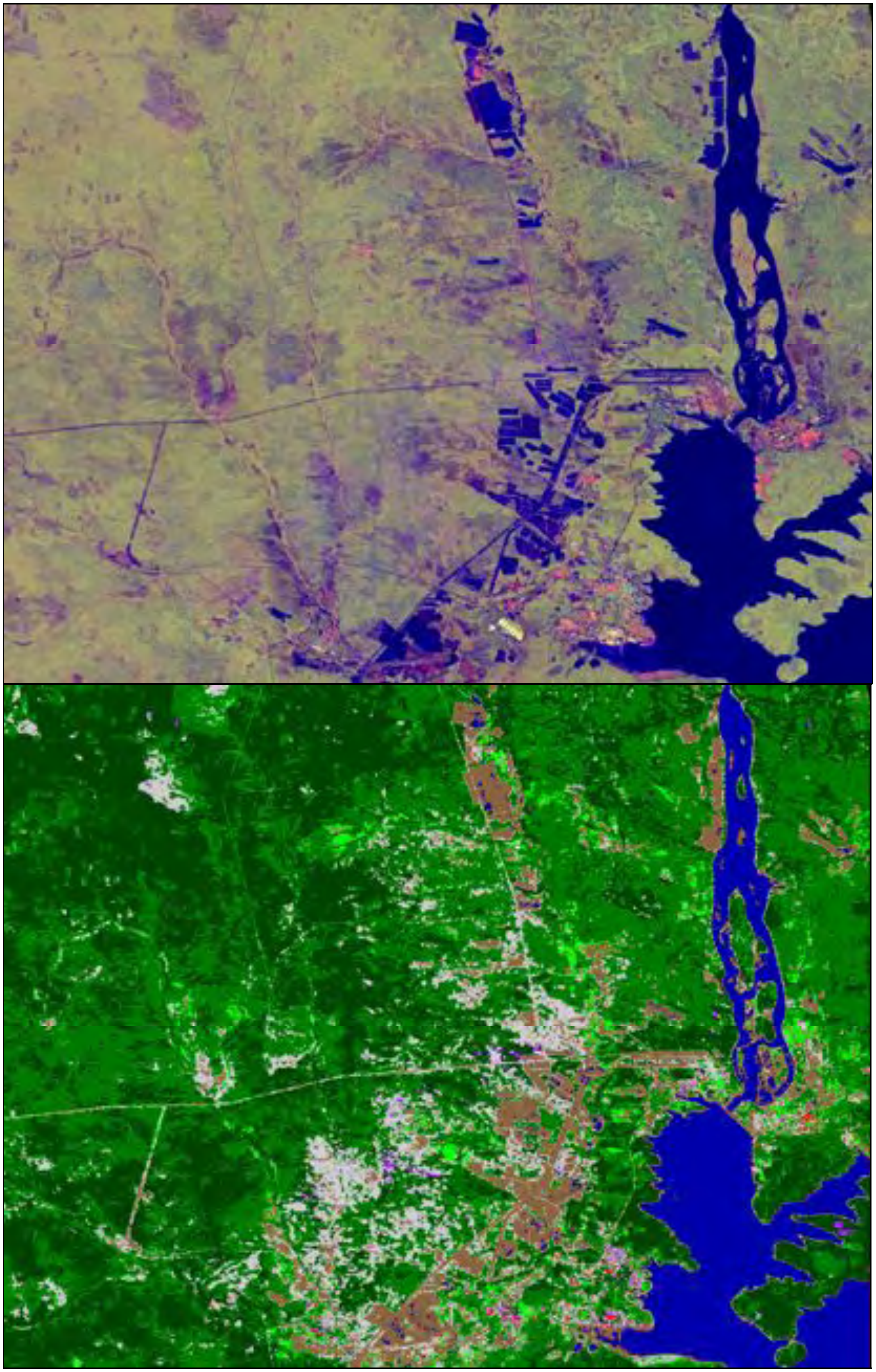

Figure 6: SAR data (top) and classification result (bottom) for part of subset. SAR data composite: HH mean / HV mean / HV std. dev.; Colour coding map: water (blue), forest dense (dark green), forest low biomass (green), forest very low biomass (light green), settlement (red), agriculture (brown), clear-cuts & burnt areas (grey), new clear-cuts and fire scars (purple), ALOS K&C © JAXA/METI

TEST AREA AND RESULTS

The result of the basic landcover classification for the whole prototype area is provided by Figure 7 (bottom) for the complete area and by Figure 8 for a subset of the area. The subset covers the same area as the map provided by Figure 6. Even if no accuracy assessment has been conducted so far it is obvious, that misclassifications are occurring. In particular the separation of water and very low biomass areas is not satisfying at all. In particular the steppe area in Tuwa (south-western edge of the area) produces very low backscatter and cannot be separated from water. A similar problem can also be observed at the subset of this map (Figure 8, compare with Figure 6). Very low biomass areas are in general well detected, however further separation of this mixes class is not feasible. Also at this subset significant confusion between water and very low biomass is obvious. Multitemporal data (important for agricultural areas) or even better coherence data would overcome this separation problem.

C. CLASSIFICATION OF CHANGES

CLASSIFICATION METHODOLOGY

Aim of the classification of changes is to detect areas with short term changes in land cover. Changes refer to deviation in land cover between cycle 12 and cycle 20. Due to radiometric deviations between the stripes the changes have to be detected stripe-wise. The classification of changes was not conducted for the whole prototype area, but for a subset. The subset is defined by the data coverage of track 468.

Input for the classification was the normalised backscatter difference index *NDBI*. This change measure was derived as follows:

$$NBDI_{XX} = \left\langle \frac{\sigma^0{}_{XX_{f_{t1}}} - \sigma^0{}_{XX_{f_{t2}}}}{\sigma^0{}_{XX_{f_{t1}}} + \sigma^0{}_{XX_{f_{t2}}}} \right\rangle \tag{4}$$

The *NBDI* is computed for each polarisation separately. The indices *t1* and *t2* denote the two different acquisitions. The idea of normalising the backscatter difference was to achieve a better comparability between the different tracks and to reduce the impact of different weather conditions. No change and equal radiometric properties of both strips result in an *NBDI* of zero. Negative values flag areas with a decrease in backscatter and vice versa. Potential changes in the investigated area are related to agricultural activities and forest management. New fire scars and in particular clear-cuts will cause a reduction of backscatter and thus negative *NBDI* values. Forest regrowth could result in increasing backscatter. However, only minor effects can be expected. Major source of positive *NBDI* values are agricultural areas with respective crop rotations.

Basing on the *NBDI* thresholds have been defined. These thresholds are summarised in the following table. All conditions per line in the table must be fulfilled. The class significant decrease of backscatter is defined twofold. At least on of the definitions must be fulfilled. The considered classes do not allow a statement on the actual change regarding the land cover type. These classes can be interpreted as change indicators. However, the combination of the change classification with the information derived by means of the multitemporal classification can close this gap.

	$NBDI_{HH}$	$NBDI_{HV}$
Significant increase of backscatter	0.25	0.10
Significant decrease of backscatter	-0.04	-0.02
Significant decrease of backscatter	-0.15	

TEST AREA AND RESULTS

Input data and results for the change classification are presented in following. Figure 9 depicts the input data represented as *NBDI* RG (red-green) colour composite, where red represents the *NBDI* for HH and green for HV. Thus, bright areas flag areas with increasing backscatter, dark areas vice versa. Different hues are caused be unequal change of backscatter regarding the two polarisations. The change map is provided by Figure 10. Although only one year passed by between the two acquisitions, much change is visible. However, most of the change is due to agricultural activities. Such areas can be recognised by a heterogeneous pattern of increasing and decreasing backscattering intensity (as e.g. in the middle of the fourth tile of track 468).

Figure 11 provides two subsets of the above presented dataset. The upper image pair represents a forest dominated area, the lower pair an agricultural area. The clear-cuts in the forest dominated section are obviously well captured by the change map. The massive change signal at the lower pair is most likely caused by crop rotation effects. Although the change map product is not yet validated, it seems to be a promising indicator for forestry related changes. Major issue is to separate the impacts of agriculture and clear-cutting (and forest fires). One solution could be the implementation of the multitemporal classification (section A).

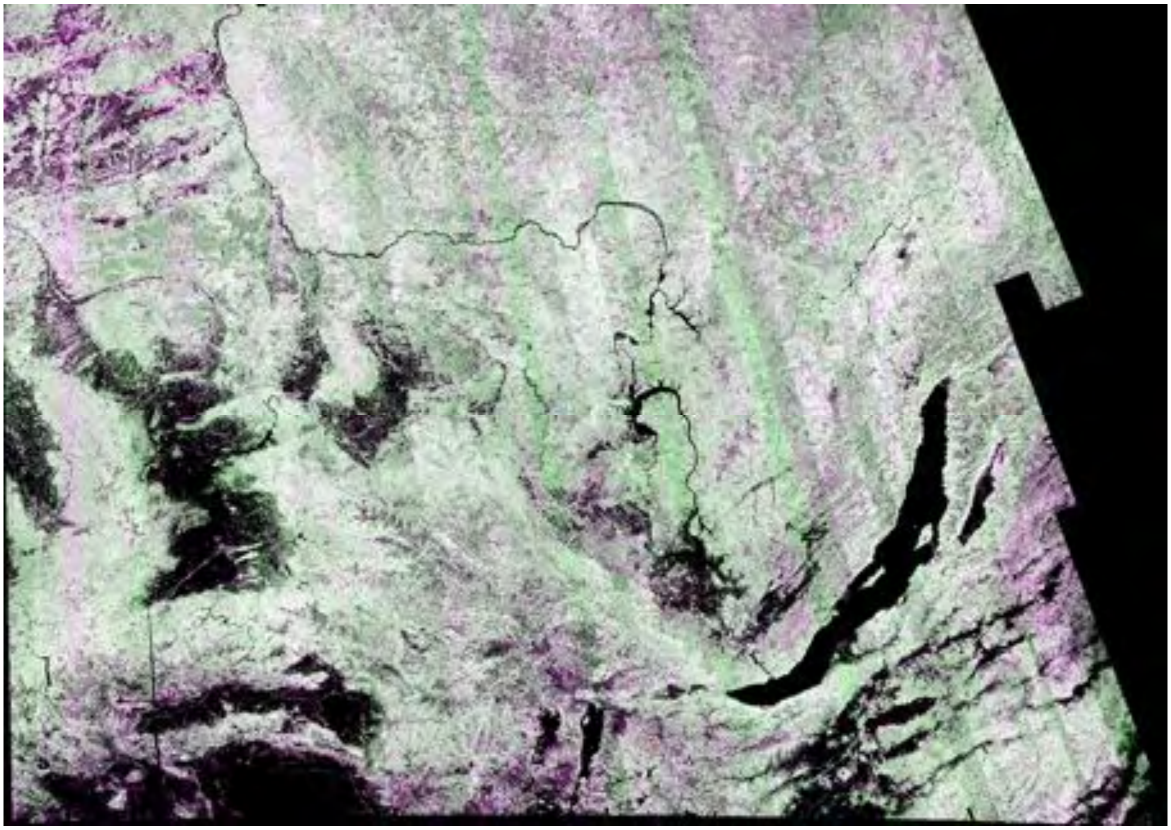

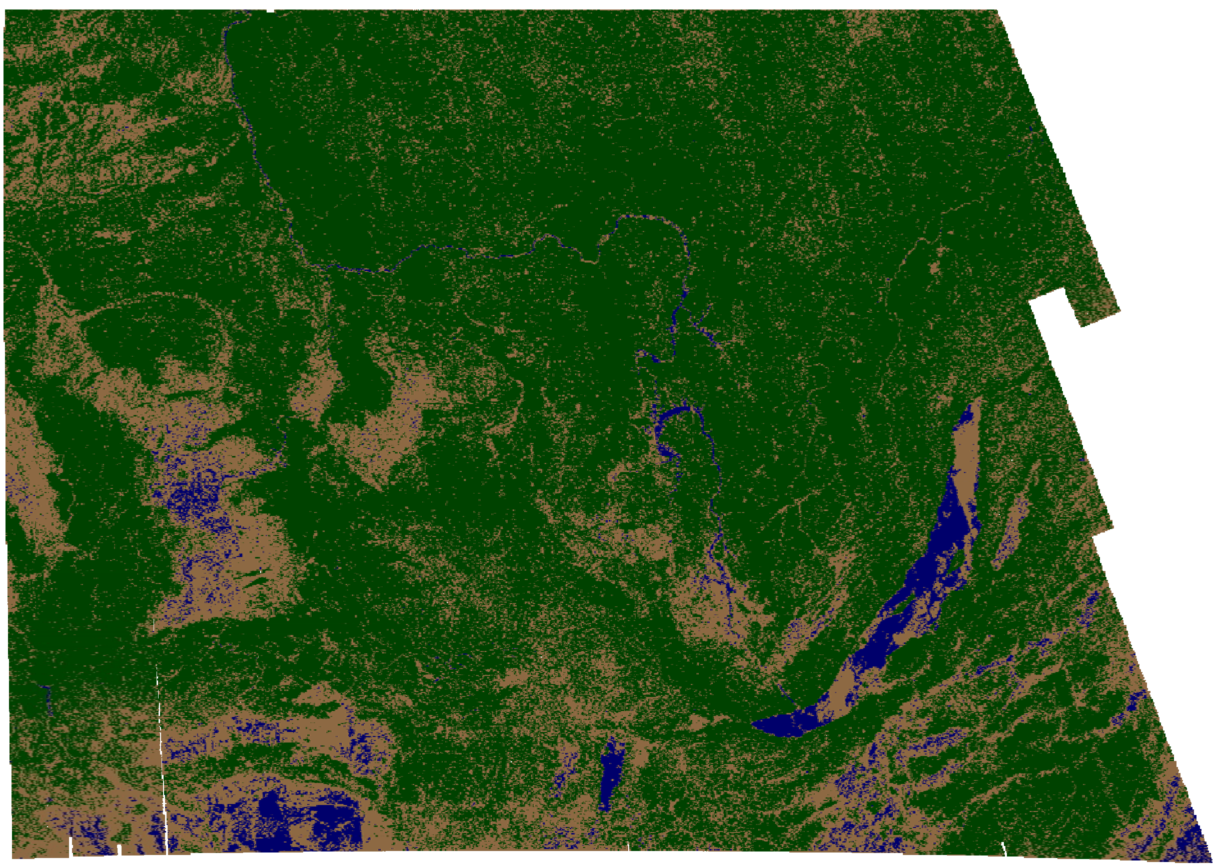

Figure 7: SAR data (top) and classification result (bottom) of prototype area. SAR data composite: HH/HV/HH; Colour coding map: water (blue), forest/settlements (dark green), very forest low biomass (brown) , ALOS K&C © JAXA/METI

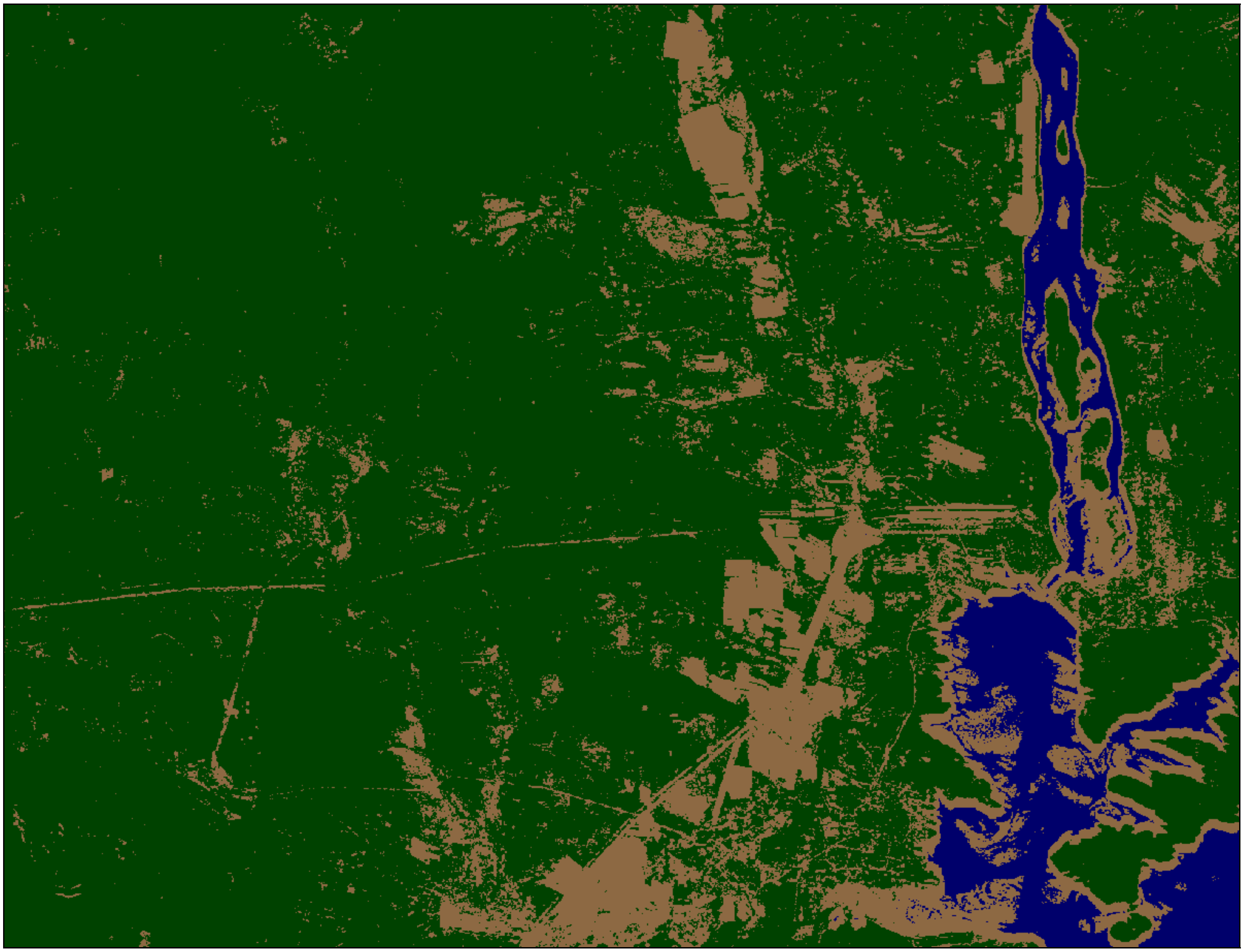

Figure 8: Classification result for subset of prototype area. Colour coding map: water (blue), forest/settlements (dark green), very forest low biomass (brown) , ALOS K&C © JAXA/METI

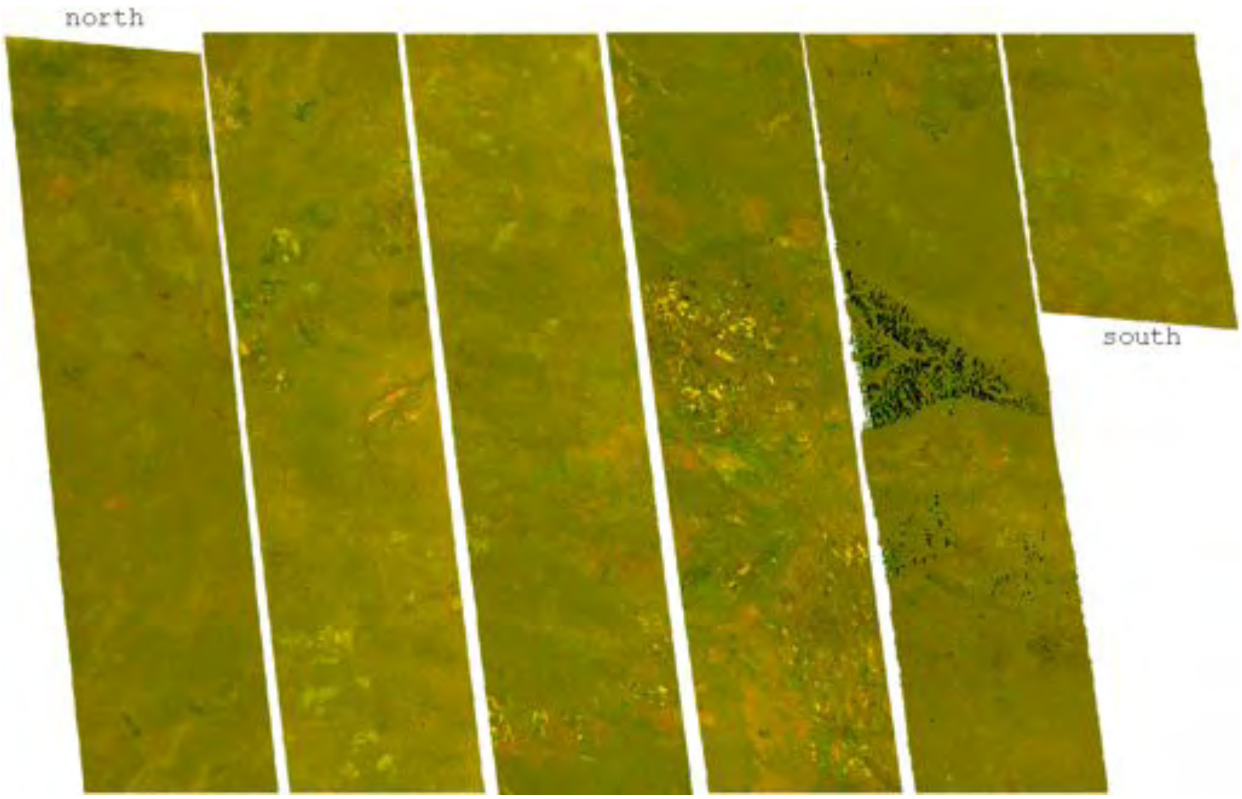

Figure 9: Input data for change map generation: Normalised Backscattering Difference Index (NBDI) of cycles 12 and 20 (RG composite: HH NBDI /HV NBDI). Data taken from track 468, fragmented for better overview, ALOS K&C © JAXA/METI

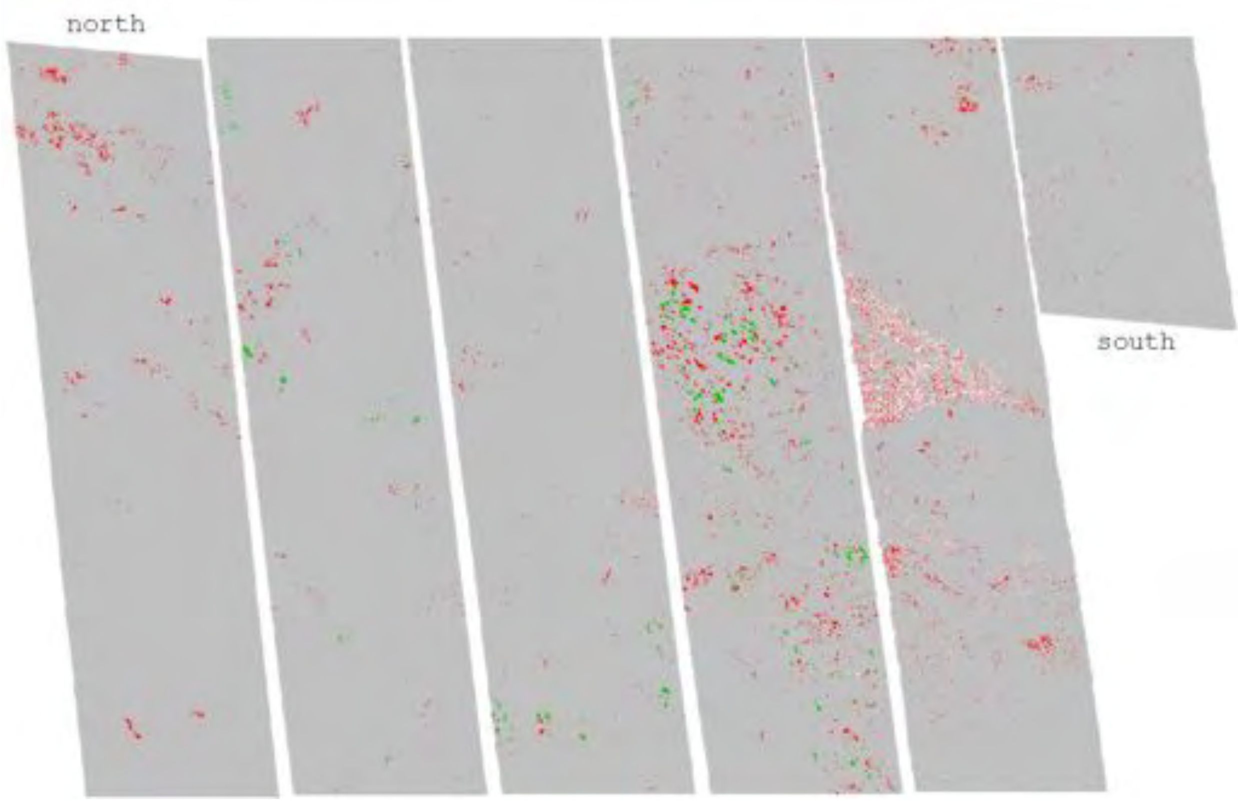

Figure 10: Change map. Colour coding: grey: no change, white: no data, red: decrease of backscatter, green: increase of backscatter. Data taken from track 468, fragmented for better overview, ALOS K&C © JAXA/METI

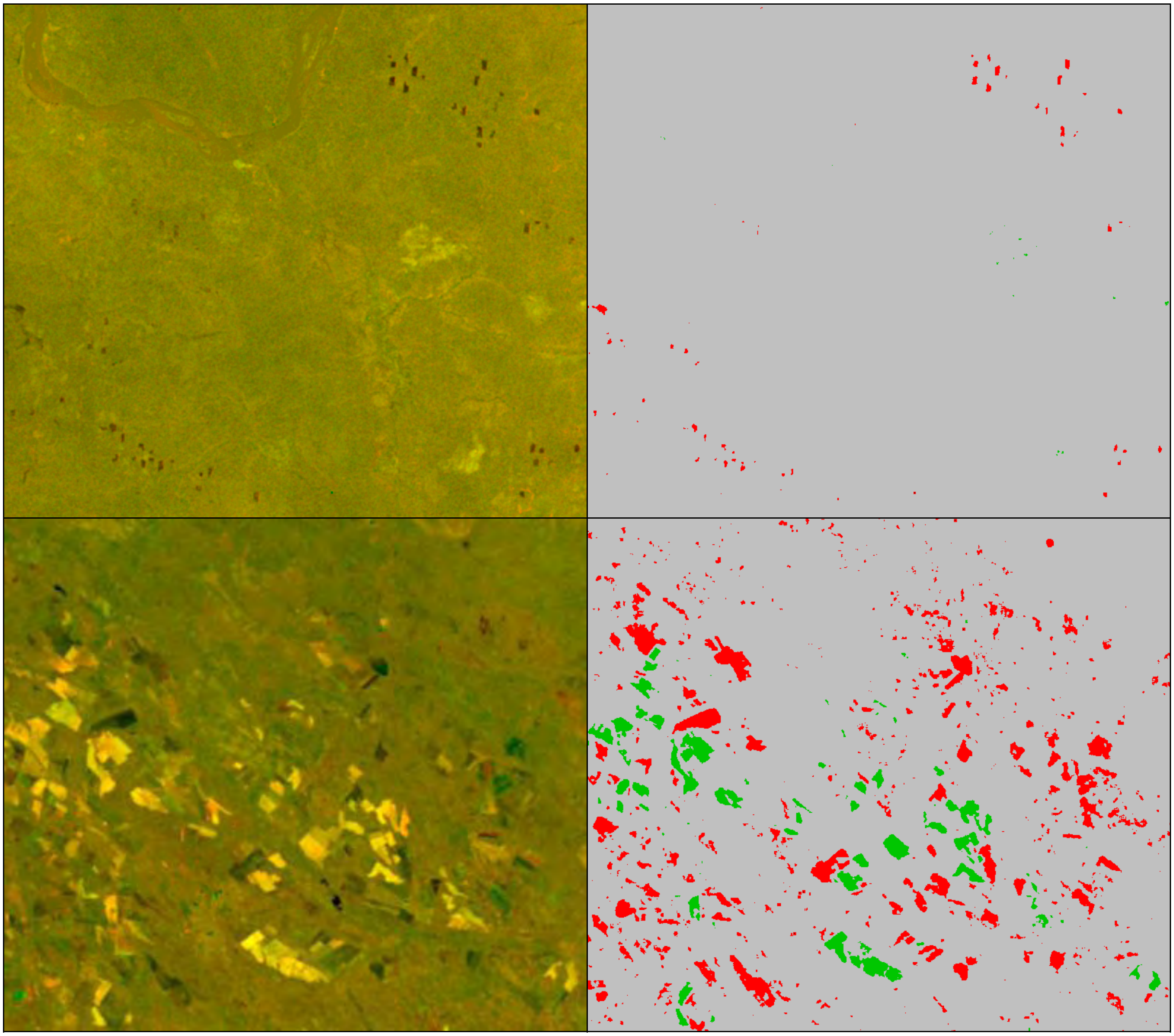

Figure 11: Input data (left column) and change map (right column). Composite and colour coding as above (Figure 9 and Figure 10). Top: forest dominated area, Bottom: agriculture dominated area, ALOS K&C © JAXA/METI

D. FOREST COVER MAPPING USING INTENSITY AND COHERENCE

Summer intensity and winter coherence images are used for forest monitoring. The intensities (FBD HH/HV) have been acquired during summer 2007 and feature the K&C intensity stripes. This initial investigation was carried out in the framework of GSE Forest Monitoring.

COHERENCE PROCESSING AND COMPOSITES

For the coherence estimation standard level 1.1 FBS scenes were applied. The path numbers range from 461 to 473. The 43 pairs have been acquired during the winters 2006/2007 (cycles 8 & 9) and 2007/2008 (cycles 16 & 17). Each pair stems from consecutive cycles (46 days temporal baseline). During both winters suited weather conditions (temperatures during and between acquisitions steadily far below 0°C) have been reported by representative weather stations. Interferometric processing consisted of SLC data co-registration at sub-pixel level, slope adaptive common-band filtering in range (Santoro et al. 2007), and common-band filtering in azimuth. Texture was used for the coherence computation procedure which employs an adaptive estimation approach (Wegmüller et al. 1998). All SAR images (K&C intensities and coherence) were orthorectified using SRTM elevation data. The final pixel size of the coherence is 50 by 50 m² and thus equal to the K&C data. The mosaic of the 43 coherence images is depicted in Figure 12.

A first impression of the potential of the synergistic usage of backscattering intensity and coherence can be caught from Figure 13. This RGB composite is based on the backscattering intensities HV and HH as well as the coherence. Some landcover classes can be visually separated. Water appears in black, unforested areas show up in blue, and forest covered sections appear in orange, yellow and light green colour shades. These variances are due to differing forest types and biomass levels. The light blue patch in the middle of the subset corresponds to a fire scar. Eastward from that position another small light blue patch is visible next to the water body. This one corresponds to the city of Novaja Igirma (ca. 11,000 inhabitants).

CLASSIFICATION METHODOLOGY

The presented SAR data (backscatter and coherence) provides the input for operational forest monitoring. The defined target classes as follows: forest, very low biomass forest and non-forest. Consequently, the large spectral variability of the non-forest class needs to be considered during the classification process. In fact, ten classes have been considered during the classification process. These are the classes old clear-cut, recent clear-cut, fire scar, agriculture, water, and urban plus four forest classes. For each class 20 samples have been selected under consideration of a good distribution over the whole site and accounting for the class internal variations. The class merge resulting in the three named target classes was conducted after the classification. For the classification the Nearest Neighbour algorithm was used.

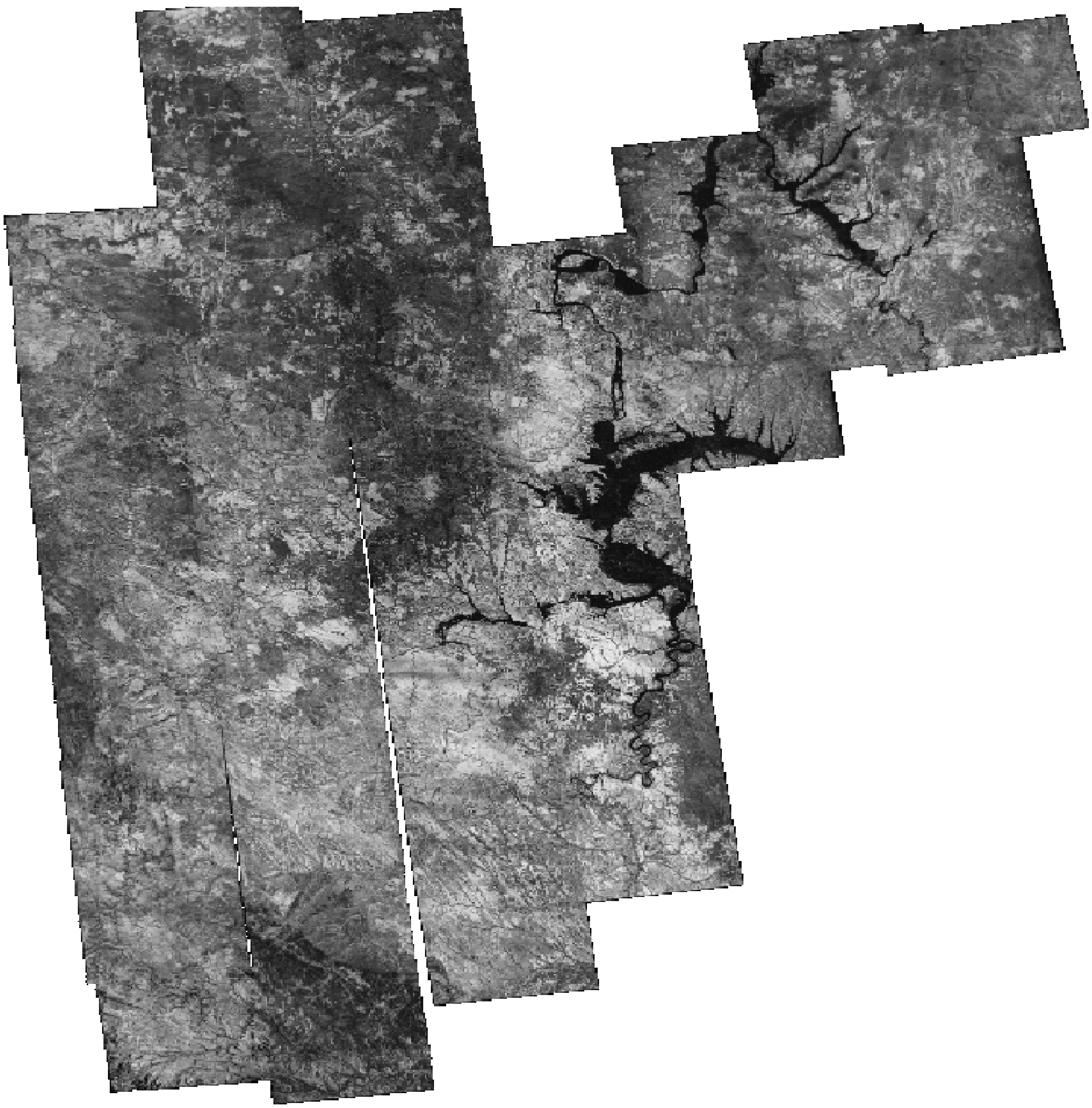

Figure 12: Mosaic of interferometric coherence images: 53°-58°N, 97°-105°E, ALOS K&C © JAXA/METI

The classification is based on image segments. The segments are identified using the multiresolution segmentation algorithm discussed by (Baatz & Schäpe 2000, Benz et al. 2004) and realised by means of the Definiens Developer software. The segments do not necessarily represent the forest compartments, but in general identify homogeneous patches. The segment size is determined by a scale parameter and can range from single pixels to the entire scene. Due to the targeted minimum mapping unit (MMU) of 1 ha, small image segments have been created. The segmentation parameter set is summarised at the following table.

Parameter	Value
Scale	2.0
Shape / Colour	0.9 / 0.1
Compactness / Smoothness	0.0 / 1.0

The segmentation process only considers the summer intensity data with the same weight of both polarisations, as the edges between the image objects are more distinct (sharp) as for the coherence. An example of a segmented image is provided in Figure 14. The provided example shows evidently, that the borders of differing adjoining patches are clearly framed. Dark blue segments represent clear cut areas which have been recently clear felled; yellow, orange and greenish sections represent different types of forest. Low biomass forest stands appear in violet shades. Although the contrast of these patches is not as strong as for the recent clear cuts, these low biomass forest stands are well captured by the segmentation.

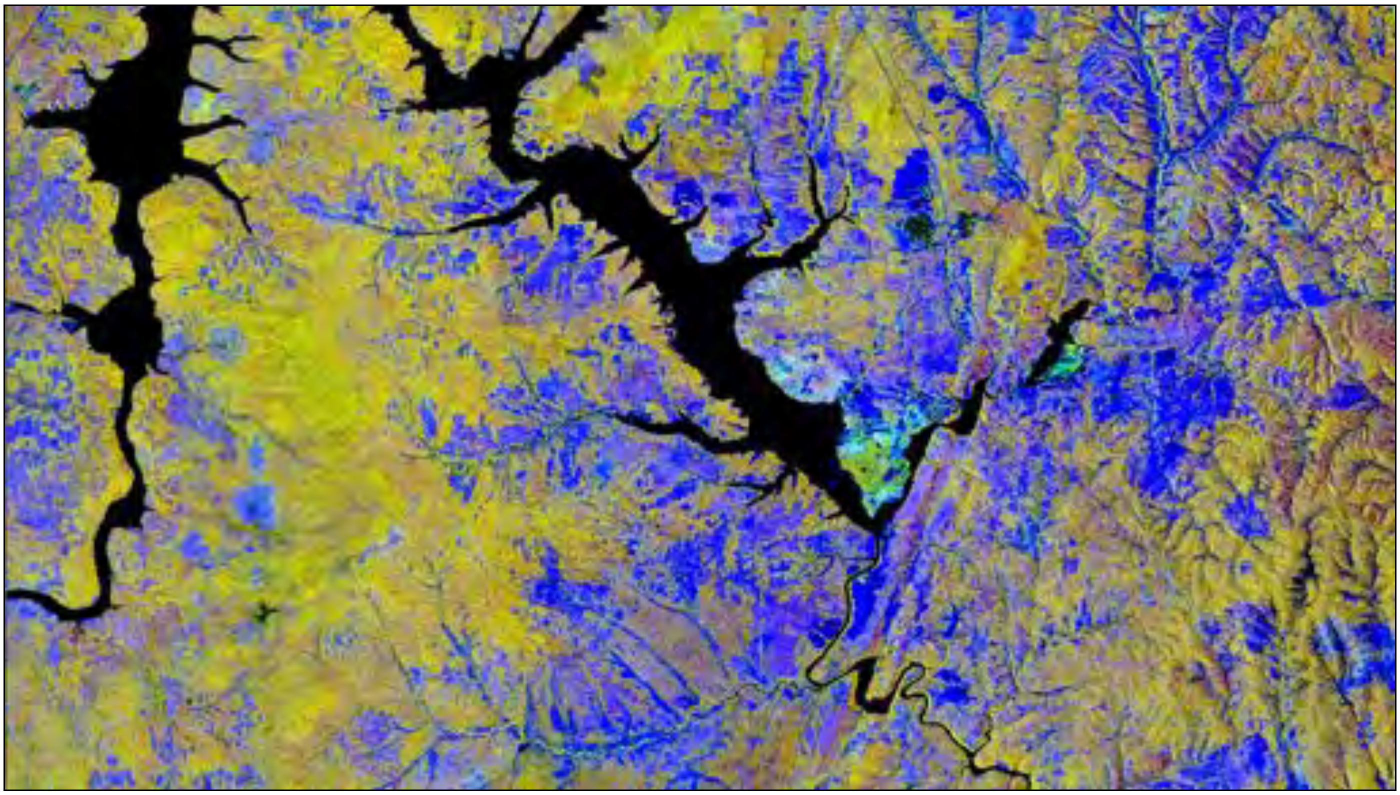

Figure 13: Composite of HV & HH backscatter and winter coherence for a subset of the monitoring area (taken from north-eastern section) , © JAXA/METI

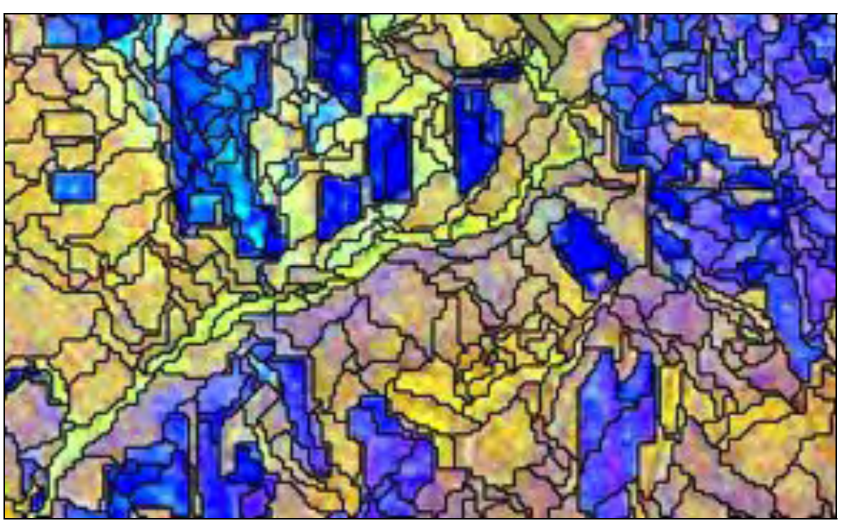

Figure 14: Example of segmented dataset, ALOS K&C © JAXA/METI

TEST AREA AND RESULTS

The test area is located in central Siberia (in the centre of the prototype area) and comprises an area of about 100,000 km² (Figure 15).

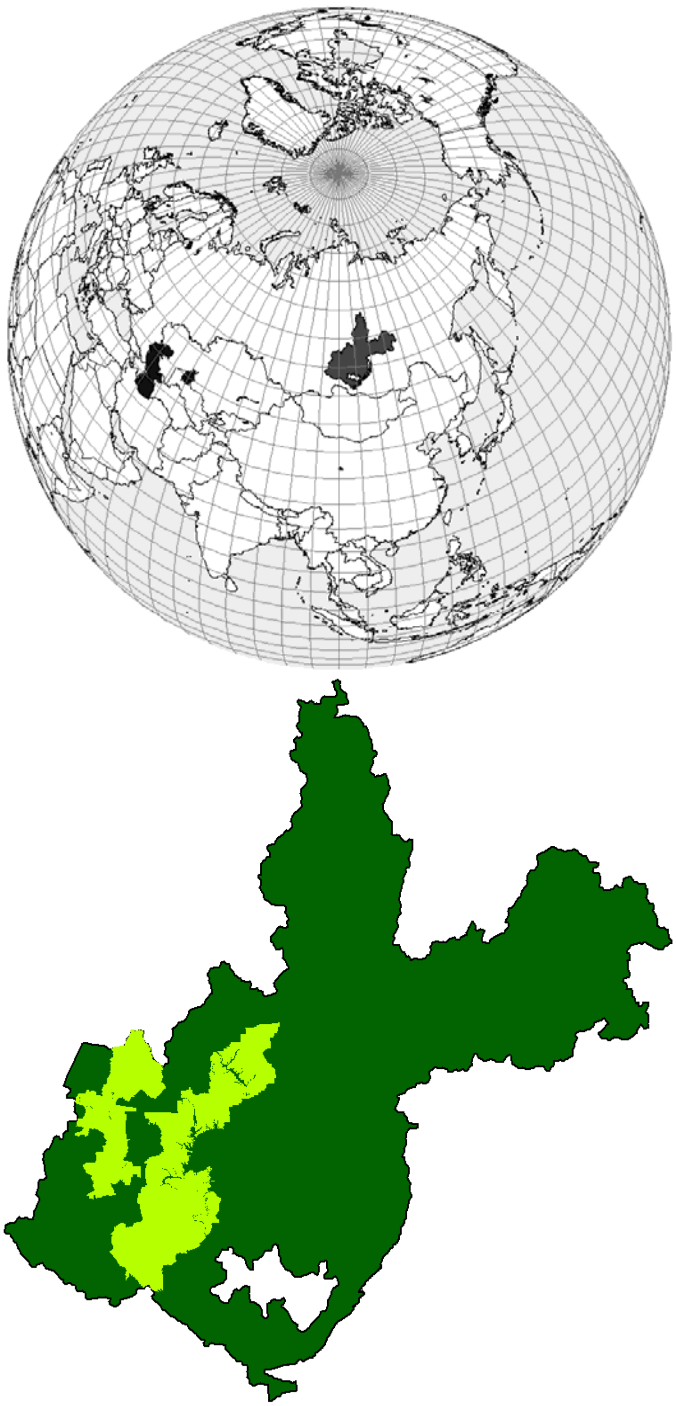

Figure 15: Test area (light green patch, right image) in the centre of the prototype area

The Middle Siberian Plateau in the southern part of the territory is characterised by hills up to 1,700 m. The northern part is flat with heights up to 500 m. Taiga forests (spruce, birch, larch, pine, etc.) dominate and cover ca. 82% of the region. The site exhibits continental climatic conditions. The yearly amount of precipitation is generally below 450 mm; the winters are very cold and dry, the summers are warm and include the precipitation season. Reference data has been available in terms of very high resolution optical data, very high resolution SAR data (TS-X), a digital forest compartment GIS data base on forest stand level, and analogue maps comprising recent and planned forest cover changes.

Figure 16 provides the SAR data and the forest cover map for the monitoring area. Figure 17 depicts a subset taken from the northern part of the provided forest cover map. The accuracy assessment for the whole monitoring area is basing on 1,000 point samples. The random sampling was stratified by class proportion. The sampling results provided the input for a standard confusion matrix. The overall accuracy of the forest cover map including the class water accounted for 90.87%. Although only three classes have been separated, an overall accuracy of 91% can be considered an excellent result. Major source of errors was some confusion between very low biomass forest and non-forest. This is due to the fact that a landscape with indiscrete landcover was separated into discrete classes. The introduction of more forest classes related to different biomass levels could overcome this handicap. However, a new potential source of confusion would be introduced. On the other hand, some confusion between diverse forest classes might be seen as awkward as between diverse land cover types. A further source of errors is the partly inexact delineation image segments. This in particular affects the classification accuracy at the edges between unlike landcover types.

Regarding the achieved map results it gets obvious, that PALSAR data are very suited for large scale forest monitoring in Siberia. In particular, the implementation of winter coherence adds a new powerful dimension to the intensity data set. Due to the well intended ALOS observation strategy coherence images can be produced for whole Siberia.

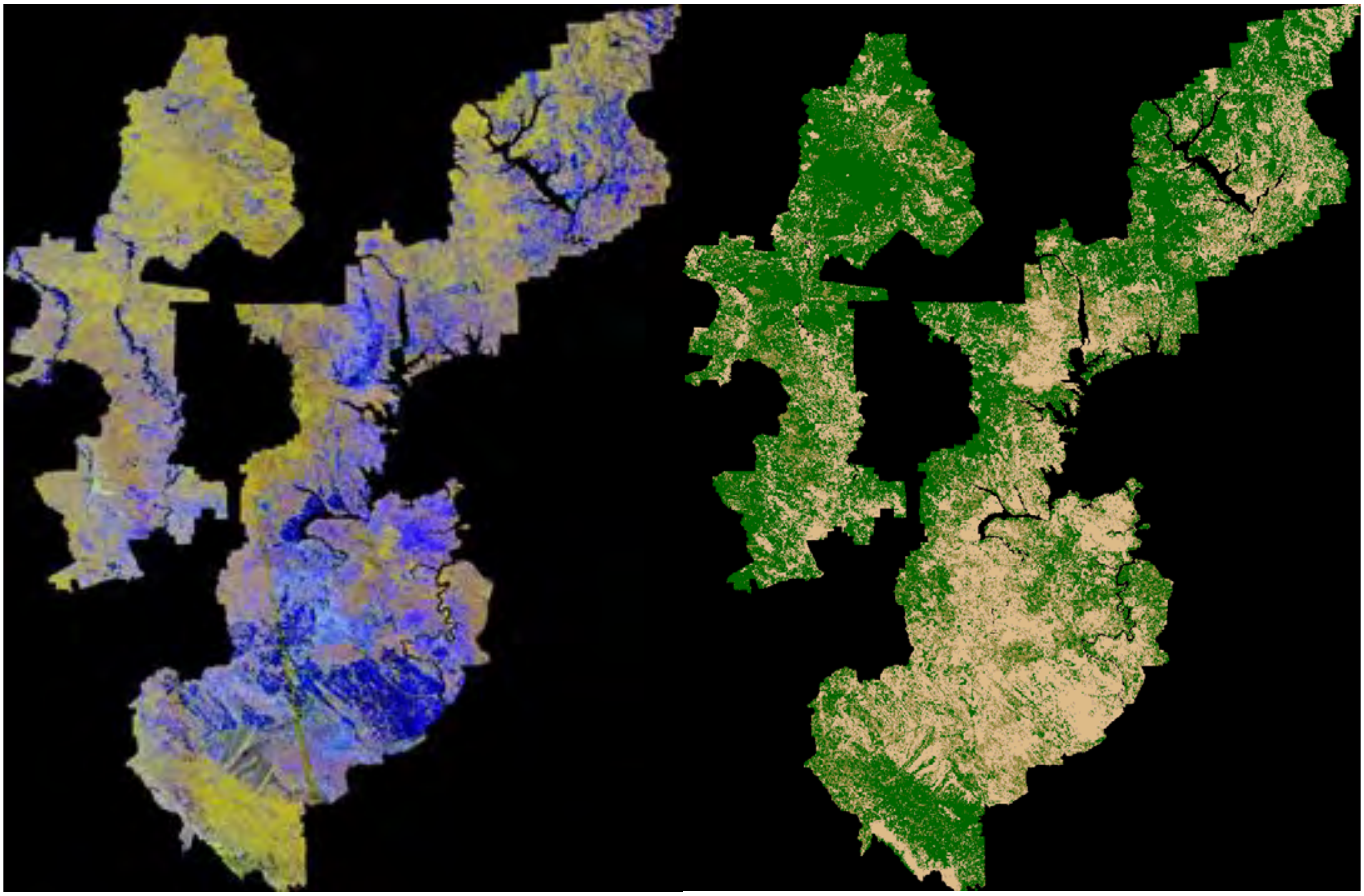

Figure 16: SAR data (left: HV/HH/Coherence) and forest cover map for the monitoring area; forest: green, very low biomass forest: brownish green, non-forest: light brown, ALOS K&C © JAXA/METI

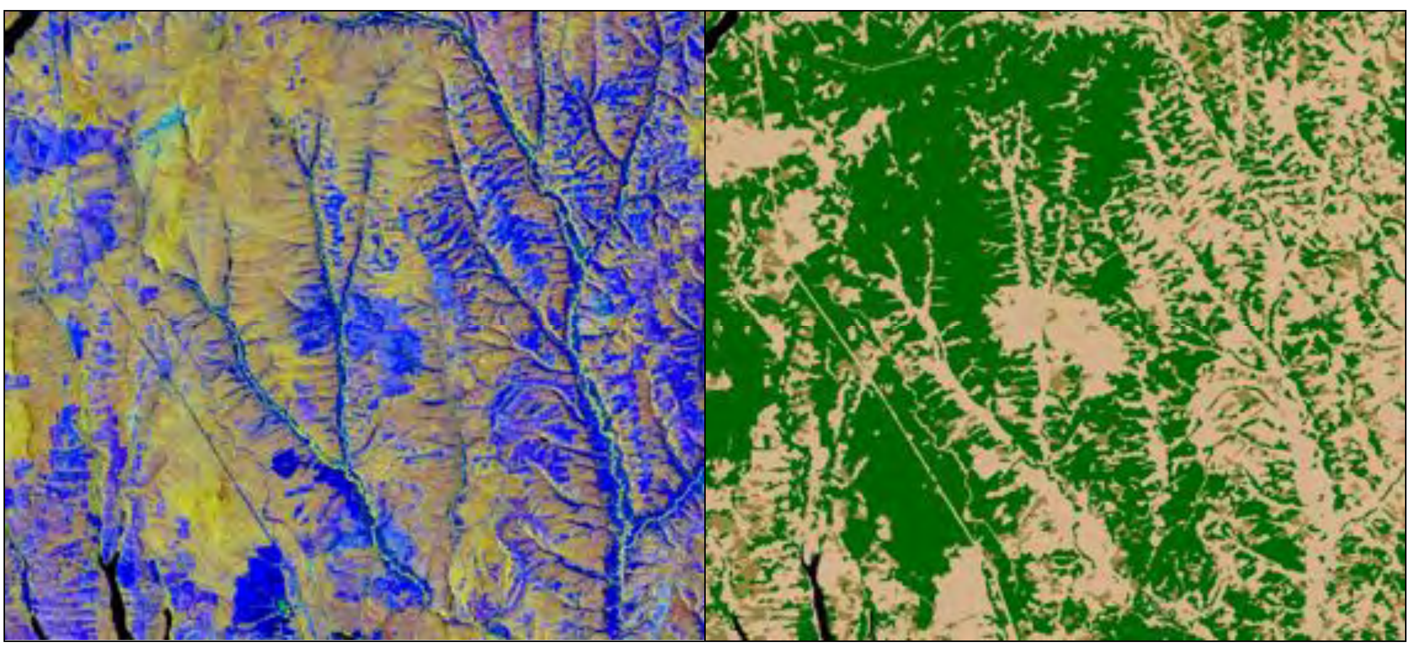

Figure 17: SAR data (HV/HH/Coherence) and forest map for subset (taken from north-eastern part) of the monitoring area; forest: green, very low biomass forest: brownish green, non-forest: light brown, ALOS K&C © JAXA/METI

4. REFERENCES

[1] Baatz, M. & A. Schäpe, “Multiresolution segmentation - an optimization approach for high quality multi-scale image segmentation” In: Strobl, J., T. Blaschke & G. Griesebner (eds) Proc. AGIT-Symposium Salzburg, Austria: 12–23, 2000.

[2] Benz, U.C., P. Hofmann, G. Willhauck, I. Langenfelder & M. Heynen, “Multi-resolution, objectoriented fuzzy analysis of remote sensing data for GIS-ready information”. ISPRS J. of Photogr. and Rem. Sens. 58: 239-258, 2004.

[3] Castel, T., A. Beaudoin, A. Stach, N. Stussi, T. LeToan & P. Durand (2001), “Sensitivity of space-born SAR data to forest parameters over sloping terrain. Theory and experiment”, Int. J. Rem. Sens. 22 (12): 2351-2376, 2001.

[4] Santoro, M., C. Werner, U. Wegmüller & O. Cartus, “Improvement of interferometric SAR coherence estimates by slope-adaptive range common band filtering”, Proc. IGARSS, Barcelona, Spain, 2007.

[5] Wegmüller, U., C. Werner, & T. Strozzi, “SAR interferometric and differential interferometric processing”, Proc. IGARSS, Seattle, USA, IEEE Publications: 1106-1108, 1998

[6] Wegmüller, U., “Automated terrain corrected SAR geo-coding”, Proc. IGARSS, Hamburg, Germany, 1999.

.

ACKNOWLEDGEMENTS

This work has been undertaken within the framework of the JAXA Kyoto & Carbon Initiative. ALOS PALSAR data have been provided by JAXA EORC.

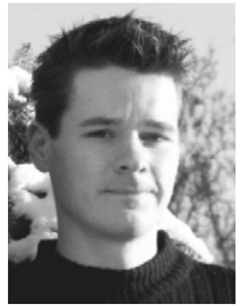

Christian J. Thiel received the Dipl. degree from the Friedrich Schiller University of Jena, Germany, in 2000 and the Ph.D. degree (with honours) from the Friedrich Schiller University of Jena, Germany, in 2004. Topic of his Ph.D. work was the investigation of polarimetric and interferometric airborne SAR data for the derivation of biophysical parameters.

Since 2004 he works as Research Project Assistant and was involved in various projects. Subject-matters have been the synergistic usage of optical and SAR-data for landcover classification, earth observation in support for transboundary aquifer management, utilisation of JERS-1 SAR-data for forest cover detection, and the operationalisation of earth observation based forestry applications. Dr. Thiel is also involved in the Kyoto and Carbon Initiative, dealing with large area PALSAR data applications focussing on forest.

Since 2006 he is chair assistant at the Earth Observation Department of the Friedrich-Schiller University Jena and head of the Radar Science and Applications section. His main scientific interests are the development and application of methods for retrieving geophysical parameters over land from active remote sensing data with a particular interest in soil moisture retrieval, forest cover mapping, and forest biomass assessment.

Forest Theme

Change in Forest Cover in Central Siberia using ALOS PALSAR

Thuy Le Toan *et al.*
CESBIO (France)

K&C Science Report – Phase 1

Change in forest cover in Central Siberia using ALOS/PALSAR

Thuy Le Toan
Centre d'Etudes Spatiales de la Biosphère
18 Avenue Edouard Belin, 31401 Toulouse Cedex 9, France
Thuy.Letoan@cesbio.cnes.fr

Collaborators
Mihai Tanase, Juan de la Riva
University of Zaragoza, Pedro Cerbuna 12, 50009, Zaragoza (Spain),
Email: mihai.tanase@tma.ro, delariva@unizar.es
Alexandre Bouvet
Centre d'Etudes Spatiales de la Biosphère
18 Avenue Edouard Belin, 31401 Toulouse Cedex 9, France
Alexandre.Bouvet@cesbio.cnes.fr
Maurizio Santoro
Gamma Remote Sensing AG, Worbstr. 225, CH-3073 Gümligen (Switzerland),
Email: santoro@gamma-rs.ch
Christiane Schmullius
Friedrich-Schiller-Universität (FSU), Jena, Germany
c.schmullius@uni-jena.de

***Abstract*— This paper presents a preliminary assessment of ALOS/PALSAR data from the Kyoto and Carbon Initiative program for monitoring changes in forest in terms of biomass loss and gain in central Siberia. The changes in forest area occurred during the last ten years were estimated using PALSAR data acquired in 2007 as compared to the forest map in 1997 using data from ERS1-ERS2 combined with JERS satellites (the SIBERIA-I project).**

The results obtained for the two study regions of Irkutsk and Krasnoyark which cover each about 5 millions of hectare indicate that the forest areas where biomass is lost (logging and fires) in 10 years are 12.2% of the area in Irkutsk and 16% in Krasknoyarsk, whereas the areas with increase in biomass account for 3.2 and 4.5% respectively in these two regions. This high rate of net loss (9% and 11.5% in 10 year) , around 1% per year, if validated, could be a concern for future development of the Siberian forests.

ALOS PALSAR data proved particularly useful for providing information relevant to carbon budget calculation and to the assessment of forest states, from logging to regrowth during the first decades after disturbances in Siberia.

***Index Terms*—ALOS PALSAR, K&C Initiative, forest biomass, SIBERIA-I.**

I. INTRODUCTION

The loss and degradation of forests worldwide has significant implications for the Earth system. The burning of forest biomass and removal or felling of timber have contributed to the additional burden of CO_2 in the atmosphere and the associated changes in climate. Clearance, degradation and fragmentation of forests have also resulted in significant losses of biodiversity and resources of social and economic importance.

Increased awareness of these impacts has led to a number of international conventions including the UN Framework Convention on Climate Change (UNFCCC), its Kyoto Protocol contributing to the preservation, enhancement and long-term sustainability of global forest carbon stocks. Large areas of forest are also regenerating naturally and these forests play a key role in the recovery of the carbon lost.

For this reason, there is a need to continue the mapping of forests on a regular basis and to assess the changes in extent and condition (in terms of structure and biomass) so that processes and drivers of change can be better quantified. For reporting to international agreements, there is also a requirement to retrieve specific data relating to the carbon budgets associated with these forests. Although considerable advances have been made in these areas in recent years,

significant obstacles still remain in terms of collecting and collating relevant and timely data.
In this context, the objective of this study is to assess the contribution of ALOS PALSAR data to provide better estimates of biomass losses and gains associated with the clearance and growth of regenerating forests. The focus is put on the boreal forests in central Siberia where forest, and which retains much less attention of the scientific community as compared to tropical and temperate forests.

The forests of Siberia constitute about 20% of the total world forested area and nearly 50% of the total world coniferous-forested areas. The Siberian forests have recently become an important topic of debate. The first reason of interest is that Siberian forests are considered in recent studies only as a weak carbon sink, however the studies show large uncertainties in the sink estimates. The second reason for this interest is concerned with the ongoing exploitation of forest resources. When combined with natural hazards, over exploitation may cause deterioration of the environment, especially when considering the boreal forest low recovery rate.

I. OBJECTIVE

The objective of this study was to quantify the change in forest cover and biomass occurred during the last ten years in two selected sites located in central Siberia. This has been achieved by comparing ALOS PALSAR data acquired in 2007 and the biomass/land-cover map obtained in the SIBERIA-I (SAR Imaging for Boreal Ecology and Radar Interferometry Applications) Project based on data acquired in 1997.

II. DESCRIPTION OF THE PROJECT

A. Relevance to the K&C drivers

The use of ALOS data to quantify changes in forest condition, is in accordance with the Carbon driver outlined in the K&C Science Plan [1]. The ALOS PALSAR is expected to facilitate estimation of changes in biomass associated with deforestation and degradation (clearing, felling of timber) and to monitor regeneration through temporal comparison of SAR backscatter data up to the levels of saturation. Relating such changes to fluxes of carbon is difficult given uncertainties in the processes of decomposition and regeneration and the rates of change [2]. For example, Schulze *et al*. (1999) [3] suggest that several decades may pass before the Net Primary Productivity (NPP) of regenerating forests on cleared land in Siberia exceeds heterotrophic respiration, largely because of the decomposition of dead biomass. Nevertheless, by integrating models and observations of carbon dynamics with forest cover or change information generated using PALSAR data (either singularly or in combination with other remote sensing data), improved estimates of carbon flux may be obtained [4], [5] .

B. Work approach

ALOS PALSAR K&C data have been first assessed for mapping of forest cover and biomass classes, using high resolution optical data and forest inventory database. In order to compare the mapping results with the map provided by SIBERIA-I, the biomass class definition is based on the SIBERIA-I classification scheme. Detection of changes is conducted in the second phase, where areas of biomass loss and gain are highlighted.

C. Satellite and ground data

Site selection was conditioned by the availability of PALSAR data and the extent of SIBERIA-I product. The SIBERIA-I Project was an international effort to map Siberian boreal vegetation using SAR backscatter and interferometric data acquired by the ERS-1/2, and JERS satellites [6]. Data were classified in four growing stock volume classes (0-20, 20-50, 50-8- and > 80 m3/ha), a smooth area class and a water body class [7]. This SIBERIA map represents a snapshot of the forest cover for a 1,000,000 km2 area of Central Siberia (see also Fig. 1) for the years 1997-1998.

Two sites covering about 50.000 km^2 each were selected. The first is the Irkutsk site situated about 250 km north of Bratsk. The second is the Krasnoyarsk site, located westwards at about 190 km north of Kansk city. The relief is represented mainly by plateaus and hills, almost 90% of the surface lying below 500 meters a.s.l. More than 95% of the slopes are below 8^0, the whole territory being within the typical boreal forest zone.

PALSAR data used in the study were acquired during summer 2007 (cycles 12 and 13) in fine beam dual polarization (FBD) mode (polarizations HH and HV). Data from paths 460 to 468 and 473 to 484 were processed and geocoded using a Shuttle Radar Topography Mission (SRTM) derived digital elevation model (DEM).

Figure 1 shows the SIBERI-I map and the location of the two testregions analysed using PALSAR data.

Very high resolution optical data (available in Google Earth) are used for analysis and qualitative validation, whereas forest database provided by IIASA (ref) are used in the analysis.

D. Processing and results

PALSAR data were provided as long strips multi-looked intensity images in slant range geometry [8]. The processing steps described in [9] includes transformation to backscattering coefficient and geocoding, strip mosaicking, and co registration to SIBERIA-I map.

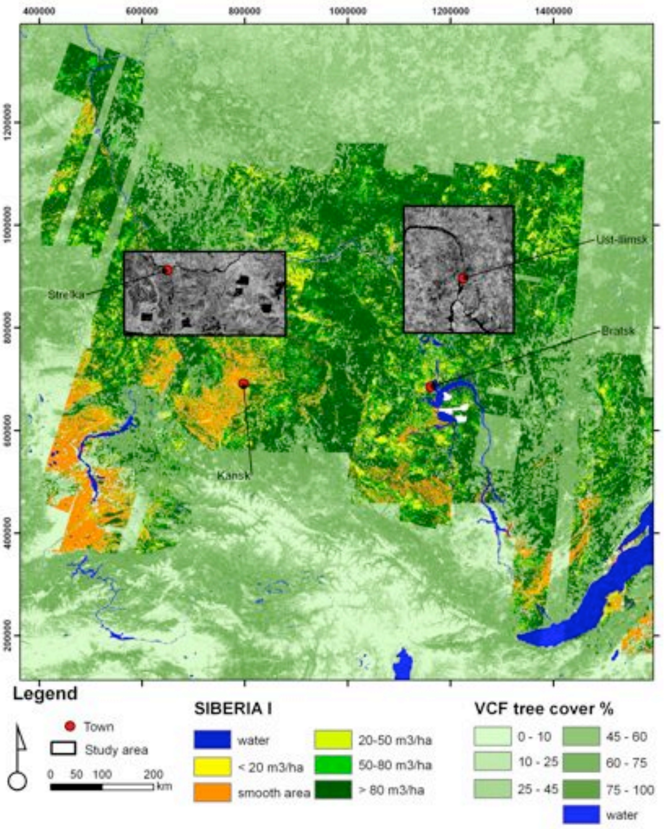

Figure 1: Map of Central Siberia (Baikal lake in the bottom right), where SIBERIA-I and the two PALSAR study regions are localized.

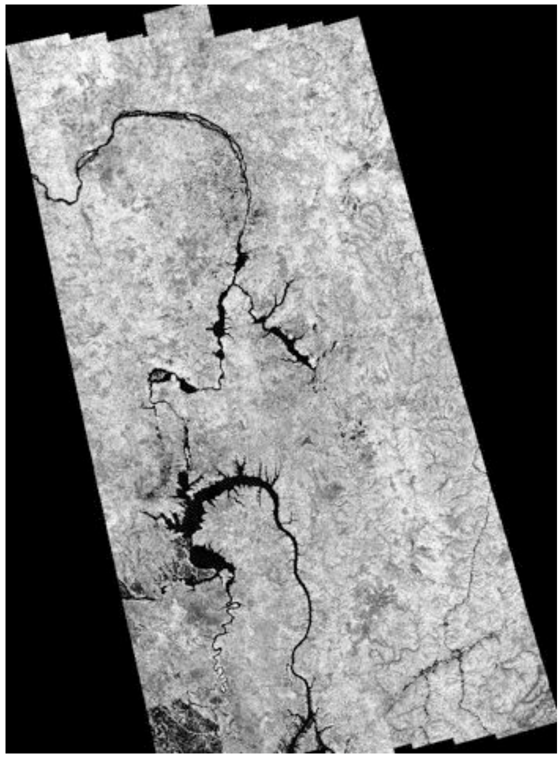

Figure 2: Mosaic of the PALSAR strip images of the Krasknoyarsk region.

Efforts have been put to compensate some of the error sources in strip mosaicking (i.e. errors related to data acquisition - radiometric accuracy, changing weather, and errors related to SAR processing - inter-strip co-registration).

Figure 2 shows the resulting mosaic covering the region of Krasknoyarsk.

E. Classification

The classification scheme was developed based on the data analysis results and the need of matching SIBERIA`s classes. A classifier based on HH and HV backscatter and their ratio was used. The analysis of the backscatter values was done based on sample polygons digitized using very high resolution optical satellite imagery (VHR). More than two hundred samples, equally distributed between three provisional classes (*open areas, low biomass forests* and *high biomass forests*) were selected for the Irkutsk site. These classes were preferred because their visual discrimination was possible on VHR optical imagery.

To fine tune these classes into SIBERIA like classes (*i.e. forests <50 m^3/ha, forests 50-80 m^3/ha and forests >80 m^3/ha)* a second backscatter analysis was carried out in 1067 polygons of Russian forest inventory parcels [10]

The classification method based on the data analysis has been described in [9] and applied to the two test regions. Figure 3 shows a subset of classification result for the region of Krasknoyarsk, where the percentage cover was found to be 59% of forests > *80 m^3/ha, 15% for class 50-80 m^3/ha, 19% for forests <50 m^3/ha, 5% of smooth area, and 1.5% of water.* This is interesting to note that only 60% of the pixel area are forests of more than *80 m^3/ha (or about 50 ton/ha).*

F. Change detection

To evaluate the percentage of area with forest biomass loss and gain, the classification scheme of both SIBERIA and PALSAR data are compared on a pixel basis. Due to the high confusion errors for the intermediate forest classes (50-80 m3/ha) a reduced number of classes was implemented, where classes 50-80 m^3/ha and > 80 m^3/ha are merged to a class of > 50 m^3/ha. Reducing the number of classes greatly diminishes classification uncertainties, assessed using validation data even though it reduces the sensibility of the change detection algorithm to small biomass changes. In Siberia small changes (for the considered time interval) represent mostly growing processes.

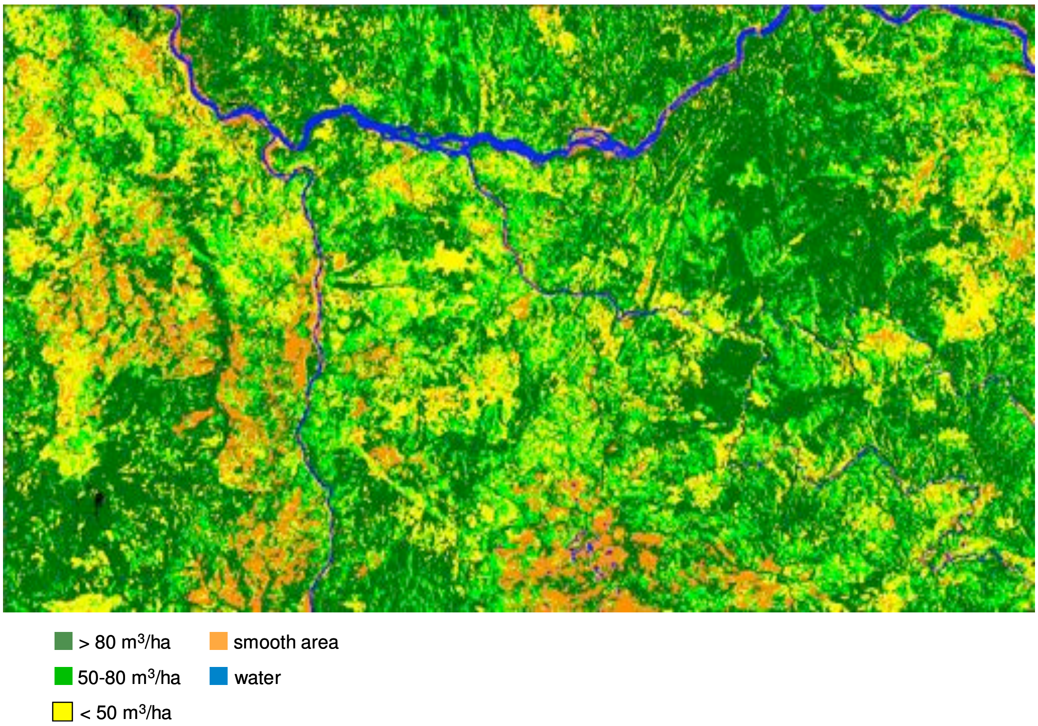

Figure 3: Map of land cover in the region North of Krasknoyarsk, central Siberia, using ALOS PALSAR FBD data acquired in 2007. The forests are mapped in three classes of growing stock volume (< 50 m^3/ha, 50-80 m^3/ha and > 80 m^3/ha) and smooth areas including agriculture and grassland. The map covers an area of 314 km x 163 km, crossed by the large Angara river in the North.

Due to slow growth ten years are not always sufficient for forests to pass from 0 m^3/ha to the 50 m^3/ha, and thus only some of the areas classified as less than 50 m^3/ha will be recorded by the change detection algorithm as surface with biomass gain. Consequently areas presenting biomass gains will be to a certain degree underestimated. On the other side clear cuts and fires will be certainly recorded since changes from forest to open area take place much faster and there are less chances of confusion. Therefore, a certain overestimation of the net forest surface loss is unavoidable when considering this method. In addition, the values registered by area with biomass loss and gain could be partially resulted from misclassification especially between classes *forest <50 m^3/ha* and *forests >50 m^3*

Class	*SIBERIA*	→	*PALSAR FBD*	*Irkutsk (%)*		*Krasnoyarsk (%)*	
Biomass loss	forest >50 m^3/ha	→	forest <50 m^3/ha	9.6		11.4	
	forest >50 m^3/ha	→	smooth areas	1.1	**12.2**	1.2	**16.0**
	forest <50 m^3/ha	→	smooth areas	1.5		3.4	
Biomass gain	smooth areas	→	forest <50 m^3/ha	0.1		0.1	
	smooth areas	→	forest >50 m^3/ha	0.02	**3.22**	0.04	**4.54**
	forest <50 m^3/ha	→	forest >50 m^3/ha	3.1		4.4	
Stable forest	forest >50 m^3/ha	↔	forest >50 m^3/ha	69.1		58.5	
Stable smooth fields & open areas	smooth areas	↔	smooth areas	0.5		2.3	
	forest <50 m^3/ha	↔	forest <50 m^3/ha	7.9		6.7	
Water	water	→	water	2.7		1.2	
	not classified	→	water	0.3		0.3	
Other changes	all other changes			0.4		0.4	
Not classified	not classified Siberia or Palsar			3.8		10.1	

Table 1. Change detection - class correspondence SIBERIA ↔ PALSAR FBD of the two test regions.

Figure 4 shows a part of the map of changes in the Krasknoyarsk region. The subset PALSAR image shows clearly areas of forest exploitation of geometrical shape. The over all dynamics of biomass loss and gain in the 10 year interval can be thus materialized.

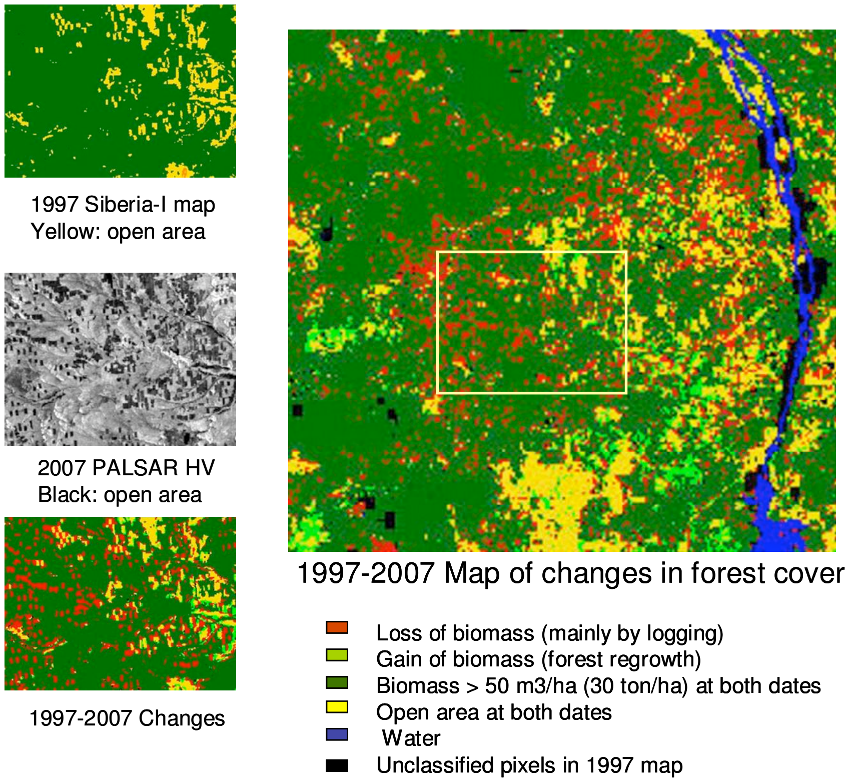

Figure 3: Right: map of changes in forest biomass in ten years (1997-2007) in the region North of Irkutsk. The map covers an area of about 120 km x 120 km, with the Angara river on the East. Left: Details of the 1997 and 2007 data and mapping result for the 40 km x 30 km subset delineated in the right figure. This includes SIBERIA-I forest map in 1997 (top), PALSAR HV image 2007 (middle) and map of changes in biomass (bottom). Note the large size of logged areas visible on the subset images.

III. CONCLUSIONS

This paper illustrates the change in forest areas associated to biomass loss and gain in Siberia as assessed using PALSAR data and the SIBERIA-I map. Two sites covering around 100.000 km^2 (or 10 Million hectares) located in the central part of Siberia have been studied.
During the last decade the percentage of the area where biomass is lost are 12.2% in Irkutsk and 16% in Krasknoyarsk, whereas the areas with increase in biomass account for 3.2 and 4.5% respectively in these two regions. The rate of net loss is thus 9% and 11.5% in 10 years, or about 1% per year. In addition, forest net loss estimates are higher for Krasnoyarsk site (11.5%) than for Irkutsk area (9%) suggesting a more active deforestation process in the eastern part of central Siberia. The similar forest net loss amount on both studied sites indicates comparable management practices at the level of the whole central Siberia.
The results and their uncertainties still need further assessment. However, the study shows clearly that area of biomass increase is much smaller than area of biomass loss. This may suggest unsustainable management policies.

The study needs to be pursued using multi year PALSAR data to detect area of forest exploitation and to evaluate the rate of exploitation. ALOS K&C Initiative provides the opportunity for such assessment during its timelife, and hopefully, during the ALOS follow-on mission.

.

IV. ACKNOWLEDGMENTS

This work has been undertaken within the framework of the JAXA Kyoto & Carbon Initiative. ALOS PALSAR data have been provided by JAXA EORC. We warmly acknowledge M. Shimada and A. Rosenqvist. This work has been financed by the Spanish Ministry of Science and Education and the European Social Fund: FPI grant BES-2006-11684 and project CGL2005-04863.

V.REFERENCES

[1] A. Rosenqvist, M. Shimada, R. Lucas, J. Lowry, P. Paillou, B. Chapman [eds.], “The ALOS Kyoto & Carbon Initiative, Science Plan (v.3.1),” JAXA EORC, March, 2008. [Online] Available: http://www.eorc.jaxa.jp/ALOS/kyoto/KC-Science-Plan_v3.1.pdf

[2] Houghton RA (2005) Above Ground Forest biomass and the global carbon balance, Global Change biology, 11, 945-958, 2005.

[3] Schulze, E. D., Lloyd, J., and Kelliher, F.M.: 1999, 'Productivity of forests in the Euroboreal region and their potential to act as a carbon sink - a synthesis', Global Change Biology 5, 703-722.

[4] Kurz W.A., and Apps M.J.: 1999, 'A 70 year retrospective analysis of carbon fluxes in the Canadian forest sector', Ecological Applications 9, 526-547.

[5] Le Toan T., S. Quegan, I. Woodward, M. Lomas, N.Delbart and G. Picard, "Relating radar remote sensing of biomass to modelling of forest carbon budgets, J. of Climatic Change, Volume 67, Number 2, pp. 379 - 402 , December 2004.

[6] 3. Schmullius, C. (ed.). SIBERIA final report. FSU Jena. Available at http://www.siberia1.uni-jena.de/, last accessed June 2008

[7] 1. Wagner, W., Luckman, A. , Vietmeier, J, Tansey , K., Balzter, H., Schmullius, Ch., Davidson, M., Gaveau, D., Gluck, M., Le Toan, T., Quegan, S., Shvidenko, A., Wiesmann, A. & Jiong Jiong, Y. (2003). Large-scale mapping of boreal forest in SIBERIA using ERS tandem coherence and JERS backscatter data. Remote Sensing of Environment 85(2), 125-144.

[8] M. Shimada, “PALSAR and Calibration update”. 11th ALOS K&C Science Team meeting (KC#11), Tsukuba, Japan, Jan. 13-16, 2009. [Online] Available: http://www.eorc.jaxa.jp/ALOS/kyoto/jan2009_kc11/pdf/090113/shimada_calval_up_090113.pdf

[9] Tanase M., T. Le Toan, J. de la Riva , M. Santoro, ‘An estimation of changes in forest area using multitemporal SAR data’ Proceedings of the ALOS Symposium, November 2008.

[10] Schvidenko A. and Nilsson S. (2002) Dynamics of Russian forests and the carbon budget in 1961-1998: An assessment based on long term forest inventory data. Climatic Change.

VI. BIOGRAPHY

Thuy Le Toan has a PhD in atomic and nuclear physics from the University of Toulouse, France. She has been the Head of the Remote Sensing research team in the Centre d’Etudes Spatiales de la Biosphère (CESBiO). Her research activity has been in the area of microwave remote sensing for land applications, including experimentation and modelling of microwave interaction with agricultural and forested media, and analysis of SAR images. Her current interest is on the use of remote sensing data to characterise the land processes and to quantify their impacts on the carbon cycle.

She is member of the Kyoto and Carbon Initiative Science team. She is the chairperson of the Mission Assessment Group of BIOMASS, the satellite mission candidate to the ESA Earth Explorer Core mission, retained for the pre-feasibility phase, in May 2006, and for the phase A in March 2009.

Forest Theme

Synergetic Use of ALOS PALSAR, ENVISAT ASAR and Landsat TM/ETM+ Data for Land Cover and Change Mapping

Francesco Holecz *et al.*
sarmap (Switzerland)

K&C Science Report – Phase 1

Synergetic Use of ALOS PALSAR, ENVISAT ASAR and Landsat TM/ETM+ Data for Land Cover and Change Mapping

Francesco Holecz, Massimo Barbieri, Alessio Cantone, Paolo Pasquali, and Stefano Monaco
sarmap – Cascine di Barico, 6989 Purasca, Switzerland – www.sarmap.ch
fholecz@sarmap.ch

***Abstract*—Interferometric ALOS PALSAR Fine Beam Single/Dual, multi-temporal ENVISAT ASAR Alternating Polarization, and Landsat-5 TM/-7 ETM+ data are used for the generation of land cover and change maps. In synthesis, the product generation foresees two main steps: The first one consists in a rigorous data pre-processing, including interferometric processing (PALSAR), geometric / radiometric calibration (PALSAR, ASAR, TM/ETM+), and multi-temporal speckle filtering (PALSAR, ASAR); as result, terrain geocoded coherence, sigma nought, and top-of-atmosphere reflectance products are obtained. The second part is dedicated to data classification and fusion. Classification is performed by means of a prior knowledge-based approach exploiting interferometric, multi-temporal intensity, and spectral signatures. Data fusion and change detection are subsequently applied at semantic level. Results – based on acquisitions over Malawi (country-wide) and on an area in Brazil – show that the synergetic use of data provided by these sensors allows the reliable identification of key land cover types (in primis cropped areas, bare soil areas, sparse and dense vegetated areas, forest clear cuts and burnt areas, water bodies) and their evolution over time, aimed at gathering essential information on the land cover status. In addition, it is shown that using the same repeat-pass interferometric ALOS PALSAR data pair, a Digital Elevation Model (DEM) with higher quality than the Shuttle Radar Topographic Mission (SRTM) can be generated unless the area is densely vegetated.**

***Index Terms*—ALOS PALSAR, ENVISAT ASAR, K&C Initiative, data calibration, prior knowledge-based classifier, data fusion, change detection.**

I. INTRODUCTION

Spaceborne Remote Sensing is the only reliable system to collect systematic data at frequent rates over large areas. Therefore, it can be considered as a tool to observe the spatial and temporal aspects of land cover changes. Although an analysis of current and forthcoming sensors pointed out that there is a wide range of information which can be derived from SAR (Synthetic Aperture Radar) and optical data – in particular high resolution – it remains a fact that its use is still limited today. In order to transform this (often) huge amount of multi-temporal multi-source data into information, automated data understanding techniques are mandatory, as ground truth data, required by traditional inductive supervised data learning image classification techniques to be trained on a scene-by-scene basis, and ancillary (e.g., atmospheric) information are typically tedious, expensive, and either difficult or impossible to gather at several locations within image area at the time of image acquisition.

Prior to the ALOS mission, JAXA in collaboration with the K&C team, performed a careful PALSAR data acquisition planning, leading – for the first time – to the acquisition of a multi-temporal, multi-scale L-band data set at global level. Thanks to the availability of this unique multi-temporal data set and to the synergy with other remote sensing spaceborne systems, valuable remote sensing based products – country-wide – can be generated for the mapping and monitoring of land use and natural resources of our planet.

The work proposed within this initiative is essentially focused on the synergetic use of SAR (ALOS PALSAR and ENVISAT ASAR) and optical (Landsat TM/ETM+) data, by considering:

- A rigorous data pre-processing aimed at obtaining terrain geocoded coherence, sigma nought and top-of-atmosphere reflectance products.
- A first level prior knowledge classifier requiring, as input, data radiometrically calibrated into physical values belonging to a common radiometric scale.
- A second level prior knowledge classifier requiring, as input, the semantic layers of the first level classification and temporal features derived from SAR intensity time-series.

II. METHOD

The processing chain, as illustrated in the data flow diagram in Figure 1, consists of six modules (yellow boxes). Each module, which includes one or a set of functions (grey boxes), provides an intermediate (bright purple boxes) or final product (dark purple boxes). Remote Sensing input data are highlighted in magenta, while Digital Elevation Model (DEM) data are in cyan.

Purpose and functionality of each module are:

1. First Level Optical Classifier

The purpose of this module is to generate, based on top-of-atmosphere calibrated reflectance data, spectral classes. Recently, an original fully automatic modular hierarchical top-down prior spectral knowledge-based classifier capable of detecting a set of kernel (i.e. reliable) spectral layers in calibrated optical data was proposed by Baraldi et al. [1].

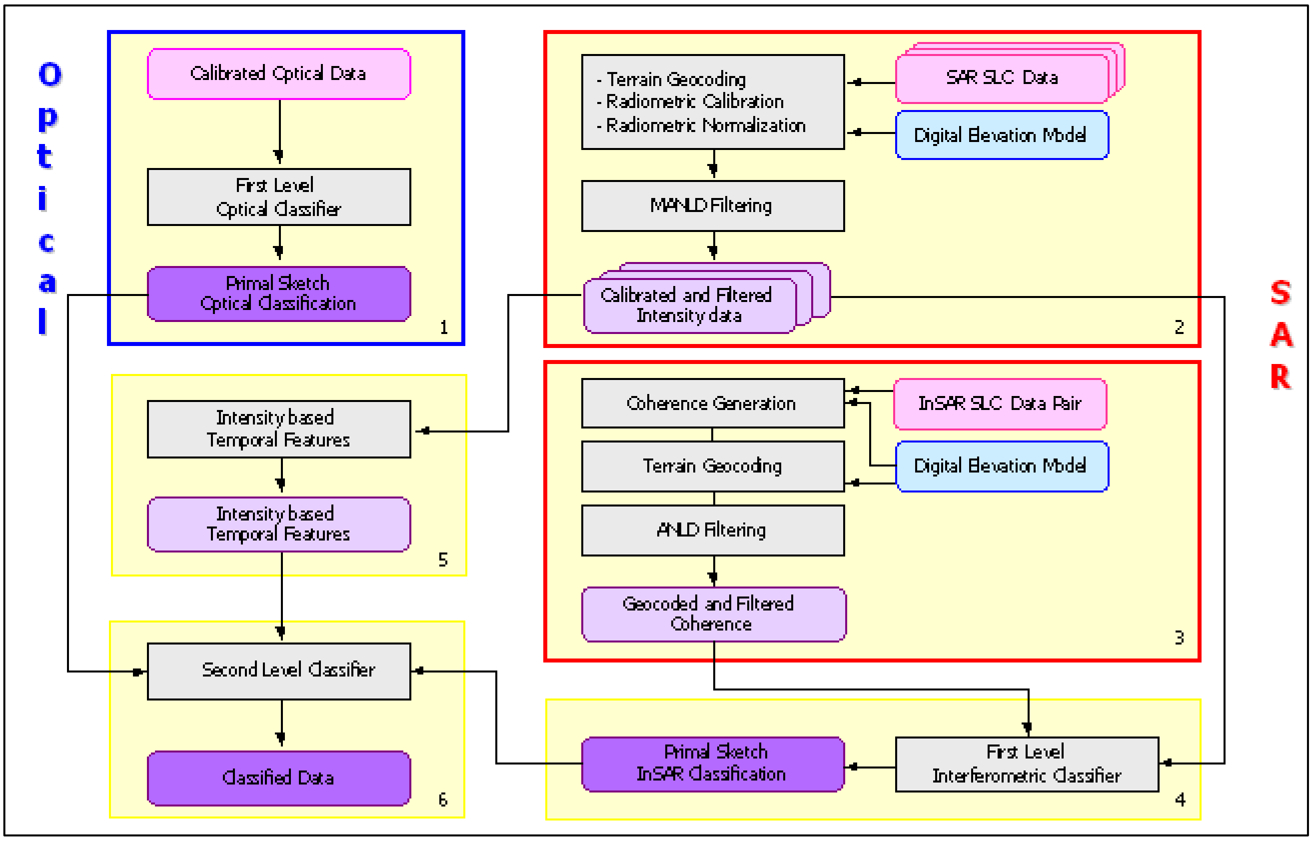

Figure 1. Data Flow Diagram.

In essence this system uses kernel spectral to mimic well-known spectral signatures of target land covers. Based on prior knowledge exclusively, the proposed classifier requires no training and supervision to run, i.e., it is fully automatic. Its output map consists of spectral classes provided with a symbolic meaning. Each of the identified spectral classes is associated with a USGS land cover index, thereby enabling a link between spectral and thematic categories. Furthermore, the proposed algorithm allows to generate a set of spectral features – such as Canopy Chlorophyll Content, Canopy Water Content, Greenness Index, and Water Index – determining, for each pixel, additional (and complementary) quantitative information.

Although this work is based on the use of Landsat TM/ETM+ data, the same approach can be applied to other optical sensors, as the implemented algorithms fully support data acquired by AVNIR-2, SPOT-1,2,4,5, LISS III,IV, AWiFS, and MODIS data.

2. Processing of multi-temporal SAR Intensity

The aim of this module is to generate calibrated (in geometric and radiometric terms) and multi-temporal speckle filtered SAR intensity data. It is anticipated that the provided algorithms [2,3] are sensor independent, hence supporting the process of SAR Single Look Complex (SLC) data of all existing spaceborne, prior the availability of the necessary processing and platform parameters.

Within this initiative, three data types are considered, i.e. ALOS PALSAR Fine Beam Single / Dual polarization and ENVISAT ASAR Alternating Polarization data.

For what concerns the SAR filtering method, conventional single-date and multi-temporal approaches which are based on probability density functions, perform well under strictly controlled conditions, but they are often limited with respect to sensor synergy and to the temporal aspect, where complex joint probability density functions must be considered. The drawback of existing speckle filters is that they are strongly sensor and acquisition mode dependant, because based on the scene statistic. Moreover, if features masks are used, an accuracy loss is introduced when regarding particular shape preservation. This is mainly due to the lack of a priori information about size and type of the features existent in the image. By taking advantage of the redundant information available in multi-temporal series, while being fully independent regarding the data source, a multi-temporal anisotropic diffusion scheme is proposed [4].

3. Interferometric Processing

The purpose of this module is to generate terrain geocoded coherence data. As in the previous module, the provided algorithms are sensor independent. Within this initiative ALOS PALSAR Fine Beam Single and Dual polarization interferometric data are exploited. Due to the temporal decorrelation at C-band, ENVISAT ASAR could not be used.

Concerning coherence estimation, usually it is estimated by setting a moving window with fix dimensions. The drawback of this method is that, due to the fix window size, coherence values are not optimally estimated (in particular when the window is too small), because the filter is not spatially adaptive. For this reason an alternative approach is proposed, which takes advantage from an anisotropic non linear diffusion method.

4. First Level Interferometric Classifier

An interferometric data pair enables the estimation of coherence, which is a measure of the phase noise of the interferogram, and it depends upon sensor parameters, parameters related to the imaging geometry, and object parameters. A general rule of thumb is that high coherence values correspond to small changes (coherent changes) or no temporal variations – meaning that the objects are stable – while volume scattering and temporal changes (incoherent changes) are related to low coherence values. In this latter cases, where the coherence values tend to approach the noise level, the backscattering coefficient of both acquisitions – in primis in terms of average and difference – provides useful information to determine the main land cover types and their changes.

The proposed algorithm has been developed based on the characteristics of interferometric Fine Beam Single and Dual polarization data. It is worth mentioning that the use of these images for interferometric applications have been extensively demonstrated within the ESA project *Prototype Processor for ALOS PALSAR Data and Polarimetric Interferometric Products Generation* [5]. The adopted algorithm's strategy has been derived from [1]: obviously, in this case, kernel spectral rules are not designed to mimic well-known spectral signatures of land covers, but to the object's single- and multi-date backscattering properties at L-HH and/or L-HV polarization and to the corresponding coherence signature. The classification therefore, intrinsically, does not include only main classes related to the object, but also classes linked to the object's temporal changes. It has to be pointed out that the rules have been derived from the literature, in particular from [6], and through the analysis of PALSAR interferometric scenes acquired over different agro-ecological zones, geographic areas and time periods. Finally, the class names, indicate general land cover categories (for instance dense vegetation) rather than thematic classes (for instance forest).

5. Temporal Features

The purpose of this module is to generate key temporal features based on multi-temporal ENVISAT ASAR Alternating Polarization data set.

6. Second Level Classifier

The purpose of this module is twofold. The first one is to provide a classification based on the synergy of interferometric PALSAR Fine Beam Single polarization and multi-temporal ENVISAT ASAR Alternating Polarization data. The second one is to derive a land cover and change detection map based on interferometric PALSAR Fine Beam Dual polarization data and optical (Landsat-5 TM in this case). It is anticipated that, in both cases, a prior knowledge-based approach underpins the inference of land cover classes and changes. In the first case, the primal sketch interferometric classification (outcome module 4) drives the use of temporal features derived from SAR intensity time-series (outcome module 5). In the second one, primal sketch classifications (outcome module 1 and 4) are inputted into the classifier.

The fundamental idea, in both cases, is based on the fact that thematic information and/or changes can be retrieved in a semantic way (since a common denominator between the different data sources has been established) rather than at signal level, as conventionally done. In fact, knowing the symbolic (spectral, interferometric, multi-temporal or pseudo-thematic) name of two input classes, the output class can be assigned by means of logic relationships. For instance, if in the first acquisition date, the identified pseudo-thematic class is snow, and, in the second date, the pixel is classified as clear water, the resulting class will be melted snow.

III. DATA SETS

Two different data sets are used: Malawi – country-wide, i.e. around 100,000 sqkm area coverage – and Brazil – the area covered by an ALOS PALSAR standard frame.

Malawi – The following data are used:

- ALOS PALSAR Fine Beam Single polarization SLC data acquired on:
  - 20 November 2007
  - 05 January 2008
  - 20 February 2008
- ENVISAT ASAR Alternating Polarization Mode SLC data acquired on:
  - 23 July 2007
  - 27 August 2007
  - 01 October 2007
  - 05 November 2007
  - 18 November 2007
  - 10 December 2007
  - 14 January 2008
  - 18 February 2008
  - 02 March 2008
- Shuttle Radar Topographic Mapping Digital Elevation Model.

All products are referenced to the UTM zone 36, Northern hemisphere, WGS-84 system, grid size of 15m.

Brazil – The following data are used:

- Landsat-5 TM data acquired on September 1986;
- ALOS PALSAR Fine Beam Dual polarization SLC data acquired on 20 June and 5 August 2007;
- Shuttle Radar Topographic Mapping Digital Elevation Model.

All products are referenced to UTM zone 22, Southern hemisphere, WGS-84 system, grid size of 15m (PALSAR) and 30m (Landsat-5 TM).

IV. RESULTS AND SUMMARY

The results based on the two data sets – and illustrated in Figure 2, 3, and 4 – are generated according to:

- Malawi: modules 2,3,4,5,6;
- Brazil: modules 1,2,3,4,6.

Note that all data processing are performed using SARscape® a sarmap proprietary software.

The results obtained so far indicate that the synergetic use of interferometric PALSAR Fine Beam Single and Dual polarization data with multi-temporal ASAR Alternating Polarization or single-date Landsat TM/ETM+ data enables the reliable identification of main land cover types and their evolution over time. Furthermore, the proposed approach provides, additionally and in an automated way, the location (where) and the type (what) of the change.

Concerning product's reliability, the obtained accuracy is in the order of 80% for Malawi [7], and significantly higher than 90% for Brazil [8]. It is worth mentioning that, in both cases, the products have been validated using in situ data: 1,213 points in 76 clusters for Malawi, 30 points for Brazil. The main reason of the lower accuracy reported in Malawi, with respect to the Brazil, is primarily due to the fact that some features (for instance cropped areas), in general, are heterogeneous and of limited dimension (i.e. less than 1 ha).

In these specific cases, due to the mixed nature of the pixels, classification inaccuracies are observed. A higher spatial resolution, which will be available with ALOS PALSAR-2, would strongly reduces the presence of mixed pixels, hence significantly contributing to improve the overall accuracy.

Furthermore, given the spatial resolution of ALOS AVNIR-2 data (10 meters) and the radiometric high quality of these data, it is planned, in the next phase (2009-2011), to additionally exploit images acquired from this sensor. Moreover, very high resolution stripmap SAR data (3 meters), acquired by the COSMO-SkyMed satellite constellation [9], will be integrated in the current processing chain. Based on this new data scenario, it is thereby planned to extend the second level classifier to support the use of textural features and geometric descriptors.

Finally, given the availability of suitable interferometric ALOS PALSAR data pair, the capability of, and the limitation to, the generation of a Digital Elevation Model in the two areas is additionally analyzed. In synthesis: in Brazil – due to the presence of very dense forest – the quality of the resulting DEM is very poor. In Malawi, on the other hand, the obtained quality is doubtless higher than the SRTM DEM, particularly with respect to the spatial details resulting from the better spatial resolution (10 meter of PALSAR Fine Beam Single polarization against the 90 meter interpolated SRTM DEM).

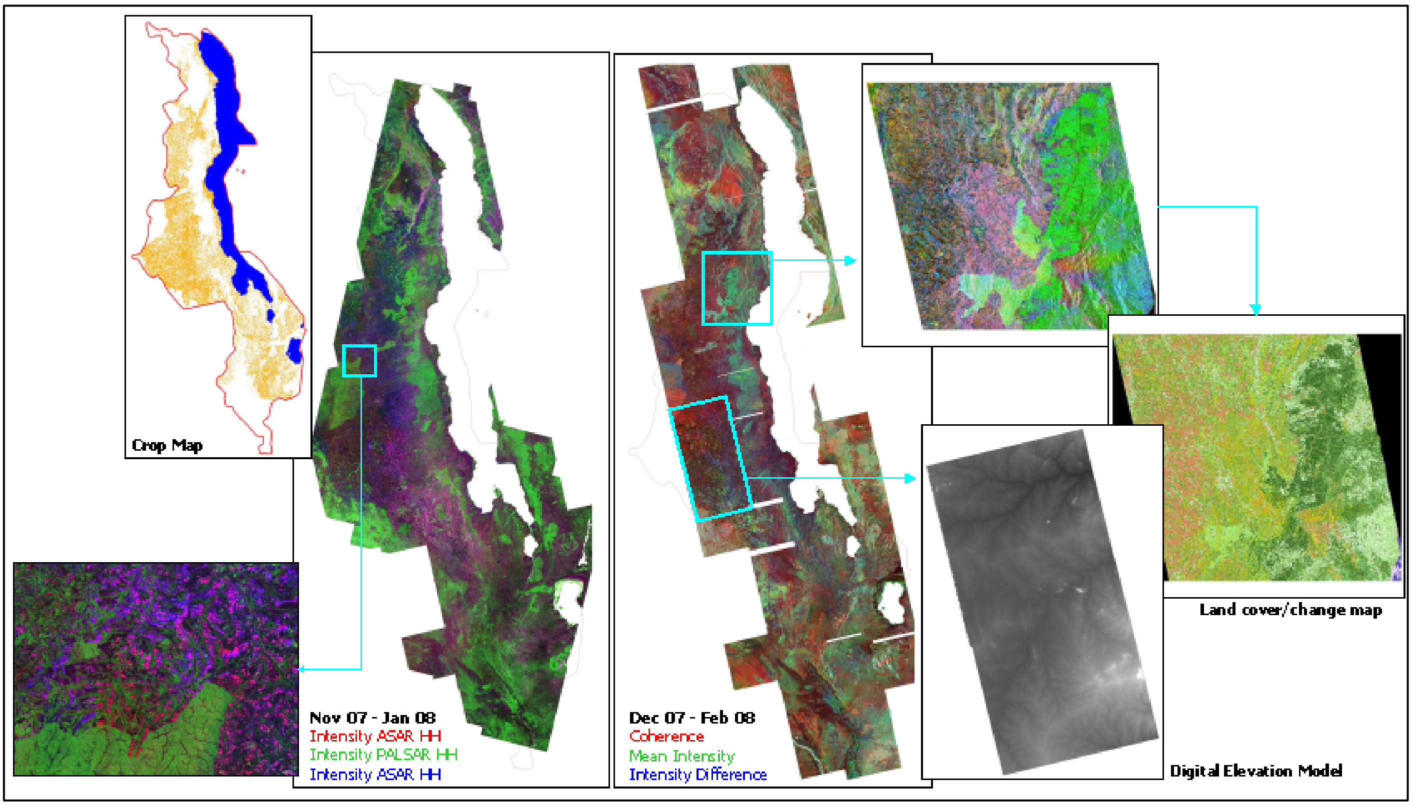

Figure 2. The color composite on the left illustrates a multi-temporal data set based on 120 ENVISAT ASAR AP images and 70 ALOS PALSAR FBS scenes ("© *JAXA/METI)* data covering the whole Malawi (100,000 sqkm, 15m resolution). The image on the right shows an interferometric color composite based on ALOS PALSAR FBS data (70 image pairs). The enlargements highlight the extensive information included in this type of multi-temporal multi-source data set, which allows the generation of products such as crop map, main land cover/change classes, and digital elevation model. All processing has been performed starting from SLC data. ALOS K&C © *JAXA/METI.*

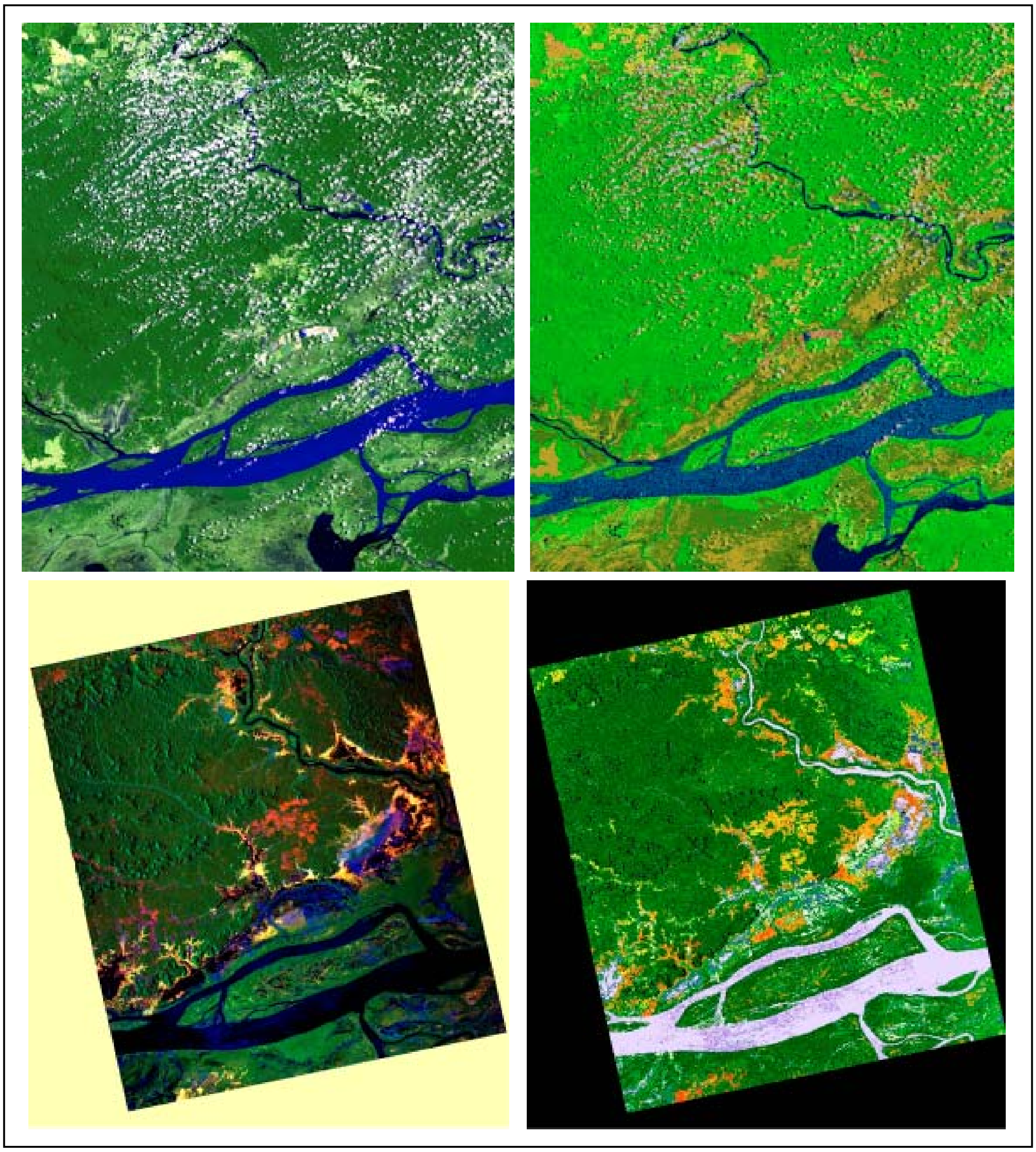

Figure 3. Landsat-5 TM color composite acquired on 1986 (top left) and corresponding classification (top right). ALOS PALSAR interferometric color composite acquired on 2007 (bottom left) and corresponding classification (bottom right).

<u>Legend Optical</u> (main classes): Green tones: Forest and sparse vegetation; Brown tones: barren land and built-up areas; Blue tones: water types; White tones: clouds.

<u>Legend SAR</u> (main classes): Green tones: Thick and sparse forest; Brown tones: Bare soil; Yellow tones: short vegetation and short dry vegetation; Blue tones: water types; Red: rocks/settlements.ALOS K&C © *JAXA/METI.*

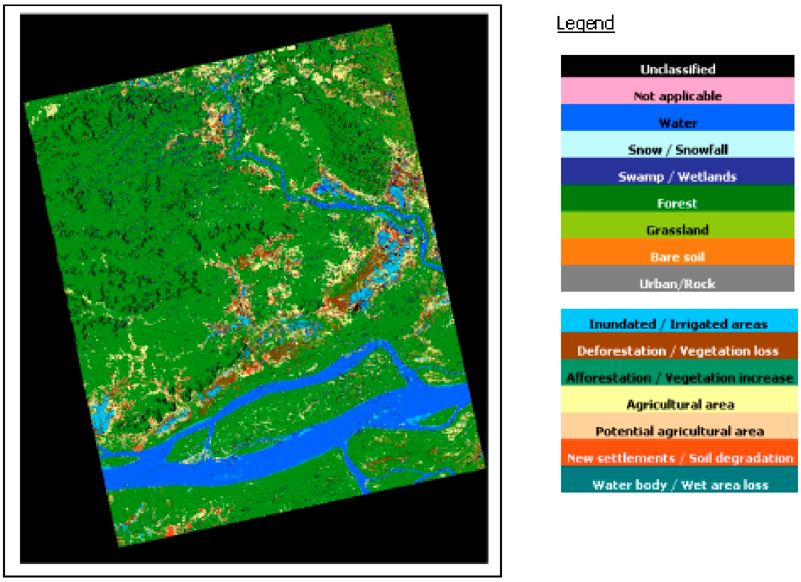

Figure 4. Land cover and change map between 1986 and 2007.

ACKNOWLEDGEMENTS

This work has been undertaken within the framework of the JAXA Kyoto & Carbon Initiative. ALOS PALSAR data have been provided by JAXA EORC, ENVISAT ASAR data by ESA, Landsat-5 TM data by USGS. ESA is additionally acknowledged to financially support the work performed in the Global Monitoring for Food Security and EOMD project.

REFERENCES

[1] Baraldi A., V. Puzzolo, P. Blonda, L. Bruzzone, and C. Tarantino, Automatic Spectral rule-based preliminary mapping of calibrated Landsat TM and ETM+ Images, IEEE Transactions on Geoscience and Remote Sensing, Vol. 44, No.9, 2006.

[2] Meier E., U. Frei, and D. Nuesch, Precise Terrain Corrected Geocoded Images, SAR Geocoding: Data and System, Wichmann Verlag, 1993.

[3] Holecz F., E. Meier, J. Piesbergen, D. Nüesch, and J. Moreira, Rigorous derivation of backscattering coefficient, IEEE Geoscience and Remote Sensing Society Newsletter, No. 92, 1994.

[4] Aspert F., M. Bach Cuadra, J.P. Thiran, A. Cantone, and F. Holecz, Time-varying segmentation for mapping of land cover changes, Proceeding of ESA Symposium, Montreux, 2007.

[5] sarmap, Aresys, and RSL, Prototype Processor for ALOS PALSAR Data and Polarimetric Interferometric Products Generation, Final Report, ESA/ESRIN, 2007.

[6] Ulaby F.T. and C. Dobson, Handbook of Radar Scattering Statistics for Terrain, Artech House, 1989.

[7] Global Monitoring for Food Security Consortium, Malawi Service Validation Report, Report to ESA/ESRIN, 2009.

[8] Aon, sarmap, FSC, and Ambiental, Earth Observation in Support of Corporate Social Responsibility – Forestry Sector, Service Validation Audit Report, Report to ESA/ESRIN, 2009.

[9] sarmap, COSMO-SkyMed AO Programme: Global Monitoring for Food Security , 2009.

sarmap S.A. – a Swiss company, www.sarmap.ch – currently constituted by 6 employees, was founded in January, 1998 to provide product / service development in the field of remote sensing (SAR and optical), particularly airborne and spaceborne Synthetic Aperture Radar (SAR) data processing. Training courses are also offered to extend the understanding of the utilization of SAR data, products and services. Application areas of expertise include Digital Elevation Model, agriculture, forestry, ground deformation, and change detection. In the past 10 years, sarmap has been involved in around 80 projects: approximately 2/3 on algorithm/product/service developments at the European Space Agency. The remaining 1/3 focused on the developments of innovative remote sensing based products/services for the World Bank, EC Joint Research Centre, JAXA, and private sector (re-insurance sector in primis). sarmap developed SARscape®, a software tool for the processing of airborne and spaceborne SAR data integrated in ENVI® and world-wide commercialized by Creaso GmbH, ITT Visual Information Solutions Ltd., and Sierra Atlantic Ltd..

Forest Theme

Forest Height Estimation by means of Pol-InSAR
Limitations posed by Temporal Decorrelation

Kostas Papathanassiou *et al.*
DLR (Germany)

K&C Science Report – Phase 1

Forest Height Estimation by means of Pol-InSAR

Limitations posed by Temporal Decorrelation

S.K. Lee, F. Kugler, K.P. Papathanassiou and A. Moreira

Microwaves and Radar Institute (DLR-HR)

German Aerospace Center (DLR)

D-82234 Wessling, Germany

E-mail: SeungKuk.Lee@dlr.de; Florian.Kugler@dlr.de; Alberto.Moreira@dlr.de; Kostas.Papathanassiou@dlr.de

***Abstract* — Polarimetric Synthetic Aperture Radar (SAR) Interferometry (Pol-InSAR) is a radar remote sensing technique, based on the coherent combination of radar polarimetry (Pol-SAR) and SAR interferometry (InSAR) which is substantially more sensitive to structural parameters of forest volume scatterers (e.g. forest) than conventional interferometry or polarimetry alone. However, temporal decorrelation is probably the most critical factor towards a successful implementation of Pol-InSAR parameter inversion techniques in terms of repeat-pass InSAR scenarios. This report focuses on the quantification of the effect of temporal decorrelation at L-band as a function of temporal baseline based on multi-temporal airborne experimental data acquired in the frame of dedicated air-borne experiments. Conclusions on the suitability of ALOS/PalSAR for Pol-InSAR applications are drawn and recommendations for mission characteristics of a potential follow on mission are addressed.**

***Index Terms*—ALOS PALSAR, K&C Initiative, Forest Theme, Polarimetric SAR Interferometry (Pol-InSAR), Forest Height Estimation, Temporal Decorrelation.**

I. INTRODUCTION

Towards a continuous quantitative forest monitoring, information about horizontal and vertical structure and/or about integrative forest parameters such as forest biomass is essential. In contrast to qualitative applications, quantitative approaches by means of SAR are less developed especially in tropical environments due to the limited data availability and the complexity of such environments. Most of the quantitative approaches are developed on temperate and/or boreal test sites where reference and validation data are easier to collect. The very different structure of tropical forests makes an offhand generalization not possible and requires dedicated experiments for development and validation. Pioneering work based on early airborne SAR experiments addressed tropical forest biomass classification and estimation hence demonstrating the potential of low frequency polarimetric SAR (PolSAR) measurements [3][4]. However, the complexity of radar scattering in forest environments makes the interpretation and inversion of individual SAR and PolSAR observables on the basis of empirical, semi-empirical or theoretical models difficult. The establishment of interferometric SAR (InSAR) techniques for forest monitoring in the late nineties triggered first InSAR experiments in the tropics that indicated the potential of interferometric observables at low frequencies for the estimation of vertical structure parameters [5][6][7][8][9].

Table 1: ALOS Quad-Pol Mode Parameters.

RF-centre frequency	*1.270 GHz (L-band)*
System bandwidth	*14 MHz*
Sampling Frequency	*16 MHz*
PRF	*1500-2500Hz*
Transmit Peak Power	*2 kW*
Incidence Angle	*21.5° (selective on 18.5 °)*
NE Sigma Zero	*< - 31dB*
Observation Swath	*30.6 Km (@ 21.5°)*
Range Resolution	*31.2m (ground range @ 21.5°)*
Azimuth Resolution	*20m (4 looks)*
A/D Convertion	*5bit*
Data Rate	*249 Mbps*
Repeat-Pass Time	*46 Days*

In the last years, the coherent combination of both, interferometric and polarimetric observations by means of Polarimetric SAR Interferometry (Pol-InSAR) was the key for an essential break through in quantitative forest parameter estimation [10][11]. Indeed, quantitative model based estimation of forest parameters - based on a single frequency, fully polarimetric, single baseline configuration - has been successfully demonstrated at L- and P-band and more recently even at X-band. Several experiments demonstrated the potential of Pol-InSAR techniques to estimate with high accuracy key forest parameters like forest height over a variety of natural and commercial; temperate, boreal and tropical test sites characterized by different stand and terrain conditions.

Validated results for boreal forests at X- and L-band are shown by [12] [11][13][14][15].

The launch of JAXA's ALOS in January 2006 provided - for the fist time since the SIR-C/X-SAR mission's in the 80's - the opportunity to acquire Pol-InSAR data from space. Indeed, PalSAR (i.e. the SAR instrument onboard of ALOS) is able to operate in a Quad-pol mode - declared by JAXA as an "Experimental Mode" - that allows the acquisition of Pol-InSAR data in a repeat-pass mode. The main characteristics of the PalSAR Quad-pol mode are summarized in Table 1. In this sense, ALOS-PalSAR allows the application, validation and development of Pol-InSAR inversion techniques on a much wider range of sites distributed world-wide and accessible to a much wider scientific user community than possible with airborne sensors.

A. *Importance of Forest Height*

An estimation of the 3-D forest structure allows retrieving quantitative forest parameters. One parameter providing information about the 3- D structure of forests is forest height, a key parameter for a wide range of applications in forest management and forest conservation, such as biomass estimation, illegal logging, stand delineation and disaster management.

Especially information about forest biomass and the detection of changes in forests on a global scale are highly valuable information. Forest height is correlated with biomass; this means by using allometric equations dependent on the ecosystem (boreal or tropical) biomass can be easily derived from forest height. Biomass is a parameter going directly into climatic modelling or carbon balancing and is therefore in a globally changing environment of high interest. In the frame of a changing climate, but also for the conservation of ecosystems and biodiversity a documentation of changes in forest ecosystems is essential. This includes the detection of forest clearings but also the detection of changes in the 3-D structure of forests for which height is an important parameter. Full area forest height maps resolve the horizontal forest canopy structure allowing a classification and evaluation of forest ecosystem. In contrary to this wood industry and forest management require quantitative forest information to guarantee a sustainable forest management and wood supply also here forest height is a basic parameter for the planning of logging activities.

Until now, quantitative information about forests is mainly based on the sampling of ground measurements. Their accuracy and reliability depend on the used grid and the uniformity of the forest. For remote forest types such as boreal or tropical forests, the available information becomes particularly poor due to a lack of measurements. Ground measurements are generally expensive and staff intensive. Therefore they are normally conducted only once every 10 years or more. 3-D remote sensing techniques could provide complete information in short time periods.

II. PROJECT DESCRIPTION & OVERVIEW

ALOS provided, for the first time, the possibility to **demonstrate quantitative Pol-InSAR techniques from space**. This demonstration in terms of forest height estimation was the **core objective of the original project.** Based on repeat-pass fully polarimetric interferometric SAR data acquired by the ALOS/PalSAR sensor - during its early CAL-VAL phase - model based estimation of forest height was proposed. Towards higher estimation accuracy, the observation vector was planned to be extended including the two dual-pol single-baseline data sets acquired on the latter ALOS/PalSAR operation phase. There where three tasks foreseen:

Task 1: Inversion methodology development adapted / optimised to the actual ALOS/PalSAR acquisition scenario: I.e., a limited number of Quad-Polarimetric (Quad-pol), repeat-pass interferometric acquisitions with a temporal baseline of about 46 days. Assessment of the impact of temporal decorrelation on Pol-InSAR inversion techniques.

This task has been **successfully completed.** Using L-band airborne Pol-InSAR data acquired by DLR's E-SAR system in a repeat-pass mode an optimised methodology for the inversion of Pol-InSAR data affected by moderate levels of temporal decorrelation, has been developed. The performance of the developed methodology was validated in the frame of dedicated experiments/campaigns against ground-measurements, and Lidar data. **Unfortunately the 46 days temporal baseline of ALOS lead to severe temporal decorrelation that restricts dramatically the application of Pol-InSAR techniques**. The emphasis was then moved towards the assessment of temporal decorrelation levels at different temporal baselines ranging from days to weeks and the evaluation of its impact on forest height estimation techniques. The analysis, the results and the conclusions are reported in Section 3 & 4.

Task 2: ALOS/PalSAR data inversion and validation of the obtained forest height estimates over a limited number of selected test-sites. Evaluation of the performed estimation accuracy and feasibility assessment for global scale application. Evaluation of the option for the collection of a global data set for forest height mapping.

This task has been **completed.** Based on repeat-pass quad-pol interferometric SAR data acquired by the ALOS/PALSAR sensor during its early calibration/validation phase it was possible to demonstrate model based Pol-InSAR inversion over single isolated stands (see Figure 1). However, the high temporal decorrelation levels induced by the 46-day repeat-pass cycle reduce the estimation performance of forest structure parameters significantly and prevent the demonstration of Pol-InSAR inversion on a large scale.

The decorrelation levels are similar to the ones obtained in airborne experiments (see Task 1) for similar temporal baselines, a fact that can be seen as a validation of the ALOS-PalSAR sensor and data quality.

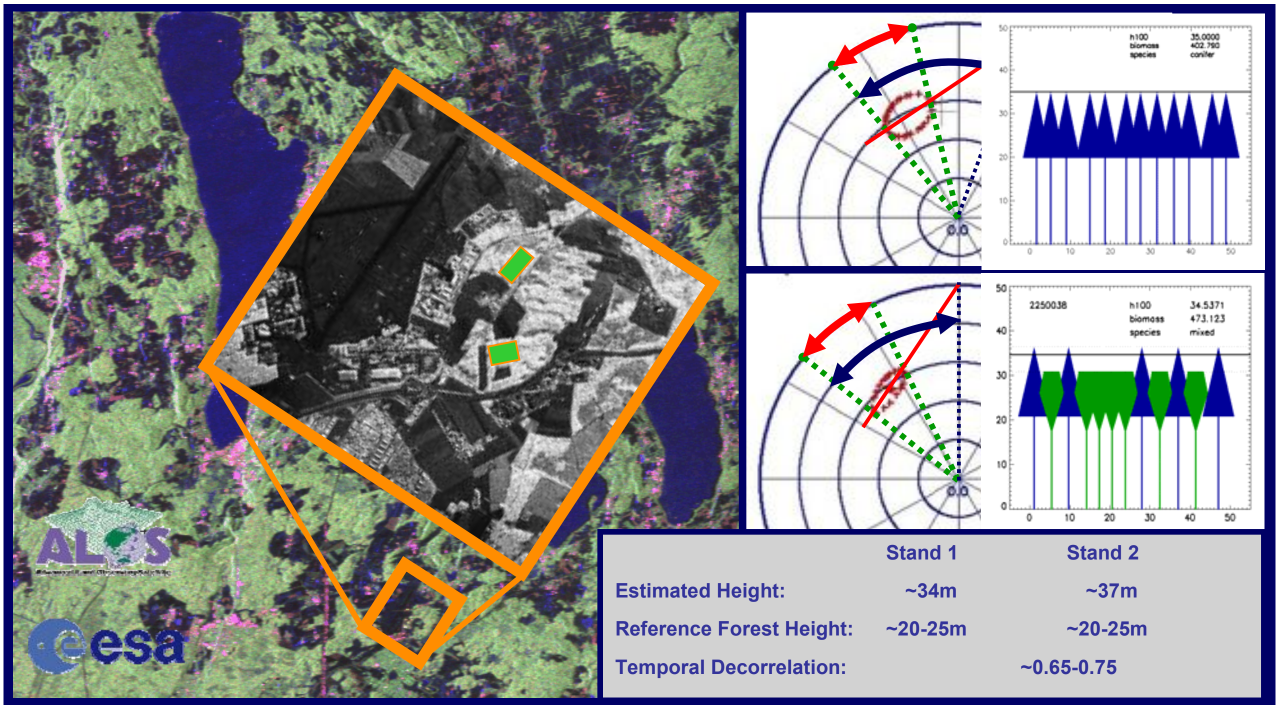

Figure 1: Forest height estimation for a mixed forest stands located within the Oberpfaffenhofen test site obtained from the inversion of dual-baseline Quad-Pol-InSAR ALOS-PalSAR data "© JAXA/METI".

Task 3: Inversion methodology development adapted to the Dual-pol ALOS/PalSAR global coverage acquisition scenario for an optimised forest height estimation performance on a global scale. The proposed methodology was proposed to be tested against ground measurements over selected test-sites worldwide in order to state about estimation accuracy and potential limitations.

This task has been **not-completed** because of the high temporal decorrelation levels that make quantitative Pol-InSAR inversion not meaningful. The very low coherence levels over forest areas degrade the value of interferometric information and make a successful performance of this task not possible.

III. POL-INSAR FOREST HEIGHT INVERSION

The key observable used in Pol-InSAR applications is the complex interferometric coherence $\tilde{\gamma}$ (including both, the interferometric correlation coefficient and interferometric phase) measured/estimated at different polarizations (indicated by the unitary vector $\vec{w}$ [10][11]). $\tilde{\gamma}$ is given by the normalized cross-correlation of the two SAR images obtained from the interferometric acquisition s_1 and s_2

$$\tilde{\gamma}(\vec{w}) := \frac{< s_1(\vec{w}) s_2^*(\vec{w}) >}{\sqrt{< s_1(\vec{w}) s_1^*(\vec{w}) >< s_2(\vec{w}) s_2^*(\vec{w}) >}} \tag{1}$$

The coherence depends on instrument and acquisition parameters as well as on dielectric and structural parameters of the scatterer. A detailed discussion of system induced coherence errors can be found in [18]. After calibration of system induced decorrelation contributions and compensation of spectral decorrelation in azimuth and range the estimated interferometric coherence can be decomposed into three main decorrelation processes [19]:

$$\tilde{\gamma} := \tilde{\gamma}_{Temp} \ \gamma_{SNR} \ \tilde{\gamma}_{Vol} \tag{2}$$

-- Temporal decorrelation $\tilde{\gamma}_{Temp}$ can be real (i.e. effecting the absolute value of $\tilde{\gamma}$ only) or complex (i.e. biasing the phase of $\tilde{\gamma}$). It depends on the structure and the temporal stability of the scatterer, the temporal baseline of the interferometric acquisition and the dynamic environmental processes occurring in the time between the acquisitions.

-- Noise decorrelation γ_{SNR} introduced by the additive white noise contribution on the received signal [20][21]. It affects primarily scatterers with low (back-) scattering and is in general of secondary importance when looking on forest at conventional frequencies.

-- Volume decorrelation $\tilde{\gamma}_{Vol}$ is the decorrelation caused by the different projection of the vertical component of the scatterer into the two images $s_1(\vec{w})$ and $s_2(\vec{w})$. $\tilde{\gamma}_{Vol}$ is directly linked to the vertical distribution of scatterers *F(z)* through a (normalized) Fourier transformation relationship

$$\tilde{\gamma}_{Vol} = \exp(i\kappa_z z_0)\frac{\int_0^{h_V} F(z')\exp(i\kappa_z z')dz'}{\int_0^{h_V} F(z')dz'} \tag{3}$$

where h_v is the height of the volume and κ_z the effective vertical (interferometric) wavenumber that depends on the imaging geometry and the radar wavelength λ

$$\kappa_z = \frac{\kappa\Delta\theta}{sin(\theta_0)} \quad \text{and} \quad \kappa = m\frac{2\pi}{\lambda} \tag{4}$$

and $\Delta\theta$ is the incidence angle difference between the two interferometric images induced by the baseline. z_0 is a reference height and $\varphi_0 = \kappa_z z_0$ the corresponding interferometric phase. For monostatic acquisitions, as flown in the case of ALOS PalSAR, *m:=2,* while for bistatic acquisitions *m:=1.* Accordingly, $\tilde{\gamma}_{Vol}$ contains the information about the vertical structure of the scatterer and is therefore the key observable for quantitative forest parameter estimation [10][11].

The estimation of vertical forest structure parameters from interferometric measurements can be addressed as a two step process: In the first step (*modelling*) *F(z)* is parameterized in terms of a limited set of physical forest parameters that are related through (3) to the interferometric coherence. In the second step (*inversion*), the volume contribution of the measured interferometric coherence is then used to estimate *F(z)* and to derive the corresponding parameters. A widely and successfully used model for *F(z)* is the so called Random Volume over Ground (RVoG), a two layer model consisting of a volume and a ground layer [22], which can be described as

$$F(z) = \tilde{m}_V\ e^{\left(\frac{2\sigma}{\cos(\theta_0)}z\right)} + m_G\ e^{\left(\frac{2\sigma}{\cos(\theta_0)}h_V\right)}\delta(z-z_0) \tag{5}$$

where m_V and m_G are the ground and volume scattering amplitudes and σ a mean extinction coefficient. Equation (5) leads to

$$\tilde{\gamma}_{Vol} = \exp(i\kappa_z z_0)\frac{\tilde{\gamma}_{V0}+m}{1+m} \tag{6}$$

The phase $\varphi_0 = \kappa_z z_0$ is related to the ground topography z_0 and m the effective ground-to-volume amplitude ratio accounting for the attenuation through the volume $m = m_G/(m_V I_0)$. $\tilde{\gamma}_{V0}$ is the volume decorrelation caused by the vegetation layer only, given by

$$\tilde{\gamma}_{V0} = exp(i\kappa_z z_0)\frac{\int_0^{h_V} exp(i\kappa_z z')exp\left(\frac{2\ \sigma\ z'}{cos\theta_0}\right)dz'}{\int_0^{h_V} exp\left(\frac{2\ \sigma\ z'}{cos\theta_0}\right)dz'}. \tag{7}$$

Neglecting temporal decorrelation and assuming a sufficient calibration/compensation of system (e.g. SNR) and geometry (range/azimuth spectral shift) induced decorrelation contributions (6) can be inverted in terms of a Quad-pol single baseline acquisition [11],[13],[23],[24]. Assuming no response from the ground in one polarization channel (i.e. $m_3 = 0$) the inversion problem has a unique solution and is balanced with five real unknowns ($h_V, \sigma, m_{1-2}, \varphi_0$) and three measured complex coherences [$\tilde{\gamma}(\vec{w}_1)\ \ \tilde{\gamma}(\vec{w}_2)\ \ \tilde{\gamma}(\vec{w}_3)$] each for any independent polarization channel [23]

$$\min_{h_V,\sigma,m_i,\varphi_0} \left\| \left[\tilde{\gamma}(\vec{w}_1)\ \ \tilde{\gamma}(\vec{w}_2)\ \ \tilde{\gamma}(\vec{w}_3)\right]^T - \left[\tilde{\gamma}_V(h_V,\sigma,m_1)\ \ \tilde{\gamma}_V(h_V,\sigma,m_2)\ \ \tilde{\gamma}_{Vo}exp(i\varphi_0)\right]^T \right\| \tag{8}$$

Equation (8) is used to invert data sets at L-band using m_3=0 for regularisation. Note that the assumption for no ground response is not necessarily linked to the HV channel.

IV. The Effect of Temporal Decorrelation

Equation (6) accounts only for the volume decorrelation contribution of the interferometric coherence while other decorrelation effects are ignored. Such decorrelation contributions reduce the interferometric coherence, and increase the variation of the interferometric phase. The impact of such non-volumetric decorrelation effects is evaluated in the following. One has to distinguish between real and complex decorrelation contributions: Both of them bias (reduce) the absolute value of the interferometric coherence and increase variance of the interferometric phase. But, while complex decorrelation biases the expectation value of the (interferometric) phase, the expectation value remains the same in the case of real decorrelation.

A. Temporal Decorrelation

One of the most prominent decorrelation contributions in the case of non-simultaneous acquisition is temporal decorrelation caused by dynamic changes within the scene occurring in the time between the two acquisitions. Such changes can effect the location and/or the (scattering) properties of the scatterers within the scene inducing in the most general case a complex decorrelation.

Temporal changes within the scene occur, in general, in a stochastic manner and cannot be modeled accurately even when detailed information about the environmental conditions in the time between the two observations are available. The fact that everything within the scene may change and affect all or some of the polarimetric and/or interferometric observables in different ways make a general model-based consideration of temporal effects, if not impossible, very difficult.

Hence, temporal decorrelation effects - in the absence of detailed knowledge about the occurring dynamic process - can be incorporated in scattering models in a rather abstract way. Regarding Equation (6) model, temporal decorrelation may affect both, the volume component that represents the vegetation layer and the underlying ground layer

$$\tilde{\gamma}(\vec{w}) = \exp(i\varphi_0)\frac{\gamma_{TV}(\vec{w})\ \tilde{\gamma}_V + \gamma_{TG}(\vec{w})\ m(\vec{w})}{1+m(\vec{w})} \qquad (9)$$

γ_{TV} denotes the correlation coefficient describing the temporal decorrelation of the volume scatterer and γ_{TG} the correlation coefficient describing the temporal decorrelation of the underlying surface scatterer. As indicated, both coefficients may be polarisation dependent and complex: For example, changes in the dielectric properties of the canopy layer (due to changes in moisture content) or even more changes in its structural characteristics (caused by the annual phenological cycle or fire events) lead to different amount of change at different polarisations in the volume scatterer. Furthermore, a change in the dielectric properties of the ground scatterer - as for example due to a change in soil moisture - effects the scattering properties in each polarisation in a different way and leads to a polarisation dependent temporal decorrelation of the ground scatterer.

An important, and missing today, information is the behavior of γ_{TV} and γ_{TG} as a function of time. The decorrelation processes within the volume layer occur at different - in general much smaller - time scales than the decorrelation process on the ground (that includes both surface and dihedral scattering). While the vegetation layer starts already to decorrelate at temporal baselines on the order of seconds to minutes and is completely decorrelated for temporal baselines on the order of 1-2 months, the ground scattering remains partially coherent for even for baselines on the order of a half year. Especially dihedral scattering mechanisms - related in forest environments to the ground-trunk interaction - appears to be very stable in time and remain coherent even over the period of several months. However, the individual values and temporal characteristics of γ_{TV} and γ_{TG} are, of course, frequency dependent but depend also on the tree/stand canopy and architecture characteristics. The overall temporal decorrelation is then depending – according to Equation (9) – on the ground to volume ration *m* that defines the ratio of more to less temporal stable components. In other words, stands with a higher ground contribution are obviously expected to have a higher temporal coherence than stands characterized by a weak 'visible' ground scattering component.

From the parameter inversion point of view now, the RVoG model with general temporal decorrelation – as addressed in Equation (9) - cannot be solved under any (repeat-pass) observation configuration, as any additional measurement – at a different polarisation and/or baseline – introduces always two new unknowns, γ_{TV} and γ_{TG}. However, even if the general temporal decorrelation scenario leads to an under-determined problem, special temporal decorrelation cases may be accounted under certain assumptions, as it will be discussed in the next section.

B. Wind Induced Temporal Decorrelation

The most common temporal decorrelation effect over forested terrain is wind-induced movement of scatterers within the canopy layer as for example leaves and/or branches etc. In terms of the RVoG model, this corresponds to a change of the position of the scattering particles within the volume. However, in this case the scattering amplitudes as well as the propagation properties of the volume remain the same. Assuming further that the scattering properties of the ground do not change the RVoG model with temporal decorrelation in the volume component becomes [37][23]

$$\tilde{\gamma}_{Vol}(\vec{w}) = exp(i\kappa_z z_0)\frac{\gamma_{Temp}\tilde{\gamma}_{V0} + m(\vec{w})}{1+m(\vec{w})} \qquad (10)$$

The inversion of Pol-InSAR coherences contaminated by temporal decorrelation using Equation (6) by means of Equation (10) leads to overestimated forest height estimates: The lower coherence values (due to the temporal decorrelation) are interpreted by Equation (6) as to be caused by higher forest heights. Figure 2 shows the height error obtained by inverting Equation (10) for different levels of temporal decorrelation (γ_{Temp}=0.90 to 0.75) using Equation (6) as a function of forest height.

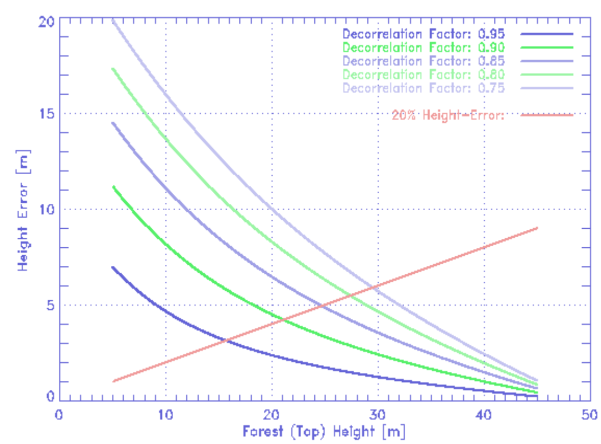

Figure 2: Height error induced by different levels of temporal decorrelation as a function of forest heights assuming as a vertical wavenumber of κ_z=0.1 rad/m.

A vertical wavenumber of κ_z=0.1rad/m has been assumed that corresponds to an 1100m horizontal spatial baseline for the ALOS Quad-pol mode. Clearly, one can see that the estimation errors induced by a constant level of temporal decorrelation are significantly higher for short than for high heights and that the errors increase with increasing temporal decorrelation. Note that even for low temporal decorrelation levels (on the order of 0.9) the height error is critical for low forest heights.

Figure 2 makes clear that for achieving acceptable height estimates temporal decorrelation has to be suppressed or compensated. Unfortunately, as already discussed, temporal decorrelation occurs in a stochastic manner within the scene [39] and can be only difficult accounted/modeled on the basis of detailed information about the environmental conditions over the time between the two observations. The first best option to reduce the impact of non-volumetric decorrelation contributions on the forest height estimation is to increase the volume decorrelation contribution with respect to the non-volumetric decorrelation by increasing the spatial baseline of the acquisitions. Figure 3 shows the height error obtained by inverting Equation (11) for different levels of temporal decorrelation (γ_{Temp}=0.90 to 0.75) using Equation (6) as a function of vertical wavenumber (and horizontal spatial baseline referred to the ALOS Quad-pol mode), assuming a constant forest height of 20m. Even for low temporal decorrelation levels (on the order of 0.9) the height error is critical at small baselines (60% for κ_z=0.05) but degreases with increasing baseline: for the same level of temporal decorrelation the height error degreases to 20% for a vertical wavenumber of 0.1. This makes clear that larger spatial baselines are advantageous in the presence of weak to moderate temporal decorrelation as they minimise the introduced bias by increasing the temporal baseline. The price to be paid is a lower overall coherence level - due to the increased volume decorrelation contribution - that caused an increased phase variance. This can be compensated by multilooking on the expense of spatial resolution. For small bandwidth systems additionally the low of common bandwidth due to the increased baseline may be an issue. However, the realisation of large baselines is, in the case of ALOS PalSAR, limited by the acquisition scenario that foresees small spatial baselines optimized for deformation applications. On the other side, the 46 days repeat-pass time of ALOS PalSAR lead to temporal coherence levels that are by far to low to be compensated by spatial baseline optimisation.

In the next sections the quantification of temporal decorrelation and its impact on forest height inversion for different repeat-pass intervals is discussed.

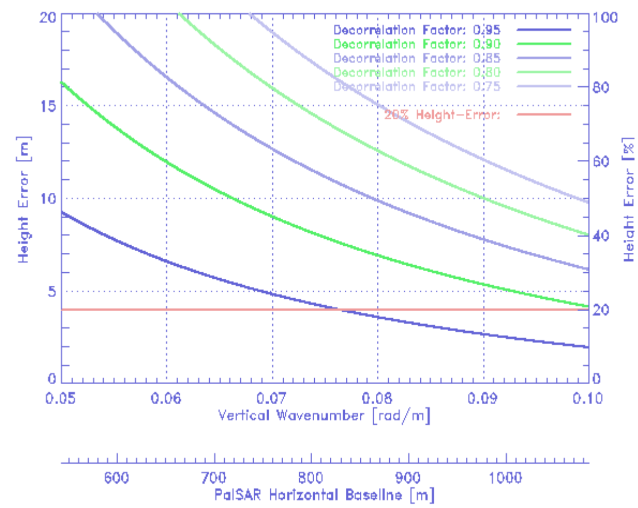

Figure 3: Height error induced by different levels of temporal decorrelation as a function of vertical wavenumber (and horizontal spatial baseline referred to the ALOS Quad-pol mode), assuming a constant forest height of 20m.

V. Airborne Experiments & Test Sites

In order to asses the effect of temporal decorrelation at L-band, temporal baselines smaller than the ones obtained by ALOS-PalSAR, i.e. 46 days, two main airborne experiments have been conducted and data from an experiment in 2003 have been evaluated.

The BioSAR-I campaign was performed over the Remningstrop test site located in Sweden in 2007. DLR’s experimental airborne SAR system (E-SAR) flew over the Remningstrop forest at three different times: 09 March, 31 March, 02 May 2007. During the three data acquisitions, L-band Quad-polarimetric data have been acquired in a repeat-pass interferometric mode. The configurations flown and the available L-band data sets are summarized in Table 2 The experiment allows to investigate temporal baselines on the order of 32 days and 54 days.

The TreeSAR campaign was conducted in October 2003 over the Traunstein test site. This was an early experiment to investigate the temporal behavior of forests for a temporal baseline in the order of weeks. L-band data have been acquired by DLR’s E-SAR system in a fully polarimetric mode. Data base for this campaign is summarized in Table 2.

The TempoSAR campaign was performed in June 2008 DLR’s E-SAR system collected fully polarimetric and interferometric SAR data at L-band over the Traunstein test site located in Germany six times within 13 days. The experiment was designed to investigate temporal baselines on the order of days up to two weeks. The configurations flown within the frame of TempoSAR and the available L-band data sets are summarized in Table 2.

Table 2 Campaigns and Data base

Campaign	Acquisition Date	Temporal baseline	Spatial baselines
TempoSAR	2008/06/07 2008/06/08 2008/06/10 2008/06/12 2008/06/19 2008/06/20	1 – 13 days	15, 10, 5, & 0m
TreeSAR	2003/10/11 2003/10/26	15 days	0, 5, & 10m
BioSAR-I	2007/03/09 2007/03/31 2007/05/02	32 & 54 days	0, 8, 16, & 24m

A. The Remningstrop test site

Remningstrop test site (see Figure 4 left) is located in southern Sweden (58°28' north, 13°38'east). The forest is part of the southern ridge of the boreal forest zone in transition to the temperate forest zone. Topography is fairly flat with some small hills and ranges between 120m and 145m amsl. It is a managed forest, divided into several stands with similar forest structure. Prevailing tree species are Norway spruce (*Piceaabies*), Scots pine (*Pinus sylvestris*) and birch (*Betula spp.*). Forest height ranges from 5m to 35m, with biomass levels from 50t/ha to 300t/ha. For this test site a large area lidar data set is available for validation. Lidar systems are an established technique to measure forest height. In this case the lidar data are used to validate the radar measurements.

B. The Traunstein test site

The Test Site Traunstein (see Figure 4 right) is situated in the southeast of Germany (47°52' north, 12°39' east), next to the city Traunstein to the east. Geologically, the test site is placed in the pre- alpine- moraine landscape of southern Germany. Topography varies from 530 – 650m amsl, with only few steep slopes. The climatic conditions with a mean annual temperature of 7.8°C and precipitation of more than 1600 mm/a favor mixed mountainous forests, dominated by Norway spruce (*Picea abies*), beech (*Fagus sylvatica*) and fir (*Abies alba*). On a global scale this forest type is part of the temperate forest zone. It is a managed forest composed of even-aged stands which cover forest heights from 10m to 40m. Mean biomass level is on the order of 210t/ha while some old forest stands can reach Biomass levels up to 500t/ha. Compared to other managed forests in this ecological zone (mean biomass of 121 t/ha) the biomass values at Traunstein test site are significantly higher. Validation is based on forest inventory, which was done by means of a plot system on a 100m by 100m grid.

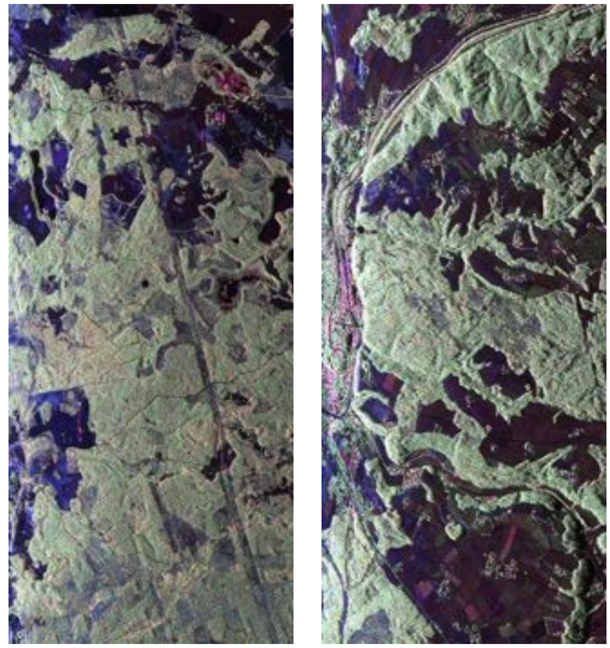

Figure 4: Remningstrop test site: left, Traunstein test site: right. Radar image Pauli decomposition, red: double bounce scattering, blue: surface scattering, green: volume scattering.

VI. Assessment of Temporal Decorrelation

A. Pol-InSAR Inversion Height and Validation

Forest height was estimated and validated against ground measurements for Traunstein test site as well as for Pol-InSAR inversion results (left side figure 5) and forest height estimates from lidar measurements (right side figure 5) for Remningstrop test site (April flights) are shown. Figure 7 right shows the Pol-InSAR forest height map for Traunstein test site (left side) and an amplitude image containing all ground plots for validation. All height images are scaled from 0m to 50m.

The Traunstein test site was validated against forest inventory data. A forest stand map was provided and forest heights origin from ground measurements based on a 100m x 100m grid (see Figure 7 right, colors represent H100). All together, 224 inventory points are located within the test site. However, in heterogeneous forests even a small misregistration between inventory coordinates and radar image may deteriorate the results. Also, the certainty of the estimated parameters increases for larger sampling areas. For these reasons it was tried to select large forest areas which were as homogeneous as possible in terms of species, height, biomass and stadium. In total, 20 validation stands covering 123 ha and including 133 inventory points were selected. A comparison of Pol-InSAR forest height against H100 of inventory data is shown in Figure 8: with an R^2 of 0.90 and RMSE of 3.16 m, over a height range from 10 to 35m.

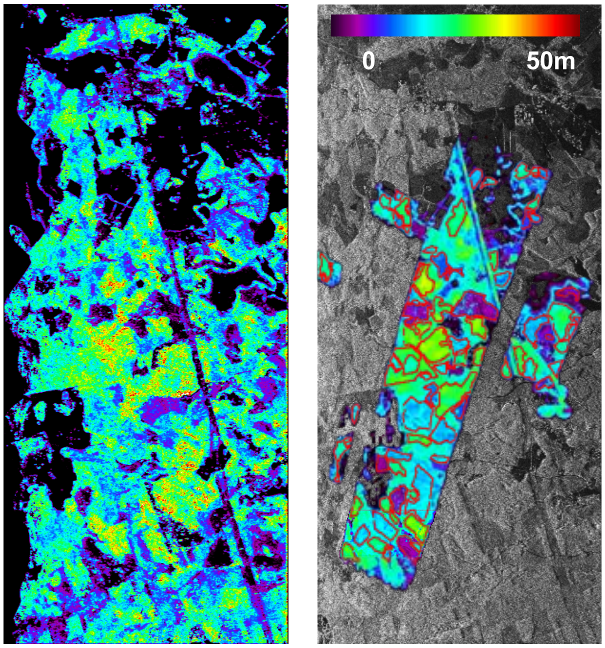

Figure 5 Forest height map Remningstrop forest; scaled from 0m to 50 m; Left: Pol-InSAR inversion height, Right: L-band amplitude image overlaid with lidar height (H100).

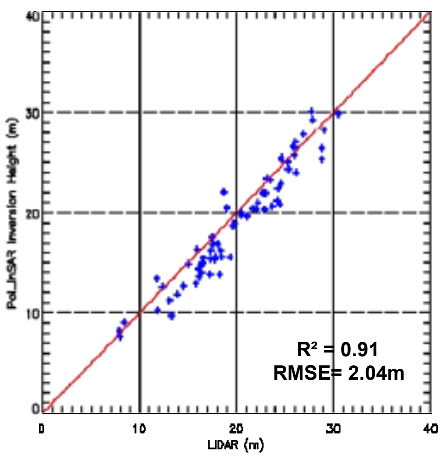

Figure 6: Validation Plot Remningstrop test site: LIDAR H100 versus Pol-InSAR height estimates.

The results of both campaigns demonstrate in an impressive way that Pol-InSAR forest height inversion provides consistent forest height maps at different type of forests if there is low temporal decorrelation.

B. The Impact of Temporal Decorrelation

After demonstrating the potential of Pol-InSAR inversion with data not affected by temporal effects, in this part data quality and inversion results for repeat pass acquisitions with temporal baselines from 0 day to 54 days are presented.

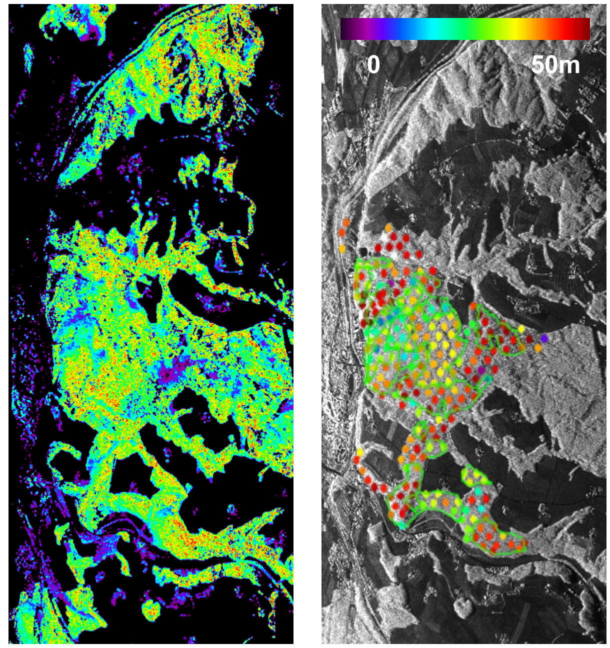

Figure 7: Forest height map Traunstein; scaled from 0m to 50 m; Left: Pol-InSAR inversion height, Right: L-band amplitude image overlaid with inventory points.

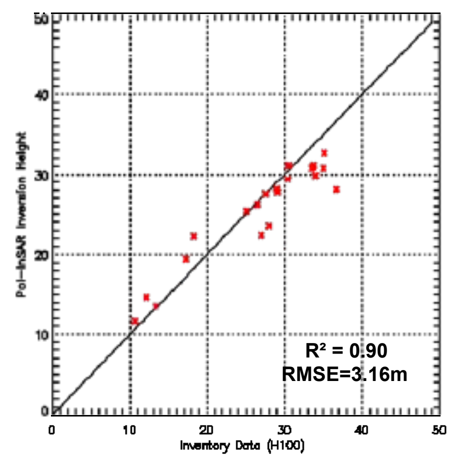

Figure 8: Validation Plot Traunstein test site: Inventory H100 versus Pol-InSAR height estimates.

During the BioSAR-I campaign data with temporal baselines of 0 days, 32 days and 54 days have been acquired. Effects of temporal decorrelation are shown in Figure 9. Coherence histograms in HH, VV, and HV polarizations over the whole scene for three temporal baselines (all acquired with 0m nominal spatial baseline) are plotted.

As expected, temporal decorrelation decreases with time independent from polarizations. Even in the 0 day scenario some decorrelation effects can be observed. Also here the data are acquired in a repeat pass mode with temporal baselines in the order of one hour. As seen in Figure 9 temporal decorrelation reduces coherence level to 0.65 (32 days) and 0.30 (54 days). Coherence with 54 days temporal baseline is too low to apply valuable Pol-InSAR application. Pol-InSAR height estimates were calculated for a 32 days temporal baseline, results are shown in Figure 10. In this case Inversion forest height all over the image is fairly overestimated originated by temporal decorrelation effects.

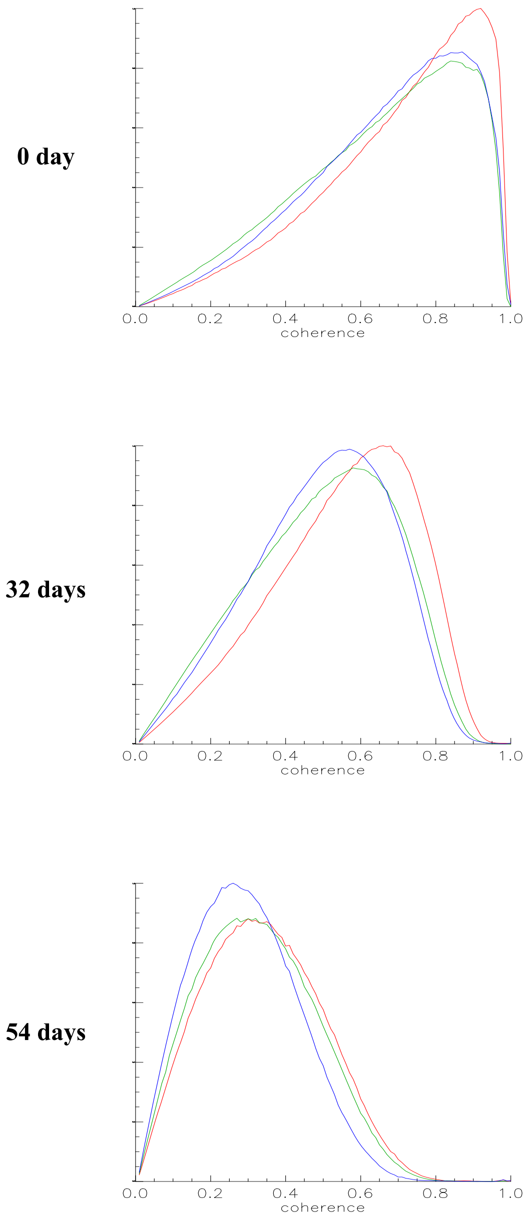

Figure 9: Coherence histograms for 0days (top), 30days (middle) and 54 days (bottom) temporal baseline; HH= red, HV= green, VV= blue.

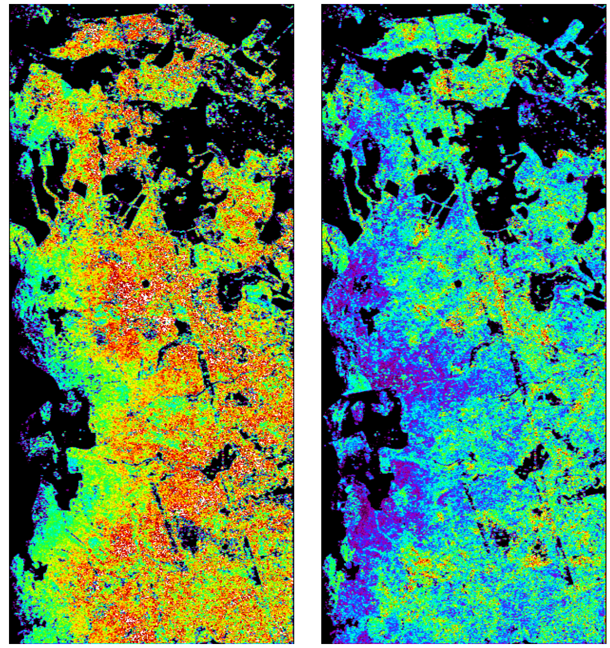

Figure 10 Forest height maps for Remningstorp forest, scaled 0 to 50m. Left: Inversion height map with one month temporal baseline, Right: Different height map between left image and the left image of Figure 5.

The level of temporal decorrelation with one month repeat-pass cycle of L-band makes a height inversion still feasible, but introduces a large height bias.

During the TempoSAR campaign data have been acquired on six days within a 13 days period. This enables to generate several temporal baselines ranging from 1 day to 13 days. Pol-InSAR forest heights for 6 temporal baselines are shown in Figure 13. As expected, overestimation tends to increase in time (comparing the results with Figure 7 left). Height errors induced by temporal decorrelation were estimated and plotted in Figure 11. There is a tendency that height errors increase with decreasing forest height, caused by the Pol-InSAR model. Low forests are more affected by uncompensated decorrelation contributions than high forests (see Figure 2). Even 1 day of temporal decorrelation can lead, dependent on forest height, to 20-100% overestimation of forest height. Usually L-band height estimates are affected by rather stochastic temporal effects due to the variable wind induced motions see also [39].

Temporal decorrelation yields always in an overestimation of forest height as indicated by Equation (10). Using the behavior of the height error in time (see Figure 11), enables us to correct forest height and volume coherence can be estimated by corrected forest height and Equation (7) under the assumption that extinction is constant in time. Under this assumption temporal decorrelation can be decomposed from volume decorrelation see Equation (2).

Estimated temporal decorrelation coefficients for different temporal baselines are shown in Figure 14. From this two main points become obvious. First: γ_{TV} decreases with increasing temporal baseline. Second: γ_{TV} is not constant in time, it depends on forest height and additionally on the random behavior of wind induced motion of forests [39]. Figure 12 shows the estimated γ_{TV} against temporal baselines. If there is no temporal decorrelation, as we can find in single pass systems, γ_{TV} should be 1. γ_{TV} tends to decrease with increasing temporal baseline. Looking on temporal baselines in the order of days a rapid drop of coherence can be observed (see Figure 12), but coherence values are still greater than 0.3 which allows a Pol-InSAR inversion. Temporal effects for temporal baselines on day level are caused by wind-induced movements of unstable scatterers within the canopy layer like leaves, branches or birds.

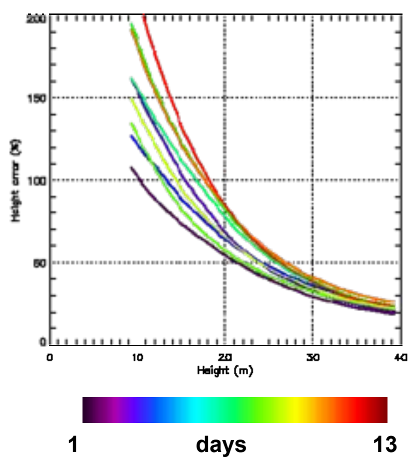

Figure 11: Height error (%) with temporal baselines (1 - 13 days).

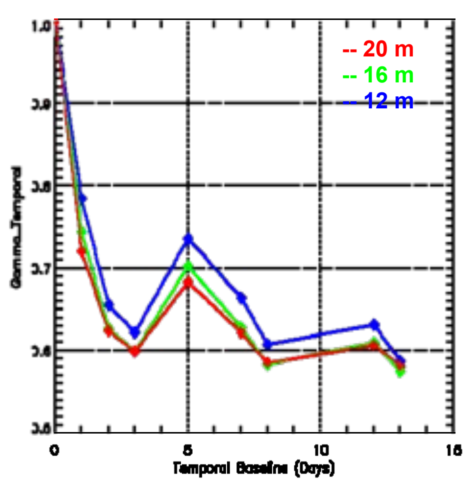

Figure 12: Temporal decorrelation (γ_{TV}) against temporal baselines. Color mean forest height (red: 20m, green: 16m, blue: 12m).

Going to temporal baselines in the order of weeks or month (as it is the case for ALOS –PalSAR) coherence is more decorrelated, there are not only the wind induced motions but also other events, for example precipitations (rainfall, snow), changes in soil moisture, breaking branches, fall of leaves, etc. Taking everything into consideration coherence level becomes too low (<0.3) to perform any kind of quantitative evaluation and/or analysis of the data.

VII. Results and Summary

With respect to quantitative Pol-InSAR applications there are several "sub-optimum" aspects on the ALOS system, mission and operation design that constrain - more or less - a large scale demonstration:

- *Coverage:* The Quad-pol mode does not provide global coverage for the defined ALOS orbit. The 30Km wide swath has on the equator - and therefore on the sensible tropical region - gaps on the order of 30Km and covers therefore only approx. 50%.

- *Repeat-Pass Time:* The repeat-pass interval of 46 days - required in order to ensure global coverage of the optical PRISM and AVNIR2 instruments - is to large to limit the impact of temporal decorrelation on the interferometric coherence.

- *Observation scenario:* The fact that the Quad-pol mode is declared as an experimental mode reflects on the observation scenario for ALOS-PalSAR: Only two consecutive Quad-pol observations (cycles) every year are foreseen allowing the formation of a single Quad-pol baseline. This, combined with the fact that the Dual-pol modes are operated at a different incidence angle - limits drastically the formation of an adequate Pol-InSAR observation space.

- Orbit Control: The ALOS orbit control allows the realisation of orbital tubes of about 500m leading to a zero mean distribution of baselines up to 1Km. Having in mind that for compensating temporal decorrelation effects large baselines are of advantage, the expected small baselines are sub-optimal.

Acknowledgements

This work has been undertaken within the framework of the JAXA Kyoto & Carbon Initiative. ALOS PALSAR data have been provided by JAXA EORC

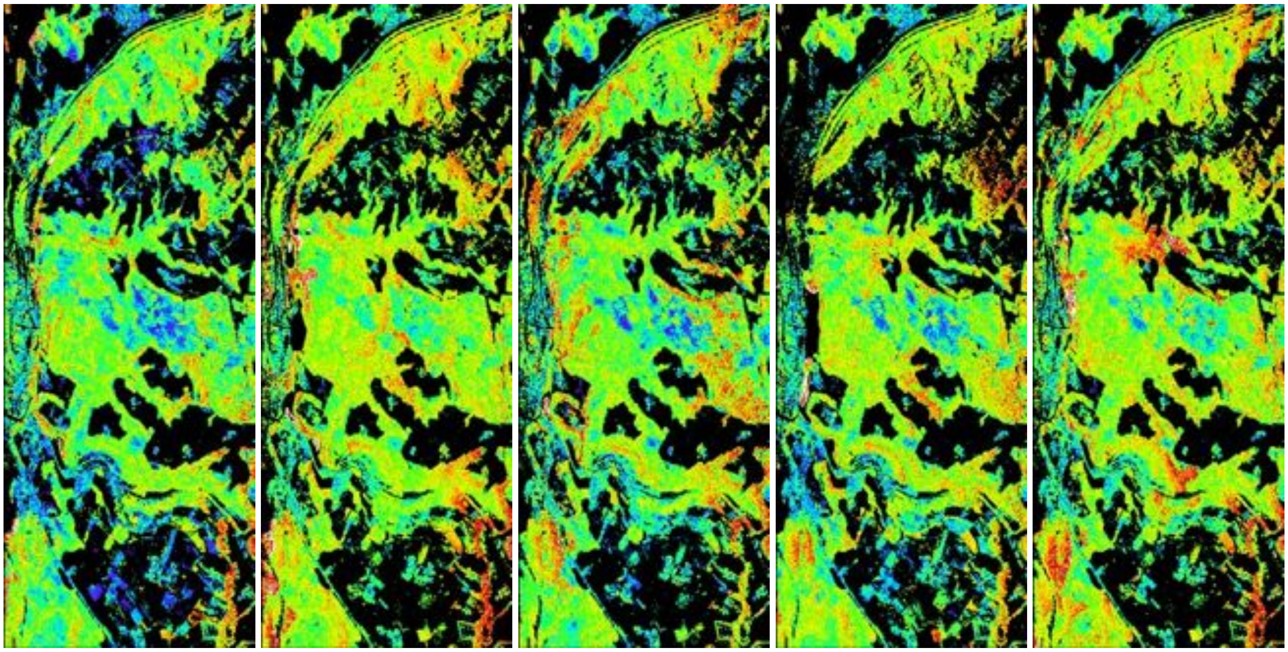

1 day **5 days** **7 days** **12 days** **13 days**

Figure 13 Forest height maps Temposar campaign with temporal baselines, from 1 to 13 days; scaled from 0m to 50m; color table in Figure 7.

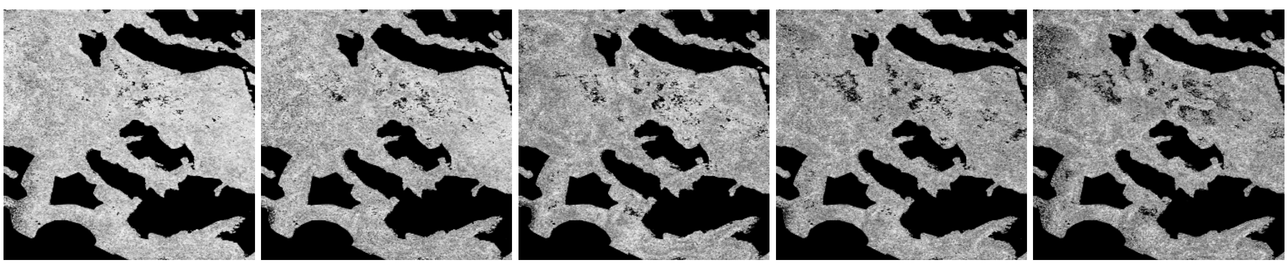

1 day **5 days** **7 days** **12 days** **13 days**

Figure 14 Temporal decorrelation TempoSAR campaign from 1 to 13 days, scaled from 0 (black) to 1 (white).

REFERENCES

[1] [1] A. Rosenqvist, M. Shimada, B. Chapman, A. Freeman, G. de Grandi, S. Saatchi, and Y. Rauste, " The Global Rain Forest Mapping Project – a review", International Journal of Remote Sensing, vol.21, No.6&7, 1375-1387, 2000

[2] A. Rosenqvist, T. Ogawa, M. Shimada and T. Igarashi, "Initiating the ALOS Kyoto & Carbon Initiative", Proceeding of IEEE Geoscience and Remote Sensing Symposium (IGARSS'03), 21. - 25. July, Toulouse, France, 2003

[3] M. J. Quinones and D. Hoekman, "Exploration of Factors Limiting Biomass Estimation by Polarimetric Radar in Tropical Forests", IEEE Transactions of Geoscience and Remote Sensing, Vol 42, NO.1, January, 2004

[4] D. Hoekman, M. J. Quinones, "Biophysical Forest Type Characterisation in the Colombian Amazon by Airborne Polarimetric SAR", IEEE Transactions on Geoscience and Remote Sensing, Vol 40, NO.6, June, 2002

[5] J. Mura, L. Bins, F. Gama, C. Freitas, J. Santos & L. Dutra, "Identification of the tropical forest in Brasilian Amazon based on the DEM difference from P- and X- band interferometric data.", Proceedings of the IEEE International Geoscience and Remote Sensing Symposium (IGARSS), 9-13 July, Sydney, Australia, vol. 2 pp.789-791, 2001

[6] T. Neef, G. S. Biging, L. V. Dutra, C. C. Freitas, J. R. d. Santos, "Markov point processes for modelling of spatial forest paterns in Amazonia derived from interferometric height", Remote Sensing of Environment 97 , pp: 484-494, 2005

[7] T. Neef, , L. V. Dutra, J. R. d. Santos, , C. C. Freitas, L. V. Dutra, "Tropical Forest Mesaurments by Interferometric Height Modeling and P-Band Radar Backscatter", Forest Science 51(6), pp: 585-594, 2005

[8] D. H. Hoekman and C. Varekamp, "Observation of Tropical Rain Forest Trees by Airborne High-Resolution Interferometric Radar", IEEE Transactions of Geoscience and Remote Sensing, Vol 39, NO.3, March, 2001

[9] C. Varekamp, D. Hoekman, “High-Resolution InSAR Image Simulation for Forest Canopies”, IEEE Transactions of Geoscience and Remote Sensing, Vol 40, NO.7, July, 2002

[10] S.R. Cloude and K.P. Papathanassiou 1998, "Polarimetric SAR Interferometry", IEEE Transactions on Geoscience and Remote Sensing, vol. 36, no. 5, pp. 1551-1565, September 1998.

[11] K.P. Papathanassiou and S.R. Cloude, ‘‘Single-baseline Polarimetric SAR Interferometry’’, IEEE Transactions on Geoscience and Remote Sensing, vol. 39, no. 11, pp. 2352-2363, 2001.

[12] J. Praks, F. Kugler, K. P. Papathanassiou, I. Hajnsek, M. Hallikainen, “Tree height estimation for boreal forest by mreans of L- and X- band POLInSAR and HUTSCAT profiling scatterometer”, IEEE Transactions on Geoscience and Remote Sensing letters, Vol. 4, No. 3, pp. 466-470, July 2007

[13] F. Kugler, F.N. Koudogbo, K.P. Papathanassiou and K. Gutjahr , “Frequency Effects in Pol-InSAR Forest Height Estimation”, Proceedings of European Conference on Synthetic Aperture Radar, EUSAR'06, Dresden, Germany, May 16-18, 2006.

[14] T. Mette, K. P. Papathanassiou, I. Hajnsek, “Estimating Forest Biomass from Polarimetric Interferometric SAR Data in Combination with Forest Allometry - Results from temperate spruce forest test site Traunstein”, Proceedings on Retrieval of Bio and Geophysical Parameters from SAR data for land applications, Innsbruck, Austria, 16 - 19 November 2004

[15] F. Garestier, P. C. Dubois-Fernandez, K. P. Papathanassiou, “Pine Forest Height Inversion Using Single-Pass X Band PolInSAR Data”, IEEE Transactions on Geoscience and Remote Sensing, Vol 46, NO.1, January, 2008

[16] S. Magnussen, P. Eggermont, and V. N. La Ricca, “Recovering tree heights from airborne laser scanner data,“, Forest science, 45, pp. 402-422, 1999

[17] J. Hyyppä, H. Hyyppä, M. Inkinen, & M. Engdahl, ”Verification of the potential of various remote sensing devices for forest inventory“,Proceedings of the IEEE International Geoscience and Remote Sensing Society, pp. 1812-1814, Pasadena, California, 1998

[18] G. Krieger, K. P. Papathanassiou, S. R. Cloude, “Spaceborne Polarimetric SAR Interferometry: Performance Analysis and Mission Concepts”, EURASIP Journal of Applied Signal Processing, Vol. 20, pp 3272-3292, 2005

[19] R. Bamler, P. Hartl, “Synthetic aperture radar interferometry”, Inverse Problems, vol.14, no. 4, pp. R1-R54,1998

[20] I. Hajnsek, K. P. Papthanssiou, and S. R. Cloude, “ Removal of Additive Noise in Polarimetric Eigenvalue Processing”, Proceedings IGARSS’01, Sydney Australia, 2001

[21] H. A. Zebker, J. Villasenor, “Decorrelation in interferometric radar echoes”, IEEE Transactions of Geoscience and Remote Sensing, Vol 30, NO.9, January, 1992

[22] R.N. Treuhaft, S.N. Madsen, M. Moghaddam, and J.J. van Zyl, “Vegetation Characteristics and Underlying Topography from Interferometric Data”, Radio Science, vol. 31, pp. 1449-1495, 1996.

[23] S.R. Cloude and K.P., Papathanassiou, “Three-stage inversion process for polarimetric SAR interferometry”, IEE Proceedings - Radar Sonar and Navigation, vol. 150, no. 3, pp. 125-134, 2003.

[24] F. Kugler, K.P. Papathanassiou, S. K. Lee, I. Hajnsek and H. Pretzsch, “Forest Height Estimation by Means of Airborne Repeat-Pass Polarimetric SAR Interferometry”, in preparation.

[25] S.R. Cloude, & E. Pottier, “A Review of Target Decomposition Theorems in Radar Polarimetry”, IEEE Transactions on Geoscience and Remote Sensing, vol. 34, no. 2, pp.498-518, 1996

[26] Izzawati, E. D. Wallington, I. H. Woodhouse, “Forest Height Retrieval From Commercial X-Band SAR Products”, ”, IEEE Transactions on Geoscience and Remote Sensing, Vol. 44, No. 4, 2006

[27] H. Balzter, C. Rowland, R. Milne, O. Stebler, G. Patenaude, T. Dawson, and P. Sachi, “Potential of Polarimetric SAR Interferometry for Forest Carbon Accounting”, Proceedings IGARSS 2003, Toulouse, France, 2003

[28] J.C. Mura, L. Sant` Anna Bins, F.F. Gama, C. Da Costa Freitas, J.R. dos Santos, LV. Dutra, ”Identification of the Tropical Forest in Brazilian Amazon based on the DEM difference from P and X bands interferometric data”, Proceedings IGARSS 2001, Sydney, Australia, 2001

[29] M. Tabb, J. Orrey, T. Flynn, and R. Carande, “ Phase diversity: a decomposition for vegetation parameter estimation using polarimetrc SAR interferometry”, Proceedings EUSAR 2002 pp. 721-724

[30] T. Flynn, M. Tabb and R. Carande, “ Coherence region shape extraction for vegetation parameter estimation in polarimetric SAR interferometry”, Proceedings of the IEEE International Geoscience and Remote Sensing Symposium (IGARSS), June, Toronto, Canada, vol. 5, pp.2596-2598 , 2002

[31] E. Colin, C. Tintin-Schnaider and W. Tabbarra, “An interferometric coherence optimization method in radar polarimetry for high-resolution imagery”, IEEE Transactions on Geoscience and Remote Sensing, vol. 44, no. 1, pp. 167 - 175, January 2006

[32] R.T. Fomena and S.R. Cloude, “On the Role of Coherence Optimization in Polarimetric SAR Interferometry”, CEOS SAR Cal / Val Workshop, Adelaide, Australia, September 28-30, 2005

[33] T. Mette, K. P. Papathanassiou, I. Hajnsek, “Biomass estimation from polarimetric SAR interferometry over heterogeneous forest terrain”, Proceeding of IEEE Geoscience and Remote Sensing Symposium (IGARSS 2004), 20. - 24. September, Anchorage, Alaska, 2004

[34] H. Kramer, A. Akca, ”Leitfaden zur Waldmesslehre“, Sauerländer, Frankfurt, 1995 p. 145

[35] T. Aulinger, T. Mette, K. P. Papathanssiou, I. Hajnsek, M. Heurich, P. Krzystek, “Validation of heights from Interferometric SAR and Lidar over the temperate Forest Site Nationalpark Bayerischer Wald”, Proceedings of the 2nd International Workshop POLinSAR 2005 (CD), 17-21 January, Frascati, Italy 2005

[36] R. Horn, “ The DLR airborne SAR project E-SAR”, Proceedings of IEEE Transactions of Geoscience and Remote Sensing, Symposium, Lincoln, Nebraska, Vol 3, May, 1996

[37] K.P. Papathanassiou and S.R. Cloude, “The Effect of Temporal Decorrelation on the Inversion of Forest Parameters from Pol-InSAR Data”, Proceedings IGARSS'03 (CD-ROM), Toulouse, France, 2003

[38] G. Krieger, A. Moreira, H. Fiedler, I. Hajnsek, M. Werner, M. Younis, M. Zink, “TanDEM-X: A Satellite Formation for High Resolution SAR Interferometry”, IEEE Transactions on Geoscience and Remote Sensing, 45 (11), pp. 3317 – 3341, 2007

[39] I. Hajnsek, F. Kugler, S.-K. Lee, K. P. Papathanassiou, “Tropical-Forest-Parameter Estimation by means of Pol-InSAR: The INDREX II Campaign, *IEEE Transactions on Geoscience and Remote Sensing*, vol. 47, no. 2, pp. 481 – 493, February 2009

Seung-Kuk Lee received the B.S. and M.S. degrees in earth system sciences from the Yonsei University, Seoul, Korea, in 2000 and 2005, respectively. In 2007, started working at German Aerospace Center (DLR) as a guest scientist on scholarship from Korea Research Foundation (KRF). He is currently a PhD student at DLR. His interest is in Polarimetric SAR interferometry.

Florian Kugler was born in Bavaria, Germany, in 1974. He received a Diploma degree (Dipl. Ing. silv.) in forestry science from the Technische Universität München, Freising, Germany, in 2004. Since October 2004, he is a Ph.D. student at the German Aerospace Center (DLR). His research focuses on Remote Sensing on forests, by using Polarimetric SAR Interferometry.

Konstantinos Panagiotis Papathanassiou (*IEEE M' 02, SM' 03*) received the Dipl. Ing degree (Honors) in 1994 and the Dr. degree (Honors) in 1999 from the Technical University of Graz, Austria. From 1992 to 1994 he was with the Institute for Digital Image Processing (DIBAG) of Joanneum Research, in Graz, Austria. Between 1995 and 1999 he worked at the Microwaves and Radar Institute (HR) of the German Aerospace Center (DLR), in Oberpfaffenhofen, Germany. From 1999 to 2000 he was an EU post-doctoral fellow with Applied Electromagnetics (AEL) in St. Andrews, Scotland. Since October 2000 he is again with the Microwaves and Radar Institute (HR) of the German Aerospace Center (DLR). Actually he is a senior scientist within leading the SAR System research group at DLR-HR. His main research interests are in polarimetric and interferometric processing and calibration techniques, polarimetric SAR interferometry, and the quantitative parameter estimation from SAR data, as well as in SAR mission design and SAR mission performance analysis. He has more than 100 publications in international journals, conferences and workshops. He was awarded with the IEEE GRSS IGARSS Symposium Prize Paper Award in 1998, the Best Paper Award of the European SAR Conference (EUSAR) in 2002 and the DLR science award in 2002.

Alberto Moreira was born in São José dos Campos, Brazil, in 1962.

He received the B.S.E.E. and the M.S.E.E. degrees from the Aeronautical Technological Institute, São José dos Campos, in 1984 and 1986, respectively, and the Eng. Dr. degree (with honors) from the Technical University of Munich, Munich, Germany, 1993.

In 2003, he received a full professorship from the University of Karlsruhe, Karlsruhe, Germany, in the field of microwave remote sensing. As its Chief Scientist and Engineer, he managed from 1996 to 2001 the Synthetic Aperture Radar (SAR) Technology Department,-Microwaves and Radar Institute, German Aerospace Center (DLR), Oberpfaffenhofen, Germany. Under his leadership, the DLR airborne SAR system, E-SAR, has been upgraded to operate in innovative imaging modes like polarimetric SAR interferometry and SAR tomography. Since 2001, he has been the Director of the Microwaves and Radar Institute, DLR. The Institute contributes to several scientific programs and space projects for actual and future air-and spaceborne SAR missions like TerraSAR-X and Sentinel-1. In 2006, the mission proposal TanDEM-X led by his institute has been approved for the realization phase. He is the Principal Investigator for this mission. His professional interests and research areas encompass radar end-to-end system design and analysis, innovative microwave techniques and system concepts, signal processing, and remote-sensing applications.

Dr. Moreira is serving as a member of the IEEE Geoscience and Remote Sensing Society (GRSS) Administrative Committee (1999–2001, 2004–2007, 2008–2009 as Executive Vice-President), was the Founder and Chair of the German Chapter of the GRSS (2003–2008), was an Associate Editor for the IEEE GEOSCIENCE AND REMOTE SENSING LETTERS (2003–2007), and is serving as Associate Editor for the IEEE TRANSACTIONS ON GEOSCIENCE AND REMOTE SENSING. Since 2003, he has also been serving as a member of the Board of Directors of the Information Technology Society, German Association for Electrical, Electronic and Information Technologies. In 1995, he was the recipient of the DLR Science Award. He and his colleagues received the GRSS Transactions Prize Paper Awards in 1997 and 2001, respectively. He is also the recipient of the IEEE Nathanson Award (1999) and the IEEE Kiyo Tomiyasu Award (2007). He has contributed to the successful series of the European SAR conferences since 1996 as a member of the Technical Program Committee, Technical Chairman (2000), Awards Chairman (2002–2004), General Chairman (2006), and Cochairman (2008).

Forest Theme

SAR, InSAR and Lidar Studies for Measuring Vegetation Structure Over the Harvard Forest Region

Paul Siqueira *et al.*
University of Massachusetts (U.S.A.)

SAR, InSAR and Lidar Studies for Measuring Vegetation Structure Over the Harvard Forest Region

Paul Siqueira
University of Massachusetts, Amherst, MA, siqueira@ecs.umass.edu

Razi Ahmed (UMass), Bruce Chapman (JPL)
rahmed@ecs.umass.edu, bruce.chapman@jpl.nasa.gov

Abstract— **This short paper details the current work for utilizing repeat-pass ALOS/PALSAR observations for characterizing vegetation in the Harvard Forest of Western Massachusetts. A significant number of repeat-pass measurements in both polarimetric and single/dual-polarization mode were made by PALSAR in the three years since its launch. To date, our team has been analyzing the co-polarized horizontal channel of the quad-pol mode over this region, and compared it to full waveform lidar data collected by the LVIS instrument in 2003. From these analyses, it has been possible to derive a lidar based estimates of biomass over a large geographic region, and to create relationships between the radar backscatter and the lidar derived biomass. Further, it is also possible to test the ability of the radar to estimate biomass directly, as well as to explore alternate observing scenarios, such as polarimetric interferometry and single-pol interferometry for estimating vegetation characteristics. This short paper summarizes these studies, and reinforces the well known association of backscatter power in the cross-pol L-band channel with biomass as well as showing the degree of temporal decorrelation over the PALSAR 46 day repeat cycle is sufficiently large to preclude the use of this observing mode for estimating height, or other structural characteristics, of vegetation.**

Index Terms—**ALOS PALSAR, K&C Initiative, Forest Theme, above-ground biomass, etc. etc.**

I. INTRODUCTION

Among the areas necessary for continued scientific development identified by United Nations Framework Convention on Climate Change via the Kyoto Protocol and REDD (Reducing Emissions and Deforestation and Degredation) is the need for quantifying carbon stores held in the world's vegetation and characterization of species habitats through the measure of vegetation structure, both horizontal (on a hectare-to-hectare scale) and vertical (to a meter-level accuracy). The spaceborne instrument, ALOS/PALSAR [1,2], an L-band Synthetic Aperture Radar, and the Japanese Aerospace Agency's (JAXA) Kyoto and Carbon Cycle Initiative [3], provides unprecedented access to detailed, expansive and continued coverage of the world's forests in the form of data that can be used to characterize the current state of the vegetation and its change (both seasonal and long-term) over time.

In one study conducted by the University of Massachusetts, NASA's Jet Propulsion Laboratory, and the Japanese Aerospace Agency, scientists are using data from ALOS/PALSAR and an Airborne lidar (LVIS; from NASA's Goddard Space Flight Center) to image the vegetation structure over the Harvard Forest located in Western Massachusetts. The Harvard Forest [4] is a mixed hardwood, transitional forest that has been the subject of many studies, both large and small, for the purposes of characterizing the environment and the many species that benefit from the presence of the forest (Figure 1).

Figure 1. Image of the forest cover type near the Quabbin reservoir in the ALOS/PALSAR image swath. This image gives an indication of the vegetation and landcover type for the region.

The series of repeat ALOS observations made available from the Japanese Space Agency since the launch of the platform in 2006 has provided a rich and consistent data set which provides an opportunity to explore relationships between the SAR, InSAR and lidar data, to better understand methods of combining these fundamental data sources for studying the ecosystems, carbon balance and vegetation three-dimensional structure in the Harvard region and to extrapolate the results as they would apply to similar observations worldwide.

II. PROJECT DESCRIPTION

A. Relevance to the K&C drivers

One of the drivers of the JAXA's Carbon Cycle Program is for the quantification of carbon of the world's forested regions. In order to attain this far reaching goal, it is necessary to carry out focused studies on localized regions, so as to develop a better understanding of the types of accuracies and error sources involved in estimating carbon using a satellite based system.

To this end, this detailed study of the Harvard Forest provides a cornerstone for conducting further studies, as well as providing an important set of conclusions in its own right. Among the scientific findings that have been made as a result of this work are:

i.) we have derived a lidar based biomass map of the Harvard Forest region. This biomass is available to other scientists in JAXA's K&C program by request

ii.) a relationship of L-band cross-polarized backscatter to above ground biomass has been derived. This relationship is consistent with similar relationships published by other researchers in the field

iii.) it is demonstrated that the degree of temporal decorrelation over a 46 day repeat period makes it difficult to perform quantitative estimates of 3D vegetation structural characteristics based on the interferometric observations alone.

B. The Harvard Forest Region

Located near the Quabbin reservoir in Western Massachusetts, the Harvard Forest is a temperate zone mixed phase forest consisting of a variety of transition hardwood regrowth resulting from widespread disturbances that took place over 100 years ago. One of the nine NASA funded Bigfoot sites for connecting remote sensing measurements to ground process observations of carbon flux and net primary production, the Harvard Forest has been a resource for a wide variety of ecological studies on spatial scales extending from the microscopic to macroscopic. Typical characteristics of the region that are relevant to this study are an upper limit to carbon content range between 100 and 120 Mg/ha, an average tree height of 24m, a mean basal area of 40 m2/ha, and on the order of 1000 trees/ha [5].

In July of 2003, the Laser Vegetation Imaging Sensor (LVIS) overflew the Harvard region, collecting full waveform lidar data for determining the true ground elevation and the vertical extent of the canopy over a 30 kha area (9 km x 30 km). These data are used for comparison to the PALSAR backscatter and INSAR data (Figure 2).

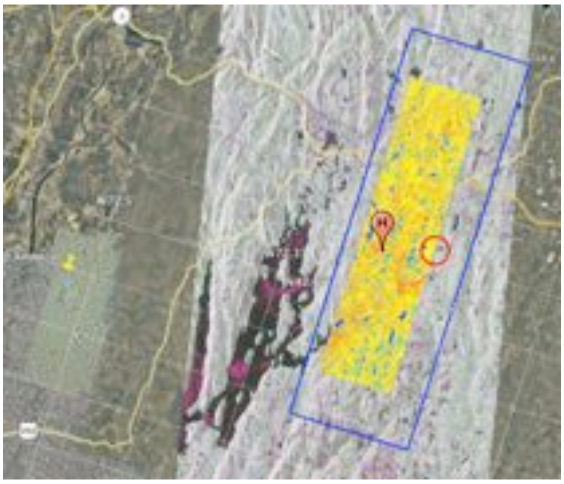

Figure 2. Location of the Harvard Forest (balloon-H) in relation to Amherst (yellow push-pin), the LVIS swath (yellow rectangle representing tree heights), the ALOS swath (white region). ALOS K&C © JAXA/METI.

C. ALOS/PALSAR Observations

Since its launch in early 2006, ALOS has made multiple observations of western Massachusetts using various observing modes, among them, fully polarimetric, single- and dual-pol, and wide beam scansar. The initial focus of this work has been on the processing of the fully polarimetric data. To date, only the co-polarized horizontal polarization has been processed. A summary of the fully polarimetric (PLR) observations (cycle number, date and season) are given in Table 1. Note that not all cycles included observations (letters monikers indicate the observations), yet some nine data collections have already been made. Each observation offers a new scene that can be interfered with the others, thus creating a matrix of possible interferograms. Table 2 provides details of the interferometric baselines between all possible pairings of these nine observations. The critical baseline being 4.5 km for this observing mode.

The sum total of all ALOS observations covers multiple years and multiple seasons. Many are in adjacent observing periods (46 days long). Hence the rich data set, especially over the Harvard Forest region, is ideal for exploring a variety of relationships relating to phenology of different target types, and repeatability of measurements over multiyear periods. All important characteristics for maximizing the utility of the existing dataset as well as for planning future ones.

Table 1. Summary of available fully polarimetric PALSAR scenes over the Harvard Forest. A letter code is given for easy reference to the different scenes.

cal	1	27-May-06	early summer
A	2	12-Jul-06	mid summer
B	3	27-Aug-06	late summer
C	4	12-Oct-06	mid fall
D	5	27-Nov-06	early winter
E	6	12-Jan-07	mid winter
	7	27-Feb-07	mid winter
F	8	14-Apr-07	early spring
G	9	30-May-07	early summer
	10	15-Jul-07	mid summer
	11	30-Aug-07	late summer
H	12	15-Oct-07	mid fall
I	13	30-Nov-07	early winter

Table 2. Interferometric perpendicular baselines (m) over the Harvard region (see table 1 for observation dates). The critical baseline for this observing mode is 4.5 km. Highlighted are those baselines of interest. Dark highlights indicate those that have baselines that are likely too large for their intended purpose.

	A	B	C	D	E	F	G	H	I
A	0	4250	3800	4500	2450	5160	4600	6180	6200
B		0	460	240	1800	910	340	1900	1970
C			0	705	1350	1360	800	2380	2460
D				0	2070	660	70	1670	1720
E					0	2730	2160	3750	3800
F						0	570	1020	1080
G							0	55	1640
H								0	52
I									0

Figure 3. Optical image (from Google Earth) of a small region covered by both LVIS and PALSAR observations. Note a variety of landcover types, ranging from open fields, open water and mixed (coniferous and deciduous hardwood) vegetation types. The size of the above image is 3 km by 5 km.

D. Work approach

The approach for performing the study has taken place in three basic steps. These are: i.) processing of the full waveform lidar data into estimates of above ground biomass based on available ground validation measurements over 43 sites within the region, ii.) processing of the ALOS data from level 1.0 into ground referenced data suitable for PolInSAR processing as well as radiometrically calibrated backscatter measurements, and iii.) investigation of relationships between the lidar derived parameters of height and biomass, and those observed with ALOS/PALSAR. First however, it is important to consider the region being studied.

Lidar data and Processing

Full waveform data from the LVIS instrument is available over a 10 by 30 km region over the Harvard Forest (see Figure 1). In addition, some 43 ground validation sites have been established [5] for studying biomass and vegetation structural characteristics. Full waveforms, like those shown in Figure 4, provide measures such as the height of mean energy (or HOME) which can be used for forming empirical relationships between vegetation characteristics of interest and the lidar measures. Several such relationships are shown in Figure 5, which relates lidar derived biomass to the biomass measured at the ground validation sites. Note that in determining the biomass relationships that make up the plot of Figure 5, the ground validation data is used two times, first to fit the data, and second, to demonstrate the quality of the fit. Given the very small sample size (43 plots, 30m in diameter), this is an acceptable approach.

Further, Figure 5 also demonstrates the goodness of fit for two different types of polynomials. One, a linear fit to the lidar measure of HOME (equivalently rh50) and the other, proportional to HOME, the square of HOME, and the variance of the HOME measure. In all, the improvement attained by the more complicated model is only 5 Mg/ha for the root mean square error, or RMSE. Because of the minor improvement, it is generally preferred to rely on the simpler model, to avoid overfitting of the ground validation data.

A last step of preprocessing for the lidar data was necessary. This involved in examining the lidar waveforms over the ground validation sites in a 3-dimensional framework to assure that the lidar waveforms were correctly aligned with respect to the true ground surface. That is, it was found that a significant number of waveforms were mis-registered in the vertical direction and had to be corrected so as not to provide false signatures related to the vegetation height. An example of a successful set of lidar waveforms over the 85th Harvard Forest Site is shown in Figure 6.

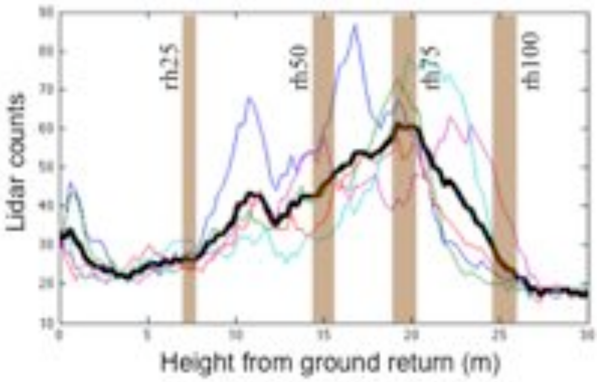

Figure 4. An LVIS waveform plot over a 700 m^2 Bigfoot test plot (#85) located at the Harvard Forest. The biomass for this area was measured to be 92 ± 10 Mg/ha. Shown are five waveforms (thin lines) and the average waveform (thick black line) and the radar metrics of rh25, rh50, rh75 and rh100, which can be used for forming empirical relationships between height and vegetation structural characteristics or biomass.

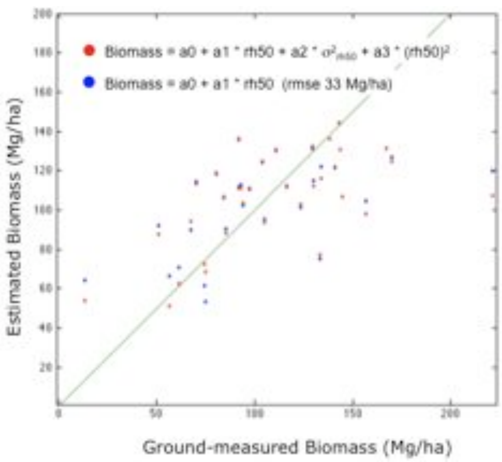

Figure 5. Results from forming a polynomial fit between full waveform derived lidar moments and measured biomass. There is a preference for the least complicated model, shown in blue, which gives a mean error of 33 Mg/hectare. ALOS K&C © *JAXA/METI.*

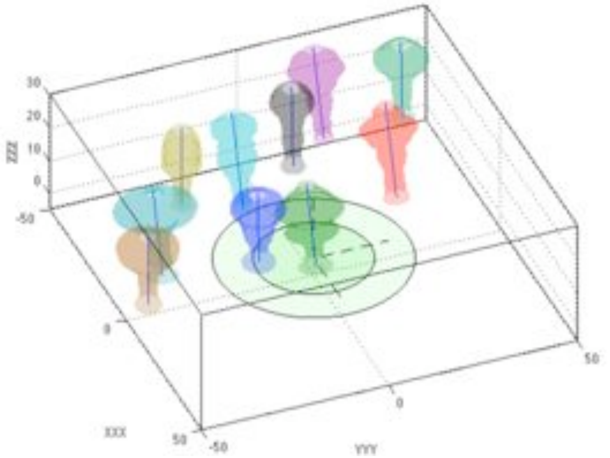

Figure 6. A 3-dimensional plot of lidar waveforms associated with the site #85 of the Harvard Forest ground validation data. Shown at center are 15m and 25m radii around the area where data were taken on the ground. Ten lidar waveforms closest to the site (shown in different colors), are plotted with different aspect angles due to the changing position of the lidar platform, and the power as a function of height, shown as a vertical cylinder with varying radius, for each lidar return. It was determined that individual lidar waveforms had to be adjusted to assure that all were correctly registered to the true ground surface for the region.

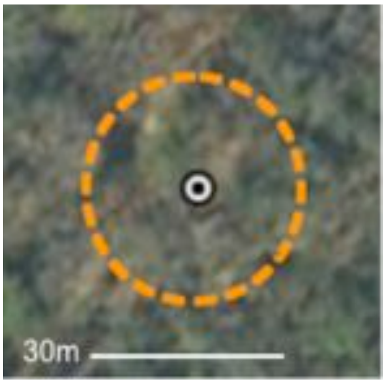

Figure 7. A close-up optical image of site #85 at the Harvard Forest. Images such as these were used to interpret the observed lidar returns for each site.

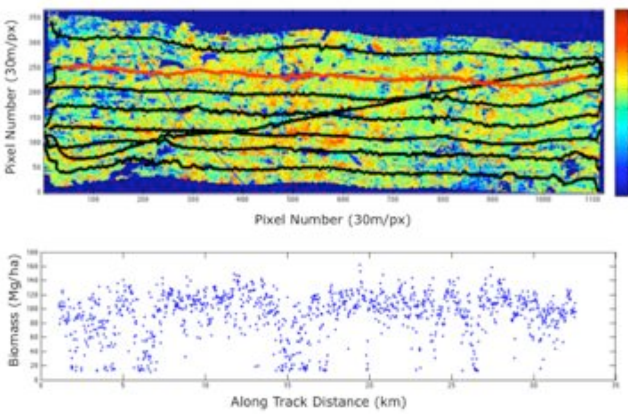

Figure 8. Image of the lidar-derived biomass map of the Harvard Forest region overlain with the nadir track of the LVIS lidar. The part of the track highlighted in red was used to extract a plot of biomass which could be compared to radar observations of backscatter power and interferometric correlation. The lower plot shows the resulting biomass estimates calculated along the highlighted LVIS nadir track.

Once the relationship between lidar and ground validation data (shown in Figure 7) was established, a full biomass map based on the observed LVIS lidar data set was derived. This is shown in Figure 8 and Figure 10. In Figure 8, this biomass map is overlain with the nadir track of the LVIS sensor. The nadir track tends to be more accurate because of the simpler viewing geometry and better ground return for the lidar in the nadir direction.

Data from this nadir track was extracted and used for comparison against radar derived measures of correlation and backscatter, thus providing a pathway for determining how well the radar can estimate the vegetation structural characteristics across the lidar swath and over wider regions where lidar data might not be available. The biomass as a function of position along one of the LVIS nadir tracks is shown in the lower half of Figure 8. The full biomass map, expanded in size to show greater detail, is shown in Figure 10.

SAR and InSAR data and Processing

SAR and repeat-pass InSAR data were collected over the Harvard Forest using multiple observing modes of the ALOS/PALSAR instrument. For the work described in this paper, we show only those results relating to the polarimetric observing mode known as PLR 21.5.

Data was requested from JAXA in level 1.0 format so that all scenes could be processed by gamma remote sensing software to the same Doppler centroid (necessary for interferometric processing). Further, data were coregistered to the SRTM DEM, using a simulated backscatter image derived from the DEM. This process allows easy exchange between radar data coordinates and map coordinates, as well as the extraction of the known DEM (C-band) from the interferometric data.

Because the processed SAR data is effectively co-registered to the SRTM DEM map-level data to the sub-pixel level, both in radar and map coordinates, the task of making comparisons between the lidar (in map coordinates) and radar data sets is a straight-forward task. An illustration of this relationship is shown in Figure 9.

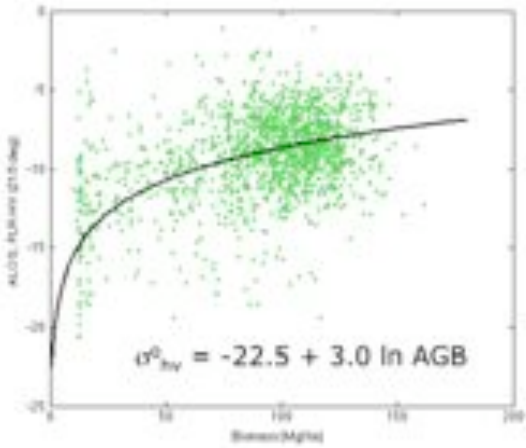

Figure 9. A relationship between ALOS measured backscatter cross-pol power (21.5 degree look angle) and lidar derived biomass. The black curve shows the equation for above ground biomass (ABS) and the backscatter power. ALOS K&C © JAXA/METI.

Processing for interferometry and polarimetric interferometry is a bit more involved (see Figure 11). It requires careful calibration of the data and processing all polarizations for the two (or more) passes of the instrument to a common Doppler centroid, nominally zero, or in the broadside direction to the flight path. After processing scenes, they are coregistered (if not already) and the coherence matrix is formed from the multiple polarizations. Based on the observing geometry and the SRTM DEM, the interferometric phase due to topography is removed, thus leaving only that phase that is associated with the difference in topography seen between the SRTM C-band observations and those from ALOS/PALSAR's L-band SAR.

The resulting interferogram for any one combination of two polarizations is a complex number. The phase, relating to the differential topography discussed in the previous paragraph, and the amplitude, which is relate to the standard deviation of the phase. For volume scatterers, this standard deviation is proportional to the vertical depth of the volume, and thus can provide a method for estimating the vegetation height.

There are other signals that affect both the volume and phase of the interferometric signature however. Related to the phase, things like a differential path length through the atmosphere (due to weather etc.) can distort the phase across the observed swath. For the correlation magnitude, the primary error source for repeat-pass systems is related to a changing electromagnetic signature of the target in the time period between observations. This signature can be altered by simple things such as active weather (wind and rain [6]), as well as long term effects related to seasonal differences in the target. Because of the 46 day repeat period of ALOS, it would be expected that this might be a dominant error source, and indeed it is. While correlation magnitudes are large enough to provide sufficient signature for estimating phase, they are large enough to preclude the use of the instrument for using the correlation magnitude signature to perform vegetation height estimation.

III. Results and Summary

In all, the detailed work has yielded a lidar-derived biomass map of the Harvard Forest region. This map was used to develop and test relationships between the L-band SAR backscatter and interferometric signature against the biomass or other forest structural characteristics. In all, it was shown that a basic signature exists between backscatter and biomass, but that the variation is a bit large (Figure 9). This would make inverting the model prone to large uncertainty. Further, interferometric correlation magnitude was studied with the intent that it might be useful for vegetation height extraction. Temporal decorrelation however proved to be a dominant error source, and hence for the PLR 21.5 observing mode over the Harvard Forest at least, it is unlikely that the correlation magnitude can be used for quantitative estimation of vegetation height or other physical characteristics.

Future work will entail the investigation of other ALOS observing modes (such as the dual-pol FBD 34.3) for estimation of vegetation characteristics. The dual-pol observing mode will have a larger cross-track swath (and thus better for mapping) as well as a larger incidence angle, which will likely amplify the polarimetric signature of the vegetation. Figure 12 provides an illustration of the breadth and depth available from these other observing modes. Shown are the LVIS observing swath, a SRTM derived DEM corigistered to PALSAR polarimetric data (FBS 21.5) and PALSAR FBD differential interferometry data.

Acknowledgement

This work has been undertaken within the framework of the JAXA Kyoto & Carbon Initiative. ALOS PALSAR data have been provided by JAXA EORC. It has been financially supported through NASA's Terrestrial Ecology program for the development of remote sensing science for vegetation and ecological applications.

References

[1] M. Shimada, "PALSAR and Calibration update". *11th ALOS K&C Science Team meeting (KC#11)*, Tsukuba, Japan, Jan. 13-16, 2009. [Online] Available: http://www.eorc.jaxa.jp/ALOS/kyoto/jan2009_kc11/pdf/090113/shimada_calval_up_090113.pdf

[2] Rosenqvist A., Shimada M., Ito N. and Watanabe M. "ALOS PALSAR: A pathfinder mission for global-scale monitoring of the environment," *IEEE Trans. Geosci. Remote Sens, vol. 45, no. 11, pp. 3307-3316, 2007.*

[3] A. Rosenqvist, M. Shimada, R. Lucas, J. Lowry, P. Paillou, B. Chapman [eds.], "The ALOS Kyoto & Carbon Initiative, Science Plan (v.3.1)," JAXA EORC, March, 2008. [Online] Available: http://www.eorc.jaxa.jp/ALOS/kyoto/KC-Science-Plan_v3.1.pdf

[4] McKain, K., "Carbon Accumulation at the Harvard Forest: A Comparison of Methods for Measuring Tree Biomass for Regional Extrapolation of the Eddy-Flux Tower Footprint," Mt. Holyoke College Honor's thesis, 2005.

[5] See Harvard forest website: harvardforest.fas.harvard.edu

[6] Ahmed, R., Siqueira, P., Hensley, S., Chapman, B., Bergen, K., "A survey of temporal decorrelation rom spaceborne repeat-pass InSAR," submitted to Rem. Sens. Env., 2008.

Paul Siqueira. Paul Siqueira is an associate professor of Electrical and Computer Engineering at the University of Massachusetts in Amherst. Previously, he has been a radar system engineer and team-X science chair at NASA's Jet Propulsion Laboratory and has earned his PhD at the Radiation Laboratory of the University of Michigan. His PhD topic was wave propagation and scattering in dense random media. Prof. Siqueira's research interests are in remote sensing applications for radar and InSAR and microwave engineering. During his spare time, he enjoys chalk drawing and listening to old records made by Jimi Hendrix and John Coltrane.

Razi Ahmed. Razi Ahmed received the B.S.E.E degree from the National University of Sciences and Technology, Pakistan, in 2002, and the M.S degree in Electrical and Computer Engineering from University of Massachusetts, Amherst, in 2006. Since 2004, he has been with the Microwave Remote Sensing Laboratory at the Univesity of Massachusetts, Amherst where he is currently a PhD student. His research interests include radar remote sensing, statistical signal processing, SAR interferometry and its application to remote sensing of vegetation characteristics.

Bruce Chapman. Bruce Chapman is a senior member of the technical staff at the Jet Propulsion Laboratory, California Institute of Technology, in Pasadena, California. He received his Bachelor of Arts degree in Physics and Astronomy from the University of California, Berkeley in 1981, and his Ph.D. in Earth, Atmospheric and Planetary Sciences from the Massachusetts Institute of Technology in 1986. He is currently an investigator in NASA's Terrestrial Ecology, Space Archaeology, and MEASUREs programs, studying forest structure measurements using Synthetic Aperture Radar, and the utilization of airborne Synthetic Aperture Radar in Mayan Archaeology regions in Central America; as well as participating in the production of an Earth Science Data Record for Inundated Wetlands using ALOS SAR data. He is also the science coordinator for NASA's UAVSAR airborne Synthetic Aperture Radar.

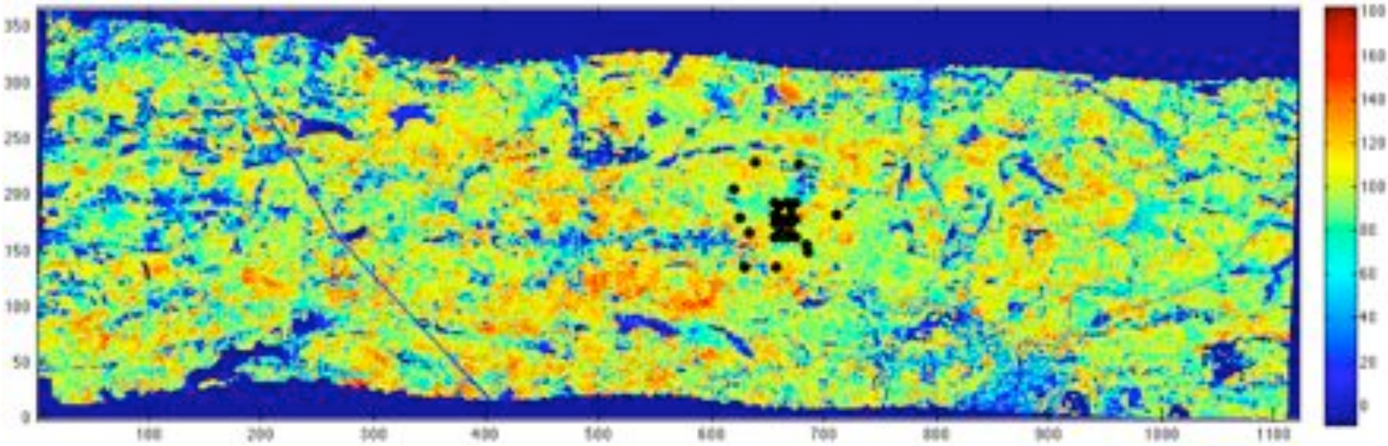

Figure 10. A biomass map of the Harvard Forest region using Goddard Space-Flight Center's LVIS (Laser Vegetation Imaging Sensor). Black dots near the center of the image indicate the locations of the 700m2 plots were biomass and other vegetation physical characteristics were measured on the ground. Horizontal and vertical (inverted) scales are in units of meters with respect to the SoutH-East corner. A depiction of the location of the LVIS swath with respect to larger geographic features and other data sets is shown in Figure ZZZ. Biomass units are in kilotons per hectare.

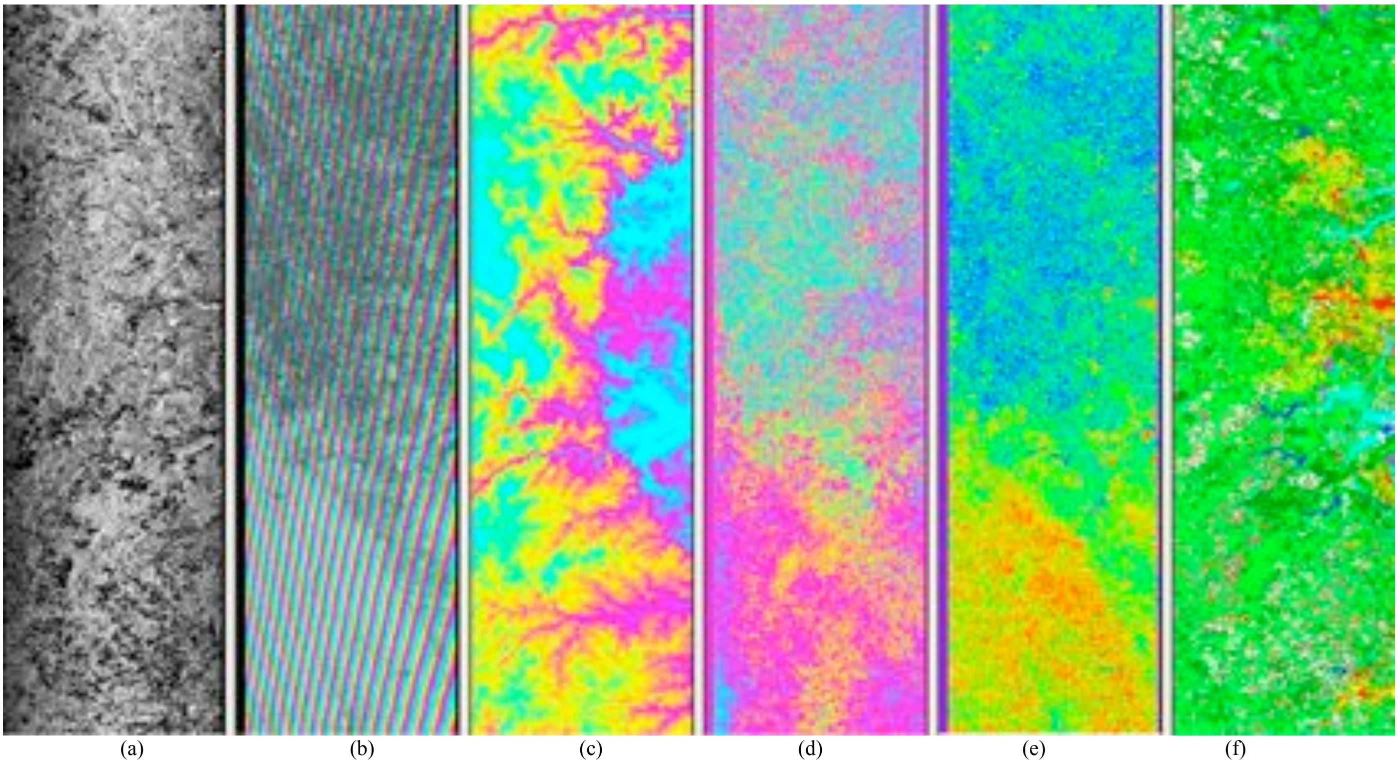

(a) (b) (c) (d) (e) (f)

Figure 11. Illustration of the various steps along the SAR processing chain. Shown is (a) the backscatter image, (b) interferometric correlation and fringes, (c) the SRTM DEM, (d) the differential interferogram, (e) the interferometric correlation magnitude and (f) a map of the national land cover data base (NLCD) from 2006.

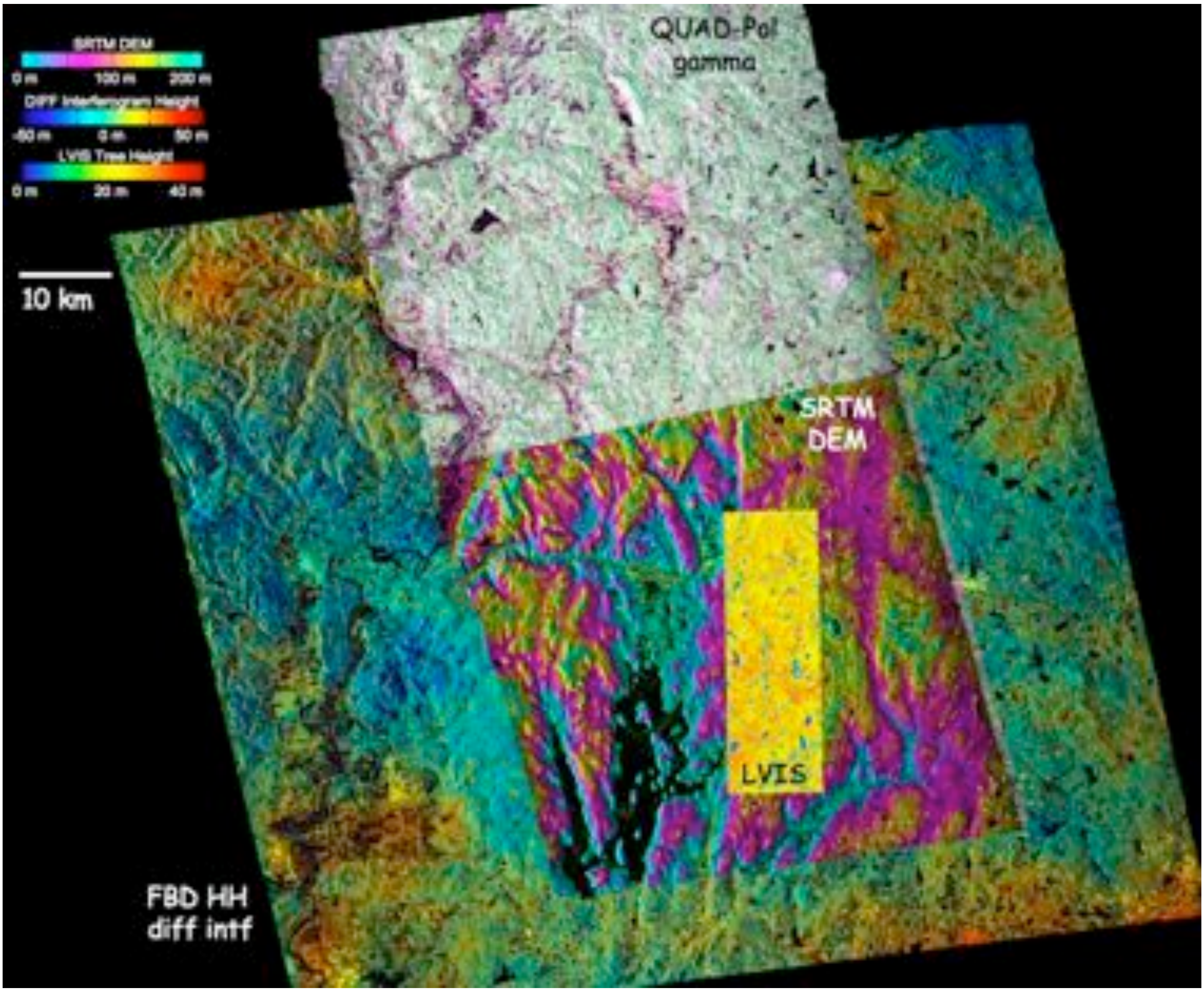

Figure 12. Image of the PALSAR coverage area over the Harvard Forest. Shown are the FBD differential interferogram, the Quad-pol, terrain corrected backscatter, a sample of the DEM derived from SRTM, and the tree height data derived from full-waveform lidar (LVIS). ALOS K&C © JAXA/METI

Wetlands Theme Reports

Wetlands Theme

Seasonal Dynamics of the Pantanal Ecosystem

Maycira Costa *et al.*
University of Victoria (Canada)

Seasonal Dynamics of the Pantanal Ecosystem

Phase 1 Report

THE PANTANAL

ALOS/PALSAR ScanSar Temporal Imagery, 2007

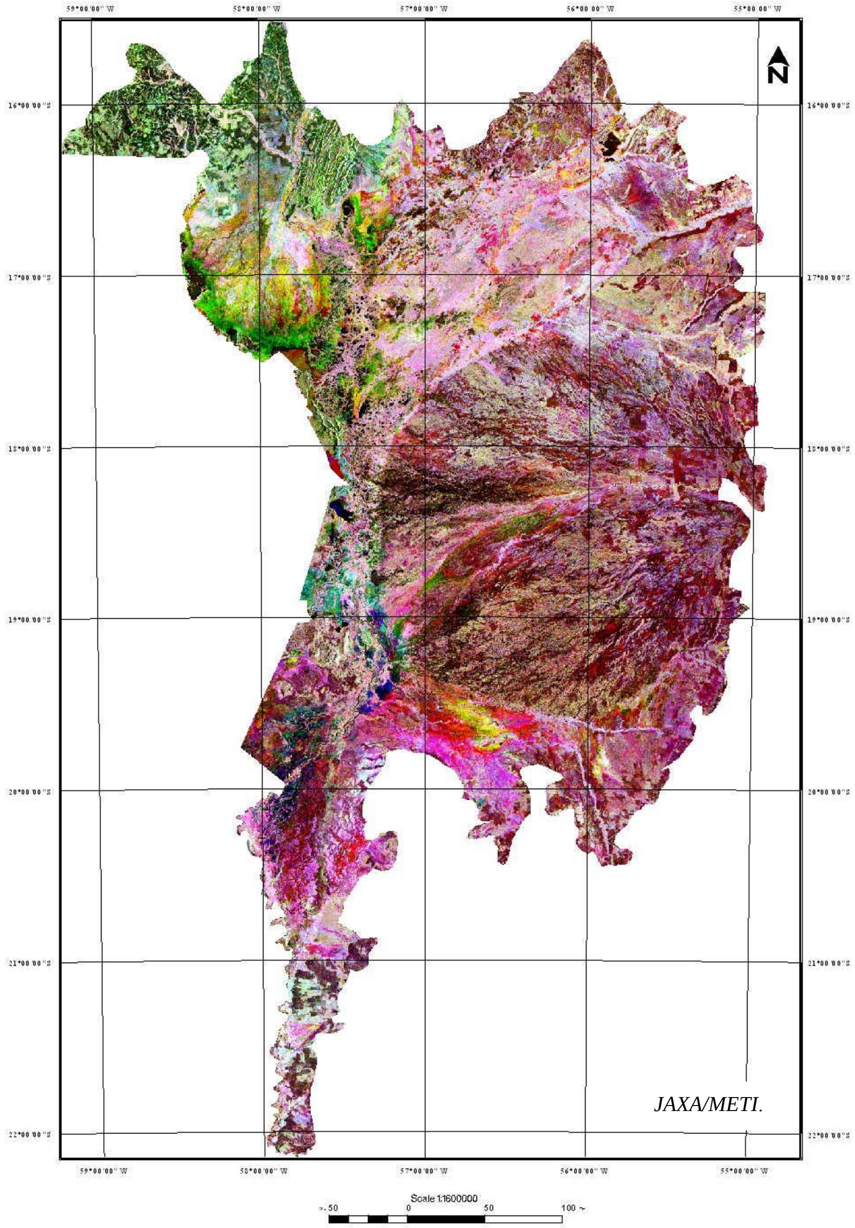

ALOS/PALSAR temporal data for 2007: Blue - February (rising water); Red - May (high water); Green - November (low water)

Seasonal Dynamics of the Pantanal Ecosystem

Maycira Costa[1] , Kevin Telmer[2] and Terresa Evans[1]

[1] Department of Geography; [2] School of Earth and Ocean Sciences, University of Victoria, 3800 Finnerty Rd., Victoria, BC Canada V8P 5C2

Email: maycira@office.geog.uvic.ca

Abstract—**The Brazilian Pantanal is a large tropical wetland with an abundance of biodiversity and varied habitats. It is defined by a seasonal inundation pattern that varies both temporally and spatially. This study uses L-band ALOS PALSAR and C-band Radarsat-2 multi-temporal SAR data to map the seasonal ecosystems and the first spatial-temporal maps of the flood dynamics of the Pantanal. First, an understanding of the backscattering characteristics of flooded and non-flooded habitats was developed. Second, maps of habitats and flooding dynamics were generated using an object based classification method. A level 1 classification defining five cover types was achieved with accuracy results of approximately 77%. A level 2 classification separating flooded from non-flooded regions for five temporal periods over one year was also accomplished, showing large interannual variability between subregions in the Pantanal. Cross-sensor, multi-temporal SAR data was found to be useful in mapping both land cover and flood patterns in wetland areas. The generated maps will be a valuable asset for defining habitats required to sustain the Pantanal biodiversity and the impacts of human development in this region.**

Index Terms—**ALOS PALSAR, K&C Initiative, Wetlands Theme, Pantanal, Conventions, Conservation, Flooding dynamics.**

I. INTRODUCTION

The Pantanal (Figure 1), the largest tropical wetland in the world, is roughly located in the center of South America, between Brazil, Bolivia, and Paraguay. In many ways, it is a unique landscape characterized by salt and freshwater lakes, abundant aquatic vegetation, and open and dense savanna (Pott, 2000, 1989; Abdon *et al.,* 1998; Costa and Telmer, 2006). It is fed by the upper Paraguay River and its tributaries (Figure 2) and these promote a strong annual flood. The degree of flooding and its duration and amplitude vary both yearly and spatially. The complicated flood dynamics makes the delimitation of the total area of the Pantanal extremely difficult (Por, 1995). Estimates suggest that the Brazilian Pantanal occupies an area that ranges from 138,000 km^2 during maximum flood (Silva and Abdon, 1998) to 11,000 km^2 during the dry season (Hamilton *et al.,* 1996), a difference of approximately 90%. The entire watershed of the Pantanal occupies an area of approximately 362,000 km^2.

Within the Pantanal, the occurrence of different habitats such as river corridors, gallery forests, perennial wetlands, and lakes (fresh and brackish lakes), seasonally flooded grass lands, and terrestrial forest is related to the dynamics of the flood cycle and its spatial variations. During the rising and maximum water stand, the dominant habitats are the large areas of floating and rooted aquatic vegetation, open water, and flooded forest. The flooded forest is mostly comprised of shrub-like trees and tall, densely foliated riparian trees (Silva and Abdon 1998). The aquatic vegetation is dominantly floating and rooted species that grow quickly during the maximum flood and die during the dry period. This dynamics of this wetland is the foundation for the many species of plants and animals – salviniaceaes, cyperaceaes, iguanas, tortoises, crocodiles, primates, and multitudes of fish, birds, and insects. However, it is the delicate interplay between the dynamic distribution of vegetation, the high biological productivity of the aquatic plants, the climate, and the hydrological cycle, that nourishes and sustains the incredible diversity of plants and animals. Unfortunately this interplay is poorly understood and is threatened by human development.

A series of human initiatives such as modification of the natural hydrological cycles of rivers, mining, agriculture, and chemical industry, construction initiatives (hydroelectric dams, dikes, Hydrovia, GASBOL – Bolivia-Brazil Gas pipeline), clearing of land and extensive burning, and commerce of wild animals are threatening this wetland ecosystem in an irreversible manner (Hamilton 1999; da Silva and Girard 2004). Some of the resultant effects are loss of habitat and biodiversity, water pollution (mostly mining byproducts and agrochemicals), and erosion and sedimentation of waterways (Gottgens et al. 1998). For example, the five governments of the La Plata basin, Brazil, Bolivia, Paraguay, Argentina, and Uruguay, have jointly developed plans to deepen the Paraguay River, canalize many meanders, and regulate inflows along its course from Cáceres, Brazil, to Porto de Nueva Palmira, Uruguay – an astounding 3400 km, the called Hydrovia (Paraguay-Parana Waterway Project). This project was designed aiming the cheaper transport of soy beans, oil, corn, cotton, manganese, and iron ore, at the expenses of one of the largest environmental disasters ever planned, the canalization and regulation of the Pantanal major rivers. This project as it was initially idealized was waned (recently it has been re-evaluated); however, various smaller hydrological initiatives remain of interest, which are accurate described by Gottens et al., 1998 as the "tyranny of small decisions".

The state of this initiative is currently unclear, however, the Brazilian government has planned the construction of a series of small projects that when treated individually are considered too small-scale to warrant impact assessments, but that together represent potentially large scale change for the Pantanal (Gottgens 1998; da Silva and Girard 2004). The suspected consequences of these projects have been voiced by many critics – loss of wetlands, changes in water quality, reduction in the diversity of flora and fauna, and negative impacts on the livelihoods of local and indigenous people in the region. It is our hope to add to this debate and to do so provide a better understanding of the flooding dynamics of the Pantanal ecosystem. This document reports mostly the use of ScanSAR imagery for mapping the flooding dynamics; the use of fine resolution imagery requires more work on lakes classification (in progress). Also, fine resolution mosaics are not used in this report; at this time, we do not have access to these mosaics.

II. The Pantanal Project

A. *Objectives and Relevance to the K&C drivers*

As stated in the introduction, there is a lack of information on the spatial-temporal inundation pattern on the Pantanal. This is important information for understanding the biogeochemical cycles, the habitats required to sustain the Pantanal biodiversity, and the impacts of human development in the region. With this in mind, the objectives of this project were (1) to map the seasonal ecosystems and flood dynamics of the Pantanal and (2) to detail characterize lake types in the Pantanal. To attend the first objective, ScanSAR ALOS/Palsar and Radarsat 2 imagery were used to map variations in vegetation and monthly inundation extent during the year. To attend the second objective, ALOS/Palsar fine resolution imagery of a pilot area were used and fine resolution mosaics will be used when available.

Our objectives are clearly related to the Thematic drivers: **C**onventions, **C**arbon and **C**onservation, with a stronger focuses on the first and third, as we aim to map the flood dynamics that sustain the Pantanal wetland ecosystems.

B. *Field data*

Field data were acquired for 209 sites in the Brazilian Pantanal in July of 2008. Preliminary analysis of 2007 ALOS/PALSAR imagery, Landsat (provided in Google Earth Pro), and field data acquired in 2001 provided the approximate location of regions to be visited for this campaign. Three regions within the study area were chosen as pilot areas, comprised of the Nhecolandia, Aquidauana and Miranda subregions. Ground cover, as well as vegetation characteristics such as species and distribution were determined from direct observation, then recorded and photographed for each location; also 75 water samples for determining lakes geochemistry were sampled.

Figure 1. The Brazilian Pantanal displayed in grey. (GEF 2004).

C. *Satellite data*

The satellite dataset was acquired from two Synthetic Aperture Radar (SAR) systems: the Advanced Land Observing Satellite (ALOS) and RADARSAT-2. ALOS was launched in January 2006 by the Japanese Aerospace Exploration Agency, and carries onboard the variable-resolution and polarimetric Phased Array L-band Synthetic Aperture Radar (PALSAR) with a variety of spatial resolutions (Rosenqvist et al 2007). The PALSAR ScanSAR observation mode, used for this report, allows coverage of large areas of land. Radiometric accuracy of PALSAR products is reported as 1dB per scene (JAXA 2009). RADARSAT-2 was launched on December 2007 by the Canadian Space Agency, and also offers a variety of spatial resolutions and selective polarization.

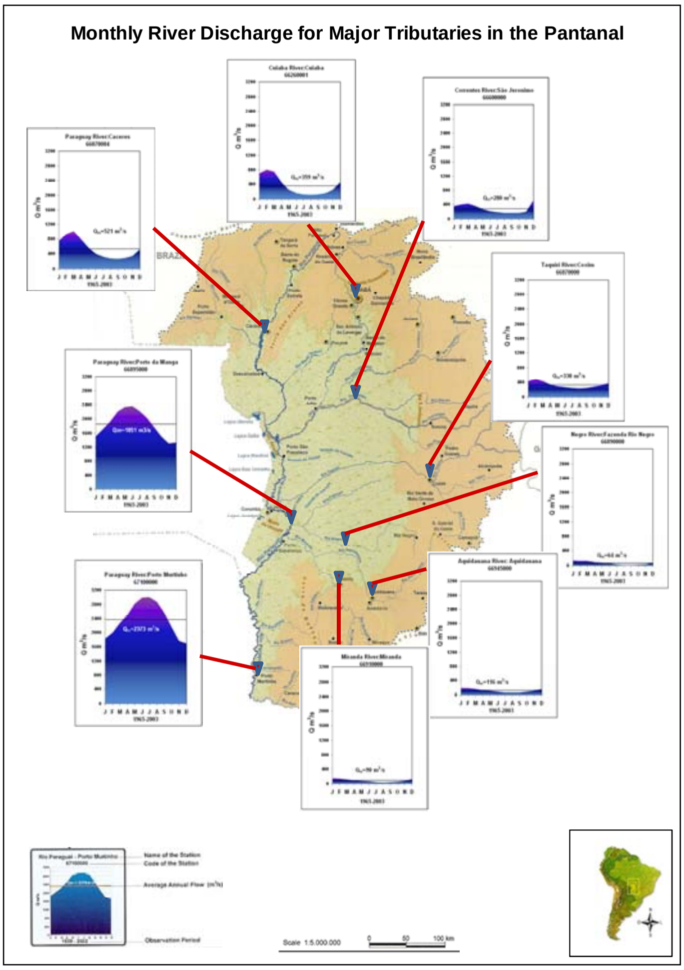

Figure 2. Monthly mean annual discharge for major tributaries in the Brazilian Pantanal. (Source: GEF 2004)

The acquired data set includes a temporal series of ALOS/PALSAR ScanSAR images from 2007, covering January, February, May, July, and November, and Radarsat-2 ScanSAR Narrow imagery from August of 2008. Each time period consists of a series of four contiguous images to be mosaicked together to provide complete coverage of the study area. The specific months of acquisition for the ALOS data were chosen due to the timing of the flood-pulse in the study region: January represents rising water; February high water; May receding; July nearly dry; and November fully dry (refer to Figure 2). The Radarsat-2 imagery was chosen as complementary information, corresponding to the timing of field data acquisition.

D. Imagery processing

Step 1: Raw data
ALOS raw image files were processed through the Alaskan SAR Facility's Map Ready software, using provided geometric and radiometric data. ALOS images were already calibrated for the antenna pattern and so were not subject to a Look-Up Table (LUT) scaling process. Radarsat-2 raw images were processed and orthorectified using PCI Orthoengine, using a SAR specific satellite orbiting model and 121 ground control points provided from MDA (MacDonald, Dettwiler and Associates Ltd.), the primary suppliers of Radarsat-2 imagery. The RADARSAT images were converted to original 32-bit format using a sigma-nought LUT (provided).

Step 2: Mosaicking
Each set of four images for each of the temporal periods was mosaicked together to form cohesive coverage of the entire Pantanal. Cutlines (the seams between individual images in a mosaic) were collected automatically based on minimum difference parameters with a blend width of three pixels. A vector file of the Pantanal floodplain provided by the Brazilian Agricultural Research Corporation (EMBRAPA) was then utilized to clip the study area from the mosaics.

Step 3: Geometry
To minimize possible geometric distortions a geometric correction approach based on ground control points collected in the images and a first order polynomial was applied. An RMS error of smaller than 1 pixel was deemed sufficient for this study. All of the images were examined visually for geometric inaccuracies: ALOS-ALOS same temporal period; ALOS-ALOS cross-temporal; RSAT-RSAT; and ALOS-RSAT. All images were projected to UTM coordinates (zone 21, row K) using the WSG84 reference ellipsoid.

There were no apparent geometric errors between ALOS images within the same time period. However, the February ALOS images displayed a slight shift in geometry compared to the other months, so a second order polynomial correction was performed using nine ground control points obtained from the January images. The RMS error for this correction was 0.31 for the x-axis and 0.51 for the y-axis. A comparison of the ALOS mosaics to the RSAT mosaics showed no significant geometric inconsistencies. However, when comparing Radarsat-2 images from 2 different satellite paths, there was a slight shift of 2 pixels in the x-axis between the western path and the eastern path. Because the error was consistent along the entire path, a simple shift of the west path to match the east executed the required correction.

Step 4: Preliminary Visual Interpretation
The series of mosaics was integrated into a single multi-layered dataset and visually examined for general patterns of ground cover. Colour composites using different temporal and cross-sensor combinations were created to aid in visual analysis and primary interpretation of the data (see example in Figure 3).

Step 5: Regions of Interest (ROI) Collection
ROI's were collected from the multi-layered mosaic, and were based on ground truth data, a priori knowledge of SAR backscattering characteristics, secondary information gathered from local inhabitants of the area, and examination of high

spatial resolution optical imagery (IKONOS and ANVIR-2). Table 1 outlines ROI categories, number of ROI per categories, and total number of pixels per category. Histograms for training sites were computed and the minimum, maximum, mean, and standard deviation for each was extracted.

Table 1. ROI categories.

Category	*Number of Training Sites*	*Total Number of Pixels*	*Class Description*
Savanna Forest	12	299	- does not flood; includes cordilhieras and capoes; 1-2m higher than terrain
Gallery/Floodable Forest	4	74	- gallery forest are riparian, occur on higher banks of major rivers; class also includes other seasonally flooded forest
Grasslands	6	39	- areas of natural grasslands
Floodable Grasslands	16	166	- areas of natural grasslands known to flood
Pasture	5	58	- cultivated, farmland and pasture
Floodable Pasture	4	35	- cultivated, farmland and pasture known to flood
Dense/Open Savanna	10	242	- herbaceous fields with shrubs and short trees
Floodable Dense/Open Savanna	3	30	- herbaceous fields with shrubs and short trees known to flood
Herbaceous Savanna	9	189	- occurs on sandy soils of alluvial fans, areas of herbaceous aquatic vegetation, vazantes and waterways
Open Water	4	327	- open water bodies; lakes and major rivers

Step 6: Backscattering Analysis

In order to understand the scattering processes of microwave radiation interaction with ground cover, as well as change in these scattering processes due to inundation, the backscattering values collected from the ROI were compared. For this comparison, the backscattering signal, minimum, maximum, and mean values of amplitude were then converted to normalized backscattering coefficients (σ^0) expressed in terms of dB. The conversion process from amplitude (DN) to backscattering in dB (σ^0) for ALOS/PALSAR is as follows:

$$\sigma^0 = 10*\log_{10}(DN^2)+CF$$

where CF is the calibration coefficient for PALSAR standard products, and equals –83 for the time of imagery acquisition and processing. (Rosenqvist et al, 2007).

Conversion of DN to σ^0 for Radarsat-2 ScanSAR images require a Look-up Table (LUT) which is included with the product, and the equation is as follows:

$$C = (DN^2 + B) / A$$

where C is the calibrated value; B is the offset (supplied in the LUT); and A is the range dependant gain (supplied in the LUT) (MDA, 2008). This step was performed during initial raw image processing in Orthoengine (PCI Geomatics). The calibrated values were then expressed in dB via the following calculation (Wessels, 2008 – personal communication):

$$dB = 10*\log(C)$$

Converted dB values were then examined visually to determine seasonal trends among classes, and any confusion between classes. After conversion of ALOS and RSAT minimum, maximum, and mean values from amplitude to dB backscattering, the values were analyzed for class specific and temporal changes.

Step 7: Speckle Filtering

For this study, three common adaptive filters were tested: Frost, Gamma and Kuan. Several tests were performed employing these three adaptive filters with a 3x3 and a 5x5 window, and using one, two and three interactions. Visual analysis of the resultant filtered images was performed to determine the best preservation of edge features and discrimination of different textured areas. After visually ruling out the 5x5 window, and the two and three interaction images, the remaining images were tested for mean backscattering preservation and decrease of standard deviation. Four samples (98, 183, 303 and 342 pixels) of a homogenous target (open water) were selected and the mean and standard deviation of each sample was calculated before and after filtering. The goal was to determine the method that best preserves the mean values, while decreasing the standard deviation (Oliver & Quegan 2004).

Once all of the mosaics were filtered, they were scaled to 8-bit images to reduce processing time during classification.

Step 8: Classification: Definiens Processing and Analysis

The classification scheme was organized in two levels aiming to capture different land cover types (Level 1) and seasonally flooded and non-flooded areas (Level 2).

Level 1 – Cover Classification

All 8-bit and amplitude ALOS image mosaics (January, February, May, July and November) as well as both 8-bit and amplitude Radarsat-2 images (August, HH and HV polarizations) were imported into Definiens. The 8-bit data was used for the segmentation processing, and the amplitude for defining the backscattering (dB) of the generated objects. The follow steps were performed:

A: Several combinations of the three multi-resolution segmentation parameters were tested in order to determine the optimal combination for this data. A scale factor of 20 resulted in object polygons that were refined enough to capture small objects such as the lakes as individual entities, without being so small as to confuse fuzzy borders. An emphasis on radiometry as opposed to shape was deemed important, therefore a factor of 0.3 was chosen as the best compromise, and the portion allotted to shape was divided evenly between smoothness and compactness as both were considered of equal importance. Only the February, the July, and the RSAT HV image were given weight for this segmentation as they were the layers deemed to have the most seasonal and spectral contrast (February being high water, July low water, and RSAT representing additional information from C-band).

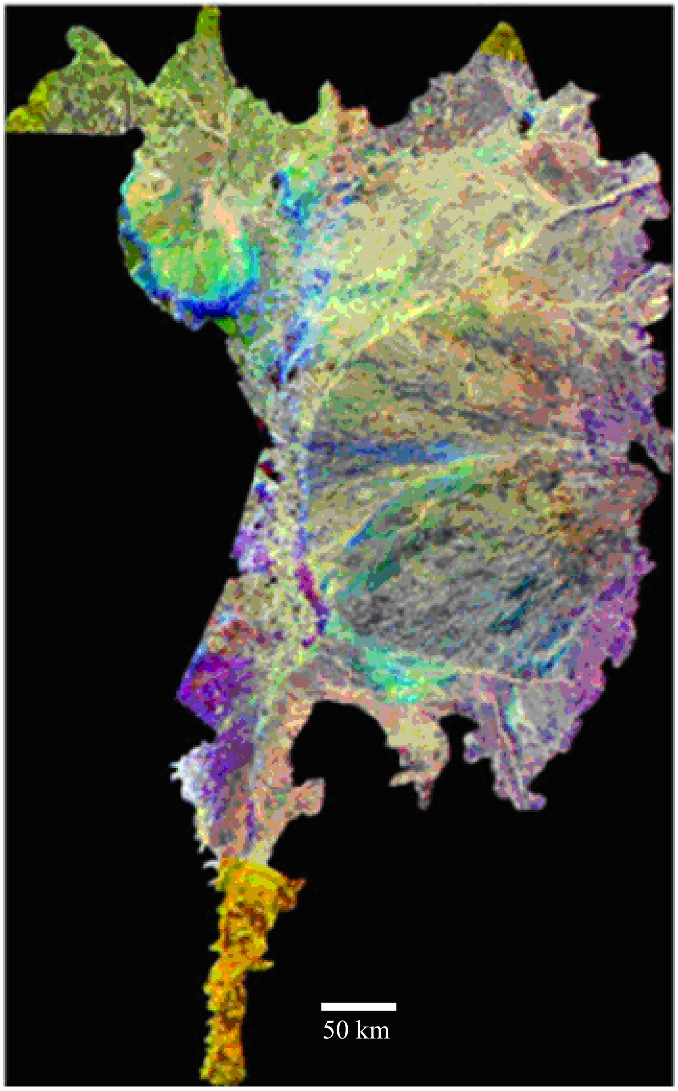

Figure 3: February (R), July (G), Radarsat HV(B) (Note: the lack of blue in the Nabileque subregion is due to the lack of C-band coverage for this area) © *JAXA/METI*.

B: The resulting objects from step A were then subjected to spectral difference segmentation with a factor of 10. This essentially merged any contiguous objects with a spectral difference of <=10 in all 3 layers, thereby reducing the overall number of objects while losing the minimal amount of spectral information. Backscattering values were recorded for the resulting objects over areas of known cover based on ground truth, a priori knowledge of SAR backscattering characteristics, secondary information regarding landscape and flood extent gathered from local inhabitants of area, and examination of high spatial resolution optical imagery (IKONOS and ANVIR-2). These backscattering values were then compared to those gathered from the previously defined ROI (Steps 5 and 6), and rules based on radiometric ranges for classes were formed.

The Level 1 classification encompassed five categories, examples of which can be seen in Figure 4:

- Gallery forest/savanna forest: includes riparian forests on high banks of major rivers, all forests subject to seasonal flooding, and non-floodable forest (cordilheiras and capoes)

- Dense savanna/open savanna: includes areas that are comprised of any combination of shrubs, short trees, herbaceous fields, fields with sparse density trees; may or may not be subject to flooding

- Grasslands/pasture – includes natural grasslands, pastures, agriculture, cultivated fields and farmland; may or may not be subject to flooding. Due to the relative inseparability of the grasslands and pasture classes they were grouped together in one class to avoid confusion

- Herbaceous savanna – includes areas of sandy soils, alluvial fans, floating emergent aquatic vegetation, herbaceous vegetation, waterways, vazantes; subject to seasonal or permanent flooding

- Open water – includes all permanent lakes and rivers

In addition, object area parameters were utilized to separate small freshwater lakes from spectrally similar herbaceous savanna.

Level 2 - Defining Seasonal Change Classification
Numerous studies utilize temporal change in backscattering characteristics of cover types to determine inundation (Martinez & Le Toan 2007; Hamilton et al 2004; Costa 2004; Hess et al 1995; Wang et al 1995). Essentially, areas subject to inundation show seasonal change in backscattering values; areas with no temporal change do not flood and therefore minimum backscattering change was observed. In light of this, algorithms designed to exploit the temporal variability in backscattering were applied to the images (Silva 2009). The first was a cumulative mean distribution algorithm designed to show areas of cumulative change over the entire year:

$$[(a-b)^2 + (a-c)^2 + (a-d)^2 + (a-e)^2 + (b-c)^2 + (b-d)^2 + (b-e)^2 + (c-d)^2 + (c-e)^2 + (d-e)^2]^{0.5}$$

Where,

a = January ALOS image

b = February ALOS image

c = May ALOS image

d = July ALOS image

e = November ALOS image

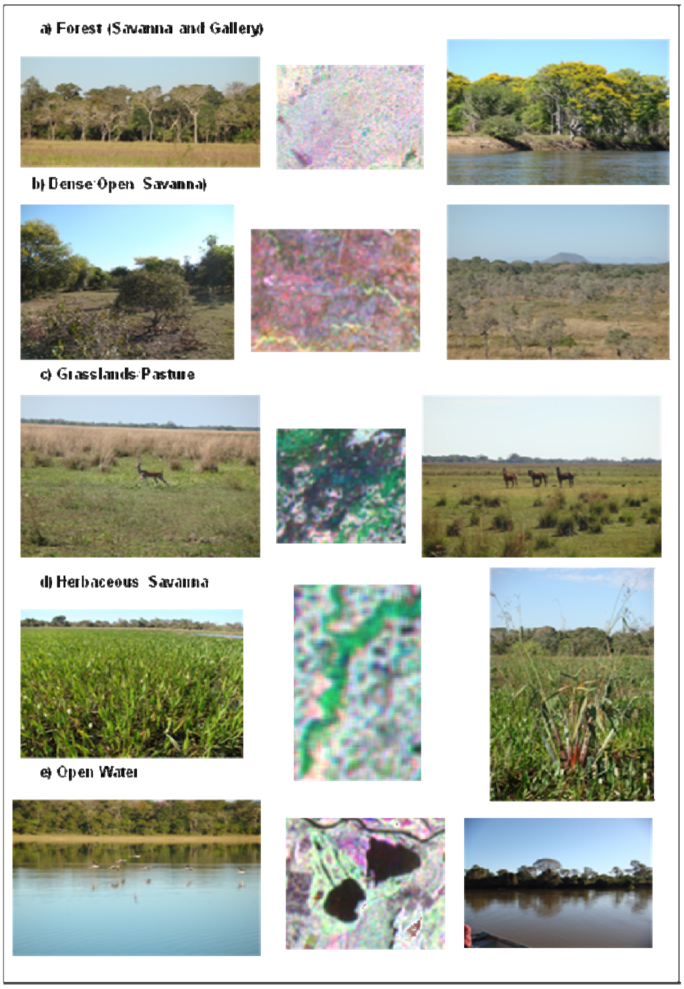

Figure 4 – Examples of Level 1 classification cover types and how they appear in the SAR colour composite Feb-red; Jul-green, Nov-blue.

Individual calculations were performed to show change between each time period.

$[(a-b)^2]^{0.5}$; $[(b-c)^2]^{0.5}$; $[(c-d)^2]^{0.5}$; $[(d-e)^2]^{0.5}$; $[(e-a)^2]^{0.5}$

Applying these algorithms resulted in outputs maps that clearly showed the areas of the most change in backscattering values within these temporal periods. Then, rules based on backscattering were applied to Level 1 Savanna Forest/Gallery Forest and Grasslands/Pasture classes to separate flooded from non-flooded areas.

III. Results and Summary

A. Backscattering Analysis

Sites used for the backscattering analysis (Figure 5) were taken from the Nhecolandia, Aquidauana and Miranda subregions, where field data was gathered. Therefore, any analysis regarding the seasonality of flood patterns is mostly applicable to these areas as other regions in the Pantanal have different flood patterns. However, it is expected that the backscattering signal behaves similarly for the other regions.

Figure 5 – Cross-temporal, multi-sensor comparison of mean backscattering values from training site classes.

(i) Forest (Figure 4a)
Forested areas exhibited the highest backscattering values of all the classes in L-band, for all seasons. Mean values during maximum flood in February ranged from –3.9dB for floodable forest to –8.1dB for non-floodable forest, and mean values during the dry season in July ranged from –6.0 for floodable forest to –7.1 for non-floodable forest. This is the result of multiple scattering mechanisms and interactions with the various components present in forested regions as suggested by Wang et al (1995):

$$\sigma^\circ_t = \sigma^\circ_s + \sigma^\circ_c + \sigma^\circ_m + \sigma^\circ_d$$

where,

σ°_s = backscattering from the canopy surface directly back to the sensor
σ°_c = volume scattering within the canopy
σ°_m = multiple interactions of the canopy and the ground
σ°_d = double-bounce scattering

At the long wavelength of L-band, the leaves of the canopy are quasi-transparent, thus the radiation penetrates through to interact with branches, trunks and the underlying surface. The combination of all of these components results in a higher backscattering return than other cover types. However, forested backscattering values are lower in C-band than in L-band as σ°_t is almost exclusively made up of σ°_c, particularly with cross-polarized (HV) C-band as suggested in Wang et al, (1995). Townsend (2002) found that C-band HH polarized radiation may penetrate the canopy structure allowing detection of inundation in forested areas; however in non-flooded conditions total C-band HH backscatter is predominantly due to volume scattering (Wang et al 1995; Townsend 2002). Our C-band data was acquired in August during the dry season, even if some of the radiation did penetrate the canopy there was no water available to cause double-bounce, therefore, C-band HH and HV exhibited only marginal differences for the two forest classes.

Overall mean backscattering values (-5.7dB to –8.1dB for non-floodable forest, and –3.9dB to –6.4dB for floodable forest) were within the expected range for that cover type (Hess et al 1995; Wang et al 1995; Costa 2004; Martinez & le Toan 2007). There was very little variability between ROI values within both of the forest classes (Figure 13). This is likely because large homogenous areas of forest were clearly visible in the data, thus there was less chance of accidentally including pixels that were not representative of the class.

Temporally, L-band signal from non-floodable forest and floodable forest showed little variation between them for May, July, November and January, but a great difference in February. This is because high water occurs in the Nhecolandia region (where the majority of the forest ROI's were located) in February, thus there was increased backscattering for floodable forest attributable to the $\sigma°_d$ component not present in the non-floodable forest class. Floodable forest exhibited slightly higher mean values in L-band than non-floodable forest (0.9dB, 4.9dB, 1.1dB, 0.6dB for Jan, Feb, Jul, and Nov, respectively) for all months except for May, where non-floodable forest was slightly higher than floodable forest (-5.7dB compared to –6.1dB). Although the variation was slight, they could be attributable to differences in tree species. Hess et al (1990) suggested that the relationship between hydrology and tree species must be kept in mind to ensure that observed backscattering differences are the result of flooded/non-flooded conditions and not due to differences in vegetation species.

(ii) Dense/Open Savanna (Figure 4b)

This class covered a wide range of landscapes from open grassy savanna with sparse trees and areas of bare soil to relatively dense areas of herbaceous vegetation, shrubs, and small trees. This diversity of the land cover resulted in the high degree of backscattering variability between sites. Also, the heterogeneous nature of mixed savanna and the relatively low spatial resolution of the data hindered the selection of pure training sites. As such, areas of open grassy savannas exhibit backscattering characteristics closer to grasslands, while dense savannas are more similar to forest.

Generally, floodable dense/open savanna exhibited consistently higher backscattering values than non-floodable dense/open savanna, regardless of the season. Furthermore, values for floodable areas did not change significantly, nor did values for non-floodable areas, regardless of season. The explanation for the differences between the two classes is likely due to different tree and vegetation species inhabiting floodable and non-floodable areas, however, the lack of temporal change is not as easy to clarify. The only possibility speculated upon lies in the nature of the backscattering characteristics of the components present in a savanna landscape; during flooded conditions, the presence of water would cause much of the signal to be specularly reflected away from the sensor, but, the presence of trees and shrubs would add an enhanced double-bounce signal. In a pixel representing $100m^2$ of savanna terrain, these two components could cancel each other out, thereby showing no discernable change between flooded and non-flooded conditions. However, this theory is speculative given the lack of literature pertaining to SAR analysis of areas of mixed terrain such as this in relation to flood detection.

Mean C-band HH and HV backscattering values both fall somewhere in between grasslands/pasture and forest classes (-8.7dB and –14.6dB for HH and HV Dense/Open Savanna, and –7.8dB and –14.6dB for HH and HV Floodable Dense/Open Savanna). This is again to be expected due to the mixed nature of the class.

(iii) Grasslands/Pasture (Figure 4c)

Due to the relative inseparability of the grasslands and pasture classes, these classes are considered together in this analysis. This class represents a variety of herbaceous, grass-like vegetation including: very short grass found around the *vazantes*; croplands of various species; cultivated fields of *Brachiaria sp*. (a hardy introduced plant species used for cattle pasture); and the very tall (~2m) wild grass found on the *campos*.

Overall, the backscattering values for grasslands and pasture, floodable and non-floodable, fell within expected values (Hess et al 1995; Hill et al 1999). The grasslands/pasture class, whether floodable or not, were found to exhibit consistently higher values at C-band HH (mean value of –10.7dB) than at L-band (11.8dB for May, the highest backscattering of the L-band imagery) due to volume scattering interactions with the vegetation. This type of vegetation is usually partially transparent to L-band, however can occasionally exhibit higher values depending on the height and density present. For example, Hill et al (1999) found that thick, lush, ungrazed herbaceous pastures had a backscattering value of –8.8dB in L-band (which is almost comparable to non-floodable forest, and not typical for grasslands). Of the 15 classes of grass tested by Hill et al (1999), the backscattering values exhibited wide divergence from –8.8dB to –23.1 dB in L-band, –5.9dB to –14.5dB for C-band HH, and –6.2dB to –13.5dB for C-band HV; this helps to explain the high variability between grasslands training sites for all our images.

Floodable grasslands and pasture showed lower mean values in January (-15.2dB) and May (-12.5dB), and far lowers values in February (-19.6) than non-floodable areas (-12.8dB, -11.1dB and –13.9dB, respectively). This is consistent with expected results as maximum flood in the region occurs in February, with rising water occurring in January and falling water in May. Low values for this class during inundation are due to increased specular reflection away from the sensor caused by the water surface. Land submergence in the

Pantanal is typically 0.5-1.5m, while the pasture and grasslands training sites covered areas from very short grass (< 0.05m) to very tall (~ 2.0 m). Therefore, flooded areas would show differing degrees of backscattering depending on whether the vegetation (grass) was fully submerged or only slightly flooded. Fully submerged areas would demonstrate a very low backscattering return, as most of the incident radiation would be specularly reflected away from the sensor. However, areas of very tall and/or very dense grass, only slightly flooded (maybe only a few centimetres) would not show as great a degree of difference between flooded and non-flooded as less of the signal would be reflected away, and more would be volumetrically scattered within the vegetation. There was a noticeable difference between C-band floodable and non-floodable pasture, for both HH (-13.0dB for floodable and –8.0dB for non-floodable) and HV (-20.2dB for floodable and –14.9dB for non-floodable) polarizations, which could only be explained by different vegetation species inhabiting the two cover types. The C-band data was acquired in August during the dry season, therefore no difference in backscattering could be attributable to actual flood conditions. Another phenomenon found in the data was the seemingly inconsistent pattern of backscattering present in the non-floodable area: high values in May and November but low in July. One possible explanation for this may be the changing dielectric properties of the vegetation (Dobson et al 1996). Although these are not floodable areas they are still susceptible to climate. July is in the middle of the dry season and the lack of precipitation, along with senescence of the vegetation, results in a lowering of the moisture content, and hence the backscattering value. May is at the end of the rainy season and November at the beginning, therefore the vegetation would like contain a greater moisture content than in July.

(iv) Herbaceous Savanna (Figure 4d)

This class encompasses herbaceous aquatic/amphibious vegetation occurring on alluvial fans, *vazantes* and waterways. The lowest L-band values for this class occurred in February (-21.2dB), during maximum flood in this region. At this time, any vegetation present is likely to be fully submerged, or of the small free-floating broadleaf variety (3-30cm in height). Therefore, the majority of L-band radiation would be specularly reflected away from the sensor, resulting in the low backscattering return. The highest L-band values were found in July (-9.8dB), during low water. At this time, a possible new group of herbaceous vegetation adapted to the drier conditions would be present, thereby increasing the backscattering return. For example, rooted forms of broad-leafed aquatic vegetation would have more ability to take hold and thrive in less turbulent low waters than in the relatively faster moving, deeper waters occurring during maximum flood. Also, more Aquatic Terrestrial Transition Zone (ATTZ) amphibious vegetation becomes exposed with receding waters further increasing the backscattering signal. This further explains the high variability in January and May as differing degrees of water level would be present depending on localized flood conditions.

C-band HH values were high (-8.6dB) compared to L-band for this class, as less of the vegetation is interacting with L-band due to the longer wavelength. The C-band imagery was acquired in August, therefore more vegetation would be exposed, increasing the degree of volume scattering and decreasing the degree of specular reflection. The backscattering of aquatic vegetation at C-band is primarily through volume scattering, although double-bounce scattering has been observed with dense, tall (~1m) aquatic vegetation (Hess et al 1995; Costa 2004, Martinez & le Toan 2007).

(v) Open Water (Figure 4e)

The open water class was expected to show consistently low values in both C-band and L-band (-18.3dB, -20.6dB, -16.9dB, -20.1dB, -20.2dB, -20.0dB and –26.3dB for L-band Jan, Feb, May, Jul, Nov, and C-band HH and HV, respectively), as the majority of the incident radiation would be specularly reflected away from the sensor. For example, Martinez & le Toan (2007) reported open water in the Amazon floodplain to have values of –17.0 dB with a negligible variation of +/-0.3dB in L-band. However, the open water training sites for this study showed slightly elevated values in May and February for L-band, and fairly high variability between training site values. One possible explanation for the variability is the presence of migrating floating *camalotes* of aquatic vegetation, which, if tall enough, and dense enough, could cause some volumetric scattering increasing the signal to the sensor from individual training sites. Another explanation could be an increase in water surface roughness caused by wind (Oliver & Quegan 2004).

B. Separability between classes

The best separability between flooded and non-flooded classes occurred in February (Figure 6). This is to be expected, as February is the high water season for the area, and would thus show the most variability between flooded and non-flooded areas. The overlap in backscattering values between forest classes, savanna classes and grasslands/pasture classes was anticipated due to the fuzzy borders between them. Dense/open savanna is a class that bridges forest and grasslands, and therefore contains varying degrees of both cover types. Although herbaceous savanna and open water were virtually indistinguishable in February during maximum inundation, they were easily separated in July. This is because lowering water levels resulted in the exposure of more vegetation cover for herbaceous savanna, thereby increasing the backscattering signal, especially in C-band, while backscattering for open water remained fairly low. The high degree of overlap between floodable and non-floodable grasslands and pastures is due to the similar nature of the two classes. They both represent areas of low vegetation devoid of trees, however height and density of both classes is variable, so they are easily confused.

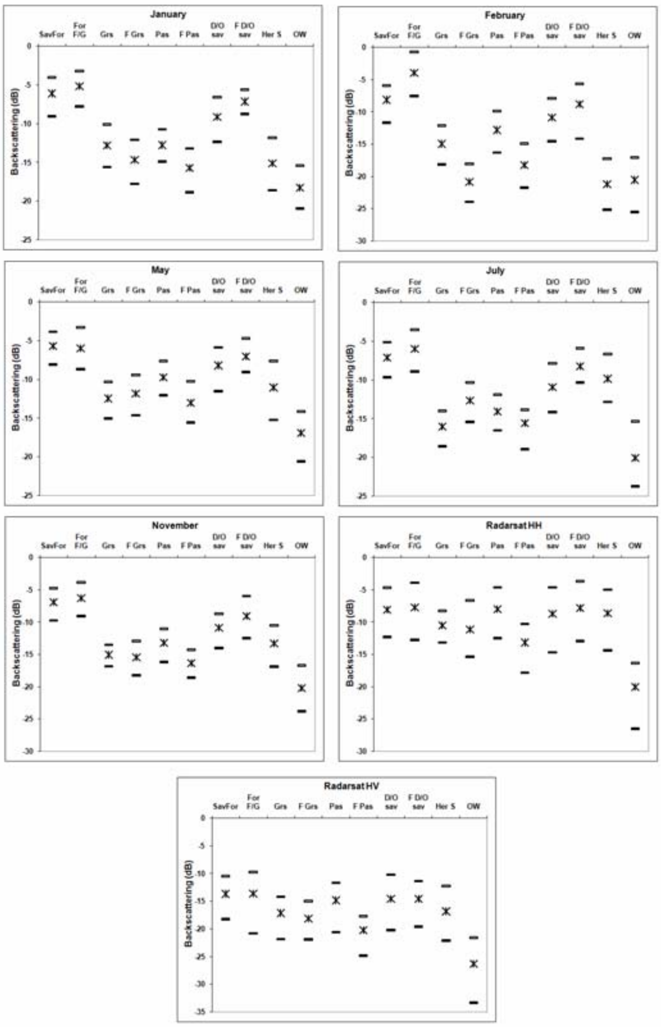

Figure 6 – Variability between classes: Savanna Forest, Forest Floodable/Gallery, Grasslands, Floodable Grasslands, Pasture, Floodable Pasture, Dense/Open Savanna, Floodable Dense/Open Savanna, Herbaceous Savanna, Open Water.

C. Level 1 Classification

The Level 1 classification map is shown in Figure 7. A classification accuracy assessment was performed on the Level 1 classification using the ROI's defined in Step 5. The confusion matrix (Table 2) shows that open water and herbaceous savanna were 100% correctly classified in Definiens. For forest, 76% were correctly classified, while 14% were misclassified as dense/open savanna. As predicted by the backscattering analysis in the previous section, there was a high degree of uncertainty between grasslands/pasture and herbaceous savanna; only 58% of grasslands/pasture was correctly classified, while 38% was classified as herbaceous vegetation and 3 % as dense/open savanna. Also as predicted, there was a considerable overlap between forest, dense/open savanna and grasslands/pasture; 50% were correctly classified while 25% were misclassified as forest and 25% were misclassified as grasslands pasture.

Large areas of aquatic macrophytes (herbaceous savanna) were observed in the data when examining the optical images. These areas were not included in the original backscattering analysis, as there was no ground truth to validate them. However, a high degree of confusion was present between forest and these large areas of herbaceous vegetation. Rules were created to separate the two classes and a visual comparison of the entire image with the optical data showed an improvement. Confusion between aquatic macrophytes and forest classes in L-band has been reported in several cases (Hess et al 1990; Hess et al 1995; Pope et al 1997). Our data exhibited high backscattering values for large areas of aquatic macrophytes similar to values found in the forest classes. Pope et al (1997) reported that L-band double-bounce interactions were possible for herbaceous aquatic vegetation at relatively steep incidence angles (25° at swath center for their study). Therefore, this could explain the high values for our study as the L-band imagery was acquired at a relatively steep incidence angle of 27.1°. Hess et al suggested that forest and macrophytes were best separated at L-band HV polarization (1995), or with a range of different incidence angles (1990). After a great degree of manual comparison of values for areas of aquatic macrophytes and forest, the greatest degree of separability between the two was found to be between the November L-band and the C-band HH imagery; thus a rule exploiting this difference was created to separate the two in the Level 1 classification. Also, areas of upland hills were misclassified due to increased elevation and shadow effects; these areas were corrected manually.

Overall, the confusion found between classes in the Definiens classification were consistent with the results established in the backscattering analysis. However, the ROI's, and resultant accuracy assessment, are only representative of the field study subregions of Nhecolandia, Aquidauana/Negro and Miranda. Due to the variable nature of the Pantanal floodplain as a whole, the same level of confidence cannot be transferred to the entire study area; however we intend to improve the accuracy of the classification during the Phase 2 of this project, where other areas of the Pantanal will be visited.

D. Level 2 Classification

The temporal series of mosaic images representing the separation between flooded forest and non-flooded forest can be seen in Figure 8. For the most part, areas representing flooded forest for the majority of the time follow riparian corridors, except for the large northern area spanning parts of the Piquiri/Sao Lourenco, Cuiaba and north Paraguay subregions mentioned previously. Areas of forest that never flood are present in all subregions, but are particularly apparent in the Nhecolandia, Taquiri Fan, and Corixo Grande subregions. The mapped flood timing is consistent with that reported in Hamilton et al (1996) and the hydrological data shown in Figure 2. For example, rising water in January and maximum flood in February have been reported for the Piquiri/Sao Lourenco, Nhecolandia, and Aquidauana/Negro subregions, and this can be seen by the darker green, representing flooded forest, along the riparian areas of these three subregions for the January and February images.

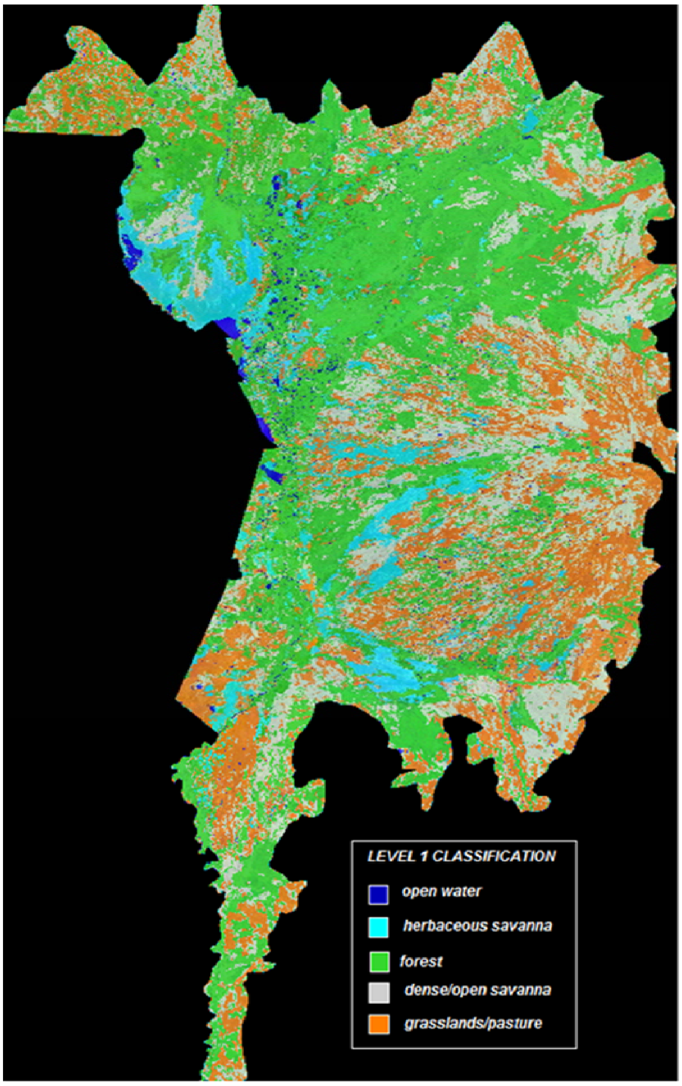

Figure 6.2 – Level 1 classification output

Figure 7 – Level 1 Classification output. ALOS K&C © *JAXA/METI.*

Table 2. Level 1 confusion matrix.

Confusion Matrix for Level 1 Classification of the Brazilian Floodplain					
	Gallery/Savanna Forest	**Dense/Open Savanna**	**Grasslands/Pasture**	**Herbaceous Savanna**	**Open Water**
Gallery/Savanna Forest	13	4	0	0	0
Dense/Open Savanna	3	6	3	0	0
Grasslands/Pasture	0	1	17	11	1
Herbaceous Savanna	0	0	0	9	0
Open Water	0	0	0	0	4

However, the dark green begins to recede and is replaced by the light green, representing non-flooded forest, in May, and particularly in July and November for these regions. Conversely, the lower Paraguay River shows more dark green (flooded forest) in July than in February, which is consistent with the timing of maximum flood found in that subregion.

We speculate that some areas of flooded forest not in agreement with the reported flooding regime for each of the subregions may be a result of the confusion between aquatic macrophytes and forest reported previously; the methods employed for separating the two classes were experimental, and therefore may not have done an adequate job. The Nabileque subregion shows flooded forest in all months except for July, contrary to GEF (2004), which reports localized flooding only along the Paraguay River itself, and to Hamilton et al (1996) who report the greatest degree of flooding in this region in July. Therefore we suggest that perhaps the species of forest in this region show higher backscattering values than other forest regions and thus fell within the range designated for flooded forest and was erroneously classified. The Nhecolandia region shows very little flooding with the forest class throughout the year indicating a high degree of savanna forest made up of *capoes* and *cordilheiras*, which is consistent with what was observed in the area during the field campaign.

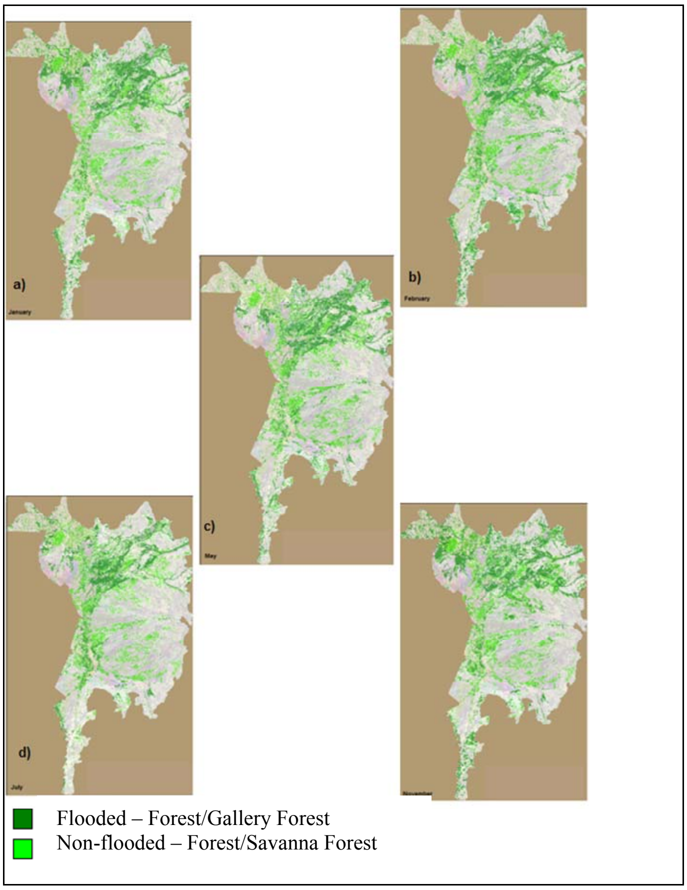

Figure 8 – Level 2 Classification output. Flooded Forest vs. Non-Flooded Forest for: a) January; b) February; c) May; d) July; e) November . ALOS K&C © *JAXA/METI.*

The temporal series of mosaic images representing the separation between flooded and non-flooded grasslands/pasture can be seen in Figure 9. Overall, the areas representing flooded grasslands are very low compared to non-flooded, however there are some notable results. The January image shows small areas of flooding in the Nhecolandia and Taquiri Fan subregions, greatly increasing in the February image. Both January and February show small areas of flooding in localized patches of the northern Paraguay and northern Nabileque subregions as well. The area of the greatest observable flooding occurs in the Nhecolandia region in February, and in the southern Paraguay River subregion in July, consistent with observed results in Hamilton et al (1996) and the maximum river discharge timing seen in Figure 2. May shows very little flooding anywhere except for the Corixo Grande subregion, and localized portions of the Paraguay. Flooded areas are apparent in the southern Paraguay/northern Nabileque subregions for July, as well localized areas in the east of the entire mosaic. November shows no flooded areas anywhere except for small areas in the southeast Taquiri Fan and east Nhecolandia.

V. CONCLUSIONS

Examination of the SAR ALOAS/PALSAR and RADARSAT-2 data used for this study, coupled with data gathered in the field, provided an understanding of the interactions between incident microwave radiation at L and C bands and ground cover, and how they change temporally with the seasonal flood in the Brazilian Pantanal. In general, the Definiens object-based Level 1 classification using both bands yield an average accuracy of 77%, in which the most confusion was between grassland/pasture and herbaceous and open savanna classes. This was expected given (1) the nature of these landscape covers, i.e., mostly grass-like vegetation and (2) the 100 m course resolution of the ScanSAR imagery. Nonetheless, our work provided the most detail classification of landscape cover available for the entire Brazilian Pantanal.

The generated flooded/non-flooded maps provided consistent separation of flooded from non-flooded forest. However, as expected due to similar backscattering values at this spatial resolution, L-band HH was not ideal for separating flooded from non-flooded grasslands/pasture, or flooded from non-flooded dense/open savanna. Nonetheless, much of the temporal pattern of inundation defined the classified maps was consistent with that found in Hamilton et al (1996), with some areas of disagreement. However, Hamilton et al (1996) used passive microwave data and did not provide an accuracy assessment or temporal output maps to validate their study. As such, we can not truly compare our spatial maps with their results.

Generally, two main factors contributed to confusion and erroneous classification in the Definiens software. First, low spatial resolution (100m), further degraded by the SAR speckle filtering process, may have led to a high degree of mixing of cover types with segmented image objects. The Pantanal is a highly heterogenous landscape where a single pixel representing 10000m^2 often contains forest, grasslands, and lake elements within the same pixel.

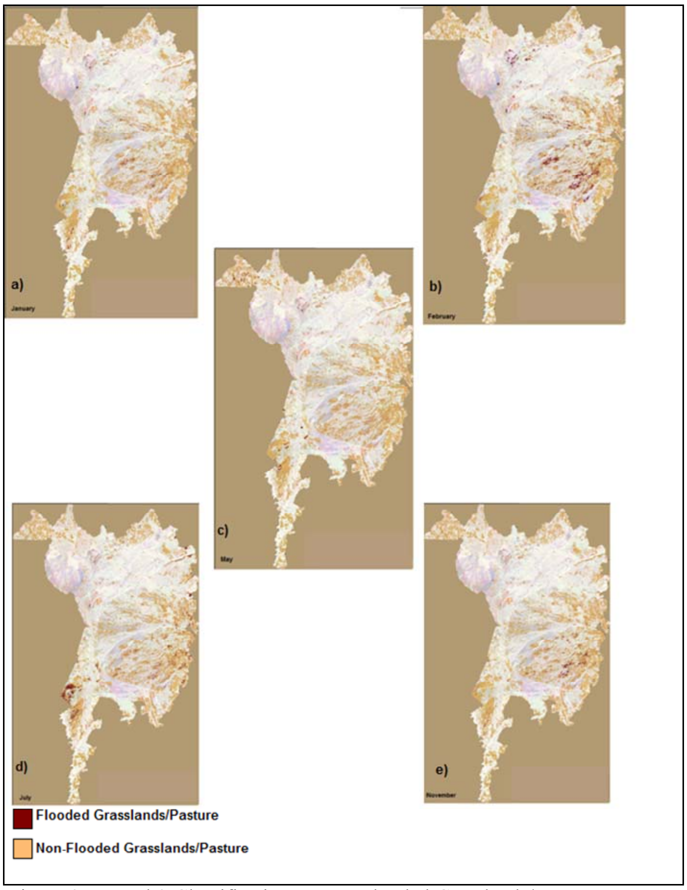

Figure 9 – Level 2 Classification output. Flooded Grasslands/Pasture vs. Non-Flooded Grasslands/Pasture for: a) January; b) February; c) May; d) July; e) November. ALOS K&C © *JAXA/METI.*

Second, varying seasonal flood regimes for the many different subregions in the Pantanal increased the difficulty in selecting rules for determining separation between classes. Interpolating what we knew to be true in the area where we had conducted field work to the rest of this complex wetland system was problematic because the timing of the flood was different for different subregions, and there were areas where ground cover information was not available.

Improvements on both land-cover and temporal flooding classifications will come by (1) splitting the Pantanal mosaic into hydrological subregions based on peak river discharge, and conducting separate classifications for each area. (2) The addition of a temporal series of C-band data corresponding to a time series of L-band, and (3) field data acquired in the wet season. Further improvement will come from the analysis of 12.5 m fine resolution mosaics of the second phase of this project and planned field work in the northern and central Pantanal.

In conclusion, utilizing multi-temporal, multi-band SAR data for defining land cover and inundation patterns in the Pantanal was accomplished. The delineation of the landcover will be used as input spatial data in future studies involving land use or habitat monitoring (part of our collaboration with EMBRAPA-

Brazil in the phase 2 project). Although there have been several previous habitat studies at a local scale in the Pantanal (Tomas et al, 2001), only a few have covered the entire Pantanal at a regional scale (Hamilton et al, 1996; but does not provide spatial maps), as the size and relative inaccessibility of the region hinders traditional methods of data collection. Ultimately, the generated data from phase 1 and 2 will aid in further understanding the spatial and temporal pattern of the flood-pulse regime in the Pantanal, and will provide seasonal habitat suitable for threatened species, and define corridors and connectivity for defining conservation areas.

ACKNOWLEDGEMENTS

This work has been undertaken within the framework of the JAXA Kyoto & Carbon Initiative. ALOS PALSAR data have been provided by JAXA EORC. The authors would like to acknowledge the K&C group for the interesting fun meetings and valuable technical information learned from this team. In special, we thank you A. Rosenqvist, M. Shimada, and M. Watanabe for all the effort and patience with us during all these years. Special thank you to JAXA for partially support all the K&C projects; it is invaluable! Thank you to the Canadian Space Agency for providing Radarsat-2 imagery under the SOAR program. Many thanks to The National Geographic Society for funds for field work.

REFERENCES

[1] Abdon M, da Silva J, Pott V J, Pott A, da Silva M P. (1998). Utilization of analogic data of Landsat-TM on screening vegetation of part of the Nhecolandia subregion of the Brazilian Pantanal. Brazilian Journal of Agricultural Research. 33:1799-1813.

[2] Costa M P F, Telmer K H. (2007). Mapping and monitoring lakes in the Brazilian Pantanal wetland using synthetic aperture radar imagery. Aquatic Conservation: Marine and Freshwater Ecosystems. 17: 277-288.

[3] Costa M P F, Telmer K H. (2006). Utilizing SAR imagery and aquatic vegetation to map the fresh and brackish lakes in the Brazilian Pantanal. Remote Sensing of the Environment. 105: 204-213.

[4] Costa M P F. (2004). Use of SAR satellites for mapping zonation of vegetation communities in the Amazon floodplain. International Journal of Remote Sensing. 25(10): 1817-1835.

[5] Costa M P F, Niemann O, Novo E, Ahern F, Mantovani J. (2002). Biophysical properties and mapping of aquatic vegetation during the hydrological cycle of the Amazon floodplain using JERS-1 and Radarsat. International Journal of Remote Sensing. 23 (7): 1401- 1426.

[6] da Silva C J, Girard P. (2004). New challenges in the management of the Brazilian Pantanal and catchment area. Wetlands Ecology and Management. 12:533-561.

[7] Dobson M C, Pierce L E, Ulaby F T. (1996). Knowledge based land cover classification using ERS-1/JERS-1 SAR composites. IEEE Transaction of Geoscience and Remote Sensing. 34(1): 83-99.

[8] GEF (Global Environment Facility) Pantanal/Upper Paraguay Project. (2004). Implementation of Integrated River Basin Management Practices in the Pantanal and Upper Paraguay River Basin. Strategic Action Program for the Integrated Management of the Pantanal and Upper Paraguay River Basin. ANA/GEF/UNEP/OAS. Brasilia: TDA Desenho & Arte Ltda. 2004.

[9] Gottgens, J. F., R. H. Fortney, J. Meyer, J. E. Perry, and B. E. Rood. 1998. The case of the Paraguay-Parana´ waterway (‘‘Hidrovia’’) and its impact on the Pantanal of Brazil: a summary report to the Society of Wetlands Scientists. Wetlands Bulletin:12–18.

[10] Hamilton, S. K., S. J. Sippel, and J. M. Melack. (1996). Inundation patterns in the Pantanal wetland of South America determined from passive microwave remote sensing, Arch. Hydrobiol., 137, 1 – 23, 1996.

[11] Hamilton, S. K. (1999). Potential effects of a major navigation project (the Paraguay–Parana Hidrovıa) on inundation in the Pantanal floodplains. Reg. Rivers Res. Manage. 15: 289– 299.

[12] Hamilton S K. (2002). Human impacts on hydrology in the Pantanal wetland of South America. Water Science and Technology. 45(11): 35-44.

[13] Hamilton, S. K., S. J. Sippel, and J. M. Melack. (2004). Seasonal inundation patterns in two large savanna floodplains of South America: The Llanos de Moxos (Bolivia) and the Llanos del Orinoco (Venezuela and Colombia). Hydrological Processes. 18: 2103-2116.

[14] Heckman, C. W. 1998. The Pantanal of Poconé: Biota and ecology in the northern section of the world’s largest pristine wetland. Kluwer Academic Publishers, The Netherlands.

[15] Hess L L, Melack J M, Filoso S, Wang Y. (1995). Delineation of inundated area and vegetation along the Amazon floodplain with the SIR-C synthetic aperture radar. IEEE Transactions on Geoscience Remote Sensing. 33: 896-904

[16] Hill M J, Donald G E, Vickery P J. (1999). Relating radar backscatter to biophysical properties of temperate perennial grassland. Remote Sensing of the Environment. 67:15-31.

[17] JAXA – Japanese Aerospace Exploration Agency. (2009). Advanced Land Observing Satellite. Internet Resource Accessed January 20 2009. http://www.jaxa.jp/projects/sat/alos/index_e.html

[18] Junk W J, da Cunha C N, Wantzen K M. (2006). Biodiversity and its conservation in the Pantanal of Mato Grosso, Brazil. Aquatic Sciences. 68(3): 278-309.

[19] Le Toan T, Ribbes F, Wand L, Floury N, Ding K, Kong J A, Fujita M. (1997). Rice crop mapping and monitoring using ERS-1 data based on experiment and modeling results. IEEE Transactions on Geoscience and Remote Sensing 35: 41-55.

[20] Martinez J M, le Toan T. (2007). Mapping of flood dynamics and spatial distribution of vegetation in the Amazon floodplain using multitemporal SAR data. Remote Sensing of the Environment. 108: 209-223.

[21] MacDonald, Dettwiler and Associates Ltd.13800 Commerce Parkway. Richmond, British Columbia, Canada V6V 2J3.

[22] Oliver C, Quegan S. (2004). Understanding synthetic aperture radar images. SciTech Publishing, Inc. Raleigh, NC.

[23] Pope K O, Rejmankova E, Paris J F, Woodruff R. (1997). Detecting seasonal flooding cyclesinmarshes of the Yucatan Peninsula with SIR-C polarimetric radar imagery. Remote Sensing of the Environment. 59:157-166.

[24] Por F D. (1995). The Pantanal of Mato Grosso (Brazil): World’s Largest Wetlands. Monographiae Biologicae. Vol 73. Dumont H J & Werger M J A (eds). Kluwer:Dordrecht.

[25] Rosenqvist A, Shimada M, Ito N, Watanabe M. (2007). ALOS PALSAR: A pathfinder mission for global-scale monitoring of the environment. IEEE Transactions on Geoscience and Remote Sensing. 45(11): 3307-3317.

[26] Silva T S F, Costa M P F, Melack J M, Novo E M L M. (2008) Remote sensing of aquatic vegetation: theory and applications. Environmental Monitoring and Assessment. 140(1-3): 131-145.

[27] Townsend P A. (2002). Relationships between forest structure and the detection of flood innundation in forested wetlands using C-band SAR. International Journal of Remote Sensing. 23(3): 443-460.

[28] Wang Y, Hess L L, Solange F, Melack J M. (1994).Canopy penetration studies: modeled radar backscatter from Amazon floodplain forests at C-, L- and P-band. Geoscience and Remote Sensing Symposium. IGARSS. Surface and Atmospheric Remote Sensing: Technologies, Data Analysis and Interpretation. International 2(8-12): 1060 – 1062.

[29] Wessels, J., PCI Geomatics. Personal communication via email, Dec 16 2008.

 Maycira Costa and Kevin Telmer, professors at the University of Victoria, Canada, Nattan, 6 years old, and Maiara, one month old. One way or the other they are all part of the K&C project.

 Terresa Evans is a student in the Geography Department at UVic. Terri is a key player in this project and will be developing her graduate thesis as part of the second phase of the K&C project - Pantanal.

Wetlands Theme

Characterisation of inland wetlands in Africa

Lisa-Maria Rebelo *et al*.
International Water Management Institute (Ethiopia)

K&C Science Report – Phase 1
Characterisation of inland wetlands in Africa

Lisa-Maria Rebelo
International Water Management Institute, P.O.Box 5689, Addis Ababa, Ethiopia, l.rebelo@cgiar.org

Collaborator: Max Finlayson
Charles Sturt University, Albury NSW, mfinlayson@csu.edu.au

Abstract - **Inland wetlands occur extensively across Sub-Saharan Africa. These ecosystems typically play a vital role in supporting rural populations and their sustainable management is thus critical. In order to prevent depletion of resources and ecosystem services provided by these wetlands, a balance is required between ecological and socio-economic factors. The sustainable management of wetlands requires information describing these ecosystems at multiple spatial and temporal scales. However, many southern and eastern African countries lack regional baseline information on the temporal extent, distribution and characteristics of wetlands. PALSAR data provides invaluable information related to the flooding patterns and vegetation characteristics of these wetlands, and is being used to document and characterise specific sites within the region which have been identified due to their vulnerability to both climatic variability and agricultural activities. The information derived from the PALSAR data is needed to assist managers in making decisions about future land uses in wetlands that are intensively used for agriculture and fisheries, and which are an important natural resource for local communities.**

***Index Terms*—ALOS PALSAR, K&C Initiative, Wetland Theme, Africa, flooding patterns, vegetation.**

I. INTRODUCTION

Throughout Sub-Saharan Africa, floodplains and wetlands are extensive [1]. These ecosystems depend on frequent flooding. They also make critical contributions to the livelihoods of many people. Many hydrological interventions (i.e. dams and irrigation schemes) either already exist within these basins, or are being planned to increase economic benefits and food security. However, these interventions will not be without consequences and both the costs and benefits need to be carefully evaluated. One likely consequence of increased flow regulation is reduced downstream flooding. Annual time series of PALSAR data are an invaluable dataset for identifying seasonal patterns of inundation, and are used here to determine flooding patterns and to map the temporal dynamics of inundation within selected sites in southern and eastern Africa. The data are also used to provide detailed maps of the vegetation for specific wetland sites.

II. DESCRIPTION OF THE PROJECT

A. Relevance to the K&C drivers

The project aims to generate knowledge to assist in the sustainable management of wetlands which are utilised for agriculture and fisheries activities, and to assist the countries concerned to put in place or enhance mechanisms that minimize degradation of the wetlands, in order to optimize the ecosystem and livelihood benefits. Project objectives also include the provision of baseline wetland information from remote sensing and GIS data, and the generation of generic guidelines, tools and methodologies for wetland mapping and characterisation.

The Wetlands Theme of the K&C Initiative focuses on the provision of remote sensing datasets that can be used to assist the global mapping and monitoring of wetlands and identifying and quantifying the threats to which these are exposed. Specifically, it aims to develop a suite of products which may be used to improve the understanding of carbon cycle science, assist the implementation of conservation and management strategies and support national and international obligations to multi-national conventions [2]. The work reported here is of relevance to all three of the thematic drivers: **C**arbon, **C**onservation, and **C**onventions i.e. the three C's. The draining and transformation of wetlands for agricultural (as well as for other) uses is likely contributing to the carbon imbalance in the atmosphere [3]. Wetlands contain and cycle a significant amount of carbon and play a key role in the global carbon cycle, not least because of the large turnover of methane within these systems; it is estimated that natural wetland sources emit about 20% of the methane entering the atmosphere each year [4] and they are responsible for a significant proportion of biogeochemical fluxes between the land surface, the atmosphere, and hydrologic systems [5]. A basic requirement for modelling regional to global methane or carbon dioxide emissions from wetlands is information on their type and distribution.

In Africa where wetlands are utilised extensively for agriculture and fisheries activities, the loss of these ecosystems will also have a more direct effect on local populations. Long-term preservation and sustainable use of these resources is therefore critical for the economic and social well being of current and future generations. Key requirements include the establishment of regional and temporal datasets of wetland extent and condition which incorporate an understanding of the inundation dynamics of an area and spatially quantifiable measures of both anthropogenic and natural pressures and threats to wetland communities [2].

The Ramsar Convention on wetlands of International Importance promotes the conservation and wise use of all wetlands through local, regional and national actions and international cooperation, as a contribution towards achieving sustainable development throughout the world (Ramsar COP8, 2002). The Convention aims to halt and reverse the global trends of wetland degradation and destruction through the dissemination of information, involvement of local communities and establishment of sustainable management plans. While Contracting Parties to the Convention have been encouraged to undertake better and more efficient wetland inventory, and to establish and maintain national inventories, many African countries lack the resources to achieve this. Remote sensing technologies are essential in providing up-to-date spatial and temporal information about wetlands and their catchment basins, and should be seen as a fundamental component in the development of wetland management plans for conservation and sustainable utilisation. While mapping of wetlands has proved difficult in many areas because of the lack of temporally and spatially consistent datasets, the systematic data acquisition strategy of ALOS PALSAR seeks to redress this [3].

B. Site description

The analyses have been conducted at two inland wetland sites located in Malawi and Mozambique (Figure 1). Both sites have been nominated by the countries as priority sites for analysis, as they are vulnerable to both climatic variability and agricultural activities. Population pressure and increased exploitation of resources within these wetlands and the surrounding catchments are leading to serious degradation and loss of biodiversity and inter-connected ecosystem services. Lake Chilwa is a transboundary wetland located in a tectonic depression in south-eastern Malawi and western Mozambique. The catchment covers a total area of 8349km^2, 97% of which is located in Malawi and 3% in Mozambique. The wetland (an area of approximately 2250km^2) is a Ramsar site, and a UNESCO Biosphere Reserve. While the Lake is fed by 7 streams, it is an endorheic system with no outflow. As the lake is shallow with an average depth of 1-2m (Figure 2), its size varies considerably depending on precipitation levels in the catchment with small increases in water level resulting in

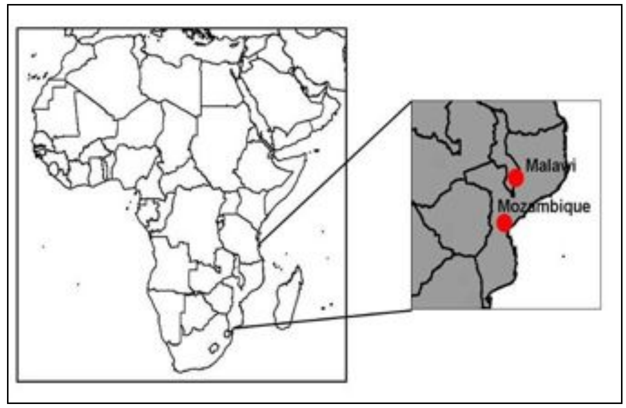

Figure 1. Site locations © JAXA/METI and acquisition date (here: Jan 15, 2009)

large increases in spatial extent. The wetland has a history of cyclic drying and filling; in the last century alone it has dried and filled eight times, with the last recession occurring in 1996/97. The hydrology of the lake is an important control on the ecology of the wetland, determining not only the water chemistry and physical properties, but also the composition of the vegetation and soil characteristics [7]. The only available information relating to the vegetation within the wetland complex was produced from a ground survey conducted in the 1970's [8], and no digital data on spatial patterns of inundation is available.

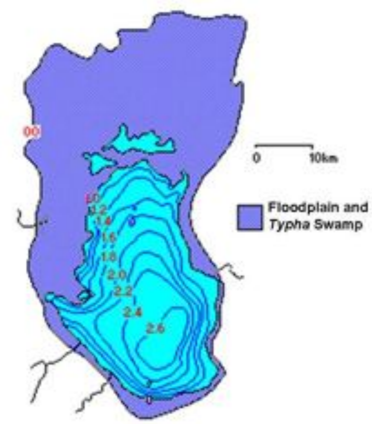

Figure 2. Bathymetric map of Lake Chilwa (source: UNESCO, 2004).

Lake Urema and the surrounding wetlands are located in Gorongosa National Park in central Mozambique. An understanding of the ecology and hydrology of the lake and wetlands is essential for the conservation of the floodplain habitats which are critical for maintaining the biodiversity of the Park. There are concerns that the hydrology and ecology of the lake have changed in recent years, possibly dues to climatic variability and land use changes, as well as tectonic activity [9]. The analyses conducted here aim to provide baseline data on the vegetation composition, spatial extent, and seasonal variations in the wetlands around Lake Urema, in order to improve understanding of their vulnerability to changes in the hydrological regime.

C. Materials and methods

The analyses were performed on multitemporal datasets of ALOS PALSAR fine beam data. Where available, optical images and topographic data were also incorporated. For both sites extensive field campaigns were conducted according to the following methods. Latitude and longitude grids were overlaid on maps of the sites, and depending on access, field sites were selected at one second intervals.

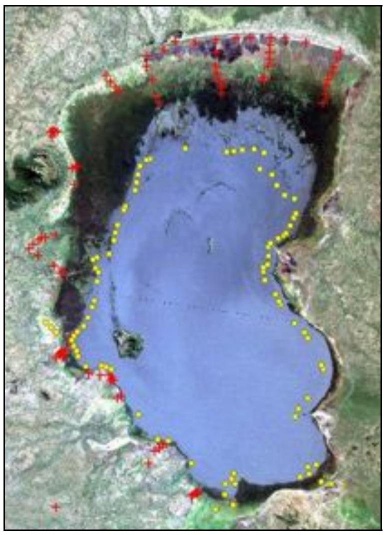

Figure 3. Air photo (yellow circles) and field site (red crosses) locations, Lake Chilwa, Malawi. Base image: Landsat TM real colour composite

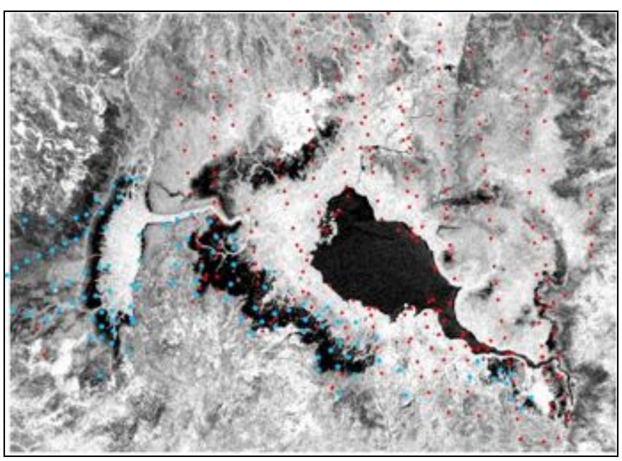

Figure 4. Air photo (red circles) and field site (blue circles) locations, Lake Urema, Mozambique. Base image: ALOS PALSAR HH, Feb 2007 © *JAXA/METI*

An area of 20x20m was demarcated at each site, and various data recorded including vegetation species, ranked biomass, species dominance, land use and hydrology. Where cloud (and smoke) free optical datasets were available, these were incorporated into the analysis. The remote sensing datasets for each site are described in Table 1. In addition georeferenced low altitude aerial photos were acquired at both sites (for Lake Chilwa courtesy of the Danish Hunters Association, DANIDA). The locations of field sites and aerial photos are illustrated in Figures 3 and 4. Data were collected at 90 field sites (92 aerial photos) around Lake Chilwa, in October 2006 (a PALSAR FBS image was also acquired this month) and at 120 sites (250 aerial photos)

Site	**Sensor**	**Wavebands/ mode**	**Acquisition date**
Lake Chilwa	Landsat TM	VNIR, TIR	18th Nov 2005
	ASTER	VNIR, SWIR, TIR	21st May 2006
	PALSAR	FBD	17th May 2006
		FBS	2nd Oct 2006
		FBS	Feb 2007
Lake Urema	PALSAR	FBS	Dec 2006
			Feb 2007
		FBD	Jun 2007
		POL	Jun 2007
		FBD	Aug 2007
			Sep 2007
		FBS	Feb 2008

Table 1. Remote sensing datasets used in the analysis

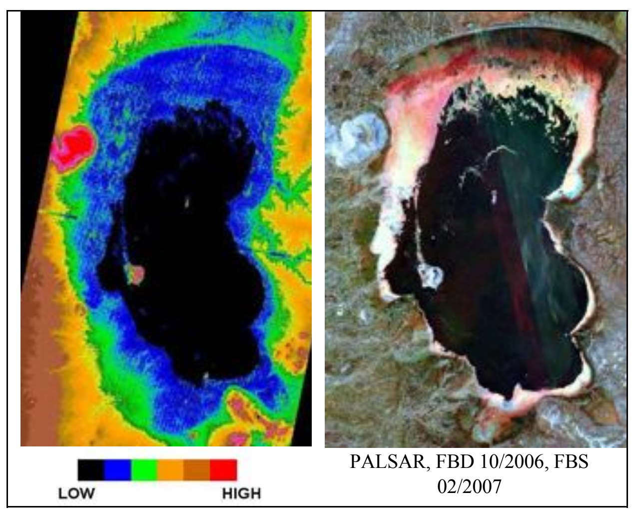

Figure 5. 15m DEM derived from ASTER, PALSAR composite image (R: HH, G: HV, B: HH) © *JAXA/METI*

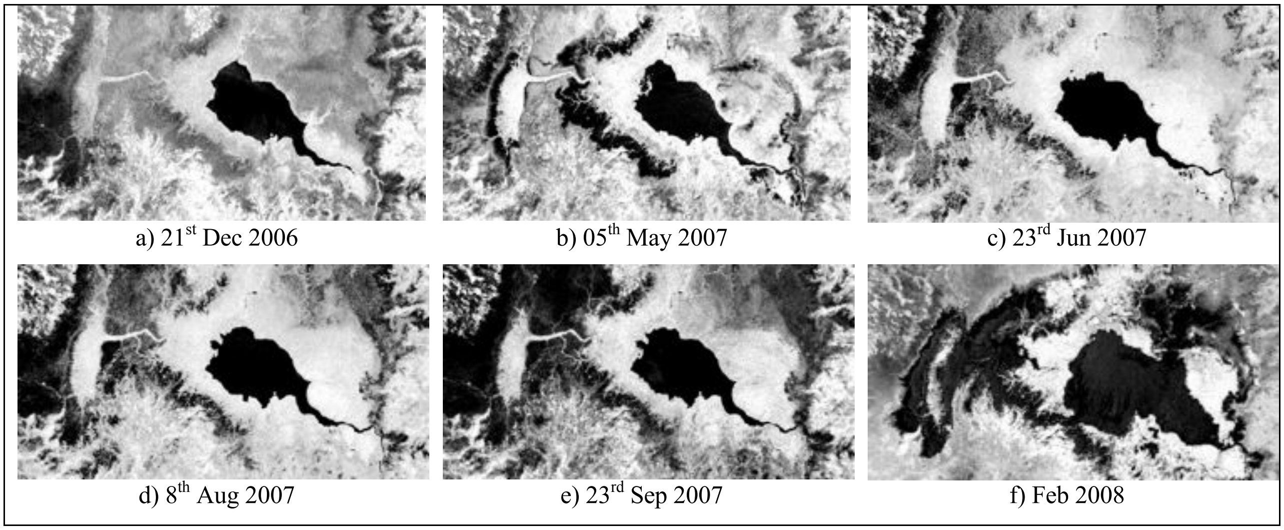

Figure 6. ALOS PALSAR scenes, Level 1.5, 12.5 pixel spacing © *JAXA/MET*

around Lake Urema in July 2007 (PALSAR POL and FBD images were acquired in June and August 2007 respectively). A 15m DEM was derived using the two visible bands of the ASTER image. This and the PALSAR data are shown in Figure 5.

For Lake Chilwa, the classification of the remote sensing data into dominant wetland types was performed using a Decision Tree (DT) classifier, based on a series of binary decision rules. DT classifiers allow multistage classifications to be performed, recursively partitioning the input dataset into increasingly homogenous subsets. A particular advantage of this approach is that datasets with different spatial resolutions, as well as ancillary datasets can be used together during the classification process. Image segmentation was performed at each node based on histogram analysis in order to separate the data into two mutually exclusive classes. The vegetation within the "wetland vegetation" class was subsequently

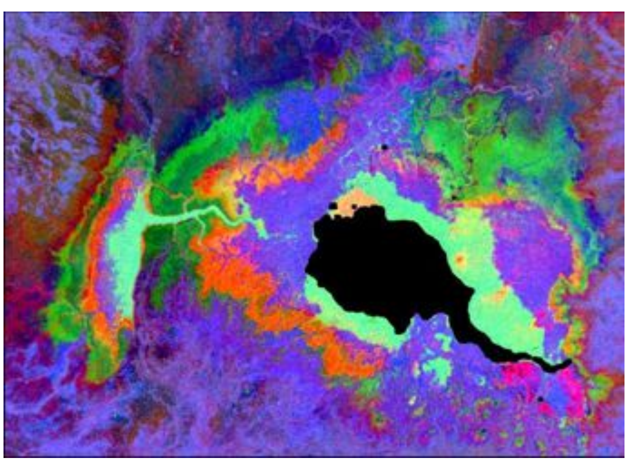

Figure 7. Principal Components Analysis of 7 ALOS PALSAR FBS, FBD and POL scenes (RGB: PCA 1, PCA 2, PCA 3), ALOS K&C © *JAXA/METI*

classified into species dominance based on a subset of the field sample sites (50% of the sites were randomly selected) and the aerial photograph locations.

Over central Mozambique cloud cover in the wet season, and smoke from burning during the dry season presents a problem in the acquisition of suitable optical datasets. All PALSAR images available (Figure 6) over a 14 month period (Dec 2006 – Feb 2008) were therefore used in the analysis, in an attempt to characterize the seasonal variations in the Lake and surrounding wetlands. The PALSAR images (with a pixel size of 12.5m) were smoothed using a 5x5 pixel median filter, to reduce the influence of speckle. This filter was chosen as it preserves edges, while smoothing the data. For wetland areas the boundaries of the wetlands are thus preserved while a more homogenous within-wetland pixel value is achieved [10]. The variations observed in the PALSAR images between the various dates (Figure 6) are predominantly due to changes in the flood condition and soil moisture.

In order to quantify the temporal variance in the data, a Principal Components Analysis (PCA) of the filtered temporal sequence of PALSAR images (Figure 6, Table 1) was performed on the filtered images, thereby providing information on the duration of the flood conditions. Figure 7 shows the results for the multitemporal PCA analysis. Areas with minimal changes across all dates exhibit very low variance (low values in each PCA band), and are represented by the black areas in Figure 7. This corresponds to the permanently flooded areas (between Dec 2006 and Feb 2008) of Lake Urema. Variations in the hydrologic regime over the time period of the study for the wetland areas surrounding the Lake are clearly evident from a visual analysis of Figure 7. A supervised classification was performed using the first three PCAs as input in addition to the individual PALSAR images, in order to identify classes within the wetland based on frequency of flooding and their hydrologic condition over the 14 month period. Visual analysis of the PCA results, the aerial photos and the field data collected suggested a high correlation between the dominant vegetation species and the time/duration of flooding. Training sites for the classification were selected based on dominant vegetation species, as identified during the field campaign. 50% of the 120 sites were selected at random for this purpose, along with 125 of the aerial photo locations. Thus based on the field data the flooding patterns have been linked to the different vegetation communities.

III. Results and summary

Two products have been created for the Lake Chilwa wetland; i)a map depicting the spatial zoning of broad wetland classes derived from the annual flood dynamics, and ii)a map illustrating the spatial distribution of the wetland vegetation. These are shown in Figure 8. In addition to the open water, the wetland consists of a band of dense reed swamps and marshes, and a seasonally inundated grassland floodplain. The distribution and dynamics of the wetland flora and fauna are dependent on the seasonal and annual fluctuations in water levels. An accuracy assessment of the classification results (Figure 8b) based on an independent sample (the 45 field sites not used in the training phase) indicated a classification accuracy of 89%. The identification of wetland classes for Lake Urema and the surrounding wetlands has been determined based on flooding regime. These results are displayed in Figure 9. Accuracy assessment of the results is currently underway.

The ALOS PALSAR datasets have been used in this project to detect spatial and temporal changes in hydrologic conditions of inland wetland ecosystems in Africa. The images have been used to provide baseline data for two biodiversity hotspots; Lake Chilwa, a Ramsar wetland site of

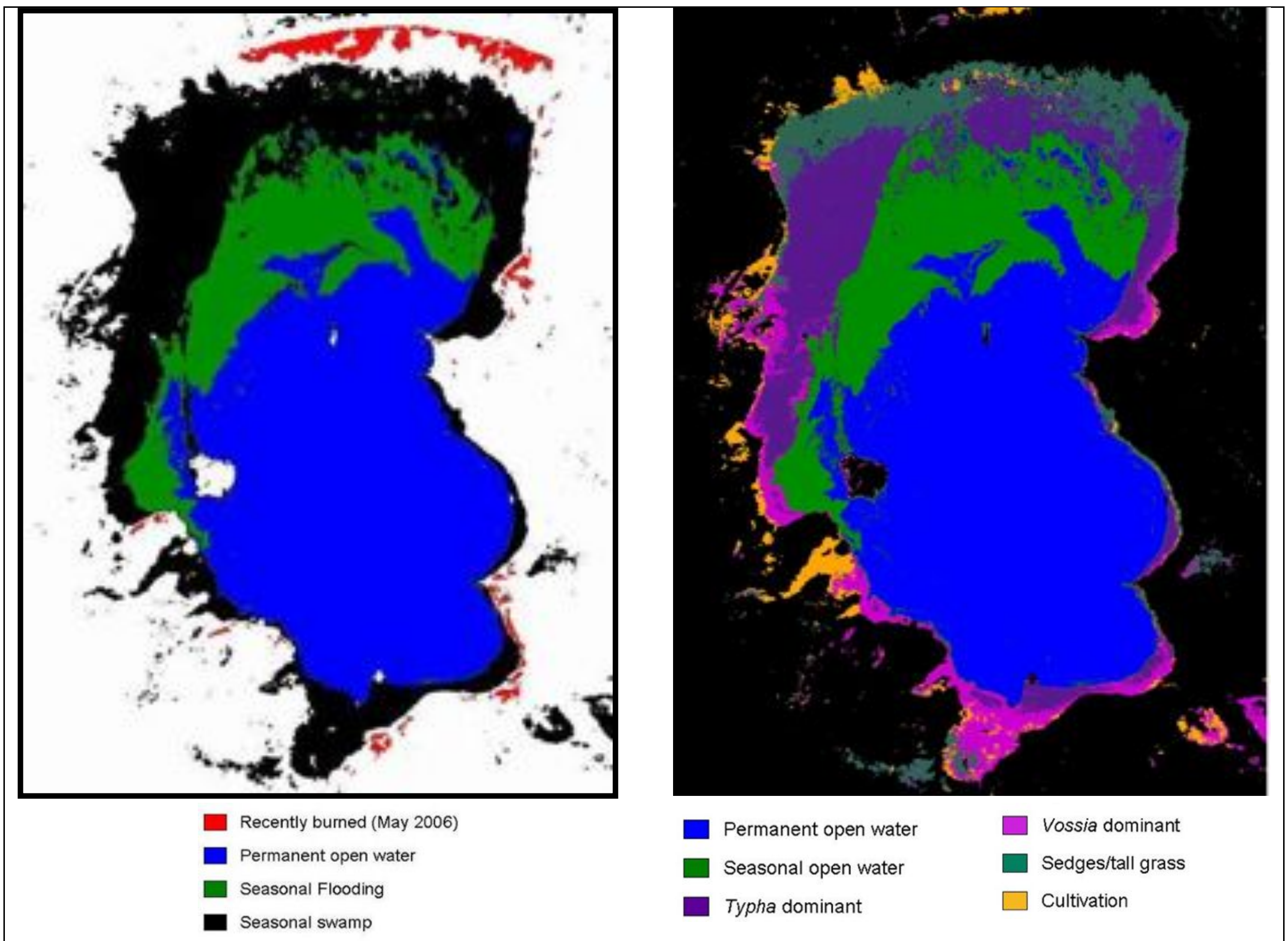

a) Broad wetland classes derived from annual flood dynamics   b) Distribution of wetland vegetation

Figure 8. Principal Components Analysis of 7 ALOS PALSAR FBS, FBD and POL scenes (RGB: PCA 1, PCA 2, PCA 3), ALOS K&C © *JAXA/METI*

International Importance, and a UNESCO Biosphere Reserve in Malawi, and Lake Urema, a key component of the Gorongosa National Park in Mozambique. The analysis has provided information on the vegetation composition and seasonal variations in the wetland extent, thereby increasing understanding of the ecology and hydrology of these ecosystems and providing information crucial for their sustainable management and conservation. ALOS PALSAR proved to be an essential data source for these analyses due to i) frequent cloud cover over the areas of interest thereby preventing the use of optical data, ii) a systematic observation strategy [11] and frequent image acquisition allowing for characterisation of the flood dynamics at a high temporal resolution, iii) FBD in addition to FBS coverage of the wetlands during the summer months enabling discrimination of different vegetation structural types.

Building on the work reported here, future work will attempt to scale out to larger areas.

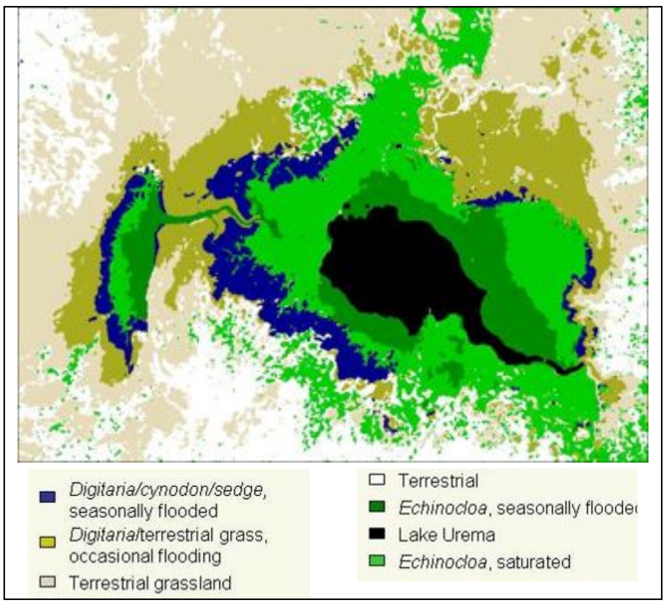

Figure 9. Lake Urema, Mozambique: Identification of wetland classes based on flooding regime. ALOS K&C © *JAXA/METI*

Annual time series of PALSAR (ScanSAR) data are an invaluable dataset for identifying seasonal patterns of inundation, and will be used to determine flooding patterns and to map the temporal dynamics of inundation across selected regions of the White Nile and the Zambezi.

ACKNOWLEDGEMENTS

In addition to any other acknowledgement you may wish to make, please include also the K&C standard acknowledgement: "This work has been undertaken within the framework of the JAXA Kyoto & Carbon Initiative. ALOS PALSAR data have been provided by JAXA EORC."

REFERENCES

[1] L-M. Rebelo, M. McCartney, C.M. Finlayson "Wetlands of Sub-Saharan Africa: distribution and contribution of agriculture to livelihoods". *Wetlands Ecology and Management*, 2009. [Online] Available: http://www.eorc.jaxa.jp/ALOS/kyoto/jan2009_kc11/pdf/ 090113/shimada_calval_up_090113.pdf

[2] A. Rosenqvist, M. Shimada, R. Lucas, J. Lowry, P. Paillou, B. Chapman [eds.], "The ALOS Kyoto & Carbon Initiative, Science Plan (v.3.1)," JAXA EORC, March, 2008. [Online] Available: http://www.eorc.jaxa.jp/ALOS/kyoto/KC-Science-Plan_v3.1.pdf

[3] W. H. Schlesinger, Biogeochemistry: An Analysis of Global Change, Academic Press; Harcourt Brace and Company, Publishers, 1997.

[4] I. Fung, J. John, J, Lerner, E. Matthews, M. Prather, L.P. Steele, P. J. Fraser, "Three-dimensional model synthesis of the global methane cycle", *Journal of Geophysical Research, Vol 96, pp 13033-13065*

[5] D. Sahagian, H. Melack, [eds.], "Global wetland distribution and functional characterisation: trace gases and the hydrological cycle", *IGBP Report No. 46,* IGBP Secretariat, Stockholm, 1996.

[6] A. Rosenqvist, M. Finlayson, J. Lowry, D. Taylor. "The potential of long-wavelength satellite-borne radar to support implementation of the Ramsar Wetlands Convention", *Aquatic Conservation, Vol 17(3 pp 229-244, 2007*

[7] C. Howard-Williams, B. H. Walker, "The vegetation of a tropical African lake: Classification and ordination of the vegetation of Lake Chilwa (Malawi)"., 1974, *Journal of Ecology, Vol 62(3), pp 831-854*

[8] M. Kalk, A. J. McLachlan, C. Howard-Williams, [eds.], "Lake Chilwa: Studies of change in a tropical ecosystem". *Monographiae Biologicae, 35.* Junk, The Hague, 1979.

[9] B. Bohme, F. Steinbruch, R. Gloaguen, H. Heilmeier, B. Merkel, "Geomorphology, hydrology, and ecology of Lake Urema, central Mozambique, with focus on lake extent changes". *Physics and Chemistry of the Earth, vol 31, pp 745-752, 2006*

[10] L. Bougeau-Chavez, K. B. Smith, S. Brunzell, E. Kasischke, E. Romanowicz, C. Richardson, "Remote monitoring of regional inundation patterns and hydroperiod in the Greater Everglades using Synthetic Aperture Radar", *Wetlands, Vol 25(1), pp. 176-191*

[11] Rosenqvist A., Shimada M., Ito N. and Watanabe M. "ALOS PALSAR: A pathfinder mission for global-scale monitoring of the environment," *IEEE Trans. Geoscience and. Remote Sens, vol. 45, no. 11, pp. 3307-3316, 2007.*

Lisa-Maria Rebelo is a researcher at the International Water Management Institute (IWMI), part of the Consultative Group for International Agricultural Research (CGIAR). With an MSc in Remote Sensing and GIS and a PhD in Remote Sensing algorithm development, both from the University of London, Dr Rebelo's current research is concerned with the provision of geospatial data for improved land and water management in Africa. As a JAXA K&C PI under the Wetland Theme, her interests lie in the characterisation of wetland ecosystems and mapping spatial patterns of inundation in the Nile and Zambezi basins.

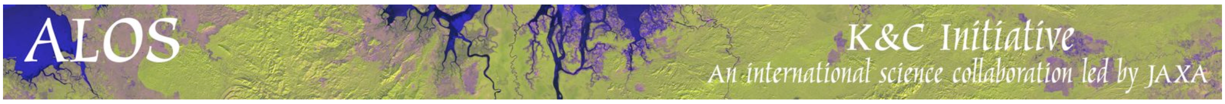

Wetlands Theme

Wetland monitoring of flood-extent, inundation patterns and vegetation, Mekong River Basin, Southeast Asia, and Murray-Darling Basin, Australia

Anthony Milne & Ian Tapley
Horizon Geoscience (Australia)

Wetland monitoring of flood-extent, inundation patterns and vegetation, Mekong River Basin, Southeast Asia, and Murray-Darling Basin, Australia

Anthony K Milne
School of Biological, Earth and Environmental Sciences,
University of New South Wales, Sydney, NSW 2052, Australia, Tony.Milne@unsw.edu.au

Ian J Tapley
Horizon Geoscience Consulting Pty Ltd, 12 Viewcrest Way, Sorrento, 6020, WA, Australia.
HGCiant@bigpond.net.au

Abstract— **It is well documented that 24cm wavelength JERS-1 and ALOS PALSAR L-band radar data are well suited to map and monitor the structural assemblage of dense vegetation cover comprising shrublands and forests. In addition, the penetration capability of L-band enables accurate detection and mapping of flooding below forest canopy. In this on-going study, ALOS-PALSAR and archival JERS-1 SAR imagery are used in conjunction with complementary datasets and field-data to develop a baseline inventory for showing the extent of flooding in the Lower-Mekong Basin in South East Asia and to analyse flood patterns in the Macquarie Marshes located in the Murray-Darling Basin in eastern Australia. These baselines will then be used to monitor subsequent seasonal changes in the extent and duration of flooding. Attention is also paid to mapping and monitoring changes in the status and condition of wetland vegetation types in these two river basins.**

Index Terms—**ALOS-PALSAR, JERS-1 SAR, K&C Initiative, wetlands, Lower Mekong Basin, Murray-Darling Basin**

I. INTRODUCTION

The Project focuses on two contrasting wetland environments: the wet-tropical Lower Mekong Basin in Southeast Asia, and the semi-arid Macquarie Marshes in the Murray-Darling Basin. Both regions are under threat from anthropogenic disturbances and from the impacts of projected climate change. Foremost among these influences are landscape degradation and declining water availability.

In this on-going project, ALOS-PALSAR and archival JERS-1 SAR imagery are used in conjunction with complementary datasets and field-data to develop a baseline inventory for showing the extent of flooding in the two study sites against which subsequent seasonal changes in the extent and duration of flood events can be mapped and assessed. Attention has also been paid to mapping and monitoring the changes in wetland vegetation types.

Within the Lower Mekong Basin (LMB), future significant changes in river flow and total discharge can expected to occur as a result of dam building in the upper reaches of the Basin. Land use and environmental planning will therefore be intimately linked and to a large extent controlled by changing river flow regimes which are likely to seriously alter the seasonal passage of discharge through the LMB.

Within the Murray Darling Basin (MDB) there are a number of freshwater Ramsar-listed wetland sites including the Macquarie Marshes, the Gwydir wetlands and the Murrumbidgee wetlands [1]. These, along with other riverine wetlands in eastern Australia, have experienced significant long-term declines in stream flow as a result of river regulation and water storage diversions to support irrigated agriculture.

II. STUDY AREAS

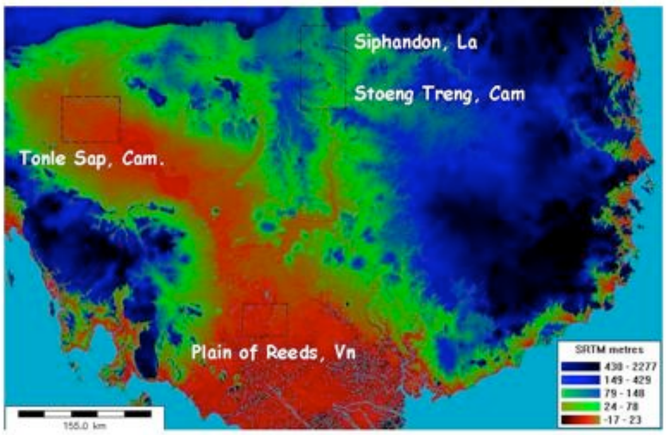

Figure 1. SRTM DEM showing location of study sites within Lower Mekong Basin

A. Lower Mekong Basin

Within the LMB analyses of PALSAR and JERS radar datasets have focused on 4 sites: Siphandon in Lao PDR, Stoeng Treng and Tonle Sap in Cambodia, and Tram Chim in the Mekong Delta of Vietnam. Wetland sites along the Songkram River floodplain, Thailand, and within Attepeu Province, Lao PDR, are yet to be included in the analysis. Siphandon and Stoeng Treng are sites along the Mekong River under threat from the development of hydro-electric dams and modification to the extent of flooded forests and disruption to the fish habitats proximal to the river channels.

Tonle Sap is the most important wetland in Southeast Asia in terms of productivity and biodiversity [2] and [3]. In addition to impacts of illegal forest logging, it too is threatened by the future availability of floodwaters which are likely to be insufficient to support Cambodia's demand for irrigated rice growing and for the supply of fish stocks.

Tram Chim National Park is a remnant wetland, representative of the ecosystem that formerly occupied the vast Plain-of-Reeds. Threats to its sensitive biodiversity include modification of the water regime in the Mekong Delta, inappropriate fire-control measures, fires, chemical pollution from agriculture development, acidification of water bodies by digging and exposure of acid-sulphate soils, and illegal logging of the natural *Melaleuca spp*. forests.

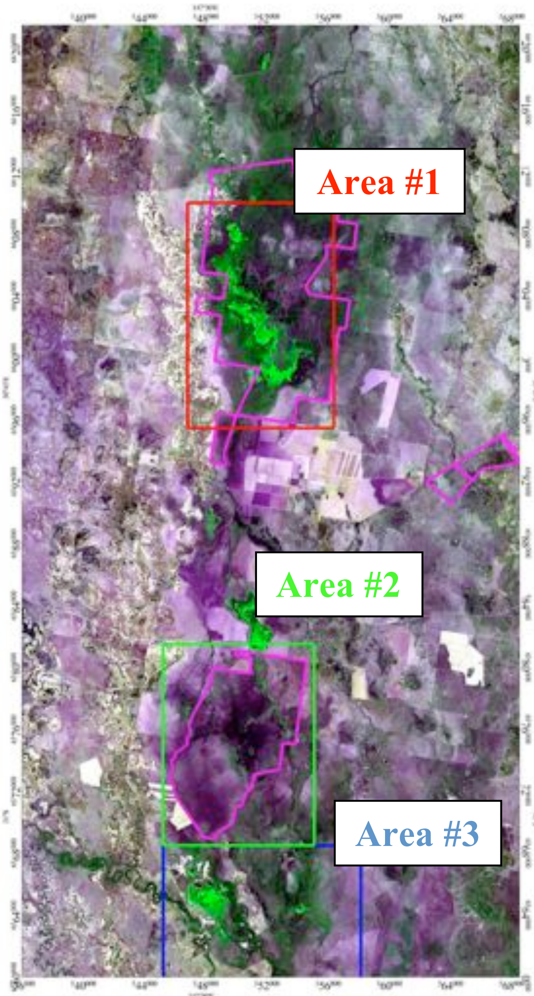

Figure 2. Target areas in the Macquarie Marshes overlain on SPOT-5 imagery (bands Red:NIR:Green in R:G:B): Area 1 (red) in the northern reserve; Area 2 (green) in the southern reserve; and Area 3 (blue) to the south of the marshes. The boundary of the Macquarie Marshes Nature Reserve is shown in magenta.

B. Macquarie Marshes

The Macquarie Marshes constitute an inland semi-permanent wetland located in the Macquarie River Catchment in central-western NSW. The wetlands have formed within an alluvial fan system which is characterised by a series of anastomosing channels running through the marshes [4]. The streams eventually drain into the Darling River (Figure 2). The Marshes depend on the inflow of water coming from up-river and outside the immediate area for their maintenance and ecological survival. In this respect they differ markedly from the Mekong wetlands which receive seasonal rainfall and an annual inflow of floodwaters in the monsoon season.

In the case of the Macquarie Marshes, 40-50% of the wetlands have already been lost and overall <10% of the original wetlands are considered healthy. Together with the impact of continued drought and water being diverted for irrigation, water availability to the marshes and inflow into this river system in general is limited to the release of controlled environmental flows from upstream.

III. PROJECT DESCRIPTION

A. Lower Mekong Basin

Objective: To detect changes in the magnitude and frequency of flood events, and identify land cover changes over selected wetland sites in the Lower Mekong Basin using a time-series of JERS-1 and PALSAR datasets.

Specific aims include:

i. Examine relative contributions of HH and VV polarizations to discriminate between wetland types;
ii. Examine data for details of wetlands, generate site specific maps of wetland type and land cover change;
iii. Create hydro-pattern maps based on individual scenes to show extent of flooding and relative water heights;
iv. Merge multiple datasets and look at spatial variations in backscatter signatures over the temporal domain.;
v. Determine disturbance parameters in the selected wetland ecosystems through land development, land clearing for rice paddies, road constructions and water diversion;
vi. Analyse for changes in wetland type and extent and impacts of disturbance.
vii. Undertake field validation of image-map products with a revisit to nominated field sites and spot-checks of additional sites of interest identified in the imagery.

Complex seasonal cycling involved in the change from wet-to-dry conditions is not captured in a single date image. This problem is resolved using multi-date imagery resulting in the likelihood of a much improved classification and monitoring scheme.

Products to be derived from this K&C Initiative include image-maps of wetland cover and of annual changes in wetland cover, along with flood maps showing flood extent and seasonal floodwater recession patterns.

B. Macquarie Marshes, Australian Murray-Darling Basin

Objective: To undertake a multi-scene stack analysis of 20+ scenes of PALSAR data to identify hydrologic and vegetation response to changed flood and in-channel discharge conditions in a semi-arid environment.

Specific aims include:

i. Process a registered and calibrated time-series PALSAR dataset of both FBS and FBD imagery acquired over a 3-5 year time period.
ii. Apply suitable image processing routines to enable class discrimination to be established between open water, saturated soil areas, bare ground and seasonal grasslands.
iii. Apply suitable image processing routines to enable class separation between different wetland vegetation types, assess vegetation condition over time.
iv. Relate class separation to periodicity and magnitude of flood events occurring over the same period.

This study is assessing PALSAR FBS data for detecting surface water beneath tree canopies and for monitoring the impact of environmental flow on soil moisture and vegetation response and condition in these marshes [5] and [6].

Ultimately, the Project aims to demonstrate the benefits of incorporating SAR into an operational system for monitoring flooding, wetland and landuse dynamics, and assessing the impacts of climate change in this semi-arid environment. This will be accomplished when a longer time-series of imagery becomes available.

IV. METHODOLOGY

The principal datasets for both investigations include JERS-1 L-band wavelength, HH-polarization for the period 1992-98, and Fine-Beam PALSAR L-band wavelength, HH- and HV-polarization collected for period 2006-2009. ScanSAR strip data at 50m resolution is now available but has not yet been processed. An important aspect of the Macquarie Marshes study is an evaluation of X-band (Terra-SAR) and C-band (Radarsat-1) datasets with PALSAR acquired for near corresponding dates. HyMap hyperspectral data and field observations complement the Macquarie Marshes radar data.

In the LMB SRTM height data and time-series radar data was used for hydrological and wetland dynamic studies, complemented with high-resolution optical imagery and stream-gauging information for flood assessment.

PALSAR and JERS image intensity data were provided by JAXA as calibrated datasets. Each was subsequently adjusted to dB values using the documented techniques allowing direct comparison between processed data of each system.

Initial assessment of the map geometry supplied in the header file for each JERS and PALSAR scene showed the coordinates to be unreliable. Therefore considerable time was spent geolocating each scene to UTM map projection using ground-control points selected from a reference optical scene. Final registration accuracy was <1 pixel. Multi-date scenes of JERS and PALSAR were assembled for each study site into a stack of registered scenes suitable for time-series analysis.

Image enhancement and information extraction procedures used include; single-date grey-tone images, ratio greytone images, RGB colour-composite images of multiple dates and polarizations, data transforms, change detection, multivariate analysis, segmentation and classification.

Advanced processing techniques were applied to quantify the land-cover and determine how the cover classes alter over time in response to variations in local topography, climatic change and anthropogenic impacts such as forest and wetland clearing, flooding, reduced water availability and urbanization.

V. RESULTS

A. Lower Mekong Basin

The capacity to map and monitor the incidence of seasonal flooding in the LMB as well as observe the larger regional responses to seasonal change are shown in Figure 3. These ScanSAR images (50 metre resolution) for 5th November, 2006, which marks the end of the wet season, records the extent of flooding in the Tonle Sap Lake. The inflow of water comes from the flooded Mekong River. Tonle Sap occupies the bottom of a shallow basin with water levels peaking at around 6-8 metres above sea level at peak flood height when the capacity of the lake increases fourfold.

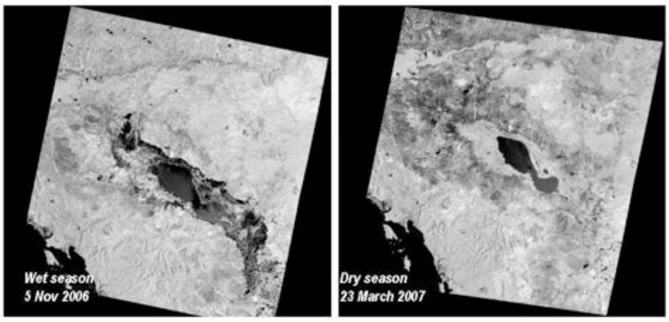

Figure 3. ScanSAR images of Tonle Sap Great Lake in Cambodia showing seasonal flood extent, wetlands and permanent surface water. Comparison indicates the extent of flooding during the wet season and open surface water bodies in the dry season. © JAXA/METI

The dry season image for 23March 2007 in contrast shows a shrunken lake area as the floodwater drains back into the main channel of the Mekong River. This annual reversal of flow dominates the ecological and human response to the prevailing environmental conditions. The expanded dark areas in the March image away from the lake and adjoining wetlands are a backscatter response from dry rice paddies and bare fields.

Figure 4 shows in more detail the impact of flooding and the effect of falling lake levels along the western end of the Tonle Sap Lake. Extensive areas of wetland forest are covered by water in the wet season but have 'emerged' as the water level in the lake falls to its lowest in the dry season. Detailed mapping and classification of this wetland is given in [2].

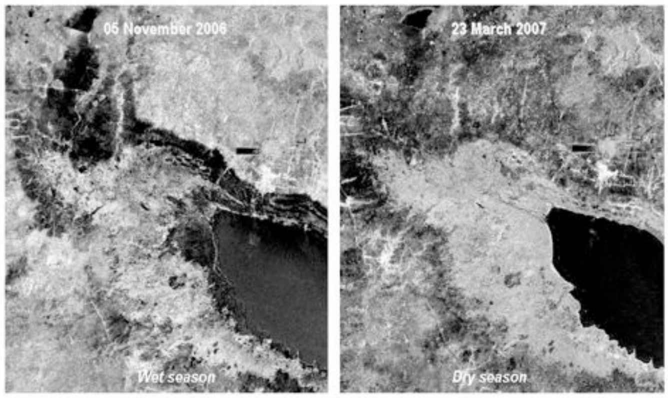

Figure 4. Northern end of Tonle Sap Great Lake - ScanSAR images acquired during the wet (November) and dry (March) seasons show clearly the seasonal differences in the level of water in the lake and also highlight flooding under tree canopies, especially apparent in the wet season.
© JAXA/MET

Calibration of JERS-1 and PALSAR into a multi-temporal dataset spanning the period 1992-2007 permits the analysis of landscape change over a much longer period.

Figure 5 displays a time-series colour-composite image of JERS-1 Sept.1992, JERS-1 Sept.1998 and PALSAR Sept.2007 as RGB, respectively. This image shows a consistency in the flood pattern of the Mekong River for the September time-frame which is the height of the wet monsoon season. The adjacent scene is a difference image from calibrated scene backscatter data for Sept 1992 and 2007. Increases or decreases in backscatter are shown in db.

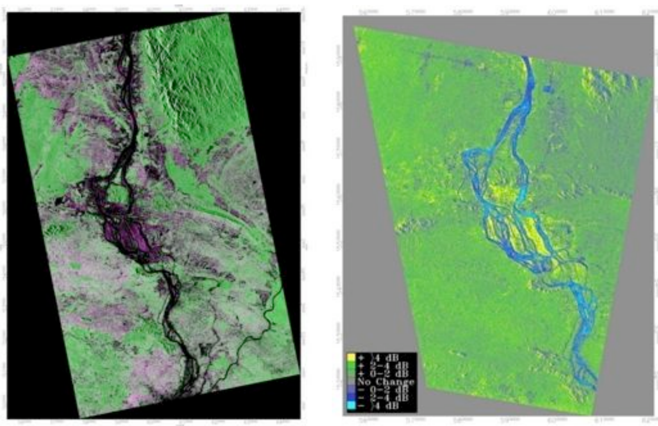

Figure 5. Siphandon, Lao PDR:
Left image: time-series RGB colour-composite image comprising JERS (Sept.1992) : JERS (Sept.1998) : PALSAR (Sept.2007), respectively.
Right image: change detection over a 15 year period, Sept.1992 to Sept.2007. Increase in biomass, maturation of rice crops etc. are shown in yellow; a general increase in the level of foliage cover as green; water surfaces, rough (Sept.1992) and smooth (Sept.07) as cyan-blue, and transport routes as blue. © JAXA/METI

The capacity to use PALSAR data to capture seasonal and intra-annual change in landscape dynamics information is depicted in Figure 6. Here a mid-dry season image (January), an end of dry season image (March) and an early wet season image (September) from 2007 are combined allowing discrimination of more land cover types than is possible with a single-date image.

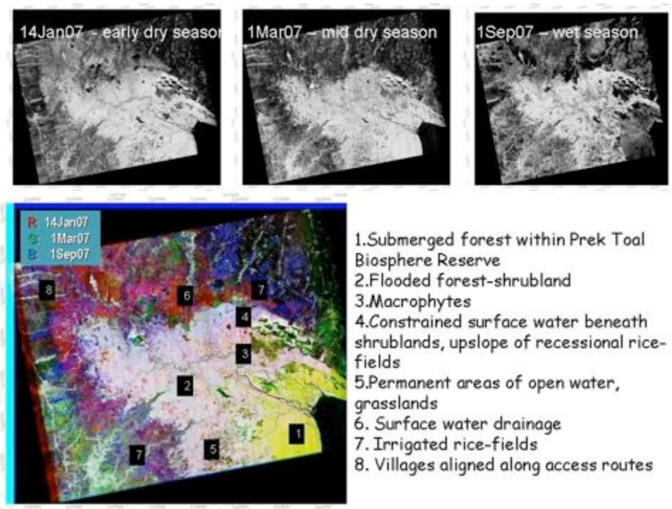

Figure 6. Three-date colour composite image of the Prek-Toal Nature Reserve, Cambodia. The colour and hues are in response to changing backscatter conditions that occur as a result of falling water levels and crop phenology. © JAXA/METI

Figure 7 shows the relative changes that have occurred over a fifteen year period (1992-2007). While the dataset has not yet been classified, an intuitive interpretation of some of the probable changes in land cover that have taken place at selected locations is noted with the image.

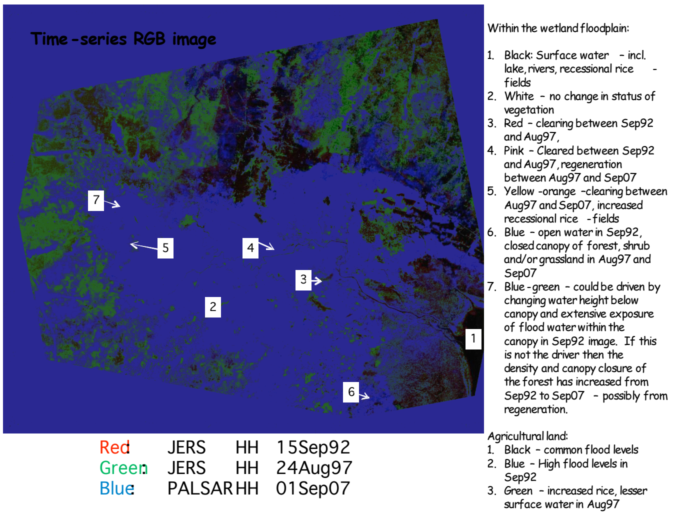

Figure 7. Tonle Sap change image resulting from the RGB combination of JERS-1 Sept. 92, JERS-1 Aug.97 and PALSAR Sep.07 - possible changes identified are described for seven locations. © JAXA/METI

A more detailed analysis in landscape change in the LMB awaits the availability of an extended PALSAR time series from the 2009 -2011 period.

B. Murray-Darling Basin

Vegetation cover in the Macquarie Marshes is must less luxuriant than that found in the LMB. Here sedges, shrubs and grassland dominate with eucalypt (River Red Gum) forests aligning the waterways, with occasional open woodlands on the periphery of the forest stands.

Analysis of PALSAR data acquired over the Macquarie Marshes in 2006, 2007 and 2008 was centred on the impact of a single flood event in January 2008. From available stream discharge records, it is not clear if in fact and to what extent overbank flows occurred within the marshes. In addition to identifying flooded forest wetlands, determining the inundation pattern, detecting areas of increased surface soil moisture and ephemeral vegetation growth on the floodplain, also became drivers in this analysis.

Flooded forests are easily recognised in PALSAR data by their bright response and enhanced backscatter at L-band HH polarisation as a result of penetration of the tree canopy and double-bounce interactions between the large branches and trunks and the underlying, highly reflective inundated surface. Strong returns from single-bounce interactions at HH and HV polarisation with large branches and trunks are also observed.

In the single-date image shown in Figure 8, areas of flooded forest are bright. Ponded areas and open water in channels (black on image) are scattered throughout the wetlands, including water flowing into the River Red Gum forest (purple arrow), Loudens lagoon (red arrow), Third Crossing Lagoon (orange arrow) and Bora Creek (blue arrow). The dark patches on the western side of the image comprise old river channels and scalded bare ground. Water has accumulated in the depressions and flat scalded areas forming a thin film of mud that induces a specular response, and so these areas appear black.

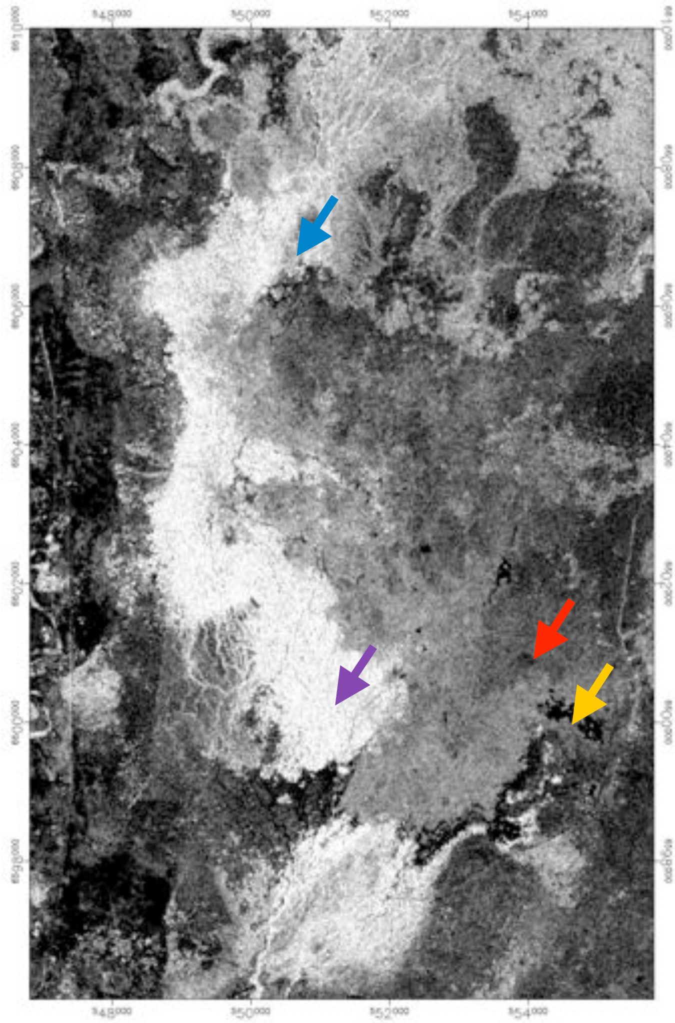

Figure 8 ALOS-PALSAR L-HH data over Area 1. The image was acquired on 21 January 2008 when the wetlands were at their wettest after a minor flood event © JAXA/METI

In Figure 9 a decorrelation stretch has been applied to highlight different surface conditions retrieved from a three-date multi-temporal dataset.

A decorrelation stretch provides a simple and effective method to remove high inter-band correlation and increase the range and diversity of colours in a colour composite image. The areas of flooded forest (yellow) have been masked from the image. There is good discrimination between open water (purple), edge wetland or marsh (red-magenta), inundated floodplain (green), other forest (pink) and surrounding wetland (blue).

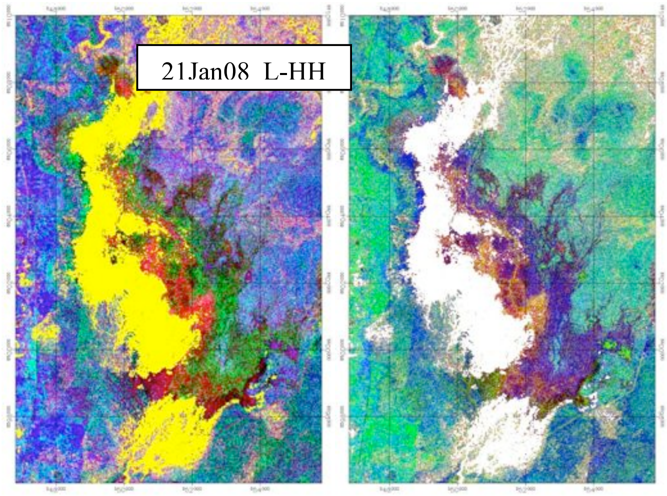

Figure 9. Decorrelation stretch of PALSAR bands Oct07 HH, Jan08 HH and Mar08 HH. Area 1, Northern Macquarie Marshes Nature Reserve. © JAXA/METI

A variety of advanced data-processing techniques are available to visually enhance and combine multiple dates of imagery for improved surface water detection. When applied to L-band PALSAR data, Independent Components Analysis (ICA) and Minimum Noise Fraction (MNF) provided good separation of flooded forests, open water, saturated soils and floodplain wetland. However, decorrelation stretching of the PALSAR dataset enhanced equally the visual detail and produced a colourful 3-band composite of the scene. Areas of open water, water with a cover of aquatic vegetation and wet soil were better discriminated in the decorrelation stretched image than in the ICA and MNF images.

Nevertheless all these techniques are effective in developing indices across dates when applied to stable calibrated data. Data acquired by ALOS PALSAR meet this criterion.

Multi-temporal PALSAR imagery can be interrogated and used to delineate wetlands, locate open water bodies, detect flooding beneath forest cover, identify flood extent and in this case, the area of the enlarged floodplain that was not flooded in January 2008.

The impact of temporary overbank flow from river channels and subsequent inundation of the heavily clayed floodplains is manifested on SAR imagery in different ways. Additional water leads to an increase in surface soil moisture and may also cause the water table to rise close to the surface. This soil moisture response can be observed at any wavelength by the increase in brightness or surface roughness caused by an increase in the dielectric and a flush in ephemeral vegetation growth. A vegetation flush is more easily confirmed in shorter wavelength data (e.g., C-band, ~5.3 cm; and X-band, ~2.5 cm), as a first surface return is received from diffuse scattering between small canopy components (leaves and stems).

End-member analysis using the Spectral Angle Mapper is a rapid classification technique that determines the L-band HH-polarimetric similarity of selected end-member spectra (average spectra from regions-of-interest representing selected surface types) to spectra of all pixels in the scene. It is essentially a physically based technique that determines the spectral similarity between two spectra by calculating the angle between them, treating them as vectors in space with dimensionality equal to the number of bands (3 dates). Smaller angles represent closer matches to the reference spectrum.

Areas that satisfy the criterion for 3 cover types, surface water, marshlands adjacent to the red-river gums, and floodplains subject to inundation, have been classified and are shown in Figure 9. Pixels further away than the specified threshold are not classified. The percentage cover of each class is also calculated (surface water 1.3%; marshland 4.3% and floodplain 7%). A median filter has been applied to suppress spuriously classified pixels. Forests and the immediate marshlands were flooded, but not part of the surrounding floodplain (blue in Figure 9).

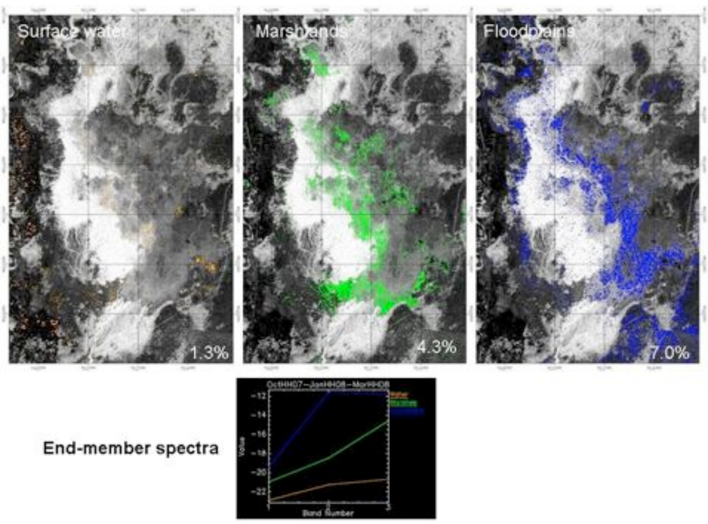

Figure 9 Spectral Angle Mapper (SAM) images based on PALSAR Oct.HH 07, Jan.HH 08 and Mar.HH 08 data of the Macquarie Marshes.
© JAXA/METI

Area 2 of the Macquarie Marshes is largely bare open ground covered with sedges and grasses which respond to flooding. Scattered trees and taller shrubs mark the watercourses. This effect is seen in Figure 10 where the areas displaying the highest component of change (+db) captured in the time-series, are covered with ephemeral vegetation underlain by soils with a high soil moisture content.

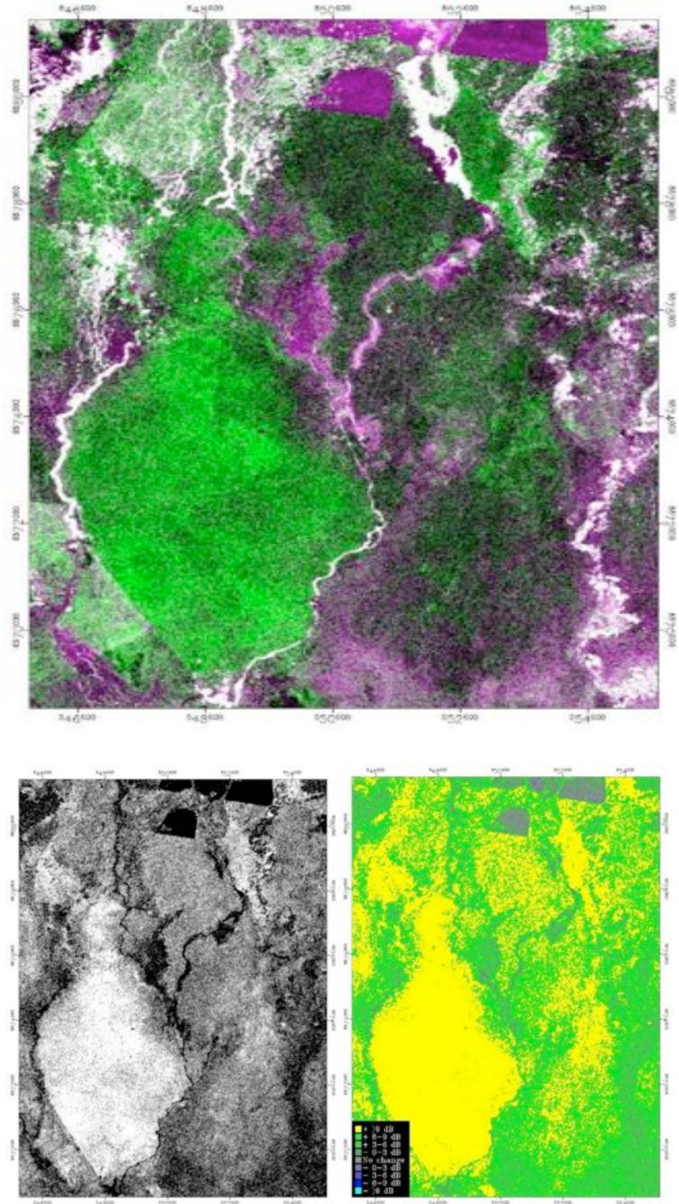

Figure 10. Area 2, Southern Macquarie Marshes Nature Reserve - colour composite and change detection images applied to HH-polarization PALSAR data acquired on 21Oct.07 and 21Jan08.
Top: R:G:B image of Oct07:Jan08:Oct07, respectively;
Bottom-left: Band difference - Jan08 minus Oct07; and
Bottom-right: Change detection, Oct07 to Jan08 – classes displayed in 3 dB increments for a +/- 9dB range. © JAXA/METI

The integration of multi-frequency SAR data in the form of PALSAR and TerraSAR-X can be shown to improve the discrimination of some wetland surfaces.

The TerraSAR-X StripMap data over Area 1 shown in Figure 11 was acquired on 2March 2008 and the PALSAR FBS data on 7March 2008. The TSX data provides a first return or largely a top of the canopy response, hence dark areas on the floodplain at X-band reveal areas where the water has flooded and overtopped the vegetation. Elsewhere there is a vegetation response from the sedges and low grasses that cover the remainder of the floodplain.

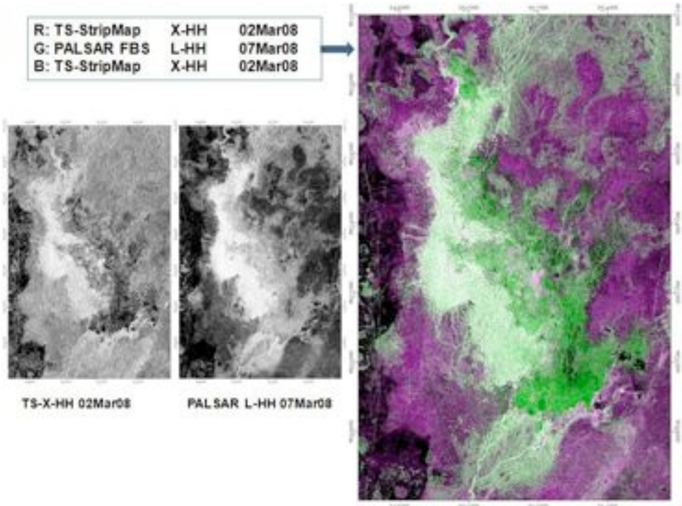

Figure 11. Integration of L-band PALSAR and X-band TerraSAR-X data for discrimination of wetlands. Area 1, Northern Macquarie Marshes Nature Reserve. ALOS K&C © JAXA/METI

An R:G:B colour composite image using bands TSX 2Mar08HH : PALSAR 7Mar08HH : TSX 2Mar08HH respectively, provides good discrimination of wetland surfaces. The backscatter over the floodplain wetland is dominated by the PALSAR Mar08 response (green on image). This is due largely to the L-band response to high soil moisture and roughness.

The backscatter over the surrounding floodplain area is dominated by the TXS Mar08 response (purple on image). The low shrubs and grasses of the floodplain provide many opportunities for volume scattering at X-band. Patches are observed in the edge wetland where the response is also dominated by the TSX Mar08 image. These are most likely areas of very high backscatter a result of ponded water with aquatic vegetation

In the PALSAR data, however, the full extent of the floodplain can be determined as flooded or not, since the longer wavelengths interact only with the woody component and not the shorter grasses.

The integration of near-coincident PALSAR and TerraSAR-X data revealed the extent of floodplain inundation and presence of aquatic vegetation in ponded areas. The PALSAR data were responsive to areas of high soil moisture and roughness, including flooded forest and wet soils. The dark areas on the floodplain at X-band reveal areas where the water had overtopped the vegetation in the wetlands. Scattered bright patches indicate high dielectric from soil moisture and or roughness from the surface of ponded water or water with aquatic vegetation.

Change detection applied to suitably calibrated SAR data reveals areas where a change in brightness has occurred in response to changes in wetland condition and provides a mechanism for understanding the hydrological and ecological changes occurring in an area. The integration of L-band PALSAR data and the shorter wavelength TerraSAR-X or Radarsat-1 data provides good opportunities for the further characterization of wetland extent and surface composition.

VI. CONCLUSIONS

This study which is ongoing demonstrates the ability of PALSAR to map and monitor changes in wetland hydrology and to discriminate between different wetland cover types.

In the Lower Mekong Basin flood mapping and determining wetland extent are clearly possible with PALSAR data. Detecting changes in the landscape response as water levels retreat can be deciphered from multi-temporal datasets. Registration and analysis of calibrated JERS-1 and PALSAR data allow scene changes over a longer period of time.

Following the release of environmental water into the Macquarie Marshes, and acquisition of a suitable short period time-series of L-band ALOS PALSAR data, the following outcomes were realized:

- The presence of and changes in surface water and soil moisture content;
- The generation of spatial map data of inundation extent over the period of image acquisition;
- The monitoring of flood extents and changing wetland dynamics over the time-frame of image acquisition;
- The discrimination of wetland cover classes using time-series analysis;
- Monitoring of changes in wetland condition using change detection techniques; and
- The generation of spatial map data of wetland community extent.

Additionally, the incorporation of multi-frequency SAR data (e.g., ALOS PALSAR and TerraSAR-X) may help achieve improved discrimination of wetland cover types based on shorter- or longer-wavelength radar response to vegetation structure, moisture content and surface roughness.

ACKNOWLEDGEMENTS

Special thanks to Dr. Anthea Mitchell from the School of Biological, Earth and Environmental Sciences at the University of New South Wales who was heavily involved in all studies related to the Macquarie Marshes.

This work has been undertaken within the framework of the JAXA Kyoto & Carbon Initiative. ALOS PALSAR data have been provided by JAXA EORC

REFERENCES

[1] Milne, A.K., Mitchell, A.L., Tapley, I.J. and Powell, M.J. 2007. Use of L-band radar to interpret inundation patterns in the Macquarie Marshes and Gwydir wetlands. Report submitted to the NSW Department of Environment and Climate Change (DECC), Sydney, November, 2007 pp77.

[2] Milne, A.K. and Tapley, I.J. 2004. Mapping and Assessment of Wetland Ecosystems in the Northwestern Tonle Sap Basin with AIRSAR Data, Results of a Pilot Study jointly Funded by the Mekong River Commission and the University of New South Wales, April 2004, pp129.

[3] Milne, A.K. and Tapley, I.J. 2007. Assessment of wetland ecosystems and change in the Tonle Sap Basin, Cambodia, using AIRSAR and JERS-1 radar data. *Asian Journal of Geoinformatics*, 7, 2: 21-29.

[4] Kingsford, R.T. and Thomas, R.J. 2001. Changing water regimes and wetland habitat on the Lower Murrumbidgee floodplain of the Murrumbidgee River in arid Australia. National Parks and Wildlife Service, Sydney.

[5] Milne, A.K and Mitchell, A.L. 2006. Remote sensing requirements of Riverbank: monitoring environmental water flows and their effects. Research report prepared for the Department of Environment and Conservation, Sydney, August 2006, pp99.

[6] Milne, A.K., Tapley, I.J., Mitchell, A.L., and Powell, M.J. 2008. Trial of L-band radar for mapping inundation patterns in the Macquarie Marshes, Volumes I, II and III, Consultancy Report Prepared for the NSW Department of Environment and Climate Change (DECC), Sydney, December 2008 pp280

Anthony Milne received his B.A degree in Geography from the University of New England, Armidale in 1967; Honours Masters in Geomorphology, University of Sydney in 1974 and a PhD from the University of Colorado, Boulder, in 1977.

He is currently a Visiting Professor of Geography and Remote Sensing in the School of Biological, Earth and Environmental Sciences at the University of New South Wales, Sydney, Australia and Remote Sensing Science Manager in the Australian Government sponsored Cooperative Research Centre for Spatial Information. He is also a Co-Director of Horizon Geoscience Consulting Pty. Ltd founded in 1992. His research interests lie in radar remote sensing, vegetation assessment and the mapping of wetlands.

Ian Tapley received his Ph.D in 1989 from the Curtin University of Technology in Perth. Formerly a Principal Research Scientist with CSIRO Australia, he is now a Co-Director of Horizon Geoscience Consulting based in Perth, Western Australia. His current interests lie in radar polarimetry and interferometry for landcover mapping, landform definition and change detection.

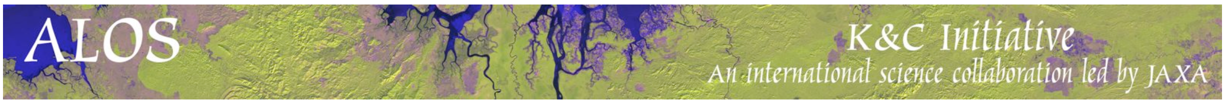

Wetlands Theme

Characterisation and Monitoring of Mangroves using ALOS PALSAR Data

Richard Lucas *et al.*
Aberystwyth University (Wales/U.K.)

Characterisation and Monitoring of Mangroves Using ALOS PALSAR Data

Richard M. Lucas, Peter Bunting and Dan Clewley,
Institute of Geography and Earth Sciences, Aberystwyth University, Aberystwyth, Ceredigion, United Kingdom, SY23 2EJ
Christophe Proisy
IRD/UMR AMAP, 34398, Montpellier cedex 5, France
Pedro Walfir Martins Souza Filho
UFPA-Universidade Federal do Pará.Centro de Geociências/Laboratório de Análise de Imagens do Trópico Úmido. Cx. Postal, 8608. CEP 66.075-110, Belém-Pará, Brasil.
Karin Viergever
Ecometrica, Top Floor, Unit 3B, Kittle Yards, Edinburgh, EH9 1PJ, UK, Scotland.
Iain Woodhouse
School of GeoSciences (Geography), Edimburgh Earth Observatory, The University of Edinburgh, EH8 9XP, Scotland.
Catherine Ticehurst
CSIRO Land and Water, Black Mountain Laboratory,
Joao Carreiras
Instituto de Investigação Científica Tropical (IICT), Departamento de Ciências Naturais, Unidade Desenvolvimento Global, Rua João de Barros, 27, 1300-319 Lisboa, Portugal.
Ake Rosenqvist
Institute for Environment and Sustainability, EU Joint Research Centre (JRC), Via E. Fermi 2749, T.P. 440, Ispra, VA, 210 27, Italy.
Arnon Accad
Queensland Herbarium, Environmental Protection Agency, Brisbane Botanic Gardens, Mt. Coot-tha Road, Toowong, Brisbane, Queensland, 4066, Australia.
John Armston
Queensland Department of Natural Resources and Water (QDNRW), Climate Building, 80 Meiers Road, Indooroopilly, Queensland, 4068.

Abstract*—Methods for classifying mangrove communities from remote sensing data has primarily focused on extent, structure, biomass and/or dominant/species or genus. However, many algorithms have been developed on and applied to local regions but are not applicable at regional levels. For the tropical and subtropics, data from the Japanese Space Exploration Agency's (JAXA) Advanced Land Observing Satellite (ALOS) Phased Arrayed L-band Synthetic Aperture Radar (PALSAR) have been acquired routinely since 2006. As part of the JAXA Kyoto and Carbon (K&C) Initiative, regional mosaics of L-band HH and HV data have been generated for insular and mainland Southeast Asia, northern Australia, Belize and the Amazon-influenced coastline of South America. By using these data in conjunction with Shuttle Radar Topography Mission (SRTM)-derived estimates of mangrove canopy height, a classification of forest structural types was developed which could be applied regionally and potentially across the range of mangroves. Across the tropics and subtropics, mangroves are also subject to change in response to natural or anthropogenic drivers. Identifying such change requires, in many cases, the establishment of baseline datasets of mangrove extent although spatial information on the distribution of dominant species and both structure and biomass as a function of growth stage is desirable. For the same regions, comparison with existing baseline datasets established areas of significant change in French Guiana, Southeast Asia and northern Australia, with each attributable to different causes. The study highlighted the benefits of ALOS PALSAR for detecting change, particularly given the prevalence of cloud-cover in many regions. The utility of and requirements for the inclusion of PALSAR data within a global mangrove mapping and monitoring system are highlighted.

***Index Terms*—ALOS PALSAR, K&C Initiative, Forest Theme, mangroves, structure, change.**

I. INTRODUCTION

A. Characterisation of mangroves

The mapping of mangrove extent and type in many regions has focused largely on the use of optical remote sensing data and especially that acquired by Landsat, SPOT and ASTER sensors. A particular advantage of using optical data is that mangroves are relatively distinct from non-mangrove areas, although confusion with adjoining tropical forests often leads to errors in the mapping of mangrove extent. Approaches to classification have varied and have included the use of standard classification supervised and unsupervised classification algorithms. However, typically only 2-3 mangrove classes have been mapped with these relating primarily to species, structure and/or biomass. Many of the classifications have also been developed and applied to local areas of mangroves and often cannot be applied more widely.

Whilst Synthetic Aperture Radar (SAR) have been used for characterising and mapping mangrove extent in some regions, most SAR have operated at higher frequency C-band (~ 2.6 cm wavelength) microwaves which interact primarily with the upper surface of the canopy. For this reason, separation between mangroves and other vegetation types and those with different structure and biomass has proved difficult, although some success has been obtained using combinations of SAR and optical data.

The launch of the Japanese Space Exploration Agency's (JAXA) Advanced Land Observing Satellite (ALOS) Phased Arrayed L-band SAR (PALSAR) in 2006 therefore represented a milestone in the global observation, characterisation, mapping and monitoring or mangroves, largely because these provide more information on the three-dimensional structure and biomass of woody vegetation and the presence and extent of (primarily tidal) inundation. As data can be day or night regardless of weather conditions, mangroves can be observed more frequently, even in regions with prevalent cloud cover.

B. Detection of change

Mangroves are dynamic ecosystems, responding to changes in the coastal environment by colonising areas where sediment has accumulated and facilitating further accretion [1]. Where changes are adverse (e.g., changes in tidal flow, flooding or storm damage), degradation or dieback of mangroves may occur with subsequent impacts on the distribution and state of the substrate. In the past, such changes have been the consequence of natural processes (e.g., sea level fluctuation) or events (e.g., cyclones or tsunamis). However, the trajectories of change are being altered by human-induced climate change which is manifesting itself as increases in the number and intensity of climate-related events (e.g., storms), longer term shifts in climate (e.g., temperature) and rises in sea level. Disaggregating the influence of climatic change on mangroves distributions and state from that associated with natural processes is therefore presenting a major challenge.

The situation is made more complex by the more direct impacts of human activity on mangroves. In many regions, extensive areas of mangrove have been cleared to support urban development, agriculture (e.g., rice production), mariculture (e.g., oyster and mussel fisheries) and pond culture (mainly shrimps) [2]. The influence of climate change processes on such mangroves is therefore often masked as such activities often lead to artificial changes in hydrological and tidal flows and recolonisation of mangroves is often prevented as the land previously available for expansion is otherwise designated for human use. Many mangroves areas, which might have been indicators of a changing climate, have been and continue to be cleared despite their importance (e.g., as a breeding ground for fish and sustainable source of natural materials). Even so, the role of mangroves in protecting coastlines is also becoming increasingly apparent, particularly since the 2004 Asian tsunami, and efforts are ongoing to ensure their long-term preservation in many regions.

C. Research objectives

Focusing on northern Australia, the Amazon-influenced coast of South America, central America (Belize) and southeast Asia, the research had two main objectives:

a) To establish the potential of the ALOS PALSAR, either singularly or in conjunction with other remotely sensed data, for consistent regional characterisation of mangroves. In particular, the research sought to provide better information for discriminating structural or biomass classes.

b) To investigate the use of these data for detecting changes in mangroves and to establish the causative factors.

These areas were primarily selected as they are supported extensive areas of mangrove and were subject to natural and human-induced influences, including that associated with climate changes.

II. BACKGROUND

L-band microwaves (wavelength approximating 25 cm) emitted by the ALOS PALSAR penetrate through the foliage and interact primarily with the woody components of vegetation [3]. Horizontally transmitted waves are either depolarised through volume scattering by branches in the canopy, with a proportion of vertically polarised microwaves returning to the sensor, or penetrate through the canopy and interact with the trunks, returning primarily through double bounce scattering, as a horizontally polarised wave However, where extensive prop root systems occur, as in the case of higher biomass mangroves dominated by *Rhizophora* and, to a certain extent, the sapling stage of *Brugeiria* and *Ceriops* species [2], multiple scattering results in little energy returning to the sensor, particularly in the HH polarisation [3,4]. This scattering behaviour is captured in the dual polarised L-band HV and HH data respectively.

Whilst these interactions are well known, the use of L-band HH and HV data for mapping and/or characterising mangroves is complicated by the following:

a) Similarities in the L-band response of mangroves and adjacent forest areas often prevent their discrimination and mapping.

b) Where mangroves with extensive prop root systems occur, these often exhibit a low L-band backscatter (particularly at HH polarisation), which leads to confusion with non-vegetated areas.

c) L-band backscatter is enhanced when mangroves are tidally-inundated.

For these reasons, additional information has to be referenced to assist their characterisation.

For global mapping of mangrove extent, optical remote sensing (e.g., Landsat sensor) reflectance data have been widely exploited. Derived products, such as the Landsat-derived Foliage Projected Cover (FPC; [5]) used for mapping the extent of woody and non-woody vegetation in Australia, have also shown promise. However, whilst the use of optical remote sensing data can assist the mapping of mangroves, these data are often difficult to use in combination with regional SAR data as the prevalence of cloud in many areas limits opportunities for acquisition. Nevertheless, many of the World's mangroves have been mapped using these data, and often in conjunction with aerial photography. Such data have been collated into regional to global reference datasets (e.g., the Global Atlas of Mangroves; [6]) and maintained and/or published by national and international organisations, such as the United Nations Environment Program (UNEP) World Conservation Monitoring Centre (WCMC). Whilst much of these data have come from different sources and been generated using a range of methods, they nevertheless provide a baseline of current knowledge. Within the mapped area, mangroves can then be characterised using, for example, SAR data, and variations from the baseline used to detect and describe change.

The characterisation and mapping of mangroves across their range requires consistent and systematically acquired global datasets, which necessarily obtained using satellite sensors. The ALOS PALSAR archive represents one of these datasets. Two other datasets are associated with the Geoscience Laser Altimeter System (GLAS) carried on the ICESat Mission; [7]) and the Shuttle Radar Topography Mission (SRTM; [8]). The ICESAT GLAS is a full waveform LiDAR that provides height profiles for footprints 70 m in dimension and with a post spacing of 14.5 km at the equator. These data have been shown to be sensitive to the heights of mangroves [9]. The SRTM took place in 2000 during which C-band SAR interferometric sensors onboard the Space Shuttle Endeavour acquired data that was used subsequently to generate a Digital Surface Model (DSM) for the majority of the Earth's surface. However, the dominant interaction of C-band microwaves with the leaves and small branches of the upper canopy [9] resulted in the overestimation of ground surface height for many forested areas. Whilst the potential for direct retrieval of forest height was recognized early on (e.g., [10], this required a reliable Digital Terrain Model (DTM) which was not always available. However, as mangroves occur at sea level, the height determined by the SRTM approximates the average stand height. The major limitation was that the SRTM data were distributed at 90 m spatial resolution, although finer (30 m) resolution data were or will be released for some regions. Using SRTM data, calibrated with both field and ICESat data, [9] reported that the crown weighted mean height (H_{CWM}) for mangroves was related to the SRTM height (H_{SRTM}) by:

$$H_{CWM} = 2.1 + 0.94\, H_{SRTM} \quad \text{(Equation 1)}$$

with the margin of error being +/- 1.9 m.

Individually, data from the ALOS PALSAR, optical sensors and the SRTM provide unique information on the extent and characteristics of mangrove ecosystems. However, when combined, considerable insight into the extent and structure of mangroves can be obtained which can be exploited to assist their classification. As these data are globally available, the potential exists for the development of a regionally-consistent algorithms for characterization and detection of change.

III. METHODS

A. Study areas

The method for characterising mangroves using the available datasets was developed initially for mangroves occurring in northern Australia, Belize and the Amazon-influenced coast of South America and is currently being applied to areas within southeast Asia. In all regions, the structural diversity of mangroves is similar in that canopy heights can 30 m in some areas, a closed canopy is commonplace, and the same types of rooting systems are evident. Levels of biomass are also similar although vary across the coastal environment as a function of environment and growth stage.

Mangroves in Australia are extensive (1.5 million ha in 2005; [2]), particularly along the northern and eastern coastlines. As with southeast Asia, the species diversity is high. Whilst urban expansion has been primarily responsible for the loss of mangroves in Australia, the majority remains relatively pristine and, as such, are useful barometers of environmental change

The mangroves of French Guiana and Brazil cover 55,000 and 1.0 million ha respectively (FAO, 2007). Those occurring along the 1600 km stretch of coastline north of the Amazon mouth are particularly dynamic because they receive vast amounts of sediment from the Amazon River. [10] describe this area as being under the influence of the Amazonian Dispersal System whereby alternate sequences of substantial accretion and erosion occur. Changes in mangroves are therefore associated primarily with these processes, although some human-disturbance is evident. Sediment delivery may also be affected by changes in climate within the Amazon region and also the amount and nature of deforestation activities over time. This low-lying area is vulnerable to sea level rise and also storm and wave damage.

The Southeast Asia region supports approximately 4.9 million ha of mangrove, with these distributed primarily in Indonesia, Malaysia and Myanmar (Table 1). Whilst rates of change have generally been reported as < 1 % for many regions, this translates to significant losses for Indonesia and Malaysia in particular with most associated with land use change (e.g., for mariculture) and extensive logging [2].

Table 1. Area of mangroves, Southeast Asia (FAO, 2007)

Country	Area (ha)	Year[1]	Country	Area (ha)	Year[1]
Brunei Darussalam	18418	1996	Philippines	247,362	2003
Cambodia	72,835	1997	Singapore	500	1990
Indonesia	3,062,300	2003	Thailand	244,085	2000
Malaysia	564,971	2005	Vietnam	157,500	2000
Myanmar	518,646	1999	**TOTAL**	**4,886,617**	

[1]Year for which estimates were current

B. Satellite and ground data

For Australia, Belize and the Amazon-influenced coasts, ALOS PALSAR strip mosaic data (Level 1.0) at a reduced spatial resolution of 50 m were provided by JAXA. Using Gamma SAR processing software [12], these data were calibrated and orthorectified to standard regional coordinate systems. For all areas, orthorectification was undertaken by cross correlating a SAR image simulated from SRTM with ALOS PALSAR data and using ALOS orbital state vectors and ancillary information. However, for the Australian strips, the process was refined through cross-correlation with Landsat panchromatic mosaics largely because of the lack of significant relief in many northern regions. Cross-track correction and mosaicing of the orthorectified strips was undertaken using procedures within Gamma and also developed by the European Commission's Joint Research Centre (JRC). The procedures were developed to ensure a high level of geometric accuracy (geocoding errors were typically less than one pixel and better in northern Australia where the panchromatic data had been used in the orthorectification process; Figure 1). The cross track correction and mosaicing procedures allowed the provision of relatively seamless regional mosaics for most of the study regions and particularly for areas of homogeneous cover (e.g., forested areas in South America; Figure 2). Difficulties in obtaining seamless mosaics for northern Australia were encountered but was not limiting for characterising and mapping mangroves.

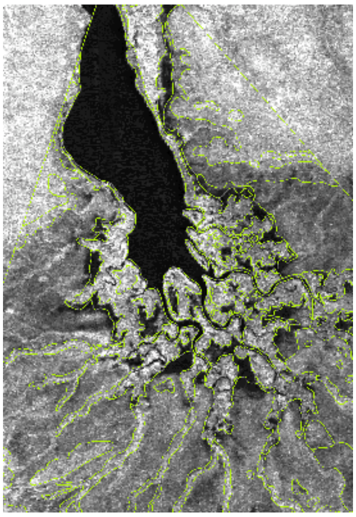

Figure 1. Extent of mangroves overlain onto orthorectified ALOS PALSAR HH mosaic (errors of registration < 50 m)

A number of existing spatial datasets were available to support the detection of change from the ALOS PALSAR. For all regions, the United Nations Environment Program (UNEP) World Conservation Monitoring Centre (WCMC) provided a global polygon dataset generated in collaboration with the International Society for Mangrove Ecosystems (ISME), 1997. A polygon dataset prepared for the forthcoming 2nd edition of the World Atlas of mangroves compiled by UNEP WCMC [13], and funded by ITTO, was also made available. Other datasets were also available for the study regions. For Australia, existing mangrove coverages provided by the Environmental Protection Agency (EPA) Queensland Herbarium (QH) were utilised. These provided a baseline map of mangroves, primarily for Queensland. For Belize, French Guiana and regions of Brazil (e.g., the Bragantina), nationally-generated datasets were available.

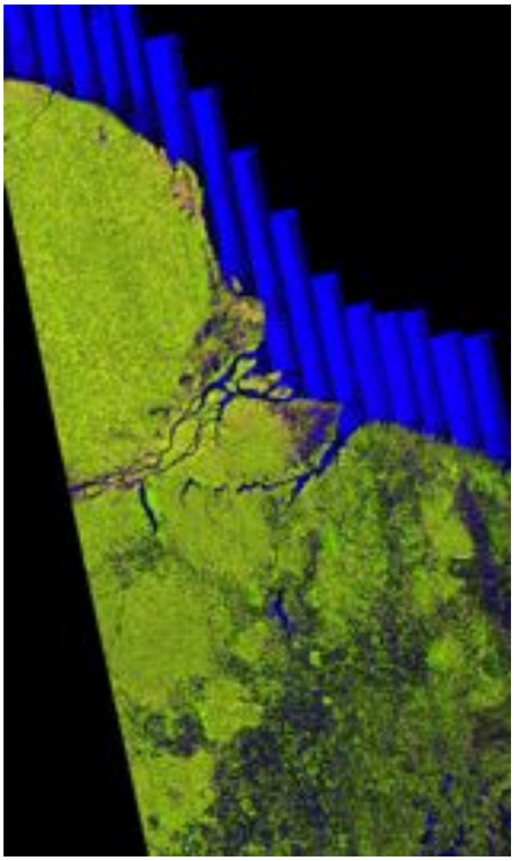

Figure 2. ALOS PALSAR mosaic of the Amazon influenced coast generated using Gamma SAR processing software (L-band HH, HV and HH/HV in RGB).

In establishing baselines of mangrove extent, information from countries in the tropics and subtropical regions was necessarily collated. However, the methods of mapping mangroves in each of the contributory countries varied as did the time-period over which the mapping was valid. Updating of estimates using, for example, Landsat sensor data was not possible because of issues relating to data availability and cloud cover [2], although these baselines could be adjusted to a common mid 1990s date using Japanese Earth Resources Satellite (JERS-1) SAR data (which were available for selected regions).

C. Ancillary datasets

For all regions, SRTM tiles at 90 m spatial resolution were combined to generate regional mosaics. As the SRTM mosaics were used in the orthorectification of the ALOS PALSAR data, errors in spatial registration were minimised. For northern Australia only, Landsat-derived FPC data were obtained from the Queensland Department of Natural Resources and Water (QDRNW).

For sites in northern Australia (Kakadu National Park in the Northern Territory and the Daintree River National Park in Queensland), a range of airborne data, including that acquired by polarimetric multifrequency airborne SAR and hyperspectral sensors, was available to support the interpretation of the ALOS PALSAR and other data. Products derived from these data included canopy height maps (generated from stereo aerial photography and SAR interferometry; [4,13,14] and species maps (classified from hyperspectral data; [15]). For Belize and French Guiana, interferometric and/or polarimetric SAR data were acquired for areas of mangrove along the coast.

D. *Approach to classification*

Based on previous studies using the available airborne datasets [3], the following observations were used to develop rules that could be used subsequently in the classification of mangroves. In particular:

a) With increases in the biomass of most mangrove communities, the radar backscatter was shown to increase to about 100-120 Mg ha^{-1} at which point, saturation of the signal was observed such that no further increases with biomass were observed. However, the exception was mangroves with extensive prop root systems where the L-band HH and HV backscatter was shown to progressively decrease with increases in biomass above 100-120 Mg ha^{-1} (Figure 3).

b) Mangroves with these high levels of biomass generally exceeded 10 – 15 m in height, as estimated from ground data and stereo aerial photographs.

c) Comparison of Digital Elevation Models (DEMs) determined from Intermap X-band SAR and SRTM C-band SAR acquired over mangroves in Belize suggested reliable retrieval of height by the SRTM where mangroves were greater than 10 m in height and the 90 m pixel was largely occupied by the mangrove canopy. Where the height was < ~10 m and the 90 m pixel area was only partially occupied by mangroves, height retrieval was less reliable.

Within all regions, mangroves could be mapped using ALOS PALSAR data alone when bordered by non-vegetated areas. However, when occurring adjacent to forests on the landward margins, discrimination was often difficult (Figure 4). For this reason, the extent of mangroves was defined on the basis of existing mapping which had primarily been generated using optical remote sensing data.

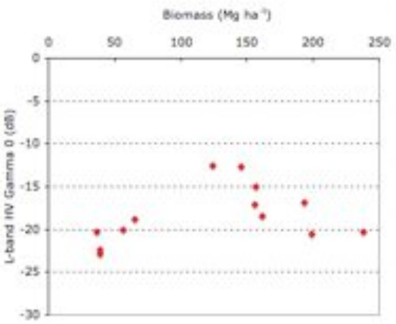

Figure 3. Observed relationships between SAR backscatter and biomass for Australian mangroves. Note the decline in backscatter above 100–120 Mg ha^{-1}

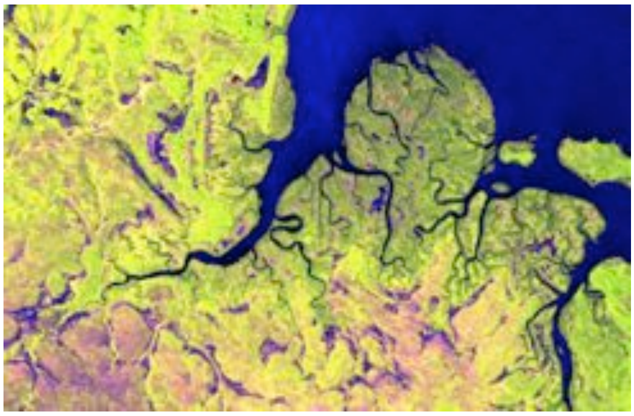

Figure 4. ALOS PALSAR image (L-band HH, HV and the ratio of HH and HV in RGB) illustrating the difficulty in discriminating mangroves from proximal rainforest and other vegetation covers.

Using Definiens Developer software [16], a segmentation of the imagery was undertaken whereby objects (one or several pixels in size) were generated within the pre-defined area of mangrove. A rule-based classification was then applied in two stages to map three forest structural types. First, mangroves <= and > 10 m (as defined using the SRTM-derived H_{CWM}; Equation 1) were separated. Second, and for mangroves > 10 m in height, an L-band HH backscatter <= or > a specified threshold was used to separate higher biomass mangroves (> ~ 100 – 120 Mg ha^{-1}) with prop roots from those without. This latter category was associated with species with pneumatophores typical to the genera *Avicennia*, *Sonneratia* and *Laguncularia* [2]. A refinement to the segmentation was undertaken in Australia where mangroves with a mean and standard deviation of Landsat-derived FPC above specified thresholds were mapped initially with these assumed to support a closed canopy and the same rules outlined above were applied. Below this threshold, mangroves were assumed to be of limited spatial extent and/or fragmented and a separate class was defined, particularly as the height estimates were then considered to be less reliable. An FPC threshold of < 12 % was used to define non- or sparsely vegetated areas.

E. *The detection of change*

For the detection of change, differences between the extent of mangroves mapped within the existing baseline datasets and that observed within 2007 ALOS PALSAR data mosaics was mapped. The change detection procedures were again developed within Definiens Developer software and focused primarily on the loss of mangroves from the existing baseline area and also on expansion of mangroves in the seaward direction. Inland extension of mangroves could be detected where expansion occurred into non- or sparsely vegetated areas but not into areas occupied previously by other forests or previously disturbed (e.g., tree plantations), because of similarities in backscatter at both L-band HH and HV polarisation. For several areas (e.g., French Guiana), regional mosaics of JERS-1 SAR data, acquired between 1992 and 1998) were available and could be used to adjust existing baselines to a common reference year. For Queensland, Landsat-derived Foliage Projected Cover (FPC) data (range 0 to 100 %) were available for 2006. Within these data, mangroves were particularly evident as their closed canopy led to FPC percentages of > 80 %, with lower values associated primarily with low and scattered mangroves. These data were used to confirm the extent of mangroves mapped within the baseline.

IV. Results

A. *Examples of mangrove classifications*

The rule-based classification was applied initially to sites for which a) ground data and/or airborne data and derived products were available or b) extensive tracts of mangrove with distinct zonations occurred. As an example, Figure 5 illustrates the distribution of the three main mangrove categories for Hinchenbrook Island, Queensland, Australia. The majority of tall mangroves with prop roots (primarily *R. stylosa*) are located on the seaward margins.

Figure 5. The distribution of mangroves < 10 m (green), > 10 m without prop roots (olive) and > 10 m with prop roots (red).

B. *Comparison with existing mapping*

Comparisons with existing classifications were undertaken, noting that the majority of these focused on the classification of species type or relative height classes. By contrast, the rule-based classification is primarily of structural classes although these can be associated with a broad species types. As an example, tall (> 10 m) mangroves with prop roots are typically dominated by *Rhizophora* or *Brugeira* species. An existing mangrove classification of species (Figure 6) is compared with the rule-based classification (Figure 7) for a coastal area near Aurukun on the Cape York Peninsula, Queensland, Australia. A general correspondence is observed between areas mapped previously as *R. stylosa* and those mapped as tall mangroves (with prop roots) using the rule-based classification is observed. Some areas dominated by *R. stylosa* are classified as low (< 10 m) mangroves, which is not incorrect but rather illustrates the complementary information these provide.

C. *Regional classifications*

For the study regions, the classification was applied to the areas mapped as mangrove. An example classification applied over Belize is presented in Figure 8, which illustrates the capacity for classifying mangroves at a regional level. Similar classifications were also generated for Australia and are to be applied to the Amazon-influenced coast and Southeast Asia.

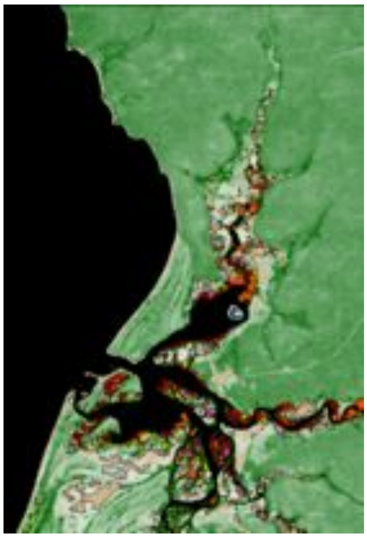

Figure 6. Classification of mangroves by species type [17].

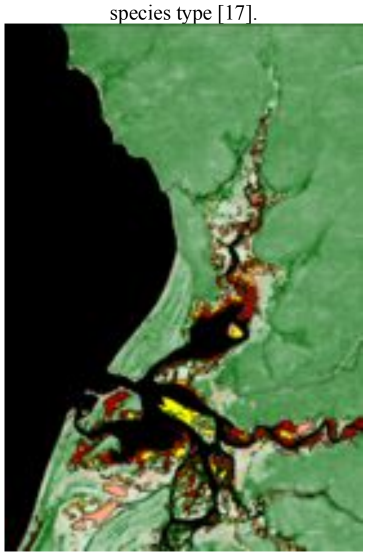

Figure 7 Distribution of mangrove classes mapped using a combination of ALOS PALSAR, SRTM and Landsat-derived FPC data.

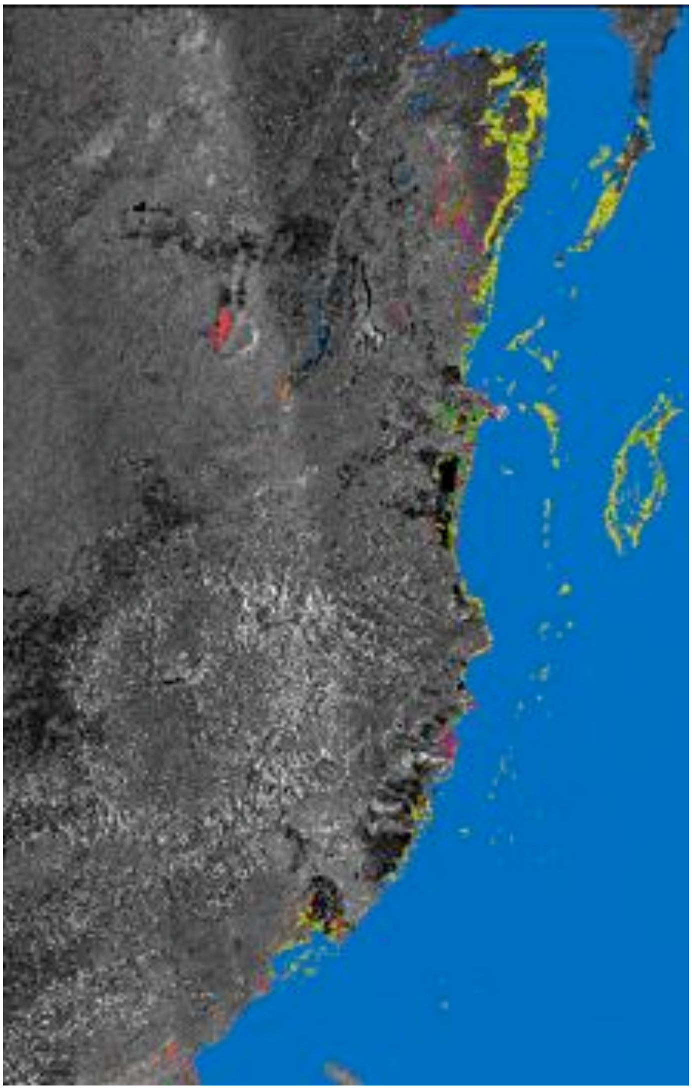

Figure 8. The distribution of mangrove classes, Belize.

Detection of change

For the north and east of Australia, and focusing primarily on Queensland, significant change away from the established baseline was not observed with the exception of the southern Gulf of Carpentaria. Here, seaward expansion of mangroves was noted along the length of the coastline (Figure 9). The cause of such change is likely to be increased sedimentation on the coastal fringe as a result of increases in rainfall and storm events. As an example, Figure 10a and b shows MODIS images of the region prior to and during the extensive flooding in 2009 [18]. The area of mangrove expansion corresponds with that influenced by the flood waters of the Flinders River.

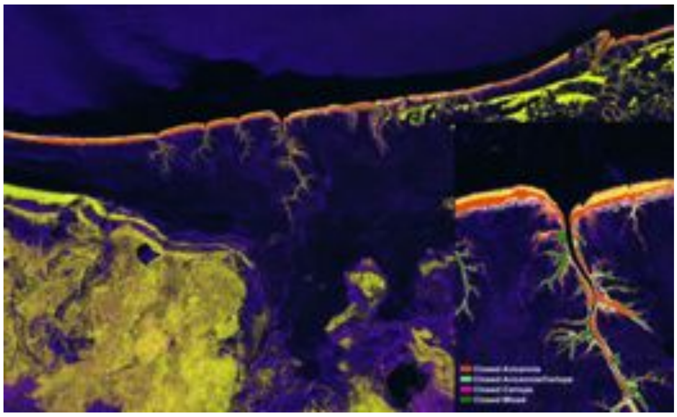

Figure 3. Seaward expansion of mangroves near Burkestown, Gulf of Carpentaria, Queensland, Australia.

Changes in the distribution of mangroves along the Amazon-influenced coast, as documented by [19], continued to be observed using ALOS PALSAR data. The baseline dataset of mangrove extent (Figure 11a), when overlain on the JERS-1 SAR image, revealed discrepancies which were adjusted for within Definiens Developer to establish a new baseline for 1995. When compared against the ALOS PALSAR data acquired in 2007 (Figure 11b), significant losses and gains in the area of mangroves relative to the 1995 baseline were mapped (Figure 11c). More stable areas of mangroves were observed, as were areas of mudflat, which exhibited a noticeably low L-band HH backscatter. These areas represented sites where future colonisation of mangroves might occur.

Within Belize, changes in mangroves from the national baseline were difficult to establish because of apparent discrepancies in definition and the mapped distribution. In particular, significant areas of mangrove savanna in the north of Belize were not mapped previously but were evident within the ALOS PALSAR mosaic (Figure 12).

Within Southeast Asia, comparison of the existing WCMC UNEP maps of mangrove extent with ALOS PALSAR mosaics (Figure 5a) indicated discrepancies in the mapped extent. These were largely associated with:

a) The resolution of the linework and the nature of digitising, which is variable between countries.

b) Registration errors between the two datasets, which led to difficulties in adjusting baselines (e.g., relative to the JERS-1 SAR mosaics) and mapping change.

c) Significant losses of mangrove with the mapped area with these associated primarily with expansion of urban areas, agriculture and fisheries.

d) Differences in the definition of mangroves.

a)

b)

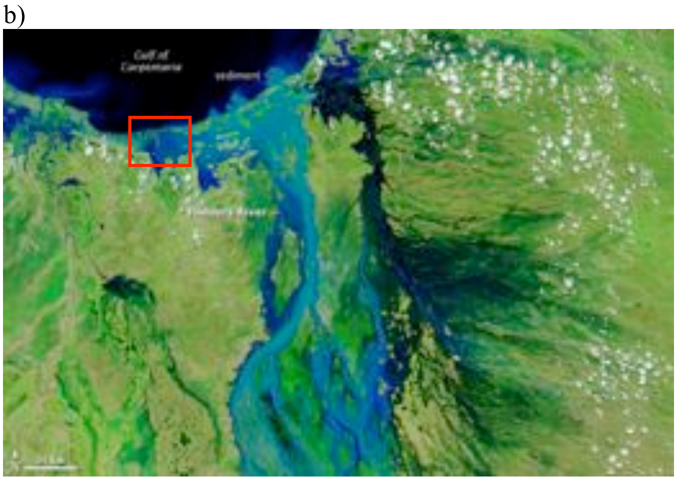

Figure 10. Changes in flooding of the Flinders River as observed from MODIS data (2009). Discharge of sediment into the Gulf of Carpentaria is evident [18]. The area corresponding to Figure 9 is shown in red.

As an example of these issues, Figure 12b illustrates the mapped extent of mangroves overlain onto the ALOS PALSAR data. The capacity for detecting change through comparison of multi-temporal JERS-1 SAR and ALOS PALSAR data is illustrated in Figure 13 [20] where the dynamics of clearance and regeneration of mangroves in Perak State, Malaysia, are evident.

a)

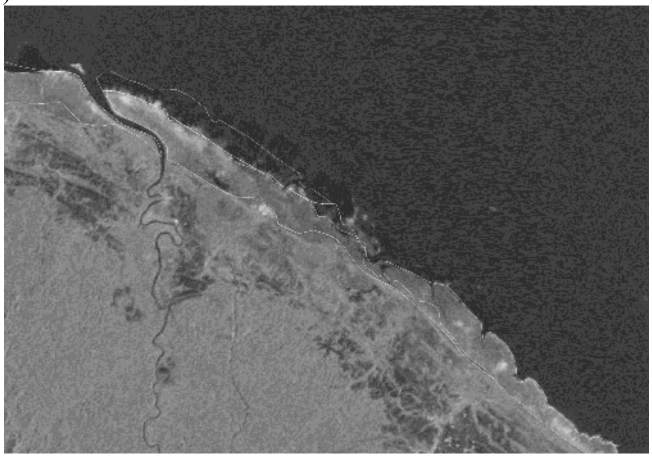

b)

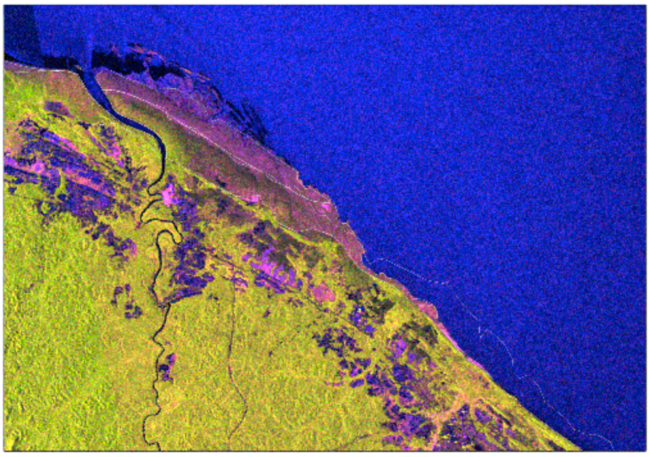

c)

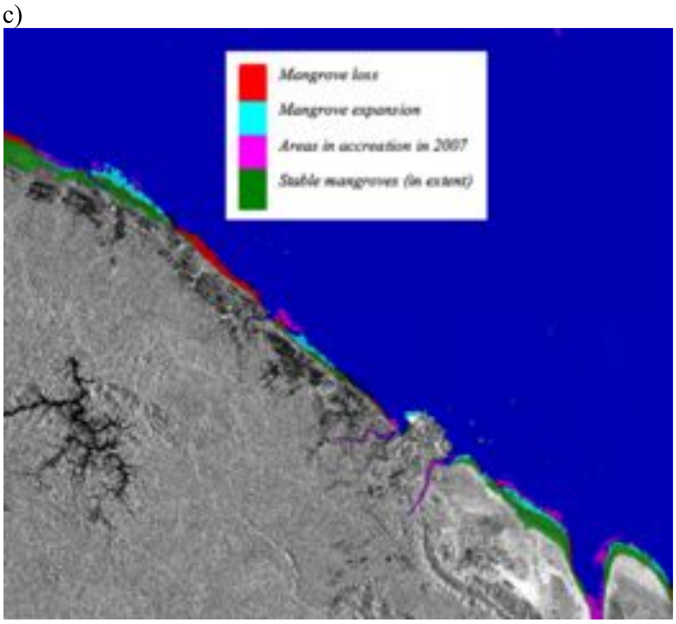

Figure 4. Mangroves along the coast of French Guiana, near Sinnamary as observed using a) JERS-1 SAR and b) ALOS PALSAR data acquired in 1995 and 2007. By comparing these datasets, areas of stable mangrove, mangrove colonisation and loss and mudflats along the French Guiana coast were identified.

Figure 5. ALOS PALSAR mosaic of Belize and baseline map of mangrove extent (white). Differences between mangroves and adjoining forests within the ALOS PALSAR data but discrepancies in the extent of mangroves are evident.

V. DISCUSSION

A. Relevance of mangrove classification

The majority of studies focusing on mangroves have largely only mapped a few classes, with most of these being specific to the area of interest and focusing primarily on species or relative height. The classification approach adopted in this study provides a more consistent approach that utilises globally available datasets (i.e., the ALOS PALSAR and SRTM) and which can be applied within and between regions. Refinements to the classification can also be made using optical data where available.

B. The detection of change

The study has highlighted the capacity of using ALOS PALSAR data in conjunction with existing mapping to detect changes in mangrove extent as a function of both natural and anthropogenically-induced change. However, only changes in a seaward direction and losses of mangroves within the known areas of mangroves were mapped. Inland or up-river extension of mangroves as a consequence of, for example, sea level rise, were not able to be mapped with confidence largely because of similarities in the backscatter of the vegetation covers being replaced. Even so, such changes were evident within some regions (e.g., northern Australia) and are important to identify, particularly given predictions of sea level rise in many regions.

a)

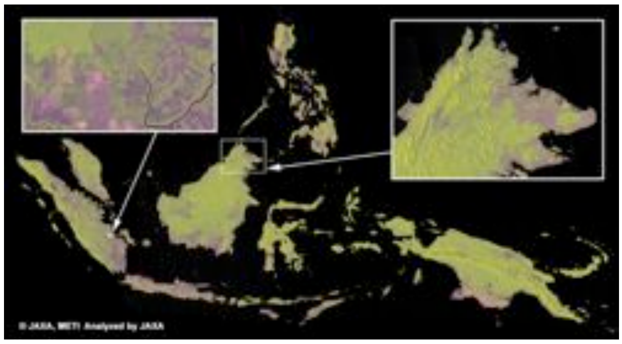

b)

Figure 12. a) JAXA K&C mosaics available for Insular Malaysia and b) UNEP WCMC map of mangroves (white line) overlain onto a subset of the mosaic. Using these data, the establishment of change is difficult because of variations in digitising, registration and the process of change itself.

Whilst the ALOS PALSAR can provide information on changes in mangroves, the cause of change can also be better understood using these and other datasets. For example, within northern Australia, time-series of ALOS ScanSAR data provide unique information on the dynamics of flooding in relation to changing rainfall patterns and runoff, factors which may explain the longer-term changes in dynamics within the Gulf of Carpentaria.

A number of limitations in the detection of change were highlighted which related to the georeferencing, digitising resolution and mangrove definitions. The relative coarse (50 m) spatial resolution of the K&C mosaics also resulted in only major changes in mangroves being identified whereas many may be extensive but associated with only a small change in terms of distance from the pre-occurring mangroves. Longer-time series, focus on areas of change using finer spatial resolution datasets, and better development of consistent retrieval algorithms is therefore required.

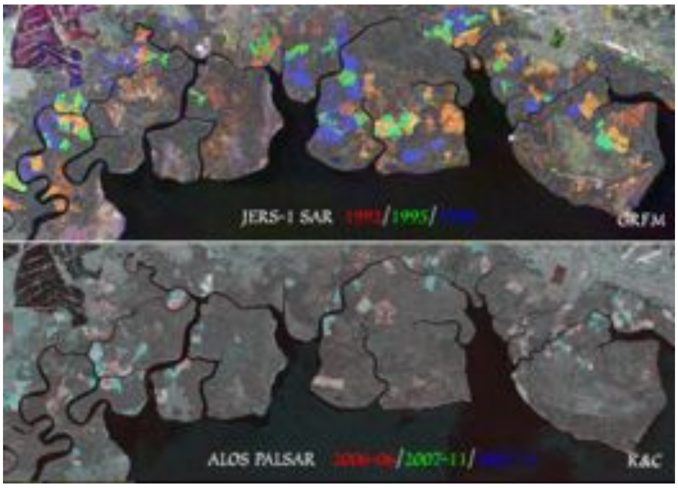

Figure 13. The Matang Mangrove Forest Reserve in Perak, Malaysia [20]. Top: JERS-1 SAR time series from 1992, 1995 and 1998. Areas logged in the period appear in blue and green, while areas of regrowth appear in orange. Bottom. ALOS PALSAR composite from 2006-2007. Red indicates regrowth in areas logged recently prior to the 2006 observation. Blue shows recent crearings. Only the HH channel has been used, as the increased double-bounce scattering from the water surface and remaining tree stumps is the key signal for the detection of logged mangroves.

C. Overview of approach

The primary benefit of using ALOS PALSAR data was the provision of cloud-free observations for entire regions over a relative short (1 - 4 month) time period during any annual cycle. The consistent provision of data over consecutive years also provides opportunities for detecting change, as illustrated in Figure 13. The use of multi-temporal ALOS PALSAR data is advocated as errors associated with classification of other remote sensing data or digitising are largely overcome. The primary objective should therefore be to establish a consistent baseline dataset for a single year (e.g., 2007/2008) against which change can be assessed.

The use of the SRTM data is adequate for retrieving the height (within certain error bounds) of extensive areas of relatively closed-canopy mangroves, the 90 m spatial resolution does limit retrieval. Therefore, the integration of finer spatial resolution DEMs (e.g., 30 m SRTM data or 10 m NextMap Intermap is advocated). The reliability and consistency of height retrieval across regions and for a range of mangrove structural types therefore needs to be quantified in order to give confidence in the approach.

Whilst maps have been generated for all or part of the study regions, the validation of these remains a challenge, particularly in relation to the detection of change, the cause of which vary considerably between regions. This needs to be achieved by strengthening collaboration with existing mapping agencies in the countries involved, at both the national and international level.

VI. CONCLUSIONS, RECOMMENDATIONS AND FUTURE STUDY

Using ALOS PALSAR in conjunction with SRTM data, extensive areas of mangrove can be categorised into a minimum of three broad classes, with these relating to relative biomass and structure. The classification is supported by observations using airborne SAR data at sites in Australia and Belize. A particular advantage of the technique is that the classification is rule-based and can be applied between regions.

The detection of change using ALOS PALSAR data currently requires reference to existing baselines of mangrove extent although it is anticipated that after adjustment to a single year, the ALOS PALSAR can form part of an ongoing mangrove monitoring system. The main benefit of the ALOS is that cloud-free observations of regions can be guaranteed.

Within the study region, both human-induced and natural change has been observed through comparison of ALOS PALSAR data against existing baselines. Key outcomes from the research include:

a) Detection of ongoing change in mangrove colonisation and loss along the Amazon-influenced coast of South America.

b) Significant seaward expansion of mangroves in the Gulf of Carpentaria in northern Australia, which is linked to increased rainfall and extreme flooding within the catchments.

c) Loss of mangrove areas in south-east Asia which have previously been reported as intact.

For several study areas, the existing baseline datasets appear to not reliablely depict the extent of mangroves, either due to issues arising during their generation or because of change occurring in the interim periods. Within Phase 2, continued development of the mangrove mapping and change detection for the study regions will be undertaken together with the development of algorithms that can be applied to other regions when regional mosaics become available.

APPENDUM: WETLANDS CLASSIFICATION, QUEENSLAND

In addition to establishing the potential of ALOS PALSAR for mangrove characterisation and mapping, the role of these data for supporting classification of wetlands in Queensland is being investigated. Across the State, regional mapping of wetlands has been undertaken previously by the Queensland Environmental Protection Agency (EPA) through reference to aerial photography and optical (primarily Landsat but also SPOT and IKONOS) sensor data supported by ground survey. The ALOS PALSAR provides complementary and often new information on wetlands, particularly in relation to inundated (woody) vegetation (Figure 14) and open water. These data are being integrated within a rule-based classification (e.g,. Figure 15; based on Definiens Developer software) with a view to refining or advancing the classification of wetlands occurring from the coastal margins to the inland semi-arid regions of the south-west of the State. These classifications makes use of the Landsat FPC and ALOS PALSAR mosaics generated for the State. These classifications will be supplemented using ScanSAR data acquired by the ALOS during Phase 2.

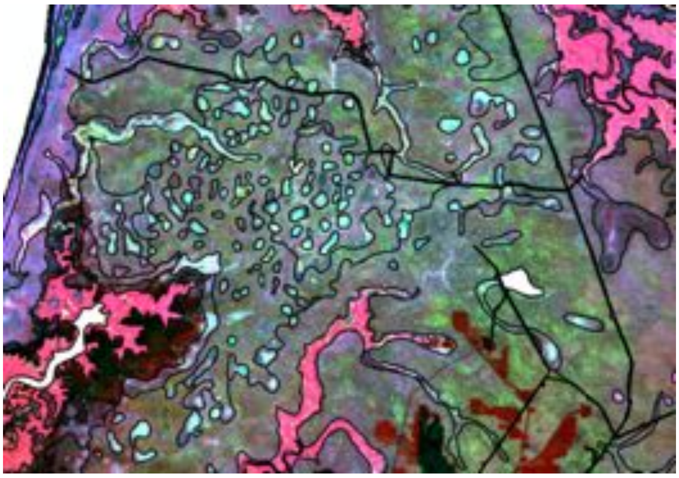

Figure 14. Composite image of Landsat-derived FPC (in red), L-band HH (green) and L-band HV (blue) showing areas of inundated vegetation (primarily paperbark swamps) in the north-west Cape York Bioregion. Queensland Regional Ecosystem mapping is overlain.

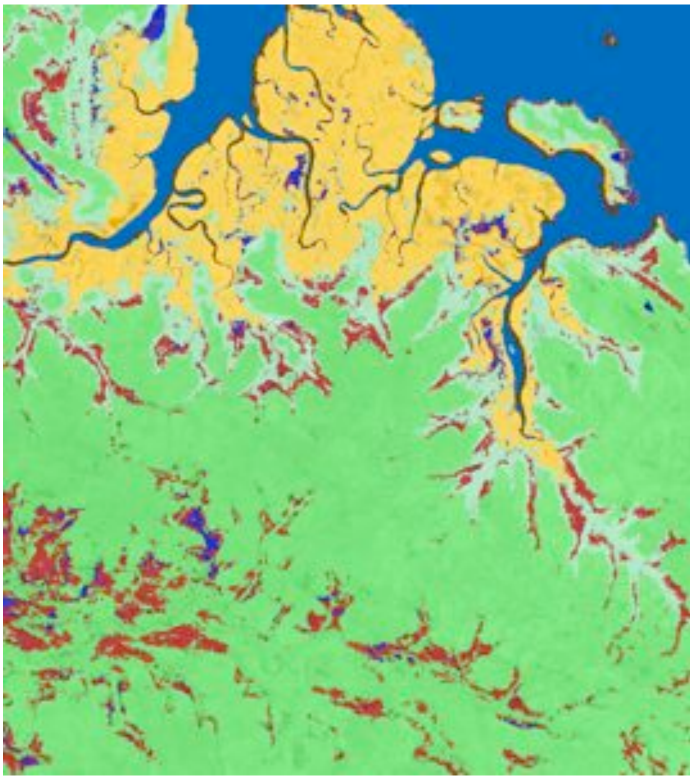

Figure 15. Preliminary classification of estuarine (including mangroves; orange), and palustrine (red) systems and open water (blue), north-east Cape York Bioregion.

ACKNOWLEDGEMENTS AND IMAGE COPYRIGHTS

This work has been undertaken within the framework of the JAXA Kyoto & Carbon Initiative. ALOS PALSAR data have been provided by JAXA EORC. All PALSAR images and derived products illustrated in this paper are copyright to the ALOS K&C © *JAXA/METI*. The authors would also like to thank the UNEP World Conservation Monitoring Centre (WCMC).

REFERENCES

[1] D.M. Alongi, "Present state and future of the world's mangrove forests", *Env. Conser.* 29, 331-349, 2002.

[2] FAO, "*The world's mangroves, 1980-2005*", FAO Forestry Paper 153, A thematic study prepared in the framework of the Global Forest Resources Assessment, 2005, 2007.

[3] R.M. Lucas, A.L. Mitchell, A. Rosenqvist, C. Proisy, A. Melius & C. Ticehurst, "The potential of L-band SAR for quantifying mangrove characteristics and change. Case studies from the tropics and subtropics.*" Aqua. Cons.: Mar. & Fresh. Ecol.*, **17**, 245-264, 2007.

[4] A. Held, C. Ticehurst, L. Lymburner, L. & N. Williams., "High resolution mapping of tropical mangrove ecosystems using hyperspectral and radar remote sensing", *Int. J. Remote Sens.,* **24(13)**, 2739-2759.

[5] R.M. Lucas, N. Cronin, M. Moghaddam, A. Lee, J. Armston, P. Bunting and C. Witte, "Integration of radar and Landsat-derived Foliage Projected Cover for woody regrowth mapping, Queensland, Australia', *Remote Sens. Environ*., vol. 100, pp. 407-425, 2006.

[6] M. Spalding, F. Blasco and C. Field, "*World Mangrove Atlas*", International Society for Mangrove Ecosystems, 178 pp, 1997.

[7] B.E. Schutz, H.J. Zwally, C.A. Shuman, D. Hancock and J.P. DiMarzio, J.P., "Overview of the ICESat mission". *Geophys. Res. Letters*, 32, L21S01, 2007.

[8] T.E. Fatoyinbo, M. Simard, R.A. Allen-Washington and H.H. Shugart, "Landscape Scale Height, Biomass and Carbon Estimation of Mangrove Forests with Shuttle Radar Topography Mission Elevation Data", *J. Geophys. Res. Biogeosciences; Special Issue on Remote Characterization of Vegetation Structure*, G02S06, 2007.

[9] M. Simard, V.H. Rivera-Monroy, J.E. Mancera-Pineda, E. Castaneda-Moya, E. & R.R. Twiley, "A systematic method for 3D mapping of mangrove forests based on Shuttle Radar Topography Mission elevation data, ICEsat/GLAS waveforms and field data: Application to Cienaga Grande de Santa Marta, Colombia", *Remote Sens. Environ*., 112, 2131-2144, 2008.

[10] J. Kellndorfer, W. Walker, L. Pierce, C. Dobson, J.A. Fites, C. Hunsaker, J. Vona and M. Clutter, "Vegetation height estimation from Shuttle Radar Topographic Mission and National Elevation Datasets", *Remote Sens. Environ*., 93, 339-358, 2004.

[11] M.A. Allison and M.T. Lee, "Sediment exchange between Amazon mudbanks and shore-fringing mangroves in French Guiana*", Mar. Geol*., 208, 169-190.

[12] Gamma Remote Sensing AG, *Modular SAR Processor – MSP. Documentation User's Guide* (Version 1.1). Gümligen, Switzerland, 2007.

[13] R.M. Lucas, A. Mitchell, B.E. Donnelly, A.K. Milne, J. Ellison and M. Finlaysson, "Use of Stereo Aerial Photography for Assessing Changes in the Extent and Height of Mangrove Canopies in Tropical Australia". *Wetlands Ecol. Management*, 10, 161-175, 2002

[14] A.L. Mitchell, R.M. Lucas, B.E. Donnelly, B.E., K. Pfizner, K., A.K. Milne and M. Finlayson, "A new map of mangroves for Kakadu National Park, Northern Australia, based on stereo aerial photography". *Wetlands Ecology and Management*, 17, 446-467, 2006.

[15] R.M. Lucas, A. Mitchell and P. Bunting, "Hyperspectral data for assessing carbon dynamics and biodiversity of forests", 47-86 In: (Eds. M. Kalacska and Gerardo-Aturo Sánchez-Azofeifa), Hyperspectral remote sensing of tropical and subtropical forests, CRC Press, 320 pp, 2008.

[16] Definiens, "Definiens Developer 7 Reference Book", Definiens AG Munich, Germany, 195 pp, 2007

[17] Danaher, K.F., Marine vegetation of Cape York Peninsula. Cape York Peninsula Land Use Strategy. Office of the Co-ordinator General of Queensland, Brisbane. Department of the Environment, Sport and

Territories, Canberra and Queensland Department of Primary Industries. 64 pp. plus appendices, 1995.

[18] NASA Earth Observatory, 2009.

[19] F. Fromard, C. Vega and C. Proisy, "Half a century of dynamic coastal change affective mangrove shorelines of French Guiana. A case study based on remote sensing analyses and field surveys", *Mar. Geol*., 208, 265-280, 2004.

[20] A. Rosenqvist, M. Finlayson, J. Lowry and D. Taylor. The potential of long wavelength satellite borne radar to support implementation of the Ramsar Wetlands Convention. *J. of Aqua. Cons., Marine and Freshwater Ecosystems*, 17, 229-244, 2007.

Richard Lucas (lead author). Received the B.Sc. degree in biology and geography (First Class) and the Ph.D. degree in the remote sensing of snow and vegetation using AVHRR and Landsat sensor data from the University of Bristol, Bristol, UK, in 1986 and 1989 respectively. He is currently Professor at Aberystwyth University in Wales, UK, where he is involved primarily in the integration of single data and time-series radar, optical (hyperspectral) and LiDAR data for retrieving the biomass, structure and speces/community composition of ecosystems ranging from subtropical woodlands to tropical forests and mangrovs. His research has and continues to focus on the carbon dynamics of these systems and their response to natural and human-induced change. He has authored or co-authored over 100 journal articles, book chapters and conference papers.

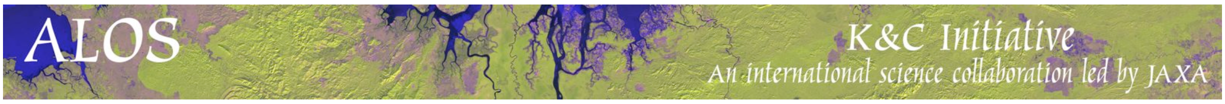

Wetlands Theme

Developing Rice Decision Support Tools

William Salas *et al.*
Applied Geosolutions (U.S.A.)

K&C Science Report – Phase 1
Developing Rice Decision Support Tools

William Salas
Applied Geosolutions, LLC
87 Packers Falls Rd
Durham, New Hampshire, USA 03857
Email: wsalas@agsemail.com
Ph: (603) 659-3363, Fax: (603) 659-0419

Collaborators
Nathan Torbick
Applied Geosolutions, LLC
87 Packers Falls Rd
Durham, New Hampshire, USA 03857

Xiangming Xiao
Department of Botany and Microbiology &
Center for Spatial Analysis
University of Oklahoma
Norman, Oklahoma, USA 73019

Changsheng Li
University of New Hampshire
Complex Systems Research Center
Durham, New Hampshire, USA 03857

Cuizhen Wang
Department of Geography
University of Missouri
Columbia, Missouri, USA 65211

Yuan Zhang
College of Environmental & Resources Sciences
Zhejiang University
Hangzhou 310029, China

Jiaguo Qi
Center for Global Change and Earth Observations
Department of Geography
Michigan State University
East Lansing, Michigan, USA 48824

Abstract*- Primary goals of JAXA's Kyoto and Carbon Initiative are to utilize ALOS PALSAR to enhance agricultural monitoring systems and improve estimates of Greenhouse Gas (GHG) emissions under the "CCC" framework. During Phase 1 of the K&C Initiative, a series of technical objectives were executed to design and apply optimal algorithms to map rice paddies, crop intensity, rice attributes (e.g., biomass), and inundation status. Multi-temporal, multi-mode, and multi-scale (FBS/FBD, AUIG ScanSAR ORT/GRD WB1, K&C GRD Strips) data were used during algorithm development at sites in Poyang Lake, Jiangxi Province and Zhejiang Province, China; Java, Indonesia; and the Sacramento Valley, California, USA. Field-level validation found the fine-beam (FBS, hh, 12.5m) rice paddy- and ScanSAR (hh, 100m) inundation status- PALSAR products to have very high overall accuracies of 95%. These thematic information products derived from PALSAR measurements were used as parameterization into a biogeochemical model to assess GHG emissions and the impacts of different agricultural managements. Biogeochemical simulations showed hydroperiod management to influence methane and GHG emissions by an order of magnitude in terms of metric tons of methane and carbon dioxide equivalence per hectare. The optimal algorithms were applied to regional orthorectified (ORT) ground-range (GRD), HH-mode imagery to create large-area maps of rice in an operational context. These operational PALSAR rice products are being used to understand human environment interactions and improve agricultural monitoring.

***Index Terms*- ALOS PALSAR, K&C Initiative, rice mapping, agriculture, biogeochemical modelling, wetlands**

I. INTRODUCTION

A. Overview

Rice is an important crop globally that influences regional economies and global trade, health and food security, and the Earth system. Rice is the predominant food staple in many regions with more than 400 million tones (milled basis) in production annually with 95% of cultivation in developing regions[1]. Rice land use globally is approximately 13048 million hectares and cultivation utilizes extensive human and natural resources[2]. Due to the important role of rice in the global ecosystem, improved rice monitoring tools are desired by a wide range of decision makers.

In the past decade a number of studies have highlighted the advantages of L-band Synthetic Aperture Radar (SAR) for wetland assessment. The primary advantage of L-band SAR data is its ability to penetrate canopies and its sensitivity to vegetation structure, water content, and biomass independent of weather conditions. The relationship between backscatter and valued ecosystem attributes (i.e., rice biomass) of interest can be modeled over large areas independent of weather making it extremely useful for rice monitoring and resource inventory. L-band rice and wetland applications have included biomass and phenology monitoring, assessing flood dynamics, and differentiating aquatic ecosystems among others.

As part of JAXA's Kyoto and Carbon Initiative (K&CI), Applied Geosolutions is developing a comprehensive Rice Decision Support System to provide end-users information required to make informed decisions. This scientific progress report summarizes progress made by Applied Geosolutions during the JAXA K&CI Phase 1activities during 2006~2008.

II. KYOTO AND CARBON INITIATIVE PHASE 1 FOCI

A. Relevance to the K&C drivers

The overarching themes of the JAXA K&CI are guided by the three **C**'s: **C**onventions, **C**arbon and **C**onservation. Under that guiding framework the rice monitoring system provides information products to address issues related to land use patterns and climate change in the context of improving our understanding of human-environment interactions. During Phase 1 the activities and rice products have contributed to:

- Map rice paddies and land use patterns;
- Assess the impacts of rice management decisions on methane and greenhouse gas emissions;
- Improve LULC datasets for scientists;
- Map and model rice growth and rice attributes;
- Monitor crop cycles.

B. Sites

Phase 1 applications and algorithm development were performed at three primary sites. Site one (fig. 1) is the Poyang Lake region in Jiangxi Province, China (centered ~116.10E, 28.50N) and an area in Zhejiang Province, China. Poyang Lake is the largest freshwater body in China and has significant ecological value with rare migratory waterfowl and extensive wetlands making the Ramsar classified-site an international recognized ecosystem of value. These factors have led to the Poyang Lake region being an international field-site with many integrated studies.

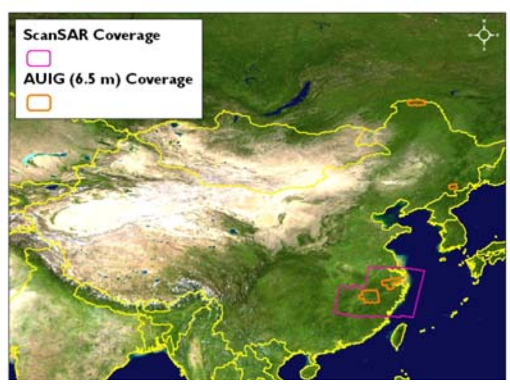

Figure 1. Algorithm development site 1 is the Poyang Lake region in Jiangxi Province, China. Image polygons highlight the development regions where PALSAR algorithms were created and evaluated using FBS and ScanSAR WB1 ORT/GRD data from AUIG.

The Poyang Lake (fig. 2) region has extremely dynamic hydrology with periodic flooding from central Yangtze River basin fluctuations and widespread levee systems altering flows. Extensive and scattered rice paddies are dispersed south of the lake within a patchy landscape of paddies, aquaculture, urban centers, villages, and natural covers. Over the past few decades of economic growth in China, many of the wetland areas are being converted for rice agriculture[3]. The site is subtropical with average annual precipitation and temperature at 170cm and 17degrees C, respectively.

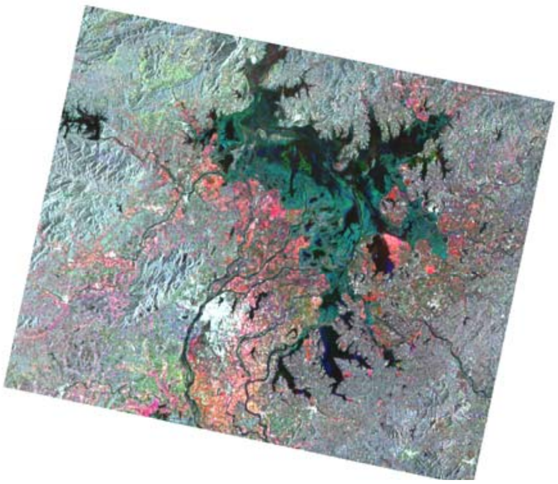

Figure 2. The Poyang Lake region, Jiangxi Province, China was a primary model development site during Phase 1. Multi-temporal AUIG ScanSAR ORT/GRD (Red: DOY241, Green: DOY149, Blue: DOY103) WB1 (HH: 100m). Bright red displays rice paddies and bright white urban land uses.

Site 2. Site two is a large, commercially important rice growing region located in the northern Sacramento Valley, California, USA (centered ~121.825W, 39.20N). Approximately 95% of rice grown in California is grown in this region and it generates nearly half a billion dollars annually to the state's economy. The eight counties in site two that have substantial rice paddy agriculture include: Butte, Colusa, Glenn, Placer, Sacramento, Sutter, Yolo, and Yuba. Other dominant LULC classes in the region include sub/urban, natural vegetation, deciduous fruits and nuts, and field crops. Average temperatures are 45 and 73degrees F in January and July, respectively. Annual precipitation in Sacramento averages 17.2 inches; whereas, annual precipitation in Redding in the northern part of the Sacramento Valley averages 40.9 inches. Intensive irrigation and agricultural management occurs in the area.

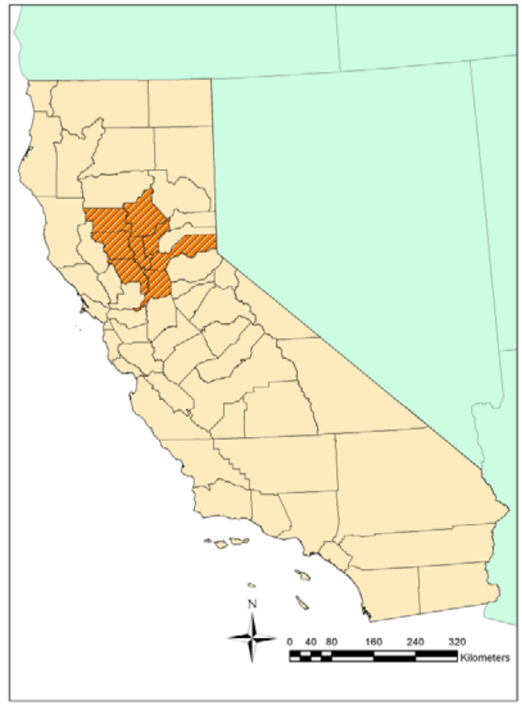

Figure 2. Development and application site 2 was the northern Sacramento Valley, California, USA. PALSAR rice products derived from FBS (HH: 12.5m) and ScanSAR WB1 ORT/GRD (HH: 100m) data were used to parameterize a biogeochemical model to assess rice management decisions and impacts on greenhouse gas emissions.

Site 3. Site three is the island of Java, Indonesia (centered ~110W, 7S). The tropical island is approximately 132,000km^2 and is one of the world's leading rice producers with more than 50 million tones annually and 13 million hectares cultivated. The region has dramatic topographic changes and rice is grown at a variety of altitudes with a range of continuous crop cycles. The majority of rice paddies in Java are under some mechanism of irrigation control with only 10% considered rainfed lowlands. Large urban populations and coastal communities tend to cultivate *indica* subspecies. Paddies range from large-area commercial farms to terraced rice and isolated communities in the highlands creating a challenging rice mapping environments in this tropical climate.

Figure 3. Development site 3 is Java, Indonesia. The algorithms were developing using FBS and WB1 imagery and are being scaled up to the Pan Asian region using K&C strip imagery.

C. Approach

A series of technical benchmarks were evaluated in order to identify optimal algorithms for rice monitoring. Costume python scripts automatically retrieve data from JAXA ftp servers. Pre-processing scripts perform multiple tasks that include: file format conversions (create geotiffs, Digital Number images, backscatter images), re-project (Albers Conic Equal Area for K&C strips and UTM for AUIG imagery), geometric viewing calculations, and file organization (fig.4). The best available Digital Elevation Model was used for each development site. International sites used 90m Shuttle Radar Topography Mission (SRTM)[4] data while USA sites used 30m SRTM data for local incident corrections.

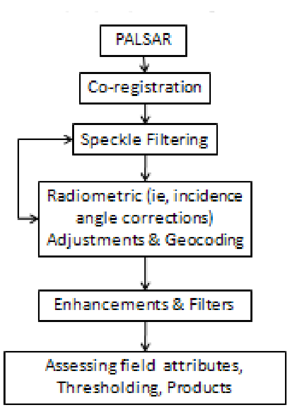

Figure 4. Secondary pre-processing steps apply a linear, multi-temporal speckling filter and perform radiometric enhancements and terrain geocoding adjustments to correct for local incident angles and viewing geometry effects using the best available Digital Elevation Model. Once secondary pre-processing is complete PALSAR imagery is ingested into the product generation stream.

Technical objectives were designed to identify optimal algorithms to monitor rice using a complementing suite of PALSAR resolutions. Initially algorithm development used AUIG fine-beam, hh-mode, 12.5m spatial resolution PALSAR. Once the algorithms were designed they were scaled up and applied to AUIG ScanSAR ORD/GRD WB1 and K&C strip imagery. The primary objectives completed during Phase 1 were to develop algorithms to:

- map rice paddies
- map rice cropping systems
- map inundations status
- map biophysical characteristics

Once secondary pre-processing (fig. 4) was complete the fully pre-processed PALSAR imagery was ingested into the second processing stream. A simple decision-tree framework based on thresholding FBS values was first used to identify rice paddies by capturing the characteristics of flooded areas and dynamic range representing rice phenology and harvest. Next, segmentation procedures are performed to create individual classified polygons or rice paddies. For each rice paddy, informative products were generated based on PALSAR K&C Strip measurements or AUIG ScanSAR ORT/GRD WB1 data. Multi-temporal PALSAR is used to identify crop cycles, flood status, and phenology/biomass changes for each rice paddy. Empirical rice growth models and various post processing tools are used to refine those products (fig. 5).

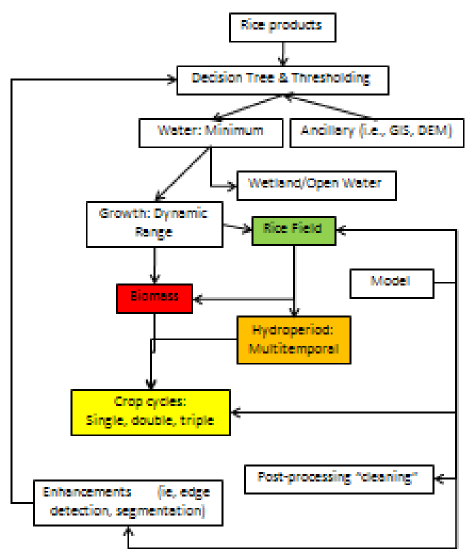

Figure 5.The product generation stream ingests fully pre-processed PALSAR imagery to provide spatially-explicit rice information products including biomass, crop cycles, and hydroperiod.

The generated products for site 2 were used to meet climate change assessment objectives and K&I "**CCC**" overarching goals. The primary objectives under the climate change assessment context during Phase 1 were to:

- Parameterize models with PALSAR rice products
- Simulate impacts of rice managements
- Assess impacts of rice managements on GHG emissions and climate change

D. Satellite data

A range of PALSAR imagery was utilized during Phase 1. FBS and ScanSAR WB1 products (level 1.5) were used at sites 1 and 2. K&C strip ORD/GRD data were utilized at site 3 for operational mapping at continental scales. Spatial resolutions ranged from 6.25m to 100m pixel spacing. Modes included single, dual, and quad pole. Processed levels ranged from JAXA level 1.0-1.5 file formats with automated scripts transforming data into DN and backscatter values (equation 1) and re-projecting to desired coordinate systems. Multiple temporal periods for each site were obtained to capture key rice phenological attributes.

- $\sigma 0 = 10 * \log10(DN2) + CF$ (eq. 1)

Table 1. AUIG PALSAR imagery used during Phase 1. Orbits include both descending and ascending, product levels 1.1 & 1.5, with ranging incidence angles.

Mode	Res (m)	Temporal	Scenes
FBS	6.25	multi (2006-2008)	58
FBD	12.50	multi (2006-2008)	55
WB	100.00	multi (2006-2008)	57

Local incident angle corrections utilized the best available Digital Elevation Model (DEM) for each development site. International sites used 90m Shuttle Radar Topography Mission (SRTM)[4] data while USA sites used 30m SRTM data.

For site 3 operational monitoring K&C strip data was utilized (Table 2). As part of JAXA's K&CI, a PALSAR acquisition strategy has been developed with a goal of having spatially and temporally consistent data at continental scales with adequate revisit frequency and timing to enable the development of continental-scale products. The wetlands science team led the development of the PALSAR acquisition strategy that includes ScanSAR data acquisitions every 46 days for regional mapping and characterization of wetlands and paddy rice in Southeast Asia. Adjacent acquisitions overlap 50%, so effectively there are 2 acquisitions every 46 days continuously from October 2006 to September 2009.

E. Field campaign & reference data

An accuracy assessment was carried out and completed during Phase 1 at Site 2. FBS (HH mode, 12.5m) rice paddy classifications and ScanSAR WB1 (HH mode, 100m) inundation status products were assessed for overall accuracy and misclassification patterns. A series of error matrices were constructed using the field-level data and high resolution color photography as reference. For the FBS HH rice products, orthorectified National Agriculture Imagery Program (NAIP) mosaics were utilized as ground control reference. NAIP data collection occurred near Day of Year (DOY) 215 and 253 which is during the rice growing season at site 2. These true-color, 1-meter, digital photos are available through the United States Department of Agriculture (USDA) Geospatial Data Gateway. Data are compressed in MrSid format with a horizontal accuracy of less than 3 meters. Mosaics are tiled using a 3.75' x 3.75' quarter quads formatted to the UTM projection system using North American Datum 1983 (NAD83). Bounding coordinates covered the entire spatial domain that PALSAR imagery covered. Additional metadata are available via the USDA data gateway.

For the FBS HH rice products a stratified random sampling scheme was utilized to insure statistical sampling rigor following well-established accuracy protocol. The validation scheme identified the maximum classified proportion to generate a specified sample number (475). A stratified random distribution with 250 rice points separated with a minimum distance of 300m was applied within the PALSAR rice product. A second suite of stratified random points were distributed among non-rice classes based on the ancillary LULC data from the Department of Water Resources (DWR) in California. Together these assessment data points provided 475 unique, statistically rigorous validation points. The accuracy points were checked using a variety of techniques. All points were compared against DWR LULC data and verified against the NAIP imagery.

For the ScanSAR inundation status products a near-simultaneous field campaign was performed to assess the accuracy of the flood products at site 2. The overpass date was January 20, 2009. ScanSAR image scene centers were 40.464N x 120.379W and 37.991N x 120.977W. From the binary FBS rice maps two large clusters were chosen as focus areas for the winter flood assessment. The clusters were approximately 50km north of the City of Sacramento and 25km west of the City of Oroville. Ground truth data were collected using a GPS-enabled camera at approximately 1000m equal intervals following the road network. "Drive-by" transects were carried out and points were systematically collected within the two pre-selected clusters. GPS photos were collected perpendicular to the road direction using the stratified approach. A total of 130 points were collected for the second portion of the rice product assessment.

Table 2. PALSAR K&C Strip imagery used during Phase 1.

AGS K&C PALSAR Archive (As of January 1, 2009)	Count	Size (GB)
Total Images	345	125
Total Processed Images (ORT Only)	284	119
By Region (China/S. Asia/Indonesia)	36/198/50	18/93/8
Unprocessed Images (SLT/GRD)	44/17	5/1
Modes Available (WB1/FBD/FBS)	285/52/8	119/5/1

F. Biogeochemical modelling

The process-oriented DeNitrification and DeComposition (DNDC) model[5,6,7] was originally developed to simulate the effects of major farming practices (e.g., crop rotation, tillage, fertilization, manure amendment, irrigation, flooding, weeding, grass cutting and grazing) and climate change (temperature and precipitation) on C and N cycles in various ecosystems. By tracking rice biomass production and decomposition rates, DNDC also simulates long-term soil organic carbon (SOC) dynamics, predicts CH_4 and N_2O emissions by tracking the reaction kinetics of nitrification, denitrification and fermentation across climatic zones, soil types, and management regimes[8]. PALSAR rice products were used as model parameterization for site 2 simulations that were completed during Phase 1.

Further, parameterization used the State Soil Geographic (STATSGO) database, which is a digital soil association map developed by the National Cooperative Soil Survey and distributed by the Natural Resources Conservation Service (formerly Soil Conservation Service) of the U.S. Department of Agriculture. It consists of a broad based inventory of soils and nonsoil areas that occur in a repeatable pattern on the landscape and that can be cartographically shown at the scale mapped. Climate data used DAYMET weather data which is a model that generates daily surfaces of temperature, precipitation, humidity, and radiation over large regions of complex terrain.

III. Results and Summary

Algorithm development has been completed during Phase 1. Figures 4 and 5 illustrates the primary image processing steps and PALSAR products generated from the rice monitoring system. To streamline reporting results are summarized by project focus and region.

A. Assessing impacts of rice managements

1. Mapping rice in the Sacramento Valley, USA

A minimum threshold identifies water within a given pixel (fig 6). Water at this stage can be a flooded rice paddy, a natural water body, or a manmade irrigation feature. A branch in the decision tree then applies a maximum or range threshold based off either empirical data or image statistics. This process results in a classification product delineating rice fields according to the rules and data used in the decision tree (fig. 7). A semi-automated data cleansing process enhances data products based on user defined rules. For example, a spatial analysis process eliminates single, isolated pixels to streamline data products.

Figure 6. Early rice paddy flood season (left) seen as dark color and full rice maturation (right) seen as light purple displayed in R:G:B (HH:HV:Difference) from PALSAR FBS/D. A decision-tree thresholding and segmentation approach identify rice paddies across the landscape using flood- and rice growth-backscatter response.

Table 3. Study area *2* inundation status monitoring Approximately half of paddies (47% or 74,292 hectares) were flooded during **December** and 75% of rice paddies were flooded during at least one winter time period.

Hydroperiod	Area (hectares)	Percent
No Winter Flood	37866	24.4
Dec Flood	**74292**	**47.8**
Mar Flood	590	0.4
Dec & Mar Flood	11176	7.2
Apr Flood	8952	5.8
Dec & Apr Flood	17341	11.2
Mar & Apr Flood	159	0.1
Dec, Mar, Apr Flood	5083	3.3

PALSAR-derived rice maps identified nearly 75,000 hectares of rice paddies undergoing cultivation during the temporal FBS overpasses in 2007. Figure 7 displays rice paddies and associated flood regimes near the Biggs Experimental Agricultural Station in the northern Sacramento Valley, California, USA. ScanSAR WB1 imagery with regional coverage twice every 46 days was used to identify inundation status for each rice paddy. Approximately half of all rice paddies in the Sacramento Valley were flooded during a portion of the month of December. During Phase 1 image dates used were 12/5/2006, 3/7/2007, and 4/17/2007 to characterize a typical winter cycle. Approximately half of paddies (47% or 74,292 hectares) were flooded during December and 75% of rice paddies were flooded during at least one winter time period (table 3, fig 8).

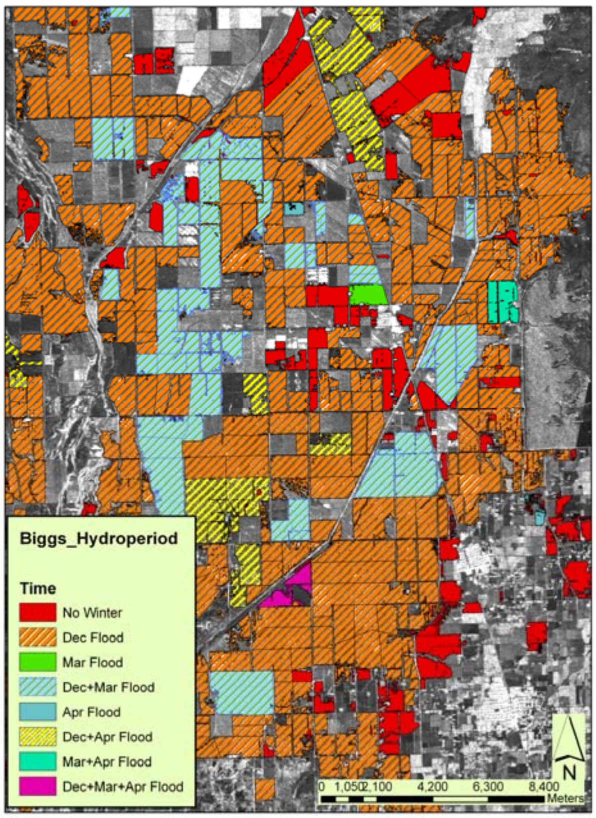

Figure 7. Mapping rice paddies and rice paddy hydroperiod with FBS (HH: 12.5m) and ScanSAR WB1 (HH:100m), respectively. Approximately 75,000 hectares of rice paddies were cultivated in the rice growing season of 2007 in the Sacramento Valley, California, USA. Of these, approximately half (47%) were identified as flooded during December.

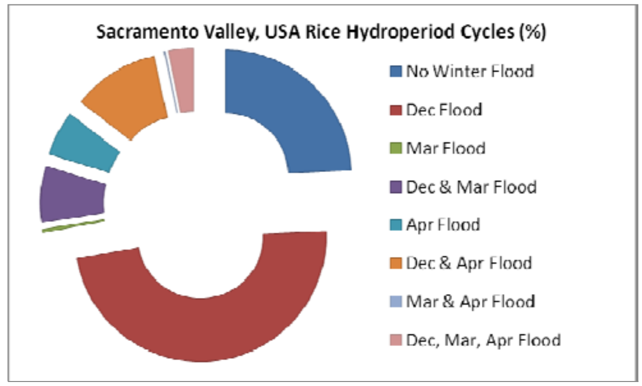

Figure 8. Study area *2* (Sacramento Valley, California, USA) inundation status monitoring with ScanSAR imagery with regional coverage twice every 46 days. Approximately half of paddies (47% or 74,292 hectares) were flooded during December and 75% of rice paddies were flooded during at least one winter time period.

2. *Accuracy of Biggs, USA rice products*

A field-campaign and ancillary reference information found the FBS rice paddy products to possess very high overall accuracy (fig 9). The rice paddy map classification had an overall accuracy of 96% (449 / 469 = 0.9573). Approximately 20 points were interpreted as misclassifications giving an overall omission error of 0.0426. Kappa statistics had a khat value of 0.912609 with a variance and z-score value of 0.00036530 and 47.748, respectively with a p-value significance of <0.00001.

Fieldwork was performed to assess the accuracy of the winter flood products for characterizing inundation status. Two ScanSAR mode scenes were pre-processed and merged to complete coverage over the Sacramento Valley, USA. The overpass date was January 20, 2009. The clusters were approximately 50km north of Sacramento and 25km west of Oroville. Ground truth data was collected using a GPS-camera at approximately equal intervals. Road transects were carried out and points were systematically collected. GPS-photos were collected to perpendicular to the road every using the major routes bisecting the two clusters. A total of 130 points were collected. Interpretation of the ground truth photos resulted in an overall accuracy of 96% (124/129). One point was thrown out due to error.

Figure 9. Two GPS-enabled camera ground truth points at Site 2 showing correct classifications of flooded rice paddies.

The misclassified points were distributed among five categories of errors (fig 10). The majority of these errors were related to temporal challenges. This means that the rules used in the decision tree classifier to define the rice paddies eliminated a potential rice field due to shifts in flood cycles, harvest date, and/or overpass timing. Three errors were related to spatial problems where a point fell just outside a rice polygon or classified rice pixel. Three were related to confusion with dynamic wetland areas.

- Temporal=12
- Spatial=3
- Riparian=3
- Grain=1
- Unknown=1

Figure 10. Ground-truth points from the Biggs, California, USA winter flood assessment found overall accuracy of 95%. ScanSAR imagery was classified into a binary map of water and nonwater pixels to characterize rice paddy inundation. Point 2 illustrates a misclassification caused by slight flooding from accumulated rain fall and saturated soil at the location.

The accurate rice products in this region then served as parameterization for the biogeochemical simulations using the DNDC model. Figure 11 illustrates simulations using the PALSAR-derived parameterizations (ie, inundation status and rice paddy). Results found that flooding regime decisions significantly impacts methane and greenhouse gas emissions.

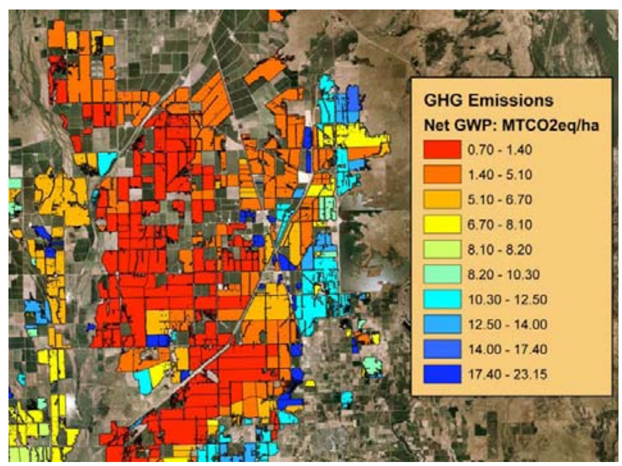

Figure 11. DNDC simulations uses PALSAR-derived rice information. Simulations found that flooding cycle decisions can substantially impact methane and GHG emissions.

B. Mapping paddy rice in China

The PALSAR backscatter coefficient (σ°) images in different dates were stacked into a three-layer composite image (fig. 12). After upland hardwoods were masked out, the non-forest composite image was put in a Support Vector Machine (SVM) algorithm for a five-class thematic map was produced.

Waterbodies were easily identified with clear boundaries. The urban area of Fuyang City was clustered in the upper center of the study area. The class map also demonstrated urbanization and intensified human settlement in lowland plains.

It was shown that rice planting was the major land use type in lowland plains in the study area. Large-area rice cultivation could be easily identified from PALSAR images. However, except for the large flat plains along the Qiantang River in the middle of the study area, paddy rice fields were often small in size and fragmented with other land use surfaces. To demonstrate classification results of these small rice fields, a subset of class map was selected in the north of Xindeng Town, 30km southwest of urban core of Fuyang City. Small rice fields were restricted by local topography and often clustered into narrow and long rice planting area. These areas were smaller and less continuous and resulted in a noisy and scattered pattern in the PALSAR class map. The under-classification of small rice fields was primarily caused by mixed pixels along field edges. These associated borders, however, were assigned rice in survey map because they were associated with rice cropping activities. In the subset, rice planting area detected in the PALSAR-derived map was 4.69×10^6 m^2 while the area in the census map was 5.13×10^6 m^2. Assuming survey map as ground truth, less than 10% of rice area was under-classified.

Two hundred (200) random points in each class were selected and served as validation sites to test the accuracy of the class map. At each validation site, the reference land use type was recorded from survey map. An error matrix of the five classes was built to compare ground-surveyed and image-classified results. The PALSAR class map in this area had an overall accuracy of 80.1% and Kappa statistics of 0.75. Paddy rice reached a user's accuracy of 90% and producer's accuracy of 76%. The relatively large commission error (24%) of rice mapping was primarily a result of misclassifying rice to dryland crop (19 out of 237) or orchard (16 out of 237). It was reasonable because of the similar backscatter amplitudes of these vegetative land use types. A large commission error also occurred where 21 out of 237 paddy rice fields were misclassified as water, a possible effect of open water in flooded rice fields. This may also partially result from land use change between PALSAR image acquisition (2006) and LULC ground survey (2005). For example, some rice fields in 2005 may be abandoned or converted to fish ponds in 2006. Nevertheless, the conditional Kappa value of paddy rice was 0.87, indicating that rice could be mapped at relatively high accuracy with multi-temporal PALSAR images.

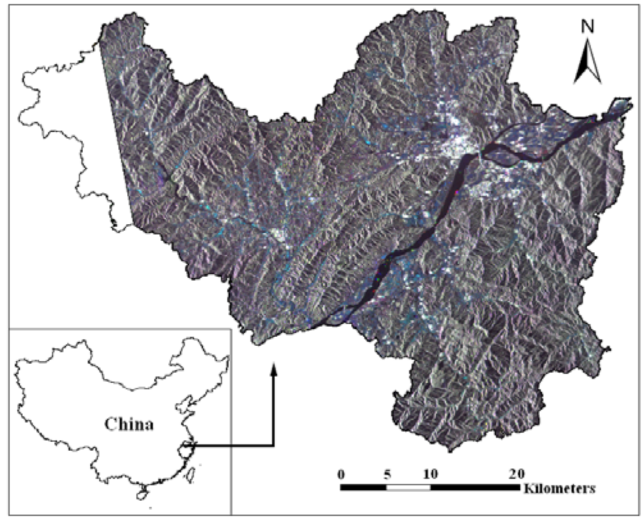

Figure 12. The PALSAR composite image (Jun.18, Aug.3, Sept.18, 2007) in Fuyang City, Zhejiang Province in the southeast China.

With the remarkably high backscatter coefficients, urban structures were classified with the highest user's accuracy of 96.5% and conditional Kappa statistics of 0.95 (fig. 13). Similarly, because of the very low backscatter, water surfaces were also easily classified with a user's accuracy of 80.5%. Some water bodies such as fishing ponds are small and shallow and sometimes covered with water vegetation, which contributed to large omission error (23.7%) of water surfaces. Dryland crops and orchards had the lowest accuracy (conditional Kappa value of 0.63 and 0.58, respectively), because of their backscatter similarity. Since the major objective of this portion of the research was rice mapping, the misclassification of these non-rice land uses was not investigated further.

Comparing with other SAR sensors, PALSAR has a great advantage in rice mapping[9]. Firstly, PALSAR has multi-mode imaging capabilities to acquire SAR imagery at varying resolutions and swaths, which provides flexible applications to fulfill tasks at various scale, extent and accuracies as well as costs. For example, the PALSAR images at FBS mode (6.25m pixel size) applied in this study could extract small and fragmented rice planting area, while the ScanSAR-mode images (100-m pixel size) could be more efficient in regional rice mapping. Among all SAR systems that are currently operating or operated in past years, only Radarsat-1/2 have the same multi-mode feature.

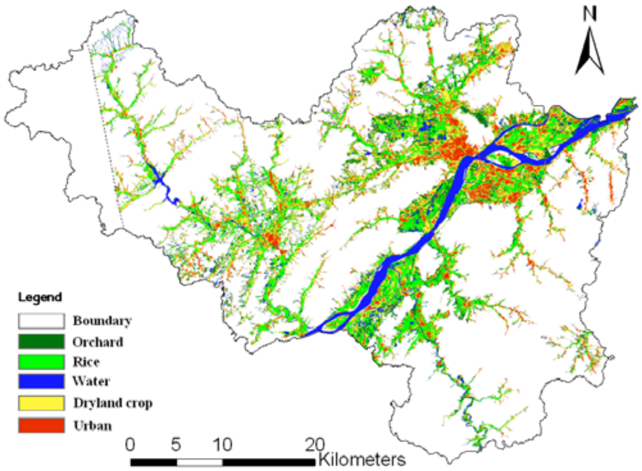

Figure 13. The class map derived from multi-temporal PALSAR images. The upland forest is masked out[9].

Secondly, except for a polarimetric sensor onboard the newly launched Radarsat-2 (in December 2007), PALSAR is the only sensor that could acquire imagery in multiple polarizations (HH, HV, and VV).

Thirdly, as a successor of JERS-1 SAR, PALSAR is the only sensor that operates in relatively low frequency (L-band). L-band signals could penetrate deeper into rice canopy and therefore, may contain more information about total rice biomass than C-band signals of other systems. It has been demonstrated in past studies that different rice biophysical parameters were sensitive to backscatter in different polarizations and frequencies[10]. This information could be applied in radiative transfer models to quantify rice biophysical properties such as leaf area index and fresh biomass, which is closely related to rice production.

C. Modeling rice attributes

This portion of the study examined L-band scattering properties of paddy rice with multitemporal PALSAR imagery, field measurements (fig 14), and a radiative transfer model[11]. Leaf volume scattering and leaf-ground double bounce in L-band were found the major scattering components that increased with plant height and leaf mass amount. In tillering and heading stages, HH backscatter was more sensitive to rice's structural variation while VV backscatter remained almost constant along rice growth cycle (fig. 15).

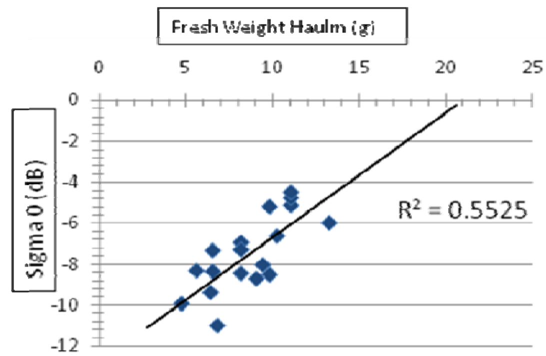

Figure 14. Top) Poyang Lake field site measuring valued rice ecosystem attribute: haulm weight, plant height, water depth, paddy density, and planting patterns. Measurements were used to develop model parameters to forecast growth cycles and PALSAR backscatter responses. Bottom) Fresh haulm weight was quantified and converted into density-adjusted biomass. These measurements were correlated against PALSAR FBS HH 12.5m to identify optimal algorithms and map paddy attributes.

These results show that multi-temporal L-HH backscatter may be more useful in rice biophysical mapping and modeling studies. HV backscatter was affected by multiple interactions between radar signals and rice canopies and cannot be accurately simulated via 1st-order canopy scattering model.

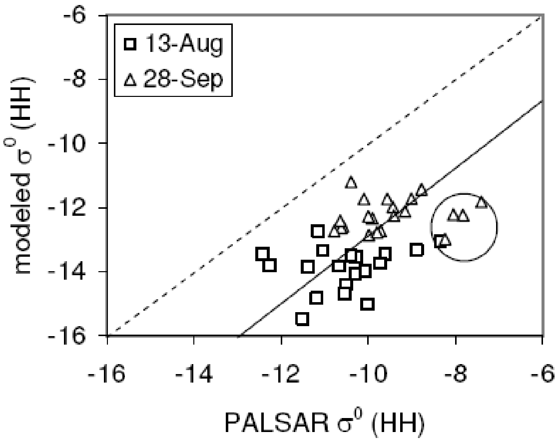

Figure 15. The scatterplot of modeled and PALSAR observed HH backscatter in three rice growth stages[11].

D. Ongoing efforts

During the extension period assessments will be performed on products for Java and Poyang Lake. Due to data delays the Pan Asian maps are now underway as well. Extensive field campaigns with partner projects will provide additional accuracy information.

ACKNOWLEDGEMENTS

This work has been undertaken within the framework of the JAXA Kyoto & Carbon Initiative. ALOS PALSAR data have been provided by JAXA EORC. Additionally support has been provided by JAXA, NASA LCLUC (#NNX08AL16G) and the National Institutes of Health (NIH).

REFERENCES

[1]International Rice Research Institute. World Rice Statistics. Statistical Database. http://irri.org.

[2]Tpriyama, K., Heong, K., Hardy, B. editors, 2005. Rice is life: scientific perspectives for the 21st century. Proceedings of the World Rice Research Conference, Tokyo, Japan. International Rice Research Institute.

[3]Jiang, L., Bergeb, K., Brown, D., Zhao, T., Tian, Q., Qi, S. 2008. Land-cover change and vulnerability to flooding near Poyang Lake, Jiangxi Province, China. *Photogrammetric Engineering & Remote Sensing*, 74, 1-12.

[4]Jarvis A., H.I. Reuter, A. Nelson, E. Guevara. 2008. Hole-filled seamless SRTM data V4, International Centre for Tropical Agriculture (CIAT); http://srtm.csi.cgiar.org.

[5]Li, C., S. Frolking, and T.A. Frolking, 1992a, A model of nitrous oxide evolution from soil driven by rainfall events: 1. Model structure and sensitivity, *Journal of Geophysical Research*, 97:9759-9776.

[6]Li, C., V. Narayanan, and R. Harriss, 1996, Model estimates of nitrous oxide emissions from agricultural lands in the United States, *Global Biogeochemical Cycles* 10:297-306

[7]Li, C., 2000, Modeling trace gas emissions from agricultural ecosystems, *Nutrient Cycling in Agroecosystems* 58:259-276.

[8]Li, C., J Qiu, S. Frolking, X. Xiao, W. Salas, B. Moore III, S. Boles, Y. Huang, and R. Sass, 2002. Reduced methane emissions from large-scale changes in water management in China's rice paddies during 1980-2000, *Geophysical Research Letters*, 29(20), doi:10.1029/2002GL015370, 2002.

[9]Zhang, Y., Wang, C., Wu, J., Qi, J., Salas, W.2009. Mapping Paddy Rice with Multi-temporal ALOS PALSAR Imagery in Southeast China. *International Journal of Remote Sensing*. (accepted/in press).

[10]Le Toan, T., Ribbes, F., Wang, L.F., Nicolas, F., Ding, K.H., Kong, J.A., Fujita, M. and Kurosu, T., 1997, Rice crop mapping and monitoring using ERS-1 data based on experiment and modeling results. *IEEE Transactions on Geoscience and Remote Sensing*, **35**, 41-56.

[11]Wang, C., Wu, J., Zhang, Y., Pan, G., Qi, J., Salas, W. 2009. Characterizing L-band scattering of paddy rice in southeast China with radiative transfer model and multi-temporal ALOS/PALSAR imagery. *IEEE Transactions on Geoscience and Remote Sensing.* (accepted/in press).

JAXA K&CI PI.

William A. Salas is President and Chief Scientist of Applied Geosolutions, LLC in New Hampshire, USA. Dr. Salas has degrees in mathematics, forestry, and natural resources from the Universities of Vermont and New Hampshire, respectively. He formed AGS in the year 2000 to promote, support and provide scientifically sound cutting-edge geo-spatial technologies, biogeochemical modeling applications, and integrated spatial information services. AGS works with private companies, universities, governments, NGOs, and federal agencies.

Collaborators.

Nathan Torbick is a Research Scientist at Applied Geosolutions In New Hampshire, USA. Dr. Torbick joined AGS after completely his graduate work at the Center for Global Change and Earth Observation at Michigan State University. His research foci are human-environment interactions, aquatic ecosystem assessment, and geospatial technologies.

Xiangming Xiao earned a Bachelor's degree in Biology from Xiamen University, China in 1982, and a Master's degree in Plant Ecology from Institute of Botany, Chinese Academy of Science and University of Science and Technology, China in 1987, and a UNEP/UNESCO's Diploma of Environmental Management and Protection from University of Technology, Dresden, Germany in 1988, and a Ph.D degree in Ecosystem Science from Colorado State University in 1994. Dr. Xiao recently began a new position at the University of Oklahoma after working at the Complex Systems Research Center at the University of New Hampshire. His research interests span a wide range of biological science, geo-science and health science, including climate change, land use and land cover change, global carbon cycle, remote sensing, and epidemiology and ecology of infectious diseases.

Changsheng Li received his Bachelor's degree in Geochemistry from University of Science and Technology of China in 1964, Master's degree in Environmental Chemistry from Chinese Academy of Sciences in 1981, and Ph.D. degree in Biogeochemistry from Chinese Academy of Sciences and University of Wisconsin in 1985. He has been devoted to biogeochemical and environmental studies since. In 1992 he moved to the University of New Hampshire where he is now Research Professor in the Complex Systems Research Center within the Institute for the Study of Earth, Oceans, and Space. His academic interest is to explore the theories and methodologies which can be used for revealing relationship between humankind and their environment. Dr. Li has been focusing his study on biogeochemical cycling of chemical elements, especially its numerical expression in time and space.

Chuizhen Wang is an Assistant Professor at the University of Missouri in the Department of Geography. Chuizhen joined UM after completing her PhD at Michigan State. Dr. Wang's primary research areas are bio-environmental remote sensing, GIS and spatial analysis. Particular interests are in biodiversity, biophysical retrieval, ecosystem and environmental mapping. Her past research experience includes Land Use/Land Cover mapping, canopy radiative transfer modeling, and quantitative biophysical estimation with optical and microwave remotely sensed data.

Zhang Yuan received the B.S. degree from Liaoning Normal University, China, in 1998, and the M.A. degrees in Dept. of Forestry, Sheyang Agricultural University, China, in 2003. He is currently a Ph.D candidate in the Institute of Agricultural Remote Sensing and Information Technology Applications, Zhejiang University, China. His research interests are in biophysical and environmental remote sensing and ecosystem simulation.

Jiaguo Qi is the Director of the Center for Global Change and Earth Observation at Michigan State University. His research is focused on using Earth observations for understanding the coupling of natural and human systems and global change research. He uses a variety of geospatial techniques to better understand the responses/feedbacks of the two coupled processes.

Wetlands Theme

Global Lake Census

Kevin Telmer *et al.*
University of Victoria (Canada)

K&C Science Report – Phase 1
Global Lake Census

Kevin Telmer[1] and Maycira Costa[2] and Jamie MacGregor[1]
1.) School of Earth and Ocean Sciences, 2.) Department of Geography, University of Victoria, 3800 Finnerty Rd., Victoria, BC Canada V8P 5C2
Email: ktelmer@uvic.ca

Abstract— **Lake size is a strong control on lake function and on how lakes interact with the environment. For example, lake size is strongly related to carbon burial rates in lake sediments. Lake size distribution (how many small, medium, and large lakes, occur per unit area) can be used to extrapolate lake function to landscapes at local, regional, and global scales. Lake size distribution can be parameterized as:**

m = log(number of lakes/unit area) / log(lake size) – b

Where m less than -1 (m < -1) indicates that small lakes occupy greater area than large lakes and vice versa. A digital database describing lake size distribution and lake shape can therefore be used to investigate and estimate lake-landscape interactions at various scales but this database does not currently exist.

Here the capability of high resolution ALOS PALSAR data is examined for mapping lakes across multiple study sites covering over 100,000 km^2 of the Canadian landscape. Classification of lakes versus land was done by expert systems based threshold analysis and also by using derivatives of the frequency histograms of the SAR image digital numbers. The expert system approach produced better accuracy but cannot be applied automatically. Accuracy varied between sample regions and across the lake size ranges, however; overall, the PALSAR lake classification differed from existing hydrographic spatial datasets for total lake area by up to 18%. Comparisons between datasets cannot be perfect because they were not created over the same time period. Due to its short time of collection and singular data source, the ALOS data is superb for capturing current conditions, establishing a baseline, and comparing to future conditions.

Estimates of carbon burial for the sample regions were made based on the lake size distribution determined from the PALSAR classification and on literature estimates of carbon accumulation for various lake sizes under different climatic conditions. Carbon accumulation in lake sediments in the Canadian boreal region alone could account for as much 13.4 Mt of CO_2 equivalent per 100,000 km^2 per year.

Index Terms—**ALOS PALSAR, K&C Initiative, wetlands, carbon, lakes.**

I. Introduction

Carbon accumulation in lake sediments has long been recognized as an important component of the global carbon cycle [1-6]. Of the many parameters which influence carbon accumulation rates, lake size has been identified as a simple predictor of carbon burial rates in lake sediments [3, 5, 7]. A database describing lake size distribution can therefore be used to investigate and estimate lake-landscape interactions.

Accurate and reliable lake census data is a fundamental first step in extrapolating carbon accumulation rates to regional and global scales. The majority of available hydrographic data is generally limited in both spatial and temporal resolution (e.g. Global Lakes and Wetlands Database [8]). This is because the majority of these datasets do not come from a single data source produced by a single method nor are they acquired from a single time period.

In Canada the CanVec hydrographic dataset produced by Natural Resources Canada (NRCan) constitutes one of the most comprehensive and freely available hydrographic datasets [9]. The CanVec dataset demonstrates very good spatial accuracy. However, its temporal resolution is limited; especially in remote areas and can span up to 50 years or more. This can limit direct application to studies examining regions undergoing potential hydrological change over short time scales such as the northern boreal forest of Canada.

The Phased Array L-band Synthetic Aperture Radar (PALSAR) sensor on board the Advanced Land Observing Satellite (ALOS) launched in early 2006 by the Japanese Aerospace Exploration Agency (JAXA) has provided a unique opportunity to construct a global lake database. PALSAR's all weather night and day acquisition capability affords continuous global coverage and allows for the construction a database from a single source over a single period of time (24 months). One of the inherent benefits of L-band radar systems such PALSAR is its capacity to detect water bodies. L-band radar can penetrate through sparse vegetation while also being less sensitive to water surface roughness. This makes it ideal for differentiating water from land under variable conditions.

A. Relevance to the K&C drivers

The objective of the global lake census is to establish a baseline map of lake size distribution and how this is controlled at regional and global levels. An up to date and temporally constrained lake database paired with existing and new carbon accumulation rates will allow for an improved first order estimate of the role lake sediments play in the storage of carbon.

Under the framework of JAXA's K&C Initiative and the three C's: Conventions, Carbon and Conservation- the global lake census will help to determine the role lakes play in the terrestrial carbon cycle now, and with changes that may occur under future climate conditions. This information in turn can be used to guide policy on carbon trading, wetland conservation, and creating and enforcing conventions needed to maximize carbon uptake from the atmosphere as well as ecological protection in general.

B. Work approach

The methodological approach in developing the global lakes census has progressed in a series of steps:

i.) Lake classification

We utilized high resolution PALSAR FBS and FBD 12.5 meter images to produce a binary classification of lakes and land for 9 pilot regions across Canada (Fig. 1). PALSAR images were filtered and reduced to 8-bit to minimize speckle and data depth. A single threshold digital number (DN) was selected for each region as cut-off value between lakes and land. This simple classification method has been applied successfully in previous studies identifying water bodies in RADAR imagery [7, 10]. The main advantage of the threshold approach over more complex classification methods is computational efficiency. This is especially important for very large datasets such as the one proposed here.

Threshold selection was first attempted quantitatively based on a first derivatives approach. This method relies on the bimodal nature of the RADAR imagery where the first mode represents water bodies and the second mode represents land (Fig. 2). The first derivative quickly identifies the inflection point between the two modes and provides a logical starting point for a threshold DN. Histograms from each pilot site demonstrated the same characteristic bimodal shape. However, each differed in how quickly and at what DN value the transition between the lakes and land occurred. This made it difficult to rely solely on first derivatives to produce an accurate classification. Therefore an expert based tuning approach was employed to improve classification accuracy. This involved increasing or decreasing the DN around the first derivative inflection point until better classification accuracy was achieved.

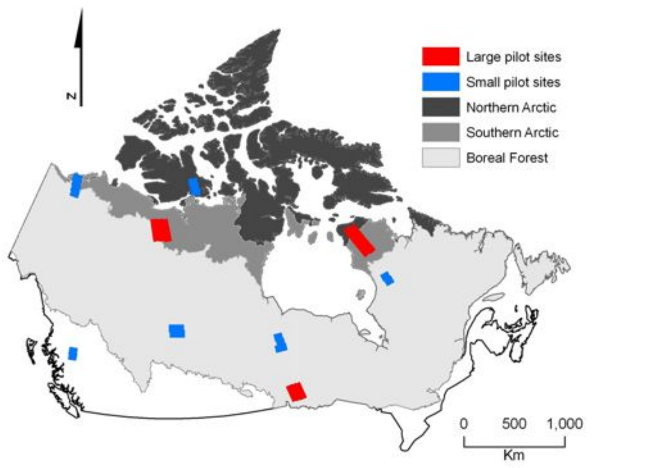

Figure 1. Pilot regions used for the methodological development of lake classification.. Each pilot region consisted of 12.5 m PALSAR FBS FBD imagery. Corresponding AVNIR-2, SPOT and Landsat imagery was also used when available to aid in accuracy assessment. All 9 regions were used in the development of the lake classification and in the extrapolation of carbon accumulation rates to regional scales. The three large pilot sites (shown in red) were used as test sites for the derived lake size distribution thematic map.

ii.) Accuracy assessment

Direct field campaigns have not been feasable up to this point becasue of the remote location and large geographic distance between study sites. Therefore classification accuracy assessment was limited to compairisons to existing hydrographic data (CanVec) and ancilliray satellite imagery from the Advanced Visible and Near-Infrared Radiometer (AVNIR-2) on board the ALOS platform, as well as SPOT 4/5 (Satellite Pour l'Observation de la Terre) and Landsat 7 imagery. When utilizing anicilliary data, the ALOS AVNIR-2 imagery provided the most accurate assessment becasue of the near simultaneous aquistion time to that of the PALSAR images. Lake area and count from both the PALSAR lake classification and the CanVec lake polygons where divided across 5 size classes ranging from less than 0.01 km^2 to over 100 km^2 allowing for direct comparison.

iii.) Carbon accumulation estimates

A preliminary assessment of carbon accumulation for Canadian lake sediments was calculated based on the PALSAR lake classification data and published lake sediment carbon accumulation rates. We used lake sediment accumulation rates from 140 Finnish boreal lakes covering a wide range of landscapes and lake sizes [5]. Finnish accumulation rates were selected because they were based on a large lake census and vary as a function of lake size. This allowed for easy application across our PALSAR lake size distributions, simplifying the process. A large part of Canada has similar physiographic conditions to boreal Finland; however there are many regions which are relatively dissimilar. In order to apply the Finnish data to these areas, a scale factor was introduced in an attempt to make the carbon accumulation rates more representative of the Canadian landscape. Here we based the scale factor on a simplified version of the terrestrial ecozones of Canada [11] to produce three regions: the boreal forest, the southern arctic and the northern arctic (Fig. 1). Combined, these regions account for almost 86% of the Canadian landmass and represent some of the major shifts in the physiographic conditions. The remainder of Canada represents some challenging and diverse landscape complexities; therefore they have been left out of the analysis for now. Future regional carbon estimates on the Canada-wide 50 meter mosaic will include other carbon accumulation rate estimates from the literature, as they come in, along with new field based measurements.

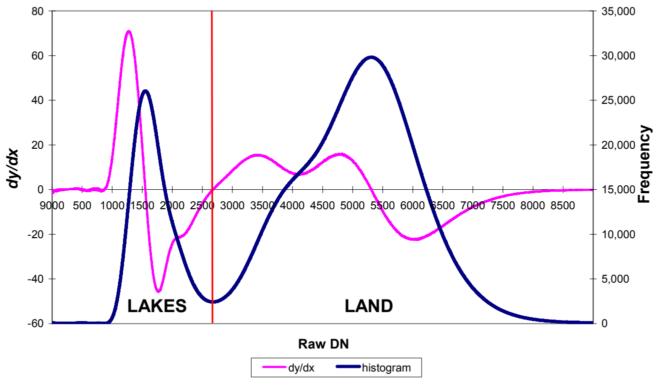

Figure 2. An example of the first derivative approach to threshold value selection. The inflection point between the first mode (water) and the second mode (land) is where the first derivative is equal to zero shown by the red vertical line. This provides a starting threshold for a classification and can be tuned according to an initial accuracy assessment.

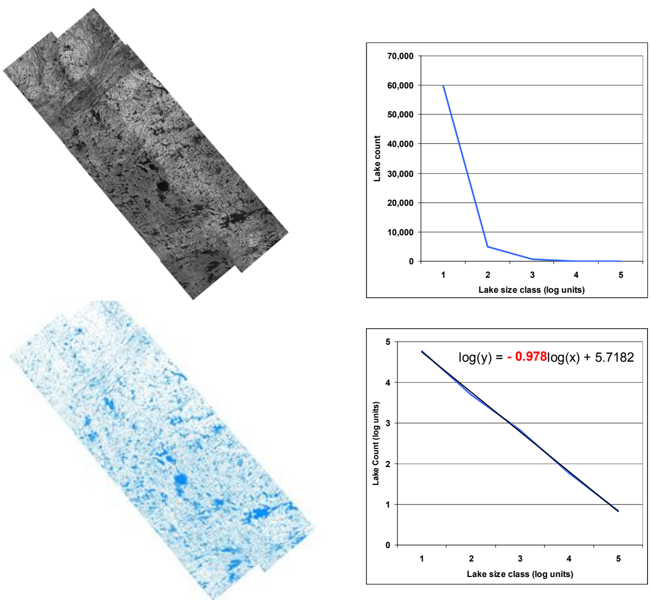

Figure 3 **Left:** The PALSAR mosaic from Northern Quebec, Ungava Peninsula and the corresponding threshold based lake classification. **Right:** Frequency of lakes within each size class (class **1:** < 0.1 km^2, class **2**: 0.1 – 1.0 km^2, class **3:** 1.0 – 10 km^2, class **4:** 10 – 100 km^2, class **5:** > 100 km^2). Lake count increases tenfold with decreasing lake size class. When frequency is log scaled the data becomes linear and can be fitted with linear best fit line where slope (shown in red) is representative of lake size distribution [12]. ALOS K&C © *JAXA/METI.*

iv.) Derived thematic product

The PALSAR lake classification describes the lake size distribution for each of the pilot areas. For the three large pilot areas (Fig. 1), size distribution was parameterized and thematically mapped to visually show how it changes across the landscape. The density of lakes generally increases from large lakes to small lakes. This increase is roughly tenfold when going from one lake size class to the next smaller class at a log scale [12, 13]. This relationship can therefore be defined by a simple log linear regression (1) (Fig. 3).

$$\mathbf{log(lake\ density) = mlog(lake\ size) + b} \qquad (1)$$

The slope (m) of the line will vary as a function of the underlying lake size distribution. A more negative slope is indicative of proportionally more small lakes whereas a more positive slope value indicates proportionally more large lakes. This simple relationship can be utilized to thematically express how lake size distribution changes across the landscape.

A grid with 100 km^2 cells was overlain on top of the lake classification for the three large pilot sites. For each grid cell the underlying lake size distribution was log transformed and fitted with the log linear regression line (1). The resulting slope values were then assigned to the corresponding grid cell (Fig.4). A cell size of 100 km^2 was selected for evaluation purposes. A final grid cell size for the 50m mosaic is under evaluation.

C. Satellite and ground data

i.) ALOS data

Analysis thus far has focused on 12.5 meter (level 1.5 processing) Fine Beam Dual (FBD) and Fine Beam Single (FBS) polarization PALSAR imagery obtained from ALOS User Interface Gateway (AUIG). All images were acquired during the summer months- between June and August- of 2007 and 2008 to minimize ice cover interference in the far north. Corresponding AVNIR-2 images (processing level 1-B2) where also obtained from AUIG for the same time period when available.

ii.) Other data

The CanVec hydrographic dataset is produced by NRCan and was obtained through the Geogratis web portal (www.geogratis.ca). The CanVec dataset is relatively new and free cartographic reference product, although the source data spans more than 50 years. CanVec aims to accurately represent topographic entities across the Canadian landmass with thematic information grouped into 11 distribution themes- including hydrographic data. Data originates from the best available sources; mainly the National Topographic Data Base (NTDB), the Geobase initiative, and recent updates from Landsat 7 imagery.

The SPOT 4/5 and Landsat 7 imagery were obtained from the Geobase web portal (www.geobase.ca) for the pilot

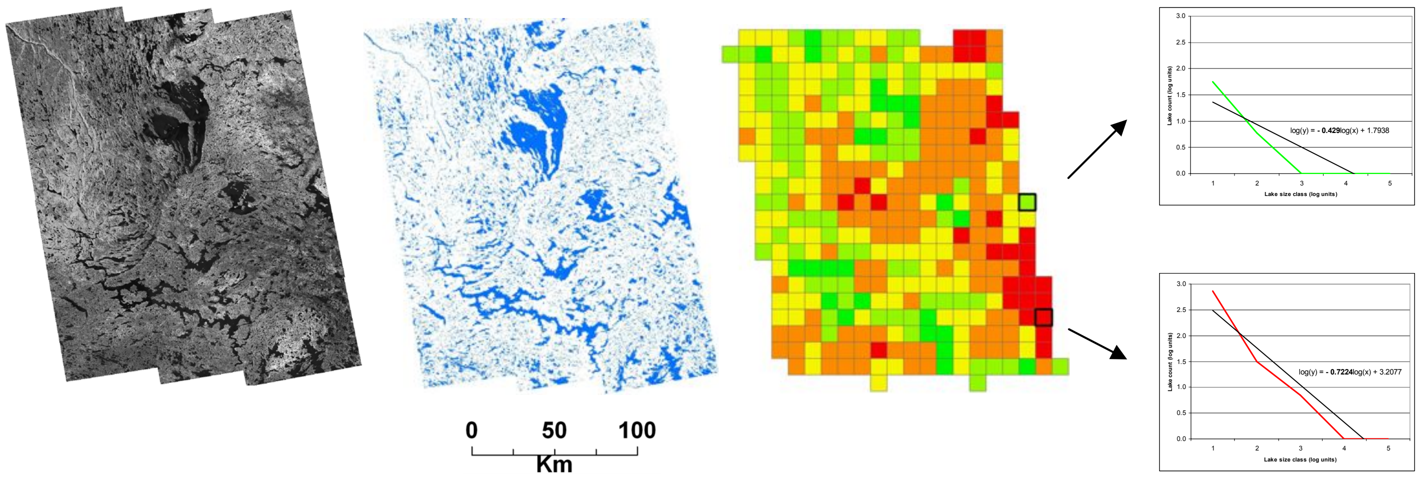

Figure 4. The development of a thematic lake size distribution map. A PALSAR image is first classified for lakes and subsequently grided to a specific cell size (in this case 100 km^2). For each grid cell the underlying lake size distribution was log transformed and fitted with the log-log linear regression line (1). The resulting slope values are then assigned to the corresponding grid cell as a raster. ALOS K&C © JAXA/METI.

Table 1. Summary lake count estimates for PALSAR lake polygons compared to CanVec lake polygons across six size classes for the 6 small pilot areas.

Pilot area	Lake Area (km^2)	< 0.1	0.1 - 1.0	1.0 - 10	10 - 100	100 <	Total
Alberta	PALSAR	20.42	58.96	118.41	151.82	205.52	555.13
	CanVec	23.23	57.51	124.98	173.20	206.54	585.46
	Difference	-2.82	1.45	-6.57	-21.38	-1.02	-30.34
	(%)	**-12.12**	**2.52**	**-5.25**	**-12.35**	**-0.49**	**-5.18**
British Columbia	PALSAR	20.97	47.83	53.17	24.20	215.03	361.20
	CanVec	11.92	36.91	63.52	27.39	228.22	367.95
	Difference	9.06	10.92	-10.36	-3.18	-13.19	-6.75
	(%)	**76.01**	**29.60**	**-16.31**	**-11.62**	**-5.78**	**-1.83**
Manitoba	PALSAR	55.44	276.06	326.00	374.69	945.66	1977.86
	CanVec	58.70	288.17	300.76	445.31	997.38	2090.32
	Difference	-3.26	-12.11	25.24	-70.62	-51.72	-112.47
	(%)	**-5.55**	**-4.20**	**8.39**	**-15.86**	**-5.19**	**-5.38**
McKenzie Delta	PALSAR	228.78	587.29	478.88	243.35	507.03	2045.32
	CanVec	281.43	654.52	543.53	542.11	248.34	2269.93
	Difference	-52.65	-67.23	-64.66	-298.76	258.69	-224.61
	(%)	**-18.71**	**-10.27**	**-11.90**	**-55.11**	**104.17**	**-9.89**
North West Territories	PALSAR	214.08	457.29	655.90	436.50	432.70	2196.47
	CanVec	286.63	571.10	715.54	358.31	574.09	2505.68
	Difference	-72.55	-113.81	-59.64	78.18	-141.39	-309.21
	(%)	**-25.31**	**-19.93**	**-8.33**	**21.82**	**-24.63**	**-12.34**
Victoria Island	PALSAR	76.32	116.20	78.78	138.74	0.00	410.04
	CanVec	113.57	139.63	82.84	164.23	0.00	500.27
	Difference	-37.25	-23.43	-4.06	-25.49	0.00	-90.23
	(%)	**-32.80**	**-16.78**	**-4.90**	**-15.52**	**0.00**	**-18.04**
ELA	PALSAR	92.16	379.71	501.66	600.46	428.94	2002.93
	CanVec	92.34	383.66	526.56	534.68	669.39	2206.62
	Difference	-0.19	-3.94	-24.90	65.78	-240.45	-203.69
	(%)	**-0.20**	**-1.03**	**-4.73**	**12.30**	**-35.92**	**-9.23**

areas. Images cover a time period from 2005 to present for SPOT 4/5 and 1999-2003 for Landsat 7.

II. Results and Summary

i.) Lake classification and Accuracy assessment

The PALSAR lake classification generally underestimated total lake area when compared directly to CanVec hydrographic data (Table 1). Differences in total lake area between CanVec dataset and the PALSAR lake classification ranged from 1.83 to 18.04%. Some of the larger differences within each size class between CanVec and PALSAR can be explained by simple class shifts. For example in the McKenzie Delta the PALSAR classification overestimates the area of lakes in the > 100 km^2 class by 104.17% compared to CanVec. If this difference is shifted into the next lower size class (10 -100 km^2) it accounts for most of this discrepancy. This is because of differences in the way PALSAR and CanVec define lakes. If a lake or water body has very narrow channels, these regions can be lost in PALSAR classification because of resolution limitations. This can result in a single lake being split into two or more lakes resulting in a different size classification. However, it may be that a lake that is split like this is behaving more like two small lakes with respect to carbon accumulation and so a PALSAR classification may be superior for this application. This is under evaluation.

Comparisons between datasets cannot be perfect because they are not time synchronous. The hydrographic data spans up to 50 years whereas the ALOS data comes from one short period of 24 months. This relatively short collection time and single data source give the ALOS product a strong advantage when comparing the current conditions as a baseline to changes in future conditions.

ii.) Carbon accumulation estimates

A summary of preliminary carbon accumulation estimates for Canadian lake sediments is shown below in Table 2. Based on these estimates for every 100,000 km^2 of boreal, south arctic and north arctic a total of 3.65, 2.45 and 0.48 Mt of carbon could be accumulating every year in Canadian lakes. This is equivalent to the CO_2 emissions of over ***4.5 million cars*** per year. Carbon estimates here were restricted to a relatively small area of 100,000 km^2 because of the limited footprint covered by the pilot areas. With improvements to carbon accumulation estimates and a complete lake size distribution based on the 50m PALSAR mosaic these estimates will be refined and extended to represent all of Canada.

Table. 2 PALSAR derived carbon accumulation in Canadian lakes per 100,000 km2 per year

Lake size km^2	Boreal	South Arctic	North Arctic
<0.1	0.15	0.24	0.08
0.1-1	1.07	0.94	0.20
1-10	1.10	0.79	0.10
10-100	0.76	0.28	0.11
>100	0.57	0.20	0.00
Total Carbon in megatonnes (Mt)	3.65	2.45	0.48
Mt CO2 Equivalent	13.39	9.00	1.77
Number of Cars[1]	2,579,000	1,733,000	342,000

1Based on EPA average annual emissions for passenger cars, April 2000. (http://www.epa.gov/oms/consumer/f00013.pdf)

Carbon accumulation rates for each size class are based on Pajunen 2004 [5]

iii.) Derived thematic product

The derived thematic slope maps for the three large pilot areas are shown in Figure 5. Each coloured box represents the lake size distribution of the underlying grid cell. Red grid cells indicate a higher proportion of small lakes to large lakes whereas green grid cells represent areas where there are more large lakes than small lakes. Carbon accumulation in lakes varies as a function of lake size [5]. With a higher density of small lakes, red grid cells will accumulate more carbon than green grid cells. Mapping lake distribution as shown allows for easy visual identification of high lake density regions and should allow for easy extrapolation of carbon accumulation rates to regional scales.

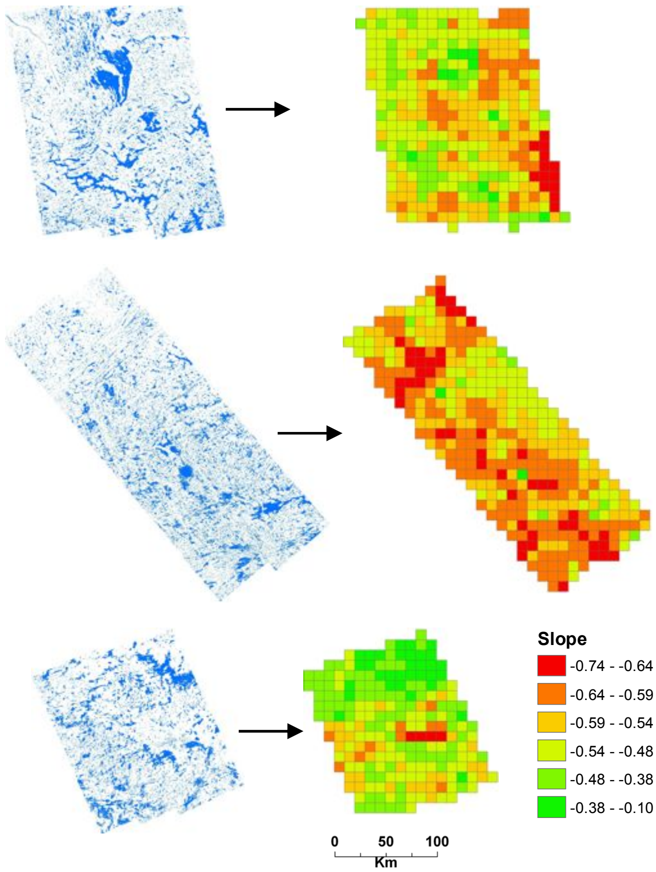

Figure 5. Lake classifications (left) and the derived lake size distribution maps (right) for each of the three large pilot areas (top to bottom): the North West Territories, Northern Quebec on the Ungava Peninsula, and the Experimental lakes in south western Ontario. Each coloured grid cell represents the lake size distribution with red indicating areas where there are more small lakes than large, and green vice versa. The grid cells were classified according to the slope of the regression fit to a classification of lake size as per Meybeck (1995) [13]. ALOS K&C © JAXA/METI.

iv.) Future work

An initial lake classification for all 9 pilot sites has been completed resulting in a digital map describing the number, size, and location of lakes. Accuracy has been validated by comparisons to other existing digital lake databases and corresponding high-resolution satellite imagery. Additionally the derived slope maps have been completed for the three large pilot sites.

Preliminary estimates of carbon accumulation in lakes have also been completed for the pilot study areas. This has provided an initial assessment of lake carbon accumulation which has been scaled up to 100,000 km^2 regions of Canada. However, these preliminary estimates are limited by the small footprint covered by the pilot sites and will improve greatly with the utilization of the Canada wide coverage 50m PALSAR mosaic to be completed during the extension phase.

ACKNOWLEDGEMENTS

This work has been undertaken within the framework of the JAXA Kyoto & Carbon Initiative. ALOS PALSAR data have been provided by JAXA EORC.

REFERENCES

[1] W. E. Dean and E. Gorham, "Magnitude and significance of carbon burial in lakes, reservoirs, and peatlands," *Geology,* vol. 26, pp. 535-538, Jun 1998.

[2] G. Einsele, J. P. Yan, and M. Hinderer, "Atmospheric carbon burial in modern lake basins and its significance for the global carbon budget," *Global and Planetary Change,* vol. 30, pp. 167-195, Oct 2001.

[3] P. Kortelainen, H. Pajunen, M. Rantakari, and M. Saarnisto, "A large carbon pool and small sink in boreal Holocene lake sediments," *Global Change Biology,* vol. 10, pp. 1648-1653, Oct 2004.

[4] P. Mulholland and J. W. Elwood, "The role of lake and reservoir sediments as sinks in the perturbed global carbon cycle," *Tellus,* vol. 34, pp. 490-499, 1982.

[5] H. Pajunen, "Lake sediments as a store of dry matter and carbon," in *Report of Investigation 160 (In Finnish with English Summary)* Espoo: Geological Survey of Finland, 2004, p. 308.

[6] M. M. Squires, D. Mazzucchi, and K. J. Devito, "Carbon burial and infill rates in small Western Boreal lakes: physical factors affecting carbon storage," *Canadian Journal of Fisheries and Aquatic Sciences,* vol. 63, pp. 711-720, Apr 2006.

[7] K. H. Telmer and M. P. F. Costa, "SAR-based estimates of the size distribution of lakes in Brazil and Canada: a tool for investigating carbon in lakes," *Aquatic Conservation-Marine and Freshwater Ecosystems,* vol. 17, pp. 289-304, May 2007.

[8] B. a. P. D. Lehner, "Development and validation of a global database of lakes, reservoirs and wetlands," *Journal of Hydrology,* vol. 296, pp. 1-22, 2004.

[9] "CanVec- http://ftp2.cits.rncan.gc.ca/pub/canvec/doc/CanVec_product_specifications_en.pdf," Natural Resources Canada, 2007.

[10] N. Kozlenko and M. O. Jeffries, "Bathymetric mapping of shallow water in thaw lakes on the North Slope of Alaska with spaceborne imaging radar," *Arctic,* vol. 53, pp. 306-316, Sep 2000.

[11] E. Wiken, "Terrestrial ecozones of Canada," 1986.

[12] M. Maybeck, *Global distribution of lakes*, 2nd ed. New York: Spinger-Verlag, 1995.

[13] J. A. Downing, Y. T. Prairie, J. J. Cole, C. M. Duarte, L. J. Tranvik, R. G. Striegl, W. H. McDowell, P. Kortelainen, N. F. Caraco, J. M. Melack, and J. J. Middelburg, "The global abundance and size distribution of lakes, ponds, and impoundments," *Limnology and Oceanography,* vol. 51, pp. 2388-2397, Sep 2006.

Jamie MacGregor is a graduate student at the School of Earth and Ocean Sciences, University of Victoria. Jamie is an outdoors enthusiast, an experienced and professional forest fire fighter, and a remote sensing expert; Dr. Kevin Telmer is a professor in the School of Earth and Ocean Sciences with expertise in the biogeochemistry of carbon and GIS and RS tools; Dr. Maycira Costa is a professor in the Department of Geography, University of Victoria specializing in applying remote sensing techniques to understand the ecology of wetlands and the ocean.

Wetlands Theme

Mapping Boreal Wetlands, Open Water, and Seasonal Freeze-Thaw Status for Assessment of Land- Atmosphere Carbon Exchange

Kyle McDonald *et al.*
Jet Propulsion Laboratory/CalTech (U.S.A.)

K&C Science Report – Phase 1:

Mapping Boreal Wetlands, Open Water, and Seasonal Freeze-Thaw Status for Assessment of Land-Atmosphere Carbon Exchange

Kyle C. McDonald, K&C Science Team Member

Jet Propulsion Laboratory, California Institute of Technology
4800 Oak Grove Drive
Pasadena, CA 91109 USA
kyle.mcdonald@jpl.nasa.gov

Collaborators

Erika Podest, Bruce Chapman
Jet Propulsion Laboratory, California Institute of Technology
4800 Oak Grove Drive
Pasadena, CA 91109 USA
erika.podest@jpl.nasa.gov

Mahta Moghaddam, Jane Whitcomb
Radiation Laboratory, Department of Electrical Engineering and Computer Science
The University of Michigan
1301 Beal Ave
Ann Arbor, MI 48109 USA
mmoghadd@umich.edu

Ted Bohn, Dennis Lettenmaier
Surface Water Hydrology Research Group
University of Washington
Seattle, WA 98195-2700
dennisl@u.washington.edu

John S. Kimball
Flathead Lake Biological Station
The University of Montana,
32125 BioStation Lane
Polson, MT 59860
johnk@ntsg.umt.edu

Abstract— **We utilize L-band Synthetic Aperture Radar (SAR) datasets from the JERS-1 SAR and the ALOS PALSAR to map and monitor wetlands in boreal North America and Boreal Eurasia. JERS SAR datasets employed include data acquired, archived and assembled as part of the Global Boreal Forest Mapping (GBFM) project. ALOS PALSAR data include data supplied by the AUIG. We utilize multi-temporal JERS-1 data extending over the last year of JERS mission operations to map variability on open water in Alaska. We apply a novel classification approach to the summertime and wintertime JERS-1 SAR mosaics to develop the first synoptic wetlands map encompassing all of Alaska. We apply this classification algorithm to map wetlands within selected hydrologic basins in northern Eurasia, utilizing both JERS SAR and PALSAR data to map wetlands ecosystem features in those regions. We show initial results for employing these mappings within a hydrologic-methane modelling construct which will eventually provide a diagnostic tool for assessing methane flux dynamics from these**

ecosystems. We demonstrate the capability of L-band SAR to observe landscape freeze-thaw state within boreal ecosystems for examining spatial and temporal character of seasonal freeze/thaw transitions in a complex boreal landscape. This work has formed the basis for assembly of extensive global-scale Earth system data record (ESDR) to include ALOS PALSAR mappings of critical wetlands regions with both fine beam and ScanSAR data sets. ESDR assembly will be supported under Phase 2 of the Kyoto & Carbon Science Panel activities.

***Index Terms*—ALOS PALSAR, JERS-1 SAR, K&C Initiative, Wetlands, Freeze/Thaw, Carbon Flux**

I. INTRODUCTION

Wetlands act as major sinks and sources of atmospheric greenhouse gases and can switch between atmospheric sink and source in response to climatic and anthropogenic forces. Despite their importance in the carbon cycle, the locations, types, and extents of northern wetlands are not accurately known, in part because suitable remote sensing data with large-area coverage, and their respective classification algorithms, have not been available. The timing of spring thaw can influence boreal carbon uptake dramatically through temperature and moisture controls to net photosynthesis and respiration processes. With boreal evergreen forests accumulating approximately 1% of annual net primary productivity (NPP) each day immediately following seasonal thawing, variability in the timing of spring thaw can trigger total interannual variability in carbon uptake on the order of 30%. Satellite remote sensing is particularly advantageous for complete synoptic study of the behavior of wetlands ecosystems, surface water dynamics, and large-scale seasonal freeze/thaw dynamics across the high latitudes, allowing useful inference of recent greenhouse gas emissions as well as supporting prediction of processes governing future land-atmosphere carbon exchange.

Phase I of our research under the Kyoto and Carbon Initiative focused on development and demonstration of capabilities for mapping and monitoring of northern wetlands ecosystems and on characterization of seasonal freeze/thaw cycles in northern high latitude ecosystems. We map wetlands ecosystems in Alaska and Northern Eurasia with L-band Synthetic Aperture Radar (SAR). We investigate the characterization of spatio-temporal heterogeneity in seasonal freeze-thaw transitions in boreal land cover with SAR.

Wetlands mapping activities include the mapping and monitoring of water bodies and demonstration of the capability of multi-temporal SAR to characterize the change in surface water seasonally. We employ a supervised decision tree approach to classify open water for all of Alaska using time series data from the Japanese Earth Remote Sensing Satellite (JERS-1) SAR collected during 1997-1998 as part of the Global Boreal Forest Mapping (GBFM) mission. We demonstrate the utility of L-band SAR for mapping and monitoring surface water dynamics.

We used the summer and winter JERS SAR mosaics, topography, ground-based measurements of land cover, our open water map of Alaska, and other ancillary data layers derived form the SAR and DEM datasets to classify wetlands regionally for all of Alaska. We develop a powerful statistically-based decision tree classification scheme to derive the new wetlands data set. The derived 100 meter resolution map is the first synoptic map of Alaska wetlands generated from a consistent and contiguous data set.

We apply these classification techniques to PALSAR data to develop open water and land cover mappings of several hydrologic basins in Northern Eurasia. Techniques for integrated these products within a process modeling construct that integrates modeling of land surface hydrology with modeling of land-atmosphere methane flux are under development. We perform an initial assessment of the potential of the utilization of the wetlands mappings for assessment of surface hydrologic processes for supporting the characterization of land-atmosphere carbon exchange, performing an initial comparison of our SAR-based products with hydro-methane model derivatives both to assess the utility of the SAR products for supporting hydro-methane modeling and to validate performance of the modeling construct. We find the SAR-based land cover products provide a capability for assessment of land surface hydrologic parameters that support the assessment of methane emissions from wetlands ecosystems.

Development of the integrated remote sensing / process modeling framework is continuing, supporting the efforts of the Northern Eurasia Earth Science Partnership Initiative (NEESPI), a program of internationally-supported Earth systems science research for developing a comprehensive understanding of the Northern Eurasian terrestrial ecosystem dynamics, biogeochemical cycles, surface energy and water cycles, and human activities and how they interact with and alter the biosphere, atmosphere, and hydrosphere of the Earth (http://neespi.org/).

II. DESCRIPTION OF THE PROJECT

A. Relevance to the K&C drivers

The overarching objective of our project is to develop products that demonstrate, support, and provide a capability for characterization of carbon cycling processes in boreal/Arctic wetlands ecosystems and as related to seasonal freeze/thaw cycles in ecosystems in boreal/Arctic regions. We capitalize on the systematic acquisition strategies implemented for the JERS SAR and the ALOS PALSAR specifically focusing on high-latitude wetland regions to prototype products over North American and Eurasian sites. We use multi-temporal datasets to address issues of seasonal change, including seasonal freeze/thaw state change. These prototype land cover classification and freeze-thaw state products are developed to provide unique and key information for use with ecosystem process models for assessing land-atmosphere carbon exchange.

Wetlands exert major impacts on biogeochemistry, hydrology, and biological diversity. The extent and seasonal, interannual, and decadal variation of inundated wetland area play key roles in ecosystem dynamics. Wetlands contribute approximately one fourth of the total methane annually emitted to the atmosphere and are identified as the primary contributor to interannual variations in the growth rate of atmospheric methane concentrations. Climate change is projected to have a pronounced effect on global wetlands through alterations in hydrologic regimes, with some changes already evident. In turn, climate-driven and anthropogenic changes to tropical and boreal peat lands have the potential to create significant feedbacks through release of large pools of soil carbon and effects on methanogenesis. Despite the importance of these environments in the global cycling of carbon and water and to current and future climate, the extent and dynamics of global wetlands remain poorly characterized and modeled, primarily because of the scarcity of suitable regional-to-global remote-sensing data for characterizing their distribution and dynamics.

In the northern high latitudes open water bodies are common landscape features, having a large influence on hydrologic processes as well as surface-atmosphere carbon exchange and associated impacts on global climate. It is therefore important to assess their spatial extent and temporal character in order to improve hydrologic and ecosystem process modeling. Spaceborne SAR is an effective tool for this purpose since it is particularly sensitive to surface water and it can monitor large inaccessible areas on a temporal basis regardless of atmospheric conditions or solar illumination.

B. *Overview of Work approach*

Our project focused on a combination of local-scale hydrological basin study sites and regional-scale study areas in North America and Eurasia. Dataset assembly, algorithm development, and algorithm prototyping were initially conducted in boreal North America, primarily in Alaska. We employed multi-temporal L-band SAR data from JERS-1 and ALOS PALSAR to map open water bodies in Alaska and Eurasia. A supervised decision tree-based approach was used to generate open water maps. We expand the JERS-based open water maps of regions within Alaska to the entire Alaska domain. Multi-temporal SAR imagery is applied to prototype the capability for monitoring seasonal hydrologic dynamics. We assembled regional-scale monthly JERS-1 SAR mosaics from data acquired during 1998. Digital Elevation Models (DEMs) and derived slope were also employed in the decision tree classifier. These supplementary data aided significantly in improving the classification performance in topographically complex regions where radar shadowing was prevalent.

We integrate the open water map with the SAR imagery into a decision tree-based classification construct to derive a wetlands map of the whole of Alaska. The resulting product is the first synoptic map of wetlands derived from a single data source covering all of Alaska. Having developed and prototyped these approaches for open water and wetlands mapping, we apply these techniques to develop open water and wetlands mappings of selected hydrologic basins in Northern Eurasia.

For study regions in Eurasia, PALSAR data was used to map open water and its change over selected study basins. We also made use of JERS SAR data in Eurasia as needed to develop open water products supporting our land surface process modeling. Supplementary data from Landsat were used to further refine the open water classification.

C. *Satellite and ground data*

We utilize JERS-1 SAR datasets acquired as part of the Global Boreal Forest (GBFM) project and PALSAR data available to us through the systematic acquisitions detailed in the Kyoto and Carbon (K&C) Science Plan. For our Alaska effort, we used JERS SAR datasets. JERS data were processed and acquired from the Alaska Satellite Facility and assembled at JPL under the Global Boreal Forest Mapping (GBFM) project. For our Eurasia effort we used fine-bean single pol (HH) and dual-pol (HH+HV) data available though the AUIG. Landscape classification approaches and associated algorithm development and testing were carried out with the JERS data in Alaska, then subsequently applied and extended using PALSAR data over the Eurasian basin-scale study sites.

Derivation of the remote sensing-based mappings makes use of important ancillary data sets incorporated within the classification construct. These include DEMs, Landsat imagery, and ground measurements acquired from external project sources and applied here for training and validation. DEMs from the Shuttle Radar Topography Mission (SRTM) were employed for the Eurasian basin regions where the basins fall within the domain of the SRTM datasets (i.e. south of 60 deg. N latitude; http://srtm.csi.cgiar.org/). For Alaska, we employ the GTOPO30 Global 30 Arc Second Elevation Data Set available from the U.S. Geological Survey (http://eros.usgs.gov/#/Find_Data/Products_and_Data_Available/gtopo30_info). Landsat data were used to supplement the landcover classification efforts in Eurasia. The Landsat data were available to us from a database assembled by the Cartography lab at JPL.

III. Wetlands Mapping: Alaska

A. *Open Water Mapping and Monitoring in Alaska*

Dual season winter and summer JERS SAR mosaics of Alaska assembled from imagery collected primarily during 1997 and 1998 were used extensively in prototyping classification schemes and in developing wetlands mappings of Alaska (Figure 1). We applied the summertime JERS SAR mosaic to map open water at local and regional scales. Figure 2 shows a map of open water for Alaska developed applying a Maximum Likelihood Estimator (MLE) to the summertime SAR mosaic. Various approaches were tested in mapping open water including supervised and unsupervised schemes. The resulting product represents open water condition for the time of acquisition of the SAR images making up the mosaic.

Time series JERS SAR imagery from 1998 was applied to map seasonal change in open water at approximately 44-day repeat intervals. Figure 3 shows a series of mappings developed over a sub-region of Alaska's North Slope near the Kuparuk River. The map of open water were developed during the 1998 non-frozen period and applied to examine change in surface open water during the non-frozen period. The open water change maps show regions where the area of open water increases relative to the early growing season as well as those locations where open water area decreases.

These efforts are being extended to develop similar mappings with PALSAR data. We are also extending the work with JERS to include Canada to support development of wetlands maps across boreal North America.

B. Wetlands Mapping in Alaska

We utilized the summer and winter JERS SAR mosaics (Figure 1) to develop a synoptic wetlands map of Alaska (Figure 4). Because of the temporal compositing time required in assembly of the mosaics, significant variability exists in land surface hydrologic features that give rise to pass-to-pass variability (striping) in the SAR mosaics. To account for this within our classification schema, we utilized a statistically-based decision tree classification approach based on the random forest software (Breiman, 2001).Random forest generates a large number of decision trees (i.e. a forest) based on ground reference (training) data and input data layers generated from remote sensing and ancillary data sources. Each decision tree is generated through an iterative process wherein nodes are split according to the pixel values in each input data layer covered by the training data. This continues until nodes can no longer be split. Each pixel to be classified is run through every decision tree in the forest. The final class assigned to the pixel is that class selected by the most decision trees in the forest. Classification accuracy is determined by comparing the final classified product to training data withheld during the generation of the forest. The resulting product represents the first synoptically-generated wetlands map available for all of Alaska.

IV. Wetlands Mapping: Eurasia

A. Open water and wetlands mapping in Eurasia

Having developed and prototyped classification and mapping approached from JERS SAR in Alaska, we utilize PALSAR data acquired form the AUIG to map open water and wetlands land cover in northern Eurasia. We focus on a selection of basins within the Northern Eurasian Earth Science Partnership Initiative (NEESPI) domain (Figure 5). The effort here is to develop remote sensing-based products to support modelling of surface hydrodynamic processes and associated methane production. Primary controls to land-atmosphere methane flux in these ecosystems include soil temperature, water table position, and vegetation productivity. Thus development of open water and wetlands vegetation maps lends itself well to supporting the needed hydro-methane modeling infrastructure for understanding present methane emissions and forecasting effects of climate and land cover changes on future methane emissions.

Fine-beam PALSAR imagery was acquired over each NEESPI sub-region. Mosaics of the PALSAR scenes covering the basins were assembled. Supplementary Landsat data were acquired and assembled over each basin. The PALSAR and Landsat data were coregistered to a DEM. Open water was derived utilizing a decision tree classification scheme applied to the combined PALSAR/Landsat/DEM datasets. Figures 6 through 10 show PALSAR an Landsat data sets and derived open water maps for five of the hydrologic basins shown in Figure 5. A random forest classification approach was employed to develop wetlands vegetation maps (Chaya basin shown in Figure 11).

B. Hydro-methane process modeling in Eurasia

Our process modeling framework (Figure 12; Bohn et al ,2007a,b) consists of the Variable Infiltration Capacity (VIC) hydrological model (Liang et al., 1994), enhanced with ecosystem process model components taken from the Biosphere Energy Transfer Hydrology (BETHY) terrestrial carbon model (Knorr, 2000), and coupled to the wetland methane emissions model of Walter and Heimann (2000). The models are linked as follows: the VIC (enhanced with carbon cycling processes from the BETHY model) component runs at an hourly time step, simulating, among other variables, soil temperature, soil moisture, and net primary productivity (NPP). At the end of the simulation, these hourly time series are aggregated to daily values, and VIC's daily soil moisture is converted to a daily distribution of water table depths across the catchment. Then, for each day, the resulting distribution of water table depths is discretized, and methane emissions are estimated (via the methane emissions model of Walter and Heimann (2000)) as a function of soil temperature, NPP, and water table depth for each water table value in the discretized distribution. The total methane emission of the grid cell, then, is the area-weighted sum of the methane emissions from all of the discrete values of the water table depth.

Initial development and testing of this modeling construct has been performed for the Bakchar Bog region of the Chaya basin (Figure13). A topographic wetness index was derived from SRTM DEM (Bohn et al ,2007a,b). This index was compared to the land cover map of the region derived using random forest classification of ALOS PALSAR imagery. Regions of high topographic wetness index correspond closely with areas of wetland as mapped with PALSAR.

Multi-temporal JERS-1 SAR data were used to produce open water maps of this region. For the modeling component, two open water image swaths were chosen based on their overlap and day of acquisition (Bohn et al, 2006). The first swath was acquired on April 10, 1995 and the second on May 23, 1995. These days represent wide variations in open water saturation. Change in saturated surface extent between day 100 and day 143, year 1995, given by JERS open water classification are compared with the process-based modeling framework estimates for change in water table depth (Figure 14).

V. Charaterization of Landscape Freeze/Thaw State

Multitemporal SAR data were applied to examine spatial and temporal heterogeneity of seasonal land surface freeze-thaw transitions for a complex boreal landscape. Figure 15 shows JERS SAR applied to map landscape freeze-thaw state for a region of complex land cover in interior Alaska. A seasonal change detection algorithm was applied to time series JERS images to derive landscape surface freeze-thaw state (Entekhabi et al., 2004). Combined with a land cover map, the freeze-thaw state may be discerned according to land cover. This approach facilitates examination of the spatio-temporal dependencies of the seasonal freeze-thaw transitions in complex, heterogeneous landcover situations (Podest 2005).

Figure 16 shows JERS SAR applied to map landscape freeze-thaw state for a region of complex topography in interior Alaska. The seasonal change detection algorithm was applied to time series JERS images to derive landscape surface freeze-thaw state. Combining these maps with a Digital Elevation Model (DEM), the influence of surface topography on the spatio-temporal character of freeze-thaw transitions can be assessed. In the time series shown, differences in the spring thaw and autumn freeze series related to slope aspect can be seen. The difference in the timing of thaw between north and south facing slopes is notable in springtime as is the similar different in autumn freeze-up timing. During spring, south facing slopes are seen to thaw earlier than the north-facing regions. In the autumn, north facing slope freeze earlier that south facing slopes.

VI. Results and Summary

The objective of our Phase I activity was to develop products that demonstrate, support, and provide a capability for characterization of carbon cycling processes in boreal/Arctic wetlands ecosystems and as related to seasonal freeze/thaw cycles in ecosystems in boreal/Arctic regions. To this end, we have applied JERS SAR and ALOS PALSAR data to demonstrate their capability for mapping and monitoring open water and wetlands ecosystems in boreal landscapes. We used multi-temporal datasets to address issues of seasonal change, including examining seasonal open water change and spatial and temporal heterogeneity in boreal landscape freeze/thaw state. The wetlands products have been used to perform an initial assessment of a process modelling scheme for examining surface hydrology and associated land-atmosphere methane flux. We have developed the first synoptic map of wetlands across Alaska.

These prototype land cover classification and freeze/thaw state products provide unique of key information for use with ecosystem process models for assessing land-atmosphere carbon exchange. In the northern high latitudes open water bodies are common landscape features, having a large influence on hydrologic processes as well as surface-atmosphere carbon exchange and associated impacts on global climate. Efforts under Phase II of our K&C work will build on the data assembly capabilities and algorithm development tasks conducted in Phase I, extending and efforts to mapping and monitoring of important wetlands regions world-wide. Data provided by the K&C Initiative will support assembly of a global-scale Earth science data record of inundated wetlands. This data record will be made available to the larger Earth science community, supporting a broad range of scientific investigations.(McDonald, 2007)

Acknowledgements

This work has been undertaken within the framework of the JAXA Kyoto & Carbon Initiative. ALOS PALSAR data have been provided by JAXA EORC. This work was carried out at the Jet Propulsion Laboratory, California Institute of Technology, under contract with the National Aeronautics and Space Administration.

References

1. Beven, K J, and Kirkby, M J, 1979, A physically based, variable contributing area model of basin hydrology, Hydrol. Sci. Bull., 24,43-69.
2. Breiman, L., 2001. Random Forests. Machine Learning, 45, 5-32. Open source software available on-line at: www.stat.berkley.edu/~brieman/randomforests
3. Bohn, T. J., D. P. Lettenmaier, K. Sathulur, L. C. Bowling, E. Podest, K. C. McDonald, and T. Friborg, 2007a. Methane emissions from western Siberian wetlands: heterogeneity and sensitivity to climate change Environmental Research Letters, 2 045015 (9pp) doi:10.1088/1748-9326/2/4/045015
4. Bohn, T. J., D. P. Lettenmaier, E. Podest, K. C. McDonald, K. Sathulur, and L. Bowling, 2007. "Methane emissions from Western Siberian wetlands: heterogeneity and sensitivity to climate change," Proceedings of the 2007b Fall Meeting of the American Geophysical Union, 10-14 December, San Francisco, California.
5. Bohn T. J., D. P. Lettenmaier, K. Sathulur, L. C. Bowling, and K. C. McDonald, 2006. Northern Eurasian Wetlands and the Carbon Cycle: Model Estimates of Carbon Storage and Methane Emissions, Proceedings of the 2006 Fall Meeting of the American Geophysical Union, 11-15 December, San Francisco, California
6. Entekhabi, D., E. Njoku, P. Hauser, M. Spencer, T. Doiron, J. Smith, R. Girard, S. Belair, W. Crow, T. Jackson, Y. Kerr, J. Kimball, R. Koster, K. McDonald, P. O'Neill, T. Pultz, S. Running, J.C. Shi, E. Wood, and J. van Zyl, 2004. The Hydrosphere State (HYDROS) Mission Concept: An Earth System Pathfinder for Global Mapping of Soil Moisture and Land Freeze/Thaw," IEEE Trans on Geosci and Remote Sensing, 42 (10) pp. 2184-2195.
7. Knorr, W., 2000, Annual and interannual CO2 exchanges of the terrestrial biosphere: process-based simulations and uncertainties, Global Ecol. Biogeogr., 9, 225-252.
8. Liang, X., Lettenmaier, D., Wood, E., and Burges. S,. 1994. A simple hydrologically based model of land surface water and energy fluxes for general circulation models, J. Geophys. Res., 99(D7), 14415-14428.
9. McDonald, K. C., 2007. "Earth Science Data Record Assembly in Support of ALOS K&C Wetlands Theme Science," The First Joint PI Symposium of ALOS Science Program, Kyoto, Japan, 19-23 November 2007.
10. Podest, E. P. 2005. Monitoring Boreal Seasonal Freeze/Thaw Transitions with Spaceborne Microwave Remote Sensing. PhD Dissertation, University of Dundee, Scotland.
11. Walter, B. and Heimann, M. 2000, A process-based, climate-sensitive model to derive methane emissions from natural wetlands: application to five wetland sites, sensitivity to model parameters, and climate, Glob. Biogeochem. Cycles, 14(3), 745-765.
12. Whitcomb, J., M. Moghaddam, K. C. McDonald, J. Kellndorfer, and E. Podest, 2009. "Wetlands map of Alaska using L-band radar satellite imagery," Canadian Journal of Remote Sensing.

Dr. Kyle McDonald is currently a Principal Scientist in the Water and Carbon Cycles Group at the Jet Propulsion Laboratory, California Institute of Technology, in Pasadena, California. He received the Bachelor of Electrical Engineering degree (co-operative plan with highest honors) from the Georgia Institute of Technology, Atlanta, Georgia in 1983, the M. S. degree in numerical science from Johns Hopkins University, Baltimore, Maryland in 1985, and the M. S. and Ph.D. degrees in electrical engineering from The University of Michigan, Ann, Arbor, Michigan in 1986 and 1991, respectively.

Dr. McDonald has been employed in the Science Division at the Jet Propulsion Laboratory since 1991. He specializes in electromagnetic scattering and propagation, with emphasis on microwave remote sensing of terrestrial ecosystems. His research interests have primarily involved the application of microwave remote sensing techniques for monitoring seasonal dynamics in boreal ecosystems, as related to ecological and hydrological processes and the global carbon and water cycles. Dr. McDonald has been a Principal and Co-Investigator on numerous NASA Earth Science investigations. He is a member of NASA's North American Carbon Program (NACP) science team, NSF's Pan-Arctic Community-wide Hydrological Analysis and Monitoring Program (Arctic-CHAMP) Science Steering Committee, and the ALOS PALSAR Kyoto & Carbon Initiative science panel. He has been a member of the NASA BOREAS and BOREAS Follow-on science teams, the NASA Scatterometer instrument team, the NASA Ocean Vector Winds Science Team, and the NASA Cold Land Processes (CLP) Steering Committee.

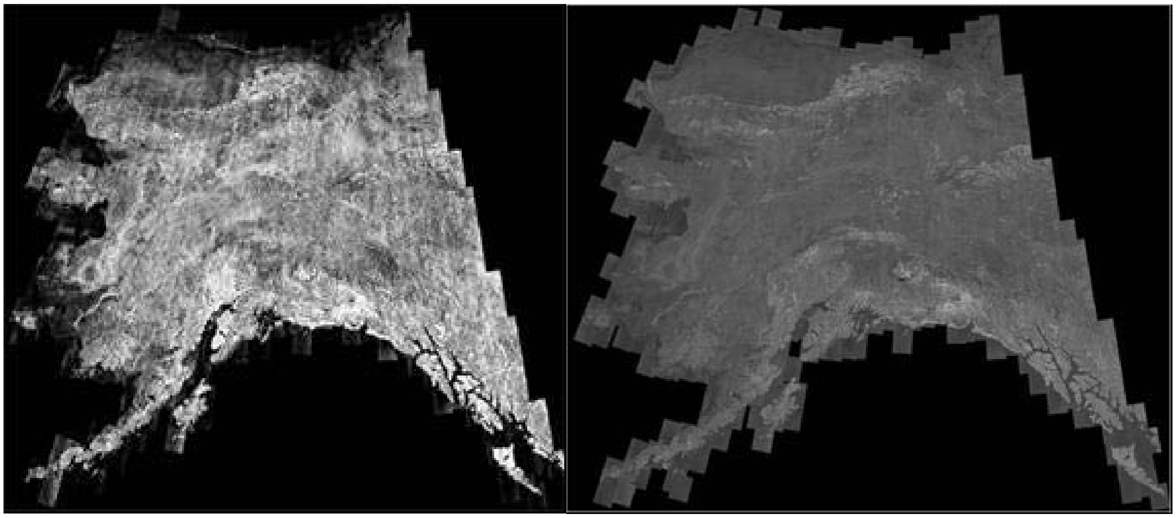

Figure 1: Mosaics of JERS-1 SAR images covering Alaska. Data are drawn from the large database of SAR images collected as part of the Global Boreal Forest Mapping (GBFM) project. Shown are mosaics representative of summertime thawed (left) and wintertime frozen (right) conditions. The complete JERS SAR dataset images collected within the Alaska Satellite Facility (ASF) receiving station mask during 1997-1998 allow mapping of open water and wetlands for the Alaska domain.

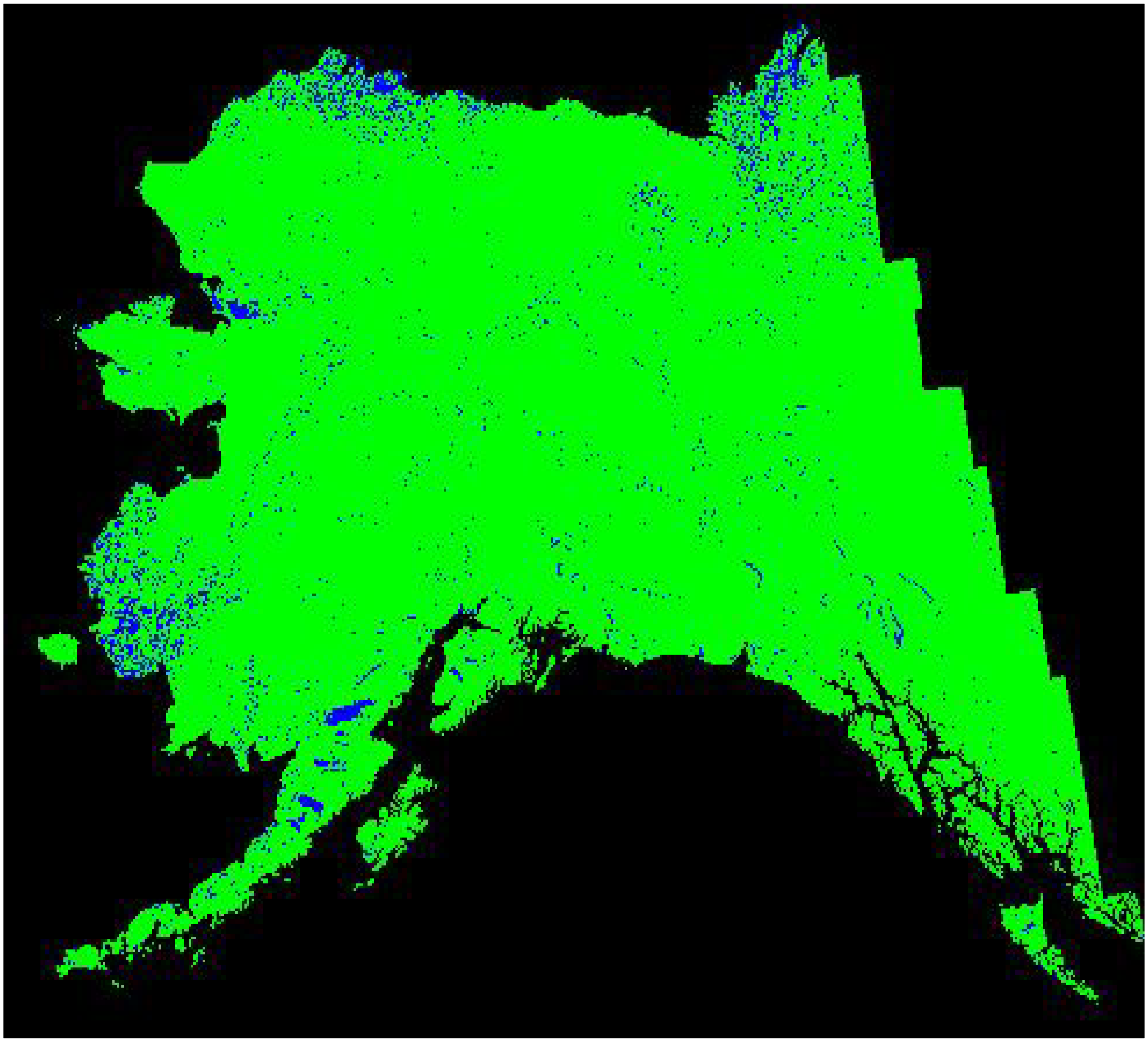

Figure 2. The open water map above was generated using an MLE supervised based approach applied to the Alaska JERS-1 summer mosaic. The product has spatial resolution of 100 meters. A DEM was used to mask out areas of high topography where radar shadowing was confused as open water.

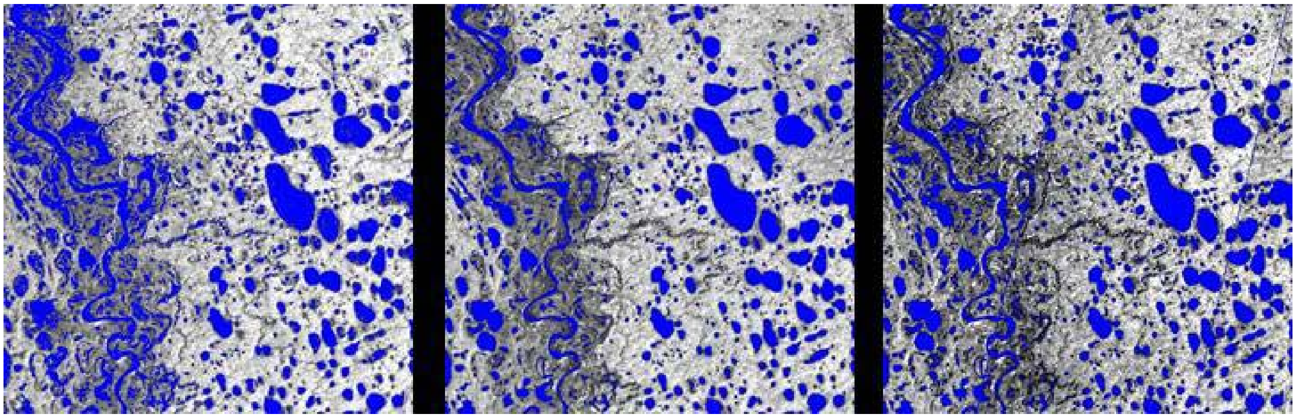

June 1998 **July 1998** **August 1998**

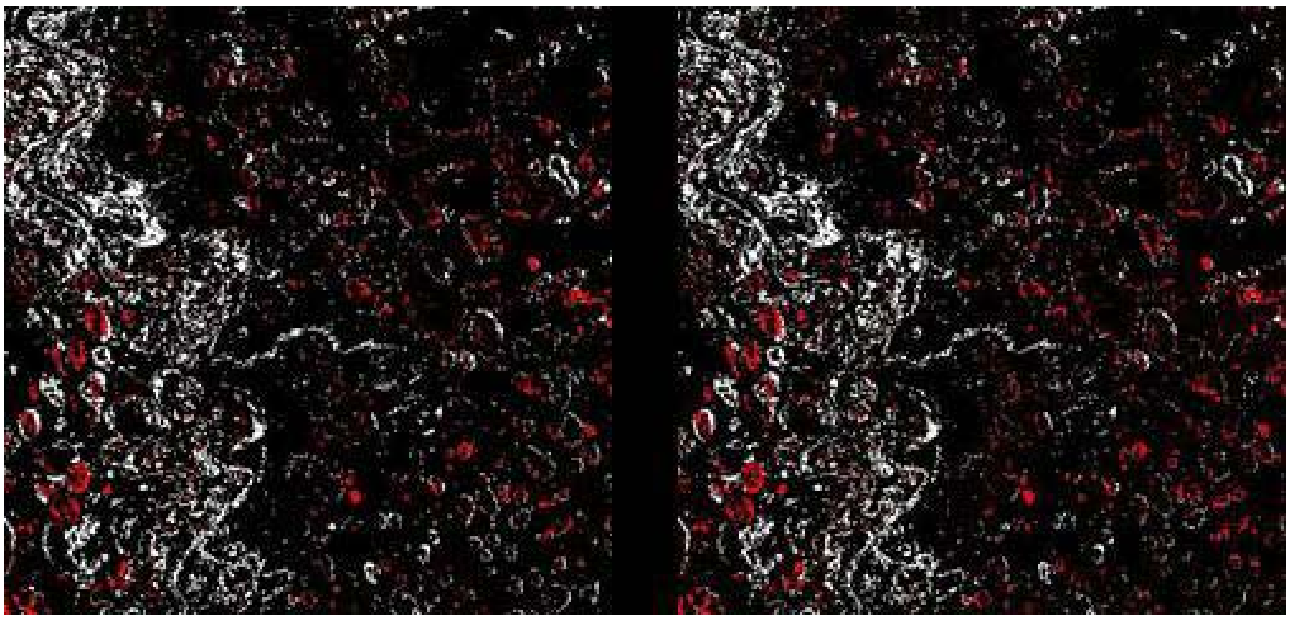

Open Water Change:
July relative to June

Open Water Change:
August relative to June

Figure 3: Time series maps of open water and change in open water for a 40 km x 40 km region of the Kuparuk River basin on Alaska's North Slope. These maps were derived from JERS SAR data collected during 1998. The top series of three maps show open water (blue) overlain on the JERS backscatter (grey scale). The lower two maps show the associated change in open water (derived from the open water maps above) during the short Arctic growing season. These change maps delineate regions of increasing (shown in red) and decreasing (shown in white) open water relative to open water conditions in June.

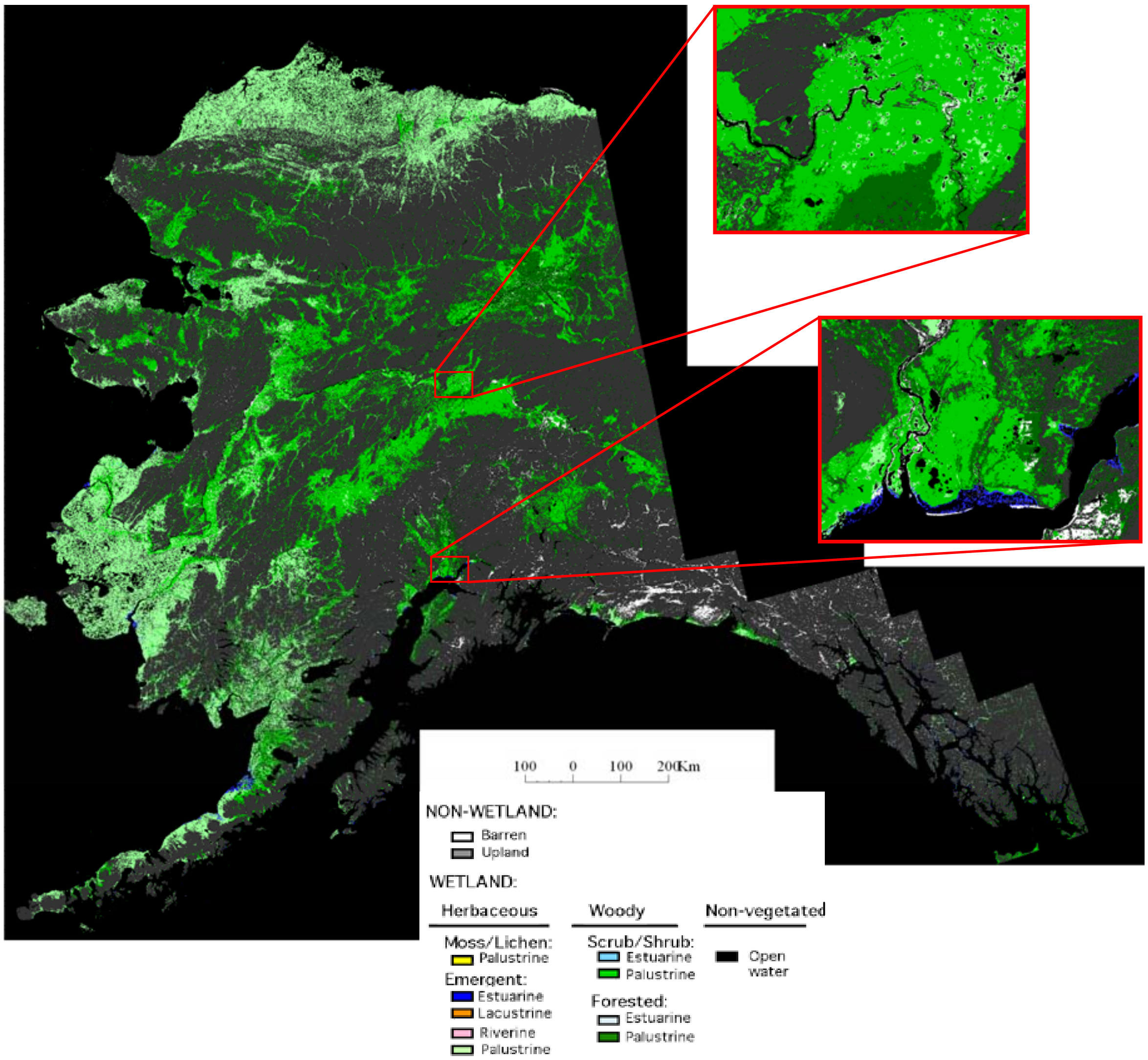

Figure 4. The wetlands map of Alaska generated from JERS radar imagery and ancillary data sets. The resolution of the map is 100 m. Top-level vegetation class accuracy rates range between 69.5% and 95% and the overall accuracy rate is approximately 89.5% based on all correctly classified pixels. The most prominent vegetated wetland classes are palustrine emergent, scrub/shrub, and forested. The other vegetation classes have only very small spatial coverage, not easily visible at the scale of this figure (Whitcomb et al., 2009).

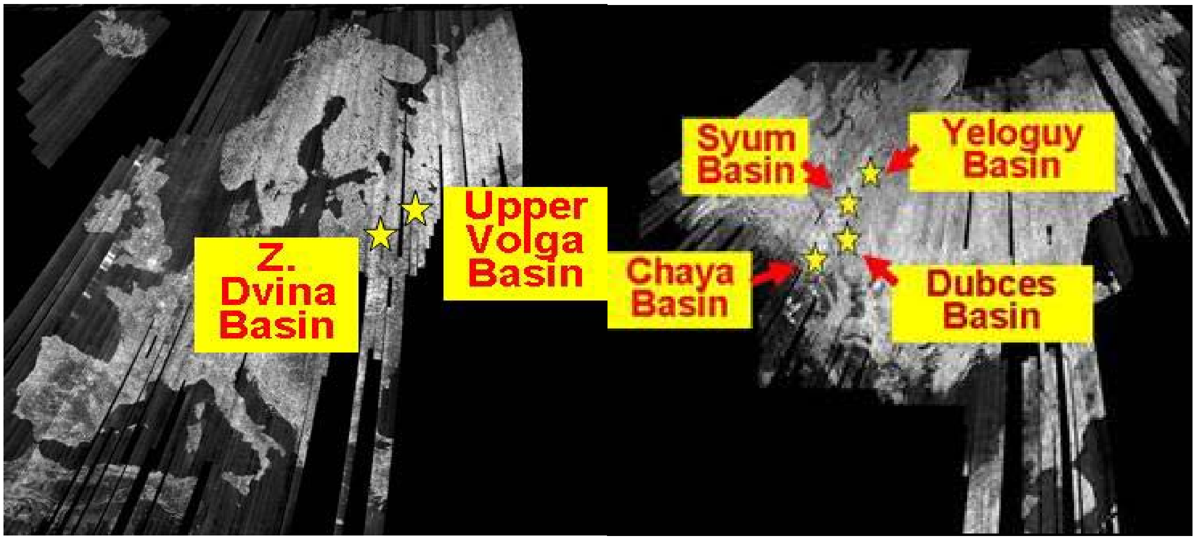

Figure 5: Location of the hydrologic basins for which PALSAR fine-beam datasets were utilized in derivation of landcover mappings to support hydrologic and carbon cycle science. Located northern Eurasia, this research supports research being conducted as part of the Northern Eurasian Earth Science Partnership Initiative (NEESPI). PALSAR-based mappings of wetlands features within these basins are being used to validate and calibrate results from hydro-methane process models under development to provide a diagnostic capability for assessing the effects of climate change on land-atmosphere water and carbon fluxes in boreal wetlands regions.

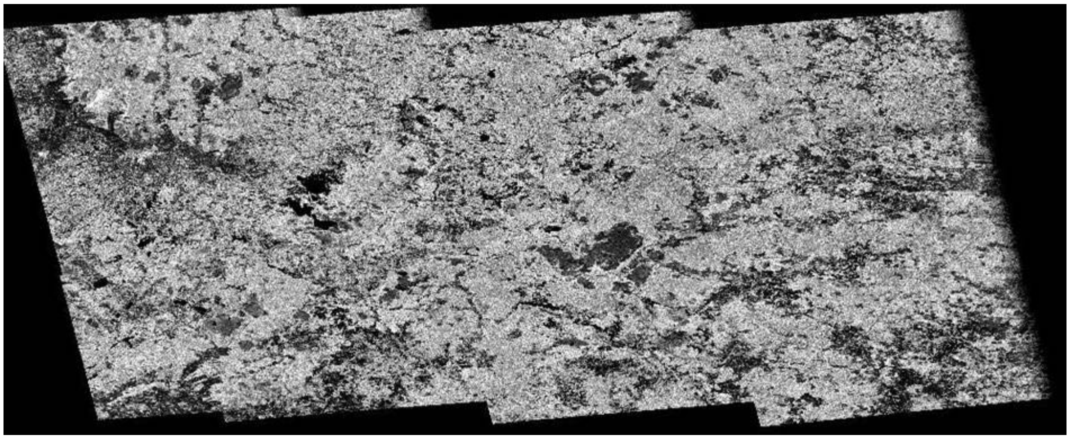

Z. Dvina (PALSAR mosaic)

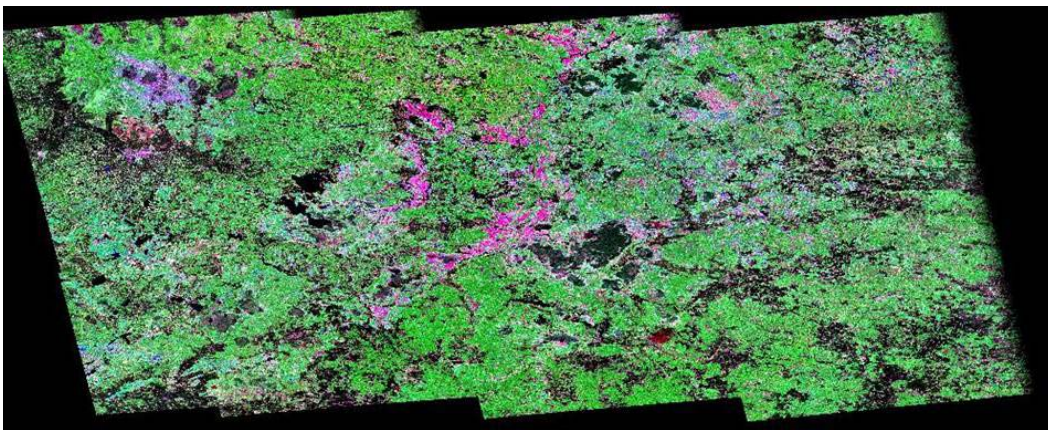

Z. Dvina (PALSAR fused with Landsat)

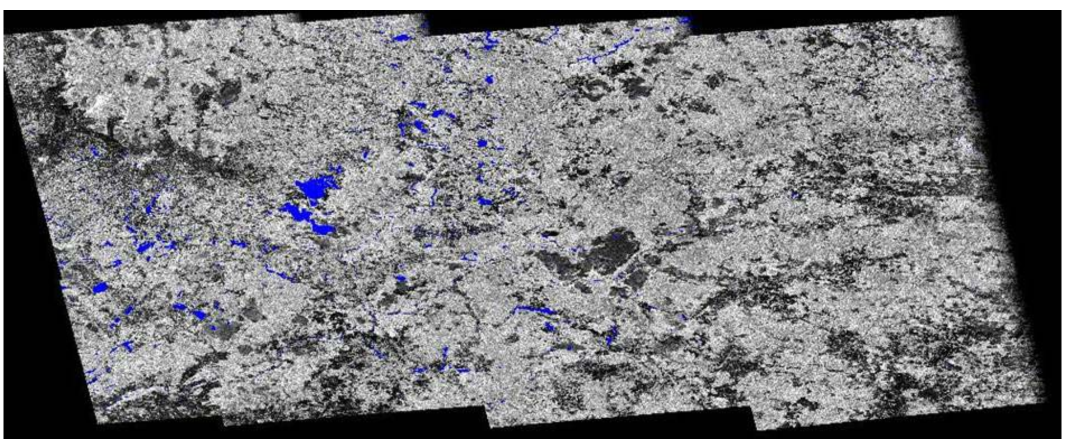

Z. Dvina (Open Water)

Figure 6: Derivation of open water for the Z. Divina basin. A mosaic of fine-beam PALSAR images is assembled (top) and fused with Landsat data (middle). These combined data are used together with a DEM in derivation of an open water map (bottom).

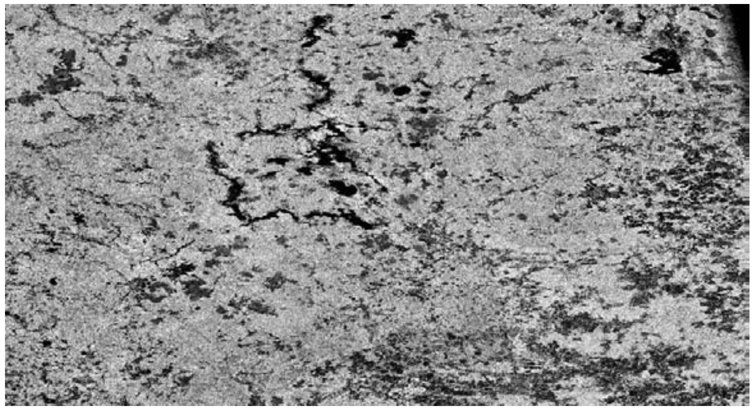

Upper Volga (PALSAR mosaic)

Upper Volga (PALSAR fused with Landsat)

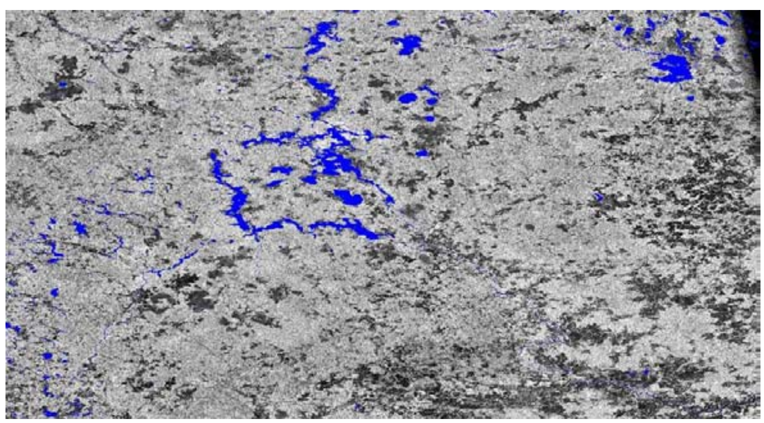

Upper Volga (open water)

Figure 7: Derivation of open water for the upper Volga basin. A mosaic of fine-beam PALSAR images is assembled (top) and fused with Landsat data (middle). These combined data are used together with a DEM in derivation of an open water map (bottom).

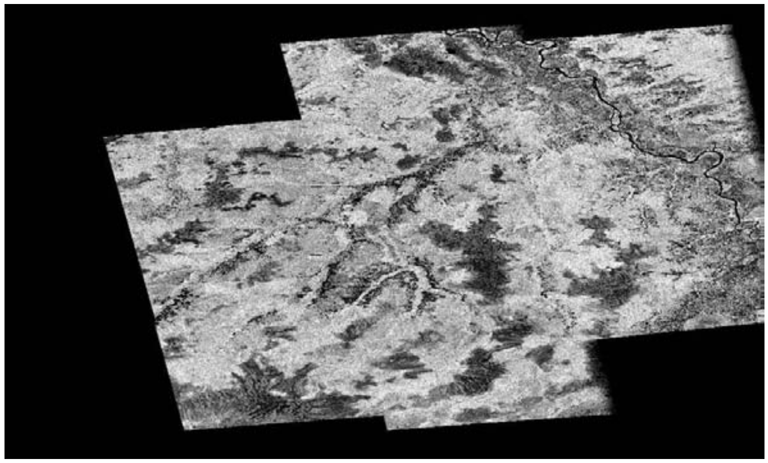

Chaya basin (PALSAR mosaic)

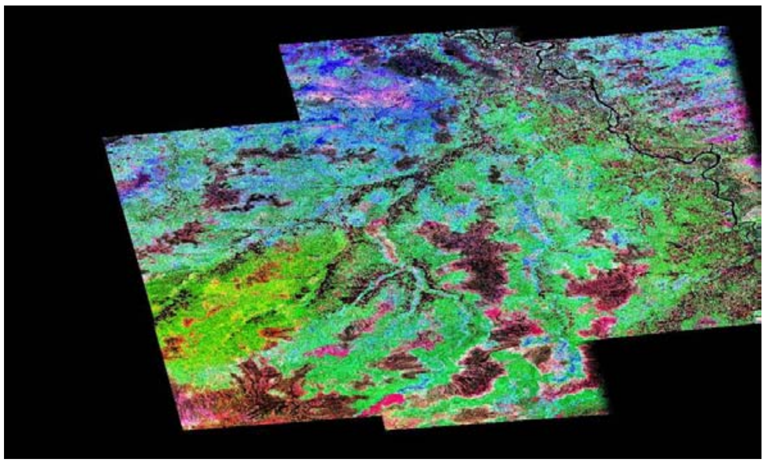

Chaya basin (PALSAR and Landsat fused)

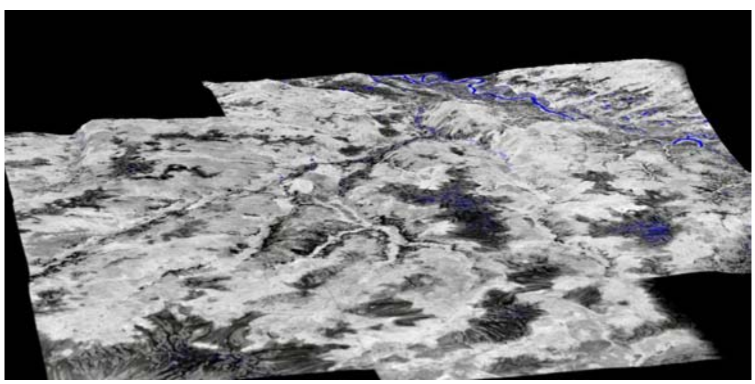

Chaya basin (open water perspective)

Figure 8: Derivation of open water for the Chaya basin. A mosaic of fine-beam PALSAR images is assembled (top) and fused with Landsat data (middle). These combined data are used together with a DEM in derivation of an open water map (bottom). The open water ma p is shown in a perspective view draped over the DEM.

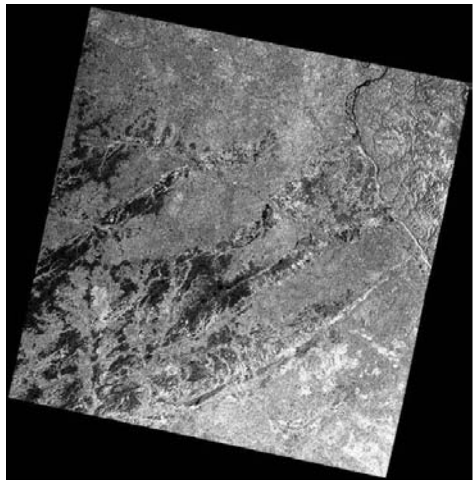

Syum (PALSAR mosaic)

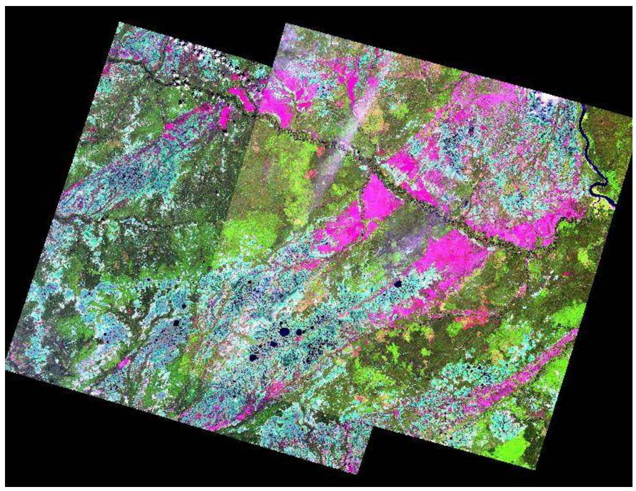

Syum (Landsat mosaic)

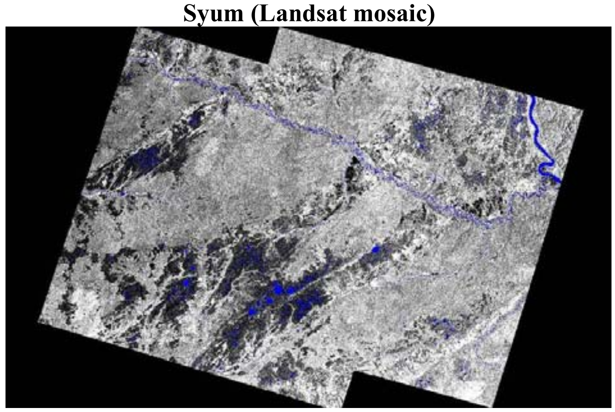

Syum (open water)

Figure 9: Derivation of open water for the Syum basin. A mosaic of fine-beam PALSAR images is assembled (top) and fused with Landsat data (middle). These combined data are used together with a DEM in derivation of an open water map (bottom).

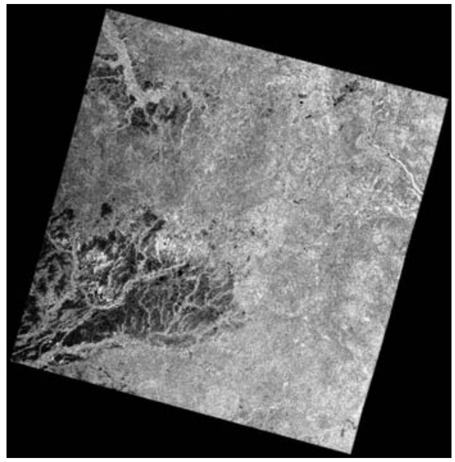

Yeloguy Basin (PALSAR image)

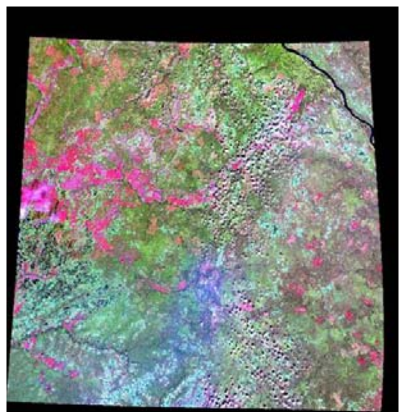

Yeloguy Basin (Landsat fused wit PALSAR)

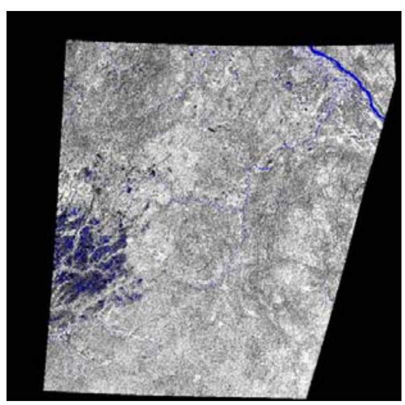

Yeloguy basin open water map

Figure 10: Derivation of open water for the Yeloguy basin. A mosaic of fine-beam PALSAR images is assembled (top) and fused with Landsat data (middle). These combined data are used together with a DEM in derivation of an open water map (bottom).

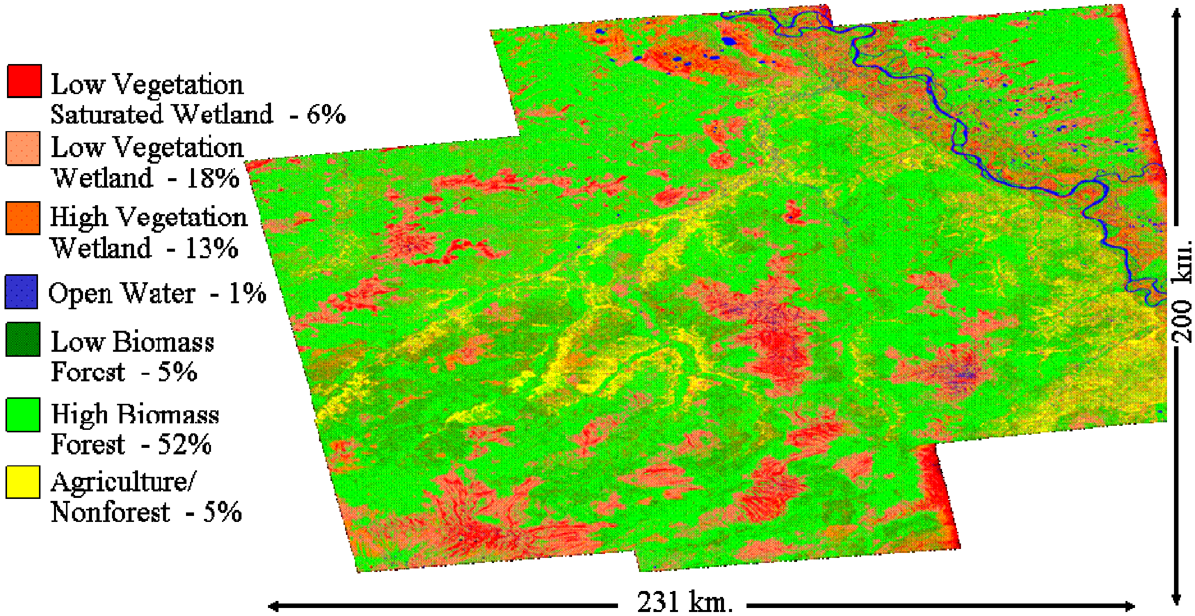

Figure 11. Landcover mapping for the Chaya Basin region, focusing on inundated wetland features and derived using ALOS PALSAR with Random Forest classification scheme applied. Landcover classes and the percent regional area covered by each are provided in the key.

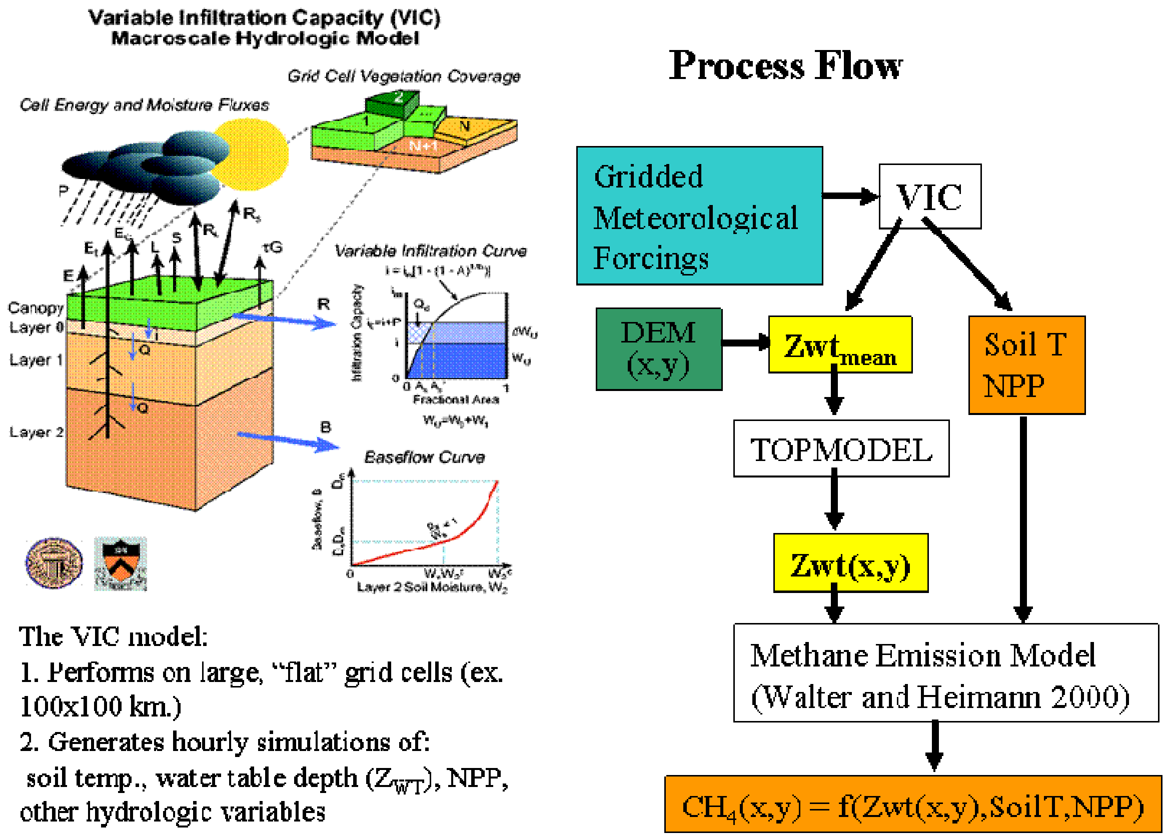

Figure 12. Modeling infrastructure utilized in the hydro-methane modeling schema. At left is the structure of the Variable Infiltration Capacity (VIC) model framework. The VIC model provides detailed information on surface hydrology processes, including soil temperature and water table depth. These are two key parameters necessary for estimation of land-atmosphere carbon exchange. At right if the process flow diagram showing the integration of the VIC model within a hydrology-methane modeling construct. This construct is being evaluated as an integrated approach for estimating land-atmosphere methane exchange, as a spatially explicit function of water table depth, soil temperature, and vegetation productivity (NPP) (Bohn et al 2007).

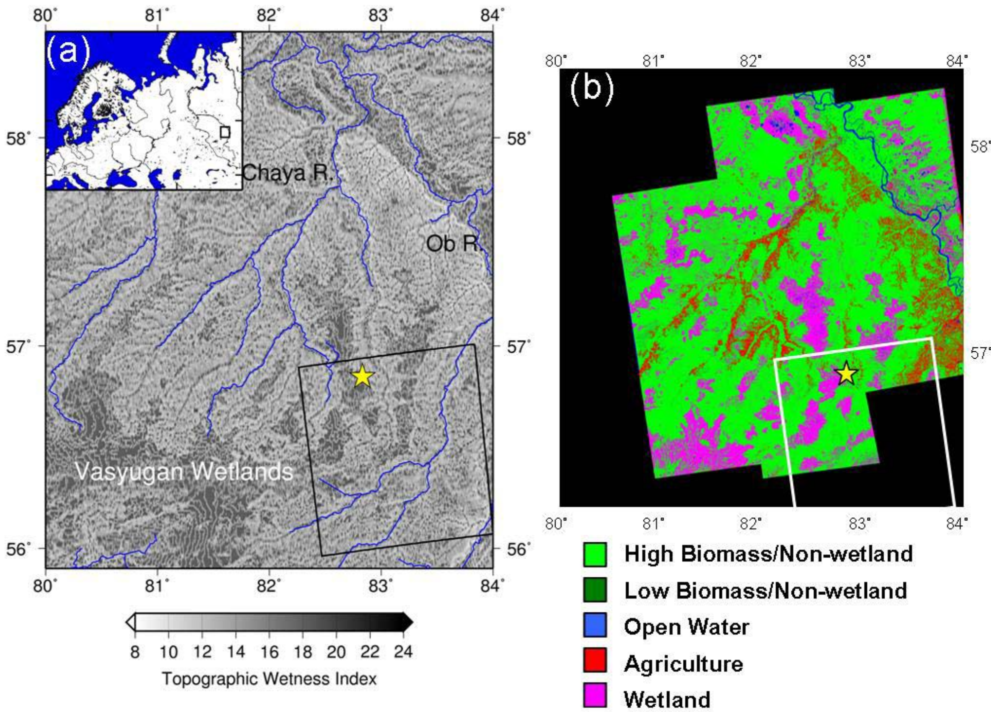

Figure 13. Location of the Chaya Basin study region where the hydro-methane modeling framework is being developed and prototyped. At left is a map of the topographic wetness index derived over the region from SRTM DEM. At right is the landcover of the region, derived using random forest classification of ALOS PALSAR imagery. The Bakchar Bog observation site is marked with the yellow star, and the 100 x 100-km EASE-grid cell centered at (56˚ 29’ N, 83˚ 09’ E) is outlined in black (at left) and white (at right). Note the close correspondence between areas of high topographic wetness index (> 14) in the panel at left and areas of wetland in the panel at right.

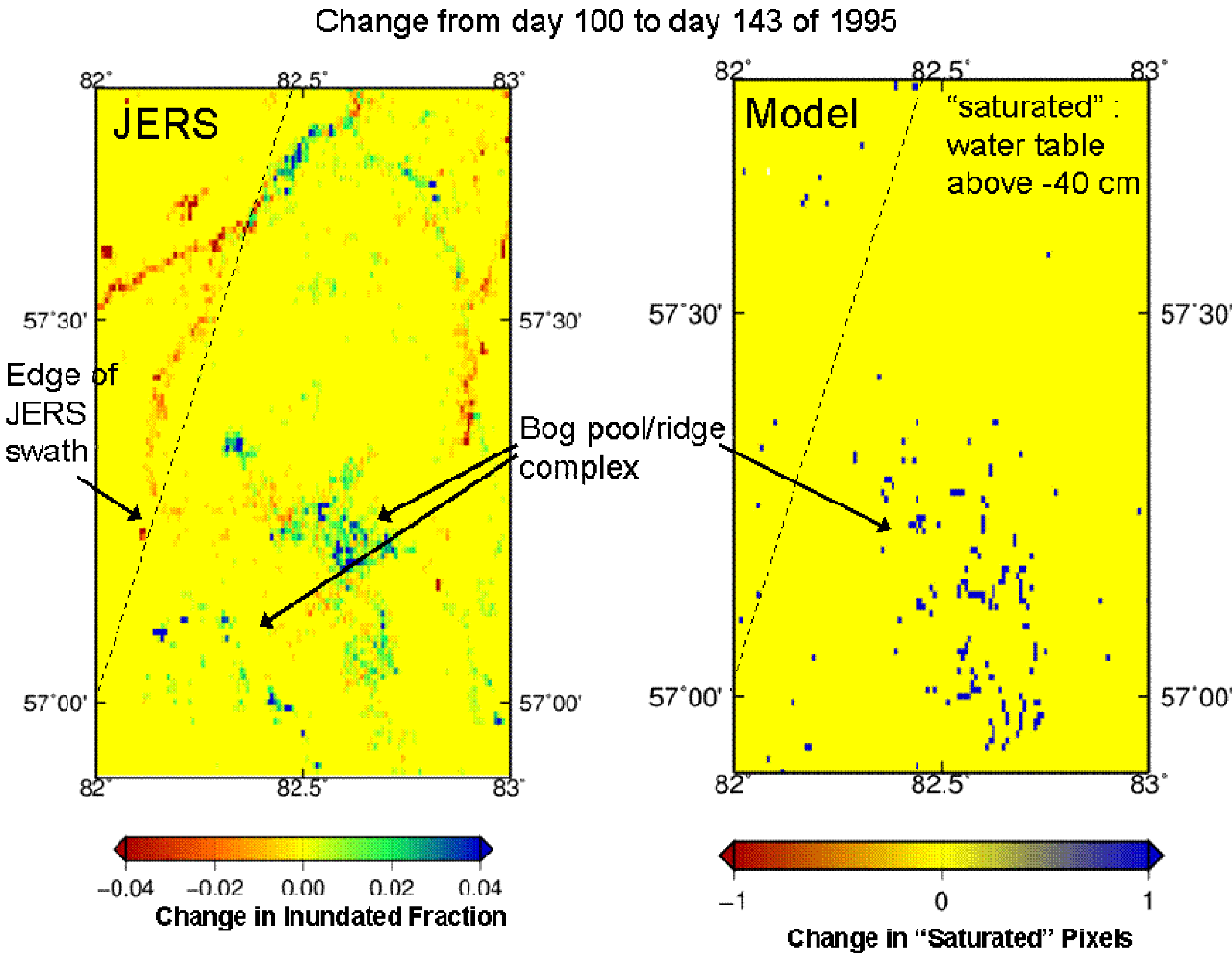

Figure 14. Comparison of change in surface inundation derived from JERS SAR (at left) with change in saturated water table derived from the hydro-methane modeling schema (at right) for the Bakchar Bog region of the Chaya Basin. JERS-based maps of open water were derived for year-day 100 and year-day 143 of 1995. Change in inundated area was computed for day 143 relative to day 100 and expressed as a change in inundated area fraction. Blue pixels contained open water on day 143 but not day 100. Red pixels contained open water on day 100 but not day 143. Model-based water table depth was computed for these same days. Saturated soil was defined as that region with water table depth less than 40 cm. The change in water table depth was determined from these modeled data. Change in saturated pixels is defined as the change in water table above 40 cm depth. At right, blue pixels had water table depth shallower than 40 cm below the surface on day 143 and deeper than 40 cm below the surface on day 100. Pixel size is 30 arc seconds. The area identified where increase in saturated pixels is evident corresponds to regions of increased surface inundation as determined from the JERS mappings.

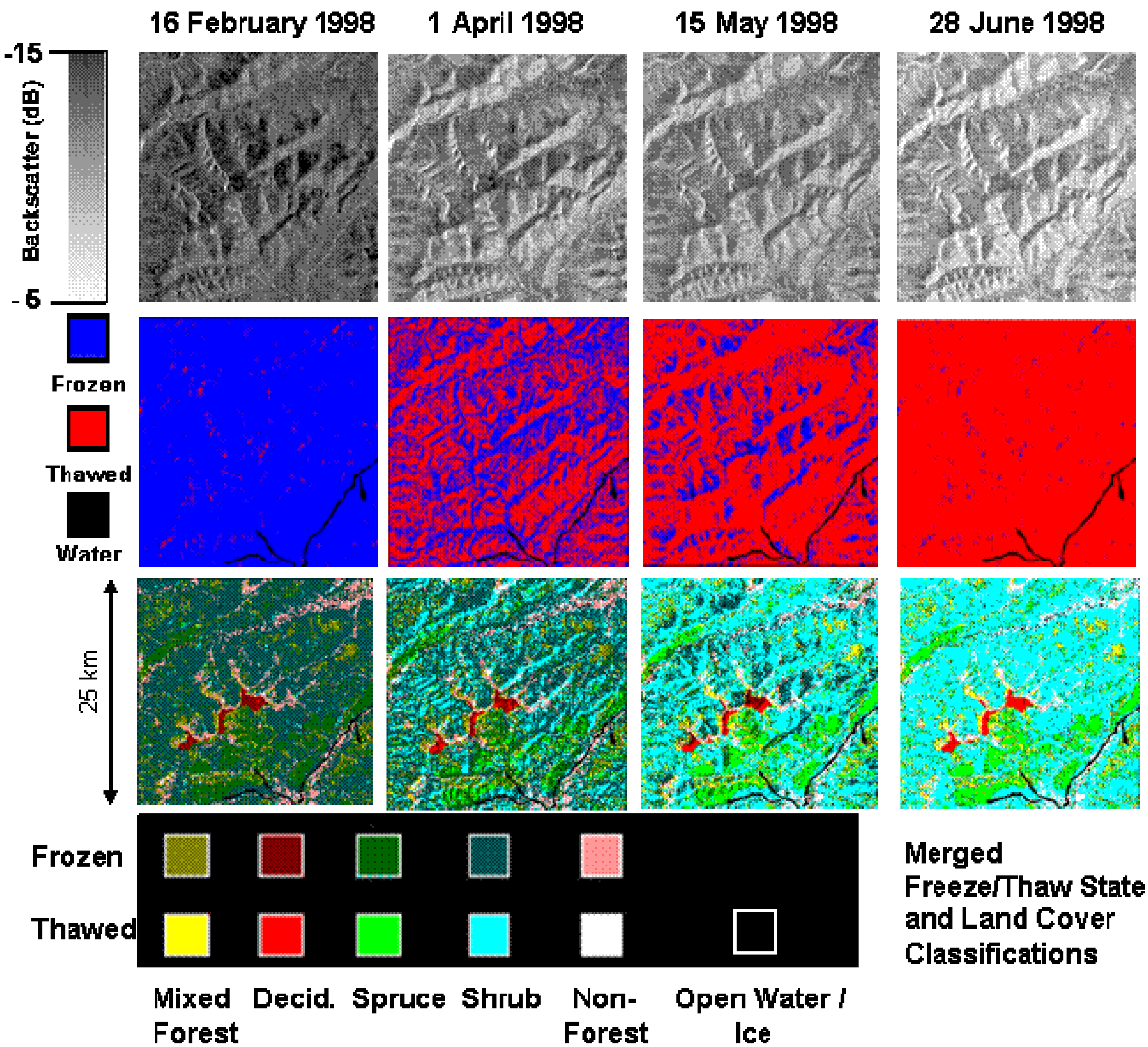

Figure 15: JERS SAR applied to map landscape freeze-thaw state for a region of complex landcover in interior Alaska. A seasonal change detection algorithm was applied to time series JERS images (top) to derive landscape surface freeze-thaw state (middle). Combined with a landcover map, the freeze-thaw state may be discerned according to landcover (bottom).This approach facilitates examination of the spatio-temporal dependencies of the seasonal freeze-thaw transitions in complex, heterogeneous landscapes.

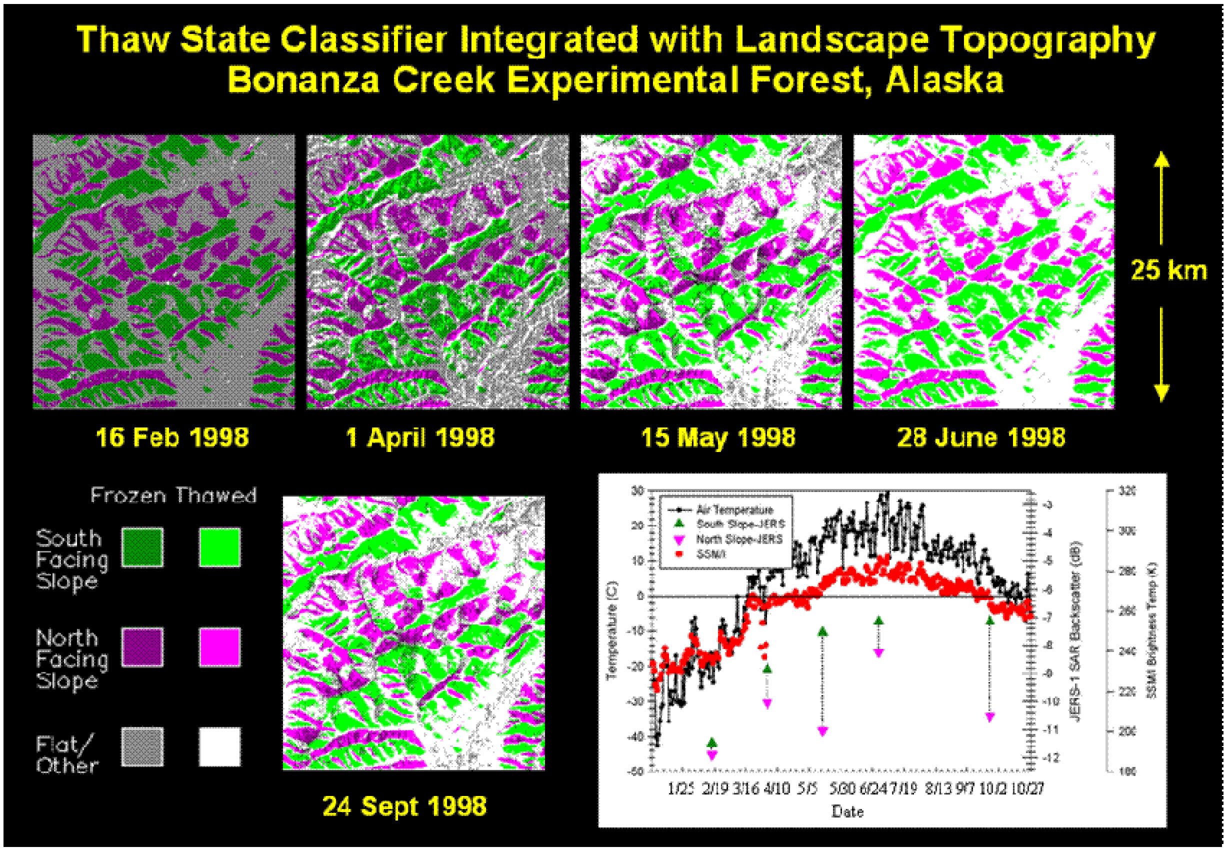

Figure 16: JERS SAR applied to map landscape freeze-thaw state for a region of complex topography in interior Alaska. A seasonal change detection algorithm was applied to time series JERS images (top) to derive landscape surface freeze-thaw state. Combined with a Digital Elevation Model (DEM), the influence of surface topography on the spatio-temporal character of freeze-thaw transitions can be assessed. In the time series shown, differences in the spring thaw and autumn freeze series related to slope aspect can be seen (e.g. bottom right graph).

Desert Theme Report

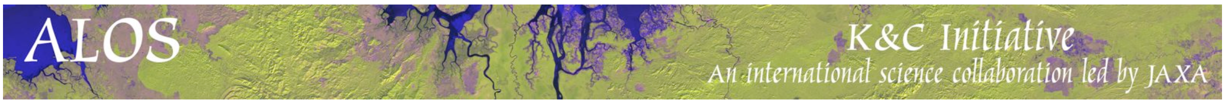

Desert Theme

Mapping Subsurface Geology in Desert Areas

Philippe Paillou
University of Bordeaux (France)

K&C Science Report – Phase 1
Mapping Subsurface Geology in Desert Areas

Philippe PAILLOU
OASU, Université de Bordeaux, France
philippe.paillou@obs.u-bordeaux1.fr

Abstract—**Using JERS-1 and PALSAR radar images provided by JAXA, we built regional and continental scale mosaics of Sahara that allowed to discover major geological features. The unique capability of L-band SAR to map subsurface structures in arid areas revealed several impact craters and paleo-rivers in Egypt and Libya.**

Index Terms—**ALOS PALSAR, K&C Initiative, Sahara, subsurface geology, impact craters, paleo-hydrology.**

INTRODUCTION

Low frequency orbital Synthetic Aperture Radar (SAR) has the capability to probe the subsurface down to several meters in arid areas. Previous studies have shown that L-band SAR is able to penetrate meters of low electrical loss material such as sand. The first Shuttle Imaging Radar (SIR-A) obtained some of the first subsurface imaging results for a site located in the Bir Safsaf region, in southern Egypt: SIR-A L-band radar revealed buried and previously unknown paleodrainage channels, which afterwards were confirmed during field expeditions. Subsequently, SIR-C data were used to map subsurface basement structures that control the Nile's course in northeastern Sudan : numerous hidden faults were detected, thus helping to better understand the Cenozoic uplift of the Nubian Swell. More recent studies have shown that combining SRTM – Shuttle Radar Topography Mission – topographic data with SAR images better reveals subsurface features which still present a topographic signature. New paleodrainage flow directions have been mapped in the eastern Sahara, allowing better definition of drainage lines leading to oases and valleys, as well as a better understanding of the Nubian aquifer in Libya.

While the geographical coverage of the Shuttle Imaging Radar missions was limited, a more complete L-band radar coverage of the eastern Sahara by the Japanese JERS-1 satellite was used to realize the first regional-scale radar mosaic covering Egypt, northern Sudan, eastern Libya and northern Chad. This data set helped discover numerous unknown geological structures, particularly impact craters: a double impact crater was found in southern Libya, in a flat and hyper arid area covered by active aeolian deposits. More than 1300 small crater-like structures, distributed over an area of 40,000 km2, were also detected in the western Egyptian desert. Continental-scale exploration is now being conducted using higher quality data from the new high-performance PALSAR L-band radar of the Japanese ALOS satellite. A new mosaic of the eastern Sahara made from PALSAR scenes shows excellent data quality, allowing a better detection of subsurface features. Using this unique data set, we discovered a major paleodrainage river in eastern Libya.

SUBSURFACE IMAGING USING JERS-1 DATA

JERS-1 was launched in 1992 and acquired L-band (1.275 GHz) SAR images of the Earth until end of 1998. It provided 18m resolution images in HH polarization, with an off-nadir angle of 35^o. Due to power feed problems, the data present a high $NE\sigma_0$ (noise equivalent σ_0) of -18dB. It is a crucial parameter for subsurface imaging since buried structures are likely to have a low backscattering return. Also, geocoding of JERS-1 SAR data was poor, with location errors reaching several hundreds of meters. A complete L-band radar coverage of the eastern Sahara by the Japanese JERS-1 satellite exists and was used in 2003 to realize the first regional-scale radar mosaic covering Egypt, northern Sudan, eastern Libya and northern Chad [1]. The production and scientific analysis of more than 1600 SAR scenes was used to study the near-surface geology hidden by the superficial sand layer, and we discovered numerous unknown geological structures.

We thus revealed a double impact crater in southern Libya: the structure is located 110 km west of Djebel Arkenu and 250 km south of Kufra oasis in Libya, at coordinates 22°04'N, 23°45'E. It is a flat and hyperarid area covered by active aeolian deposits. The optical Landsat 7 image of the region shows a sandy region with large sand dunes trending SW-NE, while the corresponding L-band radar image extracted from our JERS-1 mosaic reveals two circular structures partially hidden by Quaternary deposits (fig. 1). The NE crater, 6.8 km in diameter, is composed of concentric inner and outer rings separated by a depression filled with sediments. Its morphology is very similar to the Aorounga crater in Chad, corresponding to a typical complex crater. Shatter cones and breccia were observed during field work in April 2003. Planar fractures were also found into rock samples, confirming the impact origin of the craters [2].

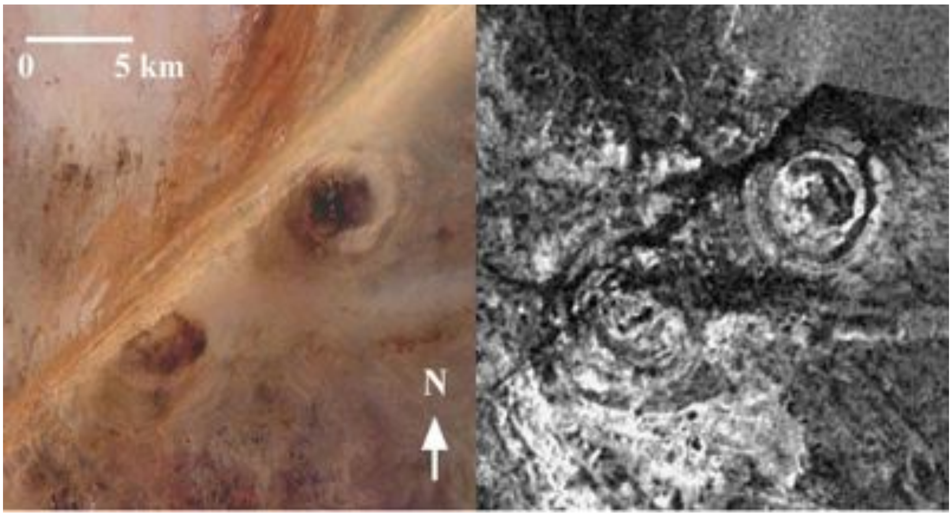

Figure 1. Landsat 7 ETM+ image of the Arkenu double crater (left), and corresponding JERS-1 radar image (right) at a resolution of 50m (JAXA/METI).

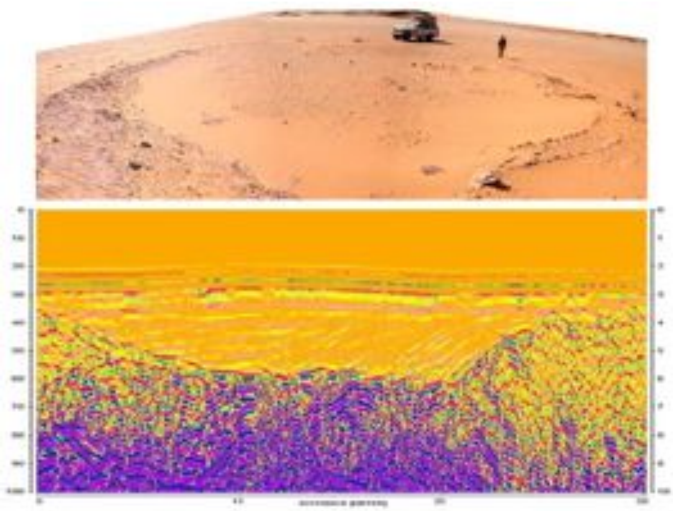

Figure 2. Surface view of the outcropping part of GKCF28 crater (40m in diameter, top) and corresponding GPR profile at 270 MHz (bottom) showing its subsurface shape.

We also detected more than 1300 small crater-like structures distributed over an area of 40,000 km^2 in the Western Egyptian Desert, close to the Gilf Kebir plateau. Sixty-two of them were visited in the field during February and December 2004 [3, 4]. Morphological observations, rock samples and ground-penetrating radar data were obtained [5] (fig. 2). Shatter cone-like features, breccia and sub-planar fractures were observed in the vincinity of most of the craters, but the impact origin of the field still has to be confirmed: hydrothermal vent complexes could also explain some of our observations [6]. Whatever its origin, the Gilf Kebir crater field is of great scientific interest and is a major element of the geological history of Western Egypt. Further field and laboratory studies are required in order to better understand its nature and origin.

FIRST RESULTS USING ALOS/PALSAR DATA

In January 2006, the JAXA successfully launched the Advanced Land Observing Satellite (ALOS). It carries two high resolution optical sensors (AVNIR-2 and PRISM) and one full polarimetric L-band SAR, PALSAR. This phased array SAR provides high resolution (10m) imagery with variable incidence angle, with a much improved value of NEσ_0 around -25dB. The geolocation accuracy is better than 10m and the radiometric accuracy is better than 1dB. The PALSAR instrument is operated to provide systematic wall-to-wall observations of all land areas on the Earth on a repetitive basis. First acquisitions over North Africa took place during ascending cycle 9 in January 2007 (Fine Beam mode, HH polarization, incidence angle 34.3^o). We produced a first small mosaic of 50 PALSAR scenes, extending between 18-23^{o}N and 24-30^{o}E over southern Egypt and northern Sudan. Comparison between the JERS-1 SAR and PALSAR data clearly shows the superior capacity of the PALSAR sensor to map subsurface features (fig. 3). Due to its improved NEσ_0 and finer resolution, PALSAR allows in particular a better detection of fine paleo-hydrological networks [7].

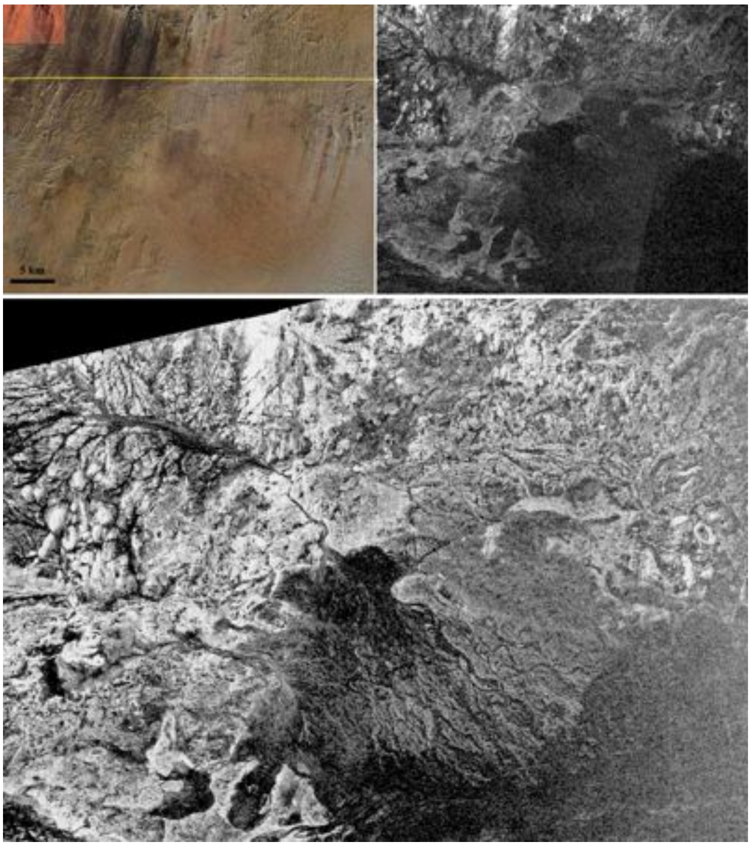

Figure 3. Landsat (top left), JERS-1 (top right) and PALSAR image (bottom) of a region located around 21^{o}55'N, 26^{o}36'E. PALSAR much better reveals paleodrainage channels in the lower part of the scene (JAXA/METI).

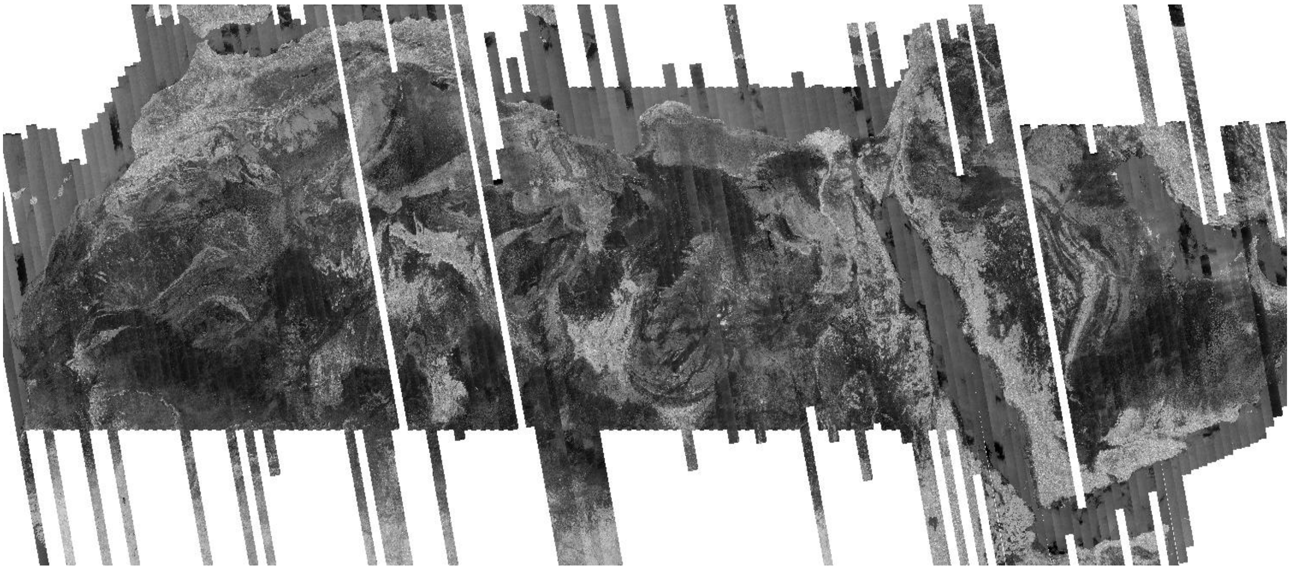

Figure 4. PALSAR mosaic from acquisition cycles 12 and 13, covering Sahara and Arabia (JAXA/METI).

A full coverage of Sahara in HH and HV polarizations was acquired in June and July 2007 (ascending cycles 12 and 13). Using our own data processing chain, we produced a geocoded mosaic of Sahara and Arabia from more than 400 dual-polarization PALSAR strips (fig. 4). It covers latitude between 17-37°N and longitude between 17°W and 60°E. This dataset constitutes a unique tool for the scientific community to study the paleo-environment and paleoclimate of North Africa. It will also help build more complete geological maps in support to future water prospecting in arid and semi-arid regions [8].

We started the analysis of the PALSAR mosaic over eastern Sahara. As a first result, we mapped a major paleodrainage system in eastern Libya, that could have linked the Kufrah Basin to the Mediterranean coast through the Sirt Basin, possibly as far back as the middle Miocene. Images from the PALSAR sensor clearly reveal a 900 km-long river system (fig. 5), which starts with three main tributaries (north-eastern Tibesti, northern Uweinat and western Gilf Kebir / Abu Ras) that connect in the Kufrah oasis region. The river system then flows north through the Jebel Dalmah, and forms a large alluvial fan in the Sarir Dalmah. The sand dunes of the Calanscio Sand Sea prevent deep orbital radar penetration and preclude detailed reconstruction of any possible connection to the Mediterranean Sea, but a 300 km-long link to the Gulf of Sirt through the Wadi Sahabi paleochannel is likely. If this connection is confirmed, and its Miocene antiquity is established, then the Kufrah River, comparable in length to the Egyptian Nile, will have important implications for the understanding of the past environments and climates of northern Africa from the middle Miocene to the Holocene [9]. Future work concern the analysis of tha PALSAR mosaic to map paleodrainage networks in western Sahara (Mauritania, Niger, Mali). We aslo plan to apply the same approach to study subsurface geology in arid regions of northen China (Sinkiang and Badain Jaran deserts).

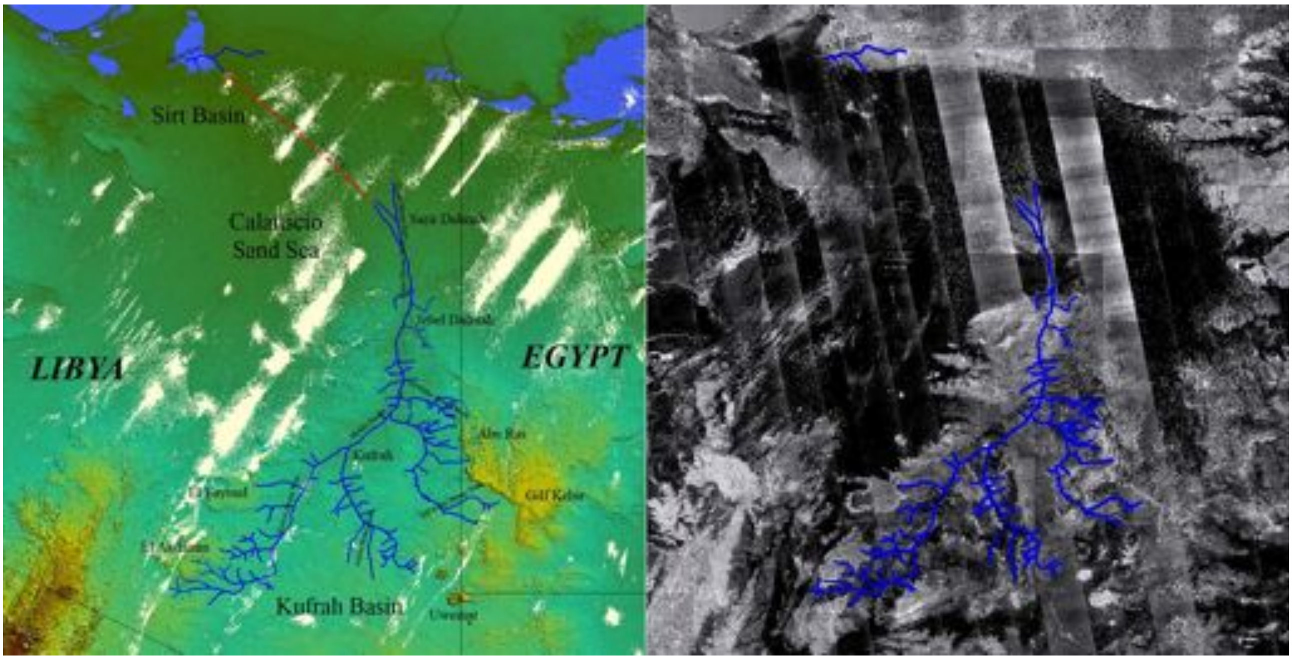

Figure 5. The Kufrah River (in blue) mapped onto SRTM topography (left) and PALSAR mosaic (right). The red dotted line represents a possible path to the Mediterranean coast (JAXA/METI).

ACKNOWLEDGMENTS

This work has been undertaken within the framework of the JAXA Kyoto & Carbon Initiative. ALOS PALSAR data have been provided by JAXA EORC. The author acknowledges financial support from CNES.

REFERENCES

[1] Ph. Paillou, A. Rosenqvist, T. Farr, “A JERS-1 radar mosaic for subsurface geology mapping in East Sahara”, IGARSS’03, Toulouse, France, july 2003.

[2] Ph. Paillou, A. Rosenqvist, J.-M. Malézieux, B. Reynard, T. Farr, E. Heggy, “Discovery of a double impact crater in Libya: the astrobleme of Arkenu”, C.R. Acad. Sci. Paris, Geoscience, vol. 335, pp. 1059-1069, 2003.

[3] Ph. Paillou, A. El Barkooky, A. Barakat, J.-M. Malézieux, B. Reynard, J. Dejax, E. Heggy, “Discovery of the largest crater field on Earth in the Gilf Kebir region, Egypt”, C.R. Acad. Sci. Paris, Geoscience, vol. 336, pp. 1491-1500, 2004.

[4] E. Heggy, Ph. Paillou, “Mapping structural elements of small buried craters using GPR in the southwestern Egyptian desert: Implications for Mars shallow sounding”, Geophysical Research Letters, vol. 33, L05202, 2006.

[5] Ph. Paillou, B. Reynard, J.-M. Malézieux, J. Dejax, E. Heggy, P. Rochette, W. U. Reimold, P. Michel, D. Baratoux, “An extended field of crater structures in Egypt: Observations and hypotheses”, LPSC 37, Houston, USA, march 2006.

[6] Ph. Paillou, B. Reynard, J.-M. Malézieux, J. Dejax, E. Heggy, P. Rochette, W. U. Reimold, P. Michel, D. Baratoux, Ph. Razin, J.-P. Colin, “An extended field of crater-shaped structures in the Gilf Kebir region – Egypt: Observations and hypotheses about their origin”, Journal of African Earth Sciences, vol. 46, pp. 281-299, 2006.

[7] Ph. Paillou, A. Rosenqvist, S. Lopez, Y. Lasne, T. Farr, “Mapping subsurface geology in arid Africa using L-band SAR”, IGARSS’07, Barcelona, Spain, july 2007.

[8] Ph. Paillou, T. Farr, A. Rosenqvist, S. Lopez, “A PALSAR mosaic of Sahara to map subsurface geology”, IGARSS’08, Boston, USA, july 2008.

[9] Ph. Paillou, M. Schuster, T. Farr, S. Tooth, A. Rosenqvist, S. Lopez, J.-M. Malézieux, “Mapping of a major paleodrainage system in Eastern Libya using orbital imaging Radar: The Kufrah River”, Earth and Planetary Science Letters, vol. 277, pp. 327-333, doi: 10.1016/j.epsl.2008.10.029, 2009.

Philippe PAILLOU obtained the Engineer Diploma from the Ecole Nationale Supérieure de Physique of Strasbourg in 1989, and a PhD in Image Processing from the University of Strasbourg in 1992. Since 2004, he is full professor at the University of Bordeaux. His research interests concern image processing and electromagnetic modelling applied to radar remote sensing. He conducts several projects related to the study of arid regions on Earth using low frequency radar.

Mosaic Theme Reports

Mosaic Theme

ALOS Image Mosaics for Wetland Mapping

Bruce Chapman *et al.*
Jet Propulsion Laboratory/CalTech (U.S.A.)

K&C Science Report – Phase 1

ALOS Image Mosaics for Wetland Mapping

Bruce Chapman
Jet Propulsion Laboratory, California Institute of Technology, bruce.chapman@jpl.nasa.gov

Kyle McDonald
Jet Propulsion Laboratory, California Institute of Technology, kyle.mcdonald@jpl.nasa.gov

Laura Hess
University of California, Santa Barbara, lola@icess.ucsb.edu

***Abstract*—**

ALOS PALSAR, an orbiting L-band SAR launched by the Japanese Aerospace and Exploration Agency (JAXA) in 2006, has been pursuing a global observation strategy through its ALOS Kyoto and Carbon Initiative (ALOS KC) [6]. The objectives of the ALOS KC project, lead by JAXA, include systematic global scale acquisitions by ALOS PALSAR, and the production of products quantifying the geographic extent of forested, desert, and wetlands [2]. As a component of this task, large collections of dual polarization (HH and HV) data are being acquired over wetland areas around the globe. Through the NASA MEASURES program, JPL will be leading an effort to utilize this data to produce a global inundated wetlands product. One of the first steps will be to produce dual polarized continental-scale mosaics of SAR imagery. Image mosaics are desired to simplify image classification. However, flexibility in constructing the mosaic is required, in order to produce representative products. The distribution and visualization of the image mosaics and products is also an important component of this work.

***Index Terms*—ALOS PALSAR, K&C Initiative, Wetland Theme, Mosaic Theme, inundated wetlands**

I. INTRODUCTION

A. Science objectives

A NASA funded research task will be generating an Earth Science Data Record for global inundated wetlands. Wetland extent and dynamics will be characterized using ALOS PALSAR imagery and other sensors. The extent and seasonal, inter-annual, and decadal variation of inundated wetland area play key roles in ecosystem dynamics. Wetlands contribute approximately one fourth of the total methane annually emitted to the atmosphere and are identified as the primary contributor to inter-annual variations in the growth rate of atmospheric methane concentrations. Climate change is projected to have a pronounced effect on global wetlands through alterations in hydrologic regimes, with some changes already evident. In turn, climate-driven and anthropogenic changes to tropical and boreal peatlands have the potential to create significant feedbacks through release of large pools of soil carbon and effects on methanogenesis.

B. Image mosaics

In assembling the ALOS SAR mosaics for the global inundated wetlands product, the mosaics will be ortho-rectified to the SRTM DEM (where available). The images to be mosaicked will be lower resolution image ‘strips’, often thousands of kilometers along track, rather than image frames which are roughly as long along track as the cross track dimension. These image strips are produced as a special product of the ALOS KC project by the JAXA Earth Observation Research Center (EORC), and have a pixel spacing of under 100 meters. These acquisitions also include the cross-pol channel, for which the same georeferencing information may be used to project the imagery to the ground topography.

C. Display and distribution of imagery and products

The display of ortho-rectified Earth Imagery can be facilitated through Earth Image browsers such as Google Earth. These Earth image browsers are easy to use, and enable visual comparison of ALOS imagery and derived products with high-resolution optical imagery. They can also be a means for data discovery, in which you use the Earth image browser to geographically find the imagery or data that you require. They can provide a public presentation at multiple resolutions of ALOS imagery and data, which is important due to the simultaneously fine resolution and large geographic extent of the ALOS Kyoto and Carbon Initiative products. They also provide a platform for interaction with the data.

II. DESCRIPTION

A. Relevance to the K&C drivers

The Wetlands theme of the ALOS KC initiative [2] will utilize ALOS image mosaics that have been ortho-rectified and projected to a simple ground projection. This simplifies quantitative analysis (i.e. overlap regions are eliminated) and validation and verification (i.e. it is easy to geographically compare with validation data sets). The mosaic theme of the ALOS KC initiative therefore enables this work by producing ortho-rectified image products. The specific objective of ALOS KC phase 1 work was to produce prototype dual polarization mosaics of North and South America, and begin analysis of ScanSAR regions where rich multi-temporal image data will be acquired. Another objective of this work is to explore how this image data may be visualized and distributed using commonly available and easy to use tools for this purpose.

The most basic requirement for modeling regional to global methane or carbon dioxide emissions from wetlands is a digital wetlands map with an appropriate scale and classification scheme [2]. The ultimate results of this project to map the extent and dynamics of inundated wetlands will therefore improve our understanding of the carbon cycle as well as facilitate conservation of wetland areas simply by identifying the location and maximum and minimum extent of wetlands.

B. Work approach

The JAXA Earth Observation Research Centre (EORC) provides slant range image strips for use by the ALOS Kyoto and Carbon Initiative [2]. These image strips can be thousands of km in length, but have a reduced resolution compared to that obtained during standard processing. The calibration is the same as that performed during standard processing, but the file format is slightly different.

First step for image mosaicking is the ortho-rectification of the image data. For these results, we use the software package from Gamma Remote Sensing [7] to orthorectify the data to a supplied digital elevation model (DEM). The DEM data was constructed from the SRTM DEM, and other available DEM's outside of the SRTM coverage area [8]. Since the image strips extend across continental scale regions, we project the imagery to SRTM–like 'tiles' of topography information, approximately 1deg x 1 deg in size. The tiles are actually reconstructed from the SRTM data slightly larger than this to accommodate edge effects. The SRTM-like tiles of imagery may then be mosaicked into the desired larger regional image mosaics (see figure 1).

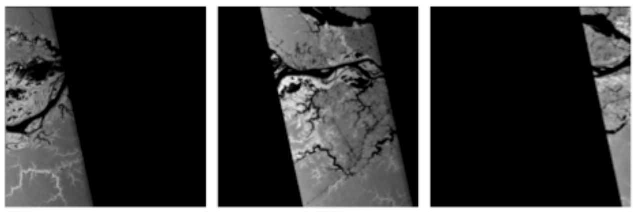

Figure 1: Three SRTM-like tiles (S04W062). This tile is imaged by ALOS on three image strips. During mosaicking, they would be assembled into a single image tile. . © *JAXA/METI*

Once the data has been ortho-rectified, the original strip map data may still be recalibrated, as an intermediate file describing the ortho-rectification is saved and may be reused. Some image strips require radiometric corrections due to a cross track systematic error. The tendency is that the brightness of the image falls off in the near and far range.

In order to assess the magnitude and character of the radiometric calibration, multiple single image strips were examined with similar results. The data were averaged in the along track direction for the entire duration of the image strips. Then, the mean and standard deviation of the image brightness was determined for each range pixel. After averaging over more than a thousand kilometres, the resultant mean trend for each image strip could represent the inverse of the required radiometric correction. As can be seen in figure 2, the nature of the trend for HH and HV are slightly different.

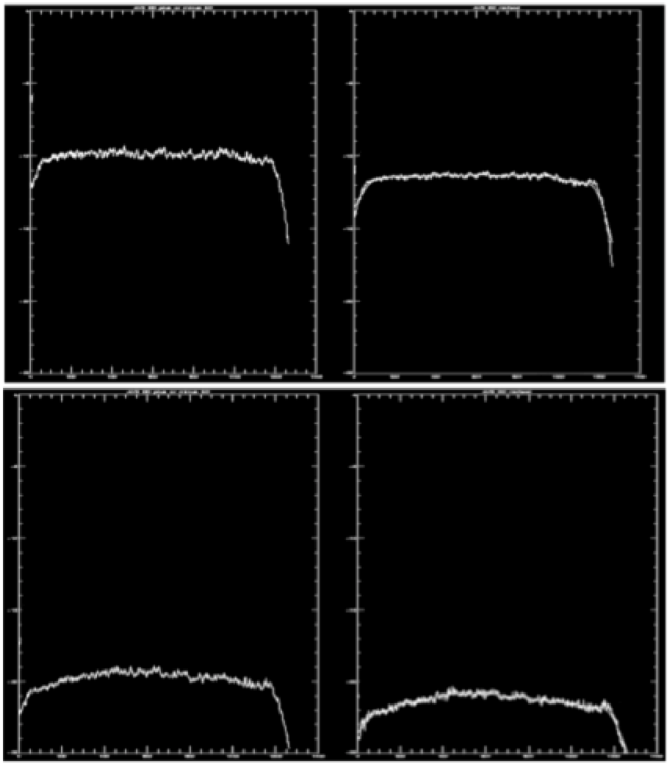

Figure 2: Top graph: mean HH cross track (range) radiometric trend. A) All data. B) Data within 1 standard deviation of mean. Bottom graph: mean HV cross track (range) radiometric trend. A) All data. B) Data within 1 standard deviation of mean.

However, when three strips were mosaicked together after correction for the inverse of this average radiometric trend, figure 3 shows that while this correction improves the radiometric accuracy required for a usable image mosaic, there are still changes in the radiometry in the near/far range overlap regions that appear to change along the image track.

The final image mosaics will have a pixel spacing of 1 arcseconds, but the resolution of the data will be approximately 100 m.

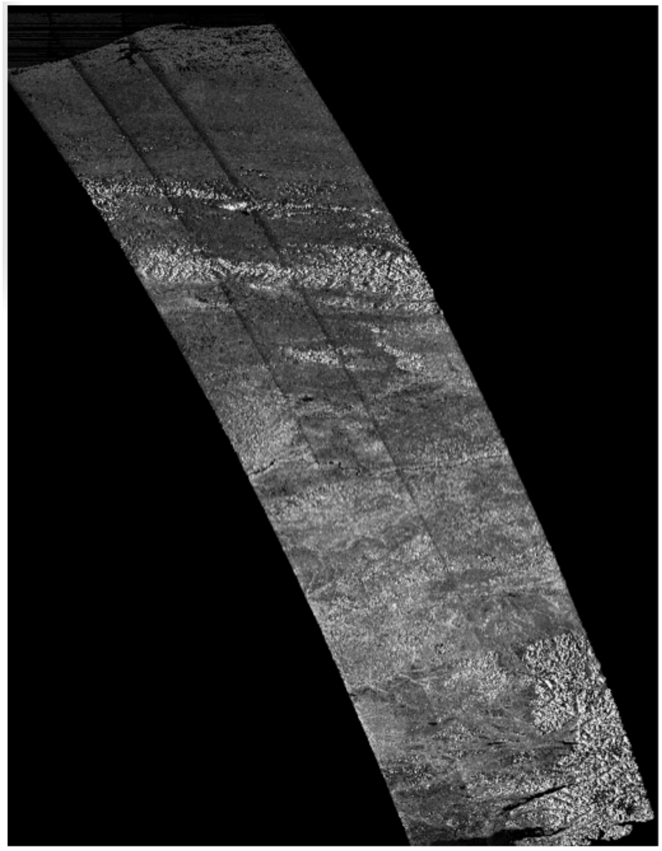

Figure 3: Mosaic of three ALOS image strips (Alaska). © JAXA/METI

Once the image mosaics are generated, the display of ortho-rectified Earth imagery can be facilitated through Earth image browsers such as Google Earth. These Earth image browsers are easy to use, and enable visual comparison of ALOS imagery and derived products with high-resolution optical imagery. They can also be a means for data discovery, in which you use the Earth image browser to geographically find the imagery or data that you require. They can provide a public presentation at multiple resolutions of ALOS imagery and data, which is important due to the simultaneously fine resolution and large geographic extent of the ALOS Kyoto and Carbon Initiative products. They also provide a platform for interaction with the data.

As can be seen in Figure 4, it is possible to control what resolutions are visible to the user. As the user zooms into the image, progressively higher resolution imagery may be seen.

Figure 5 shows how the imagery may be annotated, and displayed simultaneously with other imagery, such as Landsat imagery, which can be quite useful in interpretation of the data.

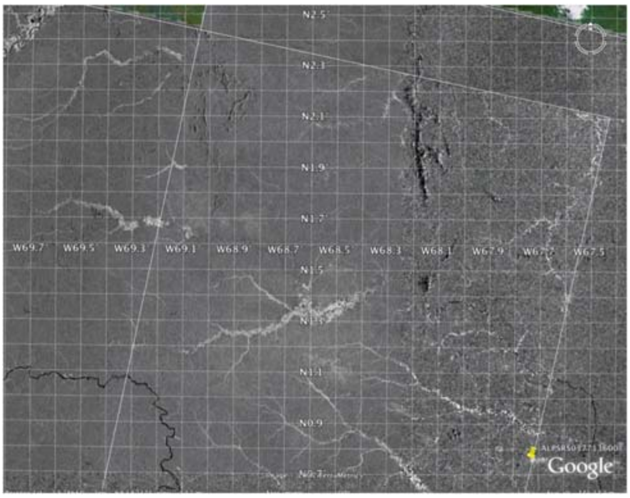

Figure 4 Imagery may be displayed at full resolution using Earth image browsing software. © JAXA/METI

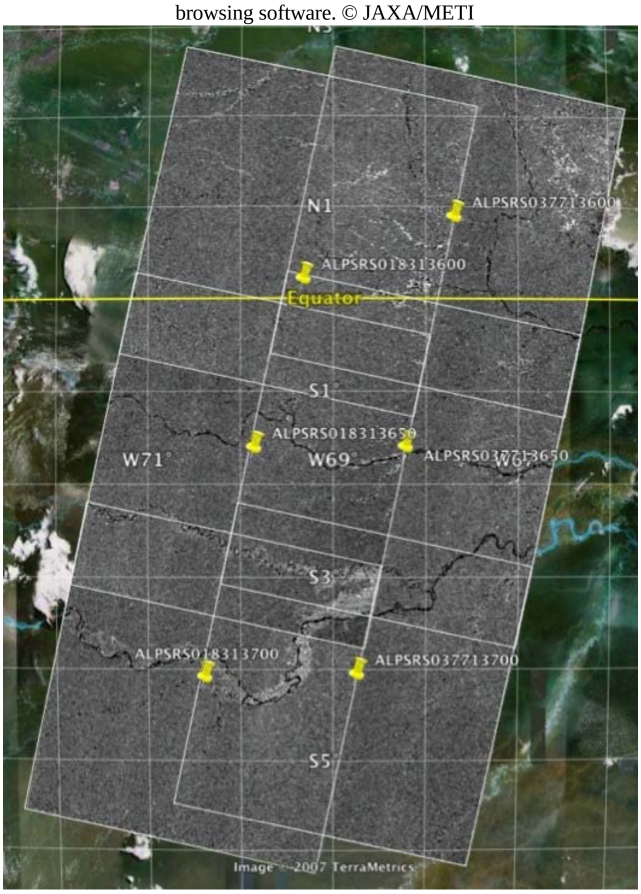

Figure 5. ALOS PALSAR image frames annotated and displayed within Google Earth. © JAXA/METI

It is also possible to view the ALOS imagery and products within an web browser. However, again, the large geographic extent and fine resolution constrain how this may be best implemented. Figure 6 shows an example of a zoomable interface, in which the regional scale imagery has been subdivided into geographic tiles that may be carefully examined within a standard web browser.

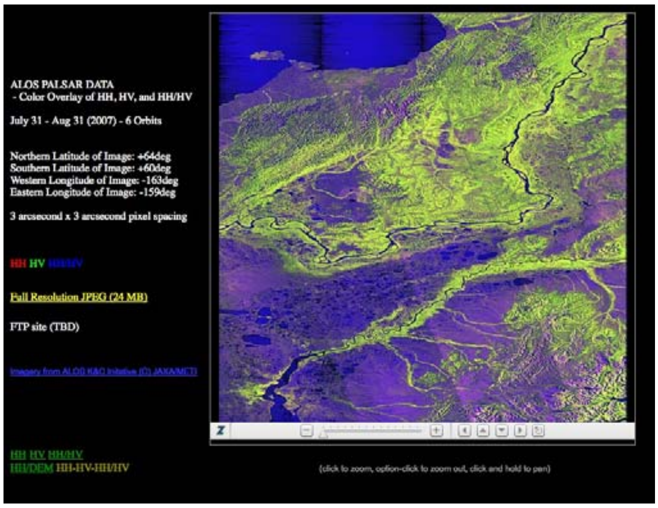

Figure 6. ALOS image mosaic subdivided into a geographic tile, and displayed within a web browser with a zoomable interface. ALOS K&C © JAXA/METI

C. Satellite and ground data

The ortho-rectification of the dual polarization ALOS PALSAR data is dependent on the DEM reference used. For this work, the SRTM 90 DEM from CGIAR-CSI [8,9] was oversampled to one arcsecond pixel spacing and padded to overlapping and padded DEM tiles. The ALOS dual polarization data is in the slant range projection from the JAXA EORC, and is from Summer 2007.

III. Results and Summary

Figure 7 shows a mosaic of the imagery from North America, without radiometric correction. This mosaic shows that while there are occasional gaps in coverage, the coverage during this period (summer 2007) was comprehensive and of good quality.

Figure 8 and figure 9 show that these data reveal fine target features at the high resolution of the final image mosaics. Once the dual polarization mosaics are completed, the use of this data in combination with multi-temporal ScanSAR mosaics of wetland regions around the world will lead to the creation of a record of the extent and dynamics of inundated wetlands for most of the worlds major wetland regions. This work is only possible using an L-band SAR with a global and multi-temporal observation strategy such as employed by ALOS [6].

In future work, the regions outside of North and South America will be processed and analyzed.

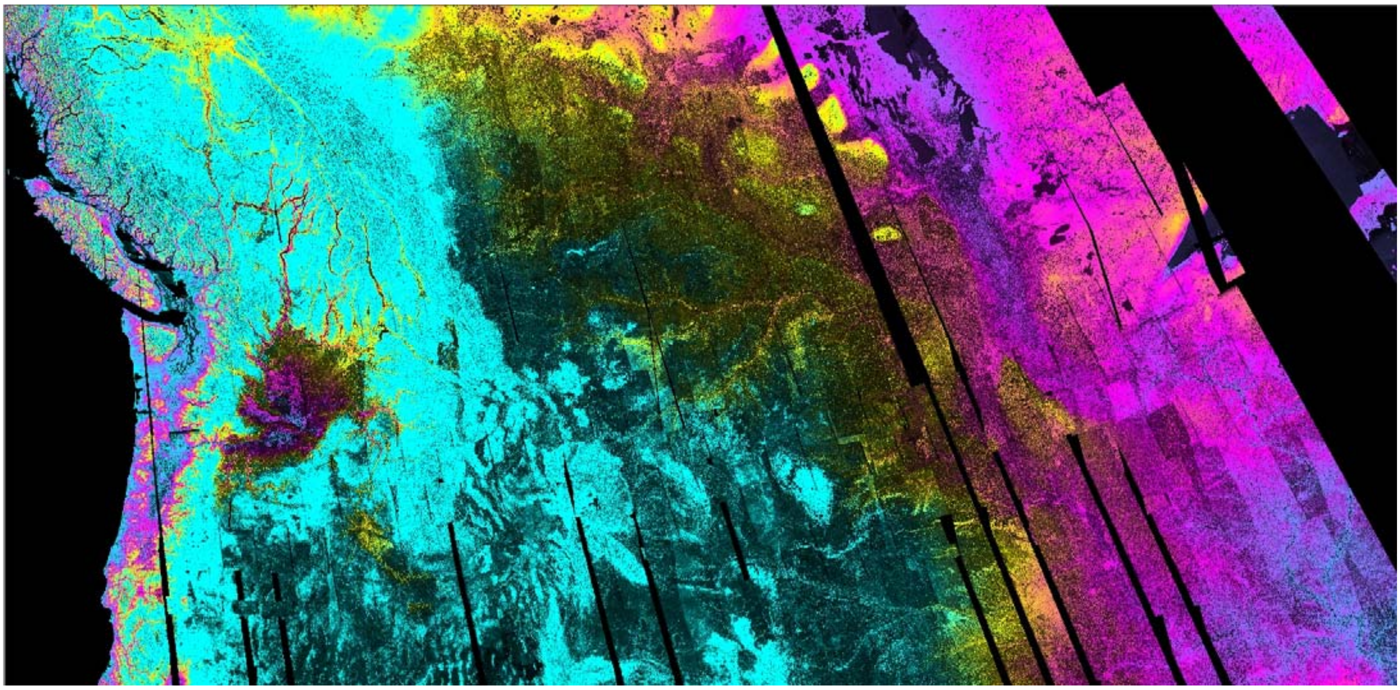

Figure 7. Image mosaic of Northern North America. Color contours correspond to ground topography. Image brightness corresponds to ALOS PALSAR HH. ALOS K&C © JAXA/METI

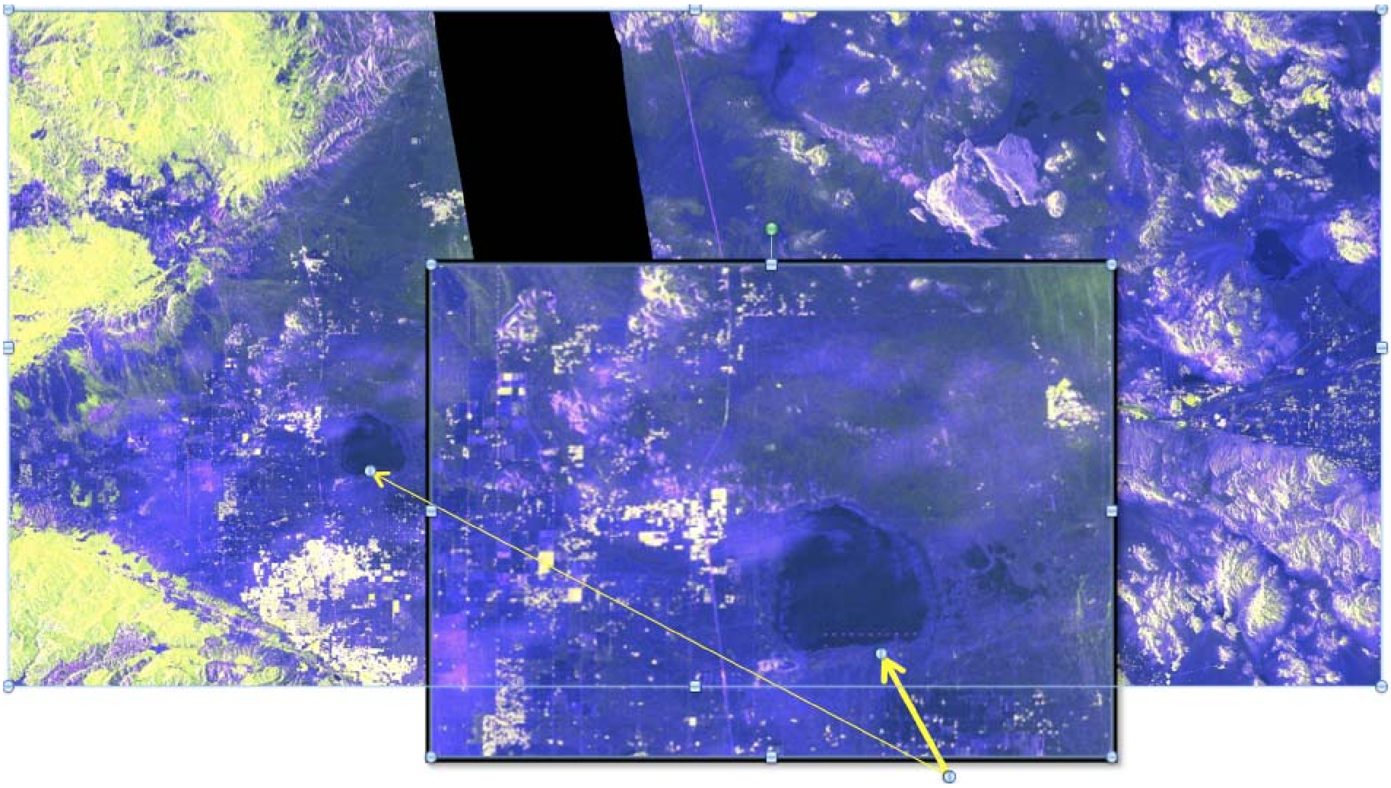

Figure 8: Mohave Desert in Southern California, USA. Rosamond Corner reflector array is visible. Colors correspond to HH – Red, HV – Green, HH/HV – Blue. © JAXA/METI

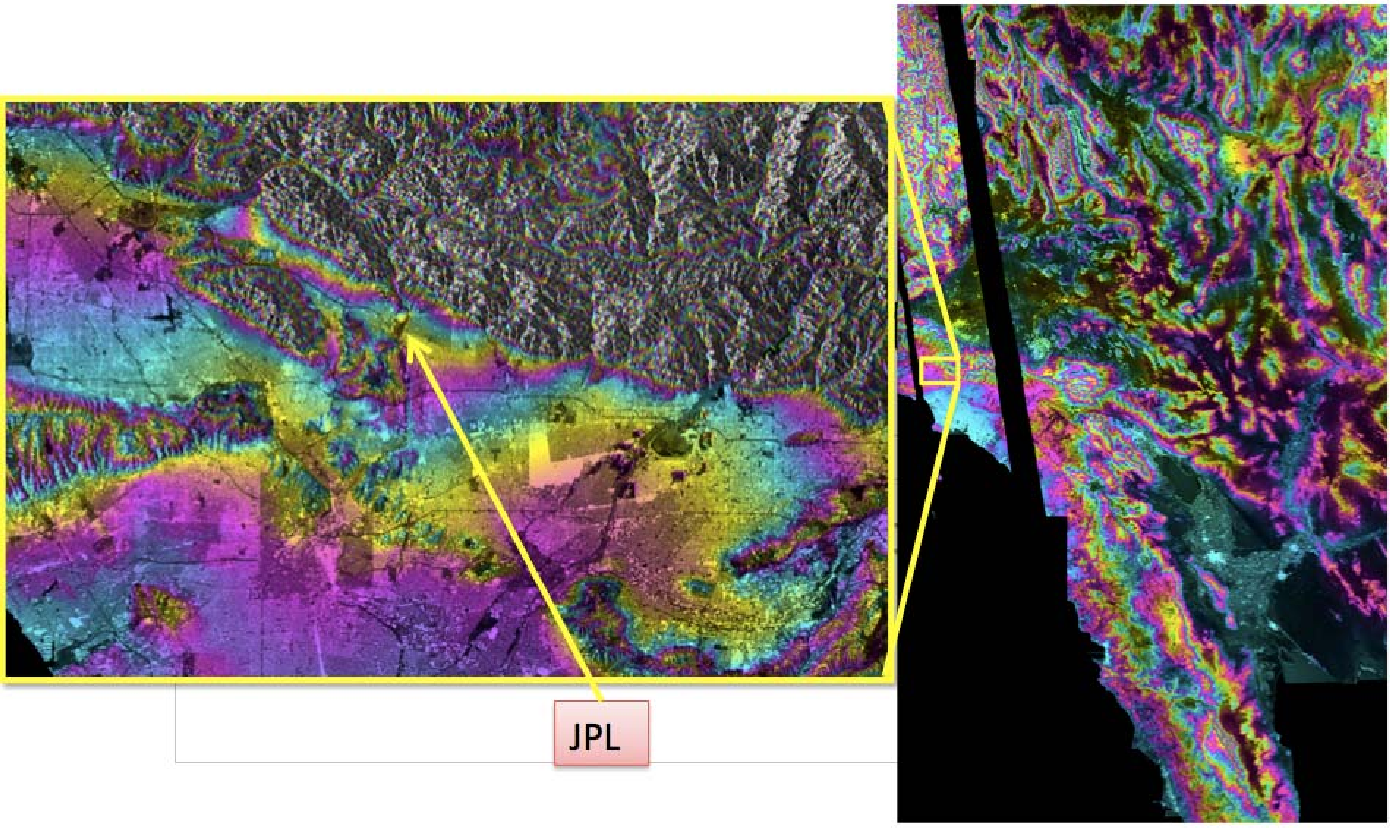

Figure 9: Los Angles, California, USA and the South Western USA. Brightness is HH image brightness, color contours corresponds to ground topography. ALOS K&C © JAXA/METI

IV. REFERENCES

ACKNOWLEDGEMENTS

This paper was partially written at the Jet Propulsion Laboratory, California Institute of Technology, under contract with the National Aeronautics and Space Administration. This work has been undertaken in part within the framework of the JAXA Kyoto & Carbon Initiative. ALOS PALSAR data have been provided by JAXA EORC.

REFERENCES

[1] M. Shimada, "PALSAR and Calibration update". *11th ALOS K&C Science Team meeting (KC#11)*, Tsukuba, Japan, Jan. 13-16, 2009. [Online] Available: http://www.eorc.jaxa.jp/ALOS/kyoto/jan2009_kc11/pdf/090113/shimada_calval_up_090113.pdf

[2] A. Rosenqvist, M. Shimada, R. Lucas, J. Lowry, P. Paillou, B. Chapman [eds.], "The ALOS Kyoto & Carbon Initiative, Science Plan (v.3.1)," JAXA EORC, March, 2008. [Online] Available: http://www.eorc.jaxa.jp/ALOS/kyoto/KC-Science-Plan_v3.1.pdf

[3] ALOS Kyoto & Carbon Initaitve home page: http://www.eorc.jaxa.jp/ALOS/kyoto/kyoto_index.htm

[4] K&C Wiki site. http://www.ies.aber.ac.uk/en/subsites/the-alos-kyoto-amp-carbon-initiative

[5] K&C Wiki site. http://www.ies.aber.ac.uk/en/subsites/the-alos-kyoto-amp-carbon-initiative/latest-news

[6] Rosenqvist A., Shimada M., Ito N. and Watanabe M. "ALOS PALSAR: A pathfinder mission for global-scale monitoring of the environment," *IEEE Trans. Geosci. Remote Sens, vol. 45, no. 11, pp. 3307-3316, 2007.*

[7] C. Werner, U. Wegmüller, T. Strozzi, and A. Wiesmann, "Gamma SAR and interferometric processing software," in *Proc. ERS-ENVISAT Symp*., Gothenburg, Sweden, Oct. 16–20, 2000.

[8] McDonald, K.C., Chapman, B., Podest, E., Jimenez, A, "Assessment of a Near-Global 30-Meter Resolution DEM Derived from the Publicly Available SRTM Data Set for Use in Orthorectification of Satellite SAR Imagery," *AGU*, FALL 2007.

[9] SRTM 90 m Digital Elevation Data from CGIAR-SCI http://srtm.csi.cgiar.org/

Bruce Chapman is a senior member of the technical staff at the Jet Propulsion Laboratory, California Institute of Technology, in Pasadena, California. He received his Bachelor of Arts degree in Physics and Astronomy from the University of California, Berkeley in 1981, and his Ph.D. in Earth, Atmospheric and Planetary Sciences from the Massachusetts Institute of Technology in 1986. He is currently an investigator in NASA's Terrestrial Ecology, Space Archaeology, and MEASUREs programs, studying forest structure measurements using Synthetic Aperture Radar, and the utilization of airborne Synthetic Aperture Radar in Mayan Archaeology regions in Central America; as well as participating in the production of an Earth Science Data Record for Inundated Wetlands using ALOS SAR data. He is also the science coordinator for NASA's UAVSAR airborne Synthetic Aperture Radar.

Mosaic Theme

Generation of PALSAR Mosaics over Africa and Eurasia

Frank De Grandi *et al.*
Joint Research Centre of the E.C. (E.U.)

K&C Science Report – Phase 1
Generation of PALSAR mosaics over Africa and Eurasia

Gianfranco De Grandi and Ake Rosenqvist
European Commission Joint Research Centre, Inst. for Environmment and Sustainability
Global Environment Monitoring Unit, TP. 440, 210 27 Ispra (VA), Italy
frank.de-grandi@jrc.it & ake.rosenqvist@jrc.it

Francesco Holecz and Stefano Monaco
sarmap – Cascine di Barico, 6989 Purasca, Switzerland
fholecz@sarmap.ch & stefano.monaco@sarmap.ch

***Abstract*—The JRC contribution to the Kyoto & Carbon Initiative constitutes the continuation of the collaboration with JAXA (then NASDA) which started more than 13 years ago within the framework of the Global Rain Forest and Boreal Forest Mapping (GRFM/GBFM) projects. The JRC is here responsible for the generation of 50 m resolution ortho-rectified PALSAR mosaics over the African continent (on-going) and subsequently, over Siberia and Europe, for the year 2007. The data used are the slant range path data processed by JAXA EORC, each some 1000~2000 km in length. Comprehensive calibration procedures have been developed to cope with the radiometric and geometric characteristics of the path image data.**

All data were acquired as a part of the systematic observation strategy implemented by JAXA for ALOS PALSAR, which is designed to provide consistent wall-to-wall coverage of all land areas twice pers year during the mission life of ALOS [1]. 319 path images were used for the generation of the Africa mosaic, out of which 276 of the passes were acquired during the main time window of June-August, 2007, another 27 passes during the next 46-day cysle (Sept-Oct, 2007), while 16 passes (i.e. 5% of the total) had to be filled in from the 2008 acquisitions.

***Index Terms*—Africa, ALOS PALSAR, K&C Initiative, Mosaic Theme.**

I. PROJECT STATUS

A. Development of methods and software tools for the generation of K&C ALOS PALSAR mosaics.

Analysis of the problems related to processing high volumes of K&C FBD dual polarization strip data has been carried out and resulted in the implementation of an automatic processing chain (see below). This effort sets the stage for the implementation of all the remaining subtasks, which is currently under way. However, please notice that improvements and refinements of methods and software code will be possibly undertaken in the extension phase if required in the course of further experiments or developments. As it always happens in science and technology, the word "completed" should be taken with due care. From this standpoint, it is proposed that the code will be delivered to JAXA only when duly consolidated. In any event the current version of the code will be included in the K&C final report for phase 2006-2008.

This task addresses the theoretical and operational requirements for the assemblage of the K&C continental scale radar mosaics. The target is the generation of geo-coded terrain corrected continental scale imagery with high radiometric quality - supporting consequently the generation of thematic products. This goal and the high data volume associated with the mosaics' generation calls in turn for the development of a bespoke and highly automated processing chain. Accordingly, a major effort has been undertaken for designing algorithms and developing software that could meet the K&C requirements. By now, a fully automatic processing chain for K&C mosaicking is in place and under test in the generation of prototype Africa radar mosaics. The processing chain consists of a blending of bespoke IDL modules and functional components supplied by SARSCAPE, a commercially available radar processing software developed by SARMAP s.a, Switzerland. The main modules and the operation flow are:

- House keeping routines to handle the ingestion and file structure of the JAXA strip data.
- Adaptive calibration revision of the original slant range data sets. This module automatically checks for the presence of radiometric anomalies (power loss in range) and calibrates accordingly the data.
- Extraction from a global Africa digital elevation model of subsets corresponding to the geographical extent of each strip data. The global Africa DEM was generated by the Consortium for Spatial Information (CGIAR-CSI). It is based on Shuttle Topographic

Mission data (SRTM) and missing data were filled using interpolation and auxiliary topographic data.

- Generation of batch files for importing calibrated JAXA strip data and SRTM tiles into SARSCAPE.
- Geo-coding into a geographic reference frame (un-projected latitude-longitude for Africa) using the solution of the range-Doppler equations (as implemented in SARSCAPE). This step also produces auxiliary data holding the effective local incidence angles for each pixel of backscatter data.
- Compression of the geo-coded data sets.
- Mosaicking of the compressed geo-coded strips within a geographic bounding box and using inter-strips blending.
- The whole process is repeated for data acquired at HH and HV polarizations, resulting finally in a co-registered set of 3 layer mosaics (backscatter HH, HV and local incidence angle).

B. Developing methodology for forest change and land cover mapping.

Methods for forest structural parameters estimation from K&C imagery have been extensively investigated both from the theoretical and experimental stand-points. However full scale application of the methods to arrive at the generation of thematic products as required by subtasks 1.d will be possible only when the final version of the mosaics will be available. This task will therefore be completed in the extension phase.

C. Developing methodology for product validation and accuracy estimation.

Classical methods were used for estimating the geometric accuracy of the geo-coded products. These methods call for tie-pointing with reference imagery (e.g. Landsat) of known accuracy. Radiometric calibration assessment is based on the assumption that slant range detected products delivered by JAXA are already nominally calibrated for range power spreading loss and effective scattering area. Radiometric checks are only performed in cases where calibration anomalies are detected (e.g. power loss in range) and consist of supervised profiling of selected areas featuring homogeneous distributed targets (e.g. forest).

D. Generation of K&C PALSAR mosaics and related products.

Two factors have delayed the task progress: i) some outliers in the PALSAR data acquisition plan, which made full coverage of the areas interest complete only later and by gap-filling acquisitions; ii) technical complexities related to the new PALSAR data sets and the target specifications of the products to generate. In our opinion, both aspects are typical of large scale projects and almost unavoidable when straddling into new terrain, as it is a case in point with the K&C continental scale mosaics. Moreover, notice that the project plan and priorities have been changed with respect to what originally stated in the JAXA-JRC agreement. This was due, on the one hand, to a change of priorities in the JRC research programs (focus shifted from Boreal towards Tropical regions)

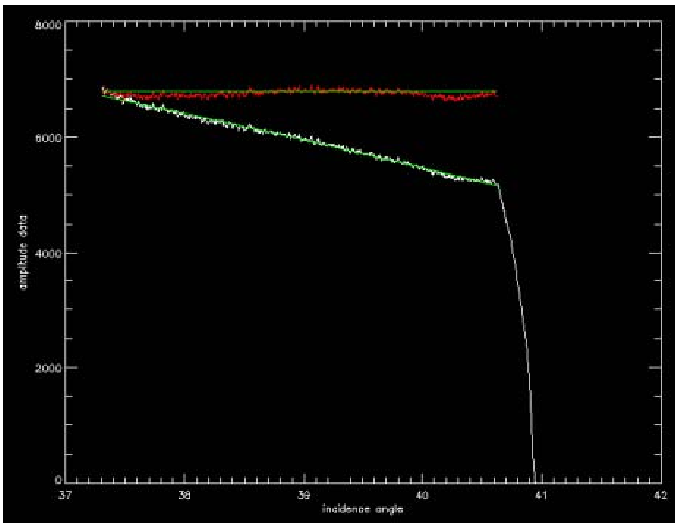

Figure 1. Example of range power loss flaw in K&C strip data, and correction by automatic flaw detection and a range-dependent empirical function

and to the other hand, to a reschedule of the overall commitments of the K&C science team. Basically, the generation of the whole Africa mosaic, not initially foreseen, has now been taken over by JRC, while the generation of the Boreal area mosaic and the related thematic products has been postponed. This point will be further elaborated in section 2.1, because it is instrumental for the definition of tasks in the requested extension phase. Major difficulties encountered in processing PALSAR data in connection with the assemblage of K&C mosaics were:

a) SAR focusing (JAXA SigmaSAR processor) in non-zero Doppler geometry. As a consequence the geo-coding algorithm, based on the solution of the range-Doppler equations, had to be redesigned.

b) Missing information on Doppler centroid estimation in some early data acquisitions. JAXA supplied code to retrofit the data.

c) Range power loss anomalies in some data sets (Fig. 1)

d) Computational problems related to the high volume of data. This problem stems from the intrinsic large coverage character of the mosaics, but also from the geometry of the long K&C SigmaSAR strip data. The raster representation of this type of imagery, once projected into a geographic reference frame (viz. geo-coded), tend to be quite inefficient, due to the large number of non significant data elements (e.g. pixels outside the imaged area). These features have an impact both on external and internal memory allocation, and on processing time. The problem has been partially alleviated by introducing a simple compression algorithm, after the geo-coding step. The mosaicking procedure then de-compresses on the fly the data sets before pasting into external memory

At the time of this writing, several prototype mosaics over Africa have been assembled. The scope of this experiments is to debug and validate the processing chain, in particular with respect to assuring a seamless assemblage of the strips, a fact that depends both on proper geometric and radiometric

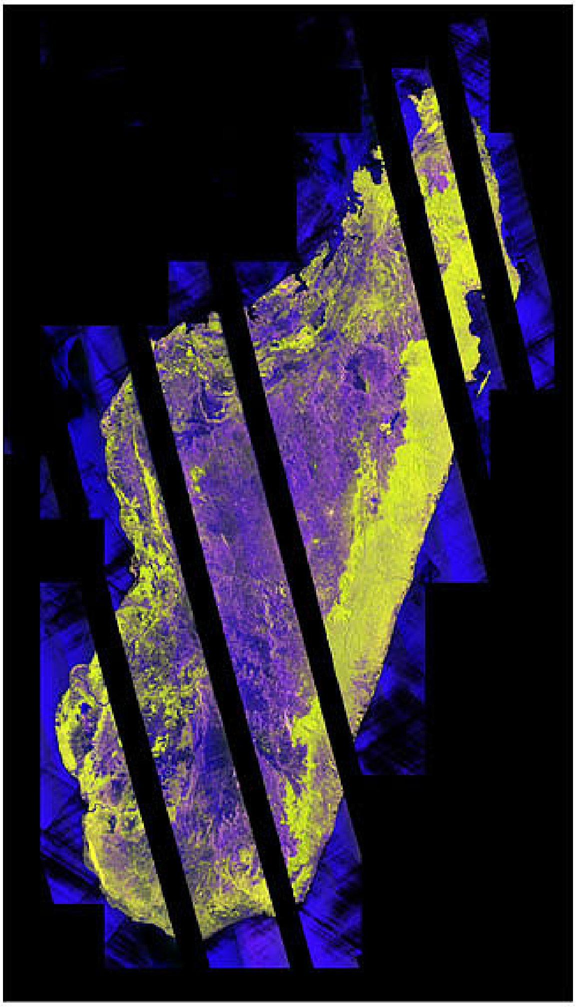

Figure 2. Prototype K&C mosaic over Madagascar.
Processed by JRC © JAXA/METI

fidelity. An inter-strip blending algorithm assures a good visual perception of the mosaic, even in the presence of residual mismatches, due for instance to temporal changes, or local incidence angle effects. Some examples are reported in Fig. 2 and 3. Processing of a prototype full Africa mosaic is scheduled to be completed by end 2008. The generation of the Europe and Siberia mosaic will have to be shifted to the requested extension phase. Additional difficulties in the generation of this mosaic stem from the unavailability of a homogeneous digital elevation model (DEM). Indeed the SRTM derived DEM covers only up to 60 N in latitude. Work is in progress to generate a global DEM over Siberia by blending SRTM and GTOPO DEMs. Notice finally that an additional product, not originally foreseen by the agreement, has been developed in the K&C context by the JRC: a full coverage of Venezuela at 200 m resolution using PALSAR data in SCANSAR mode. This product is intended as a test bed to prove the capability of the K&C processing chain with respect to SCANSAR acquisition mode, and to support a specific JRC commitment towards the European Commission's delegation in Venezuela.

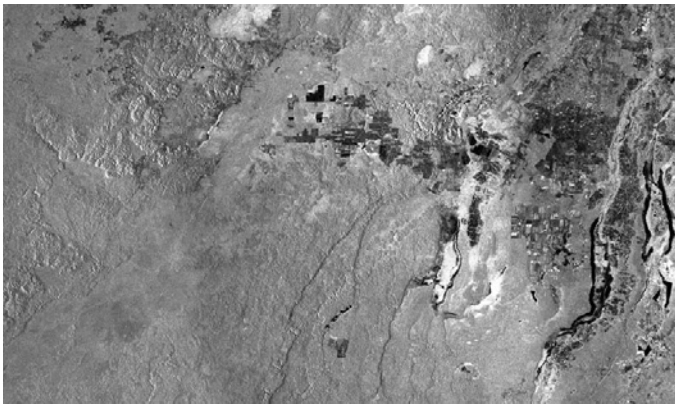

Figure 3. Subset of a prototype Africa K&C mosaic at full resolution, showing the seamless assemblage of two strips. © JAXA/METI

II. PLANS FOR PHASE 2

A. Completion of work from Phase 1

The major driving forces that caused a change in the original planning have been discussed above and can be summarized as follows:

- Complexity of the end-to-end project path, from data acquisition to generation of final products. This aspect touches upon both partners, JAXA and JRC.

- Steering of research focus at JRC from Boreal to Tropical areas and in particular to Africa. The consequences, as far as the K&C first phase is concerned, were:

1. Decision by JRC to take up the task for the generation of the whole Africa mosaic (not foreseen in the original agreement).

2. Priority allocation of resources to solving methodological and computational problems related to this product, with consequent phasing out of other commitments originally listed at point 1.2.4.

3. Delay in the task completion

Given this scenario the JRC tasks were amended to bridge over to the extension phase in a way that would still assure the delivery of comparable "value" to JAXA in terms of products and methods:

Task E1: Final version of the dual-polarization mosaic over the whole African continent. The mosaic will complemented by auxiliary data sets, such as the corresponding DEM, local incidence angle information, and a set of ground control point to document the geometric accuracy (notice that a prototype mosaic will be delivered still within phase one). Foreseen end time: April 2009.

Task E2: Compilation of the Europe-Siberia mosaic, and auxiliary data sets (e.g. dual-resolution DEM). Foreseen end time: December 2009.

Task E3: Thematic products concerning land cover mapping in Africa.

- Study of the transition zones at the border of the Congo basin, with emphasis of deforestation patterns, re-growth, forest fragmentation, embedded savannah (as detailed in the original work plan). Foreseen end time: December 2010.
- Update of the GRFM Central Africa wetlands map.
- Regional scale forest resource assessment and estimation of forest cover change with respect to years 1997 (GRFM acquisitions) in Central and West tropical Africa. Foreseen end time: Dec 2010

Task E4: Research and development of methods for forest structural and bio-physical parameters retrieval using fusion of K&C radar mosaics, orbital earth observations in the optical domain, orbital LIDARs, and topographic information. The study will be conducted using test cases in the tropical and sub-tropical domains. It will be an extension of work carried out in task 1.2.2 of phase 1 (see paper [2]). It will be conducted in collaboration with the department of geography, University of Wales at Aberystwyth. Foreseen end time: Dec 2011

ACKNOWLEDGEMENTS

This work has been undertaken within the framework of the JAXA Kyoto & Carbon Initiative. ALOS PALSAR data have been provided by JAXA EORC.

REFERENCES

[1] Rosenqvist A., Shimada M., Ito N. and Watanabe M. "ALOS PALSAR: A pathfinder mission for global-scale monitoring of the environment," *IEEE Trans. Geosci. Remote Sens, vol. 45, no. 11, pp. 3307-3316, 2007.*

[2] G.. De Grandi, R.M. Lucas, J. Kropacek," Analysis by Wavelet Frames of Spatial Statistics in SAR Data for Characterizing Structural Properties of Forests", IEEE Trans. on Geoscience and Remote Sensing, vol. 47, issue 2, 2008, in press.

[3] G. De Grandi, J. Kropácêk, T. L. Ainsworth, "Spatial Properties of Forest Clutter in Polarimetric SAR Imagery Measured by Wavelet Frames", Proc. 5th International Symposium on Retrieval of Bio- and Geophysical Parameters from SAR Data for Land Applications, Bari, 2007.

[4] G. De Grandi, J. Kropacek, A. Gambardella, M. Migliaccio, T. Ainsworth, "Analysis of Spatial Statistics in Polarimetric SAR Data Using Wavelet Signatures", Proc. EUSAR08, 2008.

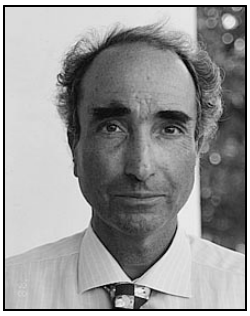

Gianfranco (Frank) De Grandi (M'90–SM'96) received the Ph.D. in physics engineering (with honors) from the Politecnico Milano, Milano, Italy, in 1973. Since 1977, he has been with the European Commission Joint Research Centre (JRC), Ispra, Italy, where he has performed research in signal processing for application areas such as gamma ray spectroscopy, data communications, and radar remote sensing. In 1985, he was a Visiting Scientist with Bell Communications Research, Morristown, NJ, where he participated in the design of METROCORE, one of the first research projects for Gb rate metropolitan area networks. From 1986 to 1989, he headed the signal processing section of the Electronics Division, JRC, where he introduced VLSI design technology and conducted research, in cooperation with Bellcore, on packet video, and in cooperation with ITALTEL Italy on the European digital mobile phone network. In 1989, he joined the Institute for Remote Sensing Applications [now Space Applications Institute (SAI)], where he started a research activity in radar polarimetry in the Advanced Techniques unit. Since 1994, he has been Principal Scientist for radar remote sensing in the Global Vegetation Monitoring unit. Since 1997, he has been Assistant Professor with the Faculte' de Foresterie et Geomatique, Universite' Laval, Quebec, PQ, Canada. His current research interests span a wide gamut, including global scale forest mapping using high resolution spaceborne SAR, multiresolution analyses based on the wavelet representation for texture measures, backscattering multitemporal estimators, topography sensing using polarimetric SAR data, and the statistics of polarimetric synthesized SAR images. Dr. De Grandi is a senior member of the IEEE Geoscience and Remote Sensing and Signal Processing Societies and a member of the Planetary Society, Pasadena, CA

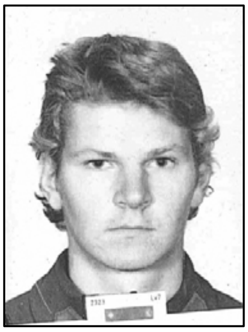

Ake Rosenqvist is Science Coordinator for the Kyoto & Carbon Initiative. He is presently a Marie Curie Fellow with the EC Joint Research Centre in Ispra, Italy, and part of the TREES group at the Global Environment Monitoring Unit. His research interests include forest- and wetlands monitoring and support to climate change science and policy needs. With a background from the Swedish Space Corporation, where he was involved in land cover and topographical mapping with SPOT, he deserted the optical field in 1993 and spent 9 years illuminated by radar at the Japanese Space Agency, JAXA/NASDA. He has been involved in the development of the JERS-1 and ALOS applications programmes, the establishment of the JERS-1 Global Forest Mapping (GRFM/GBFM) and ALOS K&C Initiative projects, and the design and implementation of systematic data observations strategies adopted by JAXA for the ALOS mission.

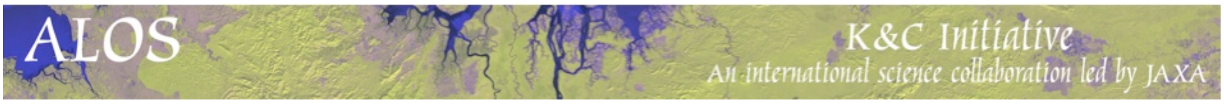

For more information about the ALOS Kyoto & Carbon Initiative,
please visit the K&C homepage at JAXA EORC:

http://www.eorc.jaxa.jp/ALOS/en/kyoto/kyoto_index.htm

Document reference: JAXA EORC, NDX-100003